Available online at www.sciencedirect.com
ScienceDirect
Talanta 70 (2006) 225–235
Talanta
www.elsevier.com/locate/talanta

Generation and characterization of polyclonal antibodies against microcystins—Application to immunoassays and immunoaffinity sample preparation prior to analysis by liquid chromatography and UV detection

Houcine Mhadhbi [a,*], Samuel Ben-Rejeb [b], Chantal Cléroux [b], Annie Martel [a], Philippe Delahaut [c]

[a] *Laboratoire de Chimie et Biochimie des Complexes Moléculaires, UMR 7576, Ecole Nationale Supérieure de Chimie de Paris, 11 rue Pierre et Marie Curie, 75231 Paris Cedex 05, France*
[b] *Food Research Division, Food Directorate, Bureau of Chemical Safety, Health Products and Food Branch, Health Canada, Sir Frederick Banting Research Centre, PL 2203D, Ottawa, Ont., Canada K1A 0L2*
[c] *Laboratoire d'Hormonologie, CER, 8, rue du Point du Jour, B-6900 Marloie, Belgium*

Received 23 September 2005; received in revised form 1 February 2006; accepted 7 February 2006
Available online 31 March 2006

Abstract

Polyclonal antibodies against microcystin-LR (MC-LR), a cyclic heptapeptide toxin, were generated in rabbits using MC-LR-BSA. An enzyme-linked immunosorbent assay (ELISA) was developed for the characterization of the antibodies and their potential use for analytical purposes. The concentration of MC-LR that inhibits 50% of antibody–antigen binding (IC_{50}) was 0.5 μg L^{-1} for the indirect ELISA format and 0.9 μg L^{-1} for the direct ELISA, using MC-LR-horseradish peroxidase conjugate. The limit of detection corresponding to IC_{80} was found to be 0.06 μg L^{-1}, well below the Word Health Organization level for drinking water of 1 μg L^{-1}. The direct competitive ELISA was applied to water samples and was shown useful for screening purposes. The developed anti-microcystin antibodies were immobilized on solid supports for use in selective solid phase extraction (SPE) systems, prior to liquid chromatography (LC) quantification. An immunoaffinity cartridge (IAC), a Sepharose®-based cartridge incorporating 2 mg of antibodies allowed the selective and quantitative recovery of a mixture of 0.2 μg of MCs showing potential use in sample preparation of real matrices. When applied to water and green algae samples, average recoveries from Sepharose®-based cartridges were in the range of 86–113% for water samples and 85–92% for blue-green algae samples. Selectivity of the IAC clean-up was proven by comparison with non-specific solid phase extraction using octadecylsilica (ODS) sorbent. Results obtained using LC/UV after IAC clean-up agreed well with results obtained using liquid chromatography and mass spectrometry detection (LC/MS and LC/MS/MS) after SPE-C18 clean-up, allowing therefore to validate the resulting technique.

Keywords: Microcystins; Enzyme immunoassay; Sample preparation; Immunoaffinity chromatography; Blue-green algae; Solid phase extraction

1. Introduction

Microcystins (MCs) are a family of hepatotoxic peptides produced by freshwater cyanobacteria (blue-green algae) belonging to the genera *Microcystis*, *Anabaena*, *Nostoc* and *Oscillatoria* (Planktothrix). All microcystins have a common cyclic heptapeptide structure (Fig. 1) consisting of -D-Ala-L-**X**-D-erythro-β-methylisoAsp-L-**Z**-Adda-D-iso-Glu-*N*-methyldehydro Ala, where Adda is a C_{20} amino acid: 3-amino-9-methoxy-2,6,8-trimethyl-10-phenyldeca-4,6-dienoic acid and **X** and **Z** refer to the variable amino acids that give its name to the molecule [1]. These molecules represent an increasing environmental and health risk as their presence in sources of water supplies has caused the death of wild and domestic animals worldwide [2] and has been linked to human fatalities [3]. MCs have been shown to inhibit protein phosphatase [4] and to promote tumors [5]. Animal studies carried out in mice administered with MCs resulted in the death of the treated animals suffering from hypovolemic shok due to loss of blood from the vasculature in the damaged liver, within 1–3 h

* Corresponding author: Tel.: +33 1 44 27 67 29; fax: +33 1 44 26 00 61.
E-mail address: elmhadhbi@yahoo.com (H. Mhadhbi).

0039-9140/$ – see front matter © 2006 Elsevier B.V. All rights reserved.
doi:10.1016/j.talanta.2006.02.029

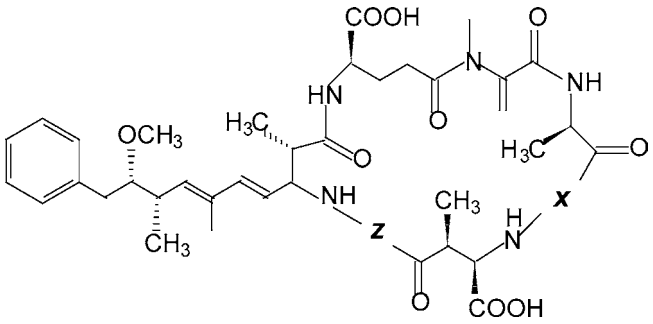

Fig. 1. Common structure of microcystins.

after MCs administration. Extensive hemorragic necrosis and disruption of sinusoids in the liver of mice or rats were reported as direct toxicological effects related to MCs [6,7]. Because of their natural occurrence, MCs can be found in drinking water supplies and some health food products based on blue-green algae such as *Aphanizomenon* and *Spirulina*, harvested from natural freshwater lakes and commercialized worldwide under a variety of brands, either individually or within vitamin supplements.

The most commonly occurring MCs are microcystin leucine-arginine (MC-LR), microcystin arginine-arginine (MC-RR), microcystin tyrosine-arginine (MC-YR) and microcystin-leucine-alanine (MC-LA) variants.

Available analytical techniques include LC/UV [8,9] and LC/MS [10–13] along with an extensive sample treatment and clean-up prior to injection into the LC system. A novel ISO norm (ISO 20179: 2005 – water quality – determination of microcystins – method using solid phase extraction (SPE) and high performance liquid chromatography (HPLC) with ultraviolet (UV) detection) is available. Some developments of more bio-analytical assays were reported as generic screening systems for different MCs. The mouse bio-assay is most frequently used to detect the toxins in cyanobacterial water blooms [14,15]. The phosphatase inhibition enzyme assay has been developed and extensively used, exploiting the characteristic of MCs to inhibit the regulatory enzymes: protein phosphatase 1 and 2A (PP1 and 2A) [16]. Although convenient for generic sample screening, these assays present the drawback of their sensitivity to the matrices and the fact that some ions such as Mn^{2+} could react as inhibitor of PP2A [31]. In addition to that, the inhibition depends on the variety of the MC and some natural compounds could inhibit the PP1A action [32]. Also, the inhibition ratio depends on the amount of protein phosphatase [33]. In the latter work, it has been shown that amounts of MCs around 0.2×10^3 $\mu g\,L^{-1}$ gave different results for the same level of MC and for the same sample, Enviroguard ELISA test gave results 10 times better than that of the protein phosphatase.

The immunochemical approach provides an excellent alternative suitable for low level detection and quantification of toxicants. Immunoassays constitute a useful screening system offering minimum sample treatment while reaching satisfactory detection limits, allowing therefore to reduce the number of samples to undergo lengthly analytical procedures. Immunoaffinity chromatography (IAC), another immunochemical-based approach, was in turn found to be an excellent sample clean-up technique for a large variety of toxic chemicals in biological samples at trace concentrations using little or no organic solvents [17–19]. This paper describes the application of both techniques to the analysis of MCs in water and blue-green algae.

The development of immunoassays was reported for a large number of low molecular weight toxins, such as mycotoxins [20] and marine toxins [21,22] and was extended to microcystins. Kfir et al. [22] reported the production of monoclonal antibodies against MCs by immunizing mice with MC-LA-polylysine. The generation of monoclonal antibodies against microcystin-LR with high affinity and the establishment of different highly sensitive immunoassays were described earlier (Weller et al. [34], Zeck et al. [35], Zeck et al. [36], Zeck et al. [37] and Lindner et al. [38]). Besides, the generation of monoclonal antibodies needs complicated protocols and high costs and then only restricted number of laboratories are able to perform it.

Polyclonal antibodies against MCs were generated by Chu et al. [23] and Brooks and Codd [21]. The sensitivity of the resulting immunoassays needed further improvement as the IC_{50} values were higher than the WHO guideline of $1\,\mu g\,L^{-1}$ in drinking water. In a recent work, McElhiney and Lawton [39] gave a comparison study between the different analysis methods of MCs, their availability, their efficiency and their field of application, showing the need of supplementary studies to be done.

This paper presents the development and the characterization of polyclonal antibodies newly generated against MCs. These antibodies were previously involved in immunoaffinity cartridges evaluated by collaborating teams [8,24] and were found to be effective in isolating the MCs from blue-green algae, fish and water samples. The resulting extracts were clean enough to enable direct LC/UV detection of the incriminated MCs. Our study has reproduced the development of larger volumes of these antibodies and attempted to demonstrate their further usefulness in analytical applications aiming at the detection of low levels of MCs in water and food supplement samples.

2. Experimental

2.1. Materials

2.1.1. Chemicals and supplies

All chemicals, organic solvents and reagents were analytical grade materials. MC-LR and MC-RR were purchased from Sigma (USA). MC-YR and MC-LA were purchased from Calbiochem-Novabiochem Corp. (USA) and were extracted from *Microcystis aeruginosa*. The purity of these microcystins estimated by HPLC was, respectively, 98.7%, 96.46%, 99.0% and 98.2%. Bovine serum albumin (BSA; RIA grade), ovalbumin (OVA), β-lactoglobulin (β-LG), goat anti-rabbit IgG peroxidase conjugate (secondary antibody), Tween 20, 30% hydrogen peroxidase (H_2O_2), 2,4,6-trinitrobenzene-1-sulfonic acid (TNBS), ethylenediamine (EDA), 1-(3-dimethylaminopropyl)-

3-ethylcarbodiimide hydrochloride (EDC), ethylchloroformate (ClCOOEt), tributylamine (NBu_3), sodium tetraborate ($Na_2B_4O_7$), 1,4-dioxane and Horseradish peroxidase (HRP) were purchased from Sigma–Aldrich Canada Ltd. (Oakville, Ont., Canada). *O*-Phenylenediamine dihydrochloride (OPD) was purchased from Pierce Chemical Co. (Rockford, USA). Freund's complete and incomplete adjuvants were obtained from Gibco (Grand Island, USA). The affinity extraction gel to extract immunoglobulin G (IgG) was the Avid-Chrom gel. IgGs were immobilized on Sepharose CL-4B® from Sigma–Aldrich (Canada) and on aldehyde activated silica gel supports from J.T. Baker (USA). Immulon-2 microtiter plates were purchased from VWR Canlab (Mississauga, Ont., Canada).

2.1.2. Buffers

Phosphate buffered saline (PBS) pH 7.4, contained 10 mM NaH_2PO_4, 10 mM NaH_2PO_4, H_2O and 140 mM NaCl. The plate coating buffer consisted of 13 mM Na_2CO_3 and 35 mM $NaHCO_3$ at pH 9.6 and contained OVA at 10^4 μg L^{-1}. Washing buffer consisted of 0.1% of Tween 20 in PBS. The blocking buffer consisted of PBS containing 0.3% of skimmed milk (PBS-BR). Citrate buffer consisted of 51 mM Na_2HPO_4 and 24 mM citric acid at pH 5.0. The substrate consisted of 17.5 mg *O*-phenylenediamine (ODP) in 25 mL citrate buffer with 10 μL of 30% H_2O_2 added.

3. Instrumentation

A microplate autowasher (EL405) from Bio-Tek Instruments (USA) was used to wash the 96-well microtiter plates. Optical densities (OD) of the wells were measured on a Multiscan Ascent® microplate reader 354 from Labsystems (Finland) with a 492 nm filter. The centrifuge device was a Mikro 22R from Hettich (Germany). The HPLC equipment consisted of a binary solvent delivery module, model LC-10AD using the Class-VP chromatography workstation as data acquisition and instrument controller and equipped with an auto-injector model SIL-9A all from Shimadzu Corporation (Kyoto, Japan).

4. HPLC conditions

The column used was a Symmetry LC-C_{18} column (5 μm ODS, 150 mm × 3.9 mm i.d.) (Waters). A diode-array detector set at 238 nm with 2 nm band length was used. The mobile phase A was acetonitrile/water (20/80) containing 0.05% (v/v) acetic acid and the mobile phase B was acetonitrile/water (80/20) containing 0.04% (v/v) acetic acid. The chromatographic programme run consisted of a gradient step from 10 to 29% B over 7 min then to 60% B over another 7 min and finally to 10% B over 5 min and for 6 min. The flow rate was set at 0.5 mL min^{-1}.

5. Preparation of the immunogen and antibody generation

Because of their low molecular weight (≈1000 Da), MCs are unable to elicit an immune response when injected to laboratory animals such as rabbits used for the immunization. MC-LR was conjugated to BSA chosen as a carrier protein to obtain an immunogen by the water-soluble carbodiimide method using 200 mg of BSA and 500 μg of MC-LR activated by EDC. Five milligrams of EDC was added to 500 μg of MC-LR dissolved into PBS buffer. The pH was adjusted to 5 and the mixture was kept under gentle stirring during 5 min at room temperature. To this solution, 200 mg of BSA was added and the mixture was kept during 4 h at room temperature. The reaction was stopped by the addition of 0.1 M sodium acetate buffer solution at pH 4.2. The solution was, then, dialyzed against PBS buffer during 1 h at room temperature and the product was kept at −4 °C before use.

Rabbits were inoculated with the immunogen (500 μg per rabbit) in complete Freund's adjuvant. A first boost was made 2 weeks later and every 4 weeks trial bleeds were recovered from rabbits 10 days after each administration boost using a mixture of immunogen/incomplete Freund's adjuvant. The titer evaluation of the antiserum was performed using an indirect immunoassay method. Once the protocol of immunization was found satisfactory to elicit the targeted antibodies, larger amounts of antiserum were produced, using several immunizations in rabbits. Antisera with similar characteristics (affinity, titer and cross-reactivity) were pooled to allow a consistent source of immunoreagents.

6. Preparation of MC-LR-OVA conjugate

A second MC-LR protein conjugate was made using OVA as a carrier protein. The conjugation of this carrier protein to MC-LR was performed using the mixed anhydride method. Five hundred micrograms of MC-LR was dissolved in 0.5 mL methanol and divided into two 250 μL-fractions, which were evaporated to dryness at 35 °C under nitrogen stream. To one residue (fraction 1), containing 250 μg of MC-LR, 0.5 mL of 1,4-dioxane was added and stirred. Eight microliters of ethylchloroformate and 15 μL of tributylamine were then added. The solution was mixed and maintained 30 min at room temperature. The solution was then added slowly and dropwise to the OVA solution (10 mg in 3 mL of bicarbonate buffer at pH 9.6). The reaction was kept 2 h at room temperature and left overnight at 4 °C and then dialyzed against 2 L of PBS for 3 days with the buffer solution changed once a day.

7. Preparation of MC-LR-HRP conjugate

Conjugation of MC-LR to HRP was achieved by the mixed anhydride method. Two hundred and fifty micrograms of MC-LR was dissolved in 1,4-dioxane and 8 μL of ethylchloroformate was added under stirring. Then, 15 μL of tributylamine was added and the mixture was stirred at room temperature for 30 min. A solution of 10 mg HRP in 0.5 mL PBS buffer 0.02 M at pH 7.4 was then added dropwise. The mixture was stirred and the pH was adjusted to 9 using sodium tetraborate. After incubation overnight at 4 °C under stirring, the mixture was dialyzed against PBS buffer 0.02 M at pH 7.4 and then carried

out overnight at room temperature. Finally, the product was concentrated, fractionated into 200 μL aliquots and stored at −20 °C.

8. Immunoassay

8.1. Microtiter plate coating

Protein conjugates or antibodies to be coated were diluted in carbonate buffer containing 10^4 μg L^{-1} OVA as a blocking reagent and were added to each well of 96-well ELISA microtiter plate (200 μL per well). Coating was allowed at 4 °C overnight. After the solution was removed, the wells were washed three times with PBS-Tween (300 μL per well).

8.2. Monitoring of antibody titers by indirect ELISA

MC-LR-OVA coated plates were used to monitor titers of antisera. To each well, 200 μL of a serial dilution of anti-MC-LR antiserum was added in triplicates and the wells were mixed gently, the plate was incubated at 4 °C for 45 min. The plate was then washed five times with 300 μL PBS-Tween 20. Goat anti-rabbit IgG-HRP conjugate (200 μL) at 1/5000 dilution in PBS-BR was then added. After allowing a 30 min incubation at room temperature, the enzyme solution is discarded and the plates washed. The substrate solution (200 μL of freshly prepared OPD substrate in citrate buffer) was then added. Colour development was allowed in the darkness at room temperature and the reaction was stopped by adding 50 μL of 2.5 M H_2SO_4. The OD was red using a 492 nm filter.

8.3. Indirect competitive ELISA

A solution of anti-MC-LR antiserum was prepared in PBS-BR at the optimum dilution previously determined by the indirect ELISA assay. Serial dilutions of MC-LR standards were prepared in water and added to the anti-MC-LR antiserum solutions. The standard solutions were pre-incubated with the antibodies for 1 h at room temperature. Two hundred microliters of each solution was then transferred in triplicates onto the plates, which were previously coated with MC-LR protein conjugate. The plate was incubated at 4 °C for 45 min and then washed with PBS-Tween buffer. Incubation with goat anti-rabbit IgG-HRP conjugate at 1/5000 dilution in PBS-BR buffer was then allowed for 30 min at room temperature. The plate was finally washed and incubated in the dark with the OPD substrate solution for 20 min at room temperature. The reaction was then stopped by adding 50 μL of 2.5 M H_2SO_4 solution and the $OD_{492\,nm}$ was recorded.

8.4. Direct competitive ELISA

Microtiter plates were pre-coated with protein A at 10^4 μg L^{-1} (200 μL per well) useful for IgG orientation. Anti-MC-LR IgG solution (10^4 μg L^{-1} or other related concentration found through optimization) was then applied to these plates and incubated at 4 °C overnight. Serial dilutions of MC-LR standards containing MC-LR-HRP conjugate at an optimum working concentration (previously determined) were then applied to these plates to generate a calibration curve. Incubation proceeded for 45 min at 4 °C. The plate was washed three times with PBS-Tween and incubated with 200 μL per well of freshly prepared OPD-substrate solution at room temperature for 20 min before the addition of the stopping solution (50 μL of 2.5 M H_2SO_4). The $OD_{492\,nm}$ was then recorded using the automatic reader.

9. Preparation and use of immunosorbents

Immunosorbents were prepared according to a previously described procedure [25]. Two commercially available sorbents have been tested for the immobilization of the purified IgGs: a CNBr activated Sepharose and an aldehydeactivated silica beads. Purified antibodies were oxidized by 0.01 M $NaIO_4$ in 0.05 M acetate buffer (pH 5) containing 0.15 M NaCl and kept under gentle stirring for 4 h at 4 °C. The excess of the oxidizing reagent was then eliminated using a 0.2 M ethanolamine solution. Solutions of about 15 mg mL^{-1} of oxidized antibodies were mixed with the Sepharose gel equilibrated in the acetate buffer. The binding reaction was allowed to proceed under gentle stirring overnight at 4 °C. The bound Sepharose gel was stored in 0.02 M PBS buffer (pH 7.4) at 4 °C. The second sorbent was an aldehydeactivated silica beads. Purified antibodies (2–6 mg mL^{-1}) were coupled to the activated silica in 0.9% NaCl solution for 8 h at 4 °C according to the procedure provided by the manufacturer. The remaining free aldehyde groups on the carrier were neutralized by flushing the gel with 0.2 M ethanolamine/HCl solution (pH 7.5). The bound silica was stored in 0.02 M PBS buffer (pH 7.4) at 4 °C. The total amounts of coupled antibodies in both cases were 2 mg mL^{-1} of gel.

The immunosorbents were packed into individual cartridges (2 mg IgG per cartridge) and washed and stored in PBS buffer 0.02 M, pH 7.4 at 4 °C when not in use. For storage period longer than 1 week, the cartridges were kept in PBS buffer containing 0.02% sodium azide (NaN_3).

10. Handling of water samples

River and ground water samples (10 mL) were filtered through a 0.45-μm disc filter (type HA, Millipore) and the filtrates were applied directly to the immunoaffinity cartridges (IACs) with a possible pH adjustment if required.

11. Sample extraction applied to blue-green algae

A 3-g portion of homogenized and grounded blue-green algae sample was placed into a 50-mL centrifuge test tube. A first extraction was performed by adding 20 mL of 75% methanol in water (v/v), and shaking on the vortex for 3 min. The sample was then centrifuged at 4500 rpm during 10 min. The supernatant was transferred into a graduated 50-mL glass tube. The residue was re-extracted with 10 mL of 75% methanol in water (v/v) as above described. The resulting supernatant

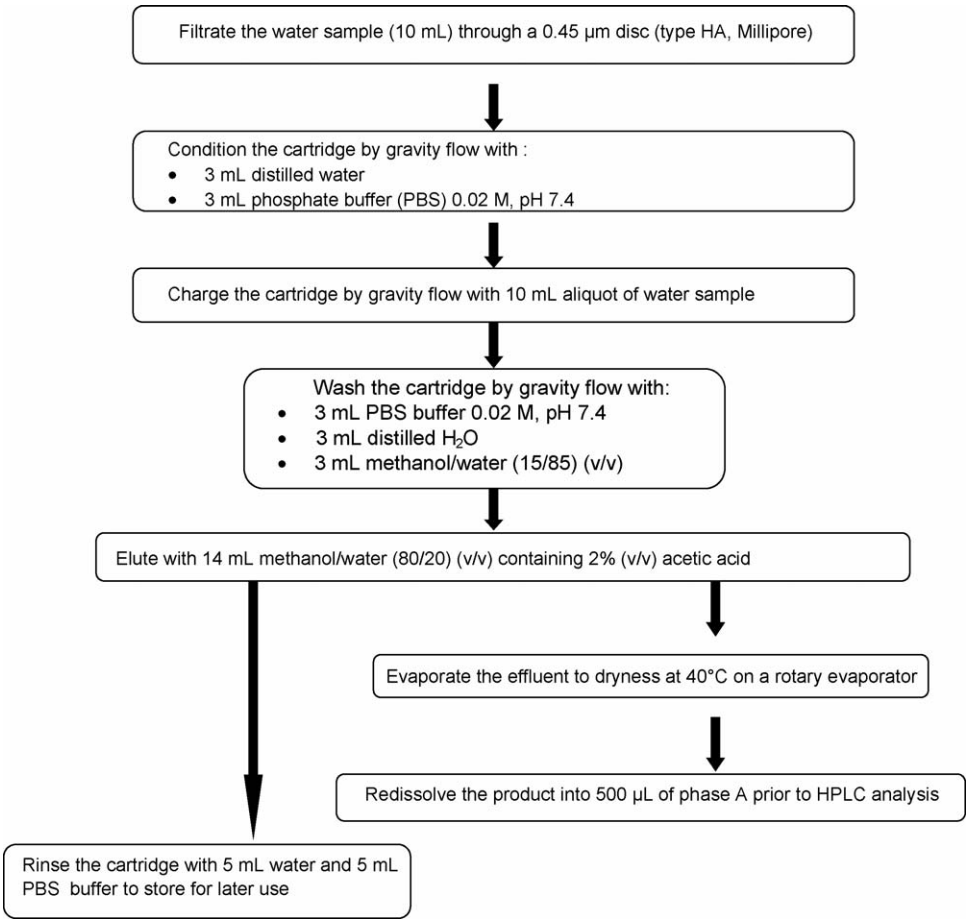

Fig. 2. Clean-up procedure of water samples and blue-green algae extracts using immunoaffinity cartridges with immobilized MC-LR IgGs prior to analysis of microcystins by HPLC.

was added to the first fraction and the volume was made up to 30 mL.

12. Evaluation of the capacity of IAC cartridges and application of to water sample clean-up

The evaluation of the IAC columns consists of the estimation of the total capacity of microcystins and the determination of their optimum conditions of use with the targeted matrices. Recoveries were first determined, for each MC individually (MC-LR, MC-RR, MC-YR and MC-LA) then using a mixture of the four MCs. A 1-mL volume of 15% methanol in PBS solution was fortified at spiking levels of 0.1 and 0.2 μg of total MCs. The obtained solution was then passed through the pre-conditioned immunoaffinity cartridge following the protocol presented in Fig. 3. First, the column was pre-conditioned with 5 mL of PBS then washed successively with 3 mL of PBS, 3 mL of de-ionized water and 3 mL of 15% methanol in water. The MCs were then eluted with 14 mL of 80% methanol in water containing 2% acetic acid. The elution fraction was evaporated at 40 °C to dryness using a rotary evaporator and then re-dissolved in 500 μL of mobile phase A prior to HPLC analysis. The IAC cartridge was then rinsed with 5 mL of water and 5 mL of PBS and stored for later use.

13. IAC clean-up procedure for blue-green algae extracts

An equivalent of 0.05–0.1 g of sample extract was diluted with PBS to obtain a maximum content of 16% methanol (v/v), the sample was then passed through the pre-conditioned IAC, following the same protocol described in Fig. 2.

14. Results and discussion

14.1. Antibody generation and evaluation

Previous studies showed that anti-MCs antibodies had little ability, if any, to neutralize the toxicity of MCs [23–26]. These antibodies recognized the common structure of MCs represented by the Adda group, which plays an important role in their toxicity and in expressing antibody specificity [27–29]. Such moiety was therefore to be preserved during the conjugation. Different proteins (ovalbumin [30], bovine serum albumin [30], Keyhole Limpet Hemocyn [30], ethylenediamine modified bovine serum albumin [23] or poly-L-lysine [23]) were described in the literature as possible carrier proteins for the synthesis of immunogens. In the present study, MC-LR-BSA conjugate was used as the immunogen to inoculate the rabbits and MC-LR-OVA conju-

gate was used as the competitor protein. The epitopic density of the generated immunogen (i.e. number of haptens attached to the carrier protein) was 13, which is in the suitable interval of 10–30 to obtain an efficient immuogen [40]. The epitopic density was evaluated by a comparative measurement of the free NH_2 functions that reacted with TNBS before and after coupling of the hapten [41,42].

Since MC-LR contains two available carboxylic acid (COOH) functions, no further functionalization was required. The harvested antibodies were evaluated by monitoring their titer and specificity. Titers were determined seeking the serum dilution giving an OD of 1 after colour development. Such target was determined aiming at using the corresponding dilution for the set-up of a competitive ELISA.

The immunization scheme was designed so as not to miss the animal optimum response against the inoculated immunogen, if bleeds are not monitored in a timely fashion. Large bleeds (20–30 mL) of serum was obtained by heart puncture, after each indicated boost period and rabbits were maintained for a maximum of 15 months. None of six immunized animals showed a significant amount of specific antibodies before 5 months of immunization. Once the protocol of immunization was proven successful, it was reproduced on several animals and the harvested fractions were characterized. Fractions with similar characteristics (titer, cross-reactivity) were gathered to constitute a pool of polyclonal antibodies with consistent properties. Under the conditions described for the titer determination, a solution of anti-MC IgGs set at $10^4\ \mu g\,L^{-1}$ induced an OD of 1.0 and could be used for the development of the intended competitive immunoassay. The specificity of the antibodies was evaluated by the midpoint value (IC_{50}) causing 50% inhibition of binding of the competitor MC-LR-OVA conjugate to the antibodies by free MC-LR. The concentration of the coating conjugate was varied from 0.5 to $10^4\ \mu g\,L^{-1}$ and various pre-incubation times (60 min, 90 min and overnight) were tested. An optimum value of the IC_{50} was found to be equal to $0.5\ \mu g\,L^{-1}$ of MC-LR when the coating conjugate was used at $0.5 \times 10^3\ \mu g\,L^{-1}$ and the pre-incubation time was set to 1 h at 4 °C, using an IgG solution set at $8 \times 10^3\ \mu g\,L^{-1}$. The background (%) due to non-specific binding of antibodies on the plate did not exceed 10% of the maximum OD obtained with the same concentration of reagents (antibody, coating protein). The IC_{50} value appears to be below the WHO level for drinking water of $1\ \mu g\,L^{-1}$ allowing therefore, to predict the possible use of these reagents for the development of an ELISA-based screening procedure for water samples.

14.2. Development of an enzyme immunoassay for the detection of microcystins

Two different immunoassay formats were investigated. The previously described steps of antibody characterization allowed the development of a competitive indirect ELISA possibly useful for analytical purposes. Two protein conjugates of MC-LR such as MC-LR-βLG and MC-LR-OVA were tried. Optimum results were obtained with MC-LR-OVA conjugate coated at $0.5 \times 10^3\ \mu g\,L^{-1}$ on microtiter plates. However and despite the achieved sensitivity ($IC_{50} = 0.5\ \mu g\,L^{-1}$), this format is relatively lengthy and may not be suitable for high throughput sample handling. A second format was developed using antibodies directly immobilized on microtiter plates and oriented by protein A. In this direct format, for a known antibody concentration and a given MC-LR-HRP conjugate concentration, the response is related to the amount of the analyte bound to the supported antibodies on the plate. The more analyte is present in the sample, the less the immobilized antibodies retain the conjugate, resulting in a low amount of enzyme bound to the immobilized antibodies and then a weaker enzyme response. Results are featured in $\%B/B_0$ versus log(concentration of MC-LR) or other related microcystins, where B is the $OD_{492\,nm}$ of a spiked sample and B_0 is that of a blank. A linear transformation of the calibration curve was given with Logit-log transformation, where $\mathrm{Logit}(\%B/B_0) = \ln[(\%B/B_0)/(100 - \%B/B_0)]$. The concentration causing 50% inhibition of binding of the antibodies (IC_{50}) was found to be of $0.9\ \mu g\,L^{-1}$ and the detection limit defined as the IC_{80} was found to be $0.06\ \mu g\,L^{-1}$. The linear transformation of the calibration curve allowed a simple and direct quantification of MCs in the spiked water samples at a concentration as low as 0.06 ppb. Considering the guideline of $1\ \mu g\,L^{-1}$ for MC-LR in drinking water, fixed by the World Health Organi-

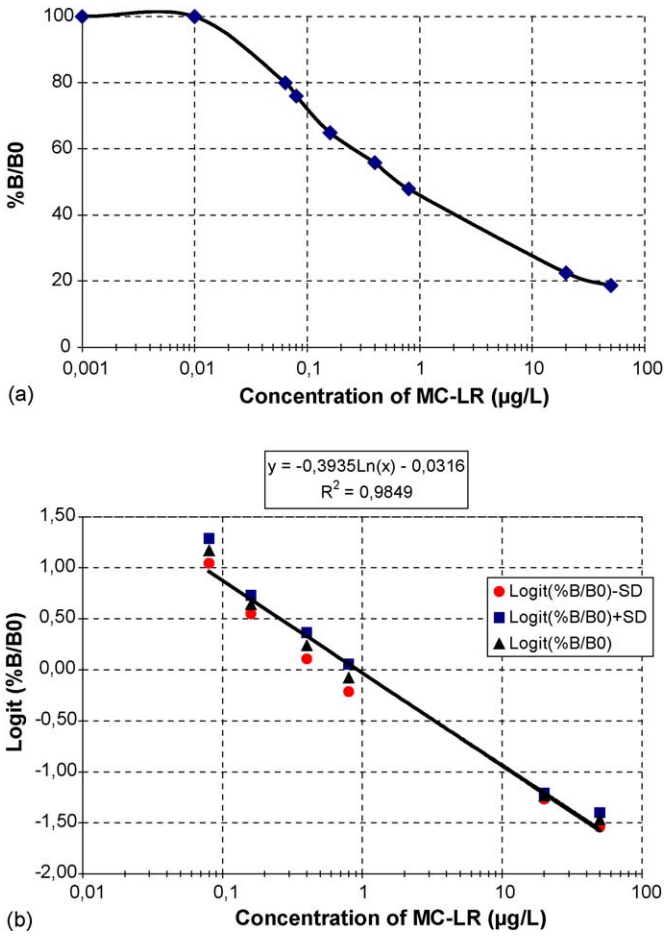

Fig. 3. (a) $\%B/B_0$ calibration curve for spiked PBS-BR buffer using anti-MC-LR and (b) Logit-log calibration curve transformation for spiked PBS-BR buffer using anti-MC-LR.

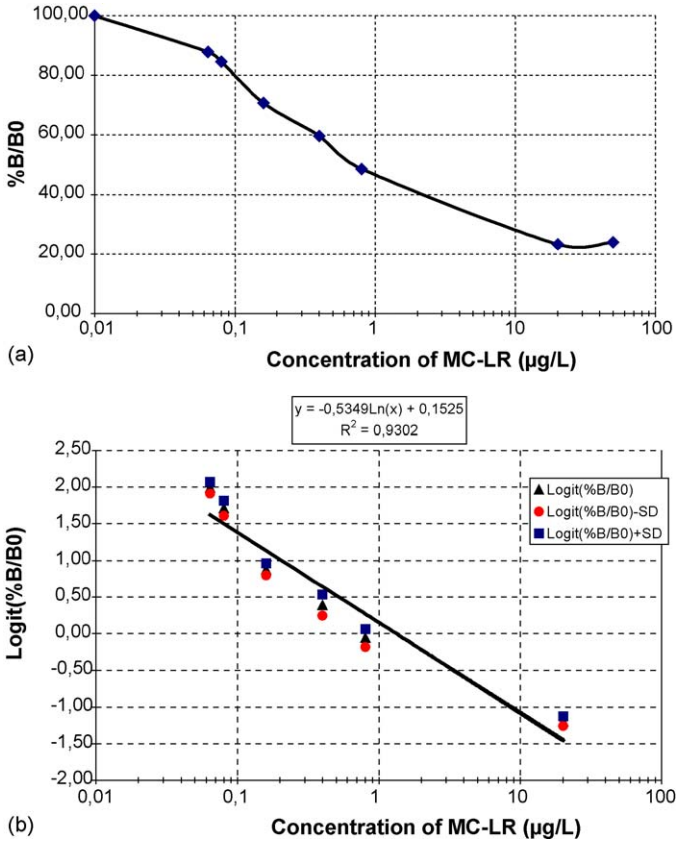

Fig. 4. (a) $\%B/B_0$ calibration curve for spiked river water using anti-MC-LR anti-serum and (b) Logit-log calibration curve transformation for spiked river water using anti-MC-LR anti-serum.

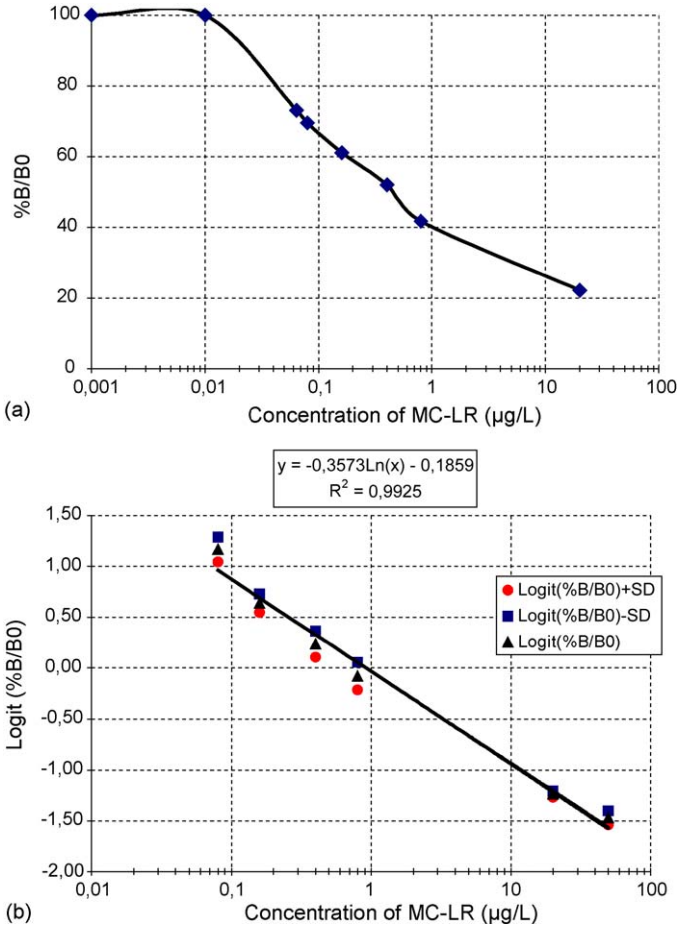

Fig. 5. (a) $\%B/B_0$ Calibration curve for spiked two-fold diluted river water in PBS-BR buffer using anti-MC-LR anti-serum and (b) Logit-log calibration curve transformation for spiked two-fold diluted river water in PBS-BR buffer using anti-MC-LR anti-serum.

zation (WHO), the sensitivity reached by the developed ELISA is adequate. Similar values of IC_{50} were found for other major MCs, respectively, 1.7, 1.6 and 1.8 $\mu g\,L^{-1}$ for MC-YR, MC-LA and MC-RR. Quantification would be expressed in equivalent concentration of MC-LR. The short incubation periods and the limited number of steps made it possible to perform the assay on real-life water samples in less than 2 h.

This ELISA test was adapted for use with river water. A calibration curve was performed in a PBS-BR buffer solution (Fig. 3a and b) and a model river water obtained from the Ottawa river (Fig. 4a and b). Recovery results were attempted using water samples fortified with known amounts of MC-LR. Best results were obtained by elimination of sediments with centrifugation and adjustment of pH to 6.5, prior to addition of reagents and application onto the plate.

Due to the observed matrix effect, calibration curves were made by diluting standards in a solution of blank river water diluted 1:2 with PBS at pH 7.4 containing 0.5% BSA and 0.2% Tween 20 as blocking reagents (Fig. 5a and b). Such calibration curves gave acceptable values of IC_{50} (0.53 $\mu g\,L^{-1}$) and IC_{80} (0.012 $\mu g\,L^{-1}$). Table 1 presents characteristics of calibration curves in different media, while Table 2 shows the calculated concentrations obtained with three spiking levels using different calibration curves performed in two different media: the regular ELISA dilution buffer (PBS-BR) and centrifuged blank river water diluted 1:2 in PBS-BR. It is recommended to use the latter calibration curve for better consistency and reproduction of the matrix effect. Such approach is commonly followed with ELISA screening systems where matrix interferences are encountered. Further investigation is required to test other sources of fresh water samples. However, this assay presents a good potential of use for screening purposes with little or no sample preparation prior to analysis.

Table 1
ELISA characteristics in different dilution media

	Dilution made in PBS-BR buffer (pH 7.4)	Dilution made in centrifuged river water with no pH adjustment	Dilution made in centrifuged river water diluted 1:2 in PBS-BR buffer (pH 7.4)
IC_{50} ($\mu g\,L^{-1}$)	0.903	1.215	0.531
IC_{80} ($\mu g\,L^{-1}$)	0.026	0.071	0.012

Table 2
Concentrations determined from artificially fortified Ottawa river water samples with MC-LR, using calibration curves performed in two different media

Experimental concentration ($\mu g\,L^{-1}$)	Calculated concentration from calibration curve performed in PBS-BR ($\mu g\,L^{-1}$) ($n=5$)	S.D. (%)	Calculated concentration from calibration curve performed in river water diluted 1:2 in PBS-BR ($\mu g\,L^{-1}$) ($n=5$)	S.D. (%)
0.22	0.181	26	0.138	17
0.56	0.571	2	0.447	17
1.11	1.776	6	1.453	14

14.3. Development and characterization of IAC cartridges for selective extraction of MCs

The extraction of environmental and food contaminants from chemically complex matrices is always problematic. Many interferents are co-extracted with the target compounds and hinder their analysis especially if residue determination is considered. Classical methods employ one or two liquid–liquid partition steps followed by liquid–solid chromatography to isolate the analytes of interest. This approach is not effective particularly for the most polar analytes. In addition, relatively large volumes of organic solvents (often chlorinated solvents) may be required.

The determination of MCs in complex matrices presenting massive interferences requires a clean-up step to remove these interferences, followed by LC/MS or LC/MS/MS quantification [10]. However, these methods are time-consuming and require expensive equipments, which are accessible to a handful of laboratories. Immunoaffinity chromatography (IAC) was considered as an alternative sample preparation technique, based on the high specificity and recognition between the developed antibodies and the target analytes. Purified anti-MC-LR antibodies were bound to two different solid supports, Sepharose® and silica. The evaluation of these IAC cartridges was performed by passing a mixture of MCs at the level of 0.2 μg of total MCs made in 15% methanol in PBS. Average recoveries ($n=3$) from the Sepharose® cartridges were found to be 100% for MC-LR, 103% for MC-RR, 100% for MC-YR and 98% for MC-LA with standard deviation (%S.D.) of 7%, 7%, 5% and 4%, respectively. The capacity of the Sepharose® IAC cartridge was evaluated to be 0.2 μg each MC passed through the cartridge separately or 0.2 μg of a mixture of MCs (0.05 μg of each MC-LR, RR, YR and LA). The capacity of the silica IAC cartridge was found to be 0.135 μg of MC-LR or of a mixture of the four MCs studied.

14.4. Use of MC-specific IAC cartridges for sample preparation

The efficiency of the developed MC-specific IAC columns was determined on two types of matrices: river water and blue-green algae-based food supplements. Spiked extracts were treated according to the protocol described in Fig. 2.

14.4.1. Water samples

A potentially blank river water was run through the clean-up and analysis steps in order to determine the possible presence of MCs. The sample was confirmed blank (Fig. 6a) and could therefore be used for spiking purposes. A ground water sample

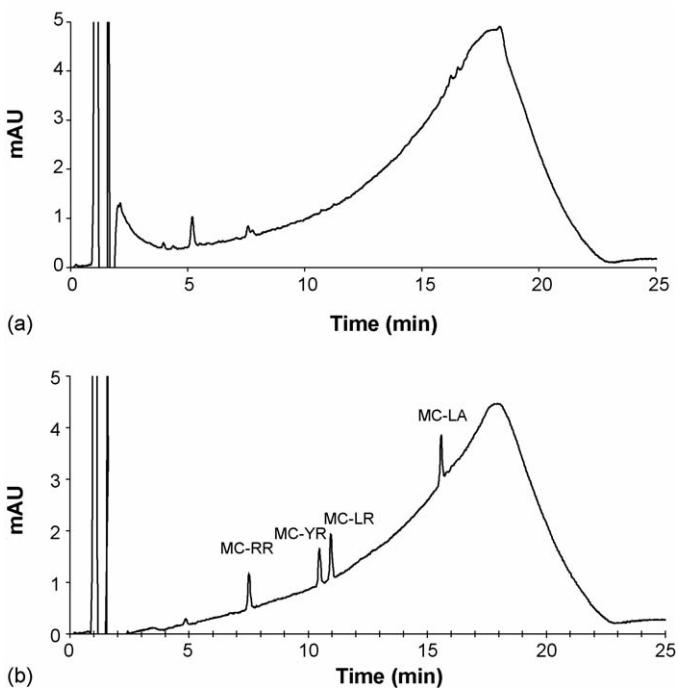

Fig. 6. (a) Chromatogram of river water sample before spiking, considered as a blank, on the MC-specific IAC cartridges and (b) chromatogram of a mixture of MC standards at the level of 0.2 μg (0.050 μg each) useful as a reference for the evaluation of recoveries from MC-specific IAC cartridges.

from the Ottawa region was also treated similarly. Both sources of ground and river water samples were spiked with 0.2 μg of total MCs and passed through both the silica and Sepharose®-based IAC columns. Fig. 6b presents the chromatogram of a mixture of MCs spiked at the level of 200 $\mu g\,L^{-1}$ (0.05 μg each), allowing the determination of the retention time of each MC for further identification. This chromatogram will serve as a reference to determine how clean an extract is once passed through the IAC columns. Recovery results are presented in Table 3. While both Sepharose®- and silica-based IAC columns gave satisfactory retention/elution results, the silica-based cartridges retained less MC-LR and required more eluent buffer to release the retained analytes. Moreover, and as it will be further discussed, silica-based cartridges were not as efficient to eliminate all interferences that may be encountered in treated extracts. Such differences may be explained by different yields of antibody immobilization, orientation of these antibodies and variation of antibody efficiency once immobilized on the various solid supports. From these limited observations, it appears that the more hydrophilic Sepharose®-based supports are more

Table 3
Average recoveries ($n = 3$) from river and ground water of a mixture of 0.2 μg of MCs using Sepharose®- and silica-based IAC cartridges

	Ground water		River water	
	% Recovery	% S.D.	% Recovery	% S.D.
Results from Sepharose®-based IAC				
MC-LR	105	4	97	4
MC-RR	112	5	89	2
MC-YR	113	6	102	4
MC-LA	86	4	87	5
Results from silica-based IAC				
MC-LR	73	4	78	5
MC-RR	112	5	98	4
MC-YR	94	4	83	6
MC-LA	76	3	43	7

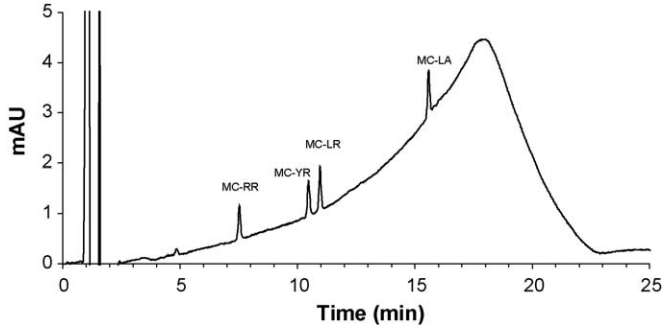

Fig. 7. LC/UV chromatogram obtained after IAC clean-up of blue-green algae sample extract AT-04, spiked with 0.2 μg of MCs using Sepharose® IAC cartridges.

appropriate than the silica-based counterparts for the intended applications.

14.4.2. Blue-green algae samples

Blue-green algae samples were obtained from food supplements collected during a monitoring campaign of *Spirulina*-based health food products. This study was limited to eight samples of blue-green algae: AT-04 which was proven to be a negative sample and OR-01, OR-02, OR-22, WR-02, WR-21, WR-26 and WR-29, which were found to be containing one or more of the MCs studies at various levels of contamination. To validate the use of the IAC clean-up for extract preparation purposes, sample AT-04 was used for artificial fortification. The extract was proven to be clean of MCs prior to fortification of an equivalent of 0.1 g sample extract with a mixture of MCs at the levels of 0.1 μg and 0.2 μg g^{-1}. IAC clean-up proceeded according to the protocol described in Fig. 2. The resulting LC/UV chromatogram is presented in Fig. 7. A recovery study was performed on the same blank sample extract and is summarized in Table 4. All MCs were recovered with satisfactory values when fortification was made on 3 g portions of homogenized and ground blue-green algae solid (sample AT-04).

The efficiency of the IAC column clean-up was clearly demonstrated by comparing results of clean-up for positive samples using such supports with those of a commercial solid phase extraction cartridge: ODS SPE-C18 (Supelco, USA). The chromatogram thus obtained (Fig. 8) has far more interferences

Table 4
Average recoveries ($n = 3$) of a spiked mixture of 0.02 μg of MCs made in 0.1 g of blank algae reconstituted in 15% methanol in PBS buffer and cleaned-up using Sepharose®-based IAC cartridges

	% Average recovery	% S.D.
MC-LR	87	10
MC-RR	85	3
MC-YR	93	9
MC-LA	90	6

than that resulting from the same extract clean-up (sample OR-22) using the Sepharose®-based IAC columns (Fig. 9). Chromatogram profiles show the clear advantage of Sepharose®-based IAC in comparison to silica-based IAC ones. Another advantage of the former columns is the level of reproducibility achieved from one experiment to the other and between various IAC cartridges prepared according to the same protocol. Each Sepharose®-based IAC column could be used for clean-up with blue-green algae extracts, more than 10 times, without a significant decrease of capacity and specificity.

Further validation of use of such specific clean-up supports was demonstrated when results of MC determination obtained with the simplified IAC sample clean-up and LC/UV detection were compared to those obtained in a previous study using LC/MS and LC/MS/MS after non-selective ODS SPE-C18 clean-up of the same samples [10]. Table 5 shows this comparison and confirms the usefulness of the IAC clean-up prior to

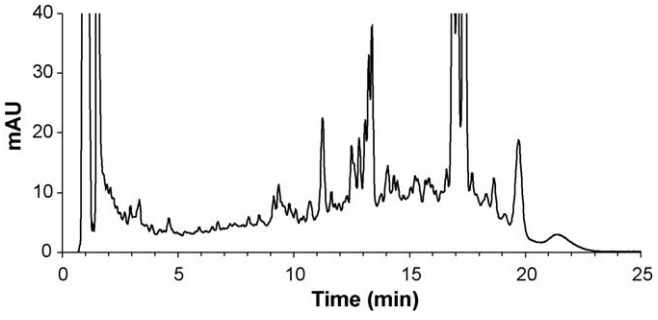

Fig. 8. LC/UV chromatogram obtained after IAC clean-up of blue-green algae sample extract OR-22 using a commercial ODS SPE-C18 cartridge.

Table 5
Comparison of quantitative results for microcystins by LC/UV after IAC clean-up and by LC/MS and LC/MS/MS after ODS SPE-C18 clean-up

Samples	IAC LC/UV(LR + LA) ($\mu g\,g^{-1}$)	S.D. (%)	Lawrence et al. [10]	
			SPE-C18 LC/MS (LR + LA) ($\mu g\,g^{-1}$)	SPE-C18 LC/MS/MS (LR + LA) ($\mu g\,g^{-1}$)
AT-04	n.d.	–	n.d.	n.d.
OR-01	1.4	4	1.4	–
OR-02	1.3	6	1.5; 1.4	1.9; 1.6; 1.3
OR-22	5.7	3	5.7	5.5
WR-02	2.8	4	3.0	4.1; 3.6
WR-21	4.3	3	2.8; 4.2	4.9; 6.6
WR-26	1.7	5	2.4	2.8
WR-29	3.4	4	1.7; 1.8	3.1

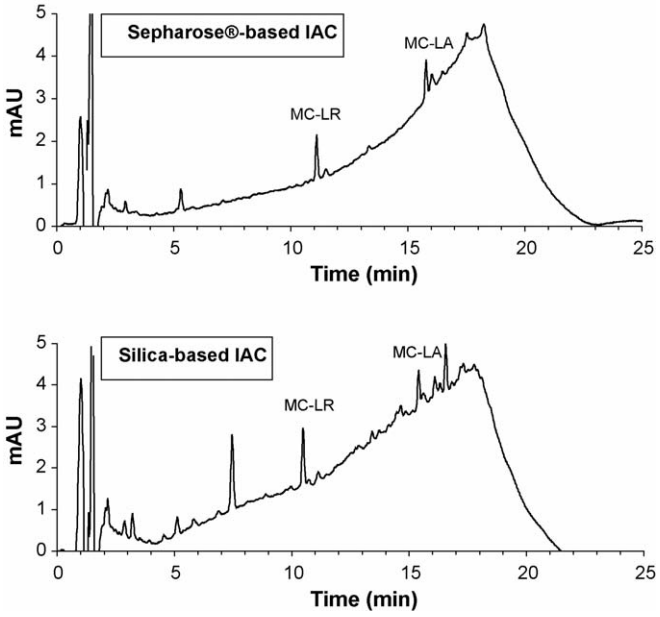

Fig. 9. LC/UV chromatograms of blue-green algae extracts from sample OR-22 using Sepharose®- and silica-based IAC cartridges.

LC/UV detection as an equally alternative to determine MCs in food supplements.

15. Conclusion

This paper presented the development and characterization of newly generated polyclonal antibodies specific to MCs. These antibodies were demonstrated to be useful for the development of immuno-analytical techniques such as immunoassay screening test and immunoaffinity sample preparation. The latter technique resulted in the development of a simple sample handling procedure to be associated with LC/UV determination of MCs that may be potentially present in blue-green algae food supplements or in sources of production of drinking water. Further investigation is required to enable the availability of these immuno-reagents and IAC columns so that they can be integrated in regulatory and compliance analysis.

Acknowledgements

Dr. J.F. Lawrence and his team are thanked for providing the blue-green algae-based health food products and their corresponding analytical results.

References

[1] W.W. Carmichael, J. Appl. Bacteriol. 72 (1992) 445.
[2] K. Sivonen, G. Jones, in: I. Chorus, J. Bartram (Eds.), Toxic Cyanobacteria in water: a Guide to Their Public Health Consequences, Monitoring and Management, E&FN Spon, London, 1999, pp. 41–111.
[3] E.M. Jochimsen, W.W. Carmichael, J.S. An, D.M. Cardo, S.T. Cookson, C.E. Holmes, M.B. Antunes, D.A. De Melo Filho, T.M. Lyra, V.S. Barreto, S.M. Azevedo, W.R. Jarvis, New Engl. J. Med. 338 (1998) 873.
[4] M. Runnegar, N. Berndt, S.M. Kong, E.Y.C. Lee, L.F. Zhang, Biochem. Biophys. Res. Commun. 216 (1995) 162.
[5] G.A. Codd, T.M. Jefferies, C.W. Keevil, in: E. Potter (Ed.), Detection Methods For Cyanobacterial Toxins, Royal Society of Chemistry, Cambridge, 1994.
[6] G.A. Miura, N.A. Robinson, T.W. Geisbert, K.A. Bostian, J.D. White, J.G. Pace, Toxicon 27 (1989) 1229.
[7] S.B. Hooser, V.R. Beasley, R.A. Lovell, W.W. Carmichael, W.M. Haschek, Vet. Pathol. 26 (1989) 246.
[8] J.F. Lawrence, C. Menard, J. Chromatogr. A 922 (2001) 111.
[9] H.S. Lee, C.K. Jeong, H.M. Lee, S.J. Choi, K.S. Do, K. Kim, Y.H. Kim, J. Chromatogr. A 848 (1999) 179.
[10] J.F. Lawrence, B. Niedzwiadek, C. Menard, B.P. Lau, D. Lewis, T.K. Goodman, S. Carbone, C. Holmes, J. AOAC Int. 84 (2001) 1035.
[11] K.P. Bateman, P. Thibault, D.J. Douglas, R.L. White, J. Chromatogr. A 712 (1995) 253.
[12] K. Tsuji, H. Masui, H. Uemura, Y. Mori, K.I. Harada, Toxicon 39 (2001) 687.
[13] F. Kondo, Y. Ikai, H. Oka, H. Matsumoto, S. Yamada, N. Ishikawa, K. Tsuji, H.I. Harada, T. Shimada, M. Oshikata, M. Suzuki, Nat. Toxins 3 (1995) 41.
[14] W.W. Carmichael, Advances in Botanical Research, vol. 12, Academic Press, San Diego, 1986, p. 47.
[15] A.T. Tu, W.W. Carmichael, Handbook of Natural Toxin. Toxins of Freshwater Algae, Marine Toxins and Venoms, vol. 3, Marcel Dekker Inc., New York, 1988, p. 121.
[16] C. MacKintosh, K.A. Beattie, S. Klumpp, P. Cohen, G.A. Codd, FEBS Lett. 264 (1990) 187.
[17] J.F. Lawrence, C. Menard, M.C. Hennion, V. Pichon, F. LeGoffic, N. Durand, J. Chromatogr. A 752 (1996) 147.
[18] J.F. Lawrence, C. Menard, J. Chromatogr. B 696 (1997) 291.
[19] J.F. Lawrence, C. Menard, J. Yeung, S. Ben Rejeb, J. AOAC Int. 83 (2000) 597.
[20] T.S. Fan, G.S. Zhang, F.S. Chu, Appl. Environ. Microbiol. 47 (1984) 526.

[21] W.P. Brooks, G.A. Codd, Environ. Toxicol. Lett. 9 (1988) 1343.
[22] R. Kfir, E. Johannsen, D.P. Botes, Toxicon 24 (1986) 543.
[23] F.S. Chu, X. Huang, R.D. Wei, W.W. Carmichael, Appl. Environ. Microbiol. 55 (1989) 1928.
[24] C. Rivasseau, S. Martins, M.C. Hennion, J. Chromatogr. A 799 (1998) 155.
[25] S. Ben Rejeb, N. Fisher Durand, A. Martel, R. Daniel, C. Jolivalt, F. LeGoffic, J.F. Lawrence, J.M. Yeung, M.C. Hennion, Food Agric. Immunol. 10 (1998) 203.
[26] S. Saito, Y. Nakano, K. Kushida, M. Shirai, K.I. Harada, M. Nakano, Microbiol. Immunol. 38 (1994) 389.
[27] K.I. Harada, K. Ogawa, K. Matsuura, H. Nagai, H. Murata, M. Suzuki, Y. Itezono, N. Nakayama, M. Shirai, M. Nakano, Toxicon 29 (1991) 479.
[28] R. Nishiwaki-Matsushima, S. Nishiwaki, T. Ohta, S. Yoshizawa, M. Suganuma, K.I. Harada, M.F. Watanabe, H. Fujiki, Jpn. J. Cancer Res. 82 (1991) 993.
[29] R.R. Stotts, M. Namikoshi, W.M. Haschek, K.L. Reinhart, W.W. Carmichael, A.M. Dahlem, V.R. Beasly, Suppl. Toxicon 31 (1993) 783.
[30] S. Nagata, H. Soutome, T. Tsutsumi, A. Hasegawa, M. Sekijima, M. Sugamata, K.I. Harada, M. Suganuma, Y. Ueno, Nat. Toxins 3 (1995) 78.
[31] B.S.F. Wong, P.K.S. Lam, L. Xu, Y. Zhang, B.J. Richardson, Chemosphere 38 (1999) 1113.
[32] J.R. Bagu, B.D. Sikes, M.M. Craig, C.F. Holmes, J. Biol. Chem. 272 (1997) 5087.
[33] J. Rappala, K. Erkomaa, J. Kukkonen, K. Sivonen, K. Lahti, Anal. Chim. Acta 466 (2002) 213.
[34] M.G. Weller, A. Zeck, A. Eikenberg, S. Nagata, Y. Ueno, R. Niessner, Anal. Sci. 17 (2001) 1445.
[35] A. Zeck, M.G. Weller, D. Bursill, R. Niessner, Analyst 126 (2001) 2002.
[36] A. Zeck, M.G. Weller, R. Niessner, Anal. Chem. 73 (2001) 5509.
[37] A. Zeck, A. Eikenberg, M.G. Weller, R. Niessner, Anal. Chim. Acta 441 (2001) 1.
[38] P. Lindner, R. Molz, E. Yacoub-G-George, A. Durkop, H. Wolf, Anal. Chim. Acta 521 (2004) 37.
[39] J. McElhiney, L.A. Lawton, Toxicol. Appl. Pharm. 203 (2005) 219.
[40] J.M. Carter, in: B.M. Dunn, M.W. Pennington (Eds.), Methods in Molecular Biology, vol. 6, Humana Press Inc., Totowa, NJ, 1994, pp. 155–163.
[41] S.L. Snyder, P.Z. Sobocinsky, Anal. Biochem. 64 (1975) 284.
[42] K. Satake, T. Okuyama, M. Ohashi, T. Shinoda, J. Biochem. 47 (5) (1960) 654.

Available online at www.sciencedirect.com
ScienceDirect
Talanta 70 (2006) 236–243
Talanta
www.elsevier.com/locate/talanta

Simultaneous determination of tetracyclines in pharmaceuticals by CZE using experimental design

Mónica Cecilia Vargas Mamani [a], Jaime Amaya Farfán [b], Felix Guillermo Reyes Reyes [c], Susanne Rath [a,*]

[a] *Institute of Chemistry, Department of Analytical Chemistry, State University of Campinas, P.O. Box 6154, 13084-971 Campinas, SP, Brazil*
[b] *Department of Food & Nutrition, State University of Campinas, P.O. Box 6121, 13083-862 Campinas, SP, Brazil*
[c] *Department of Food Science, State University of Campinas, P.O. Box 6154, 13083-970 Campinas, SP, Brazil*

Received 22 November 2005; received in revised form 9 February 2006; accepted 9 February 2006
Available online 24 March 2006

Abstract

An optimized capillary zone electrophoresis (CZE) method for the analysis of tetracycline (TC), chlortetracycline (CTC), oxytetracycline (OTC) and doxycycline (DXC) is described. Using fused-silica capillaries, the influence of the electrolyte composition, pH and concentration, as well as temperature and applied voltage were investigated. A factorial and central composite design was performed to optimize the method in a simple way. The optimal separation conditions were 50 mmol L^{-1} sodium carbonate + 1 mmol L^{-1} EDTA, pH 10; voltage 13 kV and temperature 23 °C. The method was validated for TC determination in pharmaceuticals through the following performance criteria: linearity and linear range, sensitivity, selectivity, intra-assay and inter-assay precision, detectability, accuracy and ruggedness. In comparison with the recommended HPLC method in the United States Pharmacopeia, this CZE-method exhibited the same performance as the official method, with the advantage that the same method could be used for the simultaneous determination of the different tetracyclines in pharmaceutical formulations.

Keywords: Antibiotics; Tetracyclines; Capillary electrophoresis; Validation

1. Introduction

Tetracycline (TC), chlortetracycline (CTC), oxytetracycline (OTC) and doxycycline (DXC) are members of the tetracyclines group of broad-spectrum antibiotics [1], widely used in human and animals. In animals, they are used in the treatment of bovine mastitis and are added at sub-therapeutical levels to animal feeds for prophylactic purposes [2]. They have also found application in the postharvest preservation of fruits and vegetables and the extermination of insect pests [3]. The structures of these compounds are shown in Fig. 1.

In recent years, methods using capillary zone electrophoresis (CZE) for the determination of tetracyclines and their impurities have been reported and several electrolytes like phosphate, phosphate and triton-X, phosphate and tris and methanol, sodium carbonate and EDTA, citric acid and β-alanine was employed [4–9]. Several approaches have also been followed for the determination of TC, CTC, OTC and DXC by the United States Pharmacopoeia (USP) using high performance liquid chromatography (HPLC) for quality control of these antibiotics [10]. The physicochemical properties of tetracyclines, their ionic nature, multiple ionization sites, and water solubility, however, make these compounds more suitable for electrophoretic analysis. CZE continues to grow rapidly as an analytical technique for a wide range of application areas, including the analysis of pharmaceuticals. CZE has several advantages over HPLC for the determination of tetracyclines while not sharing some of the difficulties associated with peak tailing and low efficiency of HPLC arising from interaction with residual silanol groups on silica-based packing materials. CZE has also the advantages of shorter analysis time and lesser consumption of sample and solvent, in comparison with HPLC [11,12].

The official monographs of the United States Pharmacopeia describe a different method for each tetracycline. For CTC a microbiological assay is recommended while OTC, DXC and TC are quantified by HPLC. Furthermore, the HPLC analytical

* Corresponding author. Tel.: +55 19 37883084; fax: +55 19 37883023.
E-mail address: raths@iqm.unicamp.br (S. Rath).

0039-9140/$ – see front matter © 2006 Elsevier B.V. All rights reserved.
doi:10.1016/j.talanta.2006.02.048

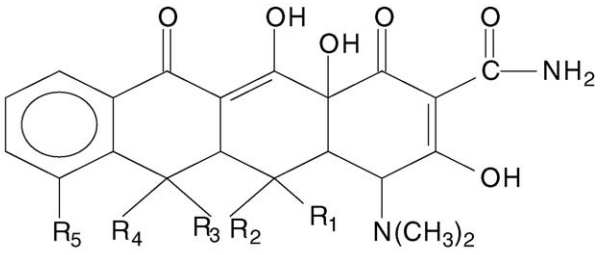

	R_1	R_2	R_3	R_4	R_5
Tetracycline	H-	H-	OH-	CH3-	H-
Chlortetracycline	H-	H-	OH-	CH3-	Cl-
Oxytetracycline	H-	OH-	OH-	CH3-	H-
Doxycycline	H-	OH-	H-	CH3-	H-

Fig. 1. Structures of the tetracyclines.

conditions are quite different for the different compounds. The stationary phases employed for OTC and DXC determination are octadecil columns and the mobile phases comprise a mixture of tertiary butyl alcohol, phosphate buffer pH 7.5 (OTC) and pH 8.0 (DXC), tetrabutylammonium hydrogen sulfate and EDTA. The quantitation of TC is performed with an octyl column, employing a mobile phase composed of ammonium oxalate, dibasic ammonium phosphate, pH 7.6, and dimethylformamide.

This paper describes the development of a simple and general CZE-method for the simultaneous determination of TC, CTC, DXC and OTC in pharmaceutical formulations, using experimental planning. The method was validated and its performance compared with the official HPLC methods described in the United States Pharmacopeia.

2. Experimental

2.1. Instrumental and operating conditions

The capillary electrophoresis was performed on a Hewlett Packard 3D Capillary Electrophoresis system (Germany), equipped with a DAD detector. Tetracyclines were detected at 270 nm. Data were collected using the HP 3D Chemstation software from Hewlett-Packard (Germany). The separations were carried out on a fused-silica capillary (50 μm i.d.) with effective (l) and total length (L) of 52 cm and 60.6 cm, respectively. Injection was done hydrodynamically for 20 s at 20 mbar. Measurements of pH were made with a DM-20 pH-meter from Digimed (Brazil), using a combined glass electrode. When necessary, the pH of electrolyte was adjusted using 0.1 mol L^{-1} NaOH or 0.1 mol L^{-1} HCl before making up to volume.

The high performance liquid chromatographic analyses were performed using a Waters chromatographic system (USA), composed of a solvent delivery system, model 510, a Tunable Absorbance Detector model 486, a 746 Data Module and a Rheodyne 7725 injector with a sample loop of 20 μL.

Chromatographic separation was achieved using a Zorbax SB-C_8 column (250 mm × 4.6 mm, 5 μm) with a SB-C_8 guard-column (12.5 mm × 4.6 mm, 5 μm) purchased from Alltech (USA). The mobile phase consisted of a mixture of 680 mL of 0.1 mol L^{-1} ammonium oxalate, 270 mL of dimethylformamide and 50 mL of 0.2 mol L^{-1} dibasic ammonium phosphate. The pH of the mobile phase was adjusted with 3 mol L^{-1} ammonium hydroxide or 3 mol L^{-1} phosphoric acid. The flow rate was 2 mL min^{-1}. HPLC conditions were followed based on United States Pharmacopeia XXVIII [10].

2.2. Standards and reagents

Standards of tetracycline hydrochloride and doxycycline hydrochloride were purchased from Sigma (USA) while oxytetracycline dihydrate and chlortetracycline hydrochloride were from ICN Biomedical Inc. (USA).

Analytical grade disodium hydrogenphosphate, sodium tetraborate, sodium hydroxide, sodium carbonate, phosphoric acid, sodium dodecyl sulfate (SDS), ammonium oxalate, ammonium hydroxide, sodium ethylenediaminetetraacetate (EDTA), TRIZMA® hydrochloride acid and phosphoric acid were purchased from Merck (Germany). Methanol and dimethylformamide, HPLC-grade solvents, were purchased from Tedia (USA).

Throughout the study, water was obtained from a Milli-Q system from Millipore (USA). Before analysis, all the solutions were filtered through 0.45 μm nylon filters from Millipore (Brazil).

2.3. Samples

Ten commercial samples of pharmaceutical formulations (capsules) containing tetracycline, from different batches and six different brands were purchased at local drugstores in Campinas, SP, Brazil.

2.4. Standard solutions

Standard stock solutions of TC, OTC, CTC and DXC were prepared by dilution of appropriate volumes of the standards in methanol to a final concentration of 1 mg mL^{-1}. These solutions were stored under refrigeration (4 °C) until use. Working solutions in the concentration range of 5.0–100 μg mL^{-1} were prepared daily by dilution of the standard stock solution in water.

2.5. CZE procedure

Before daily use, the capillary was sequentially washed with water (10 min), 1 mol L^{-1} NaOH (2 min), 0.1 mol L^{-1} NaOH (3 min) and run electrolyte (5 min). During the analyses and after each determination the capillary was sequentially washed with water (2 min), 1 mol L^{-1} NaOH (1 min), 0.1 mol L^{-1} NaOH (1 min) and run electrolyte (2 min).

The separation conditions for the tetracycline determinations were 50 mmol L^{-1} sodium carbonate + 1 mmol L^{-1} EDTA, pH 10; voltage, 13 kV and temperature, 23 °C.

2.6. HPLC procedure

The HPLC determinations of TC in the samples followed the official monograph of the United States Pharmacopeia XXVIII [10], without modification.

2.7. Experimental design for CZE optimization

A fractional factorial design (2^{4-1}) was carried out to distinguish the significant parameters. The results of this design were used to plan a subsequent higher order 2^3 design with central composite, which was performed with the same procedure. The variables evaluated were pH (9.3–12.7), temperature (20–26 °C) and sodium carbonate concentration (43–77 mmol L^{-1}; Table 1). All statistical calculations were developed with the software Statistic, Statsoft Inc., v. 5.5 (USA).

2.8. Method validation

The method was *in-house* validated using the following performance criteria: linearity and linear range, sensitivity, selectivity, intra-assay and inter-assay precision, detectability, accuracy and ruggedness [13]. The linearity, linear range, sensitivity and detectability were established through the calibration curve obtained by triplicate analysis of TC, TCT, OTC, DXC at five concentration levels 5.0, 10, 50, 75 and 100 μg mL^{-1}. The sensitivity is the slope of the calibration graph. The detectability (D) for each tetracycline was calculated according to Miller and Miller [14], using the following expression: $D = ks_{y/x}/m$, where $k = 3$, $s_{y/x}$ is the standard deviation of the residuals and m is the slope of the calibration curve.

The intra-assay precision of the method, expressed as the relative standard deviation of peak area measurements ($n = 5$), was evaluated through the results obtained with the method operating over one day under the same conditions, using solutions of each analyte at a single concentration level, 50 μg mL^{-1}. The inter-assay precision was determined for two concentration levels, 50 and 100 μg mL^{-1}, and the analyses were performed for 4 days.

The selectivity of the method was evaluated by exposing TC, CTC, OTC, DXC, at a concentration level of 50 μg mL^{-1}, to the following stress conditions for 1 h: 0.1 mol L^{-1} HCl, 0.1 mol L^{-1} NaOH, 3% (v/v) H_2O_2 and temperature (55 °C). The solutions were analyzed considering the resolution between the analyte and other substances formed during the experiment and the analytical signal before and after the exposure of the analyte to the stress conditions, expressed as recovery.

Table 1
Nominal values corresponding to −1, 0, +1, −1.68 and 1.68 in the first experimental design

Variables	−1	0	+1	−1.68	1.68
A (pH)	10	11	12	9.3	12.7
B (carbonate concentration)[a] (mmol L^{-1})	50	60	70	43	77
C (temperature) (°C)	21	23	25	20	26

[a] In the presence of 1.0 mmol L^{-1} EDTA.

Table 2
Nominal values corresponding to −1, 0, +1, −1.68 and 1.68 in the second experimental design

Variables	−1	0	+1	−1.68	1.68
A (carbonate concentration)[a] (mmol L^{-1})	48	50	52	46.6	53.4
B (temperature) (°C)	22.5	23	23.5	22.2	23.8
C (pH)	9.5	10	10.5	9.2	10.8

[a] In the presence of 1.0 mmol L^{-1} EDTA.

The accuracy of the method was evaluated through analyses of samples of pharmaceutical formulations containing the TC by the proposed CZE method, using the procedure described below, and by HPLC according to the method described in the United States Pharmacopeia XXVIII [10].

The susceptibility of the developed analytical method to changes was tested to evaluate the ruggedness of the method. For this purpose a 2^3 experimental design was employed (Table 2), where the following variables were tested: temperature (22.2–23.8 °C), pH (9.2–10.8) and carbonate concentration (46.6–53.4 mmol L^{-1}).

2.9. Sample analysis

The content of capsules of 10 samples of each commercial formulation from the same batch containing TC were weighed and homogenized in a mortar. An accurately weighed quantity of the freshly mixed powder, equivalent to about 50 mg of tetracycline hydrochloride, was transferred to a 50 mL volumetric flask and 25 mL of water was added. The mixture was sonicated for about 5 min, allowed to cool, diluted to volume and filtered through 0.45 μm membrane filters Millipore (USA). A volume of 2.5 mL of this solution was diluted to 10 mL with water in a volumetric flask (250 μg mL^{-1}). All samples were analyzed in quintuplicate.

The analyses by CZE were carried out as described in 2.5. and quantitation was accomplished through an external calibration curve with five concentration levels in the range of 25–500 μg mL^{-1}. Two samples were also analyzed by HPLC using the method described in the United States Pharmacopeia XXVIII [10].

3. Results and discussion

3.1. CZE method development

In view of reports on the influence of the electrolyte on selectivity [15], it was deemed mandatory to first compare the performance of different types of background electrolytes for the separation of the tetracyclines. Ten different electrolytes were evaluated: sodium phosphate (pH 8.5), Tris (pH 8.5 and 11), sodium carbonate (pH 8.5 and 11), sodium tetraborate (pH 8.5),

sodium acetate (pH 4.5 and 8.5) and the mixture sodium tetraborate, sodium phosphate and sodium dodecyl sulfate (SDS), (pH 8.5 and 9.5). The electrolytes were made in concentration range of 20–140 mmol L^{-1} with steps of 40 mmol L^{-1} adding, in all cases, 1 mmol L^{-1} EDTA, to prevent the well-known interference of tetracyclines with metal ions. With the first three electrolytes all the components were separated, but with the sodium carbonate-EDTA the separation was achieved in a shorter time (8 min). Notwithstanding the recommended addition of SDS to the electrolyte by some authors [16], the mixture tetraborate-phosphate-SDS-EDTA did not allow adequate resolution of the four tetracyclines under study and longer analysis times were required.

Considering the resolution of the analytes and the analysis time, the best conditions were achieved with the sodium carbonate buffer having added EDTA. Subsequently, it was necessary to establish the electrolyte concentration, pH and temperature. Due to the fact that more than one variable was potentially important, and that it would be difficult to optimize the conditions through a uni-variant optimization procedure, the experimental CZE-conditions were obtained using an chemiometric experimental design. This procedure offers an efficient route for determining the best resolution from a selected number of conditions [17]. Moreover, by using experimental design it is possible to evaluate the interaction of factors, which have a significant effect on the separation using a small number of experiments.

For the determination of the most relevant variables an experimental design using first a $2^{4-1}{}_{IV}$ factorial design with four factors was conducted: pH (10.5–12.5), temperature (21–25 °C), concentration of the electrolyte (40–80 mmol L^{-1}) and voltage (11–15 kV). Upon verification that the voltage was not significant, a central composite 2^3 design was performed for the remaining three variables (pH, electrolyte concentration and temperature) in order to refine the optimal conditions for the separation the tetracyclines by CZE. The experimental design was thus constructed by the use of a full 2^3 factorial design with three central and four axial points, respectively. The conditions are presented in Table 1.

Fig. 2 depicts the response surfaces, showing that the separation of the four TCs under study is achieved at a concentration of 50 mmol L^{-1} sodium carbonate, pH 10 and 23 °C. The responses of the model, R^2 values, were greater than 0.94, implying that the model was well fitted by the data for the response of number of peaks. It was verified that the concentration of the electrolyte and pH had a major influence on the electroosmotic flow (EOF) and the current produced in the capillary.

It was observed that, whereas the migration time increased with pH and electrolyte concentration, the resolution diminished. At pH higher than 12 incomplete separation occurred. The longer migration time with increasing pH indicates that an increase in electrophoretic movement of the negatively charged tetracycline molecules has overcome the increase in electroosmosis.

A typical electropherogram of TC, CTC, OTC and DXC at the optimized conditions established through the experimental design is presented in Fig. 3.

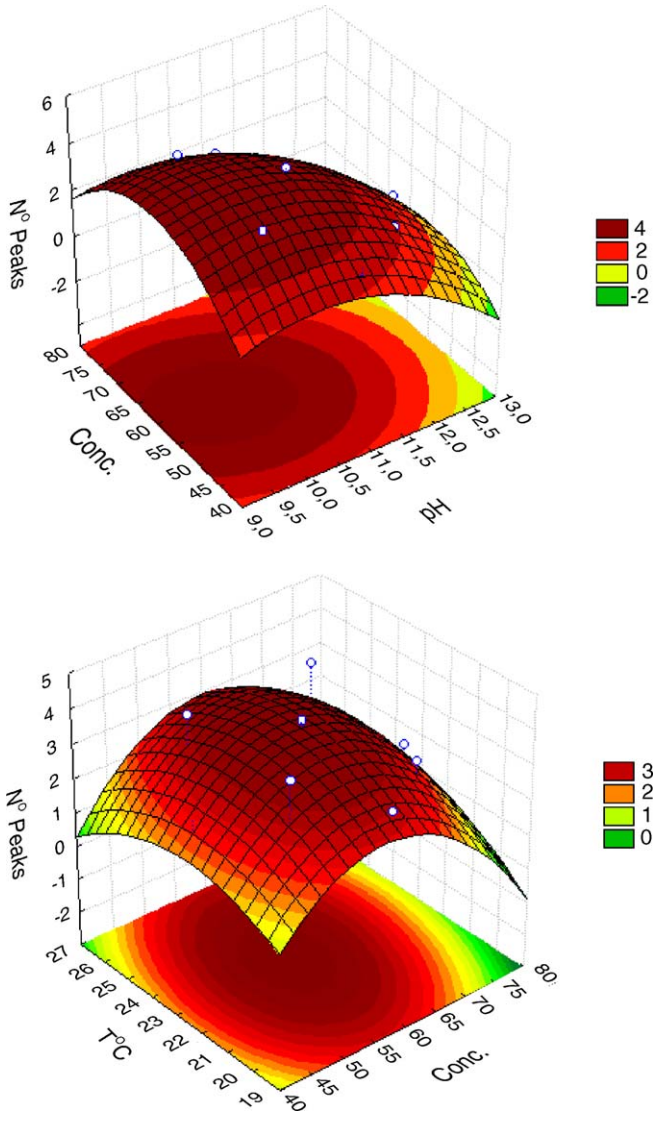

Fig. 2. Response surface for tetracyclines showing the number of separated compounds as a function of significant separation parameters using sodium carbonate plus 1 mmol L^{-1} EDTA and pH, obtained using 2^3 factorial design with the central composite design.

Before proceding to validate the CZE method for the determination the tetracyclines in pharmaceutical formulations, a system suitability test was performed, where the following parameters were evaluated: plate count (N), resolution (Rs), and tailing factor (T_F). The same procedure was also employed for

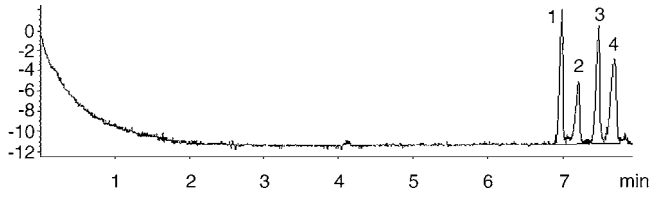

Fig. 3. A typical electropherogram of 100 μg mL^{-1} of (1) TC, (2) CTC, (3) OTC and (4) DXC (t_{m1} 6.9 min, t_{m2} 7.2 min, t_{m3} 7.5 min, t_{m4} 7.7 min, respectively). Capillary: uncoated fused silica; background electrolyte, a solution of 50 mmol L^{-1} sodium carbonate plus 1 mmol L^{-1} EDTA, pH 10; temperature, 23 °C; applied voltage, 13 kV; detection wavelength, 270 nm.

Table 3
System suitability parameters for CZE and HPLC

	CZE				HPLC
	TC[a]	CTC[a]	OTC[a]	DXC[a]	TC[a]
Plate numbers/m	227826	132570	225671	114242	26448
Resolution (Rs)	4.1	4.8	3.0	–	–
Tailing factor (T_F)	1.0	1.0	0.9	1.0	1.0
Migration time (CZE) or retention time (HPLC) (min)	7.0	7.2	7.5	7.7	8.0

The resolution was calculated between two adjacent peaks.
[a] Antimicrobial compound

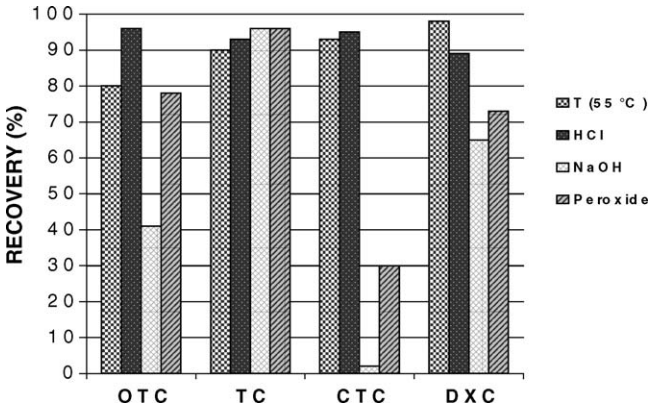

Fig. 4. Recovery (%) of tetracylines after exposure of standard solutions (50 μg mL^{-1}) to temperature (55 °C), 0.1 mol L^{-1} HCl, 0.1 mol L^{-1} NaOH or 3% (v/v) H_2O_2.

the HPLC system, due to the fact that this technique was used to evaluate the accuracy of the CZE method for TC quantitation. The results are presented in Table 3.

Both methods give adequate resolutions (Rs > 2) for all the TCs under study. Nonetheless, as expected, the calculated plates number for the CZE method were an order of magnitude higher than those for the HPLC method. The tailing factor obtained for all tetracyclines using CZE were within the acceptable range, $T < 2.0$ [18].

3.2. Method validation

The CZE method was *in-house* validated for the analyses of the tetracyclines by evaluation of the following parameters [13]: linear range, linearity, sensitivity, selectivity, detectability, intra- and inter-assay precision and accuracy. The results are summarized in Table 4. The accuracy was evaluated by comparing the results obtained from the analysis of pharmaceutical formulations by the proposed CZE method with those obtained using the recommended HPLC method described in the United States Pharmacopeia XXVIII [10].

The linearity, range and sensitivity were obtained from calibration graphs using an external standard at five concentration levels for each tetracycline under study, with triplicate analyses. The linearity was tested using a pure error lack of fit test with simple regression, which was not significant at the 5% level.

The selectivity indicates the ability of the method to accurately measure the analyte response in the presence of potentially interfering sample components or degradation products. In this study the selectivity was evaluated by exposing the analyte to stress conditions, such as acid (0.1 mol L^{-1} HCl), base (0.1 mol L^{-1} NaOH) and an oxidant (3%, v/v H_2O_2). The solutions were analyzed considering the resolution between the analyte and other substances formed during the experiment and the analytical signal before and after exposure of the analyte to the stress conditions. Co-migration of degradation products was not observed due to the fact that the peak purity for each analyte was confirmed by the overlay of the spectra before and after degradation process. The results are presented in Fig. 4. It was evident that the stability of the tetracyclines depends on their chemical structure. Under the four stressing conditions, TC was the most stable while CTC and OTC are the least stable compounds to alcaline treatment. The most significant factors that influences the stability of the tetracyclines were alkaline or oxidant media. CTC degrades completely in 0.1 mol L^{-1} NaOH. The degradation products formed under all the stress conditions migrated at shorter times (approximately 4 min) than their corresponding tetracyclines, thus confirming the selectivity of the method.

Table 4
Quantitative features for TC and CTC

Parameter	TC	CTC	OTC	DXC
Linear Range (μg mL^{-1})	10–250	10–100	10–100	10–100
Sensitivity* (aU μg mL^{-1})	0.57 ± 0.02	0.37 ± 0.01	0.57 ± 0.02	0.52 ± 0.02
Linearity (r)	0.999	0.999	0. 999	0.999
Intercept*	−0.6 ± −0.8	−0.7 ± −0.7	−0.7 ± −0.9	−2 ± −1
Intra-assay precision (R.S.D.%)				
50 μg mL^{-1}; $n = 5$	1.5	0.7	1.3	2.0
Inter-assay precision (R.S.D.%)				
50 μg mL^{-1}; $n = 4$	2.5	2.3	2.4	2.6
100 μg mL^{-1}; $n = 4$	2.3	1.7	2.3	2.6
Detectability (μg mL^{-1})	3	3	3	3

R.S.D., relative standard deviation.
* $P < 0.05$.

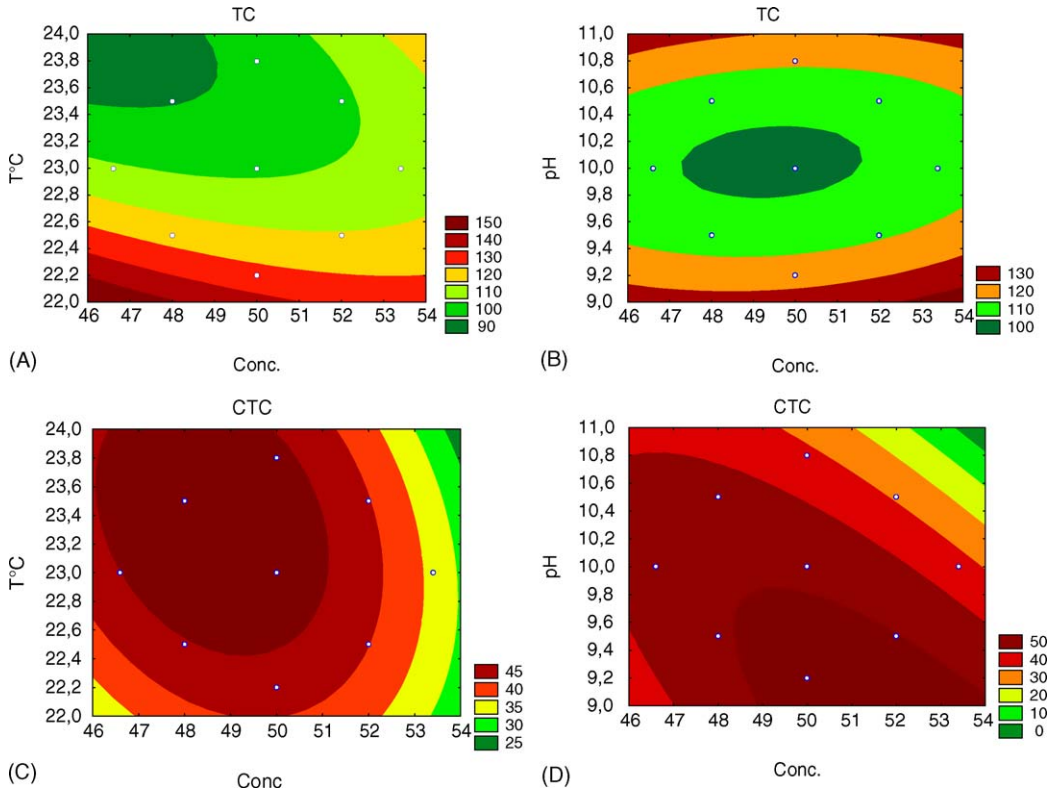

Fig. 5. Counter plots used to evaluate the ruggedness of the method selected by the 2^3 experimental design. (A) TC (temperature vs. electrolyte concentration); (B) TC (pH vs. electrolyte concentration); (C) CTC (temperature vs. electrolyte concentration); (D) CTC (pH vs. electrolyte concentration).

The precision of the method for TC, CTC, OTC and DXC was evaluated using the results obtained over one day of operation under the same conditions (intra-assay) and for 4 days (inter-assay precision). The intra- and inter-assay precisions were determined at 100% of the target concentration from 5 and 4 determinations, respectively. The results were expressed as relative standard deviations (RSD; Table 4) and were lower than 2.0 and 2.6% for intra- and inter-assay, respectively. Considering that regulatory agencies [10] recommend that the precision be lower than 2%, the values obtained by the CZE method are acceptable.

The detectability established represents the lowest concentration of an analyte in sample solutions to be introduced in the CE equipment that can be detected. The detection and the quantitation limits of the method are not presented, due to the fact that the active compound is the major constituent of the formulation and this parameter is not required for method validation for the quality control of pharmaceutical products. Furthermore, these limits would depend on sample dilution before analysis.

The accuracy of the method was assessed for TC by analyzing two commercial formulations by both the developed CZE and the recommended United States Pharmacopeia methods. The mean values obtained using the proposed method and the reference method (Table 5), for both samples, do not differ significantly ($P < 0.05$).

Finally, the ruggedness of the method was assessed introducing small changes to the procedure and examining the effect on the results (analytical signal). For this purpose, the temperature ($23.0 \pm 0.8\,^{\circ}C$), pH (10.0 ± 0.8) and electrolyte concentration ($50.0 \pm 3.4\,mmol\,L^{-1}$) were changed simultaneously using a 2^3 factorial design as described in Section 2.8. The response graphs for TC and CTC, and OTC and DXC, are presented in Figs. 5 and 6, respectively. Whereas the analytical signal of DXC and TC were less influenced by small variations in pH of the electrolyte, CTC and DXC were less affected by small variations in the temperature. Considering that the same method should be applicable for all four tetracyclines and, in order to guarantee consistent results, it is important that the range of each variable that produces acceptable results is incorporated in the analytical procedure. The results obtained in this study allowed establishing the following parameters: $50 \pm 1\,mmol\,L^{-1}$ sodium carbonate, pH 10.0 ± 0.1 and temperature $23.0 \pm 0.1\,^{\circ}C$.

Table 5
TC content per capsule determined in commercial samples by CZE and HPLC.

	Sample 6		Sample 7	
	CZE	HPLC	CZE	HPLC
Average content[a] (mg/capsule)	545	510	502	491
s (mg/capsule)	10	10	26	18
R.S.D.	1.9	1.9	4.1	3.7

[a] $n = 5$; *s*, estimate of the standard deviation (mg/capsule); R.S.D., relative standard deviation.

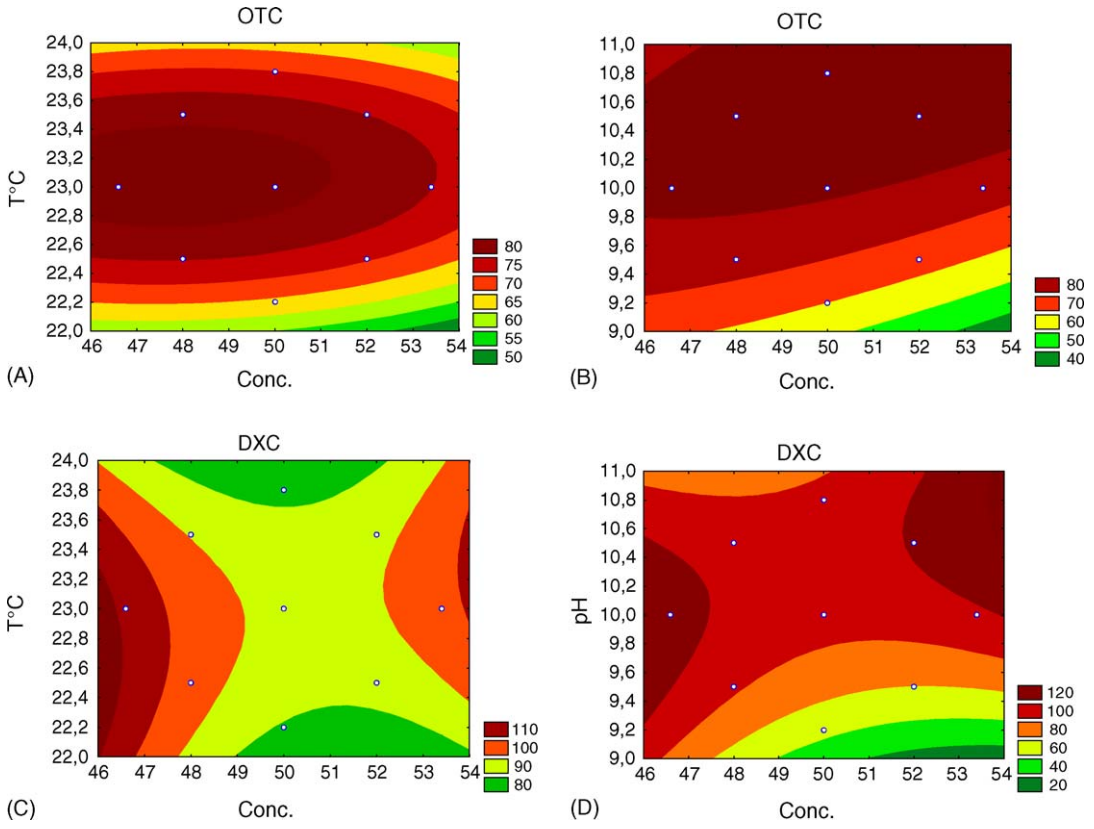

Fig. 6. Counter plots used to evaluate the ruggedness of the method selected by the 2^3 experimental design. (A) OTC (temperature vs. electrolyte concentration); (B) OTC (pH vs. electrolyte concentration); (C) DXC (temperature vs. electrolyte concentration); (D) DXC (pH vs. electrolyte concentration).

Table 6
TC content in commercial samples determined by CZE

Sample	1	2	3	4	5	6	7	8	9	10
Mean value (mg/capsule)	537	605	520	513	494	545	502	510	520	558
R.S.D. (%)	1.8	2.0	2.0	3.7	2.2	1.9	4.1	1.8	4.3	3.9

R.S.D., relative standard deviation ($n = 5$); nominal value of all samples (1–10): 500 mg of TC/capsule.

3.3. Analysis of commercial samples

After the validation, the CZE method was applied to the assay of 10 different commercial samples labeled to contain 500 mg of TC. Two of the samples were also analyzed by HPLC. The concentrations determined in the 10 samples varied between 492 and 605 mg of TC per capsule (Table 6). Considering that the active ingredient needs to be in the range of 90–125% [10], all of the samples analyzed were in accordance with their specifications and also agreed with the results of the HPLC assay.

4. Conclusions

Most of the methods for the determination of antimicrobials described in Pharmacopoeias recommend analysis by HPLC. Nonetheless, these methods are time consuming and require the use of large volumes of HPLC-grade solvents. Many CZE methods have been developed in recent decades, even though, considering their advantages such as efficiency and cost, most of them continue to be alternative methods in the quality control of pharmaceuticals.

The results obtained in this work confirm that the CZE method, when properly optimized and validated, fulfills all the pre-established requirements based on international regulations and is adequate to be used in the quality control of pharmaceuticals.

Acknowledgements

The authors gratefully acknowledge the financial support from CNPq and FAPESP (01/14072-6, 04/07312-9) and thank Professor C.H. Collins for language assistance.

References

[1] L.S. Goodman, A.G. Gilman (Eds.), The Pharmacological Basis of Therapeutics, ninth ed., McGraw-Hill Companies Inc., New York, 1996, pp. 1124–1130.
[2] F.J. Schenk, P.S. Callery, J. Chromatogr. A 812 (1998) 99.

[3] S. Croubels, W. Baeyens, C. Dewaele, C. Van Peterhem, J. Chromatogr. A 673 (1994) 267.
[4] M.F.M. Tavares, V.L. McGuffin, J. Chromatogr. A 686 (1994) 129.
[5] Y.M. Li, A. Van Schepdael, E. Roets, J. Hoogmartens, J. Chromatogr. A 740 (1996) 119.
[6] A. Van Schepdael, V.I. Bergh, E. Roets, J. Hoogmartens, J. Chromatogr. A 730 (1996) 305.
[7] Y.M. Li, A. Van Schepdael, E. Roets, J. Hoogmartens, J. Pharm. Biomed. Anal. 15 (1997) 1063.
[8] G.E. Castellanos, V.A. Schepdael, E. Roets, J. Hoogmartens, J. Chromatogr. A 895 (2000) 43.
[9] J.J. Pesek, M.T. Matyska, J. Chromatogr. A 736 (1996) 313.
[10] The United States Pharmacopoeia. The National Formulary, 28th ed., United States Pharmacopeial Convention, Rockville, 2005, pp. 1886–1887.
[11] K.D. Altria, M.A. Kelly, B.J. Clark, Trends Anal. Chem. 17 (1998) 212.
[12] M. Hernandez, F. Borrull, M. Calull, Chromatographia 54 (2001) 355.
[13] International Conference on Harmonization ICH-Q2A, Guideline for Industry: Text on Validation of Analytical Procedures, 1995. Available from (http://www.fda.gov/cder/guidance/index.htm).
[14] J.C. Miller, J.N. Miller (Eds.), Statistics for Analytical Chemistry., third ed., Ellis Horwood, New York, 1993, p. 233.
[15] A. Weston, P.R. Brown (Eds.), LC and CZE Principles and Practice, Academic Press, San Diego, 1997, p. 279.
[16] C.L. Chen, X.L. Gu, J. AOAC Int. 78 (1995) 1369.
[17] B.B. Netos, I.S. Scarminio, R.E. Bruns (Eds.), Como Fazer Experimentos, Editora UNICAMP, Campinas, 2001, p. 401.
[18] G.A. Shabir, J. Chromatogr. A 987 (2003) 57.

Available online at www.sciencedirect.com
ScienceDirect
Talanta 70 (2006) 244–250
Talanta
www.elsevier.com/locate/talanta

Multienzymatic-rotating biosensor for total cholesterol determination in a FIA system

Eloy Salinas, Valeria Rivero, Angel A.J. Torriero, Delia Benuzzi, María I. Sanz, Julio Raba*

Department of Chemistry, National University of San Luis, Chacabuco y Pedernera, 5700 San Luis, Argentina

Received 5 January 2006; received in revised form 9 February 2006; accepted 9 February 2006
Available online 31 March 2006

Abstract

Fabrication of an amperometric-rotating biosensor for the enzymatic determination of cholesterol is reported. The assay utilizes a combination of three enzymes: cholesterol esterase (ChE), cholesterol oxidase (ChOx) and peroxidase (HRP); which were co-immobilizing on a rotatory disk. The method is developed by the use of a glassy carbon electrode as detector versus Ag/AgCl/3 M NaCl in conjunction with a soluble-redox mediator 4-tert-butylcatechol (TBC). ChE converts esterified cholesterol to free cholesterol, which is then oxidized by ChOx with hydrogen peroxide as product. TBC is converted to 4-tert-butylbenzoquinone (TBB) by hydrogen peroxide, catalyzed by HRP, and the glassy carbon electrode responds to the TBB concentration. The system has integrated a micro packed-column with immobilized ascorbate oxidase (AAOx) that works as prereactor to eliminate L-ascorbic acid (AA) interference. This method could be used to determine total cholesterol concentration in the range 1.2 μM–1 mM ($r = 0.999$). A fast response time of 2 min has been observed with this amperometric-rotating biosensor. Lifetime is up to 25 days of use. The calculated detection limits was 11.9 nM. Reproducibility assays were made using repetitive standards solutions ($n = 5$) and the percentage standard error was less than 4%.

Keywords: Cholesterol; Cholesterol esterase; Cholesterol oxidase; Horseradish peroxidase; Glassy carbon electrode; FIA

1. Introduction

The clinical analysis of cholesterol (Chol) in serum samples is important in the diagnosis and prevention of a large number of clinical disorders. There is a strong positive correlation between high serum Chol level and several illnesses as atherosclerosis and hypertension which can develop into coronary heart disease, myocardial and cerebral infarction (stroke).

In conditions such as hypothyroidism, nephrosis, diabetes mellitus, myxedema, and obstructive jaundice, the patient will have increased levels of Chol and its esters above the physiological norm. Decreased levels are found in patients suffering from hyperthyroidism, anemia, malabsorption and wasting syndromes.

Normal human blood serum contains less than 5.2 mM Chol (200 mg/dl), and a high level being considered as greater than 6.2 mM (240 mg/dl) [1,2]. Plasma Chol levels increase with age, and are generally less in women than men, until menopause, when the values in women exceed those in men [3]. Chol is carried in plasma by a series of protein-containing micelles known as lipoproteins. The lipoproteins are classified into distinct subtypes according to their density, very low density lipoprotein (VLDL), low density lipoprotein (LDL), intermediate density lipoprotein (IDL) and high density lipoprotein (HDL). About 70% of total plasma Chol contained within lipoproteins is esterified by fatty acids. Hence, the concentration of free Chol within lipoproteins is approximately 1.0–2.2 mM (40–85 mg/dl) [4].

Historically, Chol was measured using non-enzymatic spectrometry, via the production of a colored substance, chiefly via cholestapolyenes and cholestapolyene carbonium ions (Liebermann–Burchard reaction). This method suffered from poor specificity, instability of the color reagent, standardization difficulties, the variable reactivity of esters and the unstable and corrosive nature of the reagents used [5,6]. The selectivity of the chemical reaction was improved with the introduction of

* Corresponding author. Fax: +54 2652 43 0224.
E-mail address: jraba@unsl.edu.ar (J. Raba).

0039-9140/$ – see front matter © 2006 Elsevier B.V. All rights reserved.
doi:10.1016/j.talanta.2006.02.043

the enzymes, cholesterol esterase (ChE) and cholesterol oxidase (ChOx).

The cholest-4-en-3-one can be reacted with 2,4-dinitrophenylhydrazine to produce a colored hydrazone [7], although the consumption of O_2 [8], or the production of H_2O_2 [4,9–11]. These are the easier methods of quantifying Chol spectrophotometrically, with the latter being the preferred method.

A number of Chol biosensors have been developed over the past 30 years. Examples of optical biosensors, which determine Chol enzymatically have been developed [12–15]. A fiber optic device has been developed by co-immobilizing ChOx and ChE on preactivated nylon membrane for free and total Chol estimations [16] and enzyme-based determination of Chol using the quartz crystal acoustic wave sensor also has been published [17].

The total Chol present in all lipoproteins fractions can be determined using amperometric and potentiometric assays specific for Chol [18–22]. Cholesterol and cholesterol esters are acted upon by cholesterol esterase and oxidase to generate H_2O_2, which could be measured amperometrically with modified electrodes [23–28].

In the present paper, we report the results of our systematic studies on the technical development and optimization of an amperometric-rotating biosensor. This is a multienzymatic system in which ChE, ChOx and horseradish peroxidase (HRP) are simultaneously immobilized on a disk rotatory. Detection is accomplished with the use of a glassy carbon electrode along with a soluble-redox mediator 4-tert-butylcatechol (TBC). ChE converts esterified cholesterol to free Chol, which is then oxidized by ChOx with hydrogen peroxide as product. TBC is converted to 4-tert-butyl-*o*-benzoquinone (TBB) by hydrogen peroxide, catalyzed by HRP, and the glassy carbon electrode responds to the TBB concentration. Besides, the system has integrated a micro packed-column with immobilized ascorbate oxidase (AAOx), that works as prereactor to eliminate L-ascorbic acid (AA) which is very important electroactive interferent.

2. Experimental

2.1. Reagents and solutions

All reagents used, except as noted, were of analytical reagent grade. Horseradish peroxidase (HRP, EC 1.11.1.7 Grade II, 181 IU mg^{-1}), cholesterol oxidase (ChOx, EC 1.1.3.6, from *Pseudonomas fluorescens*, 4.2 UI mg^{-1}), cholesterol esterase (ChE, EC 3.1.1.13 from *Pseudomonas* sp., 5.9 UI mg^{-1}), ascorbate oxidase (AAOx; 1000–3000 UI mg^{-1}), cholesterol and Triton X-100 were all purchased from Sigma (St. Louis, USA). A stock 0.01 M cholesterol solution was prepared in phosphate buffer (0.01 M, pH 7) containing 10% (w/w) of Triton X-100 in a thermostated bath at 65 °C. This solution was stored at 4 °C in the dark and was stable for at least 10–15 days (until turbidity was observed). More dilute working solutions of cholesterol were prepared by dilution of the stock solution using a 0.01 M phosphate buffer solution containing 1% (w/w) of Triton X-100. This solution was used as the carrier solution in the FIA system.

Synthetic Chol serum samples were prepared with the concentrations of interferents indicated in the text. Quality controls human serum (QC) with a lower, medium and higher (1.50 mM (QC1), 3.96 mM (QC2) and 7.77 mM (QC3)) concentrations, respectively (*Accutrol*™ Chemistry controls, A-2034, Sigma Diagnostics), were used. The kit for spectrophotometric determination of Chol (*colestat enzimatic*®) was purchased from Wiener Lab., Argentina, and was used accordance with manufacture instructions. 4-Tert-butylcatechol (4-TBC), ascorbic acid (AA), uric acid, lysine, lactate, glucose and glutaraldehyde used were purchased from Merk, Darmstadt. 3-Aminopropyl-modified controlled-pore glass, 1400 Å mean pore diameter and 24 m^2 mg^{-1} surface area, was from Electro-Nucleonics (Fairfield, NJ) and contained 48.2 μmol g^{-1} of amino groups.

Aqueous solutions were prepared using purified water from a Milli-Q-system and the samples were diluted to the desired concentrations using a 10 ml Metrohm E 485 burette.

2.2. Apparatus

The main bodies of the amperometric-rotating bioreactor were made of Plexiglas. The design of the flow-through chamber containing the rotating enzyme biosensor and the detector system was described previously [29]. Glassy carbon electrode is on the top of the rotating reactor. The rotating reactor is a disk of Teflon in which a miniature magnetic stirring bar (Teflon-coated Micro Stir bar from Markson Science Inc., Phoenix, AZ) has been embedded. Typically, a sensor disk carries 1.4 mg of controlled-pore glass on its surface. Rotation of the lower reactor was initiated by a laboratory magnetic stirrer (Metrohm E649 from MetrohmAGHerisau, Switzerland) and controlled with a variable transformer with an output between 0 and 250 V and maximum amperage of 7.5 A (Waritrans, Argentina).

Micro packed-column was made of Tygon tubing (2.0 cm long, 2.0 mm i.d.), it contained controlled-pore glass with AAOx immobilized. A pump (Gilson Minipuls 3 peristaltic pump, Gilson Electronics Inc., Middleton, WI) was used for pumping, sample introduction, and stopping of the flow. Fig. 1 illustrates

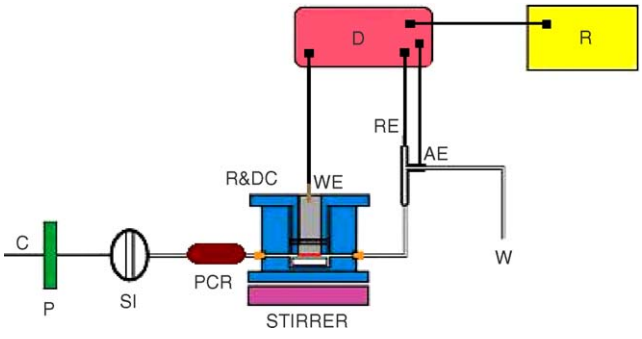

Fig. 1. Block diagram of the continuous-flow system and detection arrangement. P: pump (Gilson Minipuls 3 peristaltic pump, Gilson Electronics, Inc. Middleton, WI); C: carrier buffer line; SI: sample injection; W: waste line; R&DC: sensor and detector cell; WE: glassy carbon electrode; RE: reference electrode (Ag/AgCl/3.0M NaCl); AE: auxiliary electrode (platinum); D: potentiostat/detection unit (BAS LC-4C, Bioanalytical Systems, West Lafayette, IN); R: recorder (Varian, Model 9176, Varian Techtron, Springuale, Australia); PCR: packed-column reactor.

schematically the components of the single-line continuous-flow setup. The pump tubing was Tygon (Fisher AccuRated, 1.0 mm i.d., Fisher Scientific Co., Pittsburgh, PA) and the remaining tubing used was Teflon, 1.00 mm i.d. from Cole Parmer (Chicago, IL).

Amperometric detection was performed using a BAS LC-4C potentiostat and a BAS 100 B/W (Electrochemical Analyzer Bioanalytical System, West Lafayette, IN) was used to voltammetric determinations. The potential applied to the working electrode (Glassy carbon electrode, GCE) for the functional group detection was −150 mV versus Ag/AgCl/3.0 M NaCl reference electrode, BAS RE-6, and a Pt wire was used as counter electrode. At this potential, a catalytic current was well established.

Spectrophotometric measurements were performed with a Beckman DU 350 UV–vis spectrophotometer using 1 cm glass cells. All pH measurements were made with an Orion Expandable Ion Analyzer (Orion Research Inc., Cambridge, MA) Model EA 940 equipped with a glass combination electrode (Orion Research Inc., Cambridge, MA).

2.3. Enzymes immobilization

The rotating disk biosensor (bottom part) was prepared by immobilizing HRP, ChE and ChOx on 3-aminopropyl-modified controlled-pore glass (APCPG). The APCPG, smoothly spread on one side of a double-coated tape affixed to the disk surface, was allowed to react with an aqueous solution of 5% (w/w) glutaraldehyde at pH 10.00 (0.20 M carbonate) for 2 h at room temperature. After washed with purified water and 0.10 M phosphate buffer of pH 7.00, the enzymes mixture (constituted by HRP 40 U/ml, ChE 40 U/ml and ChOx 40 U/ml in 0.10 M phosphate buffer, pH 7.00) was coupled with residual aldehyde groups in phosphate buffer (0.10 M, pH 7.00) overnight at 4 °C.

By other way, AAOx was immobilized on 3-aminopropyl-modified controlled-pore glass (APCPG). The APCPG was allowed to react with an aqueous solution of 5% (w/w) glutaraldehyde at pH 10.00 (0.20 M carbonate) for 2 h at room temperature. After washing with purified water and 0.10 M phosphate buffer of pH 7.00, the enzyme (5 mg ml^{-1}) was coupled to the residual aldehyde groups in phosphate buffer (0.10 M, pH 7.00) overnight at 4 °C. Then the column was packed with 20 mg APCPG–AAOx preparation.

The both immobilized enzymes preparations (rotating disk and packed-column) were then washed with phosphate buffer (pH 7.00) and stored in the same buffer at 4 °C between uses. The immobilized preparations were perfectly stable throughout at least 1 month of daily use.

2.4. Validation

The samples from healthy human volunteers and Quality controls were diluted 1/10 before to carry out the measurements. Thus, the determinations were made in linear zone of the Chol calibration plot (see below).

To establish the lower limit of quantification in a single validation batch five replicates of QC sample 3.96 mM cholesterol were analyzed. The intra- and inter-day precision (CV%) and accuracy (bias%) of the assay procedure were determined by the analysis of five samples at each lower, medium and higher QC concentration (1.50 mM (QC1), 3.96 mM (QC2) and 7.77 mM (QC3)) in the same day and one sample at each QC concentration in five different days, respectively.

The freeze-thaw stability was also verified at two levels of concentrations, lower and higher, after three freeze-thaw cycles.

3. Results and discussion

The development of analytical system based on the use of immobilized multienzymes system represents one of the most rapid advancing areas of biosensors. Biosensors find a widespread application in scientific investigation as well as in medicine, biotechnological processes, food industries and environmental control.

The pioneering work of Kulys et al. [30] demonstrated that the combination of peroxidase and an oxidase makes possible to construct amperometric biosensors that work at more negative potentials avoiding electroactive interferences. This principle has also been used by other groups introducing an electroactive polymer to facilitate the HRP reduction [31,32]. However, most of the Chol in human blood is esterified with long chain fatty acids. Since cholesterol esters do not function as substrates for ChOx, biosensors based on ChE and ChOx have been developed for total Chol determination [33,34]. Cholesterol esterase catalyzes the hydrolysis of the esters to free cholesterol which can then become the substrate for ChOx oxidation. Cholesterol and cholesterol esters were acted upon by cholesterol esterase and oxidase to generate H_2O_2, which was measured amperometrically [23,35].

In our case, we have immobilized on the rotating disk HRP, ChOx and ChE in proportion 1:1:1, incorporating with the sample injection 4-TBC that works as mediator (Scheme 1). So the combination of 4-TBC and HRP, which reduces hydrogen peroxide, makes it possible to operate at a low potential and to eliminate interferents. The current developed at the detector is directly proportional to the concentration of analyte in the bulk of solution and increase with increasing rotation velocity.

Advantages of this configuration are the stability that results from immobilized enzymes in the rotatory disk and forced convection of the oxidized products to the electrode. If the flow is stopped when the sample plug transported by continuous-flow

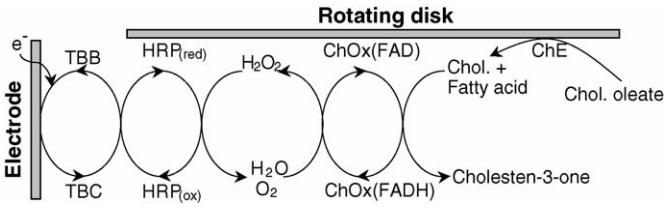

Scheme 1. Schematic representations of the reduction wave of the enzymatic process between 4-tert-butylcatechol (TBC), 4-tert-butyl-*o*-benzoquinone (TBB), hydrogen peroxide (H_2O_2), cholesterol esterase (ChE), cholesterol oxidase (ChOx), and horseradish peroxidase (HRP).

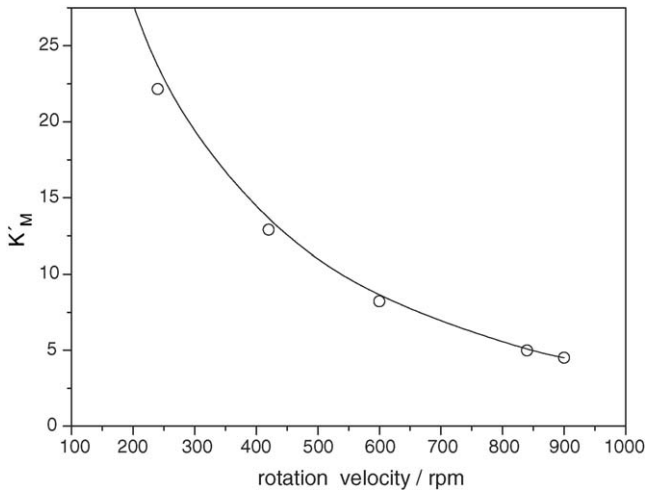

Fig. 2. The values of K'_M for the system obtained at five different rotation velocities and stopping the flow for 120 s during measurement. The calculation of K'_M was performed under conditions in which [substrate] > K'_M.

reaches the center of the reactor, detection take place under conditions similar to those of batch detection [36,37].

The implementation of continuous-flow/stopped-flow programming and the location of immobilized enzymes involved in the sequence illustrated earlier, permits: (a) utilization of relatively low enzyme loading conditions, (b) instantaneous operation under high initial rate conditions, (c) easy detection of accumulated products, and (d) reduction of apparent Michaelis–Menten constant, K'_M.

A more complete reagent homogenization is achieved, because the cell works as a mixing chamber by facilitating the arrival of substrate at the active sites and the release of products from the same sites. The net result is high values of catalytic current.

As noted at the beginning of this section, rotation is expected to decrease the values of the apparent Michaelis–Menten constant, K'_M, since the catalytic efficiency is increased. Michaelis constant which differ substantially from that measured in homogeneous solution, is not an intrinsic property of the enzyme, but of the system. This constant characterizes the reactor, not the enzyme itself. It is a measure of the substrate concentration range over which the reactor response is linear [38]. Fig. 2 shows the values of K'_M for the system obtained at five different rotation velocities and stopping the flow for 120 s during measurement. The calculation of K_M was performed under conditions in which [substrate] > K'_M, as a consequence the following applies (Eq. (1)), assuming that the Briggs and Haldane scheme [39] is of the plot of $1/S$ versus $1/[\text{Chol}_{\text{Total}}]$ plot. This is a graphical approach similar to the Lineweaver–Burk plot:

$$\frac{1}{S} = \left(\frac{m}{[\text{Chol}_{\text{Total}}]}\right) + n \quad (1)$$

where S = rate of response; $K'_M = m/n$. The apparent constant is thus obtained from the slope and intercept of the $1/S$ versus $1/[\text{Chol}_{\text{Total}}]$ plot.

Thereby, as observed earlier [40], if the sensor is devoid of rotation, there is practically no response. If a rotation of 900 rpm is imposed on the sensor located at the bottom of the cell (with immobilized enzymes), the signal is dramatically enlarged. The trend indicates that, up to velocities of about 900 rpm, a decrease in the thickness of the stagnant layer improves mass transfer to and from the immobilized enzyme active sites. Beyond 900 rpm, the current is constant, and chemical kinetics controls the overall process. Therefore, a rotation velocity of 900 rpm was used.

Advantages to these biosensors include rapid analysis, reusability, thermal stability, and linearity.

3.1. Effect of cell volume and sample size

Depending on the volume of the cell in contact with the sensors, the overall process becomes controlled by diffusion (large volumes) or by the chemical kinetics of the enzyme-catalyzed reactions (small volumes).

The cell volume was changed from 150 μl to 1 ml by removing the O-rings between the upper and lower half of the cell. The measured current, as expected, decreased linearly with an increase in cell volume, due to the dilution effect favored by rotation, and the fact that the measured current is directly proportional to bulk concentration. The smallest cell volume of 150 μl was adopted for further studies.

The measured current increased lineally with sample size up to 150 μl in a cell with a volume of 150 μl. For convenience a sample size of 150 μl was used. Sensitivity is almost tripled in the range between 50 and 150 μl.

3.2. Effect of pH

The catalytic current (nA), under stopped-flow conditions, presents a moderate increase from pH 6.5 to 7.00 and then begin to decay up to pH 8.00, the highest pH value tested (Fig. 3).

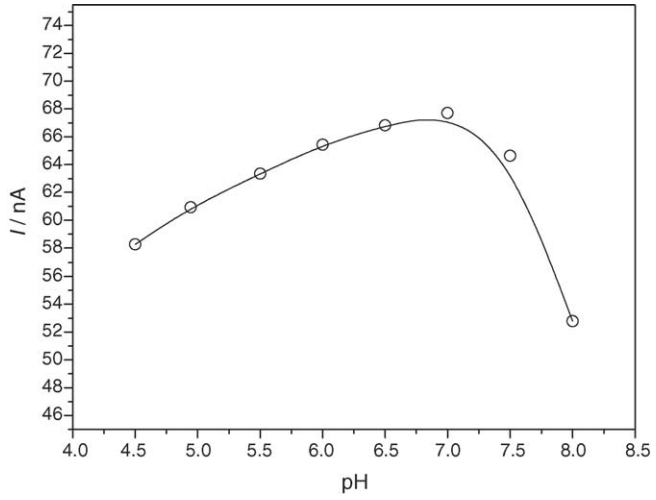

Fig. 3. pH dependence of multienzymatic-rotating biosensor signal. One hundred and fifty microliter aliquots of 3.96 mM Chol standard solution were injected into various buffers solutions. Other biosensor conditions were described in the text.

Therefore, the pH used for this system was 7.00 (0.10 M phosphate buffer).

3.3. Cholesterol measurement with multienzymatic-rotating biosensor

The working potential was selected using the cyclic voltammogram of 4-TBC at a glassy carbon electrode (GCE) in phosphate buffer [41]. For potentials values below −150 mV, the cathodic current became independent of the applied potential; therefore, this value was chosen as working potential. Furthermore, at this potential, a less contribution of the electroactive interferences present in serum is expected.

The performance of the multienzymatic-rotating biosensor for the measurement of total Chol concentration was characterized. The following procedure was used: (a) a baseline current was established with the buffer solution; (b) a solution containing the sample diluted 1/10 with buffer phosphate and 4-TBC was injected in the rotating biosensor; (c) the flow was detained, the disk was rotated to 900 rpm and the reduction current was measurement; (d) After 2 min the flow was started again. A Chol calibration plot was obtained by plotting catalytic current I (nA) versus Chol concentration. The results obtained with this method are shown in Fig. 4. A linear relation (Eq. (2)) was observed in the range of 1.2 μM and 1 mM (rotation 900 rpm):

$$I(\text{nA}) = 0.81 + 69.49[C_{\text{Chol}}] \quad (2)$$

The correlation coefficient for this type of plot was typically 0.998. Detection limit (DL) is the minimal difference of concentration that can be distinguished from the signal of baseline buffer solution. The DL was calculated as the amount of Chol required to yield a net peak that was equal to three times the SD signal. In this study, the minimal concentration of Chol was 11.9 nM. Reproducibility assays were made using repetitive standards solutions ($n = 5$) containing 1.0 mM 4-TBC and 3.96 mM Chol; the percentage standard error was less than 4%.

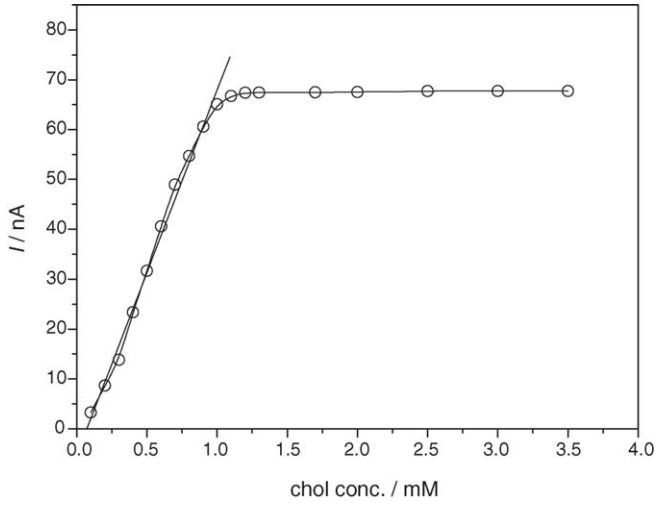

Fig. 4. Response of the multienzymatic-rotating biosensor for several Chol concentrations (mM). The flow was stopped for 2 min during measurement; cell volume: 150 μl; flow rate: 1 ml min^{-1}.

Table 1
Intra- and inter-day precision and accuracy ($n = 5$)

	Intra-day			Inter-day		
c_{nominal} (mM)	1.50	3.96	7.77	1.50	3.96	7.77
Mean c_{found} (mM)	1.47	3.93	7.72	1.39	3.83	7.59
CV (%)	0.70	1.10	1.80	1.00	1.40	2.30
Bias (%)	2.00	0.48	0.67	7.33	3.16	1.03

The stability of the biosensor was tested for nearly 3 h of continuous use in the FIA system. In this experiment, after every four samples, a standard solution containing 1.0 mM 4-TBC, 3.96 mM Chol was injected. In the FIA system using a multienzymatic sensor, there is practically no decay in the catalytic current after eight samples.

The effect of the various compounds on the response of the multienzymatic-rotating biosensor was tested. Compounds such as lysine, glucose, lactate and uric acid showed little or no effect on the current response. But the addition of 10 mM ascorbic acid resulted in ca. 4.8% decrease versus the reductive current obtained with Chol synthetic and 4-TBC. This fact can be avoided with the incorporation of a packed-column (PCR) that contains APCPG–AAOx preparation (Fig. 1).

The intra- and inter-day precision (CV%) and accuracy (bias%) of the assay procedure were determined by the analysis of five samples at each lower, medium and higher QC concentration in the same day and one sample at each QC concentration in five different days, respectively (Table 1).

Repeated analyses using a range of human serum samples, containing low and high levels of Chol demonstrate the precision of the Chol biosensor. This was found to range from 1.4 to 4.6% for within-day analyses and from 1.8 to 5.9% for day-to-day analyses. Recovery yields were performed using the clinical serum samples which were diluted with the working phosphate buffer and spiked with Chol standards. Recoveries in the range 96.6–103% with an average of 100.1% were obtained. The response study of this multienzymatic-rotating biosensor was compared with spectrophotometric methods. Table 2 gives the results obtained using the 2 methods for 5 separate determinations of 10 human serum samples.

Table 2
Results obtained using the 2 methods for 5 separate determinations of 10 human serum samples

Sample no.	Proposed method (mM)[a]	Reference method (mM)[a]
1	$3.96 \pm 4.1 \times 10^{-3}$	$3.90 \pm 6.1 \times 10^{-3}$
2	$3.83 \pm 3.6 \times 10^{-3}$	$3.89 \pm 5.2 \times 10^{-3}$
3	$1.50 \pm 3.1 \times 10^{-3}$	$1.56 \pm 4.1 \times 10^{-3}$
4	$1.46 \pm 2.9 \times 10^{-3}$	$1.40 \pm 3.9 \times 10^{-3}$
5	$7.80 \pm 3.9 \times 10^{-3}$	$7.69 \pm 5.4 \times 10^{-3}$
6	$7.60 \pm 4.5 \times 10^{-3}$	$7.57 \pm 5.1 \times 10^{-3}$
7	$5.96 \pm 3.3 \times 10^{-3}$	$5.76 \pm 6.1 \times 10^{-3}$
8	$4.36 \pm 4.5 \times 10^{-3}$	$4.47 \pm 5.5 \times 10^{-3}$
9	$6.96 \pm 3.9 \times 10^{-3}$	$6.79 \pm 4.3 \times 10^{-3}$
10	$1.96 \pm 4.1 \times 10^{-3}$	$2.09 \pm 3.1 \times 10^{-3}$

[a] $X \pm$ S.D.

Table 3
A comparison of previous methods for determining cholesterol

Detection method	Response time (min)	Linear range (mM)	Detection limit (μM)	Lifetime (days)	Known interferents	Ref.
Amperometric	1	2–10 mM for FC	500	60	Ascorbic acid, glucose were major interferents	[42]
Amperometric	1	0.05–0.50	8	25	Not tested	[43]
Potentiometric	16	0.05–3 for TC	10	–	Ascorbic acid, bilirubin and proteins had negligible effects	[44]
Amperometric	<2	0.58–3.68 for FC	60	5	Ascorbic acid, paracetamol, glutathione, uric acid were major interferents	[45]
Amperometric	5	No data for FC	–	–	Oxygen, urea	[46]
Amperometric	1	Not linear for TC	500	1	Not tested	[47]
Spectrophotometric	5	2.6–15.6 for TC	2.6	–	Negligible interference from ascorbic acid, uric acid and haemoglobin	[48]
Spectrophotometric	12	0.13–1.3 for TC	130	–	Testosterone; Vitamin D; progesterone were major interferents. NaCl; $CuSO_4$; creatinine; $NaHCO_3$; albumin; estrogen had practically no effect	[49]
Amperometric	2	0.001–1 for TC	0.012	30	Ascorbic acid, lysine, glucose, lactate, and uric acid had negligible or not effects	Proposed method

FC refers to the fact that the biosensor was used to measure free cholesterol only, while TC means total cholesterol was determined.

4. Conclusions

The usefulness of enzyme biosensor used for the determination of different concentrations of Chol was demonstrated. The proposed method was compared with another biosensor previously developed. Table 3 indicates that the results obtained by the proposed method were better than the results obtained by existing methods. This type of detection shows good promise in biological sensing, particularly in plasma and whole blood samples. Also, this biosensor is able to operate as a fast, selective and sensitive detection unit when is incorporated into a FIA system, and provides a fast and cost effective solution to the realization of quantitative information at extremely high and low levels of Chol concentrations.

Advantages to these biosensors include rapid analysis, reusability, thermal stability, and linearity. The method is highly reproducible and the values correlate well with those obtained with the colorimetric assays.

Acknowledgements

The authors wish to thank the financial support from the Universidad Nacional de San Luis and the Consejo Nacional de Investigaciones Científicas y Técnicas (CONICET). One of the authors (AAJT) acknowledges support in the form of a fellowship from the Consejo Nacional de Investigaciones Científicas y Técnicas (CONICET).

References

[1] A. White, P. Handler, E.L.R. Smith, L. Hill, I.R. Lehman, Principles of Biochemistry, 6th ed., McGraw-Hill Book, NY, 1978.
[2] National Cholesterol Education Program, Arch. Intern. Med. 148 (1988) 36.
[3] A. Kaplan, R. Jack, K.E. Opheim, B. Toivola, A.W. Lyon, Clinical Chemistry: Interpretations and Techniques, 4th ed., Williams & Wilkins, London, 1995, p. 240.
[4] C.C. Allain, L.S. Poon, C.S.G. Chan, W. Richmond, P.C. Fu, Clin. Chem. 20 (1974) 470.
[5] W. Richmond, Clin. Chem. 19 (1973) 1350.
[6] D.L. Witte, D.A. Barrett Jr., D.A. Wycoff, Clin. Chem. 20 (1974) 1282.
[7] H.M. Flegg, Ann. Clin. Biochem. 10 (1973) 79.
[8] M. Mascini, M. Iannello, G. Palleschi, Anal. Chim. Acta 146 (1983) 135.
[9] H. Huang, J.W. Kuan, G.G. Guilbault, Clin. Chem. 21 (1975) 1605.
[10] F.O. Sale, S. Marchesini, P.H. Fishman, B. Berra, Anal. Biochem. 142 (1984) 347.
[11] A. Carpenter, W.C. Purdy, Anal. Lett. 23 (1990) 425.
[12] M.D. Marazuela, B. Cuesta, M.C. Moreno-Bondi, A. Quejido, Biosens. Bioelectron. 12 (1997) 233.
[13] G. Pasin, G.M. Smith, M. O'Mahony, Food Chem. 61 (1998) 255.
[14] W. Trettnak, O.S. Wolfbeis, Anal. Biochem. 184 (1990) 124.
[15] D.M. Amundson, M. Zhou, J. Biochem. Biophys. Methods 38 (1999) 43.
[16] I. Krug, A.A. Suleiman, G.G. Guilbault, Anal. Chim. Acta 256 (1992) 263.
[17] S.P. Martin, D.J. Lamb, J.M. Lynch, S.M. Reddy, Anal. Chim. Acta 487 (2003) 91.
[18] L. Charpentier, N. El Murr, Anal. Chim. Acta 318 (1995) 89.
[19] T. Nakaminami, S. Ito, S. Kuwabata, H. Yoneyama, Anal. Chem. 71 (1999) 1068.
[20] T. Nakaminami, S. Kuwabata, H. Yoneyama, Anal. Chem. 69 (1997) 2367.
[21] M.A.T. Gilmartin, J.P. Hart, Analyst 119 (1994) 2331.
[22] M. Situmorang, P.W. Alexander, D.B. Hibbert, Talanta 49 (1999) 639.
[23] J.L. Bescombes, S. Cosnier, P. Labbe, Talanta 43 (1996) 1615.
[24] H. Kinoshita, M. Torimura, K. Kano, T. Ikeda, Ann. Clin. Biochem. 35 (1998) 739.
[25] J.C. Vidal, E. Garcia-Ruiz, J.R. Catillo, J. Pharm. Biomed. Anal. 24 (2000) 51.

[26] K.V. Gobi, F. Mizutani, Sens. Actuators B 80 (2001) 272.
[27] C. Bongiovanni, T. Ferri, A. Poscia, M. Varalli, R. Santucci, A. Desideri, Bioelectrochemistry 54 (2001) 17.
[28] H. Wang, S. Mu, Sens. Actuators B 56 (1999) 22.
[29] E. Salinas, A.A.J. Torriero, M.I. Sanz, F. Battaglini, J. Raba, Talanta 66 (2005) 92.
[30] J.J. Kulys, M.V. Pesliakinene, A.S. Samalius, Bioelectrochem. Bioeng. 8 (1981) 81.
[31] T. Ohara, M. Vreeke, F. Battaglini, A. Heller, Electroanalysis 5 (1993) 825.
[32] A. Belay, A. Collins, T. Ruzgas, P.T. Kissinger, L. Gorton, E. Csöregi, J. Pharm. Biomed. Anal. 19 (1999) 93.
[33] A.L. Crumbliss, J.G. Stonehuerner, R.W. Henkens, J. Zhao, J.P. O'Daly, Biosens. Bioelectron. 8 (1993) 331.
[34] Y. Kajiya, R. Tsuda, H.J. Yoneyama, J. Electroanal. Chem. 301 (1991) 155.
[35] H. Kinoshita, M. Torimura, K. Kano, T. Ikeda, Ann. Clin. Biochem. 35 (1998) 739.
[36] R.A. Kamin, G. Wilson, Anal. Chem. 52 (1980) 1198.
[37] J. Wang, M.S. Lin, Anal. Chem. 218 (1998) 281.
[38] B.A. Gregg, A. Heller, Anal. Chem. 62 (1990) 258.
[39] E.G. Briggs, J.B.S. Haldane, Biochem. J. 19 (1925) 338.
[40] A.A.J. Torriero, E. Salinas, F. Battaglini, J. Raba, Anal. Chim. Acta 498 (2003) 155.
[41] J.J.J. Ruiz-Díaz, A.A.J. Torriero, E. Salinas, E.J. Marchevsky, M.I. Sanz, J. Raba, Talanta 68 (2006) 1343.
[42] A. Kumar, R. Malhotra, B.D. Malhotra, S.K. Grover, Anal. Chim. Acta 414 (2000) 43.
[43] J.C. Vidal, J. Espuelas, E. Garcia-Ruiz, J.R. Castillo, Talanta 64 (2004) 655.
[44] M. Situmorang, P.W. Alexander, D.B. Hibbert, Talanta 49 (1999) 639.
[45] M.A.T. Gilmartin, J.P. Hart, Analyst 119 (1994) 2331.
[46] T. Nakaminami, S. Kuwabata, H. Yoneyama, Anal. Chem. 69 (1997) 2367.
[47] T. Nakaminami, S. Ito, S. Kuwabata, H. Yoneyama, Anal. Chem. 71 (1999) 1068.
[48] C.C. Allain, L.S. Poon, C.S.G. Chan, W. Richmond, P.C. Fu, Clin. Chem. 20 (1974) 470.
[49] Suman, C.S. Pundir, Curr. Appl. Phys. 3 (2003) 129.

Available online at www.sciencedirect.com
ScienceDirect
Talanta 70 (2006) 251–256
Talanta
www.elsevier.com/locate/talanta

Measurement of peroxidase activity in single neutrophils by combining catalyzed-enzyme reaction and epi-fluorescence microscopy

Wenpeng Li, Wenrui Jin *

School of Chemistry and Chemical Engineering, Shandong University, Jinan 250100, China

Received 8 November 2005; received in revised form 11 February 2006; accepted 11 February 2006
Available online 11 April 2006

Abstract

An epi-fluorescence microscopy for determination of peroxidase in individual neutrophils was developed by a combination of enzyme-catalyzed reaction and fluorescence detection. In this method, an individual cell was transferred into a microliter-volume vessel and lysed by freeze-thawing and ultrasonication. The peroxidases-catalyzed reaction was initiated by adding the buffer solution containing nonfluorescent substrates 10-acetyl-3,7-dihydroxyphenoxazine and H_2O_2 to the vessel. Peroxidase activity could be determined via measuring the fluorescent signal of the product resorufin of enzyme-catalyzed reaction. When the slope of kinetic curve of the enzyme-catalyzed reaction was used to quantify peroxidases in single cells, the effect of the time difference between each measurement and the interference from other intracellular compounds that could emit fluorescence can be eliminated.

Keywords: Single-cell analysis; Enzyme; Peroxidase; Laser-induced fluorescence detection; Epi-fluorescence microscopy; Neutrophil

1. Introduction

Single-cell analysis is of significant interest to the chemical, biotical, medical, and pharmaceutical communities [1–3]. Enzymes are important biological substances in cells. Early in 1950s, Lowry has developed a histochemistry method with fluorescence detection for rough measurements of a few enzymes in large single nerve cell bodies [4]. However, the method is unsatisfactory in regard to precision, and fragments of nerve tissue of known composition give low results. After that, Lowry's group reported a more accurate method for enzyme analysis in single large cell bodies using the enzyme-catalyzed reaction and the fluorescence detection [5]. The similar methods have been used to measure different enzymes [6]. In 1970s, qualitative measurements of glucose-6-phosphate dehydrogenase (G6PDH) activity in single fibroblasts have been performed by fluorescence microscopy with epi-illuminaton [7]. In the method, single frozen-dried fibroblasts were put into droplets of liquid contained substrates for enzyme-catalyzed reaction and the fluorescence of the products was detected for each cell during 3 h of incubation. The flow cytometric assay for β-galactosidase activity in single yeast cells has been reported [8]. Capillary electrophoresis (CE) has been successfully used to determine a variety of enzyme activity in different single cells. Lactate dehydrogenase isoenzymes [9,10], kinase [11–13] and α-1,3-*N*-acetylgalactosaminyltransferase [14] in single mammalian cells can be separated and determined by using CE with laser-induced fluorescence (LIF) detection. CE with electrochemical detection (ECD) has been developed for analysis of G6PDH [15] and alkaline phosphatase isoenzymes [16]. Particle-counting immunoassay in a capillary environment for determination of G6PDH has been described [17,18]. Recently, other methods for single-cell analysis of enzymes such as fluorescence imaging analysis with electroporation [19], optical sensor [20], fluorescence microscopy and flow cytometry [21], fluorescence microscopy and CE with LIF detection [22], and resonance Raman microscopy [23] have been developed.

In this work, we developed a new method for determination of enzyme activity in single cells based on the enzyme kinetics using epi-fluorescence microscopy. Peroxidase (PO) is a green heme enzyme that plays a crucial role in infection and inflammation [24,25]. It is required for neutrophils to kill a variety of microorganisms and has been implicated in promoting tissue damage in numerous inflammatory diseases including

* Corresponding author. Fax: +86 531 8856 5167.
E-mail address: jwr@sdu.edu.cn (W. Jin).

0039-9140/$ – see front matter © 2006 Elsevier B.V. All rights reserved.
doi:10.1016/j.talanta.2006.02.033

rheumatoid arthritis [26], adult respiratory distress syndrome [27], lung cancer [28] and acute myeloid leukemia [29]. Thus, analysis of PO activity within cells has attracted considerable attention to understand cellular function [30]. Therefore, PO in human neutrophils was chosen as the model enzyme. The strategy of amplifying detection signal via enzyme-catalyzed reactions is commonly used [31–33]. The protocol based on the enzyme-catalyzed reaction was also used in this work to determine PO in a single cell. Fluorescence detection is very sensitive for the products of enzyme-catalyzed reactions [34–37]. PO could catalyze nonfluorescent enzyme substrate 10-acetyl-3,7-dihydroxyphenoxazine (ADHP) to fluorescent resorufin in the presence of H_2O_2. The PO activity could be determined through measuring the fluorescence of resorufin based on the slope of linear line on the plot of the fluorescence intensity versus the reaction time. When the slop was used to quantify the PO activity in single cells, the effect of the time difference between each measurement and the interference of other compounds that could emit fluorescence could be eliminated.

2. Experimental

2.1. Chemicals

ADHP was purchased from AnaSpec Inc. (San Jose, CA, USA). A 4.3×10^{-3} mol/L stock solution of ADHP was prepared by dissolving ADHP in dimethyl sulfoxide (DMSO) and stored at −20 °C. Horseradish peroxidase (HRP, R.Z ~ 3.0, 250 U/mg) was obtained from Shanghai Lizhu Dongfeng Biotechnology Co., Ltd. (Shanghai, China). A 375 U/mL stock solution of HRP was prepared in water. The 4.5% dextran T-500 separation solution was purchased from Pharmacia (Uppsala, Sweden) and the lymphocyte separation medium was obtained from Shanghai Huajing Biological High-Tech. Co., Ltd. (Shanghai, China). Other reagents were of analytical grade and purchased from standard reagent suppliers. The ADHP stock solution and H_2O_2 solution were diluted to 4.8×10^{-4} mol/L with 2.0×10^{-2} mol/L phosphate buffer (pH 7.0) before use. Other aqueous solutions were prepared with doubly distilled water. All solutions were prepared in disposable plastic ware using disposable pipette tips and stored at 4 °C. All disposable plastic wares and disposable micropipette tips used in the assay were autoclaved prior to use in order to denature any contaminants. A resorufin solution was prepared by the following procedures: 100 μL of phosphate buffer (pH 7.0), 4 μL of 4.3×10^{-3} mol/L H_2O_2, 4 μL of 4.3×10^{-3} mol/L ADHP and 2 μL of 7.5×10^{-4} U/mL HRP were mixed in a plastic ware and sealed. After incubation for 48 h, the solution was heated for 20 min at 88 °C to disable the HRP. The solution was stored at 4 °C and diluted 1000 times just before use.

2.2. Epi-fluorescence microscopy

The schematic of the epi-fluorescence microscope is shown in Fig. 1. The excitation source was a He–Ne laser (Melles Griot Laser Group, Carlsbad, CA, USA) with 543 nm and 5 mW. The microscope frame was an Olympus IX81 inverted microscope body with a filter cube containing three filter elements (8–10). The laser passed through a 520−550 nm excitation filter (8), reflected by a 565 nm dichroic mirror (9), and focused to the sample vessel via a 10× microscope objective (NA 0.40). The fluorescence was collected by the same objective, transmitted through the dichroic mirror, filtered by a cut-on 580 nm emission filter (10) and detected by CCD camera (Cascade 512B, Roper Scientific, Inc. Tucson, AZ, USA) equipped with a 512 pixel × 512 pixel array (16 μm pixel × 16 μm pixel). An 800 μm × 800 μm area could be imaged with the CCD controlled by MetaMorph software and a 10×objective. All images were acquired with the exposure time of 100 ms, intensifier gain of 2375 and readout speed of 5 MHz.

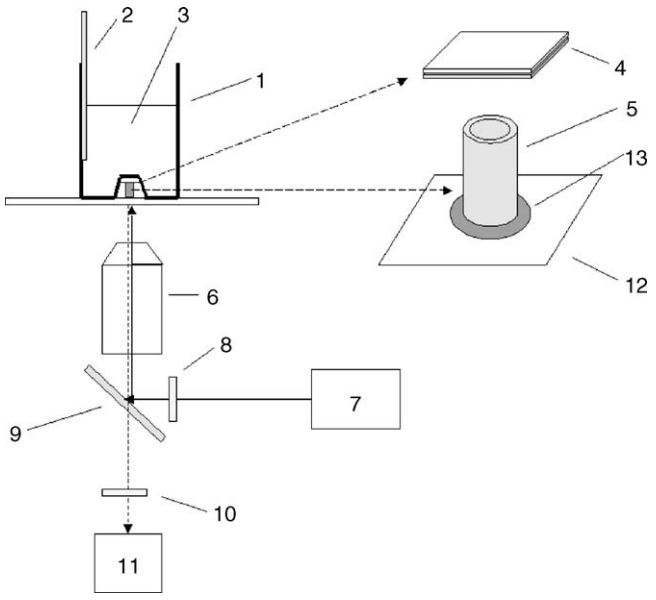

Fig. 1. Schematic diagram of the epi-fluorescence detection system: 1, plastic bottle with a recessed bottom; 2, thermometer; 3, constant-temperature water; 4, cover; 5, vessel; 6, objective; 7, He–Ne laser; 8, excitation filter; 9, dichroic mirror; 10, emission filter; 11, CCD; 12, coverslip; 13, epoxy. Dimensions are not in scale.

The vessel was fabricated by fixing a ~1.2 mm i.d., ~8 mm long plastic tube upon a 0.17-mm-thick microscope coverslip with cyanoacrylate and sealing the outside of the tube with epoxy. A 5 mm × 5 mm coverslip as the cover of vessel was glued to the plastic tube with a double-face adhesive-tape after addition of the solution. The vessel and its cover were also shown in Fig. 1.

2.3. Preparation of human neutrophils and their lysate

Human neutrophils were isolated as described previously [38]. Briefly, five portions of human blood and one portion of 4.5% dextran T-500 separation solution were mixed in a 10-mL centrifuge tube. The mixture was allowed to stand for 40 min at 4 °C. The supernatant transparent liquid in light red contained neutrophils, a few lymphocytes and erythrocytes. Three portions of the supernatant liquid were put on one portion of lymphocyte separation medium and then were centrifuged for 15 min at 1000 rpm. The supernatant and the middle foggy layer

containing lymphocytes were discarded. The cell mixture at the bottom contained neutrophils and a small amount of erythrocytes. Following washing with 2 mL PBS, the cell mixture was centrifuged for 3 min at 2000 rpm. The supernatant was discarded. Then 2 mL of H_2O was added. After vibrating the solution for ca. 20 s, erythrocytes were lysed. Two milliliters of 1.8% NaCl was immediately added into the cell mixture and the mixture was centrifuged for 3 min at 2000 rpm. The supernatant was discarded again. Following two washing steps, ~10 μL of neutrophil solution could be obtained. Then 1 mL of PBS was added to the neutrophil solution to obtain the neutrophil suspension. The cell suspension was counted using a hemocytometer (Shanghai Medical Optical Instrument Plant, Shanghai, China) under an inverted biological microscope and immediately used to determine PO activity in single cells. To prepare the cell lysate, the cells were subjected to both freeze-thawing and ultrasonication for cytolysis. The neutrophil suspension of 1 mL was centrifuged for 4 min at 2500 rpm. The supernatant was discarded. Then 1 mL of H_2O was added. The suspension was maintained at −20 °C for 30 min in a refrigerator. Then, the suspension was taken out and remained at room temperature for defrosting. Next, the suspension was ultrasonicated for 10 s in an ice bath, following stopping the ultrasonication for 10 s to cool the cells. The ultrasonication process was repeated about 30 times until the cells were lysed. Thus the lysate was obtained and stored at −20 °C.

2.4. Determination of HRP activity in the standard solution and PO activity in the cell lysate

Since the activity of all peroxidases is defined and determined with the same method. Therefore, HRP served as a standard to quantify PO activity and the same activity unit for both HRP and PO was used in this work. Before both HRP activity in the standard solution and PO activity in the neutrophil lysate were detected, the laser was focused on the resorufin solution in a vessel. For that, the vessel containing the resorufin solution was put on the microscope stage. The objective was adjusted to the position, at which the largest average-gray-level (AGL) of image was obtained. The vessel was taken off and rinsed with water. The rest water in the vessel was allowed to evaporate. The HRP solution or cell lysate, ADHP and H_2O_2 (each 2 μL), which were preheated at 25 ± 0.3 °C previously, were added into the vessel, respectively. The solution in the vessel was stirred with a ~0.3 mm-diameter quartz stirring rod for 20 s. A bottle with water of 25 ± 0.3 °C shown in Fig. 1 was put on the vessel to form an air bath to preheat the solution. After the solution was preheated for 30 s, six LIF images were taken by the CCD camera with an interval of 1 min and an exposure time of 100 ms. The laser was turned off at the imaging interval to avoid fluorescence quenching.

2.5. Single-cell analysis

For sampling a single cell, the electromigration technique reported in single-cell analysis by using capillary electrophoresis [15] was used here. The setup of single-cell injection is shown in Fig. 2. A stainless steel tube (1) (0.4 mm i.d., 0.8 mm o.d., 23 mm long) and a copper wire of 0.4 mm diameter (2) as the electromigration anode for electrokinetical injection of a single cell were immobilized on a microscope slide (3) with epoxy. There was a gap of 2 mm between the copper wire and the stainless steel tube. An epoxy ring of ~5 mm diameter (4) was formed on the slide as the container of the cell suspension. The tip of the needle of a 5-mL syringe was cut off partly. A silicon washer (5) was inserted into the fitting sleeve of the syringe needle (6). The syringe was previously drilled a hole with ~5-mm diameter (8) to insert the cathode wire (9). A capillary (25 μm i.d., 375 μm o.d., 60 mm long) (10) previously filled with phosphate buffer of 2.0×10^{-2} mol/L was inserted into the syringe needle through the silicon washer. To see the opening of the injection end of capillary, a ~15-mm section of the polyimide coating at the injection end of capillary was removed by burning before use. The syringe (7) with the capillary was fixed on a laboratory-made *xyz* stage. The capillary in the needle was inserted into the stainless steel tube by means of the *xyz* stage. The phosphate buffer of 2.0×10^{-2} mol/L was added into the syringe from the hole (8). Then, the piston of the syringe was pushed until the buffer in the syringe was over the capillary. After the microscope slide was placed on the inverted biological microscope with a magnification of 400×, a 50-μL aliquot of the neutrophil suspension was placed in the epoxy ring. When a neutrophil drifted toward the injection end under the field of vision of the microscope, an injection voltage of 500 V was applied to transport the cell into the capillary tip. The syringe needle with the capillary containing the injected cell was quickly removed from the syringe and reconnected to another empty syringe. The cell was immediately transferred to the vessel shown in Fig. 1 by pushing the piston of the empty syringe. The cell in the vessel was subjected to both freeze-thawing and ultrasonicating for cytolysis. For that,

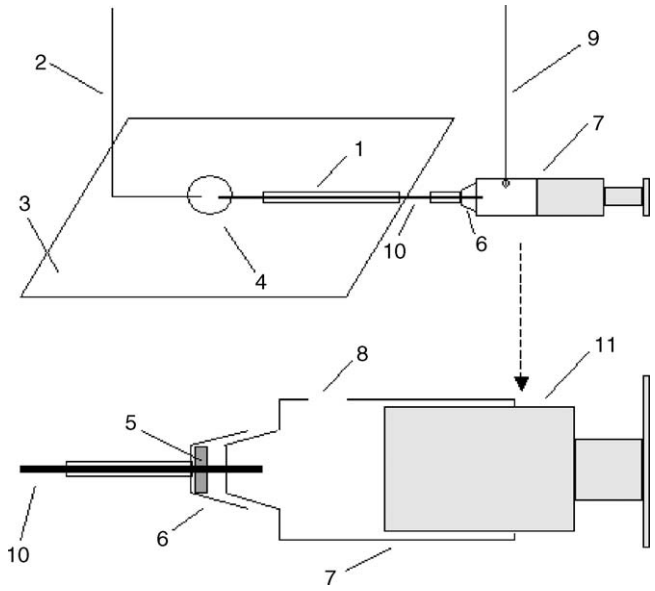

Fig. 2. Schematic diagram of the cell injector: 1, stainless steel tube; 2, copper wire; 3, microscope slide; 4, epoxy ring; 5, silicon washer; 6, syringe needle; 7, syringe body; 8, hole; 9, cathode; 10, capillary; 11, piston of the syringe. Dimension is not in scale.

~0.1 μL of water was added into the vessel with a single cell and the vessel was maintained for 30 min at −20 °C in a refrigerator. The vessel was taken out and kept at room temperature for refreezing. The liquid in the vessel was allowed to evaporate. Then, 2 μL of doubly distilled water was added into the vessel and the vessel was covered with a microscope coverslip to prevent evaporation. The vessel was put in an ice bath placed in an ultrasonicator and ultrasonicated for 5 min to lyse the cell. Thus, the single-cell lysate containing intracellular substances involving PO was obtained. The vessel containing the single-cell lysate was positioned on the microscope stage. Two microliters of H_2O_2 and 2 μL of ADHP were added to the vessel with the final concentration of 1.6×10^{-4} mol/L for the both. The solution was stirred, preheated and the LIF image of the solution was taken according to the procedure for determining PO activity in the cell lysate described above.

2.6. Data analysis

All images were analyzed with MetaMorph software (Molecular Devices Corp. Downington, PA, USA) to measure the AGLs. Corrected AGL was obtained by subtracting the value of the first image, which was corresponding to both the inherent fluorescence from intracellular components and the fluorescence from the product of enzyme-catalyzed reaction. The slope of linear relationship between the corrected AGL and the enzyme concentration, dF/dt, was used for quantification by using the standard calibration method.

3. Result and discussion

3.1. Optimization of detection conditions

The fluorescence intensity was heterogeneous in the images taken by the epi-fluorescence microscopy because of asymmetric irradiation of laser through the objective to the vessel. Therefore, AGL of the whole image was measured. It was found that both fluorescence signal and its relative standard deviation, R.S.D., increased with the laser power for the determination of the resorufin solution. R.S.D. of the fluorescence signal has a minimum value for the laser power in the range of 1.00–1.25 mW. We selected 1.10-mW power in our experiments.

Since both PO and HRP are the peroxidase, they can catalyze the same substrates with the same mechanism and HRP could be used to obtain the optimal conditions for detection of PO activity. pH 7.0 and 25 °C, which were the suitable environment for PO determination [39], were used in our experiments. ADHP can be catalyzed by PO to fluorescent resorufin, following to nonfluorescent complex polymer [40]. However, when ADHP is incubated with an equimolar concentration of H_2O_2, the substrate is quantitatively transformed into resorufin [41]. Fig. 3 shows the relationship between dF/dt and the concentration of ADHP and H_2O_2. The largest value at the concentration of 1.6×10^{-4} mol/L for both was obtained. The values were chosen in our experiments. Since the concentration of fluorescent product increased with the reaction time of the enzyme-catalyzed reaction, AGL of images was dependent on the reaction time.

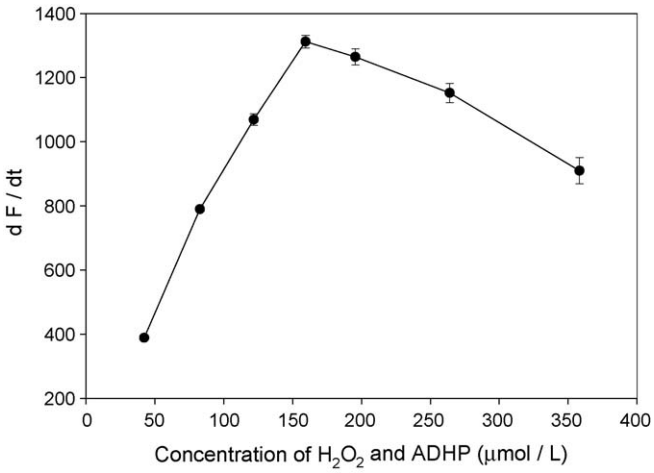

Fig. 3. Relationship between dF/dt and the concentration of substrates. 1.33×10^{-2} mol/L phosphate buffer (pH7.0); 1.5×10^{-4} U/mL HRP; laser power, 1.1 mW; laser wave length, 543 nm; exposure time, 100 ms; readout speed, 5 MHz; intensifier gain, 2375; 10× objective (NA 0.40).

To eliminate the effect of the reaction time from adding enzyme substrates to taking the fluorescent image on AGL of image, the slope of the kinetic curve, dF/dt, corresponding to the reaction rate of the enzyme-catalyzed reaction, was used for quantification. We measured AGL until 10 min. The relationship between AGL and the reaction time was linear. dF/dt was independent on the reaction time within 10 min and proportional to the activity concentration of HRP. Thus, use of dF/dt for quantification of PO activity could enhance the precision and accuracy of the method. To reduce the detection time, 5 min was used in the experiments. Fig. 4 shows the kinetic curves (the plot of AGL versus the reaction time) within 5 min for different HRP activity concentrations.

The linear relationship of the activity concentration covered a range of 7.5×10^{-8}–2.3×10^{-4} U/mL with a correlation coefficient of 0.998. The linear range of the activity calculated according to the solution volume of 6 μL was 4.5×10^{-10}–1.5×10^{-6} U. The dF/dt values obtained for a series of nine measurements of blank resulted in an average value of 1.4 AGL/min and a standard deviation, σ, of 0.2. It could be calculated that the limit of detection, LOD, of the method was 7×10^{-8} U/mL based on the equation LOD = 3σ/S [42], where S was the slop of the calibration curve. LOD of the activity was 4×10^{-10} U according to the volume of 6 μL. The relative standard deviation of the method for a series of 6 measurements of 7.5×10^{-6} U/mL HRP was 3.9%.

3.2. Determination of PO activity in the cell lysate

For determination of PO activity in the cell lysate, the thawed lysate of 1 μL was diluted 200 times and the kinetic curve of the diluted lysate was measured. From the dF/dt values, the mean activity concentrations of PO in three neutrophil lysates obtained by using the standard calibration curve described above were 1.29×10^{-4} U/mL, 1.28×10^{-4} U/mL and 1.24×10^{-4} U/mL, respectively. According to the activity concentrations determined and the cell concentrations of

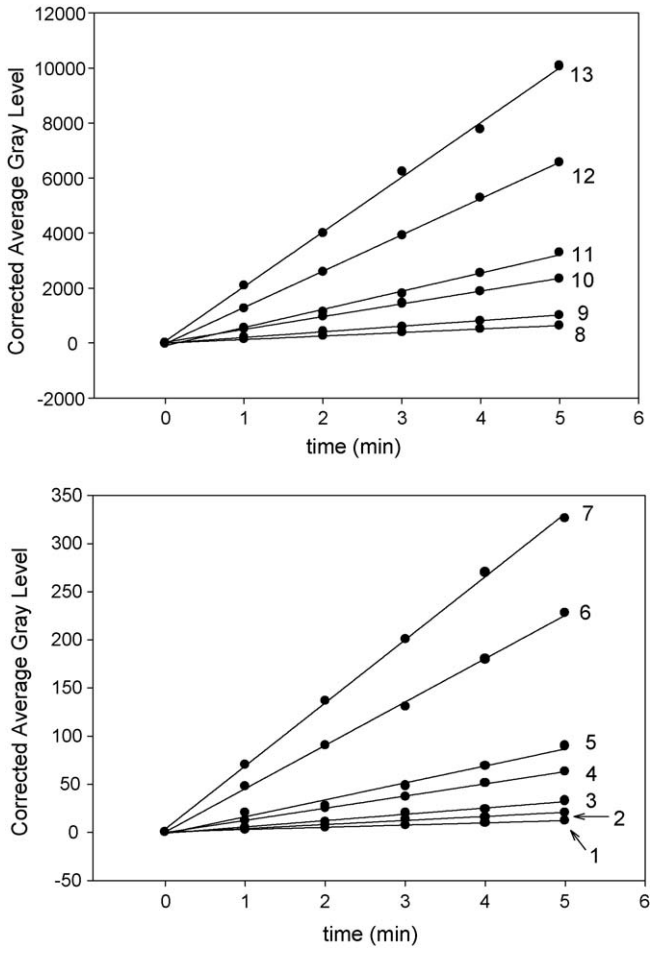

Fig. 4. Relationship between the corrected AGL and the reaction time at different HRP concentrations (10^{-7} U/mL): (1) 0.75; (2) 2.25; (3) 7.50; (4) 15.0; (5) 22.5; (6) 52.5; (7) 75.0; (8) 150; (9) 225; (10) 525; (11) 750; (12) 1500; (13) 2250. 1.6×10^{-4} mol/L H_2O_2; 1.6×10^{-4} mol/L ADHP. Other conditions as in Fig. 3.

4.3×10^3 cells/mL, 2.2×10^3 cells/mL and 1.1×10^3 cells/mL for the three lysates, the calculated mean PO activities in a single neutrophil were 2.7×10^{-8} U, 2.9×10^{-8} U and 3.0×10^{-8} U, respectively, which were within the range of values (0.11–6.4×10^{-8} U) determined in single-cell analysis by using voltammetry [43], implying that the results was reliable. To prove the reliability of the method, a certain amount of standard HRP was added to a lysate and then the lysate was measured. From the detected activity concentration in the lysate with and without the standard HRP, the recovery calculated was between 97 and 104%.

Some metal ions can catalyze the decomposition of H_2O_2 [44,45]. In order to know whether they disturb the determination of PO activity in lysates, following experiments were done: PO in a lysate sample was disabled by heating the sample to 88 °C for 30 s. The lysate was then cooled to room temperature. After the phosphate buffer containing the substrates was added, the sample was detected. The dF/dt value measured was about 1/600 of the signal of PO activity in the lysate. Thus, the disturbance of metal ions could be neglected. It was found that total fluorescence intensity of intracellular substances in the lysate without both phosphate buffer and substrates was constant during measurement, indicating dF/dt = 0. Therefore, intracellular substances did not interfere with the determination of PO activity in lysates.

3.3. Single-cell analysis

After a single cell with PBS was transferred into the vessel, water in the vessel was evaporated quickly. Therefore, water should be added to the vessel before cytolysis. In order to prevent that some chemical reagents such as NaOH, SDS and some organic solvents that often are used to lyse cells may denature PO, the cell transferred in the vessel was lysed by the freeze-thawing and ultrasonicating.

In order to estimate whether metal ions interfere with PO activity determination in single neutrophils, a similar identification used in lysates mentioned above was used. A neutrophil in the vessel was heated to 88 °C for 30 s to disable PO, then, the cell was lysed according to the procedure described in Section 2. After the phosphate buffer containing the substrates was added in the vessel, the sample was detected. It was found that the dF/dt value was near the blank value, implying no disturbance of intracellular metal ions in single-cell analysis. From the dF/dt value, the PO activity in single neutrophils could be calculated by the standard calibration method. The PO activity determined in nine neutrophils was between 8.0×10^{-9}–8.5×10^{-8} U. The corresponding value in the lysate (3.0×10^{-8} U) was within the range of values found in the present single-cell analysis.

4. Conclusions

A simple and sensitive epi-fluorescence microscopy for single-cell analysis of intracellular PO was developed on the basis of the enzyme-catalyzed reaction with ADHP and H_2O_2 as the substrates. LOD of the method is as low as 7×10^{-8} U/mL. When the slope of the kinetic curve corresponding to the reaction rate of the enzyme-catalyzed reaction was used for quantification, the time effect from adding enzyme substrates to taking the fluorescent image and the fluorescence from intracellular compounds can be eliminated, implying that the results were reasonable.

Acknowledgment

This project was supported by the National Natural Science Foundation of China (No. 20235010).

References

[1] E.S. Yeung, J. Chromatogr. A 830 (1999) 243.
[2] L.A. Woods, T.P. Roddy, A.G. Ewing, Electrophoresis 25 (2004) 1181.
[3] S.M. Buck, H. Xu, M. Brasuel, M.A. Philbert, R. Kopelman, Talanta 63 (2004) 41.
[4] O.H. Lowry, Science 116 (1952) 526.
[5] O.H. Lowry, N.R. Roberts, M.L. Chang, J. Biol. Chem. 222 (1956) 97.
[6] H.E. Hirsch, J. Histochem. Cytochem. 18 (1970) 268.
[7] J.F. Jongkind, J.S. Ploem, A.J. Reuser, H. Galjaard, Histochemistry 40 (1974) 221.
[8] K.D. Wittrup, J.E. Bailey, Cytometry 9 (1988) 394.

[9] Q. Xue, E.S. Yeung, Anal. Chem. 66 (1994) 1175.
[10] Q. Xue, E.S. Yeung, J. Chromatogr. B: Biomed. Appl. 677 (1996) 233.
[11] G.D. Meredith, C.E. Sims, J.S. Soughayer, N.L. Allbritton, Nat. Biotechnol. 18 (2000) 309.
[12] A. Zarrine-Afsar, S.N. Krylov, Anal. Chem. 75 (2003) 3720.
[13] H. Li, C.E. Sims, M. Kaluzova, E.J. Stanbridge, N.L. Allbritton, Biochemistry 43 (2004) 1599.
[14] G.K. Shoemaker, J. Lorieau, L.H. Lau, C.S. Gillmor, M.M. Palcic, Anal. Chem. 77 (2005) 3132.
[15] X. Sun, W. Jin, Anal. Chem. 75 (2003) 6050.
[16] X. Sun, W. Jin, D. Li, Z. Bai, Electrophoresis 25 (2004) 1860.
[17] Z. Rosenzweig, E.S. Yeung, Anal. Chem. 66 (1994) 1771.
[18] W. Tan, E.S. Yeung, Anal. Biochem. 226 (1995) 74.
[19] K. Nolkrantz, C. Farre, K.J. Hurtig, P. Rylander, O. Orwar, Anal. Chem. 74 (2002) 4300.
[20] P.M. Kasili, J.M. Song, T. Vo-Dinh, J. Am. Chem. Soc. 126 (2004) 2799.
[21] S. Hasegawa, J.W. Choi, J. Rao, J. Am. Chem. Soc. 126 (2004) 7158.
[22] N. Gunasekera, S.W. Lee, S. Kim, K. Musier-Forsyth, E. Arriaga, Anal. Chem. 76 (2004) 4741.
[23] H.v. Manen, Y.M. Kraan, D. Roos, J. Phys. Chem. B 108 (2004) 18762.
[24] C.C. Winterbourn, M.C. Vissers, A.J. Kettle, Curr. Opin. Hematol. 7 (2000) 53.
[25] M. Allegra, P.G. Furtmuller, G. Regelsberger, M.L. Turco-Liveri, L. Tesoriere, M. Perretti, M.A. Livrea, C. Obinger, Biochem. Biophys. Res. Commun. 282 (2001) 380.
[26] S.W. Edwards, M.B. Hallett, Immunol. Today 18 (1997) 320.
[27] F. Chabot, J.A. Mitchell, J.M. Gutteridge, T.W. Evans, Eur. Respir. J. 11 (1998) 745.
[28] S.J. London, T.A. Lehman, J.A. Taylor, Cancer Res. 57 (1997) 5001.
[29] W.F. Reynolds, E. Chang, D. Douer, E.D. Ball, V. Kanda, Blood 90 (1997) 2730.
[30] A.J. Kettle, C.C. Winterbourn, Biochemistry 40 (2001) 10204.
[31] P. Fanjul-Bolado, M.B. González-García, A. Costa-García, Talanta 64 (2004) 452.
[32] E. Salinas, A.A.J. Torriero, M.I. Sanz, F. Battaglini, J. Raba, Talanta 66 (2005) 92.
[33] R. Koncki, B. Rozum, S. Głąb, Talanta 68 (2006) 1020.
[34] Y. Andreu, J. Castillo, S. de Marcos, J. Galbán, Talanta 64 (2004) 196.
[35] I. Sanz-Vicente, J.R. Castillo, J. Galbán, Talanta 65 (2005) 946.
[36] T. Tsukatani, K. Matsumoto, Talanta 65 (2005) 396.
[37] B. Tang, L. Zhang, K. Xu, Talanta 68 (2006) 876.
[38] W. Jin, L. Jiang, Electrophoresis 23 (2002) 2471.
[39] B. Stellmach, Bestimmungsmethoden Enzyme (für Phamazie, Lebensmittel -chenie, Technik, Biochemie, Biologie, Medizin), Steinkopff Verlag, Darmatadt, 1988 (Chapter 26).
[40] International Union of Biochemistry, Enzyme Nomenclature: Recommendations 1964 of the International Union of Biochemistry, Elsevier, Amsterdam, 1965 (Chapter 4).
[41] M. Zhou, Z. Diwu, N. Panchuk-Voloshina, R.P. Haugland, Anal. Biochem. 253 (1997) 162.
[42] F.H. Hernandez, J.M. Escriche, Analyst 109 (1984) 1585.
[43] N. Gao, M. Zhao, X. Zhang, W. Jin, Anal. Chem. 78 (2006) 231.
[44] K. Saitoh, T. Hasebe, N. Teshima, M. Kurihara, T. Kawashima, Anal. Chim. Acta 376 (1998) 247.
[45] S.R. Paik, H.J. Shin, J.H. Lee, Arch. Biochem. Biophys. 378 (2000) 269.

Available online at www.sciencedirect.com
ScienceDirect
Talanta 70 (2006) 257–266
Talanta
www.elsevier.com/locate/talanta

Simultaneous preconcentration of uranium(VI) and thorium(IV) from aqueous solutions using a chelating calix[4]arene anchored chloromethylated polystyrene solid phase

V.K. Jain *, R.A. Pandya, S.G. Pillai, P.S. Shrivastav

Chemistry Department, School of Sciences, Gujarat University, Ahmedabad 380009, India

Received 7 November 2005; received in revised form 12 February 2006; accepted 12 February 2006
Available online 30 March 2006

Abstract

A new chelating polymeric sorbent is developed using Merrifield chloromethylated resin anchored with calix[4]arene-*o*-vanillinsemicarbazone for simultaneous separation and solid phase extractive preconcentration of U(VI) and Th(IV). The "upper-rim" functionalized calix[4]arene-*o*-vanillinsemicarbazone was covalently linked to Merrifield resin and characterized by FT-IR and elemental analysis. The synthesized chelating polymeric sorbent shows superior binding affinity towards U(VI) and Th(IV) under selective pH conditions. Various physico-chemical parameters that influence the quantitative extraction of metal ions were optimized. The optimum pH range and flow rates for U(VI) and Th(IV) were 6.0–7.0 and 1.0–4.0 ml min^{-1} and 3.5–4.5 and 1.5–4.0 ml min^{-1}, respectively. The total sorption capacity found for U(VI) and Th(IV) was 48734 and 41175 μg g^{-1}, respectively. Interference studies carried out in the presence of diverse ions and electrolyte species showed quantitative analyte recovery (98–98.5%) with lower limits of detection, 6.14 and 4.29 μg l^{-1} and high preconcentration factors, 143 and 153 for U(VI) and Th(IV), respectively. The uptake and stripping of these metal ions on the resin were fast, indicating a better accessibility of the metal ions towards the chelating sites. The analytical applicability of the synthesized polymeric sorbent was tested with some synthetic mixtures for the separation of U(VI) and Th(IV) from each other and also from La(III), Cu(II) and Pb(II) by varying the pH and sequential acidic elution. The validity of the proposed method was checked by analyzing these metal ions in natural water samples, monazite sand and standard geological materials.

Keywords: Merrifield chloromethylated resin; Solid phase extraction; GFAAS; ICPAES; Preconcentration; Calix[4]arene-*o*-vanillinsemicarbazone

1. Introduction

Uranium and thorium find extensive application as nuclear fuel in power plants and their main sources are pitchblende, monazite sand and sea water. Their selective extraction simultaneously in presence of each other and closely associated metal ions has drawn much attention of the chemists world over because of their importance in energy related applications [1]. The separation of these economically important metal ions is also a matter of concern as the nuclear waste coming out of reactors cause serious and irreversible environmental and biological damage [2]. Both the metal ions are known to cause acute toxicological effects in mammals and their compounds are potential occupational carcinogens [3]. Thus, there remains a need of preorganized complexing agents that discriminates U(VI) and Th(IV) from associated metal ions present in great excess in solid or aqueous media. The procedures described in the recent literature, for the separation and trace determination of U(VI) and Th(IV) are either less sensitive or time consuming due to high matrix concentration [4–13]. So far, modest work has been done towards simultaneous separation and solid phase extractive preconcentration of U(VI) and Th(IV). The reagents available for the separation and trace determination of these metal ions are either less specific as a number of diverse ions interfere during their determination or it may require further purification by ion exchange chromatography [14–20]. A separation and preconcentration is therefore mandatory ahead of their determination by highly versatile techniques like GFAAS and ICPAES. Solid phase extraction technique has

* Corresponding author.
E-mail addresses: drvkjain@hotmail.com (V.K. Jain), rapandya@hotmail.com (R.A. Pandya).

0039-9140/$ – see front matter © 2006 Elsevier B.V. All rights reserved.
doi:10.1016/j.talanta.2006.02.032

been widely used in the preconcentration/separation of trace and ultra trace amounts of inorganic and organic species, to enhance sensitivity and to separate analytical matrix [21–24]. Chelating resins are being frequently used for solid phase extraction in selective trace metal analysis. Suitable chelating agents can be chemically bonded to or impregnated onto a polymeric matrix as supports for the solid phase extraction of metal ions from aqueous solution. For solid phase extraction of these metal ions, polymeric calixarenes can play a dominant role [25–35]. Polymer supported calixarenes offer a suitable platform for their simultaneous separation and preconcentration due to their flexible operating condition, ease of synthesis, insoluble character, cost-effectiveness, lower toxicity, good stability and reusability. They also serve as eco friendly materials in contrast to the liquid–liquid extraction procedure, which results in huge environmental problem due to toxic organic diluents.

The preparation of insoluble resins by appending functionalized calixarenes to the commercially available polymeric support is relatively easy compared to polymerizing functionalized calixarene monomers. The chemistry of calixarenes, polymer supported calixarenes and their ability to complex cations have been well documented by many authors [36–44]. Shinkai et al. [45] have reported a polymer bound calix[6]arene, prepared by reacting *p*-(chlorosulphonyl)calix[6]arene with poly(ethylene-imine) and used the polymer for selective adsorption of UO_2^{2+}. Yilmaz and co-workers [46] have synthesized polymeric resins via nucleophilic substitution reactions involving 5,11,17,23-tetrakis[(propylthio)methyl]-25,26,27,28-tetrahydroxycalix[4]arene and 5,11,17,23-tetrakis[(methylthio)methyl]-25,26,27,28-tetrahydroxycalix[4]arene as precursors with Merrifield's resin. These calix[4]arene based polymeric resins have high extraction ability towards metal cations. Separation of uranium from aqueous solution by liquid–liquid extraction as well as solid phase extraction was carried out by Berhard and co-workers [47] using calix[6]arene anchored on polyester nonwoven fabric via impregnation and subsequent vitrification. As oxygen bearing *o*-vanillinsemicarbazone can act as a very good complexing agent for trace metal ions [48], it was thought to incorporate this functionality on the calix[4]arene scaffold supported by a water insoluble polymer matrix. In this article the synthesis of Merrifield resin supported calix[4]arene-*o*-vanillinsemicarbazone and its application to the separation and solid phase extractive preconcentration of U(VI) and Th(IV) in river and ground water samples, monazite sand and some standard geological materials has been reported.

2. Experimental

2.1. Apparatus

Precoated silica gel plates (Merck 60 F_{254}) were used for the analytical TLC. A Systronics digital pH meter Model 335 was used for the pH measurements. Flow rate in the column was adjusted with a Miclins peristaltic pump PP-10. Spectral measurements were done on a Hitachi 3210 UV–vis spectrophotometer using 10 mm quartz cells. FT-IR spectra were recorded on a Jasco infrared spectrophotometer as KBr pellets. Elemental analysis was done on Heraeus Carlo Erba 1108 elemental analyzer. The ^{1}H NMR spectra were recorded on Bruker operating at 100 MHz for proton in DMSO–d_6 with TMS as the internal standard. Atomic absorption measurements were performed on Perkin-Elmer model 420 atomic absorption spectrophotometer (AAS) pyrolytically coated HGA-76 graphite furnace (GF). A uranium hollow cathode lamp was used at 358.5 nm wavelength with a spectral width of 0.2 nm for U(VI) determination. The atomization temperature of 2700 °C and argon gas purge was used. Labtam plasma scan 710 sequential inductively coupled plasma atomic emission spectrometer (ICPAES) with plasma scan multitasking computer and peristaltic pump was used for Th(IV) determination under optimum working conditions: radio frequency (rf) 27.12 MHz; incident power 2000 W; Labtam GMK nebulizer; rf power 5 W; observation height 14 mm; argon coolant flow rate 10 dm^3 min^{-1}; argon carrier flow rate 1 dm^3 min^{-1}; intergraph period 10 s; resolution 0.004 nm; peristaltic pump flow rate 1 ml min^{-1}; wavelength-Th(IV) 283.73 nm.

2.2. Reagents

All chemicals used in this work were of analytical grade of Merck or Lancaster (Chennai, India). Commercially available Merrifield peptide resin [chloromethylated polystyrene divinylbenzene co-polymer or CMPDB] (1% cross-linked, 1.5 mmol equivalent of Cl/g of resin, 200–400 mesh, $C_{25}H_{25}Cl$, FW 360.92) was procured from Aldrich. All aqueous solutions were prepared with quartz distilled deionized water, which was further purified by a Millipore Milli-Q water purification system (Bangalore, India). Standard stock solutions (2000 μg ml^{-1}) of U(VI) and Th(IV) were prepared by dissolving the requisite amounts of uranyl nitrate hexahydrate and thorium nitrate tetrahydrate, respectively, in quartz distilled deionized water containing small amounts of HNO_3. Their final concentrations were standardized spectrophotometrically [49]. The adjustments of pH between 2.5 and 5.8 were made with the help of potassium hydrogen phthalate and sodium hydroxide standard buffers as described elsewhere [50] and from pH 6.0 to 7.5 with some commercially available standard buffer solutions. The glassware used were soaked in 10% HNO_3 overnight before use and cleaned repeatedly with double distilled deionized water.

2.3. Synthesis (Fig. 1)

Synthesis of 5,11,17,23-tetratert-butyl-25,26,27,28-tetrahydroxycalix[4]arene **1** and 25,26,27,28-tetrahydroxycalix[4]arene **2** were carried out as reported in literature [51,52]. 26,28-Dimethoxy-25,27-dihydroxycalix[4]arene **3** and 11,23-dinitro-26,28-di methoxy-25,27-dihydroxycalix[4]arene **4** were synthesized as reported by Arduini and co-workers [53]. Products **5**–**7** were prepared by our method reported earlier [54].

2.3.1. Synthesis of resin *8* by loading of *7* on CMPDB

A mixture containing 10 g **7** (10.8 mmol), 10 g K_2CO_3 (72 mmol) and 10 g of CMPDB in 150 ml of dimethylformamide:tetrahydrofuran = 2:1 was heated at 75 °C temperature

for 8 h under N_2 gas atmosphere. Thereafter the polymeric beads of resin **8** were separated through porous filter at pump. Repeated washing with the solvents dimethylformamide and tetrahydrofuran followed by water were carried out to ensure complete removal of unreacted **7** and the weight of the dried resin **8** was found to be 12.2 g. The amount of **7** loaded on CMPDB was evaluated by difference of mass taken before and after coupling for the dried resin and was found to be 22%:

$$\text{percentage of } \mathbf{7} \text{ hooked on CMPDB} = \frac{W_2 - W_1}{W_1} \times 100\%$$

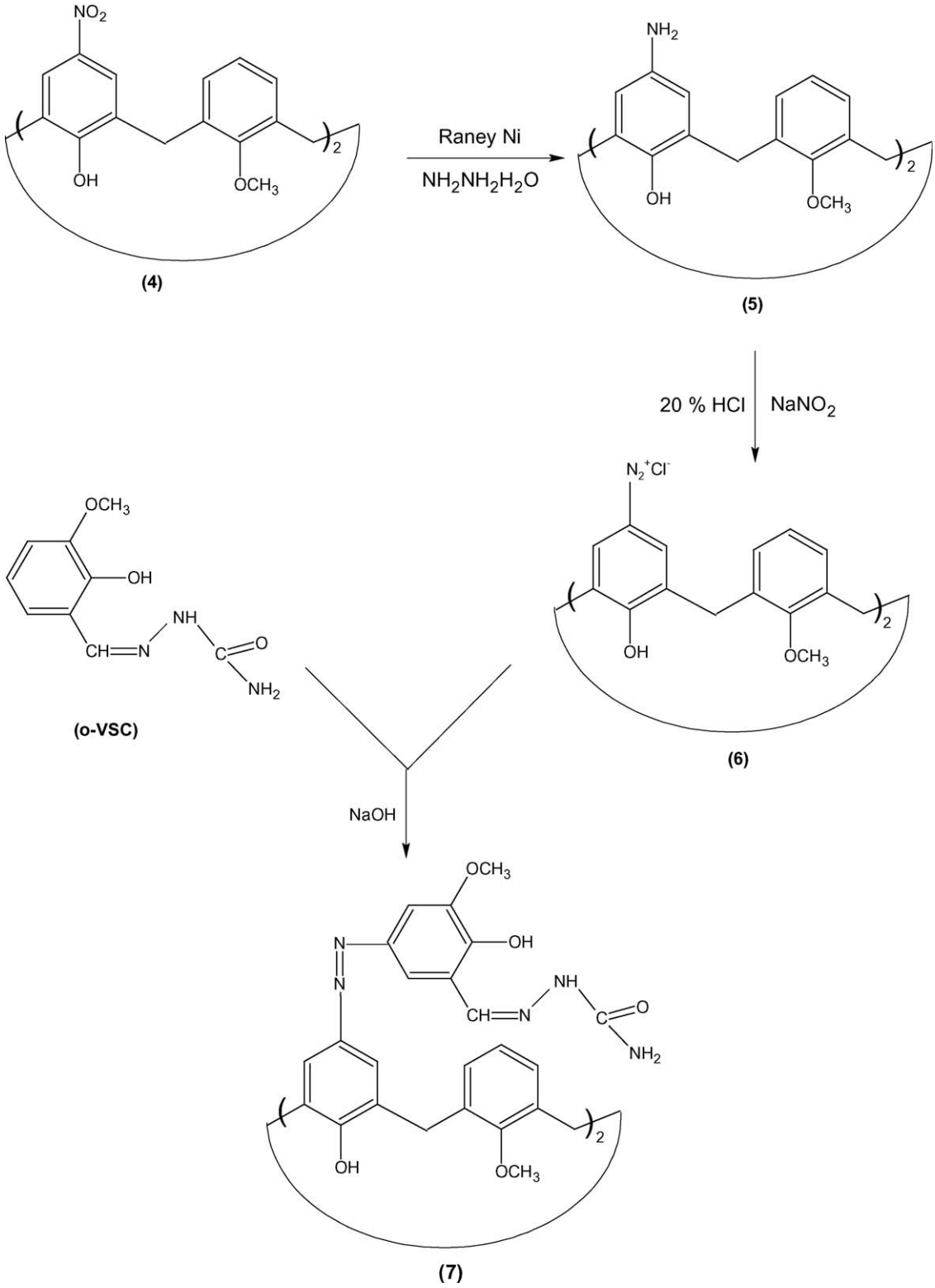

Fig. 1. Reaction flowchart.

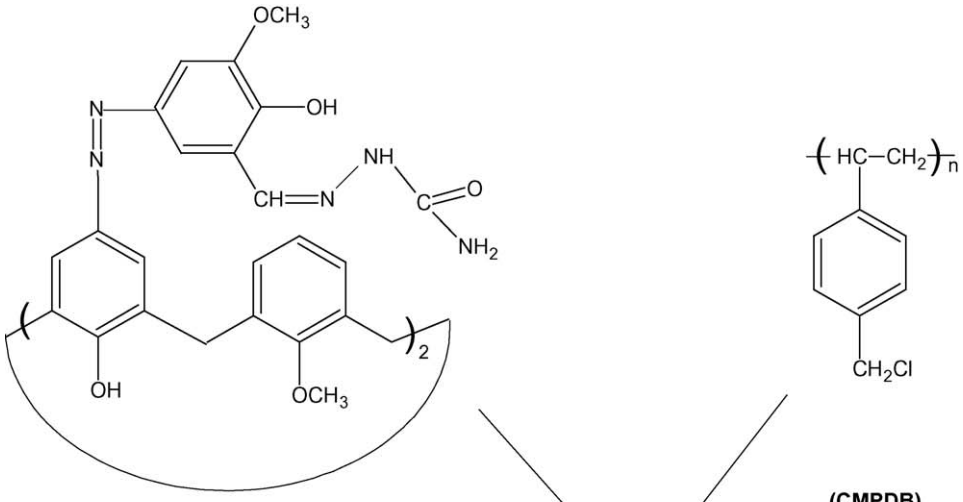

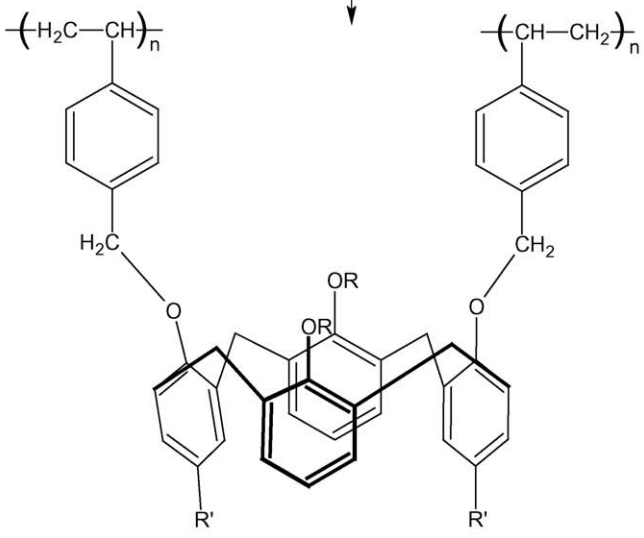

(8)

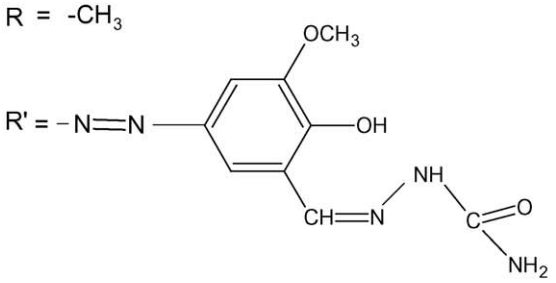

(8) : CMPDB supported calix[4]arene-o-vanillinsemicarbazone

Fig. 1. (*Continued*).

where W_1 is the weight of dried CMPDB and W_2 is the weight of dried resin **8**.

The elemental analysis of nitrogen in resin **8** was found to be 2.73%, which further confirmed the amount of loading to be 22–23%. This result shows that only 0.4 mmol, i.e. 26% of the total available Cl (1.5 mmol/g of CMPDB) reacted with 0.195 mmol of ligand **7**.

2.4. Procedure for column concentration and determination of U(VI) and Th(IV)

A glass column (200 mm × 8.0 mm) was prepared by adding the slurry of the beads of mesh size (200–400) having 1 g resin **8** in CH_3OH:H_2O (1:1). The height of the column section containing resin (bed height) was 15 mm. It was conditioned with different buffer solutions for the samples containing U(VI) and Th(IV) prior to their elution from the column. Suitable aliquot of the solution containing 0.1–15.0 μg ml^{-1} U(VI) and 0.02–3.4 μg ml^{-1} Th(IV) was passed through the column after adjusting the appropriate pH at an optimum flow rate. The stripping of the metals from resin was carried out by suitable eluting agents like HCl or HNO_3. The preconcentrated metal ions in the eluants were collected in a 25 ml volumetric flask, made to volume by double distilled water and determined spectrophotometrically and also compared by GFAAS and ICPAES (Table 1).

3. Results and discussion

3.1. Spectral interpretation of synthesized compounds

FT-IR and ^{1}H NMR spectra of compounds **1**–**4** were in good agreement with the reported values. The reduction of **4** to yield corresponding **5** is done with Raney Ni (W-2) and hydrazine hydrate. In **5**, the IR band at 3435 cm^{-1} due to N–H stretching and absence of any peak due to N–O showed complete reduction of **4**. The IR band at 3276 and 3469 cm^{-1} represented the phenolic –OH stretching at the 'lower rim' of calix[4]arene and *o*-VSC, respectively, in **7**. In **8**, disappearance of the band at 3276 cm^{-1} suggested the binding of calix[4]arene to CMPDB through the 'lower rim'. A sharp IR peak at 1593 cm^{-1} in **7** and **8** indicated the presence of CH=N stretching. In ^{1}H NMR spectra of **7**, the peak at 10.2 ppm corresponded to the phenolic –OH groups.

3.2. Parameters optimized for separation and preconcentration of U(VI) and Th(IV)

3.2.1. Effect of pH

A glass column was packed with 1 g resin **8**. One hundred milliliter solutions containing 15 μg ml^{-1} U(VI) and 3 μg ml^{-1} Th(IV), respectively, were passed through the column at their optimum flow rate by varying pH. The percentage of metal sorption was measured by desorbing resin with suitable eluting agents and then determined by spectrophotometry, GFAAS and/or ICPAES. The pH studies revealed selective sorption of Th(IV) and U(VI) in the column. The optimum pH for U(VI) and Th(IV) were found to be 6.0–7.0 and 3.5–4.5, respectively (Table 1). Their selectivity in pH of sorption suggests the possibility of separation of these metal ions in presence of each other in the column.

3.2.2. Effect of flow rate

The effect of flow rate on the extent of metal ion sorbed on the resin was studied in the column packed with 1 g resin **8** at 30 °C. Feed solutions containing 15 μg ml^{-1} U(VI) and 3 μg ml^{-1} Th(IV) were passed at different flow rates (0.5 ml min^{-1}, 1.0 ml min^{-1}, 1.5 ml min^{-1}, 2.0 ml min^{-1}, etc.) maintained by peristaltic pump at their optimum pH. The flow rate of the liquid during separation should be such that the working conditions are close to the equilibrium state as the flow rate depends upon the particle size and the temperature. Optimum flow rate may be defined as the rate of flow of the effluent through the

Table 1
Parameters optimized for sorption and desorption of U(VI) and Th(IV) on the resin

No.	Parameters	Metal ions	
		U(VI)	Th(IV)
1	pH range	6.0–7.0	3.5–4.5
2	Optimum range of flow rate (ml min^{-1})	1.0–4.0	1.5–4.0
3	Concentration of acid for desorption	0.25N HCl	2.0N HCl or 0.1N HNO3
4	Total sorption capacity (mg g^{-1} of resin)	48734	41175
5	Distribution coefficient (K_d)	3150	3995
6	Preconcentration factor (PF)	143	153
7	Breakthrough capacity (mg g^{-1} of resin)	9502	7618
8	R.S.D. (%)[a]	1.7	1.5
9	Metal sorbed (%)[a]	99.5	99.7
10	Average recovery (%)[a]	98	98.5
11	$t_{1/2}$ for exchange (min)	6.5	5
12	Linear range (μg ml^{-1})	0.1–15.0	0.02–3.4
13	Regression equation	$A = C \times 0.0997 - 0.0002$	$A = C \times 0.4959 - 0.0007$
14	Correlation coefficient	1.0000	0.9998
15	LOD (μg l^{-1})	6.14	4.29
16	LOQ (μg l^{-1})	20.48	14.32

[a] Ten determinations.

column at which more than 98% sorption takes place. The optimum flow rates obtained were between 1.0–4.0 ml min^{-1} and 1.5–4.0 ml min^{-1} for U(VI) and Th(IV), respectively (Table 1). An increase in flow rate resulted in decrease in sorption due to insufficient contact time between the resin and the metal ion solution.

3.2.3. Effect of concentration of eluting agents

The effect of eluants like HCl and HNO_3 was studied by taking their different normal concentrations. One gram of resin **8** in the column was conditioned at pH of maximum sorption and then fed with 100 ml solutions containing 15 μg ml^{-1} U(VI) and 3 μg ml^{-1} Th(IV), respectively. The metal ions were desorbed with different eluting agents and then determined by spectrophotometry, GFAAS and/or ICPAES. It was observed that quantitative elution was possible with 7 ml 0.25N HCl and 6.5 ml 2.0N HCl or 0.1N HNO_3 for U(VI) and Th(IV), respectively (Table 1).

3.2.4. Total sorption capacity

The total sorption capacity studies were carried out using the batch technique for U(VI) and Th(IV). One gram of resin **8** was equilibrated with 500 ml solution containing 100 μg ml^{-1} metal ions at their optimum pH for 2 h at 30 °C. The amount of metal ions sorbed on the resin was calculated from the difference in the metal ion concentration in the solution before and after sorption. The total sorption capacities of the resin were found to be 48,734 and 41,175 μg g^{-1} for U(VI) and Th(IV), respectively (Table 1).

3.2.5. Distribution coefficient K_d

Exchange equilibria are very often expressed in terms of the distribution coefficient. This quantity is given by the ratio of the equilibrium concentrations of the same metal ion in the resin phase and in the solution. The distribution coefficient K_d of the metal ions between the resin and aqueous phase was determined by batch experiment. One gram of resin **8** was equilibrated with 25 ml solution containing not more than 1950 and 1647 μg ml^{-1} for U(VI) and Th(IV), respectively, for 2 h at 30 °C. The solution was filtered to remove the resin and the filtrate was subjected to spectrophotometric, GFAAS and/or ICPAES determination of the metal ion content. The concentration of the sorbed metal ion was similarly measured by desorbing with suitable eluting agent. K_d for U(VI), Th(IV) were found to be 19,248 and 23,296 ml/g, respectively (Table 1). The distribution coefficient K_d or efficiency of the resin was measured using the equation:

$$K_d = \frac{\text{amount of the metal ion taken up by the resin}}{\text{amount of the metal ion remaining in the solution}} \times \frac{\text{volume of the solution}}{\text{amount of resin taken}}$$

The plots of log K_d against pH (Fig. 2) were straight lines with the slopes close to unity, slopes for U(VI) and Th(IV) were 0.85 and 1.08, respectively, indicating 1:1 stoichiometry between the metal ions and resin [55].

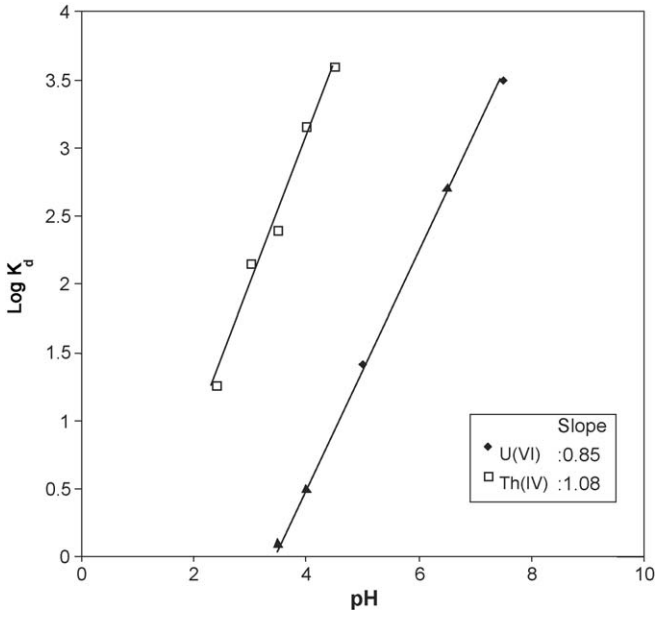

Fig. 2. Plot of log K_d against pH for sorption of U(VI) and Th(IV) on the resin. Amount of resin: 1 g; volume of the solution: 25 ml; U(VI): 1950 μg ml^{-1}; Th(IV): 1647 μg ml^{-1}

3.2.6. Exchange kinetics

The batch experiments were carried out to determine the rate of loading of U(VI) and Th(IV) on the resin: 1 g resin **8** was stirred with 100 ml feed solution containing 488 and 412 μg ml^{-1} for U(VI) and Th(IV), respectively, at their optimum pH at 30 °C. Five milliliters of the feed solution was withdrawn at predetermined intervals and analyzed. The concentration of metal ion in aqueous phase was determined by spectrophotometry, GFAAS and/or ICPAES. The amount of metal ion loaded on the resin phase was calculated by measuring the concentration of metal ion in the feed solution. The time taken for the sorption of 50% of the metal ions ($t_{1/2}$) was found to be 6.5 and 5.0 min for U(VI) and Th(IV), respectively (Table 1, Fig. 3),which indicates very good accessibility of these metal ions towards chelating sites.

3.2.7. Breakthrough studies

Breakthrough capacities are more significant and useful than total sorption capacities in ion exchange chromatographic applications as it gives actual working capacity of the resin in the column. Breakthrough capacity or the effective capacity may be defined as the capacity at the moment when the adsorbed component has appeared in the effluent with an increased concentration. It is one of the most critical parameters when working under dynamic condition. Breakthrough studies were carried out by taking 1 g resin **8** in the column having 200 mm length and 8.0 mm internal diameter with the bed height of 15 mm and passing 10 μg ml^{-1} of metal ions [U(VI), Th(IV)] at their optimum pH and flow rate. An aliquot of 2.0 ml eluant was collected each time and analyzed by spectrophotometry, GFAAS and/or ICPAES for the metal ion content. Breakthrough capacities of the resin for U(VI) and Th(IV) were found to be 9502 and 7618 μg g^{-1}, respectively (Table 1). Both the curves were

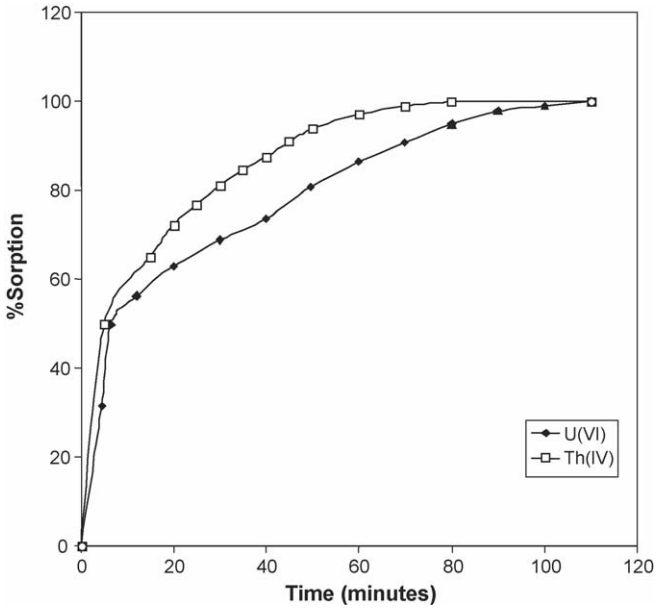

Fig. 3. Exchange kinetics of U(VI) and Th(IV) on the resin. Amount of resin: 1 g; volume of the solution: 100 ml; U(VI): 488 μg ml^{-1}, pH 6.5; Th(IV): 412 μg ml^{-1}, pH 4.0

steep at their breakthrough points at different times, indicating the possibility of separating these metal ions from their mixtures (Fig. 4).

3.2.8. Preconcentration of U(VI) and Th(IV)

The concentration of trace elements in natural water is too low for their direct determination. Therefore, preconcentration or enrichment step is unavoidable even with a sensitive detection method. The resin was studied for column concentration of U(VI), Th(IV) in terms of their preconcentration factor (PF):

$$\mathrm{PF} = \frac{\text{concentration of metal in stripping solution}}{\text{initial concentration of metal in feed solution}}$$

One thousand milliliter solutions containing 20 μg l^{-1} each of U(VI) and Th(IV) at pH 6.5 and 4.0, respectively, were passed through the column containing 1 g resin **8**. The preconcentrating ability of resin was assessed from the elution profile of metal ions by plotting the concentration of effluents as a function of the volume of stripping solutions: 7.0 ml, 0.25N HCl for U(VI); 6.5 ml, 2.0N HCl for Th(IV). The preconcentration factors were found to be 143 and 153 for U(VI) and Th(IV), respectively, with >98% recovery (Table 1).

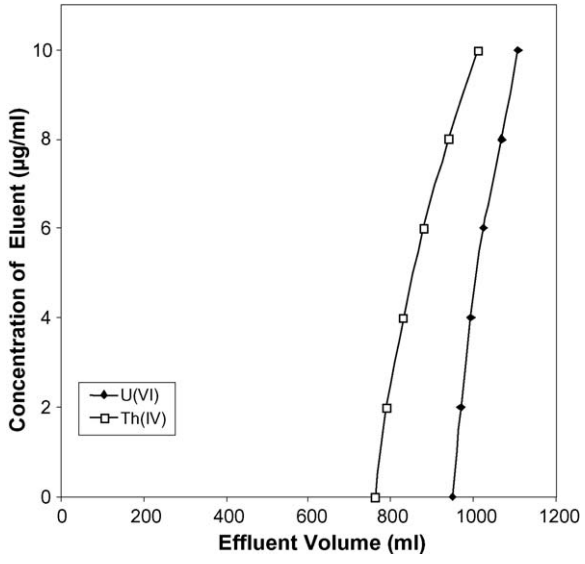

Fig. 4. Breakthrough curves for U(VI) and Th(IV) on the resin. Amount of resin in the column: 1 g; concentration of the solution passed: 10 μg ml^{-1}; U(VI): pH 6.5; Th(IV): pH 4.0

3.2.9. Resin stability tests

The stability of resin **8** was tested to evaluate its sustainability for repeated cycles of sorption and desorption with different mineral acids. It was observed that there was no detectable change in the physical and chemical properties of the resin in concentrated acidic solutions of 5.0N HCl, 3.0N HNO_3 and 3.5N H_2SO_4. To check the regenerating capacity of resin, it was subjected to repeated sorption and desorption of U(VI) and Th(IV) at their optimum conditions in the column. One gram of resin was taken in the column and 500 ml solution containing 100 μg ml^{-1} metal ions was passed through it at 30 °C. Resin was then stripped off metal ions with 25 ml of suitable eluant. Resin showed very good stability up to 20 repeated cycles of sorption and desorption, after which it showed 2–3% decrease in efficiency, which may be due to hydrolysis of resin when treated with mineral acids.

3.2.10. Effect of electrolytes and associated cations

The limit of tolerance of anions and cations on the sorption of U(VI) and Th(IV) is defined as that which causes an error of 2–3% in the recovery of these metal ions. The effect of commonly associated cations in natural water samples such as Fe(II), Fe(III), Co(II), Ni(II), Mn(II), alkali [Li(I), Na(I), K(I), Rb(I), Cs(I)] and alkaline earth [Mg(II), Ca(II), Sr(II) and Ba(II)] had been studied under optimum conditions of metal ion sorption. Mn(II) did not affect the sorption of U(VI) and Th(IV) up to 4 mg, however, for other cations the tolerance limits were much higher (Table 2). The effect of anions and their limit of tolerance on the sorption of U(VI) and Th(IV) by resin was studied by taking different concentrations of some electrolytes like NaCl, NaF, NaBr, $NaNO_2$, $NaNO_3$, Na_2SO_4, Na_3PO_4 and CH_3COONa. The results in Table 2 showed that except Na_3PO_4, all other electrolytes did not interfere between 0.2 and 0.3 M concentration range, which further augments the potential application of resin for the analysis of real samples.

3.3. Separation U(VI) and Th(IV) in the presence of La(III) Cu(II) and Pb(II)

The synthesized chelating resin was used for separating U(VI) and Th(IV) from their binary and ternary mixtures in the presence of Cu(II), Pb(II) and La(III) due to favorable kinetics and high breakthrough capacities in the column. Hence, the

Table 2
Tolerance limits of commonly associated cations and anions in water samples on the sorption of U(VI) and Th(IV) on the resin

Metal ions (100 mg each)	Interfering cations (mg)						
	Fe(II) added as $FeSO_4{\cdot}7H_2O$	Fe(III) added as $Fe(NO_3)_3{\cdot}7H2O$	Co(II) added as $Co(NO_3)_2{\cdot}7H2O$	Ni(II) added as $Ni(NO_3)_2{\cdot}6H2O$	Mn(II) added as $Mn(NO_3)_2{\cdot}6H_2O$	Alkali metal ions[a] added as nitrate salts	Alkaline earth metal ions[a] added as nitrate salts
U(VI)	12	7	10	14	8	–	–
Th(II)	8	9	13	12	4	–	–

Metal ions (2.5 μg ml^{-1})	Concentration of electrolytes (anions) (mol l^{-1})							
	NaF	NaCl	NaBr	$NaNO_2$	$NaNO_3$	Na_2SO_4	Na_3PO_4	CH_3COONa
U(VI)	1.2	1.9	1.1	2.5	2.1	1.3	0.3	1.5
Th(IV)	1.4	2	1.5	3.2	3.1	1.2	0.2	2

Experimental condition: resin, 1 g; volume of solution passed, 100 ml; U(VI), pH 6.5; Th(IV), pH 4.0.
[a] Did not interfere.

following mixtures (each 100 μg in 25 ml of buffer solution) were passed through the column at pH of maximum sorption and optimum flow rate. The separation was carried out for the following mixtures: (A) La(III), U(VI) and Th(IV); (B) U(VI), Th(IV) and Cu(II); (C) U(VI), Th(IV) and Pb(II). The column effluents were analyzed for the metal ions by spectrophotometry, GFAAS and/or ICPAES. In the separation of a ternary mixture (A) containing La(III), U(VI) and Th(IV), the mixture was passed through the column maintained at pH 6.5. Very minute amount (≤2%) of Th(IV) was retained by resin and most of it came out with the effluent as it gets hydrolysed above pH 4.0 while the other two metal ions were retained on the column. By the selective elution, La(III) was first eluted with 0.01N HNO_3 followed by U(VI) with 0.25N HCl. In the separation of a ternary mixture (B), containing U(VI), Th(IV) and Cu(II), the mixture was passed through the column maintained at pH 3.5. Most of (≥98%) U(VI) was not retained by resin and it came out with the effluent as it does not form the complex with the calixarene derivative at a low pH while the other two metal ions were retained on the column. Complete separation of Th(IV) and Cu(II) was achieved with sequential acidic elution of Th(IV) with 0.1N HNO_3 and Cu(II) by 3N HCl. In the separation of a ternary mixture (C), the mixture was passed through the column maintained at pH 6.5. Most of (≥98%) Th(IV) was not retained by resin and it came out with the effluent while rest of the metal ions were retained on the column. By selective elution, Pb(II) was first desorbed by elution with 0.1N HNO_3 followed by U(VI) with 0.25N HCl. Quantitative separation was achieved in all three mixtures as shown in their separation pattern in Fig. 5(A)–(C).

3.4. Analytical performance (calibration graph, detection limit and precision)

In the preparation of the calibration standards for U(VI) and Th(IV), their standard stock solutions were used after appropriate dilution. The precision of the proposed method was investigated based on the optimum condition for preconcentration in the column and expressed as R.S.D.: 1.7% for U(VI) and 1.5% for Th(IV) (Table 1). The limit of detection (LOD) was defined as that analyte concentration giving a signal equal to three times the standard deviation of blank signal [56]. The limit of quantification (LOQ) was then set as 10 times the standard deviation of the blank signal. The volume of initial solution for calculating LOD and LOQ for U(VI) was 0.6 and 2.0 ml of 0.1 μg ml^{-1}, respectively, and that for Th(IV) was 2.0 ml of 0.02 μg ml^{-1} and 1.4 ml of 0.1 μg ml^{-1} which was diluted to 10 ml with the buffer solution prior to elution.

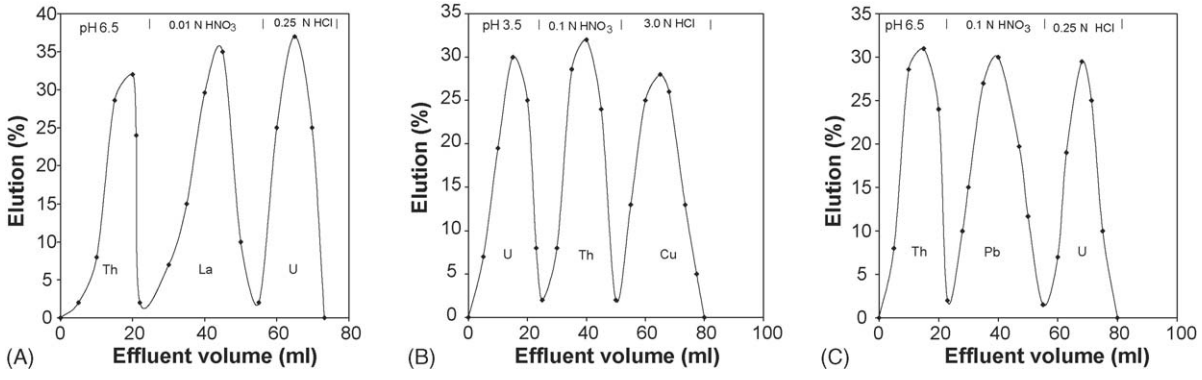

Fig. 5. Separation of ternary mixtures: (A) La(III), U(VI) and Th(IV); (B) U(VI), Th(IV) and Cu(II); (C) U(VI), Th(IV) and Pb(II) on the resin.

Table 3
Preconcentration and determination of U(VI) in river and ground water samples and U(VI) and Th(IV) in monazite sand and U.S. standard geological samples on the resin

Metal ions		U(VI)		Th(IV)	
Samples	Certified amount (μg)	Amount found (μg)	Recovery (%)	Certified amount (μg)	Amount found (μg)
Water samples[a]					
Sabarmati river, near Thermal Power Station, Ahmedabad	10 ± 0.05[b]	9.85 ± 0.03	98.5	–	–
Ground water, Gujarat University Area, Ahmedabad	17 ± 0.05[b]	16.7 ± 0.05	98	–	–
Natural geological samples[a]					
Monazite sand, Travancore, India (%)	0.0185	0.018 ± 0.0003	–	8.45	8.40 ± 0.560
USGS: BCR-1 (mg g^{-1})	1.71	1.78 ± 0.05	–	6.1	6.15 ± 0.08
USGS: GSP-1 (mg g^{-1})	2.1	2.13 ± 0.09	–	105	105.0 ± 1.49

Experimental condition— resin: 1 g; sample: 1000 ml; U(VI): pH 6.5, elution by 0.25N HCl; Th(IV): pH 3.5, elution by 2.0N HCl.
[a] Average and standard deviation from triplicate run conducted with a single column.
[b] Certified values reported by National Institute of Occupational Health, Ahmedabad, India.

3.5. Application to analysis of water samples, monazite sand and standard geological samples

The application and validation of the proposed method was verified by subjecting resin to natural water samples, monazite sand and standard geological samples. The river water samples were isokinetically collected in polyethylene bottles from Sabarmati river near thermal power station, Ahmedabad city of India and ground water samples were collected from Navrangpura region of Ahmedabad and then passed through the column as described in the general procedure for column concentration. The geological materials were obtained from United States Geological Survey USGS: BCR-1 and USGS: GSP-1 and were decomposed in the mixture of acids as described in the literature [57]. The results are given in Table 3.

3.6. Comparison with other preconcentration methods

The present method achieves high preconcentration factors (U(VI): 143 and Th(IV): 153) compared to quinoline-8-ol [26] and succinic acid [27] anchored on polymeric supports. The detection limit—a significant figure of merit obtained by this method is very low, 6.14 and 4.29, respectively, for U(VI) and Th(IV) compared to the chemically modified Amberlite XAD-16 with [(2-dihydroxyarsinoylphenylamino)methyl]phosphonic acid [28] and *N*,*N*-dihexylcarbamoylmethyl phosphonic acid [29]. The synthesized resin showed excellent stability in different acids compared to the above two methods and could be used for 20 cycles of sorption and desorption without affect the efficiency.

4. Conclusion

Solid phase extraction with a chelating calix[4]arene anchored Merrifield's chloromethylated polystyrene resin provides an effective preconcentration and separation of U(VI) and Th(IV). The calixarene ring is found to be an important platform on which ion-binding ligands can be pre-organized, resulting in high affinities and selectivities. The newly synthesized resin seems promising for trace enrichment of metal ions as apparent from the column studies. The separation curves demonstrate the efficiency of resin for the real-time separation of U(VI) and Th(IV) in the presence of each other and also La(III), Cu(II) and Pb(II) with minimum interference from alkali and alkaline earth metal ions. Resin shows high separating and preconcentrating ability for these metal ions. Resin can be successfully regenerated for 20 cycles of operation in the column. The results obtained from the analysis of natural water samples, monazite sand and standard geological samples prove the reliability of the proposed method.

Acknowledgements

The authors are thankful to GUJCOST, Gujarat for their financial assistance. The authors also acknowledge CDRI, Lucknow for providing instrumental facilities and INFLIBNET, Ahmedabad for providing online journals.

References

[1] H.F. Walton, R.D. Rocklin, Ion Exchange in Analytical Chemistry, CRC Press, Boca Raton, 1990.
[2] G.D. Clayton, F.E. Clayton (Eds.), Patty's Industrial Hygiene and Toxicology, vol. 2C, 4th ed., Wiley-Interscience, New York, 1994.
[3] Agency for Toxic Substances and Disease Registry, U.S. Public Health Service, Chapman and Hall, New York, 2000.
[4] E.R. Unsworth, J.M. Cook, S.J. Hill, Anal. Chim. Acta 442 (2001) 141.
[5] Y. Fujikawa, M. Sugahara, E. Ikeda, M. Fukui, J. Radioanal. Nucl. Chem. 252 (2002) 399.
[6] M. Kumar, D.P.S. Rathore, A.K. Singh, Microchim. Acta 137 (2001) 127.
[7] M. Merdivan, M.Z. Duz, C. Hamamci, Talanta 55 (2001) 639.
[8] J.M. Gladis, T.P. Rao, Anal. Bioanal. Chem. 373 (2002) 867.
[9] M. Kumar, D.P.S. Rathore, A.K. Singh, Analyst 125 (2000) 1221.
[10] M. Sarkar, M. Das, P.K. Datta, J. Colloid Interface Sci. 246 (2002) 263.
[11] P.E. Duru, S. Bektas, O. Genc, S. Patyr, A. Denizli, J. Appl. Polym. Sci. 81 (2001) 197.

[12] N. Demirel, M. Merdivan, N. Pirincciogluc, C. Hamamci, Anal. Chim. Acta 485 (2003) 213.
[13] I.M. Ismail, M. Nogami, K. Suzuki, Sep. Purif. Technol. 31 (2003) 231.
[14] H. Boerrigter, T. Tomasberger, W. Verboom, D.N. Reinhoudt, Eur. J. Org. Chem. (1999) 665.
[15] S.E. Matthews, M. Saadioui, V. Bohmer, S. Barboso, F. Arnaud-Neu, M.J. Schwing-Weill, A.G. Carrera, J.F. Dozol, J. Prakt. Chem. 341 (1999) 264.
[16] L.L. Saulnier, S. Varbanov, R. Scopelliti, M. Elhabiri, J.C.G. Bunzli, J. Chem. Soc., Dalton Trans. (1999) 3919.
[17] C. Fischer, G. Sarti, A. Casnati, B. Carrettoni, I. Manet, R. Schuurman, M. Guardigli, N. Sabbatini, R. Ungaro, Chem. Eur. J. 6 (2000) 1026.
[18] A. Arduini, V. Bohmer, L. Delmau, J.F. Desreux, J.F. Dozol, A.G. Carrera, B. Lambert, C. Musigmann, A. Pochini, A. Shivanyuk, F. Ugozzoli, Chem. Eur. J. 6 (2000) 2135.
[19] S. Barboso, A.G. Carrera, S.E. Matthews, F. Arnaud-Neu, V. Bohmer, J.F. Dozol, H. Rouquette, M.J. Schwing-Weill, J. Chem. Soc., Perkin Trans. 2 (1999) 719.
[20] F. Arnaud-Neu, J.K. Browne, D. Byrne, D.J. Marss, M.A. Mckervey, P.O. O'Hagan, M.J. Schwing-Weill, A. Walker, Chem. Eur. J. 5 (1999) 175.
[21] T.P. Rao, C.R. Preetha, Sep. Purif. Rev. 32 (2003) 1.
[22] V. Camel, Spectrochim. Acta Part B 58 (2003) 1177.
[23] X. Zu, P. Liu, Q.S. Pu, Q.Y. Sun, Z.X. Su, Talanta 62 (2004) 918.
[24] H. Bagheri, A. Gholami, A. Najafi, Anal. Chim. Acta 424 (2000) 233.
[25] R. Pathak, G.N. Rao, Anal. Chim. Acta 335 (1996) 283.
[26] R.S. Praveen, P. Metilda, S. Daniel, T. Prasada Rao, Talanta 67 (2005) 960.
[27] P. Metilda, K. Sanghamitra, J. Mary Gladis, G.R.K. Naidu, T. Prasada Rao, Talanta 65 (2005) 192.
[28] M. Akhila Maheswari, M.S. Subramanian, Talanta 64 (2004) 202.
[29] D. Prabhakaran, M.S. Subramanian, Anal. Bioanal. Chem. 379 (2004) 519.
[30] P. Engrand, J.R. Vains, Tetrahedron Lett. 43 (2002) 8863.
[31] J. Plutnar, J. Rohovec, J. Kotek, Z. Zak, I. Lukes, Inorg. Chim. Acta 335 (2002) 27.
[32] G. Uysal, S. Memon, M. Yilmaz, React. Funct. Polym. 50 (2002) 77.
[33] H.R. Webb, M.J. Hardie, C.L. Raston, Chem. Eur. J. 7 (2001) 3616.
[34] C.W. Hall, J.S. Cockayne, M.J. Kan, G.P. Nicholson, Green Chem. 3 (2001) 114.
[35] B. Lambert, V. Jacques, A. Shivanyuk, S.E. Matthews, A. Tunayar, M. Baaden, G. Wipff, V. Bohmer, J.F. Desreux, Inorg. Chem. 39 (2000) 2033.
[36] M. Yilmaz, N.P. Cheremisinoff (Eds.), Solution State Metal Complexes of Calixarenes and Polymeric Calixarenes, Handbook of Engineering Polymeric Materials, Marcel Dekker Inc., New York, 1997.
[37] C.D. Gutsche, J.F. Stoddart (Eds.), Calixarenes Revisited, Monographs in Supramolecular Chemistry, Royal Society of Chemistry, Cambridge, 1998.
[38] L. Mandolini, R. Ungaro, Calixarenes in Action, Imperial College Press, London, 2000.
[39] Z. Asfari, V. Bohmer, J. Harrowfield, J. Vicens, Calixarenes 2001, Kluwer Academic Press, Dordrecht, 2001.
[40] Y.K. Agrawal, V.S. Mishra, Rev. Inorg. Chem. 24 (2004) 1.
[41] P.D. Barata, A.I. Costa, P. Granja, J.V. Prata, React. Funct. Polym., in press.
[42] M. Makha, C.L. Raston, B.W. Skelton, A.H. White, Green Chem. 6 (2004) 158.
[43] R. Ludwig, Fresinus. J. Anal. Chem. 367 (2000) 103.
[44] W. Sliwa, Croat. Chem. Acta 75 (2002) 131.
[45] S. Shinkai, S. Mori, H. Koreishi, T. Tsubaki, O. Manabe, J. Am. Chem. Soc. 108 (1986) 2409.
[46] S. Memon, M. Tabakci, D.M. Roundhill, M. Yilmaz, Polymer 46 (2005) 1553.
[47] K. Scheide, G. Geipel, G. Berhard, Wissenschaftlich-Technische Berichte-Forschungszentrum Rossendorf, FZR-414, 2004, p. 1.
[48] B.S. Garg, V.K. Jain, Microchem. J. 38 (1988) 144.
[49] Z. Marczenko, Spectrophotometric Determination of Elements, Ellis-Horwood Ltd., Chichester, 1976.
[50] J.A. Dean, Lange's Handbook of Chemistry, 15th ed., McGraw-Hill, New York, 1999.
[51] C.D. Gutsche, M. Iqbal, Org. Synth. Coll. 8 (1993) 75.
[52] C.D. Gutsche, L. Lin, Tetrahedron 42 (1986) 1633.
[53] J.D. Van Loon, A. Arduini, L. Coppi, W. Verboom, A. Pochini, R. Ungaro, S. Harkema, D.N. Reinhoudt, J. Org. Chem. 55 (1990) 5639.
[54] V.K. Jain, R.A. Pandya, S.G. Pillai, Y.K. Agrawal, P.S. Shrivastav, Microchim. Acta 147 (2004) 253.
[55] M. Kanesato, T. Yokoyama, T.M. Suzuki, Bull. Chem. Soc. Jpn. 62 (1989) 3451.
[56] L.H.J. Lajunen, Spectrochemical Analysis by Atomic Absorption and Emission, Royal Society of Chemistry, Cambridge, 1992, p. 9.
[57] S.J. Hill, Inductively Coupled Plasma Spectrometry and its Applications, Academic Press, Sheffield, 1999.

Available online at www.sciencedirect.com
ScienceDirect
Talanta 70 (2006) 267–271
Talanta
www.elsevier.com/locate/talanta

A new single-well potential stochastic resonance algorithm to detect the weak signal

Zhang Wei, Xiang Bing-ren *

Center for Instrumental Analysis of China Pharmaceutical University, Mailbox 34, 24# Tong Jia Xiang, Nanjing, Jiangsu 210009, China

Received 21 November 2005; received in revised form 10 February 2006; accepted 13 February 2006
Available online 20 March 2006

Abstract

Based on the stochastic resonance theory, a new single-well potential stochastic resonance algorithm (SSR) to improve the signal-to-noise ratio (SNR) is presented. In the new algorithm, stochastic resonance takes place in a single-well potential driven only by the noise. The effect on the proposed algorithm is discussed. By using simulated and experimental data sets, it is proven that the signal-to-noise ratio (SNR) of the weak signal can be greatly enhanced by this method. The new single-well potential stochastic resonance algorithm (SSR) may be a promising tool to extend instrumental linear range and to improve the accuracy of trace analysis. The research enlarges the application scope of single-well potential to nonlinear signal processing.

Keywords: Single-well potential; Stochastic resonance; Weak signal; Gas chromatography

1. Introduction

Stochastic resonance (SR) is a nonlinear phenomenon whereby the noise can enhance the detection of a weak signal [1–3]. It generally occurs in bistable dynamical systems attacked by a weak signal corrupted by noise through the nonlinear internal dynamics of the system, the small signal is ampli1ed by the presence of noise. [4]. It was brought forward by Benzi firstly and successfully applied to the study of ancient ice age weather [5–7]. Stochastic resonance (SR) has attracted considerable interest in the last decade due, among other aspects, to its potential technological applications for optimizing the output signal-to-noise ratio (SNR) in nonlinear dynamical systems. The phenomenon shows the counterintuitive role played by noise in nonlinear systems as it enhances the response of a system subject to a weak external signal. [8]. There are lots of papers, which show the large number of applications in improving analytical detection limits for trace analysis. Such as Wang has applied double-well potential stochastic resonance (DSR) to analyze the weak laser-Raman spectrum of CCl_4. Pan et al. have improved the detectability of analytes in gas chromatography [9,10,12].

Stochastic resonance is a powerful approach to amplify subthreshold small signals, while this kind of weak signals are rarely considered by analysts before. However, it is difficult to change the optimized system parameters for the stochastic resonance in detecting weak signal. Therefore, our attention will be focused on the simple model of stochastic resonance, which has the lesser system parameters. In this paper, a new single-well potential with the only parameter b characterizing the system was applied in generating stochastic resonance. By two simulated data sets and an experimental data set, the applicability of the proposed SSR was investigated. The effect on the performance of the algorithm was also discussed in details.

2. Theory and algorithm

A model of a one-dimensional nonlinear system that exhibits stochastic resonance is the damped harmonic oscillator with the Langevin equation of motion [11,12].

$$m\ddot{x} + \gamma\dot{x} + \frac{\mathrm{d}U(x)}{\mathrm{d}x} = H(t) \tag{1}$$

where the dot represents time-derivative. This equation describes the motion of a particle of mass m moving in the presence of

* Corresponding author. Tel.: +86 25 83271180.
E-mail addresses: astdaixiong@hotmail.com, lcwangxbr@yahoo.com.cn (X. Bing-ren).

0039-9140/$ – see front matter © 2006 Elsevier B.V. All rights reserved.
doi:10.1016/j.talanta.2006.02.039

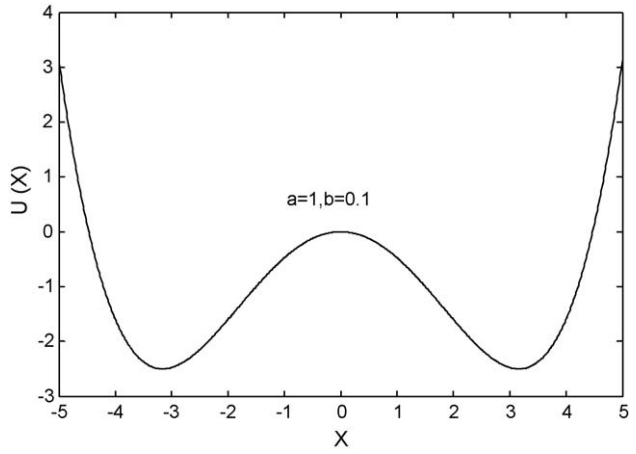

Fig. 1. Double-well potentials with the $a=1$, $b=0.1$.

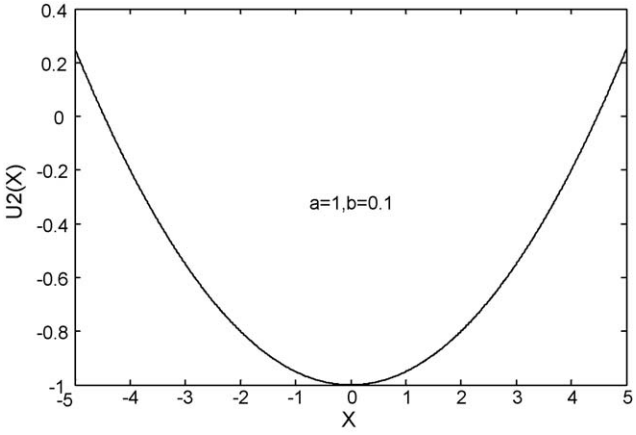

Fig. 2. Single-well potentials with the $a=1$, $b=0.1$.

friction $\gamma\dot{x}$ in a potential $U(x)$ and with an additive stochastic force $H(t)$. When the system is heavily damped, the inertial term $m\ddot{x}$ can be neglected.

Rescaling Eq. (1) with the damping term γ gives:

$$\dot{x} = -\frac{\mathrm{d}U(x)}{\mathrm{d}x} + H(t) \tag{2}$$

$U(x) = -ax^2/2 + bx^4/4$ is the simplest double-well potential with the constants a and b characterizing the system. Thus, Eq. (2) leads to:

$$\dot{x} = ax - bx^3 + H(t) \tag{3}$$

where $H(t) = h(t) + \Gamma(t)$, $h(t)$ is the input signal and $\Gamma(t)$ is the noise to induce SR.

After considering the SR phenomenon in bistable systems without excitation, Ditzinger and his coworkers investigated a system that was not bistable and concluded that bistability was not a necessary ingredient for SR [13]. In this paper, the new potential function was rendered by changing the exponent of x. Formula is as follows:

$$U(x) = -a + \frac{1}{2}bx^2 \tag{4}$$

After using the new single-well potential function, the stochastic differential equation (Eq. (2)) is as follows:

$$\dot{x} = -bx + H(t) \tag{5}$$

Fig. 1 shows the simple double-well potential which has a local unstable maximum point at $x=0$ and two stable minimum points at $x = \sqrt{a/b}$, respectively. There is a potential barrier between the two stable states with a height of $\Delta u = a^2/4b$. When SR takes place, the input signal, noise and nonlinear system cooperate well and the signal will extract energy from the noise both intrinsic and external to surmount the energy barrier and hop from one potential well to another. Consequently, the strength of signals will increase and that of noise will decrease. The output signal x of the system will be obtained by a better SNR compared with the input one.

Fig. 2 shows the single-well potential with the same a and b as Fig. 1. There is single-well potential which has no potential barrier. When SR takes place, the input signal will extract energy from the noise to move along the brim of the single-well potential. Thus, it can get the height, which the single input signal cannot reach. There may be the reason that strength of signals will increase and that of noise will decrease. Consequently, the weak signal will obtain a better SNR than input signal.

When the input signal is sine, Eq. (5) leads to $\dot{x} = -bx + A_0\sin(\Omega t + \Phi_0) + \Gamma(t)$, $\Gamma(t)$, is assumed to be zero-mean white noise of variance σ. Using an Euler scheme to discretize this equation, the following model can be obtained [14]:

$$x_{n+1} = x_n + K\sum_{i=0}^{n} s_i + K\sum_{i=0}^{n}\xi_i + K\sum_{i=0}^{n} - bx_i \tag{6}$$

where $s_i = A_0\sin(\Omega t + \Phi_0)$ and K is length of step.

When K is enough small,

$$h\sum_{i=0}^{n} s_i = \int_0^{nh} A_0\cos(\Omega t + \Phi_0)\mathrm{d}t$$

$$= \frac{A_0}{\Omega}\cos(\Phi_0) - \frac{A_0}{\Omega}\cos(\Omega t_{n-1} + \Phi_0)$$

Thus, Eq. (6) becomes as follows:

$$x_{n+1} = x_n + \frac{A_0}{\Omega}\cos(\Phi_0) - \frac{A_0}{\Omega}\cos(\Omega t_{n-1} + \Phi_0) + K\sum_{i=0}^{n}\xi_i + K\sum_{i=0}^{n} - bx_i$$

From this equation, it can be educed that the output signal is sine signal with amplitude A_0/Ω and same frequency with input signal. The small b should be used in order to avoid the effect of $h\sum_{i=0}^{n} - bx_i$.

3. Simulations

3.1. Periodic signals

For convenience, the mixed input signal reads explicitly $H(t) = A_0\cos(\Omega t) + \sqrt{2D}\Gamma(t)$. $\Gamma(t)$ is the Gaussian white

noise which means value is 0 and variance is 1. Thus, Eq. (5) becomes the following form:

$$\dot{x} = -bx + A_0 \cos(\Omega t) + \sqrt{2D}\Gamma(t) \tag{7}$$

and Eq. (3) becomes the following form:

$$\dot{x} = ax - bx^3 + A_0 \cos(\Omega t) + \sqrt{2D}\Gamma(t) \tag{8}$$

The output signal can be obtained by solving Eqs. (7) and (8). In the proposed DSR and SSR, the discrete stochastic differential equation was solved by a fourth-order Runge–Kutta method, which has more precision than Euler scheme [12,15,16]. The algorithms can be described as follows:

$$x_{n+1} = x_n + \frac{1}{6}(k_1 + 2k_2 + 2k_3 + k_4), \quad n = 0, 1, \cdots, N-1$$
$$k_1 = K(ax_n - bx_n^3 + u_n)$$
$$k_2 = K\left(a\left(x_n + \frac{k_1}{2}\right) - b\left(x_n + \frac{k_1}{2}\right)^3 + u_{n+1}\right)$$
$$k_3 = K\left(a\left(x_n + \frac{k_2}{2}\right) - b\left(x_n + \frac{k_2}{2}\right)^3 + u_{n+1}\right)$$
$$k_4 = K(a(x_n + k_3) - b(x_n + k_3)^3 + u_{n+2})$$

The algorithm of solving the double-well potential stochastic resonance (DSR)

$$x_{n+1} = x_n + \frac{1}{6}(k_1 + 2k_2 + 2k_3 + k_4), \quad n = 0, 1, \ldots, N-1$$
$$k_1 = K(-bx_n + u_n)$$
$$k_2 = K\left(-b\left(x_n + \frac{k_1}{2}\right) + u_{n+1}\right)$$
$$k_3 = K\left(-b\left(x_n + \frac{k_2}{2}\right) + u_{n+1}\right)$$
$$k_4 = K(-b(x_n + k_3) + u_{n+2})$$

The algorithm of solving the single-well potential stochastic resonance (SSR)

Where $u_n = h(t) + \Gamma(t)$ and x is the output signal. The K is length of step. All the calculations were performed by using programs written by the authors in the Matlab environment (The Mathworks, Natick, USA), running on PC with Intel (R) Pentium4 CPU 2.00 GHz and 512 M RAM.

Numerical simulation of Eqs. (7) and (8) is $K = 0.2$, $A_0 = 0.3$, $\Omega = 0.02\pi$ and $D = 0.51$. And the time is from 0 to 2000 s digitized into10000 points.

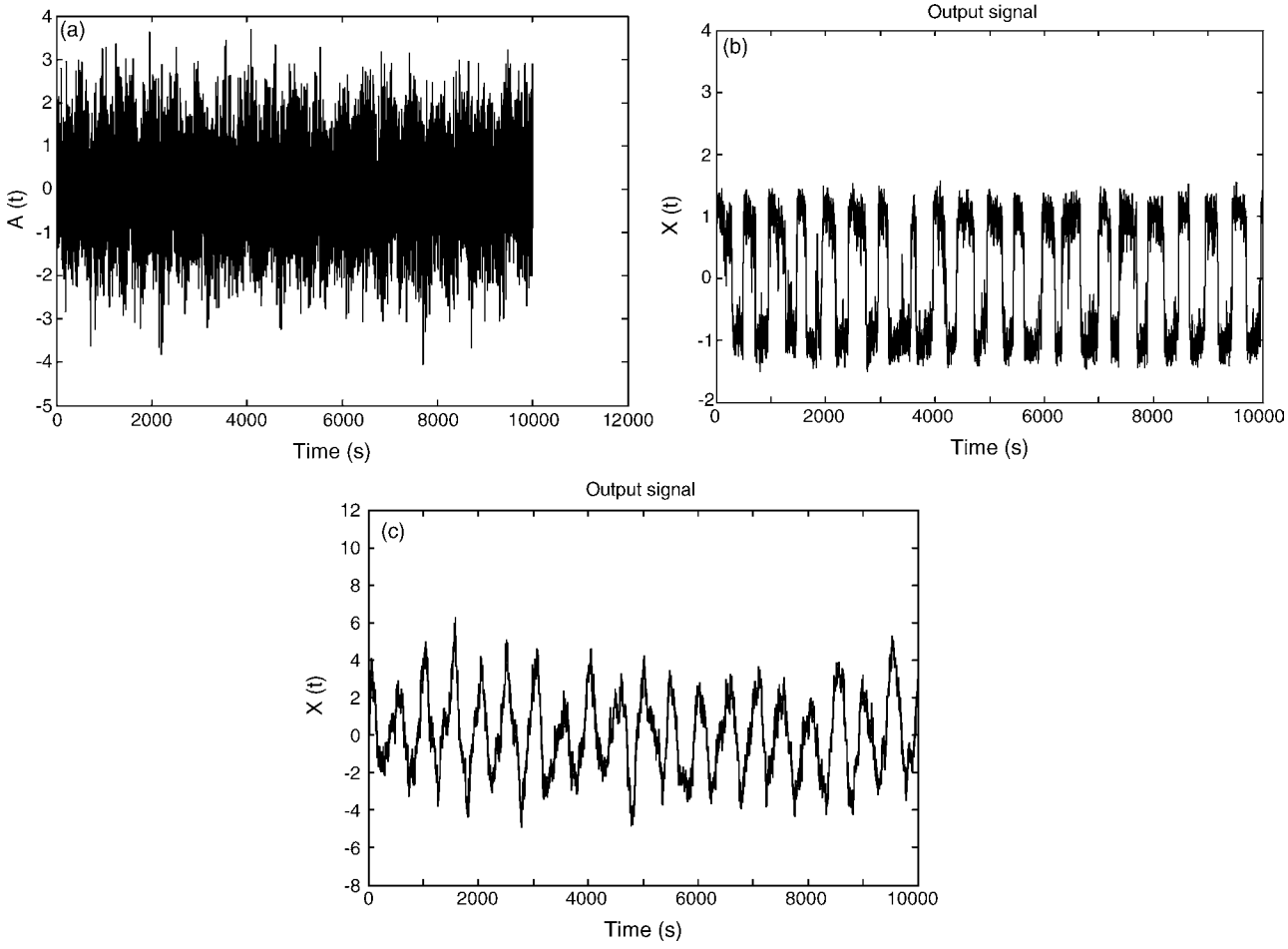

Fig. 3. (a) Numerical simulation with $A_0 = 0.3$, $\Omega = 0.02\pi$ and $D = 0.51$; (b) the output signal by the quartic bistable system with $a = 1$ and $b = 1$; (c) the output signal by single-well potential with $b = 0.1$.

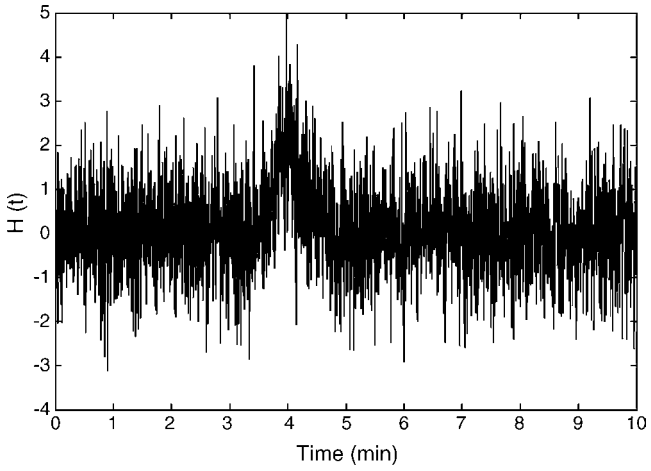

Fig. 4. Simulated chromatograms with $h_0 = 2$.

.

From Fig. 3a–c, it is can be seen that the noise was locked to the periodic signal. And the stochastic resonance as a "resonant" synchronization phenomenon, happen in the single-well potential as in the quartic bistable system.

3.2. Aperiodic signals

Simulated chromatogram was produced according to the following equation: $h(t) = h_0 \exp[-4 \ln(2)(t - t_0/w_{1/2})]$, where h_0 is the peak height; t, t_0 and $w_{1/2}$ denote time, the peak position and the peak half-width, respectively. The time is from 0 to 10 min digitized into 2500 points. t_0 is 4 and $w_{1/2}$ is 0.5. The simulated Gaussian white noise which means value is 0 and variance is 1 is added to the simulated signal to construct a noisy chromatogram. The data with $h_0 = 2$ is shown in Fig. 4 as examples.

The results of simulated data set are shown in Fig. 5. The shape of chromatograms is dissimilar because their potentials applied in generating stochastic resonance are different. But the signal-to-noise ratio (SNR) of weak signal can be greatly enhanced by the SSR and DSR.

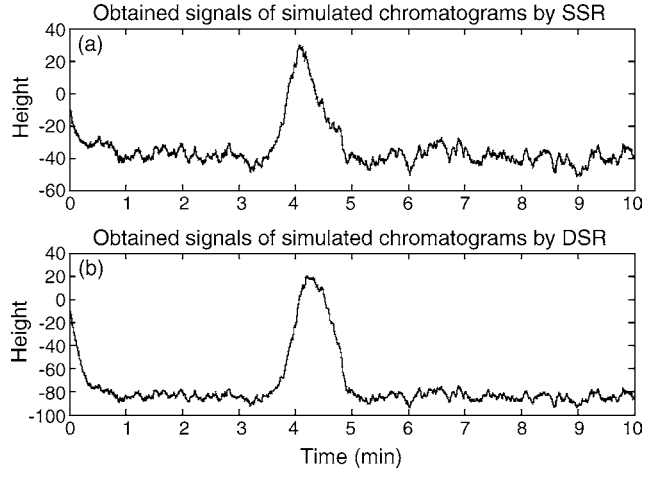

Fig. 5. (a) Obtained signal of simulated chromatogram by the single-well potential with $b = 0.026$. (b) Obtained signal of simulated chromatogram by the quartic bistable system with $a = 0.005$ and $b = 4.083 \times 10^{-5}$.

4. Experiment

4.1. Materials

Dichloromethane (99.8% purity) were obtained from the Nanjing Chemical Co. (Nanjing, China). Distilled water was used throughout the study.

4.2. Gas chromatograph determination of dichloromethane

The microanalysis of dichloromethane was performed on HP5890 gas chromatography system with FID detector, temperature at 170 °C, and attenuation factor at 2. The carrier gas was nitrogen (N_2) at a flow rate of 25 ml/min. The oven temperature was set at 50 °C. A DB5 GC-column (0.25 mm. i.d. × 30 m; film thickness 0.25 μm) was used. Reten-

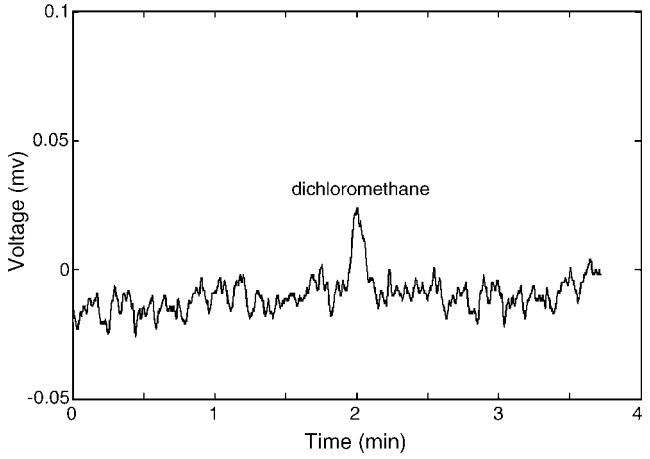

Fig. 6. Experimental chromatogram of dichloromethane at the concentration of 1.5 μg/ml.

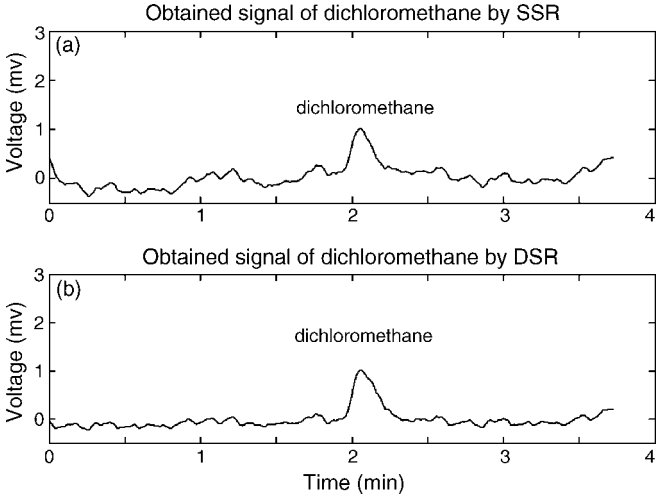

Fig. 7. (a) Obtained chromatogram of dichloromethane by the single-well potential with $b = 0.02$. (b) Obtained chromatogram of dichloromethane by the quartic bistable system with $a = 0.002$ and $b = 4.01 \times 10^{-5}$.

tion time of dichloromethane was about 2.2 min. A sample of dichloromethane was prepared in water at the concentration of 1.5 μg/ml. Fig. 6 showed the signal of dichloromethane was too weak to meet the requirement of quantitative analysis. So it was impossible to determine the concentration of dichloromethane accurately under such heavy noise. Therefore, a new and effective method of dealing data of the chromatograph signal should be adopted. The signal was chosen to perform SSR ($b = 0.02$) and DSR ($a = 0.002$ and $b = 4.01 \times 10^{-5}$). Compared with Figs. 6 and 7 presents a signal with a much larger range of strength than the former one. Consequently, the reasonable result cannot be obtained for the chromatographic data set of dichloromethane by conventional methods, such as FFT and WT. The result of experiment is same as the simulations.

5. Results and discussion

5.1. Effect of noise intensity D on the performance of stochastic resonance

The single-well potential stochastic resonance algorithm is presented in order to be applied to improve the signal to noise ratio (SNR) in the trace analysis. Thus, the effect of D to the signal of chromatogram is discussed. There is not a precise computational formula of SNR in chromatogram. So the signal-to-noise (S/N) ratios were used for a rough estimation in this paper. The same data in Fig. 5 with different values of D was selected to perform the stochastic resonance. Further increasing the noise to 2.0, the SNR of single-well potential is 3 and that of quartic bistable system is 6. This demonstrated that the quartic bistable system's detectability of the signal submerged by noise is much stronger. In the chromatogram, the noise intensity D is usually smaller than 0.5. Thus, the single-well potential stochastic resonance algorithm is enough to be applied in high performance liquid chromatography and gas chromatography.

5.2. Effect of system parameter b

The parameters a and b in Eq. (2) not only define the height of the potential barrier, but also affect the profile of the potential well. When the input signal was fixed, the parameters a and b affected the quality of final output signal directly. Same as DSR, the parameter b is very important to SSR. It is proved that strong noise needs smaller b than the weak one. In order to detect the chromatographic signal, the shape of the output signal should be taken into account. Generally, the ratio of peak height to peak half-width is evaluating indicator. And a big ratio presents a good output signal. According to the published paper [12], small a and b should be considered first. Fixing one parameter, another was adjusted until the expected output signal is obtained. By this optimization method, the satisfied value of the parameters can be obtained.

6. Conclusion

The DSR gives analysts a completely different way to improve the instrumental detectability. However, the optimization of system parameters is complicated and difficult. This paper has investigated the new single-well potential stochastic resonance algorithm (SSR). The results show that SSR transduces the signal optimally when a certain amount of noise is presented. And the parameter of SSR method is required only one. Thus, it is easier to be selected compared with the traditional double-well potential stochastic resonance. In the future it is possible that the method could be combined by or embedded in the chromatographic workstations to function online. Through the periodic signals and aperiodic signals, it can be proved that SSR can improve the SNR of weak signals. Compared with other conventional chemometrics methods, such as fast Fourier transform (FFT) [17–19], wavelet transform (WT) [20–23], the proposed SSR keeps the information of an analytical signal intact. It can be expected that the proposed SSR may be a promising chemometrics method for trace analysis.

References

[1] F. Chapeau-Blondeau, X. Godivier, Phys. Rev. E 55 (1997) 1478.
[2] L. Gammaitoni, P. HPanggi, P. Jung, F. Marchesoni, Rev. Mod. Phys. 70 (1998) 223.
[3] S. Mitaim, B. Kosko, Proc. IEEE 86 (1998) 2152.
[4] R. Zhu, Q. Shu Li, Phys. Lett. A 292 (2001) 58.
[5] R. Benzi, A. Sutera, A. Vulpiani, J. Phys. A 14 (1981) L453.
[6] C. Nicolis, Tellus 1 (34) (1982) 1.
[7] R. Benzi, G. Parisi, Tellus 34 (1) (1982) 10.
[8] M.A. Fuentes, R. Toral, Phys. A 295 (2001) 114.
[9] P. Jung, P. Hanggi, Europhys. Lett. 8 (1989) 505.
[10] L.-Y. Wang, Chem. J. Chin. Univ. 21 (2000) 53.
[11] D. Jianghai, IEEE International Conference on Neural Networks & Signal Processing, December 14–17, 2003.
[12] Z. Pan, W. Guo, et al., Chemom. Intell. Lab. Syst. 66 (2003) 41.
[13] T. Ditzinger, C.Z. Ning, et al., Phys. Rev. E 50 (1994) 3508.
[14] X. Fanghong, et al., Chin. Phys. 53 (2004) 396.
[15] B. McNamara, K. Wiesenfeld, Phys. Rev. A 39 (1989) 4854.
[16] A.S. Asdi, A.H. Tewfik, IEEE Trans. Signal Proc. 2 (1995) 1332.
[17] D.N.S. Permann, H. Teitelbaum, J. Phys. Chem. 97 (1993) 12670.
[18] M.A. Korany, O.T. Fahmy, et al., Talanta 66 (2005) 1073.
[19] M.R. Ganjali, P. Norouzi, et al., Talanta 66 (2005) 1225.
[20] L. Pasti, B. Walczak, D.L. Massart, P. Reschiglian, Chemom. Intell. Lab. Syst. 48 (1999) 21.
[21] X.G. Shao, W.S. Cai, P.Y. Sun, M.S. Zhang, G.W. Zhao, Anal. Chem. 69 (1997) 1722.
[22] C. Perrin, B. Walczak, D.L. Massart, Anal. Chem. 73 (2001) 4903.
[23] E. Dinç, A. Özdemir, D. Baleanu, Talanta 65 (2005) 36.

Available online at www.sciencedirect.com
ScienceDirect
Talanta 70 (2006) 272–280
Talanta
www.elsevier.com/locate/talanta

Creatinine sensor based on a molecularly imprinted polymer-modified hanging mercury drop electrode

Dhana Lakshmi, Bhim Bali Prasad *, Piyush Sindhu Sharma

Analytical Division, Chemistry Department, Banaras Hindu University, Varanasi-221 005, India

Received 17 December 2005; received in revised form 13 February 2006; accepted 13 February 2006
Available online 27 March 2006

Abstract

Molecularly imprinted polymers (MIP) have been elucidated to work as artificial receptors. In our present study, a MIP was applied as a molecular recognition element to a chemical sensor. We have constructed a creatinine sensor based on a MIP layer selective for creatinine and its differential pulse, cathodic stripping voltammetric detection (DPCSV) on a hanging mercury drop electrode (HMDE). The creatinine sensor was fabricated by the drop coating of dimethylformamide (DMF) solution of a creatinine-imprinted polymer onto the surface of HMDE. The modified-HMDE, preanodised in neutral medium at +0.4 V versus Ag/AgCl for 120 s, exhibited a marked enhancement in DPCSV current in comparison to the less anodised (≤+0.3 V) HMDE. The creatinine was preconcentrated and instantaneously oxidised in MIP layer giving DPCSV response in the concentration range of 0.0025–84.0 μg mL^{-1} [detection limit (3σ) 1.49 ng mL^{-1}]. The sensor was found to be highly selective for creatinine without any response of interferents viz., NaCl, urea, creatine, glucose, phenylalanine, tyrosine, histidine and cytosine. The non-imprinted polymer-modified electrode did not show linear response to creatinine. The imprinting factor as high as 9.4 implies that the imprinted polymer exclusively acts as a recognition element of creatinine sensor. The proposed procedure can be used to determine creatinine in human blood serum without any preliminary treatment of the sample in an accurate, rapid and simple way.

Keywords: Creatinine sensor; Molecularly imprinted polymer; Differential pulse cathodic stripping voltammetry; Blood serum

1. Introduction

Molecular imprinting is a generic technology, which introduces recognition properties into synthetic polymers using appropriate templates. The conventional MIPs have widely been used as selective recognition layers in sensing devices [1,2]. However, the slow diffusion and rebinding kinetics are limiting parameters which often render the application of MIPs in chemical sensor unfeasible. Few approaches such as surface imprinting techniques forming recognition sites at the membrane surface may in future lead to more efficient sensing layers. Specificity, their stability, and potentially low production costs are certainly the strongest arguments for MIPs in sensing in contrast to immobilised bio-receptors such as antibodies and enzymes. MIPs have been combined with a variety of transduction schemes like capacitance [3], impedometric [4], amperometric [5], mass-sensitive [6], and optical sensing platforms [7]. The achievable selectivity provides sensing chemistries tuned towards the templated analyte due to e.g. preferential enrichment or transport into the recognition layer. However, polymer specificity, affinity, and capacity have to be greatly improved in order to meet the requirements for real-world applications. Furthermore, most sensors require selective recognition at aqueous conditions for applications in the fields of clinical diagnostics and environmental monitoring, which remains a challenge for most MIP receptors reported to date. The absence of a general procedure for MIP preparation, incomplete template removal, difficulty in integrating MIP with suitable transducer, and the problem of transforming the binding event into processable signal are some of the major limitations encountered in the development of MIP sensor.

Despite the fact that MIP-based solid-electrode sensors have advantages such as low cost, small size, robustness, selectivities rivalling biological recognition elements and easy automation, one of the difficulties of measurement protocols involving an extraction step is the strong effects of unspecific adsorption

* Corresponding author. Tel.: +91 5422307321x112.
E-mail address: prasadbb_2000@yahoo.com (B.B. Prasad).

0039-9140/$ – see front matter © 2006 Elsevier B.V. All rights reserved.
doi:10.1016/j.talanta.2006.02.038

on the electrode surface [8]. However, voltammetry transduction adds the capacity of discriminating between species and identifying adsorption at imprinted sites either by separately optimising the binding medium and the measurement medium or by using the same medium for binding and detection. In addition, structurally related interferents can be identified by their electrochemical potentials [9]. The major drawbacks with MIP-based solid-sensors have so far been the long response time and limited senitivities for the target analytes owing to non-reproducible film thickness. Here the film thickness creates a substantial diffusion barrier across the film/solution interface. Thus, irreproducibility of the films severely influences the reproducibility of the sensors. The present work with modified-HMDE offers an alternative to the solid sensors to overcome the aforesaid problems. The mass-transfer could be enhanced by thin film grafting technique and sensitivity by coupling MIP elements to voltammetric tranducers [10,11] in the modified HMDE.

Creatine is one of the main compounds in the muscular energetic metabolism leading to phosphocreatine to maintain high ATP levels. During muscle contraction, creatine and creatine phosphate are spontaneously converted to creatinine. Creatinine is a waste product, which is eliminated from the body by renal excretion at a relatively constant rate. This leads to the fact that creatinine measurement is a clinically chosen test for indicating renal, thyroid, and muscular functions and myocardial infarction. To maintain the normal level of creatinine is important because high levels are indicative of diabetic nephropathy, eclampsia, glomerulonephritis, muscular dystrophy, preeclampsia, pyelonephritis reduced renal blood flow, renal failure, and urinary tract obstruction, while a low level may be indicative of muscular dystrophy and myasthenia [12]. The routine clinical laboratory method using spectrophotometry based on the Jaffé reaction [13] is subject to many interferences and lacks specificity [14]. Enzymatic methods are apparently costly and time consuming [15,16]. Electrochemical methods such as amperometric and potentiometric biosensors either display essential cross-reactivity with creatine, urea, glucose or are low in sensitivity [17]. The investigation of using molecularly imprinted polymer for the adsorption of creatinine was initiated by Sreenivasan and Sivakumar in 1997 [18]. They utilised γ irradiation to synthesise the polymer for the binding of creatinine [18]. Later in 2002, a reversible chemosensor was also prepared using molecular imprinting method [12]. Fluorescent MIPs, which are based on the reaction between polymerised hemithioacetal (formed by allyl mercaptan, *o*-phthalic aldehyde) and primary amine leading to the formation of isoindole complex, were also reported for the detection of creatine and creatinine [19,20]. In 2004, a synthetic monomer with Lewis acidic zinc(II) was also applied to prepare the MIP with a stereo-shape binding effect towards creatinine [21]. Many analytical methods have been reported for the analysis of creatine and creatinine in pharmaceutical formulations and biological fluids, e.g. spectroscopy [22], chemometry [23], mass spectrometry [24], fluorescence [20] and capillary zone electrophoresis [25]. Adsorption experiments to study the selectivity of creatinine-imprinted polymer in mixture solutions (consisting with different analogue compounds, for instance, creatine, *N*-hydroxysuccinimide, and 2-pyrrolinidone) were recently reported [26,27]. In these experiments, high performance liquid chromatography was found to be most suitable detection tool to simultaneously analyse the solution containing creatinine and its analogue compounds. The first reversible chemosensor to creatinine [12], based on artificial chemoreceptors and capacitive detection, displayed detection limit of 10 μM and observed no interference from NaCl, creatine or glucose. However, such impedometric (capacitive) chemosensors necessarily require an ultrathin layer of MIP grafting over the solid electrodes. It could be the irreproducibility in the film thickness which resulted in a deviation of 10% or less in experimental results [12]. Furthermore, the capacitive sensors apparently involved electrode fouling risk and therefore the deviation in capacitance data might occur with real probes.

In this paper, a MIP-modified HMDE is proposed for the selective determination of creatinine specifically from serum samples. The creatinine-imprinted polymer [abbreviated as P(Cre)] used was prepared from melamine (mel) and chloranil (chl) avoiding a higher-level of cross-linking network. It should be noted that in real time sensing applications, lower amounts of cross-linking allow better accessibility to the site [28]. The polymer P(Cre) could be regarded as an artificial receptor to recognise the target molecule by the stereo-shape ability, stoichiometric non-covalent interactions [29] as well as induced fit mutual polarisation [17] between MIP and creatinine, particularly in the aqueous and serum samples. The HMDE was preferred for electrode design, since other solid-electrodes such as mercury-film electrode and glassy-carbon electrode were proved to be highly critical owing to non-reproducible regeneration of the electrode and the excessive electrode fouling in the complex matrices of biological samples.

2. Experimental

2.1. Materials and reagents

The reagents melamine (mel), chloranil (chl), creatinine (Cre) and other chemicals (interferents) were purchased from Loba Chemie, Otto, and SD Fine, India. All chemicals were of analytical grade. The solvent dimethylformamide (DMF) was of HPLC quality. The water used in the present investigation was first demineralised and then triple distilled (conductivity range $(0.06–0.07) \times 10^{-6}$ S cm^{-1}).

2.2. Molecularly imprinted polymer preparation

The preparation and characterisation of molecularly imprinted polymer [P(Cre)] and reference non-imprinted polymer [P(Rf)] were based on the experimental methods reported elsewhere [11]. In order to study the selectivity and sensitivity of molecular imprinting, we have also studied various compositions of P(Cre) taking different molar ratios of mel, chl and template (1:1:1, 1:2:1, 2:3:3, 3:2:2) during polymerisation. The imprinting protocol (Fig. 1) presumably involved stereo-shape complementarities for template binding through non-covalent bonding interactions [11,26,30] in DMF (porogen). For template removal different solvents or mixed solvents other than water

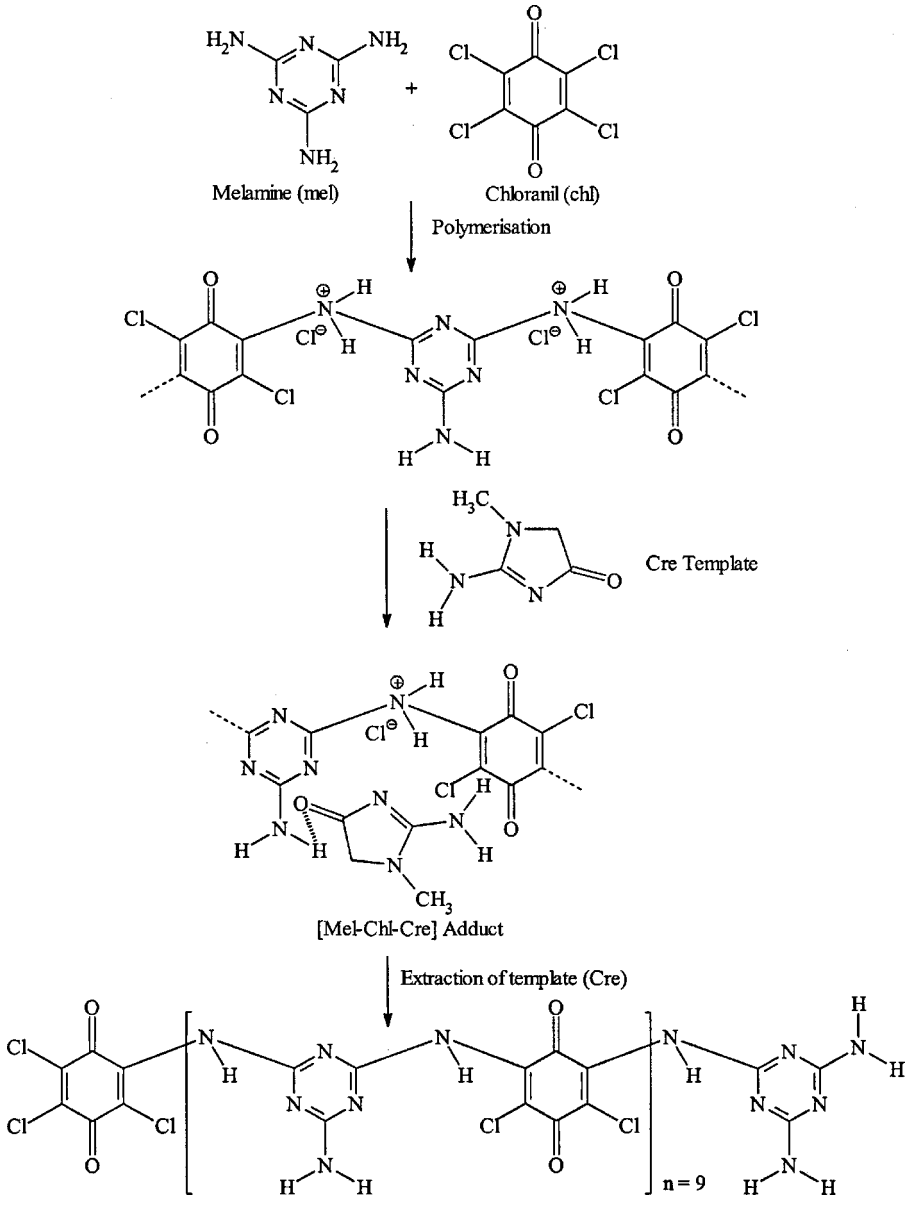

Fig. 1. Imprinted polymer with shape and functional memory [P(Cre)].

had been tried and the results were not promising. However, aqueous methanol, 10% (v/v), was found to be the most suitable solvent for the complete extraction (number of extractions 6, shaking time 10 min, 5.0 mL protions) of creatinine (polar) template from the polymer matrix. Interestingly, the molecular recognition of the creatinine in aqueous medium is most likely to proceed with the 'induced-fit' (cf., enzyme-substrate binding) (Fig. 2) [31,32] binding resulting from electronic complementarities between host and guest.

2.3. Procedure

Voltammetric measurements were performed by following the reported procedure [11] using a polarographic analyzer/stripping voltammometer (Model 264A EG & G Princeton Applied Research, USA) in conjunction with a X–Y recorder (PAR Model RE 0089) and 303A static mercury drop unit (EG & G Princeton Applied Research). The optimised amount (300 $\mu g\,mL^{-1}$) of P(Cre) in 10 mL DMF was taken into a voltammetric cell container allowing hanging mercury drop electrode (HMDE) to be submerged for 120 s at +0.4 V (versus Ag/AgCl) for electrode coating. Another cell container, containing 10 mL aqueous solution of Cre (in absence of any supporting electrolyte) was brought under this modified electrode for an optimised preconcentration period of 30 s at +0.4 V (versus Ag/AgCl) under quiescent condition. After 15 s equilibration time, differential pulse, cathodic stripping voltammograms were recorded from +0.1 V and terminated at −0.6 V (versus Ag/AgCl) at scan rate 10 $mV\,s^{-1}$ and pulse amplitude 25 mV. All runs for each concentration of Cre test analyte and subsequent quantification (standard addition method) were always proceeded with fresh mercury drops duly modified with the

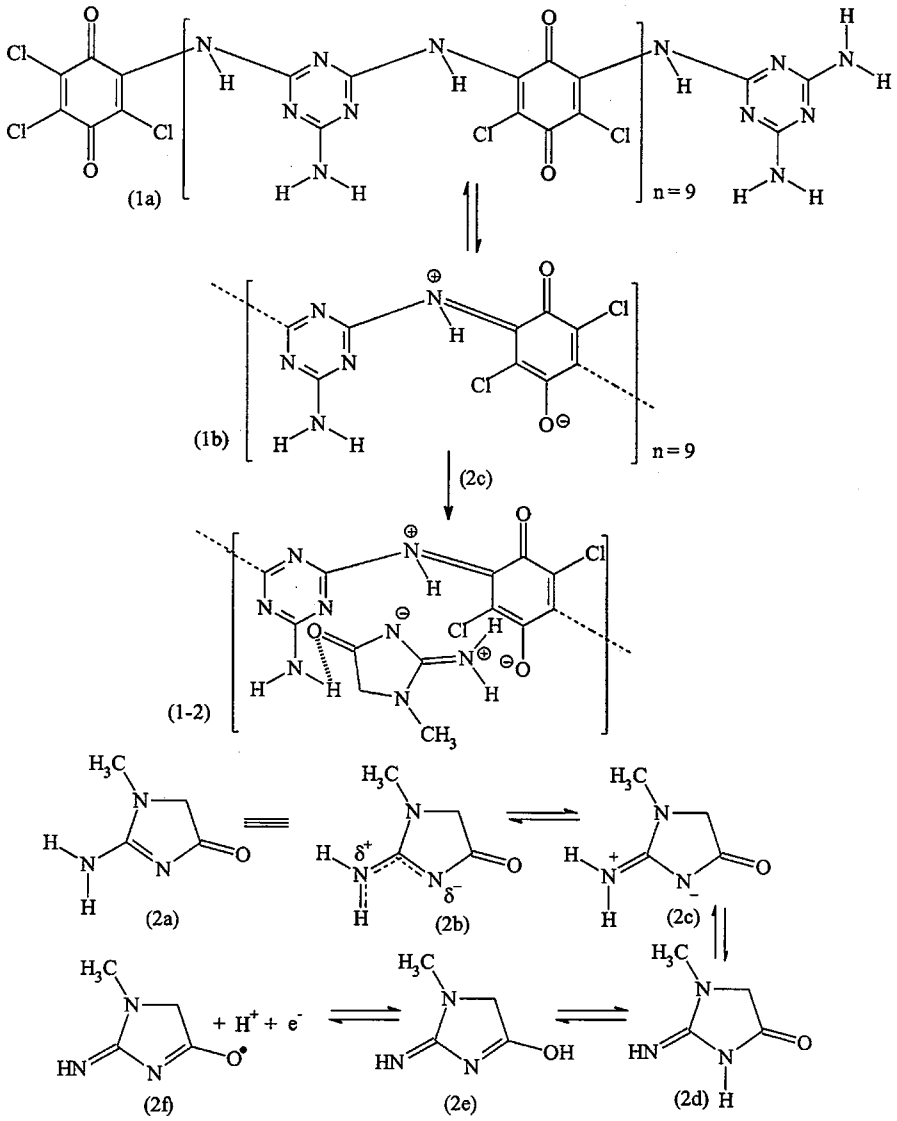

Fig. 2. Structural diagrams of possible forms of receptor and creatinine in the free and the complexed states. Form 1a is P(Cre); 1b is the rearrangement of 1a signaling receptor-template complexation (1–2) (induced fit mechanism). Diagrams 2a–e represent molecular rearrangements; 2c represent electronic distribution upon polarization of creatinine in the complexes (1–2); 2f is the Cre-radical obtained after electrochemical oxidation.

imprinted polymer at 25 ± 1 °C. Since dissolved oxygen did not interfere with the stripping voltammetry in the present instance, no deaeration was performed [33].

3. Results and discussion

3.1. Sensor development

Drop coating of the HMDE surface with a P(Cre)-DMF solution enabled preparation of modified electrode with molecular imprinted recognition capability. The approach adopted is same as described earlier [1,11]. Despite the excellent electrochemical characteristics of solid-modified electrodes, poor reproducibility is expected in terms of film thickness. The uncontrolled conformation adopted by the polymer during solidification, electrode fouling risk and critical regeneration prevent the use of drop-coating method for the production of disposable solid electrode sensor. The time consuming synthesis of MIPs and the relative lack of stability of MIP solutions limit their use as analytical tools. In contrast, HMDE was found to be a better alternative to obviate problems encountered with solid-electrodes. The imprinted polymer, P(Cre), was immobilised at the mercury drop surface via the chl and mel functionalities (>C=O and $-NH_2$) facilitating firm adherence of coating onto the positively charged surface at +0.4 V (versus Ag/AgCl) under the driving force of charge–transfer interactions. The remaining functional groups were projected outwardly making binding cavities accessible for template rebinding without any resistance. The porosity and permeability of the film were controlled by adjusting the concentration of the polymer and the template in the casting solution. The modified mercury drop could be renewed in a reproducible manner. This was evident from the fact that each voltammetric measurement was repeated thrice with a fresh HMDE duly modified with an optimised amount of 300 μg mL^{-1} P(Cre) which

Table 1
Analytical results of DPCSV measurement of creatinine (Cre) in water[a]

Cre concentration ($\mu g\,mL^{-1}$)	Cre concentration ($\mu g\,mL^{-1}$) using P(Cre)-modified HMDE				Cre concentration ($\mu g\,mL^{-1}$) using P(Rf)-modified HMDE				Imprinting factors			
	mel:chl:Cre (molar ratio)				mel:chl:Cre (molar ratio)				mel:chl:Cre (molar ratio)			
	1:1:1	3:2:2	2:3:3	1:2:3	1:1:1	3:2:2	2:3:3	1:2:3	1:1:1	3:2:2	2:3:3	1:2:3
0.00249	0.0025 (±0.06)	nd	nd	nd	nd	nd	nd	nd	–	–	–	–
0.0049	0.0049 (±0.006)	nd	nd	nd	nd	nd	nd	nd	–	–	–	–
0.02483	0.0247 (±0.15)	nd	nd	nd	nd	nd	nd	nd	–	–	–	–
5.00	5.02 (±0.01)	1.10 (±0.05)	2.05 (±0.11)	2.20 (±0.025)	1.17 (±0.53)	0.305 (±0.08)	0.559 (±0.32)	0.56 (±0.15)	4.29	3.60	3.66	3.89
14.70	14.80 (±0.11)	1.18 (±0.045)	4.88 (±0.705)	6.50 (±0.149)	2.91 (±0.08)	0.380 (±0.432)	2.32 (±0.08)	1.97 (±0.08)	5.08	3.08	2.10	3.29
28.03	28.05 (±0.05)	nd	nd	nd	6.12 (±0.07)	nd	nd	nd	4.58	–	–	–
49.03	49.90 (±0.04)	nd	nd	nd	7.20 (±0.09)	nd	nd	nd	6.97	–	–	–
58.03	58.70 (±0.08)	nd	nd	nd	8.00 (±0.28)	nd	nd	nd	7.34	–	–	–
84.10	84.10 (±0.10)	nd	nd	nd	8.95 (±0.07)	nd	nd	nd	9.40			

[a] Data in parentheses denote standard deviations based on three repeated runs (each run recorded with a fresh MIP-modified HMDE); nd, not detectable.

always responded the reproducible data (Tables 1 and 2). As the DMF solution of P(Cre) is highly stable, the conformation adopted by the polymer during solidification of the film over the HMDE surface remains intact without any cavity deformation after solvent evaporation. This was supported by a separate column chromatographic experiment in which P(Cre), as such, and P(Cre), after redissolution, in DMF had demonstrated identical imprinting effect for template retention at optimised conditions of column operations.

3.2. Different molar ratios of monomers/template in the molecular imprinting procedure

Different molar ratios of monomers (mel and chl) to template (Cre) were studied during the polymerisation. As evident from Table 1, the MIPs prepared in 1:1:1 molar ratio of monomers to template showed the quantitative adsorption of creatinine at all ranges of concentrations studied. While all the MIPs prepared in different molar ratios (other than 1:1:1) showed some Cre adsorption between 5.0 and 14.7 $\mu g\,ml^{-1}$, these polymers were found to be ineffective towards template rebinding in extreme concentration regions. On the other hand, the non-imprinted polymer, P(Rf), showed insignificant uptake of creatinine than in the case of all the MIPs studied. With the molar ratio of 1:1:1, best binding performance was achieved. It is clear from the analytical data (Table 1) that the binding capacities of the MIPs towards creatinine are drastically declined with the increase of template owing to the restricted polymerisation and moreover a steric overcrowding in the receptor network. The imprinting factors (i.e. the ratio of binding capacity of MIP for creatinine to the binding capacity of the corresponding non-MIP P(Rf) for creatinine) of the MIPs prepared from different molar ratios are listed in Table 1.At the molar ratio of 1:1:1, imprinting factors were obtained to be greater than 4.0. As the molar ratios were changed the imprinting effect declined accordingly. Hence, we may conclude that with 1:1:1 molar ratio of mel–chl–Cre, the best binding capacity as well as imprinted effect were achieved. This was supported from earlier concept of 'stoichiometric non-covalent interactions' where the interaction during the polymerisation was reportedly stoichiometric in nature [29]. Accordingly, more than 90% uptake of the template is feasible if an equimolar mixture of template and binding cavity between monomers is prepared and there is no more need to use excess binding cavities to saturate the template completely.

3.3. Voltammetric behaviour

The imprinted polymer (1:1:1), was firmly immobilized on a hanging mercury drop surface through electrostatic interactions (via Hg(II) interactions with carbonyl and amine functional groups) at +0.4 V (versus Ag/AgCl) resulting in a highly permeable monolayer during coating of 120 s. The electrode was dipped in an aqueous solution of creatinine (pH = 7.0, maintained by the addition of a few drops of $NaOH/HNO_3$) for 30 s and the cyclic voltammetry (CV) (Fig. 3) runs were scanned at a slow scan rate ($10\,mV\,s^{-1}$) in cathodic stripping mode. The *p*-chloranil incorporated in MIP film can catalyse the oxida-

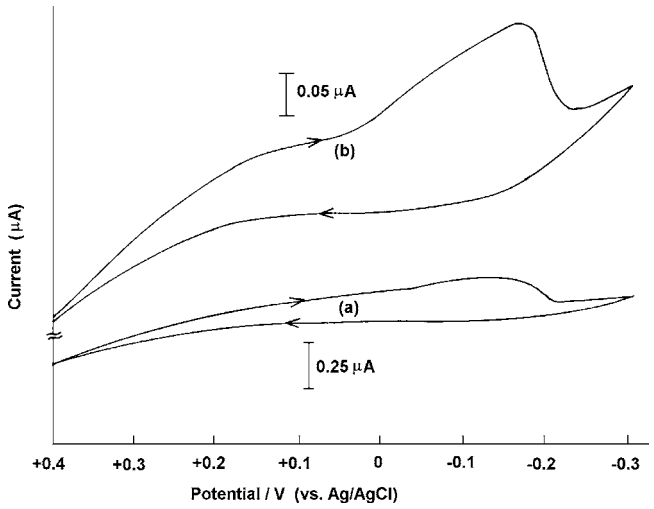

Fig. 3. Typical cathodic stripping cyclic voltammograms of Cre with MIP-modified hanging mercury drop electrode [Cre concentration; (run a) 50 μg mL^{-1}; (run b) 0.12 μg mL^{-1}; MIP concentration: 300 μg mL^{-1}; MIP and Cre preanodization potential: +0.4 V (vs. Ag/AgCl); deposition time of polymer: 120 s; preconcentration time of Cre: 30 s; pH: 7.0; scan rate: 10.0 mV s^{-1}].

tion of creatinine in aqueous solution and also it is found to be reactive toward chlorate and borate buffers [34] if used as a supporting electrolyte. Furthermore, the pre-anodisation of the modified-HMDE forbids the use of other supporting electrolytes such as KCl, KNO_3, citrate, phosphate and acetate buffers in order to avoid the possible anionic oxidation which interferes in the evaluation of electrochemical process of creatinine in the potential range studied. Therefore, no supporting electrolyte was used in this study. It has been reported that pre-anodisation can generate oxygen containing functional groups such as carbonyl, carboxylate and hydroxyl radical species in a very small quantity on the surface of electrode which can accelerate or catalyse the electrochemical process even in the absence of a supporting electrolyte [33]. In the present instance, the charge transport through redox centres was believed to occur via an electron hopping process between redox centers incorporated in the film (homogeneous electron-transfer) and eventually to the positively charged electrode (heterogeneous electron-transfer process) [35,36]. The film-entrapped creatinine molecule were readily oxidised as cre radical during preconcentration and subsequently, after 15 s equilibration time, stripped off from the electrode surface due to electrostatic repulsion (Fig. 3) during

Table 2
Analytical results of DPCSV measurements of creatinine (Cre) in human blood serum and interferent mixtures at [P(Cre)]-modified hanging mercury drop electrode

Sample	Analyte concentration (μg mL^{-1})	Determined value[a] (mean ± S.D.) (μg mL^{-1}) with MIP-modified HMDE	Recovery[b]	Relative standard deviation (%) (n = 3)	t[c]	ν[d]
Dilute human blood serum (unspiked)[e]	–	0.094 ± 0.05 (9.4)	–	–	–	–
Dilute human blood serum (spiked)[f]	0.38	0.38 ± 0.02 (0.40 ± 0.01)	100.0	5.2	t_{cal} = 3.80	1.00
	0.58	0.58 ± 0.03 (0.59 ± 0.04)	100.0	5.1	t_{tab} = 4.30	
	1.00	1.01 ± 0.01 (1.02 ± 0.03)	101.0	1.0		
Interferents[g] (in water)	0.97 (0.97 Tyr)	0.96 ± 0.01	99.0	1.0		
	1.87 (0.93 Tyr)	1.87 ± 0.01	99.9	0.5		
	0.97 (0.97 urea)	0.98 ± 0.01	101.0	1.0		
	1.87 (0.93 urea)	1.86 ± 0.14	99.5	7.5		
	0.97 (0.97 NaCl)	0.97 ± 0.01	99.0	1.0		
	1.87 (0.93 NaCl)	1.86 ± 0.02	99.5	1.1		
	0.97 (0.97 Phe)	0.98 ± 0.01	101.0	1.0		
	1.87 (0.93 Phe)	1.86 ± 0.02	99.5	1.1		
	0.97 (0.97 Glu)	0.98 ± 0.01	101.0	1.0		
	1.87 (0.93 Glu)	1.86 ± 0.13	100.0	6.9		
	0.97 (0.97 Cy)	0.98 ± 0.04	101.0	4.8		
	1.87 (0.93 Cy)	1.86 ± 0.09	99.5	4.8		
	0.97 (5.00 Crea)	0.97 ± 0.08	100.0	8.2		
	1.87 (8.00 Crea)	1.87 ± 0.13	100.0	6.9		
	0.97 (0.97 His)	0.97 ± 0.02	101.0	2.0		
	1.87 (0.93 His)	1.87 ± 0.02	100.0	1.1		
	2.81 (5.23, mix[h])	2.81 ± 0.06	100.0	2.1		

[a] Average of three replicate determinations (S/N = 3) with fresh MIP-modified HMDE.
[b] Recovery: Amount of analyte determined/amount of analyte taken.
[c] t, Student's t-test for comparison of two methods at confidence level of 95%.
[d] ν, correlation coefficient.
[e] Value in parenthesis indicates total concentration of Cre in original blood sample (undiluted) as obtained by multiplying with a dilution factor of 100.
[f] Values in parentheses indicate Cre concentration (μg mL^{-1}) determined by the standard solid phase extraction (SPE) method with P(Cre)-modified silica gel at a flow rate of 5 mL min^{-1} and pH 7.0.
[g] Values in parenthesis indicate concentration (μg mL^{-1}) of various interferent taken with Cre in aqueous mixture solution (Cy, cytosine; Ad, adenine; AA, ascorbic acid; His, histidine; Theo, theophylline; Glu, glucose; Tyr, tyrosine; Phe, phenylalanine).
[h] mix denotes mixture of NaCl, urea, Glu and Crea (concentration 5.23 μg mL^{-1} each).

cathodic scan. This could be the reason that no distinguishable anodic peak was observed on the reverse scan in spite of some adsorption of reduced product at electrode surface which gave rise to an ill-defined pre-wave to the cathodic stripping peak. The oxidation of creatinine was found to be substantial at +0.4 V. The effect of pre-anodisation of HMDE at potential ≤+0.3 V did not yield any cathodic stripping response in the present case.

In the complexes 1–2, the positively and negatively charged positions of the creatinine dipole (Fig. 2, 2b) pair with the receptor (Fig. 2, 1b) dipole's negatively and positively charged positions, respectively. Such electrostatic host–guest attraction apparently deforms the structure and alters the charge distribution of creatinine, as indicated by diagram Fig. 2c, during rebinding in aqueous medium [17]. As the recapture of the template molecule creatinine is mainly electrostatically (partly hydrogen bonding) co-ordinated to the receptor, the apparently high strength of these interactions allows analyte binding to the MIP from aqueous solution with a high affinity. Interestingly, the imprinted molecules (the oxidised form of creatinine, Cre radical) at higher concentrations were strongly adsorbed at pre-anodised MIP-coated electrode. Thus corresponding stripping current was restricted to a larger extent as compared to the lower concentration of the anlayte.

On the basis of CV behaviour as presented above, it is possible to propose a tentative mechanism (Fig. 2) for the electrochemical behaviour of creatinine at imprinted-modified HMDE. The higher electron withdrawing character of carbonyl groups as compared to imine may orient a type of keto-enol tautomerism between Fig. 2d and e. Therefore, the creatinine shown in Fig. 2e is instantaneously oxidised to the corresponding radical (Fig. 2f) at the modified electrode at +0.4 V versus Ag/AgCl.

The DPCSV runs of Cre at P(Cre)-coated HMDE are shown in Fig. 4. This depicts [as shown in Fig. 4b] multiple runs revealing the reproducible renewal of modified HMDE in the present investigation. The slight negative shift in potential at the lower concentration of analyte reveals a complexation (Fig. 2, 1–2) with high affinity for analyte binding in dilute aqueous medium. The current response in the lower concentration range primarily includes contributions from facilitated mass-transfer through electrostatic rebinding in aqueous condition. This affects the detection limit to attain as low as ng mL^{-1} level. This could be regarded as a good achievement for a MIP-based sensor. In this case the cathodic stripping of Cre radical is apparently favoured owing to the progressively increasing negative charges on the electrode. The restricted DPCSV current response in higher concentration range of analyte, like CV, could be ascribed either to the adsorption effect or the lessened contribution of migration current owing to the matrix effect of the bulk concentrated region in the absence of a supporting electrolyte.

3.4. Optimisation of analytical parameters

The optimum potential for polymer coating and creatinine rebinding was found to be +0.4 V (versus Ag/AgCl). Any potential lesser than this may cause an electrostatic repulsion at electrode/film interface owing to the induced polarisation and consequently enhanced anionic charge density of chloranil moieties in the polymeric receptor 1b (Fig. 2). An induced fit complexation by electrostatic binding to the rigid dipolar cleft suggests a better transition state stabilisation of complexes 1–2 (Fig. 2) at +0.4 V (versus Ag/AgCl) [37] than that at potentials ≤+0.3 V (versus Ag/AgCl). The maximum concentration of P(Cre) was found to be 300 μg mL^{-1} which apparently formed a thin-film monolayer coat around the mercury drop in an optimum time of 120 s. This facilitated a maximum uptake of creatinine in 30 s preconcentration time. A drastic fall in creatinine DPCSV current was observed beyond 300 μg mL^{-1} of the MIP loading probably because of slow mass-transfer and decreasing partition coefficient of test analyte from the aqueous phase to relatively thick film-layer. The thickness in the film beyond the optimum concentration of the polymer may be attributed to an intermolecular electrostatic aggregation of the rigid dipolar clefts of the receptor.

Interestingly, the reference polymer P(Rf)-modified-HMDE responded a negligible binding of creatinine below 5.00 μg mL^{-1} concentration. The current responses were

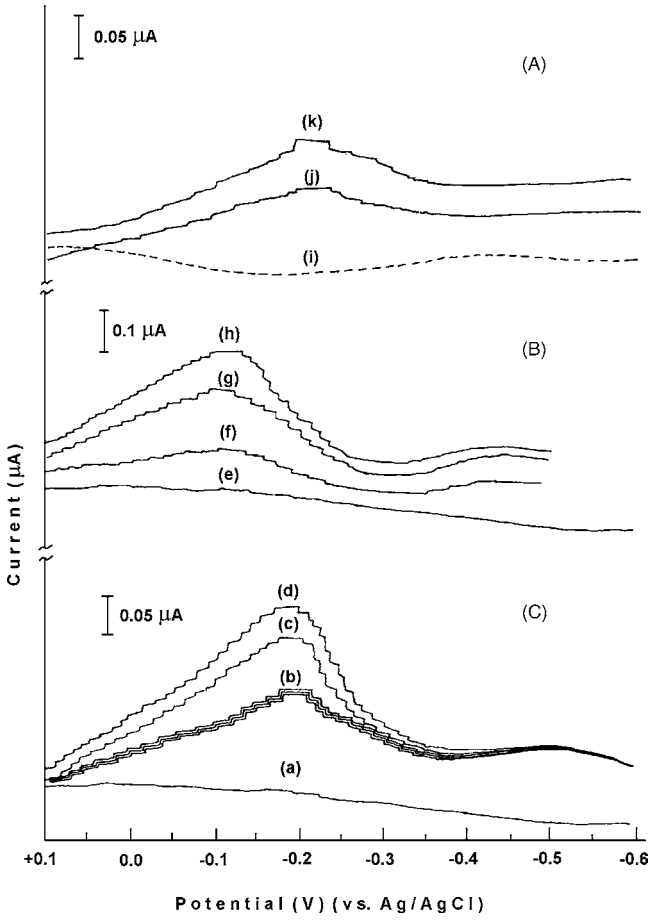

Fig. 4. DPCSV of creatinine with MIP-modified hanging mercury drop electrode in aqueous samples [Cre concentration (μg mL^{-1}): b, 0.0248; c, 0.0372; d, 0.495; f, 14.7; g, 47.93; h, 84.1] and with reference polymer P(Rf)-modified hanging mercury drop electrode [Cre concentrations (μg mL^{-1}): a, 0.0495; e, 14.7]. DPCSV in blood serum samples [Cre concentration (μg mL^{-1}): i, 0.0579 (P(Rf)-modified HMDE) and j, 0.038; k, 0.0579 (MIP-modified HMDE)]. Other conditions as in Fig. 3. DPCSV (Cre, 0.0248 μg mL^{-1}; run b) recorded for three repeated experiments (each run with a fresh MIP-modified HMDE).

reduced by one-fourth in comparison with MIP-coated electrode for Cre concentration varying from 5.0 to 84.0 μg mL^{-1}. The pH of the cell content was adjusted to neutral so as to avoid the probable hydrolysis of creatinine to creatine [38] and also to cater the need for DPCSV analysis in blood samples (pH 7.4). The average DPCSV currents were surprisingly of 10^{-2} μA (varying from 0.02–0.26 μA) order in both concentrated as well as dilute ranges of concentration under the optimised conditions (pH 7.0, P(Cre) 300 μg mL^{-1}, polymer deposition time 120 s, creatinine preconcentration time 30 s, preanodisation potential +0.4 V versus Ag/AgCl, scan rate 10 mV s^{-1}, pulse amplitude 25 mV) for the reason stated earlier. The calibration equations for creatinine were given as below:

- lower concentration range (0.0025–0.0495 μg mL^{-1});
- $I_{PC} = (4.685 \pm 0.0048)C + (0.0057 \pm 0.00087)$, $\nu = 1.00$, $n = 7$;
- higher concentration range (5.0–84.0 μg mL^{-1});
- $I_{PC} = (0.003 \pm 1.58 \times 10^{-6})C + (0.0059 \pm 0.771 \times 10^{-6})$, $\nu = 1.00$, $n = 6$.

where I_{PC} is the peak height in μA, C the concentration of creatinine in μg mL^{-1} and ν is the correlation coefficient at 95% confidence level. The limit of detection (LOD) is calculated as 1.49 ng mL^{-1} (R.S.D. 0.167%) on the basis of minimum distinguishable signals (S_m) and the slope (m) of the linear regression for lower concentrations of analyte following the equation [39]

$$\text{LOD} = \frac{S_m - \bar{S}_{bl}}{m},$$

where S_m is equivalent to the sum of mean blank signal $\bar{S}_{bl}$ plus a multiple 3 of the standard deviation of the blank (S_{bl}).

3.5. Cross selectivity studies

The DPCSV currents for creatinine and different interfering molecules such as cytosine, phenylalanine, tyrosine, urea, NaCl, glucose, histidine, creatine (Fig. 5) were studied and compared at P(Cre)-modified and P(Rf)-modified electrodes. In the case of creatinine-modified-HMDE sensor, creatinine gave a quantitative response while tyrosine and histidine were less responsive. The other interferents such as creatine, urea, glucose, NaCl, cytosine phenylalanine had shown absolutely no response. The reference polymer-modified-HMDE sensor produced no response for Cre but significant responses for all the interferents when present alone in the test solution. As regard to the mixture analysis, where most of the interferents coexists with creatinine, the creatinine uptake was found to be highly selective and quantitative at optimised conditions of analysis using P(Cre)-modified HMDE (Table 2). The ratios between the concentration of main analyte (Cre) and interferents were 1:1 and 1:2 in binary mixtures. As the major interference of creatinine detection by MIP in clinical applications might come from creatine, the binary mixture of creatinine and creatine was analysed in 1:5 concentration ratio. Insofar as multiple mixture is concerned, creatinine was analysed in a mixed solution consisted of interferents in double concentration. Here analytical results prove the selectivity of the proposed sensor over these interferents that can be generally found in the biologically fluids.

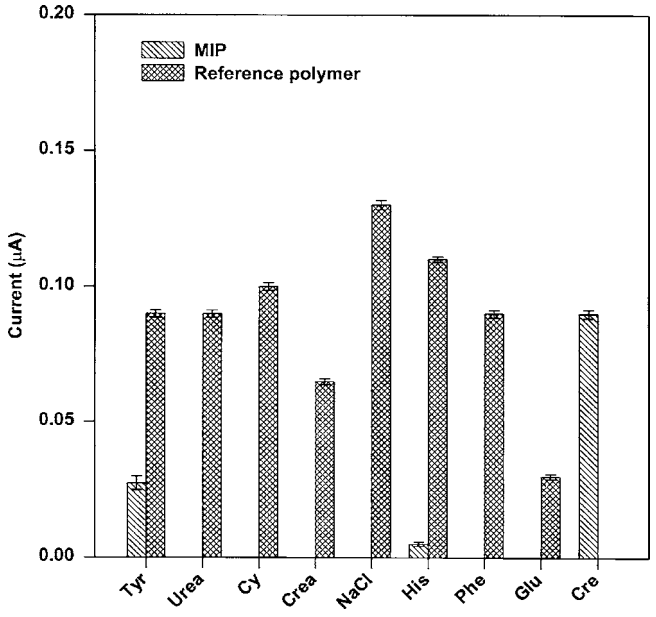

Fig. 5. Sensor response for 0.971 mg mL^{-1} solution of Cre and its interferents: tyrosine (Tyr), urea, cytosine (Cy), creatine (Crea), NaCl, histidine (His), phenylalanine (Phe), glucose (Glu) and creatinine (Cre).

4. Analytical applications

The creatinine-imprinted polymer-modified-HMDE sensor proved to be useful for the determination of creatinine in human blood serum samples (Table 2). The distortion and asymmetricity in voltammetric peak, as usually encountered due to the co-sorption of many potential interferents in human blood plasma sample, have not been found in DPCSV runs (Fig. 4) obtained with proposed P(Cre)-modified HMDE. The presence of anticoagulant species (e.g. fluoride and citrate ions) and other anions did not affect the accuracy of the desired result. The validation of proposed method was performed employing a standard technique of solid phase extraction in LC-DPCSV measurement, which revealed similar precision and accuracy of the results (Table 2) in blood serum samples on the basis of Student's t-test ($t_{cal} < t_{tab}$).

5. Conclusion

The described electrode has excellent features for the selective assay of creatinine in aqueous and biological fluids. The preparation of the electrode is simple, fast, and reproducible where the voltammetric measurement for each sample can be accomplished with a single modified mercury drop of PAR model 303A static mercury drop electrode system. The proposed method assures reliable response characteristics for the freshly renewed modified-HMDE sensor for the quantitation of DPCSV peaks.

Acknowledgements

Instrumental support from UGC-DSA programme and an UGC-SRF fellowship to one of the authors (DL) are gratefully acknowledged.

References

[1] M.C. Blanco-López, S. Gutierrez-Fernadez, M.J. Lobo-Castañón, A.J. Miranda-Ordieres, P. Tuñón-Blanco, Anal. Bioanal. Chem. 378 (2004) 1922.
[2] M.C. Blanco-López, M.J. Lobo-Castañón, A.J. Miranda-Ordieres, P. Tuñón-Blanco, Trends Anal. Chem. 23 (2004) 36.
[3] T.L. Panasyuk, V.M. Mirsky, S.A. Piletsky, O.S. Wolfbeis, Anal. Chem. 71 (1999) 4609.
[4] T. Panasyuk-Delaney, V.M. Mirsky, M. Ulbricht, O.S. Wolfbeis, Anal. Chim. Acta 435 (2001) 157.
[5] K. Sode, S. Ohta, Y. Yanai, T. Yamazaki, Biosens. Bioelectron. 18 (2003) 1485.
[6] K. Haupt, K. Noworyta, W. Kutner, Anal. Commun. 36 (1999) 391.
[7] D. Kriz, O. Ramström, A. Svensson, K. Mosbach, Anal. Chem. 67 (1995) 2142.
[8] S. Kroger, A.P.F. Turner, K. Mosbach, K. Haupt, Anal. Chem. 71 (1999) 3698.
[9] M.C. Blanco-López, M.J. Lobo-Castañón, A.J. Miranda-Ordieres, P. Tuñón-Blanco, Biosens. Bioelectron. 18 (2003) 353.
[10] B.B. Prasad, B. Arora, Electroanalysis 15 (2003) 1212.
[11] B.B. Prasad, D. Lakshmi, Electroanalysis 17 (2005) 1260.
[12] T.P. Delaney, V.M. Mirsky, O.S. Wolfbeis, Electroanalysis 14 (2002) 221.
[13] M.Z. Jaffé, Physiol. Chem. 10 (1886) 391.
[14] S. Soldin, L. Henderson, J.G. Hill, Clin. Biochem. 11 (1978) 82.
[15] N. Perakis, C.M. Wolff, Clin. Chem. 30 (1984) 1792.
[16] M.T. Jeppesen, E.H. Hansen, Anal. Chim. Acta 214 (1988) 147.
[17] T.W. Bell, Z. Hou, Y. Luo, M.G.B. Crew, E. Chapoteau, B.P. Czech, A. Kumar, Science 269 (1995) 671.
[18] K. Sreenivasan, R. Sivakumar, J. Appl. Poly. Sci. 66 (1997) 2539.
[19] S. Subrahmanyam, S.A. Piletsky, E.V. Piletska, B. Chen, R. Day, A.P.F. Turner, Adv. Mater. 12 (2000) 722.
[20] S. Subrahmanyam, S.A. Piletsky, E.V. Piletska, B. Chen, K. Karim, A.P.F. Turner, Biosens. Bioelectron. 16 (2001) 631.
[21] M. Subat, A.S. Borovik, B. Konig, J. Am. Chem. Soc. 26 (2004) 2759.
[22] A.C. Sewell, H.C. Murphy, R.A. Iies, Clin. Chem. 48 (2002) 357.
[23] P.F. Campins, L.A. Tortajada Genera, S.L. Meseger, F.G. Blasco, A.C. Sevillana, C.L. Millins, Talanta 55 (2001) 1079.
[24] T. Rozaklis, S.L. Ramsay, P.D. Whitfield, E. Ranieri, J.J. Hopwood, P.J. Meikle, Clin. Chem. 48 (2002) 131.
[25] W. Chi, Y.F. Chai, L.L. Liu, C. Yin, Y.T. Wu, Fenxi. Huaxue 29 (2001) 1144.
[26] H.A. Tsai, M.J. Syu, Biomaterials 26 (2005) 2759.
[27] R.Y. Hsieh, H.A. Tsai, M.J. Syu, Biomaterials 27 (2006) 2083.
[28] A.L. Jenkins, O.M. Uy, G.M. Murray, Anal. Chem. 71 (1999) 373.
[29] G. Wulff, K. Knorr, Bioseparation 10 (2002) 257.
[30] A. Kugimiya, T. Mukawa, T. Takeuchi, Analyst 126 (2001) 772.
[31] P. Ball, Nature 371 (1994) 202.
[32] D.E. Koshland Jr., Proc. Natl. Acad. Sci. (USA) 44 (1958) 98.
[33] X. Cai, K. Kalcher, C. Neuhold, B. Ogorevc, Talanta 41 (1994) 407.
[34] L. Meites, Polarographic Techniques, 2nd ed., John Wiley & Sons, 1965, p. 348.
[35] N. Oyama, T. Ohsaka, T. Ushirogouchi, J. Phys. Chem. 88 (1984) 5274.
[36] R.W. Murray, Molecular Design of Electrode Surfaces, Wiley, New York, 1992.
[37] J. Kraut, Science 242 (1988) 533.
[38] Y. Mo, D. Dobberpuhl, A.K. Dash, J. Pharm. Biomed. Anal. 32 (2003) 125.
[39] D.A. Skoog, F.T. Holler, T.A. Nieman, Principles of Instrumental Analysis, 5th ed., Harcourt Brace College Publishers, Florida, 1998, pp. 13–14.

Available online at www.sciencedirect.com
ScienceDirect
Talanta 70 (2006) 281–285
Talanta
www.elsevier.com/locate/talanta

Simultaneous determination of nitrite and nitrate in dew, rain, snow and lake water samples by ion-pair high-performance liquid chromatography

Yuegang Zuo [a,b,*], Chengjun Wang [a], Thuan Van [a]

[a] *Department of Chemistry and Biochemistry, University of Massachusetts Dartmouth, 285 Old Westport Road, North Dartmouth, MA 02747, United States*
[b] *University of Massachusetts, Graduate School of Marine Sciences and Technology, 285 Old Westport Road, North Dartmouth, MA 02747, United States*

Received 23 January 2006; received in revised form 12 February 2006; accepted 13 February 2006
Available online 15 March 2006

Abstract

A simple, fast, sensitive and accurate reversed-phase ion-pair HPLC method for simultaneous determination of nitrite and nitrate in atmospheric liquids and lake waters has been developed. Separations were accomplished in less than 10 min using a reversed-phase C_{18} column (150 mm × 2.00 mm i.d., 5 μm particle size) with a mobile phase containing 83% 3.0 mM ion-interaction reagent tetrabutylammonium hydroxide (TBA-OH) and 2.0 mM sodium phosphate buffer at pH 3.9 and 17% acetonitrile (flow rate, 0.4 mL/min). UV light absorption responses at 205 nm were linear over a wide concentration range from 100 μg/mL to the detection limits of 10 μg/L for nitrite and 5 μg/L nitrate. Quantitation was carried out by the peak area method. The relative standard deviation for the analysis of nitrite and nitrate was less than 3.0%. This method was applied for the simultaneous determination of nitrite and nitrate in dew, rain, snow and lake water samples collected in southeast Massachusetts. Nitrate was found being present at 4.79–5.99 μg/mL in dew, 1.20–2.63 μg/mL in rain, 0.32–0.60 μg/mL in snow and 0.12–0.23 μg/mL in lake water. Nitrite was only a minor species in dew (0.62–0.83 μg/mL), rain (<0.005–0.14 μg/mL), snow (0.021–0.032 μg/mL) and lake water (0.12–0.16 μg/mL). High levels of nitrite and nitrate observed in dew water droplets may constitute an important source of hydroxyl radicals in the sunny early morning.

Keywords: Nitrite; Nitrate; Photolysis; Hydroxyl radicals; Dew; Rain; Snow; Lake water; Ion-pair; HPLC

1. Introduction

Nitrite (NO_2^-) and nitrate (NO_3^-) are important components in atmospheric liquids and surface water because their photolysis significantly enhance the photooxidation of natural and anthropogenic pollutants by formation of hydroxyl radicals ($OH^\bullet$), the most powerful oxidant in aqueous solution [1–5]. Nitrate and its conjugated acid (HNO_3) are the end oxidative product of nitric oxide and other nitrogen species. As a major component of atmospheric aerosols, HNO_3/NO_3^- not only represents a significant nitrogen flux from the atmosphere to surface water, but also contributes substantially to the acidity of precipitation [2,6–8]. In contrast to nitrate, nitrite is only a trace component in atmospheric water droplets. However, due to the high photolytic efficiency of nitrite and its conjugated nitrous acid, HONO, the photolysis of these N(III) species has been considered a predominant source of OH radicals in the low atmosphere, particularly, in the early morning when the concentrations of other hydroxyl radical sources, such as formaldehyde and ozone, are low [1,2]. Nitrite and HONO in condensed phases are also involved in the formation of carcinogenic nitrosamines [2,9]. Given the significant influence of nitrite and nitrate on human environment and health, it is important to monitor their concentration and examine the mechanisms involved in their production, transport and decomposition in atmospheric condensed phase and surface water.

Although nitrate has been determined routinely in most rainwater surveys due to the concerns about the causes of acid rain and the eutrophication of surface water, measurements of nitrite in dew, rain, fog and cloud water are scarce [8,10–13]. The commonly used methods for nitrite determination include the spectrophotometric detection based on the Griess reaction [12,14], in which nitrite is diazotized with sulfanilamide and then reacted with *N*-(1-naphthyl)ethylenediamine to form a colored product. For the measurement of total concentration of nitrite and nitrate, it is necessary to reduce the nitrate to nitrite with copperised cadmium [15]. Nitrate concentration is then

* Corresponding author. Tel.: +1 508 999 8959; fax: +1 508 999 9167.
E-mail address: yzuo@umassd.edu (Y. Zuo).

0039-9140/$ – see front matter © 2006 Elsevier B.V. All rights reserved.
doi:10.1016/j.talanta.2006.02.034

calculated as the difference between the total inorganic nitrogen anions and nitrite. Several flow injection analysis (FIA) methods have been developed based on this spectrophotometric technique for the simultaneous determination of nitrite and nitrate [16,17]. Incomplete reduction and sample carryover have been a reported problem in the FIA analyses. The most frequently used methods for the simultaneous analysis of the nitrate and nitrite include the ion chromatography (IC) with suppressed conductivity detection [10,18,19], which requires a long analysis time if the sample contains other common anions, such as sulfate and phosphate. During the IC separation, nitrite could be partially oxidized due to the use of a mobile phase at the high pH value. Recently, capillary electrophoresis (CE) [11,20,21] is employed in the analysis of environmental and biologic samples such as rain water, human saliva and urine. In addition to traditional IC, ion-pair chromatographic methods have also been widely studied for the separation of common anions, including nitrite and nitrate [22,23]. Ion-pair HPLC methods offer, with respect to ion chromatography, advantages of relatively lower cost in both instrumentation and columns and can be advantageously employed in laboratories where only conventional HPLC systems are available. On the other hand, the theoretical column efficiency of ion-pair HPLC is better than that of an IC column, assuming that a suitable ion-pair reagent is chosen. In ion-pair LC, more parameters, such as stationary phase material, counter-ion and the concentration, pH and ionic strength of eluent, and organic modifier and the concentration, can be selected and thus provide further advantages to increase the selectivity and resolution and minimize possible interference. A comprehensive review on this technique has recently been published by Gennaro and Angelino [24]. However, little information is available on the analysis of atmospheric water samples using ion-pair HPLC.

Recently, we have reported on an indirect photometric ion-pair HPLC method for the analysis of sulfur and nitrogen anions in atmospheric liquids [13]. Because both nitrite and nitrate ions have large molar absorption coefficients in the short UV wavelength region, a direct spectrophotometric detection would generate a high selectivity and sensitivity for the measurement of these nitrogen species. In this paper, we describe a direct spectrophotometric ion-pair HPLC method for the simultaneous analysis of nitrite and nitrate in dew, rain, snow and surface water samples.

2. Experimental

2.1. Chemicals

Standards of sodium nitrite was purchased from Baker Chemical Co. (Phillipsburg, NJ, USA) and sodium nitrate from Fisher Scientific (Fair Lawn, NJ). Tetrabutylammonium hydroxide (TBA-OH) titrant (0.4 M in water, HPLC grade) and sodium phosphate were obtained from Acros Organics (Geel, Belglum, NJ). Acetonitrile was supplied by Pharmco Products (Brookfield, CT, USA). Except where noted, all reagents were of analytical grade and all solution preparations were made using doubly distilled-deionized water.

2.2. Samples

Snow, rain, and dew water samples were collected during the periods from January to June 2004, and from September 2005 to January 2006 with a Teflon container or film on the roof of Building Group-II or on the grass of the University of Massachusetts Dartmouth campus, North Dartmouth, MA. Lake water samples were collected from Buttonwood Park, New Bedford, and North Dartmouth, MA. After sampling, snow samples were stored at −20 °C; rain, dew and lake waters at 4 °C in the dark until used. The samples were centrifuged and filtered through 0.45 μm membrane filters (Fisher Scientific brand) before HPLC analysis. Precautions have always been taken to minimize sample contamination. All sample containers, glassware and filtration devices were thoroughly cleaned with 0.1 M HCl solution and then finally with doubly distilled-deionized water. The blank chromatograms with the doubly distilled-deionized water have shown no nitrite peak and nitrate below 10 μg/L.

2.3. HPLC analysis

A Dionex high-performance liquid chromatograph (Dionex Corporation, Sunnyvale, CA, USA) equipped with a P680 HPLC pump, a UVD-170U spectrophotometer detector, a Gina 50 autosampler, and Chromeleon 6.60 software was used for all experiments. Some of HPLC analyses were conducted with Beckman liquid chromatograph equipped with a Model 125 dual solvent pump, a 168 photodiod array detector, a 508 autosampler and Gold Nouveau Software. The analytical column used was a Phenomenex C_{18} reversed-phase column (150 mm × 2.00 mm i.d., 5 μm particle size) guarded by a 10 mm C_{18} guard column. The anions of interest were separated using an isocratic elution program. The mobile phase was made up of 83% 3.0 mM TBA-OH titrant and 2.0 mM sodium phosphate buffer at pH 3.9 and 17% acetonitrile organic solvent. The flow rate was 0.4 mL/min. Detection of nitrite and nitrate anions was carried out by direct UV absorbance at 205 nm.

A series of 1.5 mL standard mixture solutions of nitrite and nitrate were prepared from individual standard stock solutions. Twenty microliters of water samples or standard solutions was directly injected onto the HPLC system.

3. Results and discussion

3.1. Chromatographic separation

Charged surfactants have been widely used as mobile phase modifiers to improve the partitioning characteristics of charged solutes in reversed-phase HPLC. Various studies have been made to identify the interactions that occur between charged surfactants and ionic solutes and two retention mechanisms have been proposed. The first assumes ion-pair formation in the mobile phase prior to its adsorption on to the non-polar stationary phase, while the second assumes the hydrophobic surfactant ion is held on the surface of the hydrophobic stationary phase, and the ionic solute is retained by electrostatic attraction to the charged hydrophobic surfactants. In an earlier study, we developed a

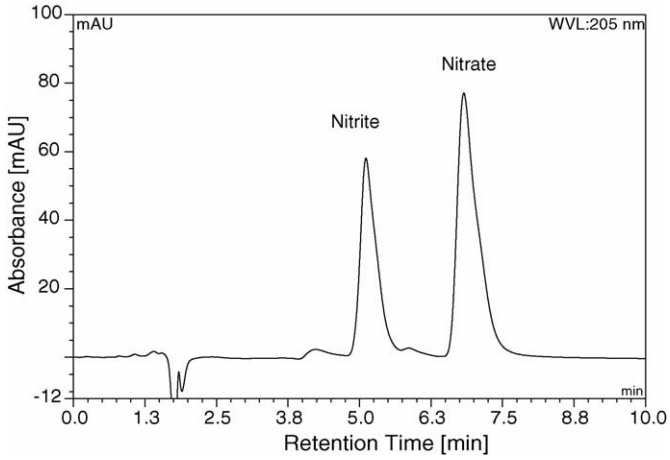

Fig. 1. Chromatogram of nitrite and nitrate standard mixture. NO_2^- and NO_3^- concentration: 6.00 μg/mL and injection volume: 20 μL.

successful method for the simultaneous determination of common sulfur, and inorganic nitrogen anions in atmospheric water samples based on this second mechanism, in which the stationary phase was recoated about every another month depending on the number of samples analyzed and their matrix complexity [13]. In this work, the short chain TBA-OH was selected to form hydrophobic ion-pairs with analyte anions to be separated in a reversed phase C_{18} HPLC column and the ion-pairs were determined using a direct photometric method. Fluoride, chloride, sulfate and sulfite are optically transparent, do not interfere the UV absorbance measurement and thus make the simultaneous determination of nitrite and nitrate with the above mentioned first mechanism possible and easier. After systematic experiments on the several mobile phase variables, including the concentration of TBA-OH, the CH_3CN/H_2O ratio (from 5% to 50%), pH of the mobile phase and mobile phase flow rate, the separation conditions were optimized and described in Section 2.

Fig. 1 shows the separation of a standard mixture of nitrite and nitrate. A good separation can be achieved in a short elution time less than 8 min. The chosen wavelength of 205 nm provides a higher sensitivity with a clean chromatogram than the wavelength of 254 or 225 nm employed in previous studies [25,26]. Nitrate in the mobile phase used in this study has a molar absorptivity of 852 L mol^{-1} cm^{-1}, and nitrite 401 L mol^{-1} cm^{-1} at 205 nm. Acetonitrile has a short absorption wavelength cut-off and was used as an organic solvent in mobile phase.

3.2. Quantitative analysis

In atmospheric liquids the concentration of nitrite is usually below 1.00 μg/mL, while nitrate has a much broader concentration range. Therefore, the calibration curve for the analysis for nitrite was made in the concentration range of 0.00–10.0 μg/mL, and for nitrate anion in the range of 0.00–1.00 × 10^2 μg/mL. Calibration curves for both nitrite and nitrate were linear over the concentration ranges tested. For nitrite a typical calibration curve followed the equation: peak area = $4.098C_{NO_2^-} - 0.001$ with a correlation coefficient of $R^2 = 0.998$ while for nitrate: peak area = $5.414C_{NO_3^-} + 1.074$ with $R^2 = 0.999$.

The mean values of retention time for nitrite and nitrate determined in standard mixtures were: nitrite 5.093 ± 0.006 min; nitrate 6.812 ± 0.012 min, respectively. The relative standard deviation (R.S.D.) values of the retention times and peak areas were generally smaller than 1%, indicating that the separation method developed was very stable and had high reproducibility. The relative standard deviations for the intra- and inter-analysis of nitrite and nitrate are less than 3.0% and 4.2%, respectively. The detection limit measured as three times the background noise was 10 μg/L NO_2^- and 5 μg/L NO_3^-. These detection limits are significantly lower than those reported for ion chromatography with a suppressor column or indirect photometric ion-pair HPLC. Increasing the injection volume of sample can further lower the detection limits.

3.3. Determination of nitrite and nitrate in dew, rain, snow and lake waters

The described method was tested in several atmospheric water matrices with known amounts of nitrite and nitrate added, and the average percentage recovery was found to be 98–101% for both analyte ions. Figs. 2–4 illustrate typical elution profile of dew, rain and lake water samples. Chromatograms of these water samples did not show interference with the same retention volume as nitrite or nitrate. Nitrite and nitrate anions were identified by matching retention times against those of standards and standard addition. In the chromatogram of lake water sample, besides nitrite and nitrate, there are two other peaks which might be due to small molecular weight organic acids but have not been identified. The concentrations of nitrite and nitrate in dew, rain, snow, and lake water samples are given in Table 1. Among all samples analyzed, the higher concentrations of both nitrite and nitrate were found in dew. This can have significant effects on vegetation and the material surfaces, since dew provides a means to hold a liquid in place for a long time (overnight) and since the concentration may further increase to a very high value during evaporation in the morning. Both nitrite and nitrate

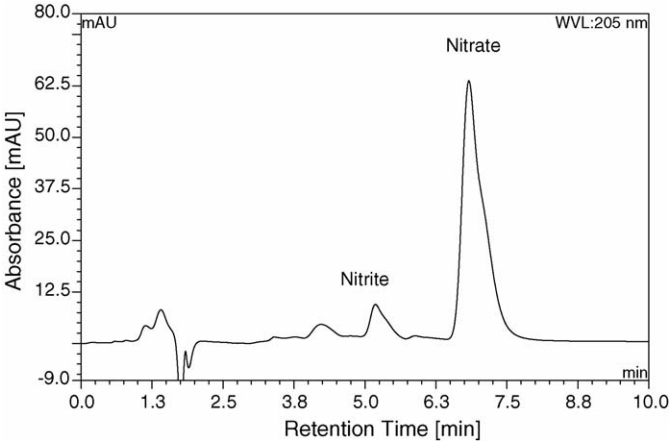

Fig. 2. Chromatogram of a dew sample.

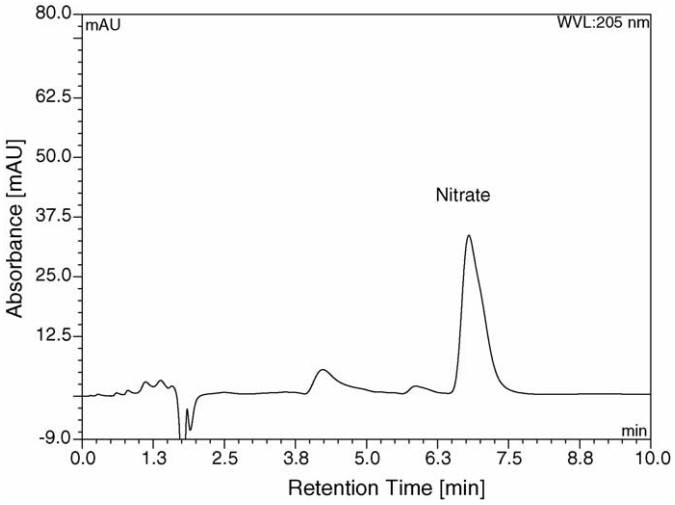

Fig. 3. Chromatogram of a rain sample.

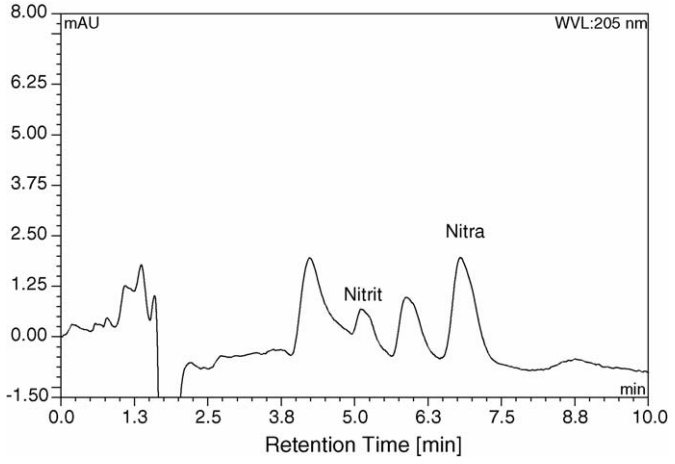

Fig. 4. Chromatogram of a lake surface water sample.

Table 1
The concentrations of nitrite and nitrate found in atmospheric and lake water samples (μg/mL)

Sample	Date of collection	pH value	Nitrite	Nitrate
Dew I	27 September 2005	6.20	0.64 ± 0.02	4.87 ± 0.15
Dew II	27 September 2005	6.32	0.62 ± 0.02	4.79 ± 0.14
Dew III	26 September 2005	6.70	0.83 ± 0.02	5.99 ± 0.18
Rain I	2 October 2005	3.86	ND[a]	2.63 ± 0.09
Rain II	2 October 2005	3.90	ND	2.62 ± 0.08
Rain III	28 May 2005	3.60	0.14 ± 0.00	1.20 ± 0.05
Snow I	29 January 2004	4.88	0.021 ± 0.001	0.320 ± 0.01
Snow II	18 January 2004	4.55	0.032 ± 0.001	0.376 ± 0.01
Snow III	12 January 2006	3.95	0.032 ± 0.002	0.60 ± 0.02
Snow IV	12 January 2006	4.02	0.026 ± 0.002	0.56 ± 0.02
Lake water I	29 September 2005	5.49	0.12 ± 0.01	0.12 ± 0.01
Lake water II	29 September 2005	5.50	0.16 ± 0.01	0.23 ± 0.02
Lake water III	29 September 2005	5.64	0.12 ± 0.01	0.14 ± 0.01
Lake water IV	29 September 2005	5.57	0.12 ± 0.01	0.17 ± 0.01

[a] ND, not detected.

undergo rapid photolysis under sunlight irradiation to form OH radicals:

$$NO_2^- + H_2O + h\upsilon \rightarrow {}^{\bullet}OH + NO^{\bullet} + OH^- \quad (1)$$

$$NO_3^- + H_2O + h\upsilon \rightarrow {}^{\bullet}OH + NO_2 + OH^- \quad (2)$$

Due to the high reactivities of hydrogen peroxide, organic peroxides and hydroxyl radicals, these photooxidants have been suggested to cause oxidative stresses in plants and be responsible for the forest decline observed in Europe, North American and Japan [27–29]. Among all the oxidants, the OH radical is known to be the most reactive one.

Nitrite and nitrate in dew and other wet precipitation could arise from the dissolution of HNO_2 and HNO_3 in the gas phase or in the atmospheric aerosols. The reactions of nitrogen oxides in water droplets can also be an important source:

$$NO + NO_2 + H_2O \rightarrow 2HNO_2 \quad (3)$$

$$2NO_2 + H_2O \rightarrow HNO_2 + HNO_3 \quad (4)$$

A reaction between NO_2 and bisulfite in water droplets could account for the formation of considerable amount of nitrite. On the other hand, the nitrite deposited and/or formed in dew water can be recycled into the mixing layer, due to the high volatility of ammonium nitrite. In this sense, the wet surface can be considered to be an active sink during the night and a source of nitrite during early morning. Given the importance of nitrite and nitrate in the atmospheric gas and liquid phase chemistry and on the health, further studies on the sources, concentration variation, transformation and fate of these nitrogen species in dew and other atmospheric precipitation is urgently needed.

4. Conclusions

The described direct photometric ion-pair HPLC method has been proved a rapid, sensitive, and accurate technique for the simultaneous determination of nitrite and nitrate. This method was successfully applied to the quantitative measurement of nitrite and nitrate in dew, rain, snow and natural surface waters. Among the samples analyzed, dew water contains high levels of nitrite and nitrate.

Acknowledgements

The authors would like to thank Dr. T. Wu, L. Zhang and J. Kang who performed some preliminary experiments. This work was partly supported by the National Science Foundation under grant ATM 9984755.

References

[1] Y. Zuo, Y. Deng, Chemosphere 36 (1998) 181.
[2] B.J. Finlayson-Pitts, J.N. Pitts, Chemistry of the Upper and Lower Atmosphere, Academic Press, San Diego, 2000.
[3] X.L. Zhou, H.J. Beine, R.E. Honrath, J.D. Fuentes, W. Simpson, P.B. Shepson, J.W. Bottenheim, Geophys. Res. Lett. 28 (2001) 4087.
[4] H. Jacobi, T. Annor, E. Quansah, J. Photochem. Photobiol. A: Chem., in press.

[5] R.G. Zepp, J. Hoigné, H. Bader, Environ. Sci. Technol. 21 (1987) 443.
[6] Y. Deng, Water Res. 32 (1998) 2249.
[7] Y. Deng, Y. Zuo, Atmos. Environ. 33 (1999) 1469.
[8] N. Poor, R. Pribble, H. Greening, Atmos. Environ. 35 (2001) 3947.
[9] J.N. Pitts, D. Grosjean, K.A. van Cauwenberghe, J.P. Achmid, D.R. Fritz, Environ. Sci. Technol. 12 (1978) 946.
[10] G. Lammel, G. Metzig, Chemosphere 37 (1998) 1603.
[11] Y. Deng, D. Hatahet, K. Douglas, M. Krzyaniak, Proceedings of the 229th American Chemical Society Annual Meeting, San Diego, CA, March 13–17, 2005.
[12] M.A. Rubio, E. Lissi, G. Villena, Atmos. Environ. 36 (2002) 293.
[13] Y. Zuo, H. Chen, Talanta 59 (2003) 875.
[14] G. Ellis, I. Adatia, M. Yazdanpanah, S.K. Makela, Clin. Biochem. 31 (1998) 195.
[15] L.C. Green, D.A. Wagner, J. Glogowski, P.L. Skipper, J.S. Wishnok, S.R. Tannenbaum, Anal. Biochem. 126 (1982) 131.
[16] R.T. Masserini Jr., K.A. Fanning, Marine Chem. 68 (2000) 323.
[17] A.A. Ensafi, A. Kazenzadeh, Anal. Chim. Acta 382 (1999) 15.
[18] P. Doble, P.R. Haddad, J. Chromatogr. A 834 (1999) 189.
[19] EPA Method 300.0, Determination of Inorganic Ions by Ion Chromatography, United States Environmental Protection Agency, Cincinnati, OH, 1993.
[20] G. Zunic, S. Spasic, Z.J. Ivanovic, J. Chromatogr. B 727 (1999) 73.
[21] N. Öztekin, M.S. Nutku, F.B. Erim, Food Chem. 76 (2002) 103.
[22] V. Rizzo, L. Montalbetti, A.L. Rozza, W. Bolzani, C. Porta, G. Balduzzi, E. Scoglio, R. Moratti, J. Chromatogr. B 798 (1998) 103.
[23] V. Jedlickova, Z. Paluch, S. Alusik, J. Chromatogr. B 780 (2002) 193.
[24] M.C. Gennaro, S. Angelino, J. Chromatogr. A 789 (1997) 181.
[25] Z. Iskandaranl, D.J. Pietrzyk, Anal. Chem. 54 (1982) 2427.
[26] D. Connolly, B. Paull, Anal. Chim. Acta 441 (2001) 53.
[27] D. Moller, Atmos. Environ. 23 (1989) 1625.
[28] C.N. Hewitt, G.L. Kok, R. Fall, Nature 344 (1990) 56.
[29] T. Kobayashi, N. Natanani, T. Hirakawa, M. Suzuki, T. Miyake, M. Chiwa, T. Yuhara, N. Hashimoto, K. Inoue, K. Yamamura, N. Agus, J.R. Sinogaya, K. Nakane, A. Kume, T. Arakaki, H. Sakugawa, Environ. Pollut. 118 (2002) 383.

Available online at www.sciencedirect.com
ScienceDirect
Talanta 70 (2006) 286–292
Talanta
www.elsevier.com/locate/talanta

Influence of different extraction methods on the yield and linalool content of the extracts of *Eugenia uniflora* L.

Mário S. Galhiane [a], Sandra R. Rissato [a,*], Gilberto O. Chierice [b], Marcos V. Almeida [c], Letícia C. Silva [a]

[a] *Department of Chemistry, Paulista State University (UNESP), P.O. Box, 473, 17033–360, Bauru (SP), Brazil*
[b] *Department of Chemistry, University of São Paulo (USP), São Carlos (SP), Brazil*
[c] *Department of Bioengineering, University of São Paulo (USP), São Carlos (SP), Brazil*

Received 3 November 2005; received in revised form 14 February 2006; accepted 14 February 2006
Available online 3 April 2006

Abstract

This work has been developed using a sylvestral fruit tree, native to the Brazilian forest, the *Eugenia uniflora* L., one of the Mirtaceae family. The main goal of the analytical study was focused on extraction methods themselves. The method development pointed to the Clevenger extraction as the best yield in relation to SFE and Soxhlet. The SFE method presented a good yield but showed a big amount of components in the final extract, demonstrating low selectivity. The essential oil extracted was analyzed by GC/FID showing a large range of polarity and boiling point compounds, where linalool, a widely used compound, was identified. Furthermore, an analytical solid phase extraction method was used to clean it up and obtain separated classes of compounds that were fractionated and studied by GC/FID and GC/MS.

Keywords: *Eugenia uniflora* L.; Extraction; Gas chromatography; Linalool

1. Introduction

The development of organic chemistry took place along with the study of plants, mainly in the 19th century, when the first studies on plants were scientifically recorded. This ended up in the isolation of some plants active principles, then, known as medicinal ones. Out of these studies, some efficient active principles were obtained, and even today, are employed in the treatment of certain diseases, e.g. morphine, quinine, camphor and cocaine [1,2].

Nature, in general, has yielded most known organic substances. Therefore, it is the vegetal kingdom that has contributed, in a more meaningful way, to the supply of useful substances for the treatment of human diseases [3]. The fantastic variety and complexity of plant bio-synthetized special metabolites, would have formed and evolved as a defense mechanism of these plants to environmental conditions, rich in microorganisms, insects, animals and also to adaptation and regulation conditions [4]. Thus, plants comprise an enormous laboratory of organic synthesis, as a result of millions of years of evolution and adaptation on Earth.

In the 1900s, the advent of antibiotics produced through microbe fermentation and the remarkable development of synthetic pharmacologicals, soon after World War II, markedly reduced the use of medicinal plants and consequently, the investment in pharmacologicals deriving from plants. In the last decades, a great change in the paradigm of western societies has caused plant products to play, once again, an important role in great populations of developed and developing countries.

Holding an extremely profitable market, the phytopharmacologicals have relighted the interest of the pharmaceutical industry in products coming from a vegetal origin. Around 1990, it was estimated that about 80% of the world population sought, in the plants, the main source of medicine [5]. It is proved, today, that a great part of the world population, mainly those from developing countries, uses as medicine, extracts or portions deriving from plants.

For some authors, out of the 200,000 species which might exist in Brazil, at least half may have some therapeutical property, but less than 1% of these, has been, so far, the object

* Corresponding author. Tel.: +55 14 3103 6135; fax: +55 14 3203 2856.
E-mail address: srissato@fc.unesp.br (S.R. Rissato).

0039-9140/$ – see front matter © 2006 Elsevier B.V. All rights reserved.
doi:10.1016/j.talanta.2006.02.040

of suitable studies. Many substances, coming exclusively from Brazilian plants, have been patented by foreign companies or governmental organs [6].

Essential oil or simply essence, are volatile oils of diverse chemical composition, which derive from vegetal materials, giving them their main odors [7,8]. The manufacturers of perfume, cosmetics and food aromatizing, nearly absorb the totality of natural essences and respective derivatives a fact that justifies the high technical level reached in their preparation and the elevated economic value which they represent. Paint and varnish industries consume important amounts of some essences and they are utilized in medicine, in the formulation of antiseptics, antispasmodics, inhalants, analgesics [7]. Furthermore, the essential oils are, almost always, bacteriostatic and often bactericide. [9].

The *Eugenia uniflora* L., the main object of this research, belongs to the Mirtaceae family [10]. The pitanga tree is a sylvestral fruit native to the Brazilian jungles, found in a range that reaches from the Guianas to the State of São Paulo; it does not survive in Southern States [11,12].

The leaves of the *Eugenia uniflora* L. are utilized in popular medicine, in infusion, in the treatment of fever, rheumatism, stomachic diseases, disorders of the digestive tract, hypertension, yellow fever and gout; to reduce weight, diminish blood pressure, act as a diuretic [13–16]. Studies have shown the odor of the leaves to have repellent properties [15]. In addition, the infusion of the fresh leaf and the green fruit is used to combat malaria and the aqueous extract of the dry leaf is utilized as a menstrual stimulant [14].

The present study aimed at assessing the influence of different extraction and purification methods on the yield and composition of *Eugenia uniflora* L.'s essential oil. The extracts obtained were submitted to analysis by high-resolution gas chromatography coupled to a flame ionization detector (GC/FID) and the results discussed.

2. Material and method

2.1. Samples

Fully grown leaves of *E. uniflora* were collected from plants cultivated on the campus of the Paulista State University, Bauru, SP, in April 2005. Plant materials were authenticated by Dr. Osmar Cavassan, Biology Department, where voucher specimen no. 2148 was deposited.

Fresh leaves, found in an intermediate position between the top (canopy) and the base of a tree, were randomly collected, always at the same time (7:30 AM). The samples were immediately sent to the laboratory to undergo the drying and extraction procedure.

The leaves were dried for 7 days, in a naturally ventilated site, sheltered from the sun, under a controlled temperature and powdered in stainless steel-cutting bladed mills, at 3800 RPM.

Following the grinding process, the samples were sifted in the GOWMAC system with sieve meshes varying between 1 and 50, being the intermediate portions used.

Fig. 1 presents a diagram with the main phases performed in the extraction, purification and analysis processes to obtain the essential oil of *Eugenia uniflora* L.

2.2. Extraction

Aiming at evaluating the best way to extract the essential oil from the *Eugenia uniflora* L. plant, four different extraction

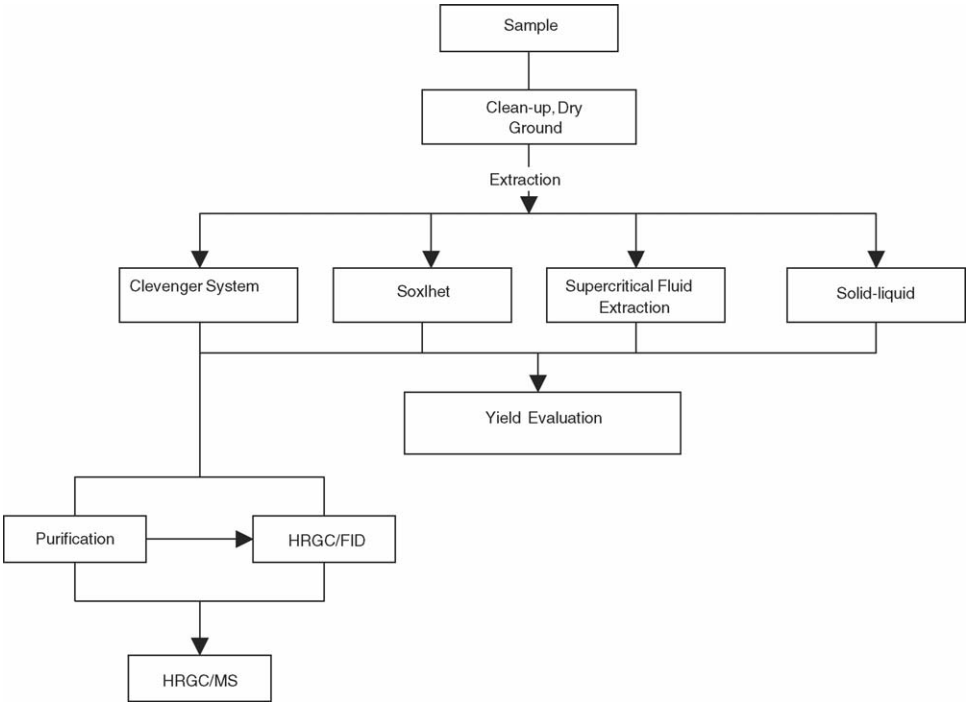

Fig. 1. Diagram of extraction, purification and analysis of *Eugenia uniflora* L. essential oil.

processes were utilized: solid–liquid, Clevenger system, Soxhlet and extraction with a supercritical fluid (SFE). The oil yield (quantitative analysis) for the tested extractions was calculated by dividing the mass obtained by the initial mass and the time of extraction (in hours).

2.2.1. Solid–liquid extraction

1.20 g of previously ground leaves were placed in a becker (250 mL) with 200 mL of distilled water under constant agitation, for 30 min, in a 45 °C temperature. Then, the extract was filtered and submitted to liquid–liquid extraction with 80 mL of petroleum ether (proposed solvent). The mixture was shaken and the operation repeated five times, so as to favor, at the maximum, the partition between the two solvents of opposed polarities, resting for 20 min to allow the separation between the two phases.

The phases were separated by the simple collection performed through the opening of the funnel's faucet. The aqueous phase was eliminated and discarded. The organic phase (clearer) was collected and submitted to concentration under a nitrogen flow and room temperature and the extract submitted to evaluation phases.

For the same purpose, different volumes of the partition solvent were tested for the same solid–liquid method, as follows.

2.2.2. Solid–liquid extraction

2.20 g of previously ground leaves were extracted with 200 mL of distilled water, for 30 min, at a temperature of 45 °C under constant shaking, being decanted for a 20-min period, in the becker itself. The aqueous part of the decanted mixture was placed in a separation funnel and the petroleum ether partition solvent was added into two portions: 40 and 20 mL, being repeated the previously described procedure. Following the collection, the organic extracts were combined, concentrated under a nitrogen flow and then, submitted to the evaluation phases.

2.2.3. Clevenger system

Thirty grams of previously ground leaves were extracted with 300 g of distilled water (proportion 1:10, m/m) in a round bottom flask at a controlled temperature (98 °C).

The study of extractions in the Clevenger system was performed in different periods: 1, 2, 3 and 4 h. The essential oil obtained was, then, submitted to evaluation.

2.2.4. Supercritical fluid extraction

SFE was carried out in the dynamic mode (the fluid passes, continuously, through the extraction cell which contains the sample) in an ISCO–SFX™ 220–Supercritical Fluid Extractor and Controller SFX™ 200 equipment. 2.5 g of ground leaves (30 mesh) were submitted to extraction using 50 mL of CO_2 as the fluid extractor, in supercritical state, in different pressures (27.58, 34.47, 41.37, 48.26, 55.16, 62.05 MPa) at flow rate of 10 mL/min during 10 min A fused-silica capillary tube (30 cm × 100 μm i.d.) was attached to the outlet of the extractor as a restrictor and the extracts were collected in an ice-cooled vial containing acetone.

After each extraction, the essential oil obtained was collected, remaining at room temperature for total CO_2 evaporation. The evaluation of the gravimetric yield was performed in relation to the initial mass, in each pressure studied.

2.2.5. Soxhlet extraction

Seven grams of previously ground leaves were inserted in a cellulose cartridge on which a piece of silanized glass wool was placed (enough to fill the cartridge). After preparing the sample, the cartridge was inserted into the Soxhlet apparatus, utilizing as the solvent, 92%-commercial ethanol, at approximately 98 °C for 4 h. The extract obtained was concentrated in a rotary-evaporator under a reduced pressure, at the temperature of 50 °C until dryness and submitted to evaluation.

2.3. Linalool purification and isolation

For the posterior application of the oil to accomplish the Lethal Dose test and other biological tests as well, the procedures to purify the sample and isolate the active principle were performed utilizing silica gel adsorption chromatography. This procedure was initially developed with a study on the extract's chromatographic behavior in the presence of solvents from different dielectric constants in thin layer chromatography (TLC). In a second step, after determining the solvent, an elution study was performed in little fractions, to define the quantity of solvent suitable for the elution procedure of compounds of interest.

Procedure: 10 g of silica gel, previously activated at 140 °C, for 4 h, were added to a preparatory liquid chromatography column, being conditioned with 50 mL of *n*-hexane, and the sample added to the column, eluted with *n*-hexane/ether (30:70, v/v) in 25 fractions of 3 mL. The extract was collected in a round bottom flask and concentrated until dryness in a rotary evaporator, under reduced pressure, at 50 °C. The extracts were finally diluted in 1 mL of hexane and submitted to analysis by GC/FID and GC/MS.

2.4. Identification of compounds

The identification of some constituents of the essential oils was achieved based on their retention indexes (determined in relation to a series of normal alkanes), and by comparison of their mass spectral fragmentation patterns (NIST database/ChemStation data system) [17], and literature data [18,19].

The results accomplished through mass spectrometry, showed the presence of linalool, which was corroborated by the injection and comparison of chromatographic retention time with its analytical standard. Thus, the present study was directed so as to quantify the linalool, owing to its great applicability as a medicine.

The quantification of linalool in the samples studied was performed by external standard method. A primary linalool standard was prepared in acetone, in concentrations of 0.1, 0.5, 1.0, 2.0 and 3.0%, being analyzed through GC/FID, so as to obtain the analytical curve.

2.5. Analysis

2.5.1. GC/FID

The extracts obtained in the studied extraction methods were solubilized in ethanol/water (1:20, v/v), being the sample volume injected, 1 μL. The analyses were performed in a HP 5890 Series II Chromatographer, equipped with a flame ionization detector and a chromatographic column CW-20 (Carbowax 20 M), length 50 m; internal diameter 0.22 mm and film thickness 0.35 μm. The operating conditions were as follows: initial temperature 40 °C (2 min), increased at 8 °C/min to 250 °C, kept for 1 min, then increased at 12 °C/min to 290 °C for 8 min; injector temperature 250 °C; H_2 carrier gas; column linear velocity (μ = 45 cm/s) operated in the split mode 1:70; injection volume 1 μL; detector temperature 300 °C.

2.5.2. GC/MS

The extracts obtained were submitted to gas chromatography analysis in a HP 5890 Series II gas chromatographer equipped with a HP 5972 (quadruple) mass selective detector and a fused silica column LM-5, 5% phenyl 95% dimethylpolysiloxane (35 m × 0.25 mm i.d., film thickness 0.25 μm). The oven temperature was from 60 °C to 25 °C/min up to 150 °C, then 3 °C/min up to 200 °C, and 8 °C/min up to 290 °C (8 min), the temperature of the injector, 250 °C; the carrier gas Helium, operated in the "splitless" mode; injection volume, 1 μL. The mass spectrometry parameters were: electrons impact at 70 eV, source temperature 250 °C, line of transference, 280 °C, electromultiplier at 1200 V, scan rate 1.5 scan/s in the mass interval 40–600 m/s.

3. Result and discussion

Medicinal plants contribute as a natural medicine source and afford great chances for a prototype molecule to be obtained, owing to their diversity of constituents. However, countless plants which are used in phytotherapeutic preparations need a greater quality control, since the scientific literature indicates that many of these may present toxic substances or variable chemical composition [20,21].

The main purpose of the present study was to investigate the extraction and purification methods by means of chromatographic methods of analysis (GC/FID and GC/MS).

3.1. Evaluation of the extraction methods studied

Table 1 presents the mean of gravimetric yield for the *Eugenia uniflora* L.'s essential oil, obtained through various extraction methods tested. In all cases, the presence of a "waxy mass", in the bottom of the becker, probably grease and hydrocarbons of a high molecular weight obtained following solvent volatilization, was confirmed. This mass was discarded in the chromatographic analyses, due to contamination risks of the chromatographic system: column and detector, mainly.

Table 1
Mean of gravimetric yield for the essential oil of the *Eugenia uniflora* L. plant obtained through the extraction methods tested

Extraction method	Mean yield (%)
Solid–liquid	0.015
Soxhlet	0.140
Clevenger	0.416
SFE	2.950

As it can be verified, the greatest yields were obtained for the SFE method (about 3.0 g) and the Clevenger system (about 0.4 g) and the smallest yield for the solid–liquid extraction (0.015 g).

The extractions accomplished by the Clevenger system still offered different results regarding the extraction time, as shown in Table 2. As it can be seen, the extraction time is an important variable in the process to obtain the oil, for, an increase of about 350% in the yield of raw oil, obtained after 5 h of extraction, as compared to the 1-h period, was confirmed.

In order to obtain better extraction conditions, that is, the greatest oil yield, ground leaves granulemetry was assessed. Table 3 presents the results obtained for the Clevenger extraction process, utilizing various ground leaves granulemetry (5, 15 and 30 mesh). The results showed the influence of pieces' sizes, which was greater in periods of 1–3 h, with differences of up to 45% in oil yield. Nevertheless, after these periods, that is, 4 and 5 h of extraction, smaller variations on the yield of oil extraction (5–10%) were observed. An increase in the yield of oil extraction was seen in all experiments, a fact that might be related to the increase in contact surface which allows a greater quantity of extracted compounds (Fig. 2).

The results obtained through supercritical fluid extraction (SFE) are reported in Table 4 and in Fig. 3. The latter demonstrates, graphically, the essential oil yield for the *Eugenia uniflora* L. plant, obtained through SFE in different extraction experiments with pressure variation. The fluid's pressure is the main parameter which influences a SFE process [19,22]. In this work, when the pressure increased from 27.58 to 55.16 MPa, the yields of the oil studied increased in

Table 2
Extraction time × yield of the essential oil obtained through the Clevenger system, for dry leaves

Time (h)	Oil yield (%)
1	0.168
2	0.328
3	0.433
4	0.556
5	0.600

Table 3
Extraction time × yield of the essential oil obtained through the Clevenger system, for different leaf granulemetries

Time (h)	Yield (%)		
	5 mesh	15 mesh	30 mesh
1	0.080	0.098	0.102
2	0.200	0.225	0.289
3	0.322	0.336	0.394
4	0.498	0.512	0.527
5	0.522	0.558	0.569

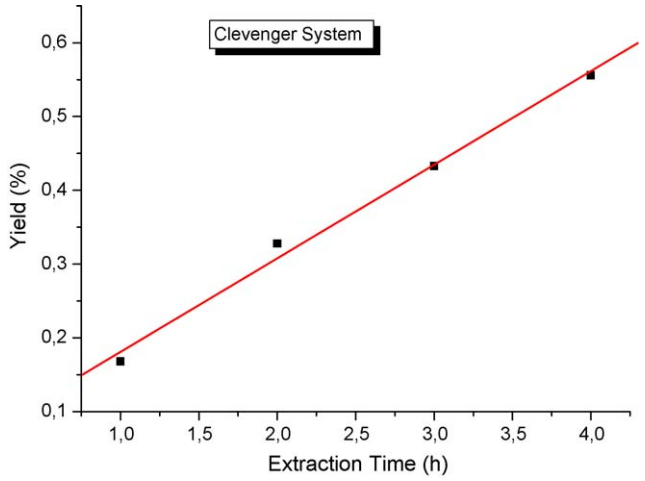

Fig. 2. Yield of the *Eugenia uniflora* essential oil obtained by Clevenger system using fresh leaves.

Table 4
Yield of the essential oil obtained through the SFE system, in different pressures

Pressure (MPa)	Yield (%)
27.58	0.832
34.47	0.500
41.37	1.044
48.26	1.548
55.16	2.512
62.05	1.268

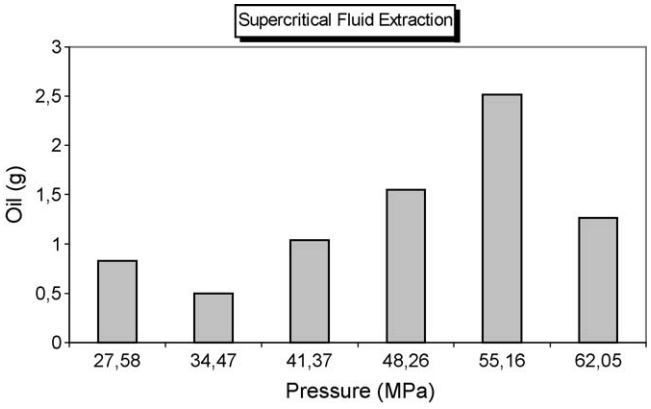

Fig. 3. Mass of *Eugenia uniflora* essential oil obtained by SFE.

about 300%. This may be related to a greater density, which increases the extraction fluid solvatation power, promoting a greater yield in oil extraction. Nevertheless, in greater densities, that is, greater pressures (62.05 MPa), the diffusion coefficient diminishes, causing a decrease in the extraction yield, owing to the kinetics of the process, which can be verified in Table 4.

Although the SFE presented an optimal quantitative yield of raw oil, the qualitative aspect was not shown to be convenient in relation to the analytes present in its composition. The diversity of the extracted compounds was probably due to the carbon dioxide's penetration strength and the conditions utilized, which showed to be little selective for our objective, besides compromising and hampering the chromatographic analysis. Hence, Clevenger was the method to present the best

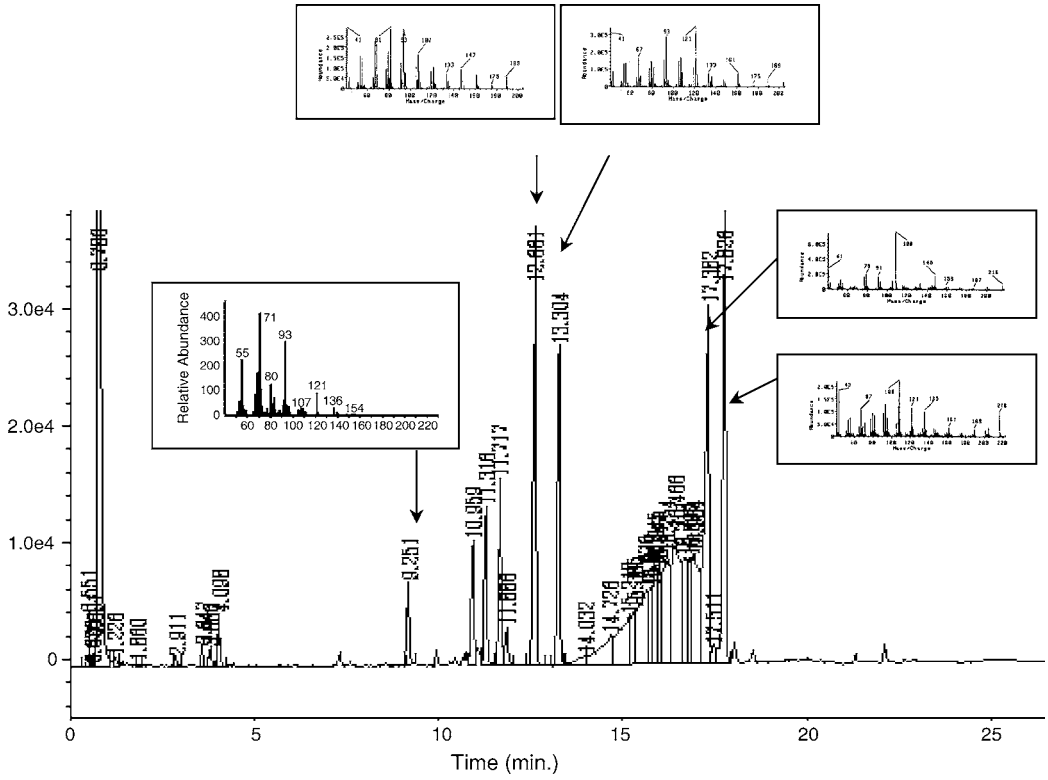

Fig. 4. Chromatogram of the *Eugenia uniflora* essential oil obtained by Clevenger system presenting the linalool and the four major compounds and their respective mass spectra.

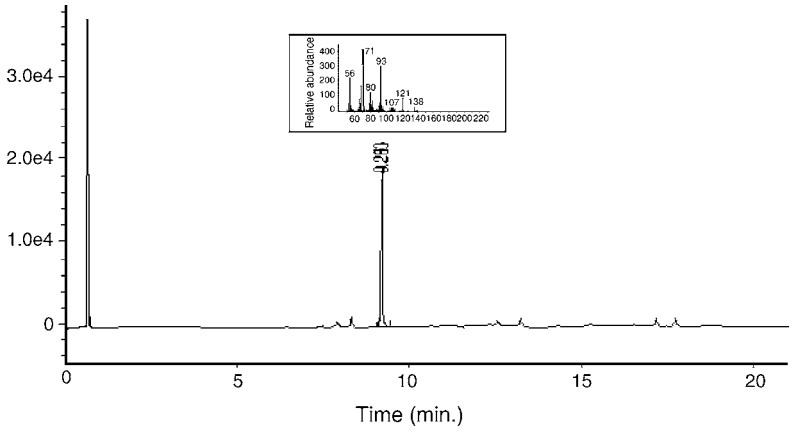

Fig. 5. Chromatogram of standard linalool at 1 μg/mL and its mass spectrum.

performance, being chosen for qualitative studies regarding its composition.

3.2. Determination of major compounds

Fig. 4 presents the chromatogram of the essential oil obtained by the Clevenger system. One can observe a great quantity of peaks, which evidence the presence of a great quantity of compounds with different polarities, since the main mechanism of separation of such column is through the value of dielectrical constant. Thus, the presence of an ample range of boiling points may be inferred, based on the programming of the temperature of the chromatograph oven.

The chromatogram of the raw essential oil (Fig. 4) obtained by GC shows various peaks, presenting four major compounds of greater concentration, which were posteriorly submitted to analysis through high resolution gas chromatography coupled to mass spectrometry. By means of a search in a database and the respective mathematical calculation in relation to the 10 peaks referring to most abundant ions in the spectrum existing in the GC/MS system, it was possible to find, experimentally, each component of interest of the essential oil.

Fig. 4 presents the chromatogram and the respective spectra of the major peaks studied in this paper.

- Cyclohexane, 1ethenyl-1-methyl;
- 1,5-Cycloundecadiene, 9-1-methylethyl;
- 5-Benzofuranacetic acid, 6-ethenyl;
- 1,2-butanediol, 1-phenyl.

The linalool compound (2,6-Dimethyl-2,7-octadien-6-ol) was also identified through the database in the GC/MS system and had its identity confirmed by the analysis of the standard, which may be observed in Fig. 5.

3.3. Purification and isolation of the linalool

The results obtained through the fractioning of the essential oil of the *Eugenia uniflora* L. plant are presented in Figs. 6 and 7. These results show that the silica's high polarity utilized in relation to the petroleum ether's polarity (*n*-hexane and other

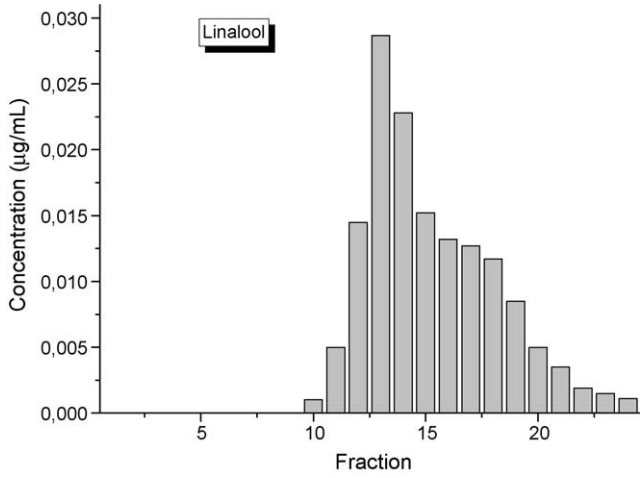

Fig. 6. Results obtained for the *Eugenia uniflora* essential oil fractioned in silica column.

hydrocarbons), enabled the retention of polar compounds and the elution of linalool, mainly in fractions of 10–24, being that fractions 1–9 did not eluate considerable quantities of the desired compound. The fractioning study was monitored by means of

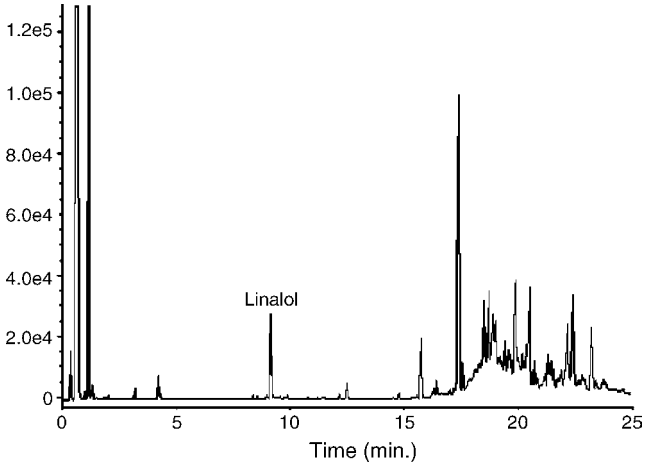

Fig. 7. Chromatogram of fraction 12 of the extract of *Eugenia uniflora* oil obtained by Clevenger system and GC/FID.

analyses carried out by GC/FID and confirmed by GC/MS, for a greater reliability of the results. Thus, it was possible to determine that the fraction of 27 initial mL could be discarded and that just another 45 mL would be necessary for the linalool, present in the sample, to be separated. This study is extremely important in plants' analytical procedures, for it contributes to a faster and more economical process, diminishing the discard of toxic solvents.

The chromatogram of Fig. 7 presents the sample of fraction 12 as an example to illustrate the purification process' effect, showing great efficiency and capacity for the concentration of the target compound (linalool).

External calibration was used to quantify the linalool in the extract of essential oil of *Eugenia uniflora*. The calibration curve obtained gave an equation of $y = 415.794 + 1.027 \times 10^7 x$ which was linear ($r^2 > 0.99$), being its average concentration around 1.70%.

In future works, the improvement of extraction and purification methods will be studied for the accomplishment of quantitative studies of other major compounds and their applications in vitro and in vivo.

4. Conclusion

This work presented several methodologies to extract the essential oil of the *Eugenia uniflora* L., and the Clevenger method showed the greatest efficiency and selectivity. More contemporary methods were also studied and, in this particular, the supercritical fluid extraction (SFE) presented excellent results, mainly by the yield and its extraction velocity, besides being a method of great solvent economy. However, it presented a low selectivity, being necessary a previous optimization to suit the purposes of the work.

The granulemetry study, in the Clevenger extraction, demonstrated that when the size of particles is diminished, the oil yield sensibly increases.

GC/FID and GC/MS showed to be valuable tools to determine the general and specific composition of complex samples such as plant extracts.

The study accomplished by chromatographic techniques pointed to linalool as one of the active principles of the *Eugenia uniflora* L.

The purification of the oil, utilizing silica, was greatly important in the active principle (linalool) isolation phase and/or cleaning, avoiding the toxic effect of co-extractives.

In subsequent phases, condition adjustments, utilizing multivariate chemometric methods with artificial computer intelligence may aid in the attainment of better extraction and purification conditions of the oil studied, prior to biological tests in vitro and in vivo.

References

[1] E.G. Wheelwrigh, Medicinal Plants and their History, Dover Publications, New York, NY, 1974, p. 288.
[2] O.R. Gottlieb, M.A. Kaplan, M.R. Borin, Biodiversidade um Enfoque Quimio-biológico, Editora UFRJ, Rio de Janeiro, 1996, p. 267.
[3] J.D. Phillpson, L.A. Anderson, J. Ethnopharmacol. 25 (1998) 61.
[4] C. Reinbothe, B. Diettrich, M.J. Luckner, Plant. Physiol. 137 (1990) 224.
[5] J. Fleuretin, J.-M. Pelt, La Recherche 2 (1990) 81.
[6] S. Sato, Amazônia já perdeu 14% de sua vegetação, em O Estado de São Paulo, São Paulo, 12 de abril de 2000.
[7] A.F. Costa, Biodiversidade um Enfoque Quimio-biológico, vol. 1, fourth ed., Fundação Calouste Gulbenkian, Lisboa, 1994, p. 1580.
[8] J.E. Robbers, M.K. Speedie, V.F. Tyler, Pharmacognosy and Pharmacobiotechnology, ninth ed., Williams and Wilkins, USA, 1996, p. 337.
[9] Encyclopedia of chemical technology, Essential Oils, vol. 16, third ed., Wiley-Interscience Publication, 1981, pp. 307–332.
[10] A.B. Joly, Botânica, Introdução à Taxonomia Vegetal, Ed. Nacional, São Paulo, 1966, p. 634.
[11] Dicionário das plantas úteis do brasil, M. Pio Corrêa (Ed.), Ministério da Agricultura-Instituto Bras, Desenvolvimento Florestal, vol. 5, 1984, p. 512.
[12] L.H. Bailey, Manual of Cultivated Plants, Ninth Printing, The Macmillan Company, New York, 1966, p. 730.
[13] A.C. Adebajo, K.J. Oloki, A.J. Aladesanmi, Phytother. Res. 36 (1989) 258.
[14] G. Schmeda-hirschmann, C. Theoduloz, L. Franco, B.E. Ferro, A. Rojas, D.E. Arias, J. Ethnopharmacol. 21 (1987) 183.
[15] P. Weyerstahl, H. Marschall-weyerstahl, C. Christiansen, B.O. Oguntimein, A.O. Adeoye, Planta Med. 54 (1988) 546.
[16] M.O. Fadeyi, U.E. Akpan, Phytother. Res. 3 (1989) 154.
[17] R.P. Adams, Identification of Essential Oil Components by Gas Chromatography/Mass Spectrometry, Allured Publishing Corporation Carol Stream, Illinois, 2001.
[18] V. Roussis, M. Tsoukatou, P.V. Petrakis, I. Chinou, M. Skoula, J.F. Harbone, Biol. Syst. Ecol. 28 (2000) 163.
[19] H.D. Skaltsa, C. Demetzos, D. Lazari, M. Sokovic, Phytochemistry 64 (2003) 743.
[20] J.B. Calixto, Br. J. Med. Biol. Res. 33 (2000) 179.
[21] R. Capasso, A.A. Izzo, L. Pinto, T. Bifulco, C. Vitobello, M. Mascolo, Fitoterapia 71 (2000) S58.
[22] B.A. Charpentier, M.R. Sevenants, Supercritical Fluid Extraction and Chromatography, Techniques and Applications, American Chemical Society, Washington DC, 1988.

Available online at www.sciencedirect.com
ScienceDirect
Talanta 70 (2006) 293–300
Talanta
www.elsevier.com/locate/talanta

Authentication of vegetable oils on the basis of their physico-chemical properties with the aid of chemometrics

Guowen Zhang [a,b], Yongnian Ni [a,*], Jane Churchill [c], Serge Kokot [c]

[a] *Department of Chemistry, Nanchang University, Nanchang, Jiangxi 330047, China*
[b] *The Key Laboratory of Food Science of Ministry of Education, Nanchang University, Nanchang, Jiangxi 330047, China*
[c] *Inorganic Materials Research Program, School of Physical and Chemical Sciences, Queensland University of Technology, Brisbane, Qld 4001, Australia*

Received 23 December 2005; received in revised form 2 February 2006; accepted 14 February 2006
Available online 29 March 2006

Abstract

In food production, reliable analytical methods for confirmation of purity or degree of spoilage are required by growers, food quality assessors, processors, and consumers. Seven parameters of physico-chemical properties, such as acid number, colority, density, refractive index, moisture and volatility, saponification value and peroxide value, were measured for quality and adulterated soybean, as well as quality and rancid rapeseed oils. Chemometrics methods were then applied for qualitative and quantitative discrimination and prediction of the oils by methods such exploratory principal component analysis (PCA), partial least squares (PLS), radial basis function-artificial neural networks (RBF-ANN), and multi-criteria decision making methods (MCDM), PROMETHEE and GAIA.

In general, the soybean and rapeseed oils were discriminated by PCA, and the two spoilt oils behaved differently with the rancid rapeseed samples exhibiting more object scatter on the PC-scores plot, than the adulterated soybean oil. For the PLS and RBF-ANN prediction methods, suitable training models were devised, which were able to predict satisfactorily the category of the four different oil samples in the verification set. Rank ordering with the use of MCDM models indicated that the oil types can be discriminated on the PROMETHEE II scale. For the first time, it was demonstrated how ranking of oil objects with the use of PROMETHEE and GAIA could be utilized as a versatile indicator of quality performance of products on the basis of a standard selected by the stakeholder. In principle, this approach provides a very flexible method for assessment of product quality directly from the measured data.

Keywords: Edible vegetable oils; Physico-chemical properties; Principal component analysis; Partial least squares; Artificial neural networks; PROMETHEE and GAIA; Chemometrics

1. Introduction

Determination of food authenticity is an important issue in food quality control and safety [1]. In general, large quantities of vegetable oils are consumed every year, and in particular, soybean and rapeseed oils are widely used in food preparation, cooking and frying. However, such oils may be spoilt naturally through rancidity, or by adulteration, which often occurs for financial gain. Spoilt oils may cause severe health and safety problems [2]. Thus, methods of detection for spoilt vegetable oils are important. Commonly available instrumental methods for such applications include gas chromatography (GC) and liquid chromatography (LC), which have been used for analysis of vegetable oil constituents such as sterols [3,4], fatty acids [5,6], triglycerides [7–9] and tocopherols [10]. However, while GC and LC are frequently-used methods for assessment of adulteration of vegetable oils, they are often time-consuming and laborious. A review of this field [11] has been published.

It is generally well known that near-infrared (NIR) spectroscopy has been applied for rapid quantitative analysis of many constituents in food and agricultural products with many applications being reported recently [12–15]. Fourier transform infrared (FT-IR) [16,17], and FT-Raman spectroscopy [18] have also been applied in this context, especially for the FT-Raman analysis with the use of the Nd:YAG laser at 1064 nm.

Chemometrics methods have been commonly applied for matching and discrimination, classification and prediction in assessing authenticity of vegetable oils. Thus, GC and LC

* Corresponding author.
E-mail address: ynni@ncu.edu.cn (Y. Ni).

0039-9140/$ – see front matter © 2006 Elsevier B.V. All rights reserved.
doi:10.1016/j.talanta.2006.02.037

methods in combination with multivariate statistical techniques such as principal component analysis (PCA), discriminant analysis (DA), cluster analysis (CA), K-nearest neighbor, partial least squares (PLS) and artificial neural networks (ANN) have been applied successfully to classify and discriminate the oils [19–22]. Quantitative assessment of oil adulteration has been similarly achieved with the use of IR [23,24] and Raman spectroscopy [25].

Traditional methods for evaluating the quality of vegetable oils have relied on the measurement of physico-chemical properties such as density, refractive index, saponification value, iodine and acid numbers [26]. Many of these methods are simple, well understood in the industry, and may be readily and cheaply applied in small food laboratories. But there are very few reports [27] of multivariate classifications of vegetable oils, which are based on such physico-chemical properties.

This paper focuses on the evaluation of the potential of multivariate chemometrics analysis for the assessment of the quality of soybean and rapeseed oils on the basis of physico-chemical properties.

In this study, we investigated physico-chemical data for both of these cases. Thus, both pure oils were available, and also samples of: (i) soybean oil adulterated with palm oil, and (ii) rancid rapeseed oil were included. Interestingly, the general physico-chemical properties of the pure and impure samples of the two types of oil were often quite similar and could not be always discriminated by, for example, the colority variable. Thus, the aim of this work was to investigate how different methods of chemometrics could facilitate the discrimination, classification or prediction of different oils and their purity on the basis of commonly measured physico-chemical properties. This aim was facilitated with the aid of the following objectives:

(1) to investigate the matching and discrimination of the oils with the aid of exploratory PCA on the basis of seven common physico-chemical properties viz, colority, moisture and volatility, density, refractive index, acid number, saponification value and peroxide value;
(2) to assess the possibility of applying PLS and RBF-ANN methods for prediction of the oil type, and quality status of the oils; and
(3) to apply the multicriteria decision making methods (MCDM) for quality ranking of the oil objects, and to demonstrate that this approach can compare the quality of the oils relative to a performance threshold introduced by the stakeholders.

2. Experimental

2.1. Soybean and rapeseed oil samples

Sixty-one soybean and rapeseed oil samples (25 quality soybean, 7 adulterated soybean, 15 quality rapeseed and 14 rancid rapeseed oil samples) from different suppliers in Nanchang, China, were provided by the Jiangxi Provincial Food Quality Safety Supervising Test Center. All the edible vegetable oil samples were examined randomly. Samples were collected in glass bottles and stored in the dark at 3–4 °C.

2.2. Methods of analysis

The seven selected physico-chemical properties, colority, moisture and volatility, density, refractive index, acid number, saponification value and peroxide value, were measured by standard methods for food analysis [28]. These are similar to those described in the well known analytical texts [29,30]. The results of the seven parameters determined for edible vegetable oil samples are summarized (Table 1) as mean values and standard deviations.

2.3. Chemometrics methods and data analysis

The data matrix consisted of 61 objects (the soybean and rapeseed oil samples) and seven variables (the physico-chemical parameters). The data were processed on a Pentium IV computer with the use of programs from: for PCA and PLS-Sirius 6.5 (PRS, Bergen, Norway), for MCDM methods (Visual Decision Inc., Version 2000), and for RBF-ANN (MATLAB 6.1, Mathworks).

Table 1
Mean values and standard deviations (S.D.) for the variables measured for the vegetable oil samples[a]

Variables	Soybean oil samples				Rapeseed oils samples			
	QS ($n=25$)		AS ($n=7$)		QR ($n=15$)		RR ($n=14$)	
	Mean	S.D.	Mean	S.D.	Mean	S.D.	Mean	S.D.
Colority	0.1	0.0	0.1	0.0	4.15	0.85	4.74	0.77
Moisture and volatility (%)	0.04	0.02	0.05	0.02	0.08	0.05	0.1	0.06
Density (20 °C)	0.922	0.006	0.915	0.002	0.918	0.003	0.917	0.002
Refractive index (20 °C)	1.474	0.002	1.471	0.004	1.473	0.001	1.472	0.001
Acid number (mg kg^{-1})	0.17	0.07	0.34	0.10	2.21	0.54	3.98	1.60
Saponification value (mg kg^{-1})	193.2	1.1	193.7	0.7	175.4	2.8	175.0	2.5
Peroxide value (meq kg^{-1})	4.73	4.5	12.0	5.7	7.7	3.0	14.3	2.6

[a] QS: quality soybean oils; AS: adulterated soybean oils; QR: quality rapeseed oils; RR: rancid rapeseed oils.

2.3.1. Principal component analysis and partial least squares

Exploratory PCA is a well-known technique of multivariate analysis [31–33]. PCA transforms an original data matrix ($X_{n\times m}$) into a product of two matrices, one of which contains the information about the objects ($S_{n\times m}$), namely scores of the n objects on m principal components (PCs), and the other, which focuses on the variables ($V_{m\times m}$), contains the loadings. PCs are extracted on the basis of data variance in a top-down order with PC1 describing the largest amount of the variance. It is common to pre-treat the data matrix before submission to a chemometrics procedure; in this work, the matrix was autoscaled. Autoscaling is a common multiple pre-treatment involving y-mean scaling followed by standardization of the variables. Since the independent variables varied in size significantly, it is useful to remove the influence of size.

PLS is a well-known factor analysis multivariate method principally applied for prediction [31,34–36]. It requires a calibration step in which a model is constructed from a number of significant factors. PLS modeling includes the dependent and independent variables in the data compression and decomposition operations, i.e., both y and x data are actively used in the data analysis. Strictly, in this work the PLS procedure could be referred to as Discriminant PLS because the objects were assigned to different classes as e.g. 0, 1, 2, etc.

2.3.2. Radial basis function—artificial neural networks

Artificial neural network modeling is widely used to solve analytical problems, especially for fitting non-linear data [37,38]. The most common ANN model involves the multilayer feed-forward net with the back-propagation (BP-ANN) learning algorithm [37]. More recently, another approach has been described – the RBF – ANN, which offers some advantages of robustness and sensitivity to noisy data as compared to the BP-ANN model. The basic theory of RBF-ANN and its application to chemical problems can be found in the literature [39,40].

In general, RBF-ANN networks use a Gaussian kernel function to account for the non-linearity of the hidden layer processing elements. The Gaussian function responds only to a small region of the input space where the Gaussian is centred. The key to a successful implementation of these networks is to find suitable centres for such a Gaussian function, which is characterized by two parameters, i.e., centre (c_j), and peak width (σ_j). The output from the jth Gaussian neuron for an input object x_i can be calculated by the following equation:

$$\text{out}_j = \Phi_j(||x_i - c_j||) = \exp\left(\frac{-||x_i - c_j||^2}{(\sigma_j)^2}\right) \quad (1)$$

where $||x_i - c_j||$ is the calculated Euclidean distance between x_i, and c_j, and the σ_j determines the portion of the input space where the jth RBF-ANN will have a non-significant zero response. This RBF-ANN hidden layer is fully connected to the output layer by the size of the weight coefficients, w_{kj}. The input value to each output node is the weighted sum of all the outputs of the hidden nodes. Finally, the response of each output node is calculated by a linear function of its input (which includes the bias, w_{k0}), i.e., the output of the hidden layer (out_k). The relationship between the value, out_k, and the input variables x_i can be represented by:

$$\text{out}_k = w_{k0} + \sum_j w_{kj}\Phi_j(||x_i - c_j||) \quad (2)$$

The weights w_{kj} are adjusted to minimize the mean square error of the net output. The two sets of parameters (the centres and the widths) in the hidden layer and a set of weights in output layer are adjusted. The adjustment for output layer is quite simple, so the RBF-ANN has a guaranteed learning procedure for convergence.

2.3.3. PROMETHEE and GAIA

PROMETHEE, a non-parametric outranking method, orders objects on the basis of a set of criteria. It and its partner, the visual display tool, GAIA, have been fully described elsewhere [41–44], and a summary of the PROMETHEE procedure follows: (a) a data matrix consisting of objects (oil samples) and the criteria (measured oil variables) was analysed with the use of MCDM Decision Lab 2000 software [45], (b) for each criterion, the user selected one of the six available preference functions for rank-ordering, and indicated whether higher or lower values were preferred i.e. maximised or minimized ranking, (c) a difference matrix was then computed from the raw data by subtraction in all possible combinations, and the preference functions were applied, (d) the global preference index was computed by summing the preference values for each object, (e) positive and negative outranking flows were calculated (where the positive outranking flow, φ^+, expressed how an object outranks all other objects and the negative outranking flow φ^-, indicated how other objects outrank the object), (f) pair-wise comparison of the outranking flows was performed for each alternative and partial ranking of the alternatives was obtained, (g) the net ranking flow, φ (where $\varphi = \varphi^+ - \varphi^-$) and complete ranking of the objects were computed i.e. the rank order was the most preferred object (highest φ value) to the least preferred one (lowest φ value), and (h) PROMETHEE results were then submitted to GAIA, which displayed them as a PC1 versus PC2 biplot with a decision axis, pi, which showed the quality of the decision. When pi is long, the best objects are in its direction and farthest away from the origin and vice versa.

3. Results and discussion

3.1. Qualitative studies: principal component analysis

The full 61 × 7 autoscaled data matrix consisting of 25 quality soybean oils and 7 soybean oils adulterated with palm oil together with 15 quality rapeseed oils and 14 rancid oils were submitted to PCA analysis. The soybean product had been mixed with another oil (palm oil), while the spoilt rapeseed oil represents oils, which had undergone normal degradation rather than being mixed with an additive. Thus, the two different methods of spoilage could show different property behavior, which could be evident on a PCA biplot.

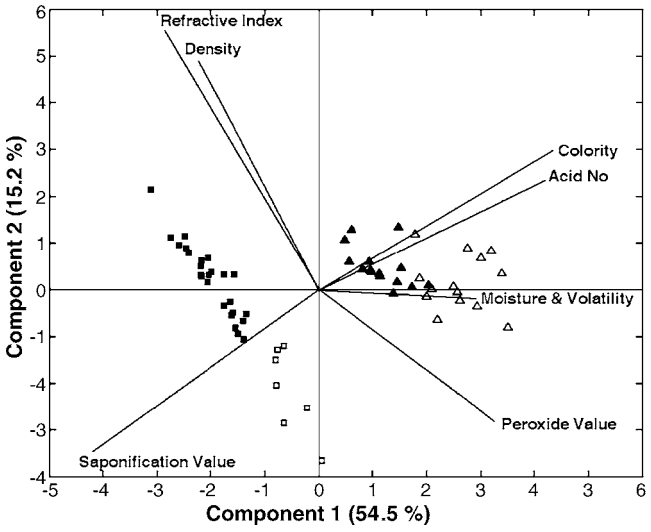

Fig. 1. PC1 vs. PC2 biplot of edible vegetable oil samples. (■) Quality soybean oils; (□) adulterated soybean oils; (▲) quality rapeseed oils; (△) rancid rapeseed oils.

The PC1 versus PC2 biplot (Fig. 1) accounts for almost 70% of data variance and shows a distinct discrimination between the soybean and rapeseed oils on PC1. The rapeseed cluster shows a trend with positive scores on this PC, and the rancid samples have the highest scores, while the soybean group has negative PC1 scores. However, interestingly, the adulterated oils form a clearly separated cluster with scores closer to zero i.e. relatively more positive. Colority and acid number loadings vectors are relatively large on PC1, and together with the shorter peroxide and moisture/volatility vectors discriminate the rapeseed oils from the soybean ones. On the other hand, saponification and the somewhat shorter refractive index and density loadings distinguish the soybean oils from the rapeseed ones. The discrimination of the oils on PC2 is much less clear. Thus, all of the quality rapeseed samples, about two thirds of the quality soybean and most of the rancid rapeseed oils are intermixed with positive scores on PC2. They are discriminated from the other oil samples on the basis of the refractive index, density and to a lesser extent colority and the acid number. It is noted that the moisture/volatility vector does not contribute to PC2. The saponification criterion is the dominant loadings vector discriminating the objects with negative PC2 scores. Together with the smaller peroxide variable, it discriminates the soybean adulterated cluster and the remnants of the soybean quality and rancid rapeseed samples from the other oils.

In addition to this PC-by-PC analysis, it is clear from the PC1 versus PC2 projection plane that the differently spoilt oil groups relate differently to their respective quality counter parts. Thus, the separate soybean adulterated oil cluster forms a rough trend along an imaginary line that passes through the soybean quality group. The refractive index and density loadings vectors, which are virtually co-linear, appear to be responsible for this trend. The saponification vector with negative loadings on both PCs is particularly related to the separation of the adulterated soybean oil. On the other hand, the rapeseed objects form a dispersed cluster. There is no obvious separation of the two groups from each other; indeed two rancid samples clearly overlap the quality ones. The strong colority and acid number loadings vectors are co-linear and reflect a clear association with the change of these properties in the rancid samples. Similarly, the peroxide vector is strongly associated with the rancid oils as well.

Thus, it is apparent from this biplot that different variables, which are commonly measured for all of the oil types considered, are specifically related to different types of spoilt samples. The biplot also indicates that spoilage by adulteration, results in sample mixtures with properties that are quite different from those of the quality oils i.e., there is a distinct discrimination between the two classes of samples. On the other hand, spoilage by normal degradation of oils resulting in rancidity produces more varied objects with the quality oil samples gradually blending in with the rancid ones.

3.2. Quantitative studies: partial least squares and artificial neural networks

In practice, the fundamental requirement is to know whether a given oil sample is suitable for human consumption or not, irrespective of the nature of spoilage. It would also be particularly useful and more efficient if the associated testing could be carried out by comparison with a composite calibration model rather than individual calibrations for different models. In this study, the soybean and rapeseed oils in the 61 sample matrix were categorised into the four sub-types of pure and spoilt oils with the use of oil category numbers 1, 2, 3 or 4, depending on the case in question, and these were included as the dependent variables for prediction modeling with the use of the PLS and RBF-ANN methods.

3.2.1. Partial least squares

For PLS modeling, the 61 × 7 data matrix was divided into a calibration and verification data sets. The former consisted of 22 soybean objects (17 pure and 5 adulterated samples) and 19 rapeseed objects (10 pure and 9 rancid samples), and the latter set consisted of 10 soybean (8 pure and 2 adulterated samples) and 10 rapeseed objects (5 pure and 5 rancid samples). All samples in the different categories were selected randomly.

For the PLS model, each type of oil was identified by a number 1, 2, 3 or 4 for quality soybean, adulterated soybean, quality rapeseed and rancid rapeseed oils, respectively. Four statistically significant PCs ($p = 0.05$) were extracted by the leave-one-sample-out-at-a-time cross-validation method [38] for the PLS calibration model, which described 67% of independent and 96% of dependant data variance. The standard error of calibration (SEC) was 0.27. In general, the predictions for the verification data set (Table 2), and the measured versus predicted plot (Fig. 2A) indicated that the results were quite acceptable (SEP = 0.26). However, one sample from the rapeseed oil group gave poor predictions (R12). On the other hand, the model suffered unavoidably from low sample numbers, because of the need to split the 61-member data set into a training and a verification groups.

Table 2
Prediction results of the calibration models constructed by PLS and RBF-ANN for the test set (quality soybean oil, adulterated soybean oil, quality rapeseed oil and rancid rapeseed oil)

Sample	Actual	Predicted[a,b]	
		PLS	RBF-ANN
1 (S2)	1	1.0	0.98
2 (S6)	1	0.89	1.0
3 (S8)	1	0.88	0.91
4 (S13)	1	1.4	1.3
5 (S16)	1	1.2	1.3
6 (S20)	1	0.65	0.68
7 (S22)	1	1.1	1.1
8 (S24)	1	1.3	1.3
9 (S27)	2	1.8	1.6
10 (S31)	2	2.1	2.1
11 (R2)	3	2.8	2.7
12 (R4)	3	2.6	2.6
13 (R10)	3	3.1	3.0
14 (R12)	3	3.5	3.4
15 (R14)	3	3.0	3.0
16 (R16)	4	3.6	3.7
17 (R18)	4	4.2	3.8
18 (R22)	4	4.3	4.3
19 (R24)	4	4.0	4.1
20 (R28)	4	3.7	3.7

[a] Values of the verification samples were set to 1, 2, 3 and 4 according to the ranges >0.5 and <1.5, >1.5 and <2.5, >2.5 and <3.5, and >3.5 and <4.5, respectively.
[b] (i) PLS model: number of significant factors = 4; (ii) RBF-ANN model parameters: 0.04, 15, 1500 and 18 for goal sum-squared error, epochs, spread (sc) radial basis function and radial neurons, respectively.

3.2.2. Radial basis function—artificial neural networks

The 61 × 7 data matrix was divided into the same training and verification data sets as for the PLS model above. The RBF-ANN predicted values are compared with the measured ones, and with those predicted by the PLS model (Table 2). An SEP value of 0.24 when compared with that from the PLS modeling of 0.26 indicates that the RBF-ANN model provides similar results.

3.2.3. The elliptic joint confidence region (EJCR) method

A statistical analysis of recoveries may be performed by applying linear regression analysis of measured versus predicted data (see Table 2). Once the intercept (a) and slope (b) are found by the LS method, the evaluated values with the ideal ones (0 for intercept and 1 for slope) may be compared by calculating the elliptic joint confidence region (EJCR) for the true intercept α and slope β parameters. The equation describing the joint region is [46,47]:

$$n(a-\alpha)^2 + 2(\Sigma x_i)(a-\alpha)(b-\beta) + (\Sigma x_i)^2(b-\beta)^2 = 2s^2 F_{2,n-2} \quad (3)$$

where n is the number of data points, s^2 the regression variance, and $F_{2,n-2}$ is the statistical F value with 2 and $n-2$ degrees of freedom at a given confidence level, usually 95%. If the point (1, 0) is inside the EJCR, it indicates that proportional and constant biases are absent. Fig. 2B shows both of these regions for PLS and RBF-ANN methods. They contain the theoretically expected value of (1, 0), but the region for PLS appears slightly better than that for RBF-ANN.

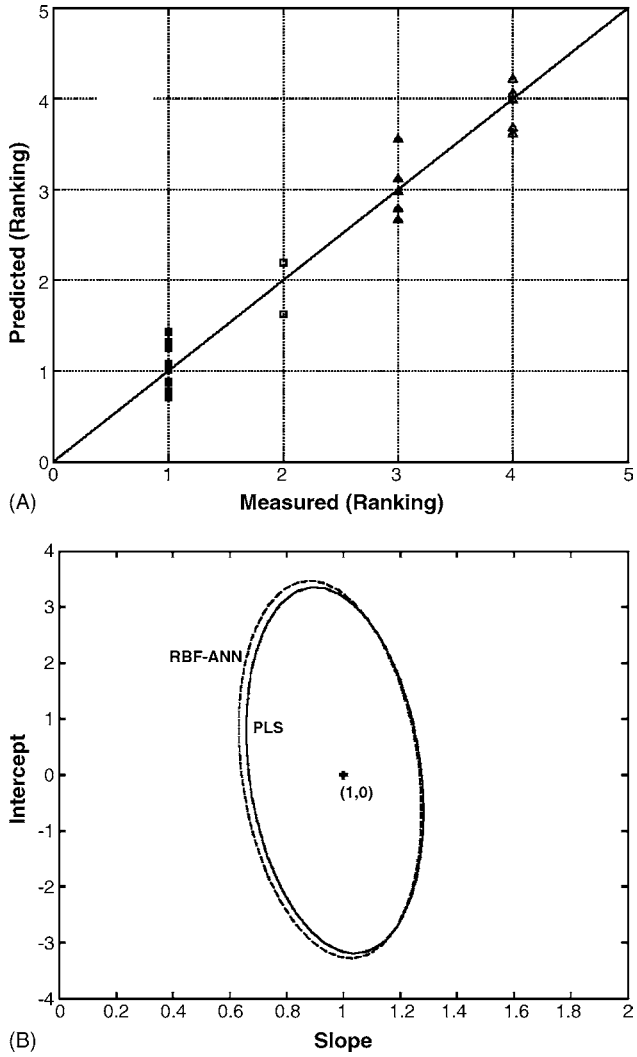

Fig. 2. (A) Plot of prediction vs. measured results for the test set in Table 3 by PLS. (■) Quality soybean oils; (□) adulterated soybean oils; (▲) quality rapeseed oils; (△) Rancid rapeseed oils. (B) Joint confidence intervals based on PLS and RBF-ANN methods ($p = 0.05$).

These investigations showed that both the PLS and the RBF-ANN methods can categorize satisfactorily the pure and the spoilt oils according to their types as identified by the oil category number. While this approach is feasible, it will always need a training set, the dependent variable of which will be subject to some other criteria required to decide the quality of the oils. An alternative potential solution to this rather cumbersome method is to apply the MCDM methods [42], which do not require model training sets, and which rank-orders the oil objects according to the criteria measurements. PROMETHEE and GAIA methods are representative of such an approach, and have recently been shown to have considerable potential for applications to problems similar to the one being discussed here [43,48,49].

3.3. PROMETHEE and GAIA analysis of the oil samples

3.3.1. Ranking of the oil samples

Recently, it has been demonstrated successfully that it is possible to differentiate the performance of sugarcane clones for resistance against disease [49] with the use of the PROMETHEE and GAIA methods. Some advantages of this approach include: (i) no training set is required; (ii) PROMETHEE is a non-parametric method based on comparisons of Euclidean distances, and thus, it is possible to rank-order not only many objects but just a few as well; (iii) reference objects or criteria may be added to the data matrix.

The same 61×7 raw data matrix was investigated in this work. The modeling parameters, preference functions and modeling rationale are summarized as follows:

(1) All the criteria were minimized because for each variable, adulterated or rancid samples have higher values than those for the quality oils.
(2) The linear preference function was chosen for modeling every criterion [41,45,49]. As there is more than one type of oil being analyzed simultaneously i.e. different types of oil of different quality, a range of ideal threshold values for each criterion could not be determined for this data set. Consequently, minimum and maximum values for each criterion in the data set were selected as the Q and P threshold values in PROMETHEE, respectively.
(3) The weighting factor for each criterion was set to the default value of 1.

The PROMETHEE II net outranking flows range from +0.18 to −0.28 (Table 3). It is clear that the two types of oil were differentiated such that the soybean oils had positive φ net outranking flow values, and the rapeseed oils had negative φ ones. Ideally, one might expect very little difference in the φ values for a given oil type, particularly for the quality samples, because for a given oil type the properties should be more or less the same. Spoilt samples should be made evident by degree rather than in large steps. Except for a few samples on both ends of the oil performance scale, the order derived from the φ net outranking flows reflected closely the above postulated ideal behavior—for the quality soybean oils φ range was 0.14–0.12, and it was somewhat wider for the quality rapeseed samples (φ range: −0.05 to −0.13). In general, for each oil, the quality products had higher (more positive) values while the spoilt samples clustered at the end of the ranking groups. However, there was no obvious separation in either group of the spoilt oils from the quality ones on the basis of the φ values. Indeed, there appeared to be some mixing of the spoilt samples with the quality ones. For the rancid rapeseed oil, two samples (R16 and R27) were picked up in the MCDM analysis. In the PROMETHEE II net outranking flows order, these samples were placed arguably at the quality boundary with φ values just above −0.16. With the adulterated soybean oil, one sample (S30) was close to the quality/spoilt boundary of the group, while the other (S29) was further up the scale. Neither sample was previously picked up by the PLS and

Table 3
Demonstration of PROMETHEE II overall rankings for the comparison of quality of the pure and spoilt soybean and rapeseed oils against the respective average oil criteria, *Savg* and *Ravg*

Object	φ Net	Group
S8	0.18	Quality soybean
S4 b	0.16	Quality soybean
S11	0.16	Quality soybean
S6	0.15	Quality soybean
S5 a	0.15	Quality soybean
S20	0.14	Quality soybean
S18	0.14	Quality soybean
S15	0.14	Quality soybean
S9	0.14	Quality soybean
S7	0.14	Quality soybean
S19	0.13	Quality soybean
S22	0.13	Quality soybean
S10	0.13	Quality soybean
S29	0.13	Adulterated soybean
S2	0.13	Quality soybean
Savg	*0.13*	*Avg. quality soybean*
S1	0.13	Quality soybean
S24	0.13	Quality soybean
S14	0.12	Quality soybean
S16	0.12	Quality soybean
S21	0.12	Quality soybean
S23	0.12	Quality soybean
S12 a	0.11	Quality soybean
S30	0.11	Adulterated soybean
S17	0.11	Quality soybean
S3	0.10	Quality soybean
S13	0.09	Quality soybean
S25 b	0.09	Quality soybean
S32	0.06	Adulterated soybean
S28	0.05	Adulterated soybean
S26	0.05	Adulterated soybean
S27	0.04	Adulterated soybean
S31	0.02	Adulterated soybean
R7 b	−0.01	Quality rapeseed
R4	−0.02	Quality rapeseed
R1 a	−0.03	Quality rapeseed
R14	−0.04	Quality rapeseed
R6	−0.05	Quality rapeseed
R2	−0.05	Quality rapeseed
R15	−0.05	Quality rapeseed
R3	−0.05	Quality rapeseed
R5	−0.06	Quality rapeseed
Ravg	*−0.06*	*Avg. quality rapeseed*
R9	−0.08	Quality rapeseed
R8	−0.08	Quality rapeseed
R10	−0.09	Quality rapeseed
R11 a	−0.10	Quality rapeseed
R16	−0.11	Rancid rapeseed
R13	−0.12	Quality rapeseed
R27 b	−0.13	Rancid rapeseed
R12	−0.16	Quality rapeseed
R24	−0.17	Rancid rapeseed
R28	−0.18	Rancid rapeseed
R23	−0.19	Rancid rapeseed
R26	−0.19	Rancid rapeseed
R19	−0.20	Rancid rapeseed
R21	−0.20	Rancid rapeseed
R25	−0.21	Rancid rapeseed

Table 3 (*Continued*)

Object	φ Net	Group
R17	−0.22	Rancid rapeseed
R18	−0.24	Rancid rapeseed
R20	−0.24	Rancid rapeseed
R29	−0.25	Rancid rapeseed
R22	−0.28	Rancid rapeseed

a, b: 1s and 2s (standard deviations) from the average quality oil (i.e. *Savg* or *Ravg*), respectively. Soybean oil: 1s range: 0.15–0.11φ and 2s range: 0.17–0.09φ; rapeseed oil: 1s range: −0.02 to −0.10φ and 2s range: 0.01 to −0.14φ.

the RBF-ANN when these were applied to the verification sets because both samples were located in the calibration models.

The GAIA biplot (Fig. 3) was produced from a matrix formed by the decomposition of the PROMETHEE II outranking flows [41], provided guidance for the detection of potential atypical samples and for the principal criteria responsible for the discrimination of the different grades of oils. Thus, all soybean samples had negative scores on PC1 and all rapeseed samples had positive ones. As with the initial PCA analysis on the autoscaled data matrix (Fig. 1), the soybean samples showed on the PC1 versus PC2 projection plane, a relatively tight roughly linear trend of the samples with a clear separation of most of the adulterated samples from the quality ones (two adulterated objects, S29 and S30, were completely immersed in the quality cluster), whereas the rapeseed oils formed a much more dispersed cluster. The quality oils formed a loose group with the more negative scores on PC1, while the rancid oils had more positive scores. The two rancid samples (R16 and R27), which appeared among the quality oils according to the PROMETHEE II net outranking flows scale were now in their corresponding rancid cluster.

The dominant criteria that were responsible for the discrimination of the soybean oils from rapeseed ones on PC1, were in order of vector length—colority, peroxide, acid number and moisture and volatility. On PC2, colority and acid number were responsible for separating mostly the rancid and the adulterated oils from the rest. Peroxide criterion was dominant for objects with positive scores on PC2, i.e., mostly the quality oils from both groups. This is in agreement with the expectation that such oils will have the lowest peroxide values consistent with the 'minimised' setting of the variable in the modeling process.

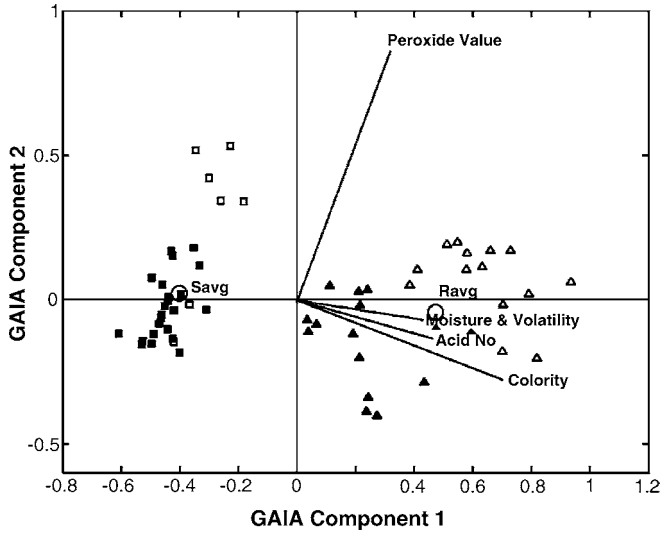

Fig. 3. GAIA biplot with average quality samples (*Savg* and *Ravg*) included. (■) Quality soybean oils; (□) adulterated soybean oils; (▲) quality rapeseed oils; (△) rancid rapeseed oils; (◯) average quality oils.

3.3.2. Performance classification of the oil samples

The PROMETHEE and GAIA analysis (Section 3.3.1) established that: (i) the soybean and rapeseed oils are clearly separated on the φ net outranking flow relative scale, and (ii) in each case, the spoilt samples formed a group at the end of each set of φ values. For the illustration of performance prediction, we chose to compare the oil samples with the average set of criteria values (*Savg* and *Ravg*) for the quality soybean and rapeseed oils respectively. PROMETHEE II rank order results for the full data show (Table 3) the positions of the *Savg* and *Ravg* objects amongst the samples according to the relative φ net outranking flows scale. The stake holder now has guidance to assess the quality of the oil against the chosen and defined decision points on the ranking scale, as well as, in this illustration, the 1s and 2s standard deviation limits. The criteria values for the objects, *Savg* and *Ravg*, can be transferred to another data set and applied in the same manner with the knowledge that they are representative of oil quality as defined. However, the φ values are non-transferable and are computed for each individual matrix.

The GAIA biplot (Fig. 3) accounted for 91% of data variance shows the position of the S*avg* and *Ravg* objects relative to the other objects.

4. Conclusion

In general, the soybean and rapeseed oils were discriminated by PCA, and the two spoilt oils behaved differently from each other. The PLS and RBF-ANN prediction models produced satisfactory results on the verification set. PROMETHEE II rank ordering indicated that the oil types can be discriminated, and for the first time, it was demonstrated how the ranking of the oil objects could be utilized as a versatile indicator of quality performance on the basis of a standard selected by the stakeholder. In general, this approach provides a very flexible method for assessment of product quality.

The proposed methodologies have been recommended to the Jiangxi Provincial Food Quality Safety Supervising Test Center for oil products quality testing.

Acknowledgements

The authors gratefully acknowledge the financial assistance of this work from the National Natural Science Foundation of China (NSFC, 20365002 and 20562009), the Jiangxi Province Natural Science Foundation (JXNSF), the State Key Laboratories of Electroanalytical Chemistry of Changchun Applied Chemical Institute (SKLEAC2004-3) and Chemo/Biosensing and Chemometrics of Hunan University (CBC2005-22), and the

Key Laboratory of Food Sciences of MOE of Nanchang University.

References

[1] M.J. Dennis, Analyst 123 (1998) 151.
[2] E. Gelpi, M.P. de la Paz, B. Terracini, I. Abaitua, A.G. de al Camara, E.M. Kilbourne, C. Lahoz, B. Nemery, R.M. Phelen, L. Soldevilla, S. Tarkowski, Environ. Health Perspect. 110 (2002) 457.
[3] E. Ballestero, M. Gallego, M. Valcarcel, Anal. Chim. Acta 308 (1995) 253.
[4] M.H. Gordon, R.E. Griffith, Food Chem. 43 (1992) 71.
[5] S.E. Woodbury, R.P. Evershed, J.B. Rossell, J. Chromatogr. A 805 (1998) 249.
[6] G.M. Wood, P.T. Slack, J.B. Rossel, P.J. Mann, P.J. Farnell, J. Agric. Food Chem. 42 (1994) 2525.
[7] J.M. Bland, E.J. Conkerton, G. Abraham, J. Am. Oil Chem. Soc. 68 (1991) 840.
[8] T. Rezanka, H. Rezankova, Anal. Chim. Acta 398 (1999) 253.
[9] R.B. Tarandjiiska, I.N. Marekov, Anal. Chim. Acta 364 (1998) 83.
[10] F. Dionisi, J. Prodolliet, E. Tagliaferri, J. Am. Oil Chem. Soc. 72 (1995) 1505.
[11] R. Aparicio, R. Aparicio-Ruiz, J. Chromatogr. A 881 (2000) 93.
[12] M.D. Guillen, N. Cabo, J. Agric. Food Chem. 45 (1997) 1.
[13] A.M.C. Davies, B. Radovic, T. Fearn, E. Anklam, J. Near Infrared Spectrosc. 10 (2002) 121.
[14] R. Rodbotten, B. Mevik, K.I. Hildrum, J. Near Infrared Spectrosc. 9 (2001) 199.
[15] E. Betran, M. Blanco, J. Coello, H. Iturriaga, S. Maspoch, Montoliu, J. Near Infrared Spectrosc. 8 (2000) 45.
[16] Y.W. Lai, E.K. Kemsley, R.H. Wilson, J. Agric. Food Chem. 42 (1994) 1154.
[17] G.F. Zagonel, P. Peralta-Zamora, L.P. Ramos, Talanta 63 (2004) 1021.
[18] V. Baeten, M. Meurens, M.T. Morales, R. Aparicio, J. Agric. Food Chem. 44 (1996) 2225.
[19] D.-S. Lee, B.-S. Noh, S.-Y. Bae, K. Kim, Anal. Chim. Acta 358 (1998) 163.
[20] D.-S. Lee, E.-S. Lee, H.-J. Kim, S.-O. Kim, K. Kim, Anal. Chim. Acta 429 (2001) 321.
[21] E.K. Kemsley, Chemom. Intell. Lab. Syst. 33 (1996) 47.
[22] S. Husain, K. Devi, D. Krishna, P.J. Reddy, Chemom. Intell. Lab. Syst. 35 (1996) 117.
[23] N. Dupuy, L. Duponehel, J.P. Huvene, B. Sombret, P. Legrand, Food Chem. 57 (1996) 245.
[24] D. Gerard, Trends Anal. Chem. 17 (1998) 418.
[25] E.C. Lopez-Diez, G. Bianchi, R. Goodacre, J. Agric. Food Chem. 51 (2003) 6145.
[26] M.Y. Bei, J.C. Zhang, Discriminatory Inspection of Adulterated Cereals, Oils and Foods, Chinese Criteria Press, Beijing, 1995, pp. 126–143.
[27] M. Wesolowski, B. Suchaez, Fresenius J. Anal. Chem. 371 (2001) 323.
[28] Y. Dai, S.C. Wang, H.F. Yang, Handbook of Food Sanitary Physical and Chemical Inspection Criteria, Chinese Criteria Press, Beijing, 1997, pp. 426–446.
[29] Z.C. Wang, Quality Analysis of Food and Oils, Chinese Light Industry Press, 2000, p. 415.
[30] D. Firestone, Official Methods of Analysis, AOAC (2), vol. 41, 15th ed., 1990, pp. 951–986.
[31] I.T. Joliffe, Principal Component Analysis, Springer-Verlag, New York, 1986.
[32] K.V. Mardia, J.T. Kent, J.M. Bibby, Multivariate Analysis, Academic Press, New York, 1979.
[33] D.L. Massart, L. Kaufman, The Interpretation of Analytical Chemical Data by Use of Cluster Analysis, Wiley, New York, 1983.
[34] D.L. Massart, B.G.M. Vandeginste, L.M.C. Buydens, S.D. Jong, P.J. Lewi, J. Smeyers-Verbeke, Handbook of Chemometrics and Qualimetrics, Elsevier, Amsterdam, 1997, p. 153.
[35] M. Otto, Chemometrics, Wiley-VCH, New York, 1999, p. 313.
[36] S. Wold, K. Esbensen, P. Geladi, Chemom. Intell. Lab. Syst. 2 (1987) 37.
[37] J. Zupan, J. Gasteiger, Anal. Chim. Acta 248 (1991) 1.
[38] J. Zupan, J. Gasteiger, Neural Network for Chemists: An Introduction, VCH, Weinheim, 1993.
[39] B. Walczak, D.L. Massart, Anal. Chim. Acta 331 (1996) 177.
[40] A. Pulido, I. Ruisanchez, F.X. Ruis, Anal. Chim. Acta 388 (1999) 273.
[41] H.R. Keller, D.L. Massart, Chemom. Intell. Lab. Syst. 11 (1991) 175.
[42] S. Kokot, G. Ayoko, in: P.J. Worsfold, A. Townshend, C.F. Poole (Eds.), Chemometrics-(I) Multi-criteria Decision Making, Encyclopaedia of Analytical Sciences, vol. 2, 2nd ed., Elsevier, Oxford, 2005, pp. 40–45.
[43] W.A.-S. Khalil, A. Goonetilleke, S. Kokot, S. Carroll, Anal. Chim. Acta 506 (2004) 41.
[44] J.F. Le Teno, B. Mareschal, Eur. J. Oper. Res. 109 (1998) 522.
[45] Decision Lab 2000, Executive Edition, Visual Decision Inc., Montreal, Canada.
[46] J. Mandel, F.J. Linning, Anal. Chem. 29 (1957) 743.
[47] A.G. Gonzalez, M.A. Herrador, A.G. Asuero, Talanta 48 (1999) 729.
[48] Y.N. Ni, C.F. Huang, S. Kokot, Chemom. Intell. Lab. Syst. 71 (2004) 177.
[49] D.E. Purcell, G.J. Leonard, M.G. O'Shea, S. Kokot, Chemom. Intell. Lab. Syst. 76 (2005) 135.

Available online at www.sciencedirect.com
ScienceDirect
Talanta 70 (2006) 301–306
Talanta
www.elsevier.com/locate/talanta

EDXRF spectrometry determination of tungsten in tobacco plants after antiviral treatment with 12-tungstophosphoric acid and its compounds

S. Uskoković-Marković [a,*], M. Todorović [b], U.B. Mioč [c], I. Antunović-Holclajtner [c], V. Andrić [d]

[a] *Faculty of Pharmacy, P.O. Box 146, Belgrade 11001, Serbia and Montenegro*
[b] *Faculty of Chemistry, P.O. Box 158, Belgrade 11001, Serbia and Montenegro*
[c] *Faculty of Physical Chemistry, P.O. Box 137, Belgrade 11001, Serbia and Montenegro*
[d] *Chemical Dynamics Laboratory, VINČA Institute of Nuclear Sciences, P.O. Box 522, Belgrade 11001, Serbia and Montenegro*

Received 18 January 2006; received in revised form 14 February 2006; accepted 14 February 2006
Available online 29 March 2006

Abstract

In this study, we have developed a sensitive, rapid and simple procedure for the energy dispersive X-ray fluorescence (EDXRF) spectrometry measurement of tungsten in tobacco plant parts. Only 0.1 g of dried plant material is needed instead of the usual 1 g. EDXRF spectrometry is used for quantitative measurement, after the foliar application of solutions of tungstophosphoric acid (WPA), its magnesium salt and compounds with glycine (Gly) and alanine (Ala), in exact quantities. After that, the leaves, trunks and summits were collected and prepared separately. Tungsten is determined directly in raw dried material, and the overlap of the tungsten peak with zinc's that is present is avoided by the spectral deconvolution to obtain quantitative results. The prepared dry tablets weighed 100 mg, and measurement time was 2000 s. The radioisotope excitation source used was ^{109}Cd and tungsten was identified and quantified at the $L_{\alpha 1}$ and $L_{\alpha 2}$ lines at the energies of 8397.6 eV and 8335.2 eV, respectively. EDXRF spectrometry was applied in a wide range of concentrations (up to 2000 mg/kg), with an estimated detection concentration limit of 15 mg/kg, calculated on dried material. Quantitative analysis of different parts of the treated plant plus the washings gave 94.47% recovery of the applied tungsten in different compound forms. After the foliar application of investigated WPA compounds, there were noticed both vertical and horizontal distributions of tungsten through out the tobacco plants, according to the EDXRF spectrometry results. This conclusion is also in agreement with the positive effects of WPA on *Tobacco mosaic tobamovirus* (TMV) infection of *Nicotiana tabacum* (*Solanaceae*).

Keywords: EDXRF spectrometry; Tungstophosphoric acid; Tobacco plant; TMV

1. Introduction

Heteropoly compounds (HPCs) have large practical interest and different applications [1–4]. HPCs with Keggin-type structure have been reported as inhibitors of several kinds of viruses, but the literature about activity of HPCs on plant viruses is very limited. In our previous work we proved significant antiviral activity of 12-tungstophosphoric acid (WPA) against the plant viruses *Tobacco mosaic tobamovirus* (TMV) and *Cucumber mosaic cucumovirus* (CMV) in curative as well as in preventive purposes [5]. TMV is very resistant and contagious and has almost 800 plant species as host plants. It survives deep in the soil for even two years as well as through all the procedures of tobacco treatment. It is worth mentioning that there is no satisfactory preparation against this virus in practice. Therefore, the investigation of compounds with antiviral activity is of special economical importance, and the present study addresses the analytical procedure for the investigation of tungsten antiviral compounds.

Tungsten in plant tissues may be determined by a variety of methods, including neutron activation analysis [6–10], X-ray fluorescence [11], spectrophotometry [12,13], atomic absorption [14] or fluorescence [15] spectrometry, ICP-MS [16], or polarography [17]. Most require extensive sample preparation,

* Corresponding author. Tel.: +381 11 3970 379.
E-mail address: snezaum@pharmacy.bg.ac.yu (S. Uskoković-Marković).

0039-9140/$ – see front matter © 2006 Elsevier B.V. All rights reserved.
doi:10.1016/j.talanta.2006.02.041

including mineralization [11,14,16,17], dry [13] or low temperature [15] ashing, chromatographic separation [8,10,12], or solvent extraction [14].

In this work we have proposed a simple and sensitive non-destructive method for HPC tungsten determination in tobacco plants in wide range of concentrations (up to 2000 ppm in the dried samples, with 15 ppm detection limit) with energy dispersive X-ray fluorescence (EDXRF) spectrometry and utilized it for antiviral activity investigation 12-tungstophosphoric acid and its compounds. The tungsten compounds in the plant materials were previously concentrated by drying the material to be analyzed, allowing small samples, and zinc spectral interference effect was eliminated by spectral deconvolution.

We have used the method to investigate transport and distribution of WPA and its compounds after their foliar application on *Nicotine tobacco, var. Samsun,* as chosen host plant. It is important to estimate the distribution profile of selected WPA compounds through the host plant and to contribute to the explanation of their antiviral activity mechanism. In order to investigate the possible phytotoxicity of the applied compounds besides the WPA, experiments with the magnesium salt of WPA, and new synthesized WPA compounds with the amino acids, glycine (Gly) and alanine (Ala) were also performed.

2. Experimental

2.1. Materials and methods

2.1.1. Chemicals

12-Tungstophosphoric acid, was made by Drachel's method [18]. Magnesium salts of WPA (MgWPA) [19], as well as glycine and alanine compounds of WPA (GlyWPA and AlaWPA) were prepared according to our previously developed procedures [20]. All chemicals were of analytical grade, provided by Merck. The content of tungsten in the obtained compounds was checked by ICP-AES, and the obtained and the theoretical values were in agreement.

2.1.2. Pot experiment

The soil used in the pot experiment was sampled from an unspoiled land in central Serbia. The plants were cultured in a green house. Systematic virus infection was carried out when the seeds had sprouted. When grown, they were placed one plant per plastic pot. Each tobacco plant involved in the experiment had at least four leaves. Systematic virus infection was caused by the mechanical inoculation of each plant by using carborundum for mechanical abrasion before applying the virus solution. Mechanical inoculation with TMV inoculums (contagious plant material containing viruses, dissolution 10^{-3}) was performed on one of the lower leaves of *Nicotiana tabacum var. Samsun*. After 3 days, the first signs of systematic infection of the plant could be observed, and the application of WPA compounds was carried out 2 days after that. The weighed WPA compounds were dissolved in distilled water to give a tungsten concentration of 5 mg/mL, and the prepared solutions were applied in portions of 50 μL per each half of leaf, on three leaves per pot. We analyzed four groups of plants: three infected and treated and one group of healthy plants (control). In the case of infected plants, we analyzed HPCs treated leaves, non-treated leaves with summits, stem and roof. Groups were treated with HPCs solutions for once, twice and thrice, with 10 days between each treatment. Plants were sampled 30 days after the first application. During growth, soil humidity was maintained by adding 50 mL of distilled water per pot every 3 days.

2.1.3. Investigation of antiviral activity

Antiviral activity of HPCs was investigated by following the number of spot damages that appeared on infected plants before and after treatment by solutions of HPCs. The effect of absorbed tungsten compounds on the growth of plants was studied too.

2.1.4. Sample and standard preparation

Six plants of each group were harvested and washed with distilled water three times. Water rinse, from the first washing of treated leaves was collected for each plant and analyzed. The whole plant in the pot experiment was separated into root, stem, leaf and the top of the plant, called summits. These sub plant samples were dried at 105 °C in an oven till constant weight and ground in a mortar with pestle. Obtained dry plant material was pressed and tablets of 100.0 mg were made.

For quantitative analysis several standards of tungsten in stable hexahydrate form of WPA (WPA-6) with various concentrations (from 10 ppm to 2000 ppm of tungsten), were made with the same matrix plant material (dried tobacco plant). Namely, it was possible to use plant material of the control group for standard preparation, as tungsten is not normally present in tobacco plant in detectable quantities. So, standards were prepared by addition of WPA-6 solutions of known concentration into dried material of healthy and non-treated plant. After drying and grinding and mixing with a mortar and pestle, the tablets of 100.0 mg were made.

2.1.5. EDXRF experimental

EDXRF measurements were performed on the EDXRF spectrometer (manufactured by Canberra) with a Si(Li) semiconductor detector and annular radioisotope excitation source ^{109}Cd (manufactured by Isotope Products). The nominal activity of the source was 740 MBq (declared on the June 15 2002) and the excitation energy was 22.1 keV. An MCA analyzer S35+ and MicroSampo Software were used for data collection. All samples and standards were measured for a period of 2000 s under the same experimental conditions on the sample holders made of Teflon rings and Mylar foil.

Peaks of tungsten, corresponding energies of 8397.6 eV ($L_{\alpha 1}$) and 8335.2 eV ($L\alpha_2$), were recorded, and analysis and deconvolution of those overlapped peaks were calculated by using Matlab 7.0, Peak Fit 4.0 and Origin 7.0 software. Each value of peak area was the mean value from three successive measurements without changing the experimental setup. The peak of zinc ($K_{\alpha 12}$ 8628.0 eV), which is present in the plant as an

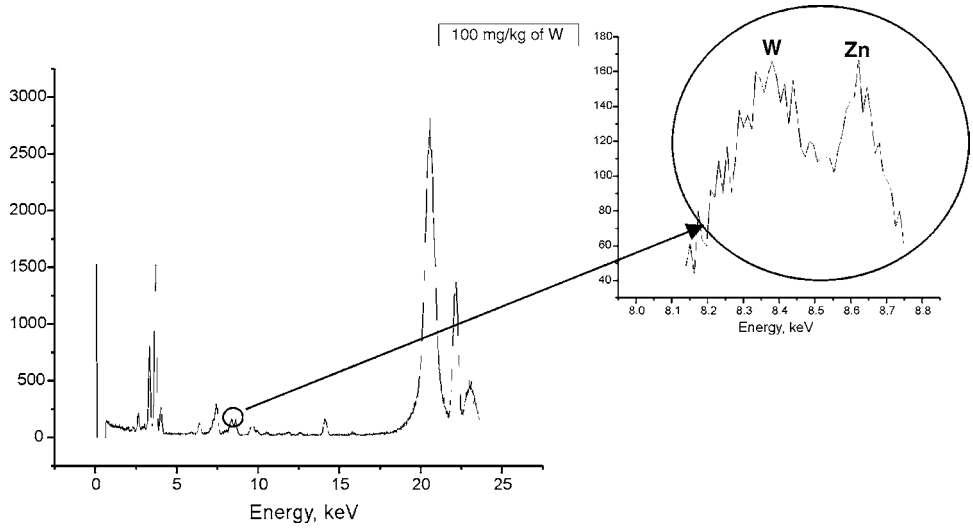

Fig. 1. Overlapping of bands characteristic for tungsten and zinc shown for EDXRF spectrum of dried *Nicotiana tabacum* leaves (standard prepared with 100 mg/kg of tungsten).

essential element tobacco plants, caused overlap with tungsten characteristic peaks, (Fig. 1). Therefore, the deconvolution procedure (Fig. 2) had to be performed, especially in the analysis of lower tungsten concentrations. The amount of zinc present varies with the plant part, but is probably not higher than about 50 ppm in the dried samples; it is typically 10–30 ppm in SRM NIST plant leaves. Zinc is highest in the parts that are in the intensive growing phase.

The tungsten detection limit was estimated to be 15 mg/kg (calculated on dry material), based on three times the standard deviation of the background. The tungsten content of 0.233 mg/kg normally present in plant (Virginia Tobacco Leaves–Ref. mat. ICHTJ-cta-VTL-2 [21]) is below the detection limit of the applied analytical technique.

The calibration curve is recorded as counts per mg/kg (content of tungsten in dried plant material) and that was used for quantitative determination of tungsten in samples. Linearity was good in a wide range of concentrations (the linear least squares line equation: $y = 18.54x - 238.3$ and $r^2 = 0.9996$).

3. Results and discussion

In comparison with literature data [22], one of the advantages of the EDXRF analytical technique in this study is the possibility of using of only 0.1 g of dried plant material instead of 1 g as usually required for multielement determination in plant materials. This was possible, as raw tobacco leaves are very succulent, and consist of about 93% of water, and the drying procedure causes sufficient pre-concentration of tungsten in samples. We analyzed different plant parts separately, along with the rinses, and it was established that the rate of tungsten recovery was not less than 93%. The average recovery of 94.47% of the tungsten indicates quantitative recovery and measurement by this method. Table 1 summarizes all the results obtained by EDXRF determination of tungsten applied, rinsed, absorbed and found in different plant parts.

The results of all the investigations confirm that tungsten was present in all analyzed sub plants after the treatment with HPCs. A translocation process of tungsten after the foliar application,

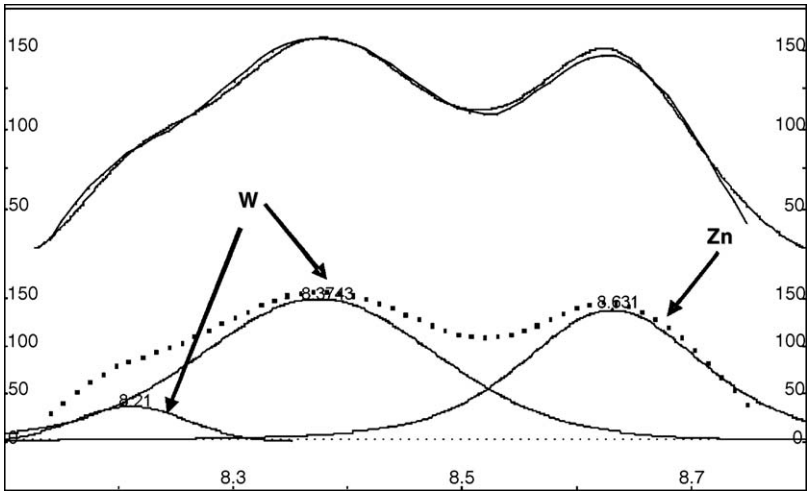

Fig. 2. Deconvolution of EDXRF spectrum of dried *Nicotiana tabacum* leaves (standard prepared with 100 mg/kg of tungsten).

Table 1
Summarized data of found and located tungsten in dried plant material

Number of treatments	Compound	Mg W, applied	Mg W, rinsed	Mg W, absorbed	Treated leaves, mg W	Untreated leaves, mg W	Stem, mg W	Root, mg W	% W found in plant[a]
1×	WPA	1.1074	0.0918	1.0156	0.2717	0.4471	0.1547	0.0837	94.23
	MgWPA	1.1027	0.0860	1.0167	0.2702	0.4371	0.1665	0.0994	95.73
	GlyWPA	1.0098	0.0862	0.9236	0.2301	0.4036	0.1428	0.0866	93.45
	AlaWPA	0.9928	0.0884	0.9044	0.2487	0.4119	0.1022	0.0838	93.61
2×	WPA	2.2149	0.2201	1.9948	0.5320	0.8516	0.2761	0.2019	93.29
	MgWPA	2.2054	0.1892	2.0162	0.5490	0.8349	0.3442	0.2030	95.78
	GlyWPA	2.0196	0.2336	1.7860	0.5235	0.7001	0.2674	0.1775	93.42
	AlaWPA	1.9856	0.2647	1.7209	0.5137	0.6835	0.2900	0.1699	96.31
3×	WPA	3.3224	0.5856	2.7368	0.9434	1.009	0.4086	0.2157	94.16
	MgWPA	3.3081	0.5614	2.7467	0.9078	1.048	0.4749	0.2269	96.74
	GlyWPA	3.0294	0.6063	2.4231	0.8764	0.855	0.3351	0.1723	92.38
	AlaWPA	2.9785	0.6117	2.3668	0.8573	0.862	0.3304	0.1884	94.57

[a] 94.47-average % of found W of totally applied amount of W.

Table 2
The concentrations of tungsten found in different sub plants in groups treated once with solutions of WPA, MgWPA, GlyWPA and AlaWPA

Concentration of W (mg/kg)	Treated leaves	Untreated leaves	Stem	Root
WPA	325 ± 14	308 ± 14	367 ± 12	329 ± 12
MgWPA	312 ± 11	302 ± 14	350 ± 11	338 ± 11
GlyWPA	281 ± 12	277 ± 12	324 ± 13	316 ± 12
AlaWPA	292 ± 11	287 ± 9	240 ± 9	287 ± 10

Mean standard deviations given for six plants in the same group in the pot experiment, with $n = 3$ for each sample.

from leaf to root, was noticed. The concentrations of tungsten in different sub plants after the first, second and third foliar applications of WPA, MgWPA, GlyWPA and AlaWPA were estimated and presented in Tables 2–4. It could be seen that after the first treatment there is no considerable difference in the concentration of tungsten in different sub plants. The only exception is in the case of WPA and MgWPA treatment, when the concentration of tungsten was slightly higher in the stem.

After the second treatment the average concentration of tungsten was approximatively doubled. The exception is in the case of GlyWPA and AlaWPA treatment, where it is evident that transport towards untreated (upper) plant parts is decreased. The possible explanation could be the slower transport of large molecules with amino acids. After the third treatment, the average concentration of tungsten is the highest in treated leaves,

Table 3
The concentrations of tungsten in different sub plants in groups treated twice with solutions of WPA, MgWPA, GlyWPA and AlaWPA (10 days between foliar applications)

Concentration of W (mg/kg)	Treated leaves	Untreated leaves	Stem	Root
WPA	597 ± 24	577 ± 21	572 ± 20	630 ± 19
MgWPA	610 ± 22	590 ± 22	607 ± 23	640 ± 18
GlyWPA	595 ± 21	492 ± 20	593 ± 24	640 ± 19
AlaWPA	587 ± 18	487 ± 19	629 ± 23	577 ± 18

Mean standard deviations given for six plants in the same group in the pot experiment, with $n = 3$ for each sample.

Table 4
The concentrations of tungsten found in different sub plants in groups treated thrice with solutions of WPA, MgWPA, GlyWPA and AlaWPA (10 days between each foliar application)

Concentration of W (mg/kg)	Treated leaves	Untreated leaves	Stem	Root
WPA	1036 ± 31	678 ± 28	814 ± 29	618 ± 27
MgWPA	993 ± 32	708 ± 27	872 ± 31	708 ± 27
GlyWPA	965 ± 30	602 ± 30	709 ± 30	551 ± 26
AlaWPA	969 ± 33	610 ± 27	691 ± 28	613 ± 29

Mean standard deviations given for six plants in the same group in the pot experiment, with $n = 3$ for each sample.

which confirms the saturation of tungsten uptake by the plant. Tungsten concentration is somewhat lower in the stem and the lowest in untreated leaves, summits and root, especially in the case of GlyWPA and AlaWPA treatment. The analysis of tungsten percentage rinsed from treated leaves shows also the saturation of tungsten uptake after the repeated HPCs treatment (Table 5). Namely, the plant attains saturation of tungsten content after absorption of WPA and MgWPA in the first two treatments. In the case of GlyWPA and AlaWPA, absorption decreases in rinse continually with repeated rinse treatments.

Increase in biomass of different parts of plants for the period of 30 days treatment is different. Therefore, it is also worth considering the percentage of tungsten in different plant parts of totally absorbed tungsten (applied–rinsed) after the repeated treatment. These results for the first, second and third HPCs applications are presented in Fig. 3a–c. The results of the analyses indicate the incorporation of exogenous tungstate in the

Table 5
Percentage of tungsten rinsed from leaves treated with HPCs (each value is mean for six plants)

% W rinsed from treated leaves	1× treated	2× treated	3× treated
WPA	8.29	9.94	17.63
MgWPA	7.80	8.58	16.97
GlyWPA	8.54	11.57	20.01
AlaWPA	8.90	13.33	20.54

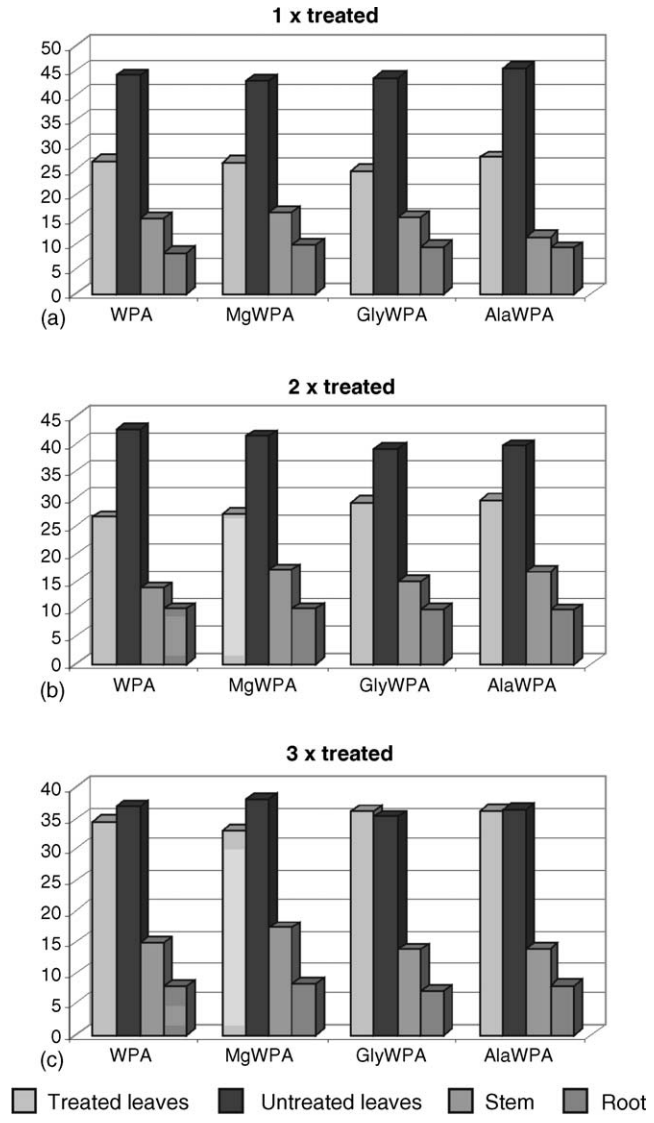

Fig. 3. Tungsten found (percentage) in different plant parts of totally absorbed tungsten (applied tungsten minus tungsten found in rinses) after the first (a), second (b) and third (c) repeated HPCs treatment.

plant and a translocation process of WPA from leaf to root when applied to leaves. A homeostatic regulation mechanism for excessive uptake of tungsten in plants is suggested to regulate the concentrations of tungsten in plant.

The effect was manifested as a decrease in the number of spots, and other damages that TMV causes on the majority of leaves. Also, treated groups of plants were considerably higher and more developed than the plants in the control group. Analysis of the results (for example, the plant height), showed slightly better activity of MgWPA.

The results of this study show that the spots and other damages caused by TMV on the majority of leaves almost completely disappeared after the HPCs treatment. The effect is obvious not only on the treated half part of the leaf but also on the other non-treated half, thus indicating the horizontal transport of HPC.

Inhibition effects were in positive correlation with the HPCs concentration. Negative effects of HPCs solutions on herbal

Table 6
Total dried plant mass of *Nicotiana tabacum* (each value is mean for six plants)

Mass of dried plants, (g)	1× treated	2× treated	3× treated
WPA	2.9642	3.1709	3.2502
MgWPA	3.0796	3.1987	3.2607
GlyWPA	2.9911	3.0561	3.1138
AlaWPA	3.0021	3.0326	3.0842

parts (phyto-toxicity is minimal) and for MgWPA almost do not exist. Negative effects could be noticed as some slightly lighter spots on leaf surfaces, probably due to slight acidity of the applied solutions. The comparison of results shows that better results could be obtained when the time between inoculation and first treatment is shorter.

Recent developments provide more data about new and interesting bioactivity of tungstate in humans and animals, such as exhibiting insulin-like [23], hepatoprotective [24], or antiobesity [25] properties. In this experiment we noticed not only the antiviral activity of WPA compounds, but also positive effects on plant growth. The results of following total dried plant mass confirmed that (Table 6) mass of the whole plants increases with the number of treatments with WPA compounds (the difference in mass is more pronounced if one takes into consideration that dried material is not more than 7% of fresh whole plant mass).

For the time being, there is not enough data about the mechanism of antiviral activity of WPA compounds against the plant viruses, but the tetrahedral structure of these compounds as well as for vanadate, tungstate, and molybdate, also appears to be a common factor important for their bio-actions [26,27]. More specialized experiments are necessary to be performed. The analytical procedure of EDXRF tungsten determination that we propose here is useful for easy and rapid measurements in such studies.

4. Conclusions

EDXRF spectrometry has been shown as a very convenient analytical technique for the analysis of plant material. The usual long and expensive treatment procedure of samples is avoided. The special advantage in this case was that tungsten is not normally present in the plant material at detectable levels by EDXRF. Therefore, standards and samples can be prepared with the same matrix. The accuracy of the method is satisfactory, as evidenced by the fact that 94.47% of the total applied amount of tungsten is located and recovered from different parts of the plant and the rinses, (Table 1).

It can be concluded that HPC with Keggin structure have positive antiviral activity on TMV, while the magnesium salt of WPA is the most efficient against plant TMV. Translocation of applied HPCs was apparent from the distribution of tungsten in different parts of plant. On the basis of the obtained results of the concentrations of tungsten in different parts of plant, it can be concluded that tungsten is transported through the plant in vertical and horizontal directions.

The obtained data are useful for consideration of possible application of this group of compounds in TMV treatment.

Acknowledgement

This work has been partly supported by the Ministry of Science and Environmental Protection of the Republic of Serbia, Project Nos. 142047 and 142037.

References

[1] M.T. Pope, Heteropoly and Isopoly Oxometallates, Springer-Verlag, New York, 1983.
[2] M.T. Pope, A. Müller, Polyoxometalate Chemistry. From Topology via Self-Assembly to Applications, Kluwer Academic, Dordrecht, 2001.
[3] J. Rhule, C. Hill, D. Judd, R. Schinazi, Chem. Rev. 98 (1998) 327.
[4] O. Delgado, A. Dress, A. Müller, M.T. Pope, Polyoxometalates: a class of compounds with remarkable topology, in: M.T. Pope, A. Müller (Eds.), Polyoxometalates: From Platonic Solids to Anti-Retroviral Activity, Kluwer Academic Publishers, Dordrecht, 1994.
[5] S. Uskoković-Marković, M. Todorović, U.B. Mioč, B. Krstić, N. Dukić, 3rd International Conference of Chemical Societies of the South-East European Countries, Bucharest, Romania, September 22–25, 2002.
[6] B. Smodis, M. Dermelj, R. Jacimovic, J. Radioanal. Nucl. Chem. 190 (1995) 3.
[7] R. Dybczynski, Fresenius J. Anal. Chem. 353 (1995) 120.
[8] B. Danko, R. Lobinski, R. Dybczynski, J. Radioanal. Nucl. Chem. 137 (1989) 145.
[9] M. Neuburger, A. Fourcy, J. Radioanal. Chem. 1 (1968) 289.
[10] H.J.M. Bowen, Biochem. J. 77 (1960) 79.
[11] H.F. Haas, V. Krivan, H.M. Ortner, Anal. Chim. Acta 149 (1983) 77.
[12] J.H. Watkinson, N. Z. J. Sci. 1 (1958) 201.
[13] B.F. Quin, R.R. Brooks, Anal. Chim. Acta 58 (1972) 301.
[14] S.A. Abbasi, Int. J. Environ. Anal. Chem. 35 (1989) 139.
[15] V. Il Rigin, I.V. Rigina, Zh. Anal. Khim. 35 (5) (1980) 929.
[16] B. Madeddu, A. Rivoldini, Atomic Spectrosc. 17 (1996) 148.
[17] P. Nangniot, Collection Czech. Chem. Commun. 30 (1965) 407.
[18] G. Brauer, Handbuch der Preparativen Anorganishen Chemie, Ferdinand Enke Verlag, Stuttgart, 1981.
[19] U.B. Mioč, M. Todorović, S. Uskoković-Marković, M. Davidović, A. Kremenović, A. Spasojević-de Bire, T. Čajkovski, V. Likar-Smiljanić, R. Biljić, Solid State Ionics 162 (2003) 217.
[20] V. Kuntić, I. Holclajtner-Antunović, S. Uskoković-Marković, U. Mioč, M.Todorović, M. Stanojević, V. Vukojević, Monatsch. Chem. (2006), in press.
[21] http://www-naweb.iaea.org/nahu/nmrm/nmrm2003/material/ichvtl2.htm.
[22] L. Guohui, F. Shouzhong, J. Geochem. Exploration 55 (1995) 75.
[23] J. Foster, S. Young, T. Brandt, R. Nordlie, Arch. Biochem. Biophys. 354 (1998) 125.
[24] S. Pawa, S. Ali Biochim, Biophys. Acta 1688 (2004) 210.
[25] M. Claret, H. Corominola, I. Canals, J. Saura, S. Barcelo-Batllori, J.J. Guinovart, R. Gomis, Endocrinology 146 (2005) 4362.
[26] S. Brichard, B. Desbuquois, J. Girard, Mol. Cell Endocrinol. 91 (1993) 91.
[27] A. Barbera, J.E. Rodrýguez-Gil, J.J. Guinovart, J. Biol. Chem. 269 (1994) 20047.

Available online at www.sciencedirect.com
ScienceDirect
Talanta 70 (2006) 307–314
Talanta
www.elsevier.com/locate/talanta

Application of factorial design in optimization of ultrasonic-assisted extraction of aluminum in juices and soft drinks

Nusrat Jalbani, Tasneem G. Kazi *, Bilal M. Arain, M.K. Jamali, Hassan I. Afridi, R.A. Sarfraz

Center of Excellence in Analytical Chemistry, University of Sindh, Jamshoro76080, Sindh, Pakistan

Received 29 December 2005; received in revised form 15 February 2006; accepted 15 February 2006
Available online 15 May 2006

Abstract

A sample preparation method based on ultrasound-assisted pseudo-digestion of Al from Juices and soft drink samples under ultrasonic effect has been described. A Plackett–Burman experimental design was used as a multivariate strategy for the evaluation of the effects of varying several variables at once. The effects of five different variables preintensification time (without ultrasonic stirring), intensification time in ultrasonic bath (UB), temperature of UB, two acid mixtures (HNO_3–H_2SO_4–H_2O_2 and HNO_3–H_2O_2), on the recovery of Al have been investigated. From these studies, certain variable showed up as significant, and they were optimized by a using 2^3 + star central composite design, which involved 16 experiments. The best conditions for pseudo-digestion were as follows: a preintensification time 10 min, intensification time 20 min, volume of acid mixtures 3.0 ml and temperature of ultrasonic bath 80 °C. A conventional acid digestion on electric hot plate was used to obtain total Al for comparative purpose. Final solutions obtained from both methods, were analysed by electrothermal atomic absorption spectrometry. Analytical results for the Al by ultrasound-assisted pseudo-digestion, and conventional wet digestion methods showed a good agreement, thus indicating the possibility of using ultrasonic-assisted digestion sample preparation instead of intensive treatments inherent with the acid digestion methods on electric hot plate. The procedure proposed allowed the determination of Al with detection limit ($3\acute{\alpha}/s$) 10 $\mu g\,l^{-1}$.

Keywords: Ultrasonic bath; Aluminum; Factorial design optimization; Electrothermal atomic absorption spectrometer (ETAAS); Soft drink; Juices

1. Introduction

Aluminum (Al) is the most popular metallic element in industries and consequently in our surroundings. However, it has attracted much attention for more than two decades in discussing whether it has any relationship with serious dementia cause Alzheimer's disease. Potential health risks associated with elevated Al intake have long been discussed among physicians and Al poisoning in patients with chronic renal failure is one of the most important clinical problems involving trace metal toxicity [1].

Despite the facts that Al is present in all foodstuffs, the question of contamination with Al from the sources arises now and then. It is well known that acidic food such as apple, rhubarb or vinegar may cause corrosion of cooking pans and that, due to this, the Al content of the food may rise during preparation [2,3]. The hypothesis that Al exposure is etiological related to Alzheimer's disease has lead to much debate. Ecological studies have suggested that concentration of Al in drinking water of 0.1–0.20 mg l^{-1} may increase the risk of Alzehiemer's disease with relative risk ranging from 1.35 to 2.6 mg l^{-1} [4,5]. Thus special efforts should be taken to prevent contamination of food and beverages, etc., with Al either directly or during preparation with special regards to infants, old people or individual with suboptimal renal functionality.

The determination of metals in complex samples by atomic absorption spectrometry (AAS) generally requires the destruction of the sample matrix to render a solution of the analyte ready for analysis. Sample digestion techniques, such as microwave,

* Corresponding author. Tel.: +92 221 771379; fax: +92 221 771560.
E-mail addresses: nusratjalbani_21@yahoo.com (N. Jalbani), tgkazi@yahoo.com (T.G. Kazi), bilal_KU2004@yahoo.com (B.M. Arain), mkhanjamali@yahoo.com (M.K. Jamali), hassanimranafridi@yahoo.com (H.I. Afridi), ras_chemist@yahoo.com (R.A. Sarfraz).

0039-9140/$ – see front matter © 2006 Elsevier B.V. All rights reserved.
doi:10.1016/j.talanta.2006.02.045

and conventional wet acid digestion (CDM) for total heavy metal determination have been used widely for the dissolution of target elemental analytes [6,7]. Such digestion techniques require the use of concentrated acids and high temperatures, and often high pressures, to affect the total dissolution of elemental analytes from liquid and solid samples [8]. For elemental analysis, the sample preparation procedure employed is, apart from sample collection, ordinarily the most time-consuming step in the overall analysis [9]. The efficiency of the wet digestion procedures can be enhanced with the use of ultrasound irradiation [9,10]. Ultrasonic radiation can be considered another alternative for sample pre-treatment, since ultrasound facilitates an auxiliary energy and accelerates some steps, such as dissolution, fusion and leaching, among others [11]. In many situations, ultrasound-assisted leaching is an expeditious, inexpensive and efficient alternative to conventional extraction techniques and, in some cases, even to supercritical fluid and microwave-assisted extraction, as demonstrated by application to both organic and inorganic analytes in a wide variety of samples [12–14].

Several means of optimization can be used for the extraction of metals from different matrixes, but some methods are time-consuming: for instance, the study of each variable separately. Procedures for optimization of factors by multivariate techniques have been encouraged, as they are faster, more economical and effective, and allow more than one variable to be optimized simultaneously [15,16]. Among the different groups of designs, Plackett–Burman designs (PBDs), introduced in 1946 by Plackett and Burman [17], allow us to discover the most significant variables for a certain system with only few experiments. They are used as a screening method in order to select the variables that have influence on a system but they do not give the optimum value for each variable.

In order to obtain the optimum values for each variable involved in a certain system, central composite designs are the most widely used design framework [18]. These design structures are based on full two-level factorial design by center point replication and inclusion of an axial portion [19]. The optimization procedures based on these approaches are nowadays being applied to optimize some sample pre-treatments and operating conditions for some analytical techniques [20–23].

The aim of this work was to improve sample preparation performance, proposing the development of an ultrasound-assisted pseudo-digestion method (UDM) for fast and reproducible recovery of Al in soft drinks and juices. Factorial designs were used for optimization of the experimental variables. Parameters influencing ultrasound-assisted pseudo-digestion, such as preintensification time (without ultrasonic stirring) intensification time (in ultrasonic bath), acid mixtures, temperature of ultrasonic bath are fully investigated. Due to there being many variables that affect the acid digestion process, in order to obtain the optimal values for each variable, experimental designs, such as Plackett–Burman and central composite designs, have been used throughout the optimization.

2. Experimental

2.1. Reagents

Through out the experimental work using ultrapure water, obtained from a Milli-Q purification device (Millipore Co., Bedford, MA, USA). For the preparation of samples, standards and blanks, Milli-Q water additionally purified by distillation. All reagents used were of analytical reagent-grade. Concentrated Nitric acid, sulphuric acid, 30% hydrogen peroxide were spectroscopic grades (Merck, Darmstadt, Germany) and were checked for possible trace Al contamination by preparing blanks for each procedure. Certified standard of Al (1000 ppm) was obtained from Fluka (Buchs SG, Switzerland) Laboratory glass wares was kept overnight in 10% (v/v) nitric acid solution, and washed with distilled water and finally with ultrapure water before use.

2.2. Instrumentation

The ultrasonic-assisted digestion experiments were carried out with an ultrasonic bath Sonicor, Model No. SC-121TH, Sonicor Instrument Corporation Copiague, NY, USA with technical specifications; programmable for temperature ranging from 0 to 90 °C, timer 0–30 min, 220 V, 50/60 Hz, intensification frequency 35 kHz for the ultrasound energy and a total volume of 4 l, was used to induce the acid digestion process. Al was determined in both digests obtained by both procedures using atomic absorption spectrometer of Hitachi Ltd., Model 180-50, S. No. 5721-2, equipped with graphite furnace G-03. The instrumental parameters are shown in (Table 1).

The calibration curves (0.1–1.0 $\mu g\, m1^{-1}$) for aluminum were established with solutions prepared from a 1000 $\mu g\, ml^{-1}$ certified stock solution.

2.3. Samples

Different eight brands of Soft drink and 10 juice samples were collected from the urban areas of Hyderabad city during 2004–2005. Five to ten samples of different batches of the same brand of both drinks packed on different dates were also

Table 1
Measurement conditions for ETAAS for aluminum

Instrumental parameters	
Lamp current (mA)	10
Wave length (nm)	309.3
Slit-width (nm)	1.3
Cuvette	Tube
Carrier gas (ml/min)	200
Sample volume (μl)	10
Temperature programming [temperature range/time (s)]	
Dry	80–120/15
Ash	400–700/15
Atomization	2700–2800/5
Cleaning	2800–2900/2

collected to observe the variation in the elemental contamination levels of the products.

For determination of Al in the mg l^{-1} range, extreme care was taken to accomplished, collection, storage, preparation, and final analysis without outside contamination from this ubiquitous element. The all samples were mechanically stirred for 1 h to degas. The accuracy of methodology was performed by standard addition method, because reference materials for soft drinks and juices are not commercially available. The triplicate samples of 7-up and Frooto was spiked with known amount of aluminum and subjected to both methods to perform a recovery test.

2.4. Procedures

Four sub-samples of each batch packed on different dates of soft drink and juice were used for analytical determinations with the conventional wet acid digestion and pseudo-digestion procedures. With each series of conventional and ultrasonic-assisted pseudo-digestions, blank were measured. Each result is the average of 20–40 readings for samples. The concentrations were obtained directly from calibration graphs after correction of the absorbance for the signal from an appropriate reagent blank.

2.4.1. Ultrasound-assisted pseudo-digestion method (UDM)

For pseudo-digestion optimization, different mixtures of concentrated acids and oxidants, HNO_3:H_2SO_4:H_2O_2 (1:1:1, v/v/v) (M1) and HNO_3:H_2O_2 (1:1, v/v) (M2), preintensification time (without ultrasonic stirring) (P) for different time interval (2–10 min), intensification or sonication times (5–20 min) and the temperature of ultrasonic bath was ranged between 40 and 90 °C were tested. To evaluate the efficiency of the process, the results obtained with the UDM were compared with those from CDM.

To optimized the different analytical variables, three replicate of 0.5 ml of five sets of sub samples of soft drink and juice were taken in Pyrex flasks (50 ml capacity), concentrated mixture of acids M1 and M2 were added at two level minimum (−) and maximum (+) separately. After different time intervals (2–10 min) at room temperature, the flasks were placed inside the ultrasonic water bath and were subjected to ultrasonic energy at 35 kHz for different time interval (5–20 min). The temperature range of ultrasonic water bath was 40 and 80 °C. After sonication for different time intervals, the supernatant liquid was evaporated to approximately 0.5 ml final volume on a heating plate. Final solution was made up to 10 ml with 2N HNO_3 and subjected to sonication for another 2 min and made volume upto 10 ml with 2N HNO_3 in volumetric flasks. The final solutions were collected in polyethylene flask, for the determinations of Al by ETAAS. Blanks were also treated in the same way.

2.4.2. Conventional digestion method (CDM)

Duplicate 0.5 ml of sub samples of soft drink and juices were placed into 50 ml Pyrex flasks. Added 5 ml volume of a freshly prepared mixture of concentrated HNO_3:H_2SO_4:H_2O_2 (1:1:1, v/v/v), to each flak and solutions were heated on electric hot plate at 80 °C, for 2–3 h, till the clear transparent digests were obtained. Final solutions were made up to 25 ml with 2N HNO_3. The final solutions were collected in polyethylene flask, for the determinations of Al by ETAAS blank digestions were also carried out. The concentrations were obtained directly from calibration graphs after correction of the absorbance for the signal from an appropriate reagent blank.

Table 2
Factors and levels used for the Plackett–Burman and central composite designs in the factorial design

Variables	Low (−)	High (+)	Optimum conditions
HNO_3:H_2SO_4:H_2O_2 (M1) (1:1:1), ml	1.0	3.0	3.0
HNO_3:H_2O_2 (1:1) (M2), ml	1.0	3.0	3.0
Preintensification time (P), min	2	10	10
Intensification time (t), min	5	20	20
Temperature (T), °C	40	80	80

Volume 0.5 ml for all experiments.

2.5. Procedure used in the factorial design

For the evaluation of five factors at two levels a Plackett–Burman design with only sixteen experiments is described instead of the $2^5 = 32$ required for a full factorial design. The Plackett–Burman matrix shown in Table 3, where the low (−) and high (+) levels are those specified in Table 2. Sixteen experiments were carried out for completing the factorial designs, the resulting values (1–16) being of three replicates. The experimental data were processed using the (Minitab 13.2 (Minitab Inc., State College, PA) and Microsoft Excel 2000.

2.5.1. Optimization strategy

Some times, the effect of some factors are less significant can lead to wrong results on the importance of the most significant variables. Plackett–Burman designs constitute a variation on saturated fractional designs, allowing the evaluation of either system with few experiments; k factors can be studied in $k+1$ runs (only the main effects are estimated). These designs can be used only when $k+1$ is a multiple of 4 (i.e., $k = 3, 7, 11\ldots$). This enlarges the opportunities offered by the saturated factorial design, which it complements [24]. Another characteristic of Plackett–Burman designs is the orthogonality property. In order to obtain the optimum values for each variable involved in a certain system central composite designs (CCDs) are the most widely used design framework for second-order RS modeling within k factor experiments [25].

The optimization process was carried out using a factorial Design 2^3 with center points. In our present work the statistically significant variables were, volume of (M1), intensification

Table 3
Plackett–Burman design

Data matrix							
Experiment Number	A (M1)	B (M2)	C (*P*)	D (*t*)	E (*T*)	%Recovery of Al[a]	Estimated variance (s^2)
1	+	−	−	−	+	66.3 ± 0.17	0.03
2	+	+	−	−	−	30.2 ± 1.05	1.11
3	+	+	+	−	−	36.2 ± 0.40	0.16
4	+	+	+	+	−	50.7 ± 0.50	0.25
5	−	+	+	+	+	94.3 ± 0.29	0.08
6	+	−	+	+	+	99.3 ± 0.21	0.04
7	−	+	−	+	+	78.5 ± 0.20	0.04
8	+	−	+	−	+	75.5 ± 0.56	0.31
9	+	+	−	+	−	38.7 ± 0.30	0.09
10	−	+	+	−	+	70.3 ± 0.30	0.09
11	−	−	+	+	−	48.9 ± 0.30	0.09
12	+	−	−	+	+	97.8 ± 0.30	0.09
13	−	+	−	−	+	70.2 ± 0.15	0.02
14	−	−	+	−	−	25.7 ± 0.20	0.04
15	−	−	−	+	−	28.9 ± 0.30	0.09
16	−	−	−	−	−	24.2 ± 0.20	0.04

Factors: 5, replicates: 1, design: 16, runs: 16, center points (total): 0.
[a] Mean values of triplicate results.

time (*t*), and temperature of the ultrasonic water bath (*T*), were regarded as factors for optimization experiment.

2.5.2. Calibration and sensitivity

Calibration and standard addition graphs were obtained for Al. However, as the acid composition of both acid mixture and different matrixes of samples, the standard addition technique was used throughout the development of Plackett–Burman and central composite designs. The mean and standard deviation, for $N = 9$, of the slopes of the standard addition graph corresponding to Al was $0.176 \pm 0.004\ \mu g\ ml^{-1}$ and good precision could be seen for the calibration.

The detection and quantification limits, given by

$$\text{LOD} = 3 \times \frac{s}{m} \quad \text{and} \quad \text{LOQ} = 10 \times \frac{s}{m}$$

respectively, where s is the standard deviation of nine measurements of reagent blank and m is the slope of the calibration or standard addition graph was obtained for Al. LOD of $10\ \mu g\ l^{-1}$ being reached, and LOQ of $25\ \mu g\ l^{-1}$ for Al was calculated.

Reproducibility of the method was assessed by using three replicates of soft drink (7-up) and juices (Frooto) taken from the same packages. The most reliable approach evaluating the accuracy of an analytical method requires analysis of certified reference materials with chemical composition and analyte concentration, which match those of the samples under investigation. To the best of our knowledge, there are no any commercially available juices or soft drink reference materials with certified Al content. Hence, spike recovery test was performed by spiking juice and soft drink samples prior to the ultrasonic-assisted and conventional wet acid digestions. Such spiking was performed in triplicate at three concentration levels 2, 4 and $8\ \mu g\ ml^{-1}$, respectively, and in this experiment we make the volume up to 25 ml in volumetric flasks and were analysed by ETAAS. Average recovery of Al spikes from juices and soft drink matrixes were shown in Table 5.

3. Results and discussion

Five factors were selected to be examined. The factors and their levels, low (−) and high (+), are described in Table 3. Two factors are related to the acid solution composition, M1 and M2 which are (HNO_3–H_2SO_4–H_2O_2) and (HNO_3–H_2O_2), respectively. Other factors correspond to the preintensification time treated samples with acid mixture M1, M2 and keep at room temperature (without ultrasonic stirring), temperature of Ultrasonic bath and the exposure time to ultrasound, which are symbolized by *P*, *t* and *T*, respectively. The sample volume kept constant for all experiment 0.5 ml. The ultrasound energy was fixed at a frequency of 35 kHz for all experiments. The effect of changing a factor from a low level to a high level value was examined on a selected response such as percentage recovery according to the following equation:

$$\text{recovery} = \frac{[]_{\text{pseudo digestion}}}{[]_{\text{conventional digestion}}} \times 100$$

where $[\text{UDM}]_{\text{pseudo-digestion}}$, the metal concentration obtained after the ultrasonic-assisted digestion procedure (each experiment 1–16 in Table 3) and $[\text{CDM}]_{\text{conventional digestion}}$ is the metal concentration found after an conventional acid digestion by heating on electric hot plate. A recovery close to (98–99%) would show quantitative of Al obtained by proposed method. Both Al, concentrations after ultrasonic-assisted acid digestion and conventional wet acid digestion procedures were measured using the standard addition technique.

3.1. Effects of variables

3.1.1. Influence of acid solvent composition

From the results of the Plackett–Burman design (Table 3), it is clearly seen that acid mixture 'M1' (HNO_3–H_2SO_4–H_2O_2) provide a significantly higher recoveries of Al. Acid volume

required for 0.5 ml of sample was 3 ml for both acid mixture for maximum recovery of Al. The second acid mixture M2 (HNO_3–H_2O_2) appears to be insignificant for the acid digestion of Al under study. The presence of high amount of sugar in soft drinks and juices, was oxidized by H_2SO_4 more efficiently as compared to M2 acid mixture. The triplicate analytical results obtained for each experiments are shown in Table 3.

It can be noted that with minimum volume (−) of acid mixture M1 have 62.3%, although the other variables (sonication time and temperature) have optimum values, while maximum acid volume (+) with maximum values of two variables (*T*) and (*t*), the extraction efficiency was found 99.3%.

3.1.2. Influence of the preintensification time

The samples after treated with of different mixture and volume of acid in flasks containing 0.5 ml samples and keep at room temperature for different time intervals in range of 2–10 min, to avoid effervesces produced due to high sugar content of soft drink and juices. Although the recovery of Al was not significantly effected due to preintensification (without ultrasonic stirring).

3.1.3. Influence of temperature

The increase in the water bath temperature showed a highly significant effect on the recovery of Al. Therefore, the temperature of the ultrasonic water bath was significant for the acid digestion of aluminum. The effects of temperature of ultrasonic bath in the range of 40–80 °C, the maximum recovery of Al was observed at 80 °C.

3.1.4. Influence of intensification time

Intensification time is in the range of 5–20 min, however, it can be seen in Table 3 that the maximum recoveries of Al were achieved after 20 min at temperature 80 °C of ultrasonic bath. The recovery of Al using ultrasonic-assisted pseudo-digestion required maximum 20 min to reach the same recoveries of Al by CDM. There was no significant difference between 20 and 30 min sonication period for Al at 0.05 probability but was 20 min. The results show that 20 min exposure time was enough for maximum recovery of Al from the studied samples.

In conclusion, three factors, acid mixture (M1), intensification time (*t*) and temperature of ultrasonic water bath (*T*), were the most significant variables for the recovery of Al in samples studied.

3.2. Final optimization by central composite design

Having screened out the variables that did not have a significant effect on the response, the remaining three factors were optimized to provide the maximum Al recovery. A central 2^3 + star orthogonal composite design with six degrees of freedom and involving 16 experiments was performed, optimizing the variables acid mixture HNO_3–H_2SO_4–H_2O_2 (M1), intensification time (*t*), and temperature of the ultrasonic water bath (*T*).

The experimental field definition for this design is given in Table 4, also showed the central composite design matrices together with the response obtained for Al. Fig. 1a and b shows the estimated response surface for each pair variables, acid mixture (M1/*t*), (M1/*T*) to obtained the maximum %recovery of Al. It can be seen from figure that the %recovery of Al is increased when the temperature of ultrasonic bath is higher, achieving the

Table 4
Central 2^3 + star central composite design ($n = 16$) for the set of (M1), (*t*) and (*T*) in Al

Run	A (M1)	B (*t*)	C (*T*)	%Recovery
1	$K_0{}^1$	$K_0{}^2$	$K_0{}^3$	63.3
2	−	−	−	24.6
3	+	−	−	31.2
4	−	+	−	35.9
5	+	+	+	99.3
6	−	−	+	55.3
7	+	−	+	71.3
8	−	+	+	62.3
9	−	−	−	24.3
10	$-a^a$	$K_0{}^2$	$K_0{}^3$	28.1
11	$+a^b$	$K_0{}^2$	$K_0{}^3$	42.8
12	$K_0{}^1$	$-a^c$	$K_0{}^3$	51.3
13	$K_0{}^1$	$+a^d$	$K_0{}^3$	78.9
14	$K_0{}^1$	$K_0{}^2$	$-a^e$	26.2
15	$K_0{}^1$	$K_0{}^2$	$+a^e$	94.8
16	$K_0{}^1$	$K_0{}^2$	$K_0{}^3$	60.2

Factors: 3, replicates: 1, design: 8, runs: 16, center points (total): 2^3. $K_0{}^1 = 2.0$ ml, $K_0{}^2 = 12.5$ min, $K_0{}^3 = 60°$, $-a^a = 0.2$ ml, $+a^b = 4$ ml, $-a^c = 7$ min, $+a^d = 25$ min, $-a^e = 30$ °C, $+a^e = 90$ °C.

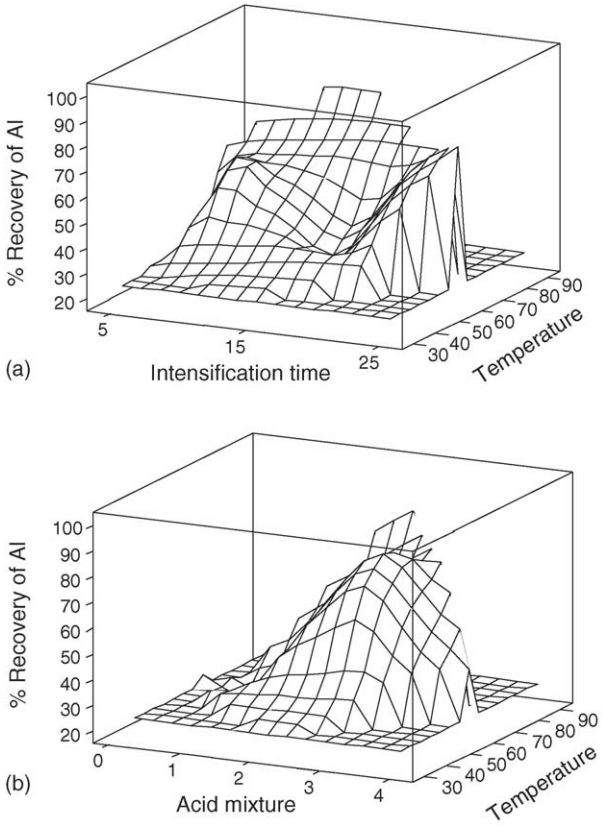

Fig. 1. a Estimated response surface from the central composite design %recovery of Al/intensification time *t*/temperature. Graph 1b: estimated response surface from the central composite design %recovery of Al/acid mixture/temperature.

Table 5
Comparison of digestion methods for %recovery of Al from soft drink and juice samples ($\mu g\,ml^{-1}$) (d.f. = 4), $t_{crit} = 2.7764$

Frooto (orange juice)					7-up (soft drink)				
CDM, $x \pm$ S.D.	RSD, %	UDM, $x \pm$ S.D.	RSD, %	t_{exp}	CDM, $x \pm$ S.D.	RSD, %	UDM, $x \pm$ S.D.	RSD, %	t_{exp}
3.52 ± 0.21	6.0	3.46 ± 0.20	5.8	0.63	4.5 ± 0.23	5.1	4.4 ± 0.21	4.8	0.83
3.53 ± 0.20	5.7	3.48 ± 0.25	7.2	0.72	4.52 ± 0.25	5.5	4.45 ± 0.19	4.3	0.51
3.54 ± 0.24	6.8	3.49 ± 0.27	7.7	0.71	4.55 ± 0.27	5.9	4.6 ± 0.23	5.0	0.19
3.56 ± 0.19	5.3	3.5 ± 0.21	6.0	0.71	4.51 ± 0.28	6.2	4.47 ± 0.25	5.6	0.75
3.51 ± 0.23	6.6	3.47 ± 0.22	6.3	0.25	4.59 ± 0.23	5.0	4.5 ± 0.24	5.3	0.69

CDM: conventional acid digestion method, UDM: ultrasonic-assisted acid digestion method.

optimum value of Al in soft drinks. The maximum temperature of ultrasonic bath is 90 °C, while maximum recovery was achieved at 80 °C, there is no any significant effect on %recovery of Al to ranging the temperature up to 90 °C.

It can be observed that the effect of acid mixture M1′ (HNO_3–H_2SO_4–H_2O_2) (variable A) and intensification time (t) shows low recovery of Al, but both of these two variables (A and B) have positive correlation with temperature (T) to release maximum recovery of Al 98.7%. In the case of high level (+) for factor A (M1), E (T), and low level of factors (−) (D) showed low recovery of Al, i.e., 71.3%, so the exposure time to ultrasonic stirring was also a significant factor. These effects show p-value less than 0.05, indicating that they are statistically significant at a 95.0% confidence level. Hence, the effects of these factors were studied more carefully.

At higher acid mixture (M1) volume + a^b (4.0 ml) and intensification time 12.5 min at the temperature of ultrasonic water bath (ko^3) 60 °C, the recovery of Al was obtained 42.8%, while at M1 2.0 ml (ko^1) and t values (ko^2) 12.5 min at maximum temperature (+a^f) 90 °C, the considerable recovery 94.8% was obtained.

For maximum recovery of Al the maximum temperature of ultrasonic bath 80 °C, intensification time 20 min and acid mixture M1′ (HNO_3–H_2SO_4–H_2O_2) was required. So the interactions of these variables were remarkable.

3.3. Accuracy

The precision of the proposed ultrasound-assisted pseudo-digestion process and ETAAS determination was evaluated through the analysis of five replicates of soft drink (7-up) and juice sample (Frooto), which were subjected to the CDM and UDM procedures under optimum conditions for each case according to Table 5. The relative standard deviations were found for CDM and UDM in the range of (5.0–6.8) and (4.3–7.7)%, respectively, which are acceptable range for this kind of studies.

3.4. Analytical application

The optimized values for the different variables (Table 2) were applied to the analysis of soft drink and juice samples, with and without Al spikes. Three replicate of 0.5 ml degassed soft drink and juice samples was used for analysis and there were spikes with 2–8 $\mu g\,ml^{-1}$. The results are showed in (Table 6) including the recovery data for added Al. The remaining all soft drink and juices samples were analysed by the optimized ultrasonic-assisted digestion.

Table 6
The results for tests of addition/recovery for Al determination in soft drink and juice samples ($N = 3$)

Added ($\mu g\,ml^{-1}$)	Al founda ($\mu g\,ml^{-1}$)			
	$\bar{x}$ CDM	Recovery of Al (%)	$\bar{x}$ UDM	Recovery of Al (%)
Juice (Frooto)				
0	3.53 ± 0.12	–	3.48 ± 0.13	–
2	5.514 ± 0.2	99.7	5.44 ± 0.14	99.3
4	7.5 ± 0.24	99.6	7.39 ± 0.19	98.8
8	11.56 ± 0.21	100.3	11.32 ± 0.23	98.6
(Soft drink 7-up)				
0	6.52 ± 0.2	–	4.47 ± 0.16	–
2	8.518 ± 0.33	99.8	6.4 ± 0.23	98.9
4	12.51 ± 0.46	99.7	8.35 ± 0.28	98.5
8	6.52 ± 0.2	99.8	12.28 ± 0.45	98.5

Confidence limit, 95%. Average values ± standard deviation ($N = 3$).

3.5. Evaluation of soft drink and juice samples for Al

Analytical results obtained by proposed method corresponding to the soft drink and juice samples analysed are shown in Table 7. Aluminum can be taken into the body from food, both as naturally occurring aluminum and as additives, and transfer of

Table 7
Determination of aluminum in juice and soft drink sample using ultrasonic-assisted pseudo-digestion method ($\mu g\,ml^{-1}$)

S. No.	Juice samples	Mean ± S.D. ($\mu g\,ml^{-1}$)	Soft drink samples	Mean ± S.D. ($\mu g\,ml^{-1}$)
1	Nestle	3.9 ± 0.13	Apple sidra	6.0 ± 1.68
2	Twist	5.8 ± 0.49	Miranda	6.6 ± 1.25
3	Fruity fun	3.6 ± 0.69	Dew	4.6 ± 0.68
4	Lemon barley	3.1 ± 0.40	Fanta	5.6 ± 1.15
5	Maza	4.9 ± 1.42	Pakola	6.4 ± 0.91
6	Shezan	3.9 ± 0.5	7-up	4.4 ± 0.56
7	Frooto	3.47 ± 0.90	Slice	12.0 ± 1.15
8	Frost	2.8 ± 0.89	Pepsi	6.8 ± 1.11
9	Classic	8.2 ± 2.12		
10	Poly	2.15 ± 0.41		

($N = 45$).

Table 8
Daily intake of aluminum by consumption of soft drinks and juices (mg of Al based on 250 ml juices/person/day) WHO values for drinking water 0.2 μg ml^{-1}

Sample name	Daily intake of Al/person/day (μg ml^{-1})	Sample name	Daily intake of Al/person/day (μg ml^{-1})
Nestle	1.0	Apple sidra	1.55
Twist	1.5	Miranda	1.675
Fruity fun	0.93	Dew	1.175
Lemon barley	0.8	Fanta	1.425
Maza	1.25	Pakola	1.625
Shezan	1.0	7-up	1.125
Frooto	0.88	Slice	3.1
Frost	0.73	Pepsi	1.725
Classic	2.1		
Poly	0.55		

aluminum from cooking implements and containers (including aluminum drink cans), aluminum in water, aerosols and dusts [26]. It is notable that aluminum accumulates with age in lung, bone and brain tissue, and this has lead in part to the controversy about aluminum and a possible association with Alzheimer's disease. When aluminum accumulates acutely in tissues such as the brain, it has the potential to cause serious adverse neurological effects [27].

Many studies have identified high levels of aluminum in the contents of some aluminum canned drinks and juices [28]. Commercially available soft drinks and juices are widely used in all cities of Pakistan especially in summer season as the reliable source for drinking. Based on investigation as cited above, the Al concentration in the different brands of soft drinks and juices from the local market of Pakistan, analysed during the present study were found in the range of (4.4–12.0) and (2.15–8.2) mg l^{-1}, respectively (Table 7). It was noted that all of the juice and soft drink samples tested have an Al concentration, above the WHO's limit for the maximum total content of Al in drinking water (0.2 mg l^{-1}, Recommendations of WHO, 1998) [29]. The separate standard values for soft drinks and juices have not been available, so in the literature people have compared them with normal drinking water standard [30,31]. All the samples show higher values than the legal recommended value indicating that soft drinks and juices producing companies are using alum for the purification of their raw water than using standard water purification methods. The dietary intake of Al via drinking of these soft drinks and juices were estimated on the consumption of 250 ml/person/day (Table 8).

4. Conclusion

Application of factorial designs allowed the development of analytical procedure for the determination of aluminum by ETAAS, based on Ultrasonic-assisted pseudo-digestion (UDM), using a smaller number of experiments. The method described offers a rapid, easy and efficient sample preparation method for direct determination of aluminum samples by ETAAS. All parameters studied (sonication time, sample volume, acid mixtures and temperature) influence the pseudo-digestion efficiency. The use of the Ultrasonic-assisted pseudo-digestion method allowed the leaching of the target analyte in a shorter time than required by the conventional wet acid digestion. The UDM is a rapid, inexpensive, easy, reproducible and selective technique for the total determination of aluminum samples, which are important in monitoring environmental pollution.

It is evident from the present studies that the level of Al in soft drinks and juices were above the permissible values by WHO for drinking water.

References

[1] J. Savory, S. Berthols, S. Brown, M.R. Wiss, Alumium, in: R.F.M. Herber, M. Stoeppler (Eds.), Trace Elements Analysis in Biological Specimen, Elsiever, Amsterdam, 1994, pp. 273–320.
[2] J.L. Greger, W. Goetz, D. Sullivan, J. Food Protect 48 (1985) 772–777.
[3] Liukkonen-Lilja, H.S. Piepponen, Food Addit. Contam. (1992) 213–223.
[4] H. Jackmin, D. Commenges, L. Lettneur, P. Barberger-Gataeu, J.F. Dartigues, Am. J. Epidemiol. 48 (1994) 57.
[5] D.R.C. McLachlan, C. Bergeron, J.E. Smith, D. Boomer, S.L. Rifat, Neurology 401 (1996) 501.
[6] Z. Sulcek, P. Povondra, Methods of Decomposition in Inorganic Analysis, CRC Press, Boca Raton, FL, 1989.
[7] H. Matusiewicz, Anal. Chem. 71 (1999) 3145.
[8] K. Ashley, R.N. Andrews, L. Cavazos, M. Demange, J. Anal. Atom. Spectrom. 16 (2001) 1147.
[9] M.D. Luque de Castro, M.P. da Silva, Trends Anal. Chem. 16 (1997) 16.
[10] J.L. Gomez-Ariza, E. Morales, R. Beltran, I. Giraldez, M. Ruiz-Benitez, Analyst 120 (1995) 1171.
[11] S. Morales-Munoz, J.L. Luque-Garcia, M.D. Luque de Castro, Crit. Rev. Environ. Sci. Technol. 33 (2003) 391.
[12] A.V. Filgueiras, J.L. Capelo, I. Lavilla, C. Bendicho, Talanta 53 (2000) 433.
[13] M.C.T. Diniz, O.F. Filho, E.V. Aquino, J.J.R. Rohwedder, Talanta 62 (2004) 469.
[14] M. Zougagh, A.G. Torres, E.V. Alonso, J.M.C. Pavon, Talanta 62 (2004) 503.
[15] S.L.C. Ferreira, M.A. Bezerra, W.N.L. dos Santos, B.B. Neto, Talanta 61 (2003) 295.
[16] W.N.L. dos Santos, C.M.N. dos Santos, S.L.C. Ferreira, J. Microchem. 75 (2003) 211.
[17] R.L. Plackett, J.P. Burman, Biometrika 33 (1946) 305.
[18] R.A. Olivero, J.M. Nocerino, S.N. Deming, in: J. Einax (Ed.), Chemometrics in Environmental Chemistry Statistical Methods, 98, Springer-Verlag, Berlin, Germany, 1995, pp. 98–99.
[19] W.P. Gardiner, G. Gettinby, Experimental Design Techniques in Statistical Practice — A Practical Software-based Approach, 335, Ellis Horwood, Chichester, Sussex, UK, 1998, p. 338.
[20] B. Lavilla, C. Perez-Cid, Bendicho, Fresen. J. Anal. Chem. 361 (1998) 164.
[21] G. Lespes, F. Seby, P.-M. Sarrandin, M. Potin-Gautier, J. Anal. Atom. Spectrom. 9 (1994) 1433.
[22] Y. Van der Heyden, K. Luypaert, C. Hartmann, D.L. Massart, J. Hoogmartens, J. de Beer, Anal. Chim. Acta 312 (1995) 245.
[23] I. Koch, C.F. Harrington, K.J. Reimer, W.R. Cullen, Talanta 44 (1997) 1241.
[24] R.A. Olivero, J.M. Nocerino, S.N. Deming, in: J. Einax (Ed.), Chemometrics in Environmental Chemistry Statistical Methods, Springer-Verlag, Berlin, Germany, 1995, pp. 95–96.

[25] R.G. Brereton, Chemometrics Applications of Mathematics and Statistics to Laboratory Systems, Ellis Horwood, Chichester, Sussex, UK, 1990, pp. 65–83.
[26] I. Rodushkina, A. Magnussonb, J. Food Compos. Anal. 365 (2005) 374.
[27] P. Zatta, R. Lucchini, S. Van Rensburg, A. Taylor, Brain Res. Bull. 15 (2003) 28.
[28] A. Sepe, S. Costantini, L. Ciaralli, M. Ciprotti, R. Giordano, Food Addit. Contam. 18 (2001) 788–796.
[29] WHO, WHO Food Additives Series: 24, Toxicological Evaluation of Certain Food Additives and Contaminants, University Press, Cambridge, 1989.
[30] Z. Yuping, X. Yunafu, w. zhuyou, Y. Zhihui, G.W. Lihua Jianyan, Huaxue Fence 36 (1998) 40.
[31] N.A. Nikno, O.I. Asubiojo, Sci. Total. Environ. 161 (1997) 208.

Available online at www.sciencedirect.com
ScienceDirect
Talanta 70 (2006) 315–322
Talanta
www.elsevier.com/locate/talanta

Isolation of individual capsaicinoids from a mixture and their characterization by ^{13}C NMR spectrometry

Robert Q. Thompson *, Michael J. Pennino, Michael J. Brenner, Manish A. Mehta

119 Woodland Street, Department of Chemistry and Biochemistry, Oberlin College, Oberlin, OH 44074, USA

Received 9 January 2006; received in revised form 15 February 2006; accepted 15 February 2006
Available online 24 March 2006

Abstract

Individual compounds were isolated from a laboratory mixture of capsaicinoids by a multi-stage approach. First, the capsaicinoids were fractionated into capsaicins and non-capsaicins by argentation solid phase extraction (SPE) on a silver-charged propyl sulfonate resin. Second, compounds in each fraction were isolated by semi-preparative liquid chromatography on a C_{30} phase in aqueous methanol. Third, the individual components of the original mixture were concentrated by reversed phased (C_{18}) SPE. The structure of each purified compound was confirmed by ^{13}C NMR spectrometry and spectral comparison to known standards, purchased or synthesized locally. The chemical shifts of 15 capsaicinoid standards were measured on a 600 MHz instrument, and their assignments to particular carbons were made by reference to Distortionless Enhancement by Polarization Transfer (DEPT) NMR experiments and NMR spectral prediction software.

Keywords: Capsaicinoids; Solid phase extraction (SPE); Argentation SPE; Preparative liquid chromatography

1. Introduction

Capsaicinoids are *N*-vanillylacylamides (Fig. 1), the spicy agents in chili peppers, and have been the focus of many analytical, biochemical, and metabolic studies over the years. Nearly all of the analytical studies [1] have been limited to just three of the more than 20 members of the natural capsaicinoids family due to the lack of readily available standards. Only 6-ene-8-methyl capsaicin (6,8-C), 8-methyl dihydrocapsaicin (8-DC), and *N*-vanillylnonanamide (NVN) are commercially available in pure form. To expand our knowledge of the capsaicinoids, especially toward the minor (low abundance) components, additional standards are needed. They must be either synthesized in the laboratory or isolated from natural sources. We present steps toward the latter goal, the isolation of individual compounds from the fruit of chili pepper.

A natural or synthetic mixture of capsaicinoids can be separated by reversed phase liquid chromatography [1]. However, direct preparative liquid chromatographic separation of the capsaicinoids is impossible due to sets of capsaicinoids with inadequate resolution. The presence of 6,8-C, the most abundant capsaicinoid in nature, makes it difficult to isolate 7-methyl nordihydrocapsaicin (7-NDC) and NVN on alkyl or phenyl stationary phases. Likewise, the homocapsaicin isomers (6,8-HC and 6,9-HC) and *N*-vanillyldecanamide (NVD) are poorly resolved.

We have taken the following multi-step approach to isolate individual capsaicinoids. First, the capsaicinoids are fractionated into capsaicins, those compounds with a double bond in the acyl chain, and non-capsaicins, those compounds with only single bonds in the acyl chain (including the dihydrocapsaicins and the *N*-vanillylacylamides). The fractionation can be accomplished by taking advantage of the strong interaction between silver ion and alkenes [2]. Argentation chromatography is well known and has been reviewed [3]. Argentation solid phase extraction (SPE) of lipids and fatty acids has been described by Christie and co-workers [4,5] and is extended here to the capsaicinoids. A propyl sulfonate or propylbenzene sulfonate resin is treated with excess silver ion to prepare a silver SPE cartridge. After loading the capsaicinoids, moderately polar solvents wash the non-capsaicins from the column. The interactions between the capsaicins and the silver-charged resin are disrupted by acetonitrile, so the capsaicins are eluted with acetonitrile.

* Corresponding author. Tel.: +1 440 775 8305; fax: +1 440 775 6682.
E-mail address: robert.q.thompson@oberlin.edu (R.Q. Thompson).

0039-9140/$ – see front matter © 2006 Elsevier B.V. All rights reserved.
doi:10.1016/j.talanta.2006.02.046

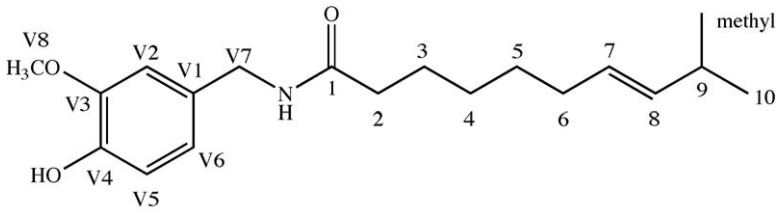

Fig. 1. Capsaicinoid numbering system with the example of 7-ene-9-methyl homocapsaicin. The vanillylamine carbons are indicated with a "V", while the carboxylic acid or acyl chain carbons are labeled with an "A" or no letter at all.

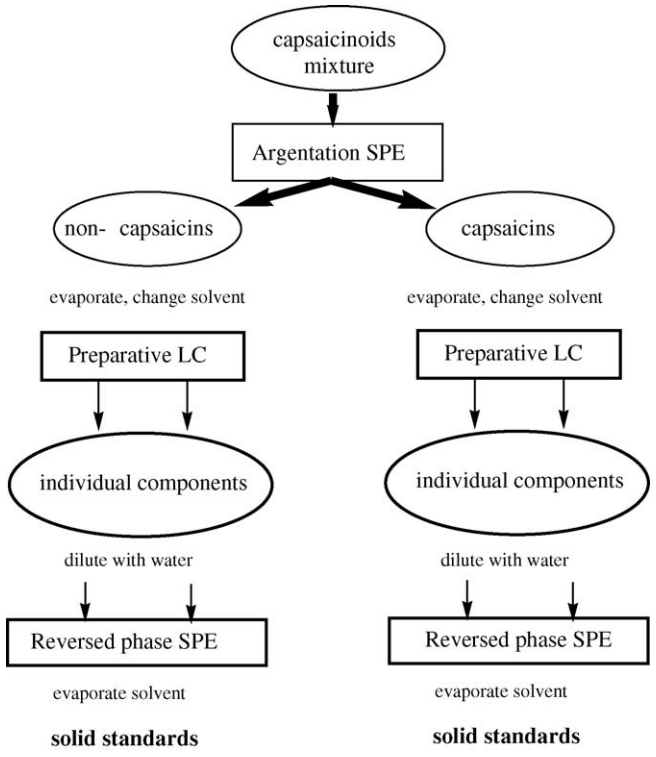

Fig. 2. Scheme for the isolation of individual capsaicinoids from a mixture.

With the two classes of capsaicinoids separated, preparative liquid chromatography (prepLC) of each fraction can proceed with effectiveness and good resolution. A C_{30} phase in aqueous methanol provides the best resolution [1]. Next, the liquids collected by prepLC are passed through a C_{18} SPE column and are eluted in a smaller volume of pure methanol. The methanol is easily evaporated to yield recovered solids, and the final result is isolated capsaicinoids with high purity. A flow chart of the method is given in Fig. 2. Literature reports of the solid phase extraction of capsaicinoids number about twenty and include SPE with a C_{18} resin [6], SPE with a mixed polarity resin [7], and solid phase microextraction [8], but not argentation SPE.

2. Experimental

2.1. Caution

The pure capsaicinoids and concentrated extracts of chili peppers are very strong irritants and must be used with care. They can cause burning, pain, coughing, and lachrymation upon skin exposure and inhalation. Use gloves and a mask when handling these solids or their concentrated solutions.

2.2. Materials and methods

Pure solids of 15 capsaicinoid compounds were obtained. Pure white powders of 6-ene-8-methyl capsaicin (6,8-C), 8-methyl dihydrocapsaicin (8-DC), and *N*-vanillylnonanamide (NVN) were obtained commercially (U.S. Pharmacopeia and Sigma–Aldrich). Pure standards of 4-ene-6-methyl norcapsaicin (4,6-NC), 4-ene-7-methyl norcapsaicin (4,7-NC), 5-ene-7-methyl norcapsaicin (5,7-NC), 5-ene-7-methyl capsaicin (5,7-C), 5-ene-8-methyl capsaicin (5,8-C), 6-ene-8-methyl homocapsaicin (6,8-HC), 6-ene-9-methyl homocapsaicin (6,9-HC), 7-ene-9-methyl homocapsaicin (7,9-HC), 7-methyl nordihydrocapsaicin (7-NDC), and 9-methyl homodihydrocapsaicin (9-HDC) were obtained from Dr. Kazuhiko Orito at Hokkaido University in Japan. *N*-vanillyloctanamide (NVO) and *N*-vanillyldecanamide (NVD) were synthesized as described in earlier work [1]. The purity of each standard was >98% as measured by UV absorbance spectrophotometry, LC-UV, and LC-MS [1]. A mixture of capsaicinoids, a purified, solid extract of chili pepper, was purchased (Sigma–Aldrich; #360376) for use in development of the isolation methods. The mixture contained mostly 6,8-C (about 60 wt.%) and 8-DC (about 30%). All of the compounds with double bonds along the acyl chain were in the trans or *E* form, unless otherwise noted.

Solid phase extraction (SPE) cartridges (Restek Corp.) of three chemistries – C_{18} (500 mg, 3 mL), propyl sulfonate strong cation exchanger (SCX; 500 mg, 3 mL), and propylbenzene sulfonate SCX (500 mg, 6 mL) – were used. Solvents for SPE (acetonitrile, ethyl acetate, methanol, water) were HPLC-grade or better. A vacuum manifold station (Restek) connected to a house vacuum system made it convenient to handle the SPE cartridges and eluates.

The SCX resins, after conditioning with methanol (10 mL at 5 mL/min), were charged with silver by exposure to a concentrated aqueous solution (up to 0.1 M) of silver nitrate (ACS grade). The 25 mL silver solution was passed through the column at 5 mL/min and was followed by a 5 mL water wash. The amount of silver adsorbed on the SCX resins was determined by measurement of the excess silver (what passed through the cartridge) using flame atomic absorption spectrophotometry (Perkin-Elmer 1100B; Ag–Au hollow cathode lamp at 328.1 nm).

HPLC-grade solvents were used to prepare the mobile phases and capsaicinoid stock solutions. Water was purified

to 18 MΩ cm by a bench-top water purifier. The mobile phase composition for the analysis of the SPE eluates and for semi-preparative liquid chromatography was 35 vol.% water:65 vol.% methanol, and the flow rate of mobile phase was 1.0 mL/min. The chromatography column (YMC Carotenoid; from Waters Corp.) was of dimensions 250 mm × 4.6 mm and packed with 5 μm silica coated with a C_{30} phase. An Agilent 1100 liquid chromatograph, equipped with an autosampler and diode array detector, was used to separate the capsaicinoids. The capsaicinoids were detected at 280 nm, a wavelength at which the molar absorptivities of the compounds are identical [9].

Solubility tests were made in the following manner. Ten milliliters of solvent were added to varying amounts (0.2–10 mg) of the capsaicinoids mixture; the mixture was stirred at moderate speed with a stir bar for 15 min; the solution was filtered (0.45 μm) until no solid particles remained and finally the clear solution was injected into the liquid chromatograph. The mass of capsaicinoids injected, assuming complete solubility, was kept constant by varying the injection volume. For example, 5 μL of the 2 mg solution was injected, but only 1 μL of the 10 mg solution was injected. Chromatographic peak areas reached relatively constant values (called standard peak areas) when the concentration of capsaicinoids was below the practical solubility limit. The fractional solubility was determined by the ratio of the peak areas of 6,8-C and 8-DC to their standard peak areas.

Proton, carbon-13, and Distortionless Enhancement by Polarization Transfer (DEPT) NMR spectra were collected on a custom-assembled system consisting of a 14.1 T, 54 mm bore magnet (600.377 MHz for ^{1}H; 150.987 MHz for ^{13}C; Magnex Scientific), a 39-channel room-temperature shim system (Resonance Research), a three-channel console (TecMag), and a 5 mm double-resonance broadband probe (Nalorac-Varian). A test solution of each standard was prepared by dissolving 3 mg of solid in 0.6 mL of chloroform-D (99.8%; Cambridge Isotopes Laboratories), containing 0.05% (v/v) tetramethylsilane (TMS) as a reference signal (0.0 ppm). A single scan of the proton spectrum was used to "shim" the magnet; this procedure enabled more definitive ^{13}C and DEPT spectra to be collected. The ^{13}C and DEPT spectra were an ensemble average of 4096 scans.

3. Results and discussion

3.1. Solubility of capsaicinoids in aqueous methanol

For the separation by reversed phase solid phase extraction (C_{18} SPE) and by reversed phase liquid chromatography (RPLC), samples were prepared in aqueous methanol. The hydrophobic nature of the capsaicinoids raised the question of the solubility of larger amounts of the compounds in such a polar solvent, so tests were performed to determine the practical solubility of the capsaicinoids mixture in aqueous methanol. In 75:25 water:methanol all of the 0.2 mg sample dissolved, but only about 80% of the 0.6 mg sample dissolved. Based on these and other results, the practical solubility of the capsaicinoids in 25 vol.% methanol was estimated to be 0.5 mg per 10 mL. In 50:50 water:methanol all of the 5 mg sample dissolved, but only about 80% of the 10 mg sample dissolved. The practical solubility was estimated to be 8 mg per 10 mL. It is clear that the percentage of methanol in the sample solvent cannot be much less than 50 vol.% for the isolation of larger amounts of capsaicinoids. Certainly 25 vol.% methanol is insufficient.

3.2. Argentation solid phase extraction: preparation of cartridges

A strong cation exchange (SCX) resin, either propyl-SO_3^- or benzyl-SO_3^- with a nominal 2×10^{-4} mol charged sites per gram, was treated with silver nitrate to create a silver-ion SPE resin. The actual amount of silver loaded was determined by difference: the amount of silver applied to the cartridge minus the amount that emerged from the cartridge. The procedures were given in Section 2.

The concentration of silver applied to the cartridge was varied from 0.1 to 1 mmol silver nitrate per 25 mL of water. The resulting silver content of the cartridge increased up to a limit of 0.11 mmol in the 500 mg, 3 mL propyl cartridge and up to a limit of about 0.2 mmol in the 500 mg, 6 mL benzyl cartridge (see Table 1). Any amount of added silver nitrate greater than ∼1.5 times the maximum silver loading appeared to fully charge the cartridge with silver.

3.3. Argentation SPE: procedure

Our goal was to separate the capsaicins and non-capsaicins (dihydrocapsaicins and *N*-vanillylacylamides) by argentation SPE. We achieved this goal with the following approach. The sample (a natural mixture of capsaicinoids) was dissolved in a less polar solvent (e.g. ethyl acetate), rather than a more polar solvent (e.g. acetonitrile), to allow full complexation between the silver ion in the stationary phase and the alkene moiety of the capsaicins. After loading the capsaicinoids in less

Table 1
Results for the silver charging of SCX resins

mmol Ag^+ applied[a]	Absorbance ratio[b]	mmol Ag^+ loaded[c]
Propyl-SCX resin		
0.095	0.169	0.08[d]
0.207	0.434	0.12
0.303	0.645	0.11
0.408	0.715	0.12
0.522	0.781	0.11
1.03	0.890	0.11
Benzyl-SCX resin		
0.117	0.254	0.09
0.216	0.352	0.14
0.311	0.413	0.18
0.389	0.539	0.18
0.513	0.628	0.19
1.05	0.757	0.25

[a] Amount of silver nitrate dissolved in 25 mL of water and applied to 500 mg of SCX resin.

[b] Ratio of the atomic absorbance of a solution derived from the cartridge eluates (sample plus wash) to the atomic absorbance of a solution derived from the silver nitrate solution applied to the cartridge.

[c] mmol Ag^+ loaded = mmol Ag^+ applied(1 − absorbance ratio).

[d] Uncertainties in the mmol Ag loaded values are ±0.01 mmol

polar solvent, successive washes of less polar solvent followed by more polar solvent removed first the non-capsaicins and then the more strongly bound capsaicins. The success of the separation was measured by the fraction of 8-DC (representing the non-capsaicins) in the sample and first less polar wash and the fraction of 6,8-C (representing the capsaicins) in the more polar eluates. The argentation SPE procedure for the fractionation is given in Table 2. The literature in the area of normal phase liquid chromatography of lipids using silver columns mentioned that strongly bound lipids could be displaced from the stationary phase by solvents containing small amounts (as low as 0.025 vol.%) of acetonitrile [10,11]. Consequently, we were careful to rinse any remaining acetonitrile from the cartridges before reuse.

Table 2
Procedure for Argentation SPE using a silver-charged SCX resin

Step	Solvent	Volume (mL)	Maximum flow rate (mL/min)
Condition	Methanol	5	5
	Ethyl acetate	5	5
Load sample (non-capsaicins)	Ethy acetate (sample)	5	2
Wash (non-capsaicins)	Ethyl acetate (EA1)	2	2
Elution (to waste)	Ethyl acetate (EA2)	2	2
	Ethyl acetate (EA3)	2	2
	Ethyl acetate (EA4)	2	2
Elution (capsaicins)	Acetonitrile (AN1)	2	2
	Acetonitrile (AN2)	2	2

3.4. Argentation SPE: separation variables

Three variables were investigated for their effect on the fractionation: SCX resin type (propyl or benzyl), amount of silver used to charge the resin, and amount of sample (capsaicinoids mixture) loaded. Each variable was investigated separately, though the three were found to interact. Data for 6,8-C and 8-DC are shown in Table 3. Acceptable fractionation was defined as >80% recovery of the compounds at >90% purity with the material contained in two or fewer SPE eluates, and is indicated by a gray background in the cells of Table 3.

Table 3
Fractionation of capsaicins (6,8-C) and non-capsaicins (8-DC) under various conditions

mmol Ag^+ applied	Compound	Percentage of compound found		
		Fraction 1 (sample, EA1)	Fraction 2 (EA2–EA4)	Fraction 3 (AN1, AN2)
Propyl SCX				
0.5 mg Sample				
0.25	8-DC	93[a]	7	0
	6,8-C	9	27	64
0.50	8-DC	85	13	2
	6,8-C	2	4	94
1.00	8-DC	83	14	3
	6,8-C	2	5	93
3 mg Sample				
0.25	8-DC	99	1	0
	6,8-C	98	1	1
0.50	8-DC	96	3	1
	6,8-C	68	20	12
1.00	8-DC	90	9	1
	6,8-C	4	33	63
5 mg Sample				
1.00	8-DC	94	5	1
	6,8-C	26	40	34
Benzyl SCX				
1 mg Sample				
1.00	8-DC	50	46	4
	6,8-C	0	1	99
3 mg Sample				
0.25	8-DC	53	44	3
	6,8-C	2	3	95
0.50	8-DC	55	39	6
	6,8-C	0	3	97
1.00	8-DC	73	19	6
	6,8-C	3	5	92
5 mg Sample				
1.00	8-DC	97	1	2
	6,8-C	96	2	2

[a] Relative uncertainties in the percentage values are about ±10%, e.g. 93 ± 9% found.

Up to 5 mg of the capsaicinoids mixture were separated on the 500 mg propyl-SCX resin. Acceptable fractionation was found with the lower amounts of sample, although in the case of 0.25 mmol applied silver the separation was not very good. The effectiveness of the separation improved in all cases as the amount of silver nitrate applied increased. This was disturbing since the silver analysis showed that the amount of silver taken up by the resin was constant (all exchange sites filled). So the total amount of silver in the resin was not a good predictor of the separation effectiveness; indeed, the amount of excess applied silver was a better predictor. One possible explanation is that two sites for silver exist—one with a low formation constant, preferred at higher silver concentrations, that displays a strong interaction with the capsaicins and a second with a high formation constant, preferred at all silver concentrations, that displays a weaker interaction with the capsaicins. Experiments are in progress to test this hypothesis. In any case, the propyl-SCX cartridge appeared to have a capacity of about 2 mg for the fractionation of the capsaicinoids.

At the higher amounts of capsaicinoids the separation under all conditions was poor, particularly in the case of the benzyl-SCX resin. In all cases the benzyl-SCX resin, compared to the propyl resin, demonstrated stronger binding of the non-capsaicins, with those compounds spilling over into the second to fourth ethyl acetate eluates. Presumably the reason for this is π–π interactions between the solutes and the benzyl moiety of the resin. The fractionations were not fully acceptable as defined (the required fractional recovery of the non-capsaicins was not met). However, if one considers the material in the sample eluate plus eluates EA1–EA3 then the separations were acceptable, even up to a sample size approaching 4 mg. So, the benzyl form had a higher sample capacity than the propyl form, but produced the non-capsaicins in a larger volume of solvent, requiring more extensive solvent evaporation and time to recover the solids.

3.5. Reversed phase solid phase extraction

With the required use of 50 vol.% methanol as the sample solvent, there was concern that the capsaicinoids would not be retained on a reversed phase (C_{18}) resin. The concern proved unfounded. The reversed phase SPE procedure is shown in Table 4 and was used to isolate the capsaicinoids (2–8 mg) from a 10 mL sample in 50:50 water:methanol. No capsaicinoids were found in the sample, wash, or 50:50 water:methanol elution, and more than 95% of the capsaicinoids were recovered by the first 2 mL elution with pure methanol. A 500 mg cartridge could separate at least 10 mg of capsaicinoids in 20 mL aqueous methanol without any breakthrough (losses during the loading or wash steps).

Table 4
Procedure for reversed phase SPE using a C_{18} resin

Step	Solvent	Volume (mL)	Maximum flow rate (mL/min)
Condition	Methanol	10	5
	Water	5	5
Load	Aqueous methanol	10	2
Wash	Water	2	2
Elution	50:50 Water:methanol	2	2
	Methanol	2	2
	Methanol	2	2

Table 5
Composition of the mixture of capsaicinoids

Peak number	Abbreviated name	Capsaicinoid	Mass (mg)
1	NVO	*N*-vanillyl octanamide	2.22[a]
2	4,7-NC	4-ene-7-methyl norcapsaicin	1.93
3	7-NDC	7-methyl nordihydrocapsaicin	2.19
4	6,8-C	6-ene-8-methyl capsaicin	4.47
5	NVN	*N*-vanillylnonanamide	2.65
6	5,8-C	5-ene-8-methyl capsaicin	3.66
7	8-DC	8-methyl dihydrocapsaicin	4.07
8	6,8-HC	6-ene-8-methyl capsaicin	2.52
9	NVD	*N*-vanillyldecanamide	2.17
10	9-HDC	9-methyl homodihydrocapsaicin	3.37

[a] Uncertainties in the mass values are ±0.02 mg.

3.6. Fractionation of a laboratory mixture of capsaicinoids

A mixture of ten capsaicinoids, four capsaicins and six non-capsaicins, was created to challenge the separation scheme. The compounds, in roughly equal amounts (see Table 5), were dissolved in 25 mL ethyl acetate to give a 1.2 mg/mL total capsaicinoids solution.

Separation of the mixture on a C_{30} phase was most efficient (see Fig. 3), but the coelution of several pairs of compounds demonstrated that direct preparative liquid chromatographic isolation of the compounds was impossible. Two-milliliter aliquots of the mixture were loaded onto each of 12 silver-charged (1 mmol silver nitrate per 500 mg resin), propyl-SCX resins, and the SPE process (Table 2) was carried out on each to produce volumes of ethyl acetate, containing the non-capsaicins, and of acetonitrile, containing the capsaicins. The SPE fractionation

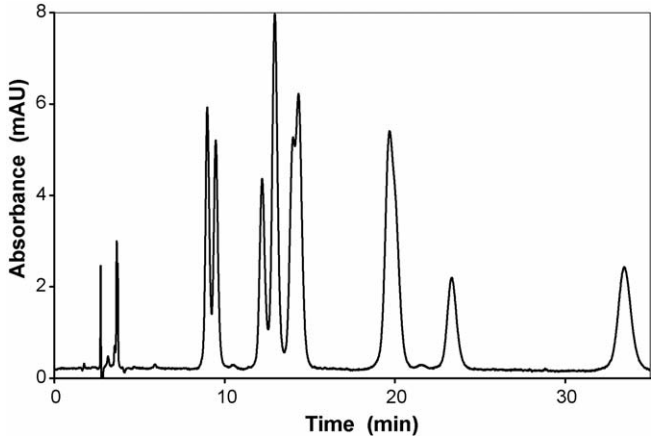

Fig. 3. Chromatogram of the laboratory mixture of capsaicinoids. YMC-Pack Carotenoid column (C_{30} phase) of 4.6 mm × 250 mm packed with 5 μm particles. Mobile phase (35:65 water:methanol) pumped at 1.0 mL/min.

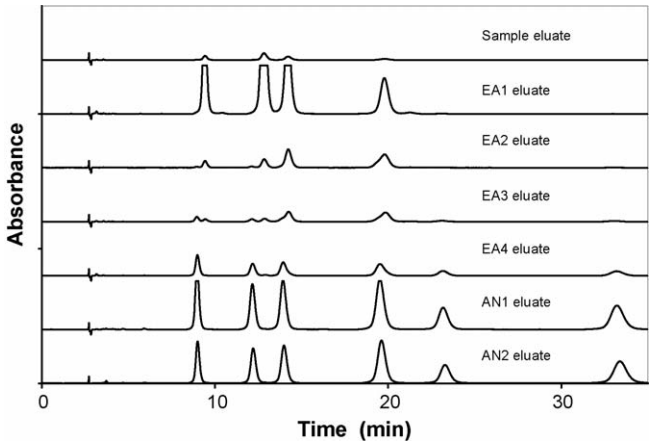

Fig. 4. Chromatograms of a set of eluates from the argentation SPE of the laboratory mixture. EA stands for ethyl acetate eluate, and AN stands for acetonitrile eluate. YMC-Pack Carotenoid column (C_{30} phase) of 4.6 mm × 250 mm packed with 5 μm particles. Mobile phase (35:65 water:methanol) pumped at 1.0 mL/min.

was very effective (see chromatograms of each eluate in Fig. 4), leading to high purity and high recovery, as described earlier. The combined ethyl acetate eluates (sample plus EA1) and the combined acetonitrile eluates (AN1 plus AN2) were separately evaporated to dryness under nitrogen with heating to 55 °C. The residue of each fraction was redissolved in 5 mL of 40 vol.% water:60 vol.% methanol.

The components of each fraction were isolated by semi-preparative liquid chromatography. Since a 4.6 mm × 25 cm column was used rather than a larger preparative column, the mass of capsaicinoids that could be injected while maintaining acceptable resolution was quite limited. Experiments revealed that up to a total mass of capsaicinoids of 0.3 mg could be injected. Representative separations are given in Fig. 5A and B. The components of the non-capsaicins fraction were fairly easily collected within volumes defined by peak start and stop times. The least resolved peak pair 3,5 showed minimally acceptable separation only on the C_{30} phase; this component pair could not be as cleanly separated on C_{18}, C_8, or phenyl columns [1]. All of the capsaicins were nearly baseline-resolved, with the peak pair 4,6 most difficult to isolate at high purity. Again, the separation was best on C_{30} compared to the more common nonpolar phases. Based on the chromatographic peak areas, the recoveries of the individual compounds ranged from 18% (8-HDC) to 70% (4,7-NC) with a median value of 45%. With five major steps in the procedure, a 90% recovery at each step would yield a 60% overall value; so our measured values were quite reasonable.

Each of the 10 aqueous methanol solutions (~20 mL) containing an isolated capsaicinoid was diluted in an equal volume of water and then loaded onto a conditioned C_{18} SPE cartridge (3 mL, 500 mg). After washing the cartridge with 50:50 water:methanol, a single 5 mL aliquot of pure methanol eluted essentially all of the analyte. The methanol was evaporated to yield the solid material. The isolated compounds at this point could undergo analysis for purity and for chemical identification. Liquid chromatographic analysis of one of the isolated capsaicinoids, 6-ene-8-methyl homocapsaicin, under several mobile

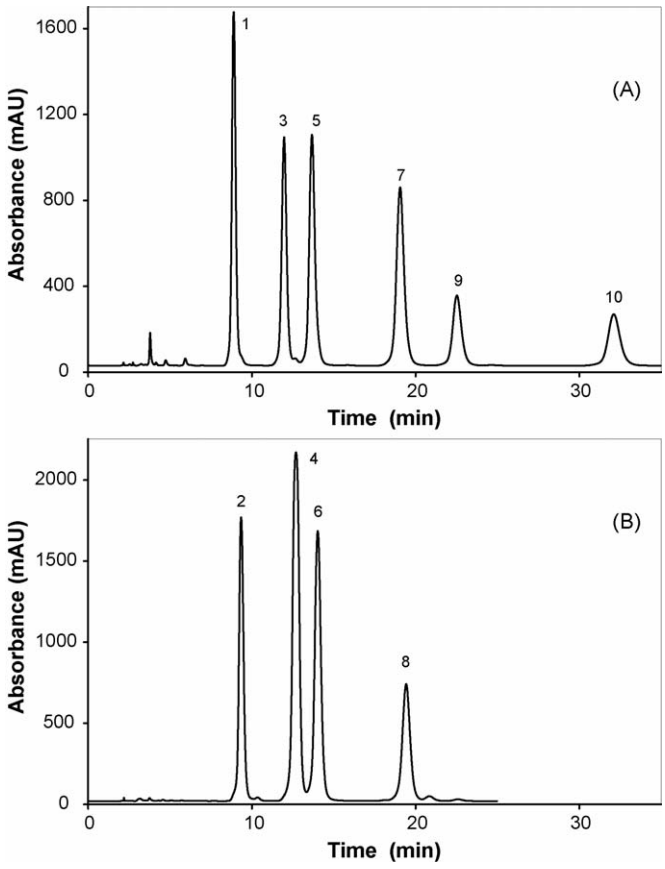

Fig. 5. Chromatograms of the fractions from argentation SPE. Part A, ethyl acetate/non-capsaicins fraction; Part B, acetonitrile/capsaicins fraction. The key to the peak numbers may be found in Table 5. About 0.3 mg total mass in 100 μL of solvent injected in each case. YMC-Pack Carotenoid column (C_{30} phase) of 4.6 mm × 250 mm packed with 5 μm particles. Mobile phase (35:65 water:methanol) pumped at 1.0 mL/min.

phase conditions and at several absorption wavelengths revealed very high purity (>98%), based on relative peak areas and the assumption of similar molar absorptivities for all components (analyte and any impurities).

3.7. ^{13}C NMR spectrometry

To conclusively identify the isolated material (as well as to identify any impurities) ^{13}C nuclear magnetic resonance spectrometry (NMR) was performed. The ^{13}C NMR chemical shifts for 15 pure capsaicinoids are listed in Table 6. The purity of the standards was checked by differential scanning calorimetry, ultraviolet spectrophotometry, liquid chromatography, and mass spectrometry as described earlier [1]. The peak assignments were made with the assistance of experimental DEPT spectra and NMR spectral prediction software (ChemDraw Ultra; CambridgeSoft).

Examination of the chemical shifts for the set of standards revealed several trends that could assist in identifications of unknown capsaicinoids isolated in the future. First, all of the chemical shifts associated with the carbons in the vanillylamine portion of the molecule and the first two carbons along the acyl chain for each capsaicinoid were identical (within ±0.4 ppm).

Table 6
^{13}C chemical shifts (ppm) for the capsaicinoid standards and the isolated compound[a]

	V1	V2	V3	V4	V5	V6	V7	V8			
All	130.4	110.7	145.1	146.7	114.4	120.8	43.6	56.0			
	A1	A2	A3	A4	A5	A6	A7	A8	A9	A10	ACH_3
4,6-NC	172.3	36.8	29.7	126.5	137.9	38.3	28.7	11.7			20.2
4,7-NC	173.0	36.8	28.7	129.3	130.8	41.9	28.3	22.2			22.2
5,7-NC	172.7	36.1	25.5	31.9	125.9	138.8	31.0	22.6			22.6
5,7-C	173.0	36.1	25.6	32.0	127.3	137.5	38.4	29.8	11.8		20.4
5,8-C	172.7	36.1	25.6	32.0	130.2	130.4	42.0	28.4	22.3		22.3
6,8-C	172.9	36.7	25.3	29.3	32.2	126.3	138.1	31.0	22.7		22.7
6,8-HC	172.7	36.7	25.3	29.3	32.3	127.9	136.7	38.4	29.8	11.8	20.4
6,9-HC	172.7	36.7	25.3	29.3	32.3	129.6	130.8	42.0	28.4	22.3	22.3
7,9-HC	173.0	36.8	25.7	28.8	29.4	32.4	126.8	137.8	31.0	22.7	22.7
7-NDC	172.8	36.9	25.8	29.6	27.1	38.8	27.9	22.6			22.6
8-DC	173.1	36.8	25.8	29.4	29.6	27.2	39.0	27.9	22.6		22.6
9-HDC	172.9	36.9	25.8	29.3	29.4	29.8	27.3	39.0	28.0	22.6	22.6
NVO	172.8	36.9	25.8	29.0	29.2	31.7	22.6	14.0			
NVN	172.8	36.9	25.8	29.2	29.3	29.3	31.8	22.6	14.1		
NVD	172.8	36.9	25.8	29.3	29.4	29.5	29.4	31.9	22.7	14.1	
Compound #8	172.7	36.8	25.3	29.4	32.4	128.0	136.9	38.4	29.9	11.9	20.5

Refer to Fig. 1 for the carbon assignments (V1–V8 and A1–ACH_3).
[a] Uncertainties in the chemical shifts are ±0.2 ppm.

Thus, these signals indicated a member of the capsaicinoids, but had no value for distinguishing individual capsaicinoids. Second, the shift of the terminal carbon along the acyl chain and the methyl sidegroup, if any, revealed the capsaicinoid type. A shift of 14.1 ppm indicated an *N*-vanillylacylamide, while a shift of about 20.5 or 22.5 ppm indicated a capsaicin or dihydrocapaicin. In addition, a signal at 11.8 ppm indicated that the methyl group was two carbons from the terminal acyl carbon. Third, in the capsaicins group, if the ene and methyl were separated widely, e.g. 4,7-NC, then the chemical shifts for the alkene carbons were within a ppm or two. A closer spacing, e.g. 6,8-C, resulted in shifts that were about 10 ppm different. The difference became slightly larger as the ene and methyl moved out along the chain, but slightly smaller as the entire chain lengthened. In conclusion, ^{13}C NMR spectra provided the means to determine the length of the acyl chain, the capsaicinoid type, and the relative positions of the ene and methyl moieties.

As far as we know, this is the first report of the ^{13}C NMR data for such an extensive list of capsaicinoids. A paper on the synthesis of some capsaicinoids and related compounds from 1988 provided confirmation of some of the NMR data [12]. The authors did not provide any carbon assignments, but the values of chemical shift for all of the carbons in 6,8-C and in 8-DC corresponded exactly (within ±0.2 ppm) to those reported here. The signals from four other compounds (5,7-NC; 7,9-HC; 7-NDC; 9-HDC) did not match quite as well. It should be noted that the 1988 data did not show constant ppm values for the vanillylamine carbons across the set of compounds, as was the outcome in our study. This suggests that the earlier data were somewhat flawed due to instrumental limitations or experimental conditions.

Table 6 also lists the chemical shifts associated with the isolated 6,8-HC (chromatographic peak #8). The correspondence of 16 values was nearly perfect (within ±0.2 ppm). Three weak lines from the reference spectrum (associated with three of the vanillyl ring carbons) did not appear in the sample spectrum, and two sample signals at 51.0 and 136.1 ppm were unique. The former is not surprising considering the noise in the sample spectrum (less concentrated sample compared to the standards), and the latter must be due to a small amount of impurity or instrumental noise. In any case, the isolated material was clearly 6,8-HC. In a similar fashion the other compounds could be conclusively identified.

4. Conclusions

The fractionation of a 30 mg mixture of capsaicinoids into capsaicins and non-capsaicins by argentation solid phase extraction was accomplished. The sets of compounds were then separated into individual members by semi-preparative chromatography through use of the uncommon C_{30} stationary phase and an aqueous methanol mobile phase. Finally, the isolated compounds were captured on a C_{18} solid phase extraction cartridge for elution with methanol and quick solvent evaporation. Pure solids, whose purities were measured by liquid chromatographic analysis and whose identities were confirmed by ^{13}C NMR, were the ultimate product of the project. Work is in progress to extend the study to larger amounts of capsaicinoid mixtures and to the extraction of capsaicinoids from chili pepper fruit.

Acknowledgements

The authors wish to thank Oberlin College and its Research and Development Committee for financial support of this project. Support from the National Science Foundation (CHE-0079470) for purchase of a 600 MHz NMR spectrometer is also gratefully acknowledged.

References

[1] R.Q. Thompson, K.W. Phinney, L.C. Sander, M.J. Welch, Anal. Bioanal. Chem. 381 (2005) 1432–1440.
[2] J.J. Lagowski, Modern Inorganic Chemistry, Marcel Dekker, New York, 1973.
[3] C.M. Williams, L.N. Mander, Tetrahedron 57 (2001) 425–447.
[4] W.W. Christie, J. Lipid Res. 30 (1989) 1471–1473.
[5] E.B. Hoving, F.A.J. Muskiet, W.W. Christie, J. Chromatogr. Biomed. Appl. 565 (1991) 103–110.
[6] N.T. Nyberg, H. Baumann, L. Kenne, Mag. Res. Chem. 39 (2001) 236–240.
[7] B. Perkins, R. Bushway, K. Guthrie, T. Fan, B. Stewart, A. Prince, M. Williams, J. AOAC Int. 85 (1) (2002) 82–85.
[8] O. Spicer, J.R. Almirall, Talanta 67 (2005) 377–382.
[9] R.Q. Thompson, K.W. Phinney, M.J. Welch, E.V. White, Anal. Bioanal. Chem. 381 (2005) 1441–1451.
[10] B. Nikolova-Damyanova, W.W. Christie, B.G. Herslof, J. Chromatogr. A 653 (1993) 15–23.
[11] B. Nikolova-Damyanova, W.W. Christie, B.G. Herslof, J. Chromatogr. A 749 (1996) 47–54.
[12] P.M. Gannett, D.L. Nagel, P.J. Reilly, T. Lawson, J. Sharpe, B. Toth, J. Org. Chem. 53 (1988) 1064–1071.

Available online at www.sciencedirect.com
ScienceDirect
Talanta 70 (2006) 323–329
Talanta
www.elsevier.com/locate/talanta

A new kinetic method for quantification phenoxyl free radicals

Jing Xu [a], Xinguo Wu [b,*], Wei Yan [b], Ruxiu Cai [a,*], Zhixin Lin [a]

[a] College of Chemistry and Molecular Science, Wuhan University, Wuhan, 430072, PR China
[b] College of Resources and Environmental Science, Wuhan University, Wuhan 430072, PR China

Received 16 October 2005; received in revised form 11 February 2006; accepted 18 February 2006
Available online 23 June 2006

Abstract

In this work, a new kinetic method was proposed for quantification phenoxyl radicals generated in enzyme reaction. Instead of direct detecting the spectral signals of phenoxyl radicals, a molecular probe, the reduced form of nicotinamide adenine dinucleotide (NADH), was employed to indicate the formation of phenoxyl free radicals. It was found that the reactions of NADH and phenoxyl radicals are very fast, but can be followed by using stopped-flow fast scanning spectrophotometric technique. The initial rate of accelerated-oxidation of NADH represents the reactivity of phenoxyl free radical, which is proportional in a certain range to the initial concentration of the parent chlorophenols of the radicals. With this method, the phenoxyl radicals generated in oxidation reaction of chlorophenols (2-CP; 4-CP; 2,4-DCP; 2,4,6-TCP and 2,3,4,6-Tetra-CP) with hydrogen peroxide, catalyzed by horseradish peroxidase, were investigated. The method is highly sensitive. Phenoxyl radicals generated from as low as 1×10^{-8} M 2,4-DCP, for example, can be readily detected with the proposed method. The results show that the reactivity of various phenoxyl radicals are in the following order: 2,4-DCP > 4-CP > 2-CP > 2,4,6-TCP > 2,3,4,6-Tetra-CP. A mechanism is proposed to explain the possible pathway of the probe reaction. The feasibility of this method was assessed by the determination of enzymatic generation of phenoxyl radicals in lake water samples.

Keywords: Phenoxyl radicals; Quantification; Kinetic analysis; Stopped-flow spectrophotometry

1. Introduction

Free radical reactions participate in the normal operation of a wide spectrum of biological events. For example, the catalytic action of many cellular enzymes and electron transfer processes, such as the mitochondrial respiratory chain, involves one-electron transfers, which yield free radical intermediates [1–3]. The pathogenesis of many disease states also involves in vivo generation of free radicals. Those reactive chemicals can take part in unnecessary chemical reactions that can damage the cell components, including DNA, protein, and lipids [4–7]. Quantification of free radical formation is thus critical for evaluation and interpretation of many radical-mediated biological processes. Numerous studies have been devoted to the determination of free radicals, but the most of the reports have been focused on oxygen-centered free radicals, the so-called "reactive oxygen species" (ROS) [8–11]. Relatively less importance has been fastened on other organic free radicals such as phenoxyl radicals, which in fact may be the primary radicals derived from the metabolism of organic pollutants in vivo [12–14]. Unfortunately, there has been no standard procedure that could be used to sensitively and reliably quantify free radicals due to their short life time and weak spectra information. The most direct measurement is the electron spin resonance (ESR) spin trapping technique, in which nitrone compounds (spin traps) react with free radicals to form spin adducts that can be detected with ESR [15–17]. Although changes in ESR signal intensity reflect the process of free radical generation and decay, the application of the ESR spin trapping protocol has been limited in biological systems due to at least two facts: first, the extremely low concentration of the organic radicals can not produce adequate spin adducts to be detected by ESR; second, some of spin adducts can easily turn to ESR-silent products by redox reaction, especially in the biological fluid [17]. Therefore, it is significant to seek for some more sensitive methods for the determination of organic radicals in biological system. As the majority of free radicals do not display sufficient spectroscopic

* Corresponding authors. Tel.: +86 27 68764184; fax: +86 27 68754067.
E-mail addresses: xujingwh@163.com (J. Xu), cai_lin@whu.edu.cn (R. Cai).

0039-9140/$ – see front matter © 2006 Elsevier B.V. All rights reserved.
doi:10.1016/j.talanta.2006.02.055

or electroanalytical properties for their direct determination, it is necessary to use indirect chemical methods. The most common indirect measurements for free radical intermediates are based on using molecular probes to compete with radical decay reaction, thus forming stable products to produce detection signals [18–22].

Peroxidases such as horseradish peroxidase (HRP) is hemeprotein having an iron–porphyrin as the active site, which catalyze the double one-electron-oxidation of substrates with hydrogen peroxide, liberating two molecules of water. The reaction mechanism seems to be already established [23–25]:

$$Per^{3+} + H_2O_2 \rightarrow Co\,I + H_2O$$

$$Co\,I + AH_2 \rightarrow Co\,II + AH^{\bullet}$$

$$Co\,II + AH_2 \rightarrow Per^{3+} + AH^{\bullet} + H_2O$$

The native HRP (Per^{3+}) is first oxidized by peroxide to compound I (Co I), after which compound I abstracts one electron from a substrate molecule (AH_2) to form compound II (Co II) and generates a radical ($AH^{\bullet}$). Subsequently, compound II oxidizes a second substrate molecule, releasing another radical and returning the enzyme to its native state [26–31]. The substrates can be chlorophenols, for example, thus give free phenoxy radicals. Using a molecular probe in situ to scavenge the phenoxyl radicals and monitoring kinetic process of the probe reaction, a kinetic method for quantification of free radicals can be developed. On basis of our experiences in researching free radical intermediates in enzymatic reactions utilizing kinetic analysis [32,33], we consider this kind of method might also be an interesting and qualified approach for phenoxyl radicals.

Owing to the rapid reaction rate of free radicals, it is difficult to trace the dynamic process of their formation and decay by conventional kinetic methods. Stopped-flow kinetic analysis has the unique characteristic to inspect the transient system of in situ, on line and real time and can be a powerful technique for investigating dynamic process of rapid reaction [23,34,35]. The stopped-flow fast scanning spectrophotometric technique was employed here to monitor the transient kinetics for phenoxyl free radical reaction.

In the present work, the oxidation of chlorophenols (CPs) with H_2O_2, catalyzed by HRP, was served as the model reaction for generating phenoxyl radicals, and nicotinamide adenine dinucleotide (NADH), an important biological molecule that participates in many metabolic processes [36–38], as the scavenger (the probe reagent). The phenoxyl radicals are scavenged in situ by NADH as soon as they were generated and, as a result, oxidation of NADH is remarkably accelerated. Therefore, the information of phenoxyl radicals can be obtained by monitoring the probe reaction, non-enzymatic oxidation of NADH with phenoxyl radicals. The presented work reports unambiguous evidences that the accelerating effect on the oxidation of NADH stems neither from chlorophenols nor from the final products of the reaction, but from the free radical intermediates generated during the enzyme reaction. The reactivity of phenoxyl radicals can be defined as the initial rate of accelerated oxidation of NADH, which is in a certain range proportional to the initial concentration of the parent chlorophenols. With this method, the phenoxyl radicals generated in oxidation reaction of chlorophenols (2-CP; 4-CP; 2,4-DCP; 2,4,6-TCP and 2,3,4,6-Tetra-CP) with hydrogen peroxide, catalyzed by horseradish peroxidase, were investigated. The feasibility of this method was assessed by the determination of enzymatic generation of phenoxyl radicals in lake water samples.

2. Experimental

2.1. Reagents

Horseradish peroxidase (RZ > 3.0) was purchased from Dongfeng Reagent Co., Shanghai, China, a stock solution of 2.27×10^{-5} M was prepared by dissolving 0.0100 g HRP in 10.00 mL water; hydrogen peroxide solution was prepared by diluting 0.10 ml of 30% H_2O_2 (standardized by titration with $KMnO_4$ standard solution) to 100 ml. NADH, disodium salt was purchased from Roche (purity > 97%), the solution was made in the concentration of 1.42×10^{-3} M with KH_2PO_4–Na_2HPO_4 buffer (PB) daily. Chlorophenols were obtained from Merck. Stock solutions for 1.00×10^{-3} M 2-chlorophenol (2-CP), 4-chlorophenol (4-CP), 2,4-dichlorophenol (2,4-DCP), 2,4,6-trichlorophenol (2,4,6-TCP) and 2,3,4,6-tetrachlorophenol (2,3,4,6-TeCP) were prepared by dissolving in double distilled water. 0.10 M KH_2PO_4–Na_2HPO_4 buffer solutions with varying pH values were prepared. All other chemicals used were of analytical reagent grade. Distilled, deionized water was used throughout. All stock solutions were stored in a refrigerator (4 °C) and diluted appropriately with KH_2PO_4–Na_2HPO_4 buffer before use.

2.2. Apparatus

Transient kinetics was monitored with an SX18MV-R stopped-flow spectrophotometer equipped with a high-intensity xenon arc lamp (Applied Photophysics, UK). Time-resolved UV–vis spectra were recorded with the same sample-handling unit equipped with a PD-1 photodiode array spectrophotometer (Applied Photophysics, UK). Mass spectrometry analysis was executed with a Finnigan Trace mass spectrometer (Thermo Electron Co., USA). Temperature was controlled with a Shimadzu TB-85 thermostat bath. For pH measurement, a TOA Electronics Model PHS-3C precision pH meter (Shanghai, China) was used.

2.3. Stopped-flow kinetic analysis

Time-resolved spectra were recorded using the photodiode array rapid-scan mode. The spectra resolution was around 1 nm with a mixing time of 1.5 ms. The time courses of the reactions were followed at 340 nm (absorbance of NADH) in the monochromatic mode and 1000 data points per trace were acquired. The initial reaction rate (denoted as dA/dt) was calculated using the data collected in the first 2.0 s of the reaction from such kinetic curves ($A \sim t$). The length of the light

path was 1 cm for both types of measurements. Temperature was controlled constant at 25 ± 0.2 °C. In a typical experiment, one syringe contained 1.14×10^{-6} M HRP in buffer solution, and the other contained mixture of 5.00×10^{-6} M H_2O_2, 1.00×10^{-4} M NADH and CPs of various concentrations in buffer solution. All data were determined from averages of five individual traces and concentrations after mixing were stated.

2.4. Mass spectrometry

The reaction products were analyzed by mass spectrometry. Aliquots of reaction mixtures containing 1.14×10^{-6} M HRP, 1.00×10^{-4} M H_2O_2, 1.00×10^{-4} M NADH and 1.00×10^{-4} M 2,4-DCP in buffer solution, were injected directly into the mass spectrometer after 1 min incubation. The settings of the mass spectrometer were as follows: ion source temperature 200 °C, electron energy 70 eV, detector voltage 350 V, scan range 40–600 amu.

2.5. Sampling procedure

Lake water samples were collected in 0.5-L acid-washed reagent bottles with Teflon-lined caps. Prior to sample collection, glassware was washed overnight in 10% HNO_3 and then copiously rinsed with water and sample. After collection, samples were filtered through 0.22-μm Nylon 66 filters and stored at 4 °C until analyzed. Immediately prior to determination, the pH of the water samples was adjusted to pH ~7.4 by adding 10% (v/v) of 1.0 M, pH 7.4 KH_2PO_4–Na_2HPO_4 buffer.

3. Results and discussion

3.1. Dynamic spectra and kinetic study of reaction systems

Time-resolved UV–vis spectra of the reaction system both in the absence and in the presence of 2,4-DCP (all the CPs investigated here have similar effects on NADH oxidation, so 2,4-DCP is chosen as representative of CPs for terseness in the following discussion) are depicted in Fig. 1a and b, respectively. It can be seen that NADH react rather slowly with H_2O_2 in the designated condition (Fig. 1a). When trace amount of 2,4-DCP (5.00×10^{-7} M) was introduced to the reaction system, oxidation of NADH was accelerated markedly. The absorbance of NADH at 340 nm disappeared rapidly within 1 s (Fig. 1b). So the phenoxyl radical reaction was studied by measuring the decreasing absorbance of NADH at 340 nm to obtain the initial reaction rate.

Time dependence of the reaction monitored at 340 nm in various 2,4-DCP concentration also exhibited its accelerating effect on NADH oxidation in a concentration-dependent manner (Fig. 2). The initial reaction rate increased linearly with 2,4-DCP concentration and that is the case for other chlorophenols investigated here. Consequently, a kinetic spectrophotometric method for the determination of phenoxyl radicals was realized by measuring the initial rate of NADH oxidation.

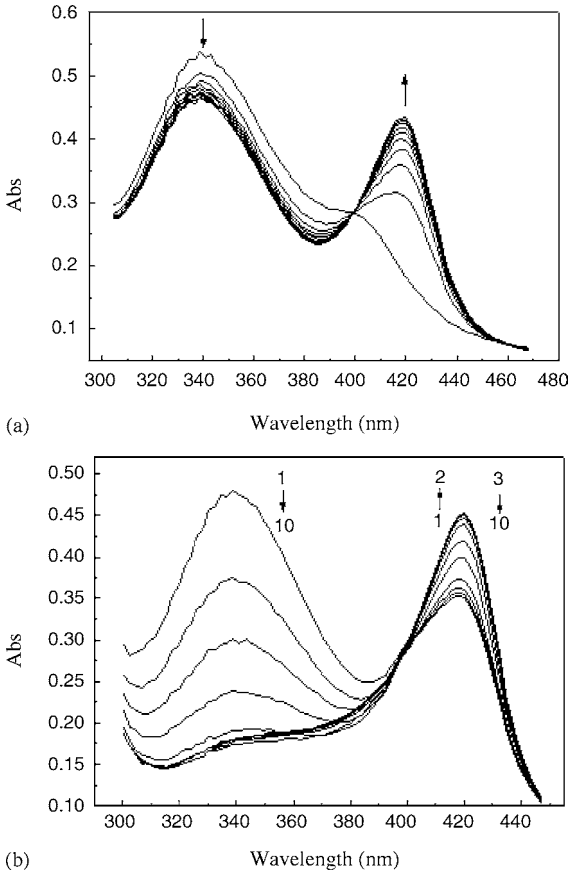

Fig. 1. Dynamic transformation of absorption spectra recorded upon mixing of 1.14×10^{-6} M HRP and (a) 0, (b) 5.00×10^{-7} M DCP with 1.00×10^{-4} M NADH and 5.00×10^{-4} M H_2O_2 in pH 7.4 PB, 25 °C. The spectrum 1 was recorded 0.019 s after mixing, and spectrum 2–10 at: (a) 0.838, 1.658, 2.477, 3.296, 4.115, 4.934, 5.754, 6.573, 7.392 s, (b) 0.224, 0.429, 0.634, 0.838, 1.043, 1.248, 1.453, 1.658, 1.862 s, respectively. The arrows show the direction of absorbance change with time.

3.2. Possible mechanism of the reaction

To exclude whether the accelerating effect stems from final products of 2,4-DCP in the reaction, two set of contrastive exper-

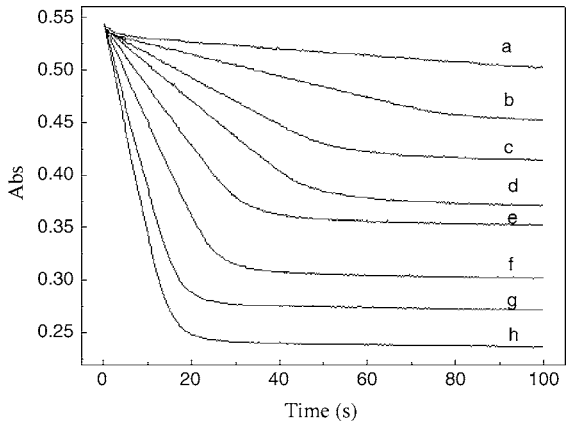

Fig. 2. Time dependence of the reaction in various DCP concentrations. The reaction mixtures contain 0, 10, 20, 30, 50, 80, 150, 200 μl 1.00×10^{-4} M DCP from curve a to h, other conditions are as depicted in Section 2.

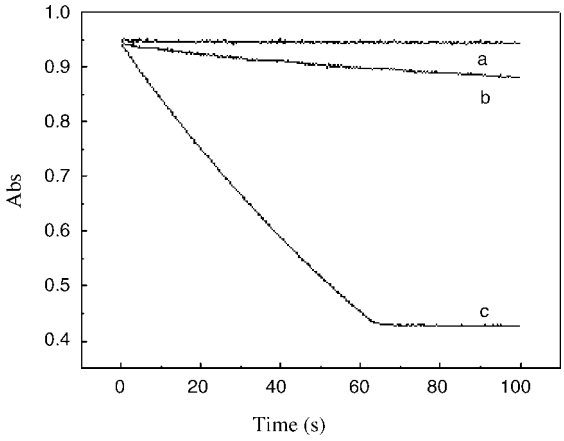

Fig. 3. Comparison of the kinetic curves of NADH oxidation in the presence of (a) final products, (c) free radical intermediates of 2,4-DCP in enzyme reaction. Curve (b) is the blank reaction of NADH oxidation. The reaction conditions are depicted in Section 2.

iments were conducted and compared with the blank reaction (oxidation of NADH without 2,4-DCP). In the first case, HRP, 2,4-DCP and H_2O_2 were premixed and incubated at 25 °C for 30 min to complete the reaction, afterwards, the mixture was rapidly mixed with NADH and time courses were followed at 340 nm. The contrastive one was carried out according to the procedure described in Section 2. As is shown in Fig. 3, the final products of 2,4-DCP show no accelerating effect on NADH oxidation, whose time course (curve a) is even slower than that of the blank reaction (curve b). These results strongly indicate a mechanism involving a role for transient phenoxyl radical formed in the investigated system, and neither 2,4-DCP nor its final products who accelerate the oxidation of NADH.

In order to clarify its mechanism, the reaction was investigated by mass spectrometry (Fig. 4). In the mass spectrum of the reaction mixture containing 1.14×10^{-6} M HRP, 1.00×10^{-4} M H_2O_2, 1.00×10^{-4} M NADH and 1.00×10^{-4} M 2,4-DCP, the strongest peaks, with a relative abundance of nearly 100%, shows the characteristic pattern of a molecular ion containing two chlorine atoms (161 *m/z*, under

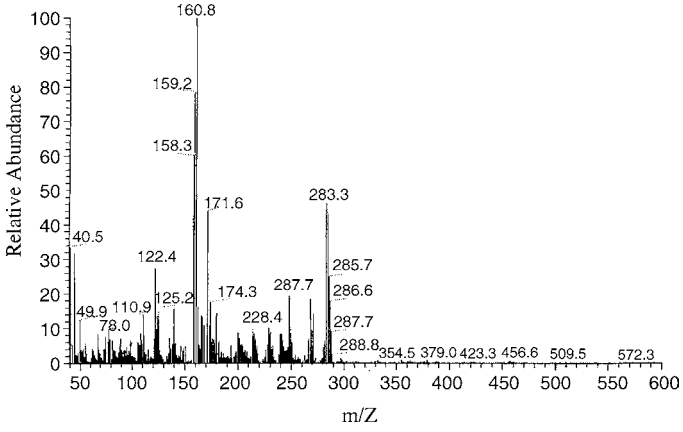

Fig. 4. Mass spectrum of the reaction mixture containing 1.14×10^{-6} M HRP, 1.00×10^{-4} M H_2O_2, 1.00×10^{-4} M NADH and 1.00×10^{-4} M 2,4-DCP after 60-s incubation.

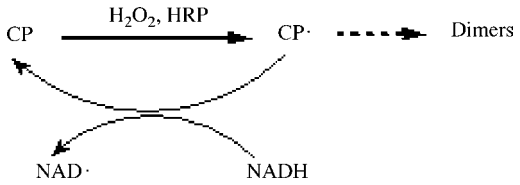

Fig. 5. Schematic illustration of the possible pathway of accelerating effect of CPs on NADH oxidation.

negative ionization). It has been assigned to 2,4-DCP (Mr = 162); the assignment of the second group, falling at 283–289 *m/z*, is not straightforward. Furthermore, peaks at *m/z* ratios corresponding to dimer products of 2,4-DCP could not be detected. In this experiment no evidence shows formation of any kind of dimers of 2,4-DCP (321, 323, 325, 327, 329 *m/z*) as were observed in oxidation of 2,4-DCP catalyzed by HRP without NADH [29]. Thus, the MS experiments rule out any depletion of CPs during the reaction.

According to the bibliography [26–30] and our own observations, the possible pathway of accelerating effect of CPs on NADH oxidation was postulated as is demonstrated in Fig. 5. HRP first catalyzes CPs to generate phenoxyl radicals ($CP^{\bullet}$), then NADH reacts with the phenoxyl radical to form $NAD^{\bullet}$. This process results in the accelerated-oxidation of NADH and returning phenoxyl radical to its initial chlorophenol state in a catalytic cycle. Hence the concentration of chlorophenol keeps constant until NADH is depleted. The dash-arrow shows the reaction pathway without NADH.

3.3. Optimization of determination conditions

The optimal condition is on the basis of obtaining maximum possible sensitivity, and at the same time, minimizing the blank reaction rate. The variables of determination were optimized in both systems, i.e. NADH oxidation in the presence of CPs (referred as "accelerated reaction") and in the absence of CPs (referred as "blank reaction").

The pH dependence of the systems was investigated over the range form pH 5.59 to 8.04 using Na_2HPO_4–KH_2PO_4 buffer solution, which is shown in Fig. 6a. It can be seen that the initial reaction rate decreases with increasing pH in both systems. Although the reaction rate is higher in lower pH in both systems, the blank is too high when pH < 7.4, which will be detrimental to the determination. Considering the potential application to the biological system, hence the Na_2HPO_4–KH_2PO_4 buffer with pH 7.40 was chosen in the subsequent experiments.

Like most work concerning enzymatic reactions, the concentration of the catalyst is always an important factor influencing the performance of the method and is essential to decide its appropriate amount. In our experiment, the reactions cannot take place at all in the absence of HRP, and the initial reaction rate increases with HRP concentration till 2.27×10^{-6} M, as is shown in Fig. 6b. With HRP concentration higher than 1.14×10^{-6} M the initial rates of phenoxyl radical generation do not increase very much, but difference between the accelerated reaction and the blank decreases. Besides, the reproducibility of the signal becomes poor with even higher HRP. Considering the

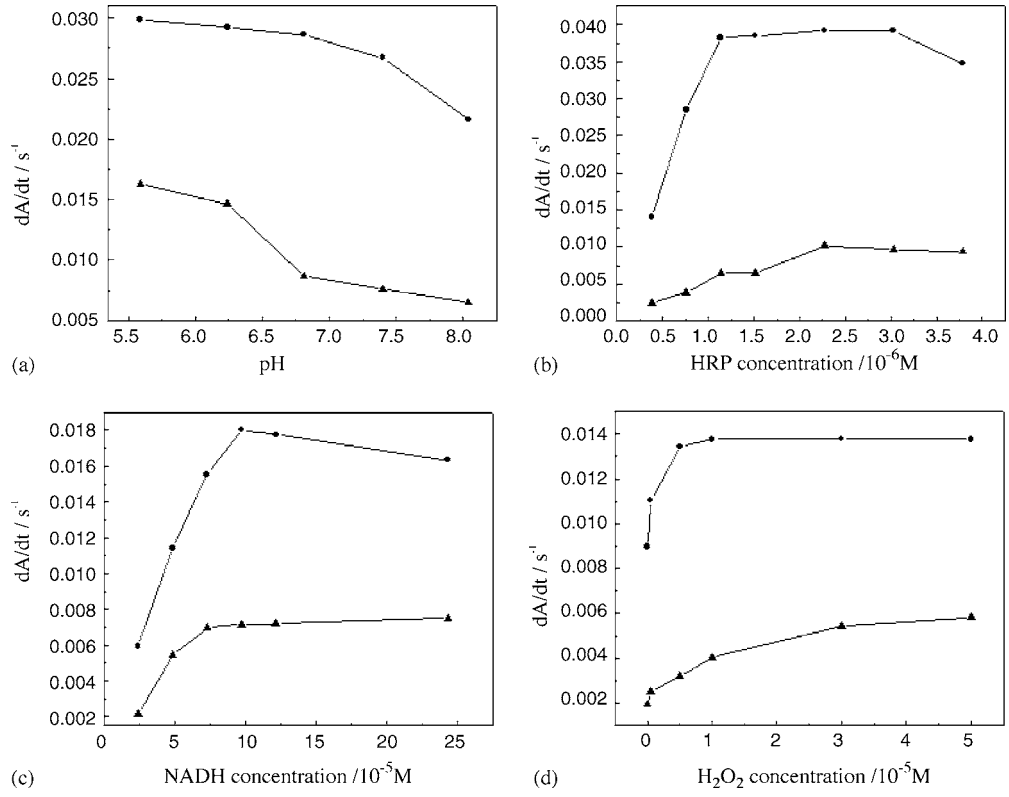

Fig. 6. Influence of: (a) pH, (b) HRP concentration, (c) NADH concentration, (d) H_2O_2 concentration on the initial reaction rate of the accelerated (●) and blank (▲) reaction.

Table 1
Analytical figures of merit for the determination of phenoxyl free radicals of various chlorophenols

Chlorophenols	Linear range ($\times 10^{-7}$ M)	Detection limit (M)	Slope ($\times 10^{7}$ s^{-1} M^{-1})	Intercept (s^{-1})	Correlation coefficient	R.S.D.[a] (%)
o-CP	0.333–16.7	3×10^{-8}	4.30E−4 ± 1.29E−5	1.58E−3 ± 5.50E−5	0.9975[b]	3.9
p-CP	0.167–8.33	7×10^{-9}	1.21E−3 ± 5.01E−5	5.22E−3 ± 4.14E−4	0.9987[b]	3.8
2,4-DCP	0.0833–16.7	3×10^{-9}	1.27E−3 ± 8.59E−5	2.38E−3 ± 1.07E−4	0.9995[b]	2.5
2,4,6-TCP	33.3–333	4×10^{-7}	7.87E−5 ± 8.13E−7	4.29E−3 ± 1.43E−4	0.9997[a]	2.3
2,3,4,6-TeCP	66.7–667	1×10^{-6}	2.94E−5 ± 6.09E−7	2.11E−3 ± 2.01E−4	0.9987[a]	3.4

[a] $n = 9$.
[b] $n = 13$.

sensitivity as well as the reproducibility, 1.14×10^{-6} M of HRP was recommended in the following determination.

The influence of NADH concentration on the initial rate in the two systems was also studied in this work. It is shown in Fig. 6c that difference of the initial rates between the accelerated reaction and that of the blank reaches to the maximum at about 1.00×10^{-4} M of NADH concentration, which was then used during the subsequent experiments.

The concentration of substrate in enzymatic reactions is always a very important factor for the system. Too low concentration of substrate will unavoidably cause signal loss because of the incompleteness of reactions. Meanwhile, improperly high concentration of substrate will be extremely detrimental to the catalyst and also contribute to the blank. The initial rate increases with the rising H_2O_2 concentration up to

Table 2
Tolerance (molar ratio of foreign substances to 2,4-DCP) of the method to some foreign substances

Foreign substances	Tolerance
Thiamine, tocopherol	10
Ascorbic acid, tyrosine	5
Glycin, glutamine, phenylalanine, tryptophan	400
Bovine serum albumin	20
Na^+, K^+, Ca^{2+}, Mg^{2+}	1000
Cu^{2+}, Fe^{2+}, Fe^{3+}, Mn^{2+}	4
SOD (U/ml)	1
DMSO, CH_3OH	500
Glutathione	1.5

Table 3
Determination of generation of phenoxyl radical in lake water samples (express as concentration of 2,4-DCP equivalent)

Sample	Found in sample[a] ($\times 10^{-8}$ M)	Added ($\times 10^{-8}$ M)	Found[a] ($\times 10^{-8}$ M)	Recovery (%)	R.S.D. (%)
1	5.22 ± 0.23	5.00	9.60 ± 0.32	94	3.3
2	8.14 ± 0.18	5.00	13.5 ± 0.62	103	4.6
3	9.65 ± 0.21	10.0	19.8 ± 0.55	101	2.9
4	12.7 ± 0.38	50.0	55.9 ± 2.4	89	4.3
5	8.98 ± 0.35	100	98.8 ± 3.8	91	3.8

[a] Values are means ± S.D. from five individual determinations.

5.00×10^{-6} M, above which it has little effect on the accelerated reaction while the initial rate of the blank reaction keeps rising. Moreover, HRP will be inactivated at too high H_2O_2 concentration [29]. So 5.00×10^{-6} M H_2O_2 was used in the recommended procedure.

3.4. Analytical performances of the method

Table 1 summarizes the figures of merit of the calibration graphs for phenoxyl radicals obtained from the above mentioned determination procedure. The calibration graphs are based on initial rate of the probe reaction plotted in function of chlorophenol concentration. The detection limit was calculated according to the three S_b/m criterion, in which 'm' is the slope of the range of the linearity used and 'S_b' the standard deviation ($n = 11$) of the blank. The relative standard deviations (R.S.D.) in Table 1 are for nine replicate determinations of 1.00×10^{-7} M *o*-CP, *p*-CP, 2,4-DCP and 1.00×10^{-5} M 2,4,6-TCP, 2,3,4,6-TeCP, respectively.

The results show excellent sensitivity as well as good reproducibility of this method. Phenoxyl radicals generated from 2,4-DCP as low as 1.00×10^{-8} M, for example, can be readily detected with the proposed method. It may be considered acceptable that apply this method for determination of phenoxyl radicals generated in enzyme reactions. The slopes of the calibration graphs in Table 1 represent the reactivity of various phenoxyl radicals, which are in following order: 2,4-DCP > 4-CP > 2-CP > 2,4,6-TCP > 2,3,4,6-Tetra-CP. These results indicate that the reactivity of phenoxyl free radicals is dependent on the structure of their parent molecules.

3.5. Interference

Interferences from some amino acids, metal ions and other bioactive molecules normally seen in biological samples, as well as several specific scavengers of $O_2^{\bullet -}$ and $HO^{\bullet}$ such as superoxide dismutase (SOD) and dimethylsulfoxide (DMSO) are considered. 2,4-DCP was chosen as the representative of chlorophenols to conduct the interference experiment. With concentration of 2,4-DCP fixed at 5.00×10^{-7} M, the foreign substances under study are added into the system with different concentrations. Their influences on the determination are presented as tolerance (molar ratio of foreign species to 2,4-DCP), which means the added intruder has lead to a variation of the initial reaction rate with less than 5%. Results in Table 2 show a fairly satisfactory selectivity of the method. It was noted that some metal ions such as Mn^{2+} tremendously enhances the extent of the reaction, but has little effect on the initial reaction rate in given concentration. DMSO (0.10 M), a specific scavenger for $^{\bullet}OH$, was introduced into the system, and the initial rate of the reaction was found to be almost unchanged, indicating that $^{\bullet}OH$ does not contribute to the accelerated oxidation of NADH. When SOD (3 U mL^{-1}), a specific scavenger for $O_2^{\bullet -}$, was added to the reaction systems, the initial rates of the reactions changed synchronously to the same extent (decreased by 12.5%) in both the accelerated reaction and the blank, proving that $O_2^{\bullet -}$ does not mediate the accelerated-oxidation of NADH. On the contrary, glutathione, a non-specific free radical scavenger, has intensive effect on the system and inhibits the reaction by 50% at concentration of 3.50×10^{-6} M.

3.6. Analytical application

The feasibility of this method was assessed by the determination of enzymatic generation of phenoxyl radicals in five lake water samples. In actual sample analysis, water sample took the placed of CPs in the standard procedure. Results were expressed as concentration of 2,4-DCP equivalent. The values of the samples determined by this method ranged from 5.22×10^{-8} to 1.27×10^{-7} M, as is shown in Table 3. Percentage recoveries were measured after adding different amounts of 2,4-DCP into the samples, which were from 89% to 103%, indicating that the lake water matrix did not significantly affect the determination.

4. Conclusion

A new kinetic method using stopped-flow spectrophotometry was proposed for detecting phenoxyl radicals generated in enzyme reaction. The accelerated-oxidation of NADH with phenoxyl radicals was observed and employed as the probing reaction to indicate the generation of phenoxyl free radicals. The information of phenoxyl radicals was obtained by monitoring the kinetic process of probing reaction. Possible pathway of the reaction is recommended. The proposed method is simple and sensitive, and shows promising to be applied to biological as well as environmental monitoring. Since peroxidase is ubiquitous in living body, the enzymatic reaction might probably be one pathway of CPs injury to cells or organism, especially in the mitochondrial respiratory chain in which NADH is abundant and plays a key roll. The mechanism of cytotoxicity of chlorophenols leaves open to further research.

Acknowledgements

The authors gratefully acknowledge financial support from the National Natural Science Foundation of China (Nos. 20275027 and 20377032).

References

[1] E. Cadenas, Mol. Aspects Med. 25 (2004) 17.
[2] N.S. Chandel, D.S. McClintock, C.E. Feliciano, T.M. Wood, J.A. Melendez, A.M. Rodriguez, P.T. Schumacker, J. Biol. Chem. 275 (2000) 25130.
[3] J.A. Knight, Ann. Clin. Lab. Sci. 28 (1998) 331.
[4] E.S. Schriner, N.J. Linford, G.M. Martin, P. Treuting, C.E. Ogburn, M. Emond, P.E. Coskun, W. Ladiges, N. Wolf, H. Van Remmen, D.C. Wallace, P.S. Rabinovitch, Science 308 (2005) 1909.
[5] A.P. Breen, J.A. Murphy, Free Radic. Biol. Med. 18 (1995) 1033.
[6] G. Cohen, S. Yakushin, D.D. Cohen, Anal. Biochem. 263 (1998) 232.
[7] D. Dreher, A.F. Junod, Eur. J. Cancer A 32 (1996) 30.
[8] H.F. Hung, C.S. Wang, Aerosol Sci. 32 (2001) 1201.
[9] C. Loetchutinat, S. Kothan, S. Dechsupa, J. Meesungnoen, J.P. Jay-Gerin, S. Mankhetkorn, Radiat. Phys. Chem. 72 (2005) 323.
[10] Y.J. Garcia, A.J. Rodríguez-Malaver, N. Peñaloza, J. Neurosci. Meth. 144 (2005) 127.
[11] D. Yao, A.G. Vlessidis, N.P. Evmiridis, Anal. Chim. Acta 467 (2002) 133.
[12] K. Midorikawa, T. Uchida, Y. Okamoto, C. Toda, Y. Sakai, K. Ueda, Y. Hiraku, M. Murata, S. Kawanishi, N. Kojima, Chem. Biol. Interact. 150 (2004) 271.
[13] K. Stolze, A. Dadak, Y. Liu, H. Nohl, Biochem. Pharmacol. 52 (1996) 1821.
[14] B. Bukowska, S. Kowalska, Toxicol. Lett. 152 (2004) 73.
[15] E.G. Janzen, Y. Kotake, R.D. Hinton, Free Radic. Biol. Med. 12 (1992) 169.
[16] R.A. Towner, R.P. Mason, L.A. Reinke, Biochim. Biophys. Acta 1573 (2002) 55.
[17] S.Y. Qian, M.B. Kadiiska, Q. Guo, R.P. Mason, Free Radic. Biol. Med. 38 (2005) 125.
[18] A.M. Osman, C. Laane, R. Hilhorst, Luminescence 16 (2001) 45.
[19] X.F. Yang, X.Q. Guo, Chem. J. Chin. Univ. 22 (2001) 396.
[20] S. Fukui, Y. Hanasaki, S. Ogawa, J. Chromatogr. 630 (1993) 187.
[21] B. Tang, L. Zhang, Y. Geng, Talanta 65 (2005) 769.
[22] E. Kilinc, Talanta 65 (2005) 876.
[23] J.N. Rodríguez-López, D.J. Lowe, J. Hernández-Ruiz, A.N.P. Hiner, F. García-Cánovas, R.N.F. Thorneley, J. Am. Chem. Soc. 123 (2001) 11838.
[24] J.E. Penner-Hahn, K.S. Eble, T.J. McMurry, M. Renner, A.L. Balch, J.T. Groves, J.H. Dawson, K.O. Hodgson, J. Am. Chem. Soc. 108 (1986) 7819.
[25] M. Mukai, S. Nagano, M. Tanaka, K. Ishimori, I. Morishima, T. Ogura, Y. Watanabe, J. Am. Chem. Soc. 119 (1997) 1758.
[26] Q. Huang, Q.G. Huang, R.A. Pinto, K. Griebenow, R. Schweitzer-Stenner, W.J. Weber Jr., J. Am. Chem. Soc. 127 (2005) 1431.
[27] A. Henriksen, A.T. Smith, M. Gajhede, J. Biol. Chem. 274 (1999) 35005.
[28] E. Laurenti, E. Ghibaudi, G. Todaro, R.P. Ferrari, J. Inorg. Biochem. 92 (2002) 75.
[29] E. Laurenti, E. Ghibaudi, S. Ardissone, R.P. Ferrari, J. Inorg. Biochem. 95 (2003) 171.
[30] A. Scheeline, D.L. Olson, E.P. Williksen, G.A. Horras, Chem. Rev. 97 (1997) 739.
[31] J.B. Marcus, Hauser, L.F. Olsen, Biochemistry 37 (1998) 2458.
[32] X.G. Wu, R.X. Cai, Anal. Chim. Acta 464 (2002) 153.
[33] X.G. Wu, R.X. Cai, L. Zhang, M. Xiao, Anal. Chim. Acta 448 (2001) 257.
[34] P. Jean-Louis, S. Grunenwald, P.L. Hagedoorn, A.M. Albercht-Gary, J. Am. Chem. Soc. 124 (2002) 1214.
[35] R.Y. Wang, R.X. Cai, Z.X. Lin, Chem. J. Chin. Univ. 25 (2004) 267.
[36] J. Xu, R.X. Cai, J. Wang, Z.H. Liu, W.X. Guo, J. Pharm. Biomed. Anal. 39 (2005) 334.
[37] Q. Zhang, D.W. Piston, R.H. Goodman, Science 295 (2002) 1895.
[38] Q. Gao, W.D. Wang, Y. Ma, X.R. Yang, Talanta 62 (2004) 477.

Available online at www.sciencedirect.com
ScienceDirect
Talanta 70 (2006) 330–335
Talanta
www.elsevier.com/locate/talanta

The interaction of recombinant *Pseudomonas aeruginosa* exotoxin A with DNA and mimic biomembrane investigated by surface plasmon resonance and electrochemical methods

Aixue Li [a,b], Zhaozeng Sun [c], Ying Ma [a,b], Fan Yang [a], Hongsheng Ouyang [c], Xiurong Yang [a,*]

[a] *State Key Laboratory of Electroanalytical Chemistry, Changchun Institute of Applied Chemistry, Chinese Academy of Sciences, Changchun, Jilin 130022, China*
[b] *Graduate School of the Chinese Academy of Sciences, Beijing 100039, China*
[c] *Biochemistry Laboratory of Veterinary College, Jilin University, Changchun, Jilin 130062, China*

Received 27 October 2005; received in revised form 16 February 2006; accepted 18 February 2006
Available online 24 March 2006

Abstract

Based on the multidomain structure of *Pseudomonas aeruginosa* exotoxin A, a fusion protein termed rPEA has been constructed, which is expected to serve as a gene carrier in vitro. The expression and purification of rPEA are described. The basal properties of rPEA as a gene carrier are evaluated by investigating its interaction with plasmid DNA and mimic biomembrane by surface plasmon resonance (SPR) and electrochemical methods. rPEA is proved to be able to bind with plasmid DNA with high affinity. It can also interact with lipid membrane and increase permeability of the membrane, so the probe molecules can easily reach the gold surface and exhibit the electrochemical response.

Keywords: *Pseudomonas aeruginosa* exotoxin A; Surface plasmon resonance; Mimic biomembrane; Electrochemical methods

1. Introduction

Recently, native peptides and proteins with amphipathic sequences which play an important role in many lipid membrane-reorganizing processes like fusion or disruption have been applied to construct fusion proteins for intracellular delivery of drugs, including oligonucleotides, peptides, or plasmid DNA [1]. One class of the membrane-active peptides is exotoxins and other bacterial proteins. The activity of these toxins depends on an efficient delivery mechanism of their toxic domain to the cytosol. One of such toxin is *Pseudomonas aeruginosa* exotoxin A (PEA), which is one of the major virulence factors of *P. aeruginosa*. The toxin is a single-chain polypeptide containing 613 amino acids and is arranged in several domains [2–5]: domain Ia (aa l–252) exerts the cell binding function (amino-terminal domain); domain II (aa 253–364) mediates membrane translocation; domain Ib (aa 365–404) of unknown function and domain III (aa 405–613) carries the mono-ADP-ribosyl transferase activity (carboxy-terminal domain). The toxin enters the cell by receptor-mediated endocytosis and internalizes by endosomes. Depending on endosomal acidification as a trigger, a conformational change within the translocation domain of the toxin and insertion into the vesicular membranes occur. Finally, the enzymatically active toxin fragment will be delivered into the cytosol of target cell, where it inhibits the eukaryotic protein synthesis by catalyzing the transfer of ADP-ribosyl moiety of NAD^+ onto elongation factor 2 [6]. Based on the multidomain structure and the endosome escape property of such toxins, fusion proteins have been engineered to be used to transport heterologous protein domains into cells by modifying the enzymatic domain [7,8], or used as immunotoxin by replacing the cell recognition domain with antibodies or natural ligands [9], or facilitated target cell-specific gene delivery by changing both the cell recognition domain and the enzymatic domain [10,11]. Alternatively, we propose to utilize the toxin to construct a fusion protein as a gene carrier that can be widely used in vitro. The fusion protein consists of three functional domains: (1) the cell-binding domain of exotoxin A confers binding to

* Corresponding author. Fax: +86 4315689711.
E-mail address: xryang@ciac.jl.cn (X. Yang).

0039-9140/$ – see front matter © 2006 Elsevier B.V. All rights reserved.
doi:10.1016/j.talanta.2006.02.056

its receptor; (2) the translocation domain of exotoxin A facilitates endosome escape; and (3) histone H3 enables high-affinity binding to plasmid DNA. Because the receptor of PEA is α2-macroglobulin receptor/low density lipoprotein receptor-related protein (α2-MR/LRP), which is found in many tissues and cells and is expressed in high levels in fibroblasts and hepatocytes [12], this fusion protein, which named rPEA, is expected to be useful in mediating the gene delivery for varieties of cells in vitro.

The traditional route for the identification of a fusion protein as a gene carrier is electrophoretic mobility shift assays and cell transfection experiments. However, for the preliminary screening, these approaches are laborious and time consuming. Here our main goal is to investigate some properties of the fusion protein that are considered important in respect of their potential use in a DNA delivery system. For a gene carrier, a basal requirement is the high affinity with plasmid DNA, so we firstly investigated the DNA binding property of rPEA. Surface plasmon resonance (SPR) is a powerful technique to monitor the interactions of biomolecules in real time without labeling. It has been widely used for measuring the reaction kinetics and affinity constants for a variety of biological systems including DNA–protein, antibody–antigen, enzyme–substrate, receptor–ligand, etc. [13–16]. SPR biosensor was used to investigate the DNA binding property of rPEA in the present paper.

The second basal requirement for a gene carrier is the capacity of translocating the biomembrane of cells' components. As rPEA would enter the cells by receptor-mediated endocytosis and internalize by endosomes, so the penetration of rPEA to the membrane of endosome is what we care about. Because of the complexity of the native biomembranes, many kinds of simplified models of biomembranes have been applied to mimic the structures and properties of native biomembranes. One of the extensively studied model biomembrane is hybrid bilayer membrane (HBM). It represents a means of stabilizing a lipid bilayer while preserving its dynamic nature and provides a way of organizing membrane proteins in a native membrane-like environment [17]. Combined with electrochemical methods, it has been used as model biomembrane to investigate the permeation mechanism of some biomolecules [18–20]. In this case, we constructed the HBM on the gold electrode and the interaction of rPEA with the model biomembrane was investigated by electrochemical methods.

2. Experimental

2.1. Materials

Escherichia coli strain BL21 (DE3 plys) cells and pET-28a vector were obtained from Novagen. HiTrap™ chelating HP was obtain from Amersham Biosciences. Isopropyl β-D-thiogalactopyranoside (IPTG), laurouyl sarcosine (SKL) and phenylmethanesulfonyl fluoride (PMSF) were purchased from Sigma. Goat polyclonal antibody to Histone H3 was purchased from Abcam. Plasmid DNA was PVAX1, preserved by our laboratory. Sensor chip C1 and hepes buffer saline solution (HBS) (pH 7.4, consisting of 10 mM 4-[2-hydroxyethyl]piperazine-1-ethane-sulfonic acid, 150 mM sodium chloride, 3.4 mM EDTA, 0.005% (v/v) surfactant P-20) were obtained from Pharmacia Biosensor AB. Poly (ethylenimine) (PEI) (average $MW = 6 \times 10^4$, 50 wt.%, Sigma) was used without further purification. Hexanethiol was obtained from ACROS. 1,2-Dimyristoyl-sn-glycero-3-phosphatidylcholine (DMPC) was purchased from Sigma. All other reagents and solvents were of analytical reagent grade. Ultrapure water was prepared with a Quartz distillatory below boiling point and then purified with a Milli-Q ultrapure water system.

2.2. Expression and purification of fusion proteins

The gene fragment of human histone H3 was inserted between the gene fragments encoding amino acids 1–364 and 604–613 of PEA. The ligated fragment was cloned into prokaryotic expression vector pET-28a directly, getting the recombinant vector pET-28a-PEA-H3. BL21 (DE3 plys) carrying plasmid pET-28a-PEA-H3 were grown at 37 °C in LB medium containing 50 μg/ml of kanamycin to $OD_{550} = 0.6$. Protein expression was induced with 0.5 mM IPTG at 37 °C for 180 min. Cells were harvested by centrifugation. Pellet was resuspended in 50 mM Tris–HCl, pH 8.0, containing 5% glycerol, 50 mM NaCl, 0.5 mM EDTA, 1 mM mercaptoethanol and 0.3 mM phenylmethylsulfonyl fluoride.

The cells were lysed by ultrasonication. Cell lysates were centrifugated at 13,000 rpm for 10 min. The inclusion bodies were washed with 0.2% deoxycholic acid twice and were lysed with 0.3% SKL overnight. The samples were loaded onto a Ni^{2+}-saturated HiTrap™ chelating HP column under the conditions of 50 mM Tris–HCl, pH 8.0, 500 mM NaCl, 0.3% SKL. Unbound proteins were removed by washing the column with equilibration buffer containing 100 mM imidazole. Bound proteins were eluted by increasing the imidazole concentration of the buffer to 500 mM. The obtained target proteins were diluted in 50 mM Tris–HCl, pH 8.0, containing 150 mM NaCl, 0.5 mM EDTA, 1 mM mercaptoethanol and dialysised in the same solution contained different concentrations of SKL (0.2, 0.15, 0.08, 0.05, 0.03, 0.02%) for 2 h each at 10 °C. The samples were concentrated with Amicon Ultra-4 Centrifugal Filter Devices. The concentrated samples were assayed by SDS-PAGE and western blotting with the polyclonal antibody to Histone H3. The concentration of the fusion protein was determined by UV–vis spectra measured on a Carry 500 Scan UV–vis-NIR Spectrophotometer (Varian, USA).

2.3. Surface plasmon resonance measurement

The SPR-based biosensor BIAcore 1000 (Pharmacia Biosensor AB, Uppsala, Sweden) was used to perform affinity experiment. The apparatus consists of a processing unit with liquid handling and optical system, a PC running BIAcore 1000 control software (version 2.1) for operating the instrument. BIA evaluation software (version 3.0) was used for data analysis.

Sensor chip C1 was inserted into the BIAcore. HBS buffer was used continuously with a flow rate of 5 μl/min, and 25 °C

was chosen for the whole process. The flow rate of 5 μl/min was maintained unless otherwise stated. Plasmid PVAX1 was selected as the immobilized ligand in the assay. The immobilization procedure was as follows: the sensor was first equilibrated with HBS buffer (10 mM, pH 7.4) until the baseline was stable. An aqueous solution of PEI (1 mg/ml, 10 μl) was injected. When the response signal was stable again, plasmid DNA (0.2 mg/ml, 10 μl, diluted in water) was injected. Then the system was programmed to run at a high flow rate (100 μl/min) for 5 min to avoid clogging by accumulation of polyelectrolyte and DNA.

The DNA-modified surface was used to determine the kinetic constants of the interaction between rPEA and plasmid DNA. rPEA was diluted in different concentrations with HBS buffer and flowed over the DNA immobilized surface. After each measurement, the surface was regenerated with 1.5 M NaCl and thoroughly rinsed with running buffer before injecting the next protein dilution.

2.4. Mimic biomembrane construction

The lipid vesicles were prepared according to the following procedure [21]: a solution of DMPC in chloroform was placed in a glass flask, and the solvent was evaporated under a stream of nitrogen, leaving a film of dried lipid in the vessel. The sample was then placed in a vacuum desiccator overnight to remove residual chloroform. The lipids were resuspended by vortexing in 0.01 M citrate buffer (pH 5.0, containing 0.1 M NaCl) to give a final concentration of 0.5 mg/ml. Sonicated unilamellar vesicles were produced from the suspension by sonication to clarity (ca. 2 h).

Prior to the formation of hybrid lipid membranes, a gold electrode was polished carefully with alumina slurries (1, 0.3, 0.05 μM) and washed ultrasonically with double distilled water. Then it was electrochemically cleaned in 1 M H_2SO_4 by cyclic potential scanning between −0.2 and 1.55 V until a standard cyclic voltammogram was obtained. Subsequently, the gold electrode was rinsed with copious amounts of double distilled water and absolute ethanol in turn.

After the electrode was cleaned, it was dried with high-purity nitrogen stream. Then it was immersed into a solution of 1 mM hexanethiol in absolute ethanol for 24 h. Subsequently, the electrode was rinsed with absolute ethanol and water to remove nonchemisorbed species. After the electrochemical characterization of the self-assembled hexanethiol, the gold electrode was immersed into a solution of phospholipid vesicles. After the formation of HBM, the gold electrode was transferred into solutions of rPEA.

2.5. Electrochemical measurements

A conventional three-electrode electrochemical system was used for the electrochemical measurements. The gold electrode was used as working electrode, an Ag/AgCl (saturated KCl) was used as reference electrode, and a Pt plate (area, 2 cm × 1 cm) was used as counter eletrode. An Autolab PG 30 electrochemical analyzer system (Eco Chemie BB, Netherlands) supplied with a FRA 2 module for impedance measurements, a SCAN-GEN scan generator, and GPES/FRA 4.9 software, were used for the electrochemical measurements. The electrochemical measurements were performed in the presence of 5 mM $K_3[Fe(CN)_6]/K_4[Fe(CN)_6]$ (1:1) mixture as a redox probe in 0.01 M citrate buffer (pH 5.0, containing 0.1 M NaCl). The impedance spectra were measured in the frequency range from 100 mHz to 100 kHz in a potential of 0.23 V versus Ag/AgCl (saturated KCl), with a root mean square amplitude of 5 mV. The frequency interval was divided into 60 logarithmically equidistant measure points. The electrical parameters of the system were fitted with a software package embedded in FRA 4.9. All measurements were carried out at room temperature.

3. Results and discussion

3.1. Production of the fusion protein

Residues 365–603 from PEA were replaced by the sequence encoding histone H3, and assembled into a single open reading frame in the bacterial expression vector pET-28a. The last amino acids (604–613) of PEA were remained, including the sequence REDLK that was required for the efficient delivery of the toxin to the cytosol [22]. The recombinant vector pET-28a-PEA-H3 encoded the target protein rPEA under the control of the IPTG inducible T7 promoter. rPEA also contained a cluster of six histidine residues allowing purification by Ni^{2+} affinity column. After transformation of BL21 *E. coli* strain, inclusion bodies were obtained by ultrasonication and then resolved by SKL. The target protein was purified through Ni^{2+} saturated chelating column and was refolded by dialysis in the gradually decreased concentration of SKL. Fig. 1 showed the typical result of the purification (>85%) that a prominent protein band migrated with the expected size of the fusion protein (57 kDa). The protein was detected as a single band after western blotting with the polyclonal antibody to histone H3.

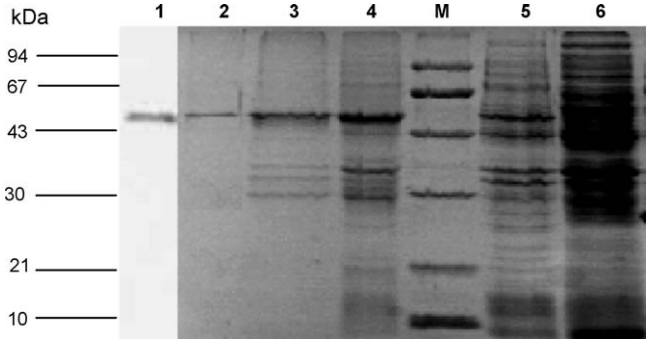

Fig. 1. SDS-polyacrylamide gel electrophoresis analysis of the rPEA protein purified from bacterial lysates. Lane 1, western blotting of the target protein with polyclonal antibody to Histone H3; lane 2, refolded and concentrated target protein; lane 3, the inclusion bodies resolved by SKL; lane 4, inclusion bodies after ultrasonication; M, molecular weight standards; lane 5, the protein of whole positive bacteria; and lane 6, the protein of whole negative bacteria.

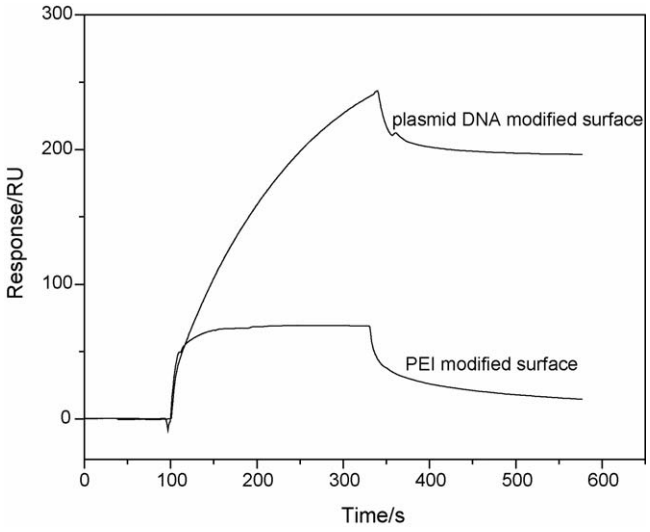

Fig. 2. Representative overlaid sensorgrams illustrating the binding of 20 μl rPEA (2.0 μg/ml) on plasmid DNA- and PEI-modified surface. The flow rate was 5 μl/min and HBS buffer was flowed over the chip surface after each injection.

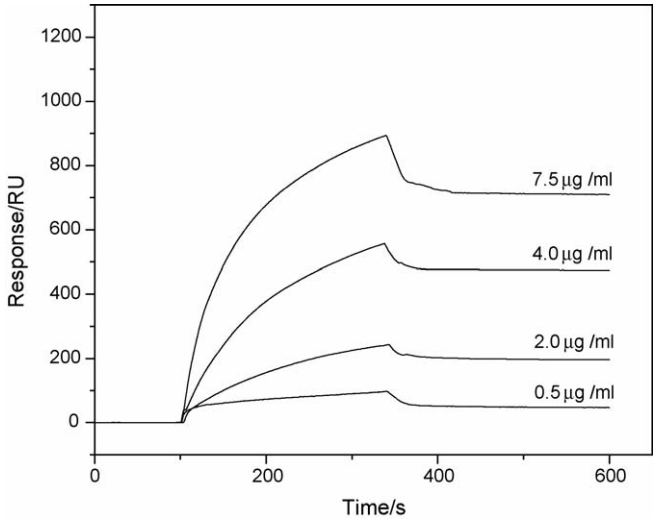

Fig. 3. Representative overlaid sensorgrams illustrating the real-time interaction of 20 μl rPEA at different concentrations (0.5, 2.0, 4.0, 7.5 μg/ml) with plasmid DNA. The flow rate was 5 μl/min and HBS buffer was flowed over the chip surface after each injection.

3.2. Interaction with plasmid DNA investigated by SPR

During real-time SPR measurement, one reagent is immobilized on the surface of the sensor chip, while the other reagent flows over the sensor surface and reacts with the immobilized one. In our work, to remain the integrated bioactivity of the rPEA, the plasmid DNA was immobilized on the sensor chip.

Usually, the linear DNA can be immobilized using streptavidin–biotin coupling method, but for plasmid DNA, this method is unsuitable. So we first modified the C1 chip with a positive charged polyelectrolyte PEI by electrostatic adsorption, then the plasmid DNA was immobilized by the electrostatic interaction with PEI. Immobilization levels of PEI and plasmid DNA were approximately 2500 and 3000 resonance units (RU), respectively. Under these conditions, the immobilization of plasmid DNA was reproducible with a relative standard deviation (RSD) of 3.5% ($n = 3$).

The immobilized surface was used to perform kinetic assay of rPEA with plasmid DNA. To eliminate the effect of the bulk refractive index, rPEA was diluted with HBS buffer (10 mM, pH 7.4). We firstly investigated the nonspecific adsorption of rPEA to the PEI-modified surface. One concentration of rPEA (2.0 μg/ml, 20 μl) was flowed over the PEI-modified surface, the result was compared with that obtained with the plasmid DNA-modified surface. As seen from Fig. 2, in the control curve with the PEI surface, the rPEA application led to an initial increase of 50 RU followed by a decrease after rinsing. This was due to a weak adsorption of the sample solution. However, the nonspecific adsorption was so small compared with the enhancement value of rPEA with plasmid DNA, it was neglected during the following experiments.

Fig. 3 was the representative overlaid sensorgrams illustrating the real-time interaction of plasmid DNA with 20 μl rPEA in HBS buffer at different concentrations. From the sensorgrams, the association and dissociation events could be directly observed. Different concentrations (0.5, 2.0, 4.0, 7.5 μg/ml) of rPEA were separately injected over the sensor surface and the amounts of bound rPEA were directly proportional to the protein concentration. The association and dissociation data were evaluated with BIA evaluation software (version 3.0). The data were analyzed with a simple 1:1 Langmuir model. The kinetic constants were given in Table 1. From the SPR study, we could conclude that rPEA has a high affinity for the plasmid DNA. The affinity constant of rPEA for the plasmid DNA was comparable with other gene carriers, such as functionalized carbon nanotubes (f-CNTs), poly (L-lysine), etc. [23,24]. Moreover, after internalization by target cells it might dissociate from the complex sufficiently. This would be desirable for the gene carriers.

3.3. Interaction with mimic biomembrane investigated by electrochemical methods

Cyclic voltammetry has been widely applied to characterize self-assembled layers on solid support surfaces [25–27]. In our experiment, a thin film of hexanethiol was firstly formed on the bare gold electrode, then the lipid layer were formed

Table 1
Kinetic parameters of the interaction of rPEA with plasmid DNA obtained with 1:1 Langmuir model ($n = 3$)

Kinetic parameters	k_a (1/M s)	k_d (1/s)	K_A (1/M)	K_D (M)
rPEA–plasmid DNA	$2.61\,(\pm 0.21)\times 10^{4}$	$5.2\,(\pm 0.33)\times 10^{-4}$	$5.02\,(\pm 0.50)\times 10^{7}$	$1.99\,(\pm 0.14)\times 10^{-8}$

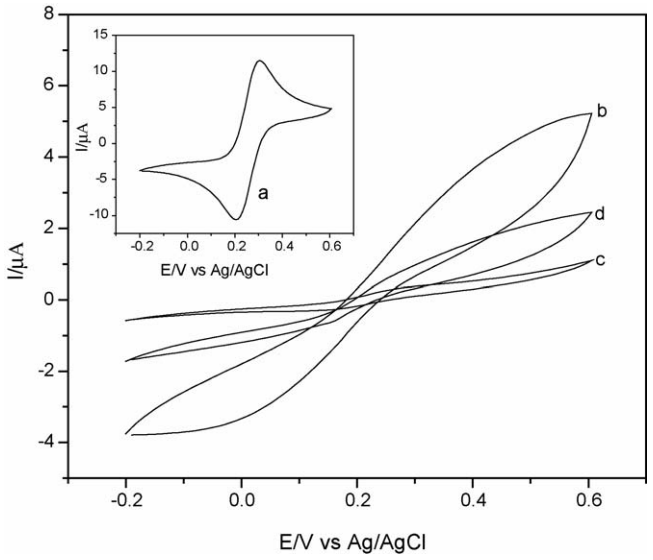

Fig. 4. Cyclic voltammogram recorded in 5 mM $K_3[Fe(CN)_6]/K_4[Fe(CN)_6]$ solution containing 0.1 M NaCl (pH = 5.0) at: (a) bare gold electrode; (b) hexanethiol-modified electrode; (c) DMPC-coated electrode; and (d) DMPC-coated electrode in the presence of rPEA (4 μg/ml). Scan rate, 100 mV s^{-1}.

on the top of the thiol layer. Fig. 4 showed CV curves of the $[Fe(CN)]_6^{4-/3-}$ redox in 0.01 M citrate buffer (pH 5.0, containing 0.1 M NaCl) on a gold electrode with different modification. After the formation of thiol layer on the gold electrode (Fig. 4b), a decrease of peak current and an increase in peak-to-peak separation between the anodic and cathodic waves were found compared with the bare gold electrode (Fig. 4a). When the thiol-modified electrode was coated with lipid membranes (Fig. 4c), a further decrease in peak current was observed and there were no obviously reversible redox peak pairs, which indicated the interfacial electron-transfer between the redox probe and the gold surface was mostly blocked and the lipid layer had been formed on the thiol-modified gold electrode. However, when the lipid-coated gold electrode was transferred to the solution of rPEA (4 μg/ml) for 30 min, which was diluted by 0.01 M citrate buffer (pH 5.0, containing 0.1 M NaCl). The amperometric response of $[Fe(CN)_6]^{4-/3-}$ was distinctly enhanced as if the mimic biomembrane were leaking (Fig. 4d). These results indicated that rPEA could bind to the HBM, insert at least partly into the HBM or disrupt the integrality of the HBM. The permeability of the membrane could be greatly enhanced, so the probe molecules could reach the gold surface easily.

Impedance spectroscopy is another effective technique for probing the interfacial properties of modified electrodes [28,29]. Fig. 5A illustrated the results of impedance spectroscopy on a bare electrode (curve a) and a hexanethiol modified electrode (curve b) and the lipid-coated electrode before (curve c) and after the interaction with rPEA (curve d) in the presence of 5 mM $[Fe(CN)]_6^{4-/3-}$. The detailed information of the impedance spectroscopy can be obtained by a simple model of a parallel resistor/capacitor in series with a solution resistor (Fig. 5B). In alkanethiol/lipid bilayer systems, the lipid monolayer specific capacitance ($C_{m\text{-}PL}$) can be calculated from the specific capacitance of the bilayer and the specific capacitance of the underlying SAM. Their relationship can be expressed by the equation [17]:

$$C_{m-PL}^{-1} = C_{m-bilayer}^{-1} - C_{m-monolayer}^{-1}$$

From the equation and the impedance spectroscopy, we obtained the value of $C_{m\text{-}PL}$ as 0.85 μF/cm^2. Considering the lipid membrane as a plate condenser, the relationship between the capacitance value and the thickness of the lipid membrane can be expressed by $C_{m\text{-}PL} = \varepsilon_0\kappa/d$, where ε_0 is the permittivity of free space ($\varepsilon_0 = 8.85 \times 10^{-14}$ F cm^{-1}), and κ the dielectric constant of the lipid ($\kappa = 2.7$) [17]. We calculated that the d-value of the lipid membrane was approximately 2.8 nm, which is about the thickness of the DMPC monolayer (2.4 nm) [30,31]. Hence, it could be concluded that the HBM was successfully formed on the gold electrode. Comparing the ac impedance spectra of the lipid membrane before (Fig. 5A, curve c) and after the interaction with rPEA (Fig. 5A, curve d), a considerable decrease was observed in the charge-transfer resistance. From the result of fitting, the value of R_m was obtained: In the absence of rPEA, the R_m was about 204.7 kΩ, while in the presence of rPEA, R_m was down to 122.5 kΩ. The impedance spectroscopy also proved that rPEA could insert at least partly into the HBM or lead to some defect or lesion in the membrane, resulting in the increased permeability of the membrane. This result was agreed with that of cyclic voltammograms.

The incorporation of native PEA into phospholipid planar bilayers or lipid vesicle and the formation of pores permeable to electrolytes are well documented [2,6,32–34]. The stimulus

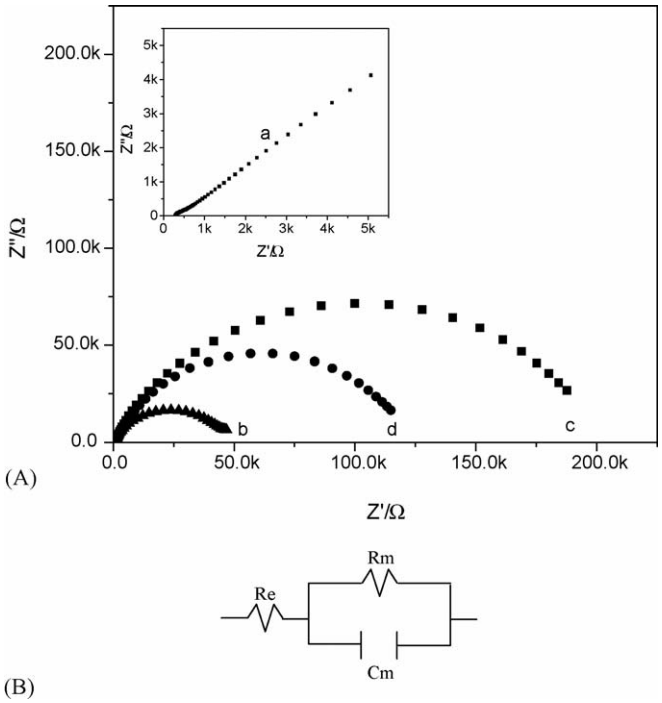

Fig. 5. (A) Complex plane impedance plots in 5 mM $K_3[Fe(CN)_6]/K_4[Fe(CN)_6]$ solution containing 0.1 M NaCl (pH = 5.0) at: (a) bare gold electrode; (b) hexanethiol-modified electrode; (c) DMPC-coated electrode; and (d) DMPC-coated electrode in the presence of rPEA (4 μg/ml). The potential was 0.23 V vs. Ag/AgCl/KCl and (B) equivalent circuit model used to fit the impedance data.

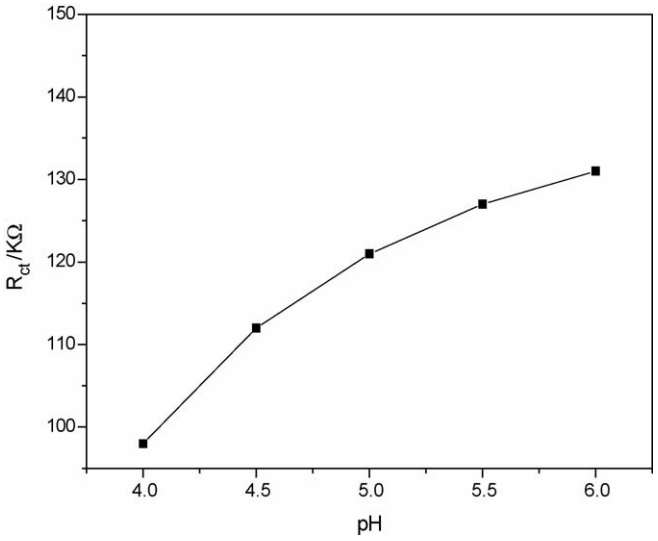

Fig. 6. R_m values of the lipid-coated electrode after the interaction with 4 μg/ml rPEA at different pH. The potential was 0.23 V vs. Ag/AgCl/KCl.

for toxin translocation is believed to be acidification of the ionic solution, which leads to protein structure changes within the toxin. In this paper, effect of pH on the penetration of rPEA to the HBM was also investigated. Fig. 6 showed the R_m values of the lipid-coated electrode after the interaction with 4 μg/ml rPEA at different pH. At lower pH values, a greater decrease of R_m was observed, which indicated that the penetration of rPEA to the HBM was dependent on the acidic environment. The result also suggested that the bacterial translocation domain in the rPEA functioned in a fashion very similar to the native toxin. Further identification of rPEA as a gene carrier in vitro is under investigation.

In summary, a fusion protein was designed for gene delivery in vitro, the whole chain from production of the fusion protein to first functional characterizations by SPR and electrochemical methods was described. We proved that the fusion protein could bind with plasmid DNA with high affinity and it could interact with lipid membrane directly and increase permeability of biomembrane. The methods we used provide a quickly and efficiently means to determine whether the fusion protein is worthy of further investigation. These techniques will especially be powerful when it is used for screening a series of substrates before setting out a large scale of cell transfection experiments.

Acknowledgements

This work was supported by the National Natural Science Foundation of China with the Grant No.20475052 and No. 20335040 and the National Key Basic Research Development Project "Research on Human Major Disease Proteomics" with the Grant No. 2001CB5102.

References

[1] C. Plank, W. Zauner, E. Wagner, Adv. Drug Deliv. Rev. 34 (1998) 21.
[2] P. Nordera, G. Menestrina, FEBS Lett. 421 (1998) 268.
[3] H. Barth, J.C. Preiss, F. Hofmann, K. Aktories, J. Biol. Chem. 273 (1998) 29506.
[4] M.J. Wick, A.N. Hamood, B.H. Iglewski, Mol. Microbiol. 4 (1990) 527.
[5] G.A. Caputo, E. London, Biochemistry 42 (2003) 3275.
[6] J.X. Jiang, E. London, J. Biol. Chem. 265 (1990) 8636.
[7] T.I. Prior, D.J. Fitzgerald, I. Pastan, Cell 64 (1991) 1017.
[8] J.J. Donnelly, J.B. Ulmer, L.A. Hawe, A. Friedman, X.P. Shi, K.R. Leander, J.W. Shiver, A.I. Oliff, D. Martinez, D. Montgomery, M.A. Liu, Proc. Natl. Acad. Sci. 90 (1993) 3530.
[9] I. Pastan, V.K. Chaudhary, D.J. Fitzgerald, Annu. Rev. Biochem. 61 (1992) 331.
[10] C. Uherek, J. Fominaya, W. Wels, J. Biol. Chem. 273 (1998) 8835.
[11] J. Fominaya, W. Wels, J. Biol. Chem. 271 (1996) 10560.
[12] M.Z. Kounnas, R.E. Morris, M.R. Thompson, D.J. FitzGerald, D.K. Strickland, C.B. Saelinger, J. Biol. Chem. 267 (1992) 12420.
[13] K. Matsumoto, A. Torimaru, S. Ishitobi, T. Sakai, H. Ishikawa, K. Toko, N. Miura, T. Imato, Talanta 68 (2005) 305.
[14] X. Liu, Y. Sun, D.Q. Song, Q.L. Zhang, Y. Tian, H.Q. Zhang, Talanta 68 (2006) 1026.
[15] R.L. Rich, D.G. Myszka, J. Mol. Recognit. 16 (2003) 351.
[16] R. Karlsson, J. Mol. Recognit. 17 (2004) 151.
[17] A.L. Plant, Langmuir 15 (1999) 5128.
[18] A.L. Plant, M. Gueguetchkeri, W. Yap, Biophys. J. 67 (1994) 1126.
[19] S.A. Glazier, D.J. Vanderah, A.L. Plant, H. Bayley, G. Valincius, J.J. Kasianowicz, Langmuir 16 (2000) 10428.
[20] L. Zhang, R. Vidu, A.J. Waring, R.I. Lehrer, M.L. Longo, P. Stroeve, Langmuir 18 (2002) 1318.
[21] H. Hillebrandt, G. Wiegand, M. Tanaka, E. Sackmann, Langmuir 15 (1999) 8451.
[22] S. Seetharam, V.K. Chaudhary, D.J. FitzGerald, I. Pastan, J. Biol. Chem. 266 (1991) 17376.
[23] R. Singh, D. Pantarotto, D. McCarthy, O. Chaloin, J. Hoebeke, C.D. Partidos, J.-P. Briand, M. Prato, A. Bianco, K. Kostarelos, J. Am. Chem. Soc. 127 (2005) 4388.
[24] T. Wink, J. de Beer, W.E. Hennink, A. Bult, W.P. van Bennekom, Anal. Chem. 71 (1999) 801.
[25] F. Auer, B. Sellergren, A. Swietlow, A. Offenhauser, Langmuir 16 (2000) 5936.
[26] S. Chen, K. Huang, Anal. Chem. 72 (2000) 2949.
[27] Z.Y. Wu, J.L. Tang, Z.L. Cheng, X.R. Yang, E.K. Wang, Anal. Chem. 72 (2000) 6030.
[28] Z.L. Cheng, E.K. Wang, X.R. Yang, Biosens. Bioelectron. 16 (2001) 179.
[29] Z.A. Xu, N. Gao, S.J. Dong, Talanta 68 (2006) 753.
[30] J.K.H. Horber, C.A. Lang, T.W. Hansch, W.M. Heckl, H. Mohwald, Chem. Phys. Lett. 145 (1988) 151.
[31] A. Watts, K. Harlos, D. Marsh, Biochim. Biophys. Acta 645 (1981) 91.
[32] F. Gambale, G. Rauch, G. Belmonte, G. Menestrina, FEBS Lett. 306 (1992) 41.
[33] P. Nordera, M. DallaSerra, G. Menestrina, Biophys. J. 73 (1997) 1468.
[34] D.M. Rasper, A.R. Merrill, Biochemistry 33 (1994) 12981.

Available online at www.sciencedirect.com
ScienceDirect
Talanta 70 (2006) 336–343
Talanta
www.elsevier.com/locate/talanta

Resolution of multicomponent overlapped peaks A comparison of several curve resolution methods

Hua Li *, Jianrong Hou, Kang Wang, Fang Zhang

Institute of Analytical Science, Northwest University, Xi'an 710069, China

Received 31 October 2005; received in revised form 18 February 2006; accepted 18 February 2006
Available online 17 April 2006

Abstract

Several curve resolution methods were compared in their performance of identification and quantification of overlapping peaks. These resolution methods are heuristic evolving latent projections (HELP), sub-window factor analysis (SFA), and orthogonal projection resolution (OPR). In this paper, HELP, SFA and OPR with the rank map produced by evolving factor analysis (EFA) or fixed size moving window-evolving factor analysis (FSMW-EFA) were applied to the simulated and experimental data. The resolved results were compared qualitatively and quantitatively. In addition, the further comparison was carried out with the results obtained from multivariate curve resolution-alternate least square (MCR-ALS) by using the initial estimates provided by EFA.

Keywords: Capillary electrophoresis-diode array detector (CE-DAD); Hyphenated instruments; Chemometric resolution methods; Heuristic evolving latent projections (HELP); Sub-window factor analysis (SFA); Orthogonal projection resolution (OPR)

1. Introduction

In recent years, hyphenated instruments, such as gas chromatography-mass spectrometry (GC-MS), high performance capillary electrophoresis-diode array detector (HPCE-DAD), high performance liquid chromatography-diode array detector (HPLC-DAD), have become routine means for qualitative and quantitative analysis. However, it is sometimes time-consuming for tedious procedures of searching optimal separation conditions. Moreover, when physical separation of some complex systems, such as chiral compounds and isomeric compounds, can often not completely accomplished because of very similar physical and chemical properties, the qualitative and quantitative analyzes are difficult for poorly resolved peaks. Fortunately, combination of hyphenated instruments with some chemometric resolution methods has been widely applied to the analysis of complex systems [1–4].

Capillary electrophoresis (CE) is a relatively new analysis and separation technique. Due to its speed of analysis, high efficiency, low solvent and sample consumption, CE has gained popularity and becomes a powerful analysis and separation technique to liquid chromatography (LC) separation. Recently, it has often been used for the qualitative and quantitative analysis of natural and biologic samples. However, it is also difficult to analyze each component of complex system qualitatively and quantitatively in CE because of above-mentioned practical problems in analysis process. Hence, combination of CE with some correlative chemometrics methods is necessary and its applications on some practical problems have been published in some papers [5–10]. Li et al. [5] and Zhang and Li [6] applied MCR-ALS method to the resolution of overlapping peaks and the quantification of each analyte in CE. Dohnal et al. [7,8] analyzed chiral compounds from unresolved peaks of CE quantitatively by using multivariate calibration with experimental design (ED) and artificial neural networks (ANN). Sentellas and Saurina reviewed the application of chemometrics in CE, in which the methods for data analysis [9] and optimization [10] were introduced. As a result, CE coupled with chemometric methods enhances its ability of separation and analysis tremendously. Some of these chemometrics methods are evolving factor analysis (EFA) [11,12], heuristic evolving latent projections (HELP) [13,14], windows factor analysis (WFA) [15], sub-window factor analysis (SFA) [16,17], orthogonal projection resolution (OPR) [18], iterative target transformation factor

* Corresponding author. Tel.: +86 29 88302942; fax: +86 29 88303488.
E-mail address: huali@nwu.edu.cn (H. Li).

0039-9140/$ – see front matter © 2006 Elsevier B.V. All rights reserved.
doi:10.1016/j.talanta.2006.02.062

analysis (ITTFA) [19], multivariate curve resolution with alternating least square (MCR-ALS) [20,21].

The above-mentioned methods can be roughly divided into iterative or non-iterative ones. Examples of iterative resolution methods are ITTFA and ALS. These methods are automatic and convenient to use, but sometimes have convergent problems [22]. Moreover, the corresponding extra information is needed for these methods such as non-negativity and unimodality constraints. Non-iterative methods such as EFA, HELP, WFA, OPR and SFA are evolutionary methods. The characteristic of this kind of resolution methods is their use of informative "windows". These methods are efficient, but usually require an experienced user.

Some papers have been published on the comparison of some curve resolution methods. Keller et al. [23] used HELP and fixed size moving window-evolving factor analysis (FSMW-EFA) to investigate their performance for peak purity control in LC-DAD. Both methods' performance in detecting a small amount of a spectrally similar impurity is identical, although they are subject to artifacts caused by instrumental and experimental problems. Grung and Kvalheim [24] used EFA, HELP and OPA to test their ability to deal with partial selectivity on simulated data. Ratios between true and predicted concentration were calculated to evaluate the performance of three methods. HELP proved to be a far better method than both EFA and OPA. Cuesta Sánchez et al. [25] used OPA, EFA and WFA to test their performance on three- and five-component mixtures of pesticides. Similarity and dissimilarity between the individual calculated and reference spectra were used as performance criterion. EFA and WFA produced better results than OPA once the concentration windows had been optimized. EFA was less than sensitive to the choice of the concentration window and gave slightly better results than WFA. van Zomeren et al. [26] applied HELP, EFA, ITTFA, and ALS with either random or iterative key-set factor analysis (IKSFA) initialization to resolve real and simulated data. Five curve resolution methods were compared systematically in their performance of identification and quantification of impurities in drug impurity profiling. For simulated data, ALS with IKSFA initialization and HELP performed better than ITTFA and EFA, which performed better than ALS with random initialization. For real data, comparison of the methods provided similar results.

Although these methods have been applied to solve some practical problems successfully and their limits have been investigated on simulated and/or experimental data, it is difficult to determine which method is most suitable under certain conditions [26]. Here, we will focus on the performance of three non-iterative methods for the progress of multivariate resolution methods developed in recent years is mainly traced to these kinds of methods [27]. HELP, SFA and OPR are all non-iterative methods using informative "windows" to resolve bilinear data matrix into electrophoretic profiles (**C**) and spectra (**S**). Thus, correct estimate of the informative "windows" based on the local rank map is crucial to obtain correct resolution results for these methods. To our knowledge, there are several kinds of chemometric methods which can obtain the local rank map of overlapping peak such as EFA, FSMW-EFA [28], eigenstructure-tracking analysis (ETA) [29], latent projective graphs (LPG) [13], needle plot (NP) [30], window target-testing factor analysis (WTTFA) [31] and sub-window comparison (ESC) [32]. In these methods, EFA and FSMW-EFA have more extensive applications than other methods to some extent.

In this paper, we will try to investigate the performance of combination of the above three non-iterative resolution methods (HELP, SFA and OPR) with two rank map estimation methods (EFA and FSMW-EFA) about the identification and quantification of overlapping peaks. These methods can be expressed simply as HELP-FSM, SFA-FSM, OPR-FSM, HELP-EFA, SFA-EFA and OPR-EFA, respectively (FSM denotes FSMW-EFA method). All resolution methods will be applied to the simulated and experimental data, respectively. The resolved results will be compared qualitatively and quantitatively. In addition, the further comparison will be carried out with the results obtained by MCR-ALS using the initial estimates provided by EFA (this method is expressed simply as ALS-EFA) [33–35].

2. Theory

A data represented by $\mathbf{X}_{m\times n}$ obtained from CE-DAD is a bilinear matrix. According to the Lambert–Beer law, it can be expressed simply as follows:

$$\mathbf{X}_{m\times n} = \mathbf{C}\mathbf{S}^{\mathrm{T}} + \mathbf{E} \tag{1}$$

where $\mathbf{X}_{m\times n}$ denotes an absorbance matrix of order $(m \times n)$ expressing n electrophoretic profiles of m migration time points measured at n different wavelength points (Eq. (1)). **C** and **S** are the pure electrophoretic matrix and the pure spectral matrix, respectively. T is the transform of matrix **S**. **E** represents the noise.

All curve resolution methods have the same goal. They try to decompose the bilinear data matrix into electrophoretic profile (**C**) and spectra (**S**). In this paper, data matrices (**X**) are expected to contain electrophoretic profiles in the columns and spectra in the rows.

For the sake of brevity, only concise theoretical explanation of each resolution method is showed here, while detail description can be found in elsewhere.

2.1. Heuristic evolving latent projections (HELP)

HELP was proposed by Kvalheim and Liang [13]. The prominent feature of this method is its emphasis on not only zero concentration information but selective information. The so-called selective information is in essence the pure component information. In generally, it is not difficult to obtain such information in the migration time direction because of the strong separation ability of CE. A thorough description of the theory of the method is given in [13], and has not been repeated here for the sake of brevity. The following procedures are carried out for each data.

(1) Detection and removing of background [13].

(2) Obtain the zero concentration information and selective information of target analysis component with the help of rank map produced by FSMWEFA or EFA.
(3) Calculate the transform vector to obtain the pure spectra and electrophoretic profile by using full rank resolution technique with the help of zero concentration information and selective information.
(4) Once the spectral and electrophoretic profiles of the first component are obtained, a component tripping procedure is used and procedure (3) and (4) are repeated to resolve next component.
(5) Decompose the whole matrix into electrophoretic and spectra profiles by repeating procedures (2)–(4).
(6) Confirm the reliability and quality of the resolved results.

2.2. Sub-window factor analysis

SFA is introduced by Manne et al. [16] as a solution to the problem of directly extracting component spectra from overlapping peaks. The theory of sub-window factor analysis is given in [16,17]. In this paper, we shall illustrate this procedure in the geometrical point of view. The following procedures are carried out for each data.

(1) Define two different sub-windows containing one and only one common component by using rank map produced by FSMW-EFA or EFA.
(2) Obtain two orthogonal basis $E = [e_1, e_2, \ldots, e_m]$, and $F = [f_1, f_2, \ldots, f_n]$ by singular value decomposition applied to above two sub-windows, respectively. So, the pure spectra **S** contained by above two sub-windows can be expressed by following equation:

$$\mathbf{S} = E\mathbf{a} = F\mathbf{b} \tag{2}$$

Here, **a** and **b** are the coefficients of **S** when expanded in the bases $[e_1, e_2, \ldots, e_m]$ and $[f_1, f_2, \ldots, f_n]$, respectively. In practice, $E\mathbf{a}$ and $F\mathbf{b}$ are not identical.
(3) Construct a target function (Eq. (3)) and calculate its minimum to obtain vectors **a** and **b**. Calculate the pure spectra **S** by Eq. (2).

$$N = ||E\mathbf{a} - F\mathbf{b}||^2 = \mathbf{a}'E'E\mathbf{a} + \mathbf{b}'F'F\mathbf{b} - 2\mathbf{a}'E'F\mathbf{b}^2 \tag{3}$$

(4) Obtain pure spectra of other components by repeating procedure (2)–(4).
(5) Obtain electrophoretic profiles by using the Eq. (4).

$$\mathbf{C} = \mathbf{X}\mathbf{S}(\mathbf{S}^{\mathrm{T}}\mathbf{S})^{-1} \tag{4}$$

2.3. Orthogonal projection resolution

There are two versions of orthogonal projection methods. One developed by Cuesta Sánchez et al. [36,37] is an iterative method and is an extension of an OPR technique used for detection of peak purity. The other described here is proposed by Liang and Kvalheim whose idea of using projection matrices to resolve the chromatographic profiles is based on Lorber's work on defining the net analytical signal (NAS) [38]. This method is identical to WFA developed by Malinowski, which has been proved by Xu and Liang [39]. The procedures can briefly be described as follows:

(1) Obtain a sub-matrix **A** containing all the analytes except the target analyte i in the studied region by using rank map produced by FSWEFA or EFA.
(2) Decompose **A** by SVD to obtain a matrix $\mathbf{V}(\boldsymbol{r})$ containing the first $\boldsymbol{r}$ orthogonal loading vector in which $\boldsymbol{r}$ is the number of principle factors.
(3) Construct an orthogonal projection matrix $(1 - \mathbf{V}(\boldsymbol{r})\mathbf{V}(\boldsymbol{r})^{\mathrm{T}})$. Obtaining $\mathbf{A}_i$ by the following equation:

$$\mathbf{A}_i = \mathbf{A}(\mathbf{I} - \mathbf{V}(\boldsymbol{r})\mathbf{V}(\boldsymbol{r})^{\mathrm{T}}) = \mathbf{C}_i\mathbf{S}_i(\mathbf{I} - \mathbf{V}(\boldsymbol{r})\mathbf{V}(\boldsymbol{r})^{\mathrm{T}}) \tag{5}$$

Here, **I** is an $M \times M$ identity matrix.
(4) By taking the norm of each column in $\mathbf{A}_i$ a normalized electrophoretic profile of analyte i is found.
(5) Each component's electrophoretic profile present is obtained by carrying out procedure (1)–(3) repeatedly.
(6) Calculating the spectra by Eq. (6).

$$\mathbf{S}^{\mathrm{T}} = (\mathbf{C}^{\mathrm{T}}\mathbf{C})^{-1}\mathbf{C}^{\mathrm{T}}\mathbf{X} \tag{6}$$

Note the electrophoretic profiles used for concentration estimation purposes can be produced by normalized spectra and Eq. (4).

2.4. ALS

ALS, also known as alternating regression (AR), is an iterative method. The original version of ALS starts the iterations with randomly estimation for the pure spectra or concentration. This version has been further developed and modified to be much more versatile [40]. The method present in this work was developed by Tauler et al. [20,21], sometimes called multivariate curve resolution-alternating least squares (MCR-ALS).

In present work, MCR-ALS decomposed a matrix once, i.e. one-order MCR-ALS. This method used initial estimates obtained by EFA. From the results of EFA analysis, an electrophoretic elution profile can be obtained. This electrophoretic profile is used as the initial values of **C** in a constrained alternating least-squares (ALS) optimization procedure. Subsequently, Spectra are estimated by using regression on data matrix and initial electrophoretic profiles. Then, electrophoretic profiles and spectra are found iteratively by using above two equations (4) and (6). The iterative process is stopped whenever the maximum number of iterations is reached or the relative difference in the SSR (sum of squares of the residuals) between two successive iterations is lower than a pre-defined threshold. When the iterative process is stopped, electrophoretic profiles (**C**) and pure spectra (**S**) are stable, and the data matrix is decomposed.

During the ALS optimization process, the corresponding extra constraints are needed. Possible constraints are (i) electrophoretic profiles are constrained to have only one maximum, i.e. unimodality; (ii) electrophoretic profiles and spectra are constrained to have only positive values, i.e. non-negativity; (iii)

selectivity; (iv) local rank and so on. Here, we used only first and second constraints for the sake of simpleness. The extensive details about ALS can be seen in [40].

3. Experimental

3.1. Reagents and solutions

The analytes were some samples of dinitro-toluene (DNT) isomeric compounds. All solutions were prepared with twice distilled water. The background electrolyte solution consisted of 5 mM sodium tetraborate aqueous solution + 100 mM sodium dodecyl sulfate (SDS) and was adjusted at pH 9. The selected analytes were 2,5-DNT and 3,5-DNT. Stock solutions for both DNT isomeric compounds were prepared in a methyl alcohol: water = 3:2 (v/v) solutions. The compositions of all mixtures were described in Table 1.

3.2. Instrument

A P/ACE Beckman capillary electrophoresis system with diode-array detector (DAD) (Beckman, Palo Alto, CA, USA) was used. Fused-silica capillaries (Reafine Chromatography, Yongnian, Hebei, China) of 75 μm i.d. with an effective length of 50 cm and a total length of 57 cm were used. Spectra were acquired in the range of 195–395 nm at regular steps of 0.25 s during the electrophoresis process. Forty-two working wavelengths with a step of 5 nm were chosen for analysis, which allowed us to define all absorption bands of spectra of isomeric compounds. The data obtained were processed with a compatible computer by using Beckman P/ACE station software (Version 2.0).

3.3. Capillary electrophoresis procedure

Before every day experiment, the capillary was rinsed with water for 2 min, 1 M HCl for 5 min, 0.1 M NaOH for 10 min and background electrolyte solution for 5 min. Between runs, the capillary was rinsed with water for 2 min and background electrolyte solution for 5 min. Sample injection was by pressure for 5 s. DNT isomeric compounds were separated at 15 kV for 18 min. The capillary was thermostated at 25 °C.

Table 1
Composition of the two-component mixture solutions analyzed

Mixture	2,5-DNT C_{true} ($\times 10^{-4}$ mol/L)	3,5-DNT C_{true} ($\times 10^{-4}$ mol/L)
M1	2.11	0.91
M2	0.84	2.29
M3	4.22	0.91
M4	0.84	4.57
M5	2.11	2.29
M6	2.11	2.29
M7	2.11	2.29
M8	2.11	2.29
M9	2.11	2.29
M10	2.11	2.29
M11	2.11	2.29
M12	2.11	2.29
M13	2.11	2.29
M14	2.11	2.29

C_{true} denotes the true concentration.

3.4. Software

All calculations were performed on a Pentium IV 3.0 GHz processor computer. All programs of the chemometric resolution methods were coded in MATLAB (Version 6.5, The Mathworks, Natick, MA, USA) for windows.

3.5. Data-sets

Experimental data were obtained by analyzing a number of samples using the CE-DAD system described above. The complete separation for DNT isomeric compounds had been done by using micellar electrokinetic chromatography (MEKC) [41]. In this paper, a MEKC separation condition was used without optimization in order to obtain overlapping peaks and the corresponding data matrices were analyzed by the above curve resolution methods. Different concentration ratios between the 2,5-DNT and 3,5-DNT were used to obtain overlapping peaks of different degree (from data M1 to M5). In order to test precision of resolved results derived from different curve resolution methods, samples were analyzed nine times repeatedly under the same as fifth experimental condition (from data M6 to M14). Therefore, a total of 14 data matrices were obtained (Table 1).

Several data containing two analytes with a varying degree of complexity were simulated. Electrophoretic profiles and spectra were produced as combinations of Gaussian peaks by means of MATLAB 6.5. Figs. 1 and 2 illustrated the profiles used in the simulations. Bilinear matrices for the analytes were produced as the outer products of the electrophoretic and spectral profiles. Every electropherogram or spectra was simulated with three parameters, i.e. peak height, peak position and variance. Nine data (from D1 to D9) were simulated according to a L9 (3^4) orthogonal design. Four factors were thought to influence the

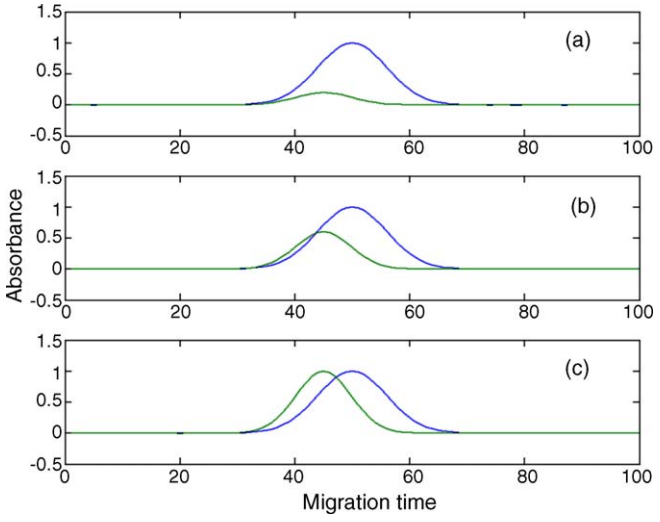

Fig. 1. Simulated overlapping peaks of CE of varying complexity (a) D3; (b) D6; (c) D9.

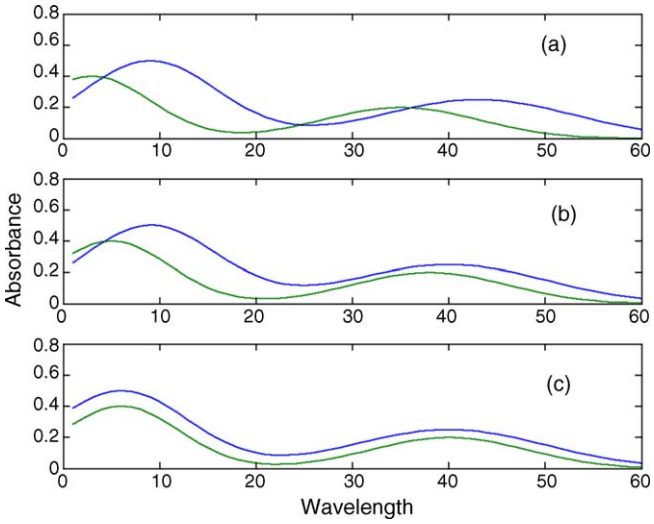

Fig. 2. Simulated spectra of different correlation coefficients between two components (a) 0.8456; (b) 0.9284; (c) 0.9919.

complexity of systems, i.e. (i) ratio of peak height with three different levels 5, 1.6667, and 1; (ii) ratio of peak position between two components with three different levels 1.4286, 1.25, and 1.1111; (iii) noise level; (iv) spectral similarity with three different levels 0.9919, 0.9284, and 0.8456. Noise was homoscedastic noise, which was added with a variance of 0.0008, 0.001, and 0.0015 to the data sets. Each data set had dimensions 100×60.

4. Results and discussion

During the calculation, the rank map produced by EFA seems more intuitionist than the one produced by FSWM-EFA for overlapping peaks. Moreover, FSMW-EFA has a problem that a correct choice of the size of the window is troublesome, although it can dramatically reduce calculation time than EFA for large data matrices because the method analyzes the data in a fix-sized window and moves the window in migration time direction instead of analyzing the data matrix in a stepwise way in EFA. Whether three non-iterative resolution methods with the rank map produced by EFA will improve their performance than those with the rank map produced by FSMW-EFA or not is also a purpose of present work.

The estimation of the number of chemical components is crucial to resolution of two-way data, which is the first step during resolution process. Without a correct estimation of the number of chemical components in the system, correct resolution seems impossible. Here, both simulated and experimental data are two-component systems. The determination of the number of chemical components is not discussed in subsequent subsections.

To evaluate the methods' performance, correlation coefficients are calculated by comparing the known spectrum of pure analytes with the resolved ones obtained by using different resolution methods from the cosine of the angle between these two vectors:

$$\cos\alpha = \frac{V_{\text{known}} \cdot V_{\text{cal}}}{||V_{\text{known}}|| \cdot ||V_{\text{cal}}||} \tag{7}$$

where $||V_{\text{known}}||$ denotes the norm of the known spectrum of pure analyte and $||V_{\text{cal}}||$ denotes the norm of the resolved spectra. The value of $\cos\alpha$ equal to one means a total agreement; deviation from one shows the level of dissimilarity [5].

Next, the quantitative analyzes are carried out with the overall volume integration method [42–44]. True and calculated concentrations of simulated data are obtained by using simulated and resolved electropherogram and spectra, respectively. Moreover, the relative error (%) between calculated and true concentration are calculated which can be used as a performance criteria quantitatively.

4.1. Case I for simulated data

Correlation coefficients between the pure and resolved spectra are obtained by several kinds of methods applied to the simulated data. One correlation coefficient obtained by HELP-FSM method is lower than 0.99, while two obtained by other methods are lower than 0.99. By comparing the average of correlation coefficients, it seems that HELP-FSM works better than other methods slightly. However, it is difficult to determine which method performs better than others because of similar results obtained by all methods. Moreover, although some correlation coefficients are higher than 0.99, the corresponding resolved results are unreasonable which can be confirmed by plotting the resolved and true electropherogram or spectra in the same plot and subsequent quantitative analysis. The possible reason is that two simulated spectra are very similar. So, the main comparison is carried out by following quantitative analysis.

Only the quantitative results of analyte 1 are shown in Table 2 in the interest of brevity as similar quantitative results are obtained by several resolution methods on analyte 2, and discussion of resolved results is detailed mainly on analyte 1. By comparing the average of relative error of calculated concentration obtained by each resolution method on analyte 1 and its standard deviation, HELP-FSM performs much better than other methods. Three non-iterative methods with the rank map produced by EFA do not perform better than those with the rank map produced by FSMW-EFA, although a fortunate choice of the size of the window and reasonable determination of selective information are exhausted for FSMW-EFA. This can be resulted from the difference between EFA and FSMW-EFA method. The noise level can be reasonably estimated for FSMW-EFA and it can provide more reliable and precision information than EFA since it is a local principal component analysis method.

Ratios of peak position between two simulated components of data D3, D6 and D9 are all 1.111. They are more complicated systems than other systems because two simulated electrophoretic profiles are overlapped strongly in these systems (see Fig. 1a). Reasonable resolution is completed by using HELP-FSM method for D9, although other methods provide inaccurate results. There are three possible reasons. Firstly, HELP method uses fully not only zero concentration information but selective

Table 2
True and calculated concentration of simulated data for analyte 1 for seven methods

Data	C_{true}	HELP-FSM C_{cal}	E (%)	HELP-EFA C_{cal}	E (%)	SFA-FSM C_{cal}	E (%)	SFA-EFA C_{cal}	E (%)	OPR-FSM C_{cal}	E (%)	OPR-EFA C_{cal}	E (%)	ALS-EFA C_{cal}	E (%)
D1	207.74	207.39	−0.17	206.86	−0.42	205.98	−0.85	206.21	−0.74	207.05	−0.33	207.07	−0.32	208.17	0.21
D2	209.51	203.46	−2.89	200.9	−4.11	193.12	−7.82	198.01	−5.49	202.9	−3.15	202.49	−3.35	199.88	−4.60
D3	195.66	202.72	3.61	137.15	−29.91	126.35	−35.42	32.786	−83.24	160.51	−17.96	142.27	−27.29	128.67	−34.24
D4	196.01	193.78	−1.13	196.69	0.345	194.48	−0.78	192.62	−1.73	195.95	−0.03	195.23	−0.40	193.46	−1.30
D5	208.04	202.32	−2.75	199.29	−4.21	200.59	−3.58	198.12	−4.77	201.64	−3.08	199.57	−4.07	198.39	−4.64
D6	209.41	239.65	14.44	142.41	−31.99	105.04	−49.84	145.17	−30.68	146.17	−30.20	145.23	−30.65	143.57	−31.44
D7	209.76	210.91	0.55	208.92	−0.40	205.86	−1.86	207.18	−1.23	209.69	−0.03	208.87	−0.42	208.07	−0.81
D8	195.84	199.68	1.96	189.72	−3.13	173.18	−11.57	179.79	−8.19	192.72	−1.59	191.11	−2.42	183.27	−6.42
D9	207.72	216.68	4.31	147.47	−29.01	147.47	−29.01	157.72	−24.07	151	−27.31	145.55	−29.93	144.84	−30.27
E_{ave}		3.53		11.50		15.64		17.79		12.37		13.82		14.67	
E_{std}		4.32		14.20		18		26.75		9.29		10.98		12.66	

C_{true} denotes true concentration; C_{cal} denotes the calculated concentration; E (%) represents relative error in percent. E_{ave} denotes average of absolute value of relative error; E_{std} expresses standard deviation of absolute value of relative error.

information. Secondly, FSMW-EFA has some advantages over EFA. Thirdly, it is possible to be resolved reasonably for D9 because its similarity between two simulated spectra is 0.8456, which is the lowest among all systems. All of methods do not provide reasonable resolution results for data D3 and D6 in which two simulated electrophoretic profiles are overlapped strongly and similarity between two simulated spectra is very high. For system D3, especially, similarity between two simulated spectra is the highest among all systems as well as ratio of peak position is the lowest, and none of methods provides accurate results. Moreover, OPR-FSM works better than ALS-EFA, which works better than SFA-FSM for these data. The results obtained by ALS-EFA are similar to ones obtained by HELP-FSM method for slightly overlapping systems such as D1, D4 and D7.

In addition, by analyzing the results of orthogonal experiment, ratio of peak position between two electrophoretic profiles is an important factor, which influences the complexity of systems and the performance of all method heavily. Secondly, similarity of spectra is also an important factor to a correct resolution. None of methods can provide reasonable results for those systems in which ratio of peak position between two electrophoretic profiles are very low and similarity of spectra are very high. Of course, several factors are found to be unable to alone say anything conclusively about the performance of different resolution methods.

4.2. Case II for experimental data

Standard solutions of 2,5-DNT and 3,5-DNT are analyzed according to above experimental conditions. Their pure spectra are extracted from the obtained data matrices at their peak maxima. Reasonable resolution is possible because of large difference of spectra. Resolved results are obtained from the produced data by HPCE-DAD with different chemometrics resolution methods.

In this paper, we investigate the performance of several methods applied to the overlapping peaks. We extract a sub-matrices from every run which only contains the overlapping peak of 2.5-DNT and 3,5-DNT (see Fig. 3a). From Fig. 3a, the electropherogram produced by CE-DAD is influenced by background and noise heavily. So, two pre-treatments are used to all matrices. One is the detection and removing of background, the other is wavelet denoising [45]. It can be seen that influences on raw data are deduced obviously after using two pre-treatments (see Fig. 3b).

Similar to simulated systems, evaluation of performance of all methods is carried out mainly by their relative error of calculated concentration because correlation coefficients obtained by these methods are similar to each other by comparing the average of correlation coefficients.

Likewise, discussion of quantitative results is detailed mainly on analyte 2,5-DNT for concision. The quantitative results of 2,5-DNT are shown in Table 3. As a whole, all of methods provide reasonable resolution results for these experimental data and HELP-FSM performs better than other methods slightly according to the average of relative error of all calculated concentration and its standard deviation. Similar to the comparison

Table 3
True and calculated concentration ($\times 10^{-4}$ mol/L) of experimental data for 2,5-DNT for seven methods

Data	C_{true}	HELP-FSM		HELP-EFA		SFA-FSM		SFA-EFA		OPR-FSM		OPR-EFA		ALS-EFA	
		C_{cal}	E (%)	C_{cal}	E (%)	C_{cal}	E (%)	C_{cal}	E (%)	C_{cal}	E (%)	C_{cal}	E (%)	C_{cal}	E (%)
M1	2.11	2.01	4.55	2.01	−4.71	1.99	−5.46	2.01	−4.52	2.01	−4.96	1.98	−5.94	2.07	−1.68
M2	0.84	0.83	−0.84	0.87	4.15	0.81	−3.17	0.86	1.89	0.82	−1.92	0.84	0.47	0.80	−4.37
M3	4.22	4.17	−1.24	4.11	−2.59	4.08	−3.31	4.04	−4.12	4.18	−1.06	3.94	−6.55	3.90	−7.67
M4	0.84	0.82	−2.65	0.78	−7.58	0.72	−14.33	0.75	−10.88	0.73	−12.95	0.68	−18.67	0.94	11.64
M5	2.11	2.05	−2.73	2.03	−3.59	2.25	6.40	2.08	−1.31	1.93	−8.52	1.97	−6.78	2.23	5.73
M6	2.11	2.15	1.86	2.11	−0.07	2.21	4.71	2.11	−0.08	2.24	6.11	2.14	1.29	2.12	0.39
M7	2.11	2.01	−4.98	1.97	−6.81	2.13	0.99	2.01	−4.61	2.22	5.33	1.92	−9.13	2.04	−3.19
M8	2.11	2.02	−4.12	2.01	−4.91	1.99	−5.77	1.96	−6.89	1.94	−8.25	1.98	−6.19	2.01	−4.72
M9	2.11	2.02	−4.17	2.06	−2.40	2.07	−1.87	1.96	−7.09	1.95	−7.63	1.98	−6.14	2.02	−4.37
M10	2.11	2.01	−4.61	2.01	−4.85	2.06	−2.28	1.98	−6.13	2.14	1.26	2.01	−5.17	1.96	−7.08
M11	2.11	2.02	−4.41	2.00	−5.31	2.05	−2.83	2.01	−4.63	2.09	−1.13	2.06	−2.45	1.94	−7.94
M12	2.11	2.04	−3.37	1.98	−5.95	2.16	2.32	1.99	−5.49	1.94	−8.17	1.94	−8.08	1.96	−7.24
M13	2.11	2.05	−2.93	1.95	−7.40	2.09	−0.82	2.05	−3.06	1.98	−6.25	2.01	−4.67	2.23	5.76
M14	2.11	2.05	−2.66	1.98	−6.28	2.02	−3.93	2.01	−4.62	1.93	−8.48	1.99	−5.84	1.96	−7.15
R.S.D.		0.041		0.047		0.083		0.0499		0.125		0.0625		0.110	
Reg		0.9997		0.994		0.9966		0.9993		0.9989		0.9990		0.9962	
E_{ave}		3.22		4.76		4.16		4.67		5.86		6.24		5.64	
E_{std}		1.31		2.10		3.40		2.70		3.53		4.32		2.85	

R.S.D. denotes the relative standard deviation of calculated concentration obtained on 10 experimental data (from M5 to M14). Reg denotes the regression coefficients of calculated concentration obtained on five mixtures (from M1 to M5); E_{ave} and E_{std} denote the average and standard deviation of relative error obtained on 14 experimental data (from M1 to M14), respectively.

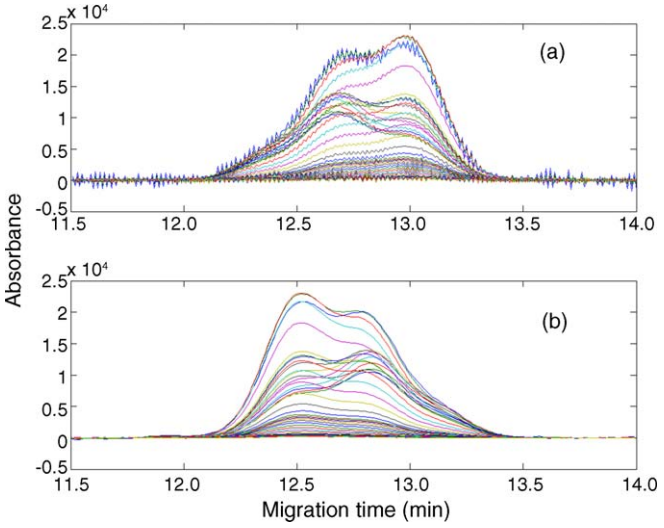

Fig. 3. The electropherograms of overlapped peaks of isomeric compounds of DNT (a) before two pre-treatments; (b) after two pre-treatments.

results of simulated data, all non-iterative methods using the rank map produced by FSMW-EFA perform better than those using the rank map produced by EFA for these data.

For mixtures containing different concentration ratios between the 2,5-DNT and 3,5-DNT (from M1 to M5), regression coefficients of calculated concentration obtained by all of methods are calculated. It suggests that HELP-FSM performs better than other methods. Example for mixtures M3 and M4, resolution difficulty is generated because of strongly overlapping peaks resulted from large concentration ratios between two DNT isomeric compounds and HELP-FSM give much better results than other methods.

In order to test the stability of performance of all resolution methods, mixtures containing same concentration ratios between the 2,5-DNT and 3,5-DNT (from M5 to M14) are analyzed and the relative standard deviation (R.S.D.) of calculated concentration obtained by each method on each analyte is calculated. It shows that HELP-FSM is a robust method. Interestingly, OPR-FSM performs better than SFA-FSM for simulated data, while the opposite is true for experimental data. The possible reason is that the heteroscedastic noise is present in experimental data while homoscedatic noise is present in simulated data, and OPR-FSM is more sensitive to the influence of heteroscedastic noise and background than SFA-FSM which can be confirmed by R.S.D. of calculated concentrations on 10 times repeated runs.

5. Conclusion

Both for experimental and simulated data, HELP-FSM performs better than other methods and HELP, OPR and SFA with the rank map produced by FSMW-EFA perform better than those with the rank map produced by EFA, respectively. Similar to HELP-FSM method, ALS-EFA works well for slightly overlapped peaks, while non-iterative methods work better than it for overlapping peaks strongly. So, when the clusters are slightly overlapped, ALS-EFA method is preferred because it is auto-

matic and convenient to use and it can converge quickly in order to economize the resolution time enormously. However, the manual non-iterative method is preferred when the clusters are heavily overlapped. At the same time, correct migration window identification is crucial to a correct resolution.

Acknowledgement

The work is supported by the National Natural Science Foundation of China [grant no. 20445002].

References

[1] A.W.M. Lee, W.F. Chan, F.S.Y. Yuen, C.H. Lo, R.C.K. Chan, Y.Z. Liang, Anal. Chim. Acta 339 (1997) 123.
[2] M. Jalali-Heravi, M. Vosough, J. Chromatogr. A 1024 (2004) 165.
[3] B.Y. Li, Y.Z. Liang, Y. Hu, Y.P. Du, Y.Q. Song, H. Cui, Talanta 61 (2003) 803.
[4] Y.X. Zhang, H. Li, A.X. Hou, J. Havel, Talanta 65 (2005) 118.
[5] H. Li, F. Zhang, J. Havel, Electrophoresis 24 (2003) 3107.
[6] F. Zhang, H. Li, Electrophoresis 26 (2005) 1692.
[7] V. Dohnal, H. Li, M. Farkova, J. Havel, Chirality 14 (2002) 509.
[8] V. Dohnal, F. Zhang, H. Li, J. Havel, Electrophoresis 24 (2003) 2462.
[9] S. Sentellas, J. Saurina, J. Sep. Sci. 26 (2003) 875.
[10] S. Sentellas, J. Saurina, J. Sep. Sci. 26 (2003) 1395.
[11] M. Maeder, Anal. Chem. 59 (1987) 527.
[12] M. Maeder, A. Zilian, Chemometr. Intell. Lab. Syst. 3 (1988) 205.
[13] O.M. Kvalheim, Y.Z. Liang, Anal. Chem. 64 (1992) 936.
[14] Y.Z. Liang, O.M. Kvalheim, H.R. Keller, D.L. Massart, P. Kiechle, F. Erni, Anal. Chem. 64 (1992) 946.
[15] E.R. Malinowski, J. Chemometr. 6 (1992) 29.
[16] R. Manne, H.L. Shen, Y.Z. Liang, Chemometr. Intell. Lab. Syst. 45 (1999) 171.
[17] H.L. Shen, R. Manne, Q.S. Xu, D.Z. Chen, Y.Z. Liang, Chemometr. Intell. Lab. Syst. 45 (1999) 323.
[18] Y.Z. Liang, O.M. Kvalheim, Anal. Chim. Act. 292 (1994) 5.
[19] B. Vandeginste, R. Essers, T. Bosman, J. Reijnen, G. Kateman, Anal. Chem. 57 (1985) 971.
[20] R. Tauler, D. Barcelo, Trends Anal. Chem. 12 (1993) 319.
[21] R. Tauler, B. Kowalski, S. Fleming, Anal. Chem. 65 (1993) 2040.
[22] F.Q. Guo, Y.Z. Liang, C.J. Xu, L.F. Huang, J. Chromatogr. A 1016 (2003) 99.
[23] H.R. Keller, D.L. Massart, Y.Z. Liang, O.M. Kvalheim, Anal. Chim. Acta 267 (1992) 63.
[24] B. Grung, O.M. Kvalheim, Chemometr. Intell. Lab. Syst. 29 (1995) 75.
[25] F. Cuesta Sánchez, S.C. Rutan, M.D. Gil Garcia, D.L. Massart, Chemometr. Intell. Lab. Syst. 36 (1997) 153.
[26] P.V. van Zomeren, H. Darwinkel, P.M.J. Coenegracht, G.J. de Jong, Anal. Chim. Acta 487 (2003) 155.
[27] Y.Z. Liang, O.M. Kvalheim, Fresen J. Anal. Chem. 370 (2001) 694.
[28] H.R. Keller, D.L. Massart, Anal. Chim. Acta 246 (1991) 279.
[29] Y.Z. Liang, O.M. Kvalheim, A. Rahmani, R. Brereton, J. Chemometr. 7 (1993) 15.
[30] A. de Juan, B. van den Bogaert, F. Cuesta Sánchez, D.L. Massart, Chemometr. Intell. Lab. Syst. 33 (1996) 133.
[31] M.T. Lohnes, R.D. Guy, P.D. Wentzell, Anal. Chim. Acta 389 (1999) 95.
[32] C.J. Xu, Y.Z. Liang, F. Gong, H. Cui, Anal. Chim. Acta 428 (2001) 235.
[33] W. Windig, J. Guilment, Anal. Chem. 63 (1991) 1425.
[34] W. Windig, S.A. Liebman, M.B. Wasserman, P.A. Snyder, Anal. Chem. 60 (1988) 1503.
[35] E. Casassas, R. Gargallo, I. Giménez, A. Izquierdo-Ridorsa, R. Tauler, Anal. Chim. Acta 283 (1993) 538.
[36] F. Cuesta Sánchez, M.S. Khots, D.L. Massart, J.O. De Beer, Anal. Chim. Acta 285 (1994) 181.
[37] F. Cuesta Sánchez, M.S. Khots, D.L. Massart, Anal. Chim. Acta 290 (1994) 249.
[38] A. Lorber, Anal. Chem. 58 (1986) 1167.
[39] Q.S. Xu, Y.Z. Liang, Chemometr. Intell. Lab. Syst. 45 (1999) 335.
[40] R. Tauler, E. Casassas, Chemometr. Intell. Lab. Syst. 14 (1992) 305.
[41] E. Sánchez, B.R. Kowalski, Anal. Chem. 58 (1986) 496.
[42] F. Gong, Y.Z. Liang, Q.S. Xu, F.T. Chau, J. Chromatogr. A 905 (2001) 193.
[43] F. Gong, Y.Q. Song, Y.G. Peng, A.K.M. Leung, F.T. Chau, Chem. J. Chin. Univ. 20 (1999) 199.
[44] F. Gong, Y.Q. Song, Y.G. Peng, A.K.M. Leung, F.T. Chau, Chem. J. Chin. Univ. 22 (2001) 1481.
[45] L. Pasti, B. Walczak, D.L. Massart, P. Reschiglian, Chemometr. Intell. Lab. Syst. 48 (1999) 21.

Available online at www.sciencedirect.com
ScienceDirect
Talanta 70 (2006) 344–352
Talanta
www.elsevier.com/locate/talanta

Assessment of infrared spectroscopy and multivariate techniques for monitoring the service condition of diesel-engine lubricating oils

Arnobio Roberto Caneca [a], M. Fernanda Pimentel [a,*], Roberto Kawakami Harrop Galvão [b], Cláudia Eliane da Matta [c,d], Florival Rodrigues de Carvalho [a], Ivo M. Raimundo Jr. [e], Celio Pasquini [e], Jarbas J.R. Rohwedder [e]

[a] *Departamento de Engenharia Química, Universidade Federal de Pernambuco (UFPE), Av. Prof. Artur de Sá S/N, Cidade Universitária, 50740-521 Recife, PE, Brazil*
[b] *Divisão de Engenharia Eletrônica, Instituto Tecnológico de Aeronáutica (ITA), Brazil*
[c] *Divisão de Ciência da Computação, Instituto Tecnológico de Aeronáutica (ITA), Brazil*
[d] *Centro Universitário Salesiano de São Paulo, Unidade de Lorena, Brazil*
[e] *Instituto de Química, Universidade Estadual de Campinas (UNICAMP), Brazil*

Received 5 November 2005; received in revised form 18 February 2006; accepted 18 February 2006
Available online 17 April 2006

Abstract

This paper presents two methodologies for monitoring the service condition of diesel-engine lubricating oils on the basis of infrared spectra. In the first approach, oils samples are discriminated into three groups, each one associated to a given wear stage. An algorithm is proposed to select spectral variables with good discriminant power and small collinearity for the purpose of discriminant analysis classification. As a result, a classification accuracy of 93% was obtained both in the middle (MIR) and near-infrared (NIR) ranges. The second approach employs multivariate calibration methods to predict the viscosity of the lubricant. In this case, the use of absorbance measurements in the NIR spectral range was not successful, because of experimental difficulties associated to the presence of particulate matter. Such a problem was circumvented by the use of attenuated total reflectance (ATR) measurements in the MIR spectral range, in which an RMSEP of 3.8 cSt and a relative average error of 3.2% were attained.

Keywords: Viscosity; Lubricating oil; Infrared spectroscopy; Multivariate calibration; Discriminant analysis; SPA

1. Introduction

Lubricants play a key role in extending the working life of rotating machines. In order to maintain a proper lubrication, it is important not only to use oils with suitable properties but also to monitor their state of degradation in a periodic manner. In fact, contaminations may compromise the lubricating capability of an oil, which increases the wear of the machine components, as well as the risk of mechanical collapse.

The tests currently employed to assess lubricant properties are time-consuming and require specific equipments for the determination of each parameter of interest (for instance, kinematic viscosity and flash point) [1,2]. In this context, the use of spectroscopy in conjunction with multivariate calibration techniques has been proposed as a multi-parametric alternative to the present methods. In particular, middle (MIR) and near (NIR) infrared spectroscopy offers several advantages for this type of application, such as high sample throughput, non-destructiveness and low cost [3]. Moreover, compact instruments in the MIR and NIR ranges can be realized for field use.

Much research has been conducted on the analysis of oil products by IR spectroscopy, for both classification and calibration purposes [3–5]. As regards lubricants, Lima et al. [6] studied the correlation between NIR spectra and the carcinogenic potential of basic oils employing principal component regression (PCR). Sastry et al. [7] used MIR spectroscopy and partial least squares regression (PLS) to determine the chemical composition (paraffins, isoparaffins, naftenes, aromatics and heteroaromatics) and

* Corresponding author. Tel.: +55 81 21267291; fax: +55 81 21267235.
E-mail addresses: mfp@ufpe.br, mf-pimentel@uol.com.br (M.F. Pimentel), kawakami@ele.ita.br (R.K.H. Galvão), ivo@iqm.unicamp.br (I.M. Raimundo Jr.), pasquini@iqm.unicamp.br (C. Pasquini), jarbas@iqm.unicamp.br (J.J.R. Rohwedder).

0039-9140/$ – see front matter © 2006 Elsevier B.V. All rights reserved.
doi:10.1016/j.talanta.2006.02.054

its influence on the physico-chemical properties (viscosity and viscosity index) in lubricants of mineral basis. MIR [8–11] and NIR [12] spectroscopy have been employed for the prediction of contaminants, degradation products and additives employing PCR, PLS and interval-PLS. The potentiality of MIR spectroscopy for the prediction of viscosity in lubricating oils for locomotives [10] and diesel engines [13] was assessed in a small-size set of samples (20 and 40 samples, respectively) by PCR and interval-PLS.

This paper proposes two strategies for monitoring the condition of lubricating oils being used in diesel engines by means of near and middle infrared spectroscopy. The first strategy is a qualitative approach formulated in the context of pattern classification. In this case, the samples are categorized in three classes according to their stage of use (short, medium, and long-term use) and classification is performed by discriminant analysis. In order to circumvent ill-conditioning problems, the dimensionality of the problem is reduced by using a variable selection algorithm. This algorithm is aimed at maximizing the discriminability of the spectral variables included in the model while avoiding multicollinearity problems. For comparison, a conventional KNN (K-nearest neighbours) classifier is also employed.

The second strategy is a quantitative approach that employs IR spectroscopy and multivariate calibration techniques in order to predict viscosity, which is the main control parameter for lubricants in service. In this case, MLR (multiple linear regression), PCR, and PLS techniques are employed in the calibration. The effect of different pre-processing procedures, as well as the utility of variable selection, is assessed by means of a factorial design study.

2. Background and theory

2.1. Qualitative analysis: Classification with respect to the stage of use

The classification method adopted in this work is based on the classic discriminant analysis technique, which assumes that the objects follow a gaussian distribution within each class. Under this assumption, the probability density function $p_j(\mathbf{x})$ for the objects $x = [x_1\ x_2\ \ldots\ x_d]^T$ belonging to the jth class is of the form:

$$p_j(\mathbf{x}) = \frac{1}{\sqrt{(2\pi)^d \det(\boldsymbol{\Sigma}_j)}} \exp\left[-\frac{1}{2}(\mathbf{x}-\boldsymbol{\mu}_j)^T \boldsymbol{\Sigma}_j^{-1}(\mathbf{x}-\boldsymbol{\mu}_j)\right] \quad (1)$$

where $\boldsymbol{\mu}_j$ $(d \times 1)$ and $\boldsymbol{\Sigma}_j$ $(d \times d)$ are the mean vector and the covariance matrix, respectively, which can be estimated from a set of training objects of known classification [14,15]. Variable x_i corresponds to the absorbance measured at the ith wavelength monitored by the spectrometer. Henceforth, with a slight abuse of language, the terms variable/wavelength and object/spectrum will be used with the same meaning.

In a problem involving C classes with equal a priori probabilities, the classification of a given object $\mathbf{x}$ is performed by calculating $p_j(x)$, $j = 1, 2, \ldots, C$ and by taking class j for which $p_j(x)$ is maximum. Such a classification rule is known as quadratic discriminant analysis (QDA) [15] because the decision boundaries defined by $p_{j1}(x) = p_{j2}(x)$, $j1 \neq j2$, are quadratic surfaces.

Simpler boundaries can be realized by adopting the regularization hypothesis that the covariance matrices are equal, that is $\boldsymbol{\Sigma}_1 = \boldsymbol{\Sigma}_2 = \cdots = \boldsymbol{\Sigma}_C = \boldsymbol{\Sigma}$. In this case, the decision surfaces are hyperplanes and the resulting classification rule is known as linear discriminant analysis (LDA) [15].

Both QDA and LDA usually benefit from a convenient selection of spectral variables [16]. In fact, if the number of variables employed in the classification model is large as compared to the number of training objects, the decision boundaries may be subject to overfitting and the resulting classifier is likely to have a poor generalization ability. Such a problem is aggravated in the presence of significant collinearity between the classification variables [17]. In the present work, a stepwise selection algorithm that takes into account both the discriminant power of each variable and the collinearity between variables is proposed.

2.2. Proposed variable selection algorithm for qualitative analysis

The proposed algorithm evaluates the individual value of each spectral variable according to its discriminability (as defined in Appendix A) with respect to the classes under consideration. At each step, the variable x_i with the largest discriminability D_i is selected, a *leave-one-out* cross-validation procedure is performed [14], and the number of errors is noted. Before the next step, the variables that are highly correlated with those already selected are discarded in order to avoid collinearity problems. The algorithm stops when no more variables are available. The set of variables that resulted in the smallest number of cross-validation errors is then presented to the analyst. Such a selection strategy can be summarized as follows.

Let A and B be the index sets for the variables already selected and those still available, respectively. Moreover let L be a correlation threshold $(0 < L < 1)$ established by the analyst. In what follows, N is a counter that indicates the number of variables already selected.

Step 0 (initialization). $A = \{\}$, $B = \{1, \ldots, d\}$, $N = 0$.

Step 1. Calculate D_i for $1 \leq i \leq d$.

Step 2. $i^* = \arg\max D_i,\ i \in B$.

Step 3. Move i^* from B to A. Let $N = N + 1$.

Step 4. Perform a leave-one-out cross-validation procedure using the variables with indexes in A. Let ECV(N) be the number of resulting cross-validation errors.

Step 5. Calculate the coefficient of multiple correlation r_i of each variable x_i with index in B with respect to the variables with indexes in A.

Step 6. Exclude from B the indexes of variables with coefficient of multiple correlation larger than L.

Step 7. If $B \neq \{\}$, return to Step 2.

Step 8. The optimum number n^* of variables is obtained from the minimum of ECV(n), $n = 1, \ldots, N$. The selected variables correspond to the first n^* indexes in A.

Remark 1. The coefficient of multiple correlation employed in Step 5 is defined, for each variable x_i, as:

$$r_i = \frac{\sigma(\hat{x}_i)}{\sigma(x_i)} \tag{2}$$

where $\sigma(.)$ denotes the standard deviation calculated in the training set and $\hat{x}_i$ is an estimate of x_i obtained by multiple linear regression from the variables already selected. If r_i is close to one, it can be concluded that the inclusion of x_i does not bring additional information into the classification model, because the values of x_i can be predicted from the variables already selected.

Remark 2. If there are several values of n associated to the minimum number of cross-validation errors ECV(n), the smallest n is chosen in Step 8. Such a choice is based on the Parsimony Principle [14], which states that, given classification models with similar prediction ability, the simplest one (smallest number of variables) should be favoured.

Remark 3. The selection procedure is performed both for LDA and QDA. If an LDA and a QDA model lead to the same number of cross-validation errors, the model with the smallest number of variables is favoured, as discussed above. If both models have the same number of variables, LDA is favoured because it employs simpler decision surfaces.

2.3. Quantitative analysis: multivariate regression for viscosity prediction

The multivariate regression methods most frequently used in infrared spectroscopy are multiple linear regression (MLR), principal component regression (PCR) and partial least squares (PLS). PCR uses principal components provided by principal component analysis (PCA) to perform regression. PCA finds directions of greatest variability by considering spectral information, whereas PLS uses both spectral and target-property information. PCR and PLS have the ability to overcome problems common to IR data, such as collinearity, band overlap and interactions. MLR is the simplest quantitative multivariate analysis method, yielding models which are simpler and easier to interpret than PCR and PLS, since these calibration techniques perform regression on latent variables, which may not be amenable to a straightforward physical interpretation. On the other hand, MLR is more sensitive to collinearity problems, and usually requires a judicious choice of spectral variables.

Selecting from the full spectrum the wavelengths that result in the maximum accuracy for regression models is still a challenging task. Several approaches have been proposed to select optimal sets of variables for multivariate calibration, such as the use of mutual information [18], simulated annealing [19,20], genetic algorithms [21–23], artificial noise introduction in PLS modelling [24], hybrid linear analysis [25], cyclic subspace regression [26], iterative predictor weighting PLS [27], and discriminant PLS [28]. Among these different variable selection strategies, genetic algorithms (GAs) have become very popular owing to their simplicity and flexibility. GAs are guided random search techniques inspired on natural selection mechanisms, which explore the solution space in an efficient manner and are suitable for parallel processing implementations.

A recently proposed wavelength selection strategy for MLR calibration, the successive projections algorithm (SPA), was specifically designed to remove collinearity from the data set in order to improve numerical conditioning and reduce noise propagation [29,30]. SPA has been successfully employed for variable selection in UV–vis [29], ICP-OES [30] and NIR [31] spectrometry. In all those applications, SPA led to MLR models with better predictive ability than PLS or PCR models employing the full spectrum. Moreover, the results reported in Refs. [30,31] provided evidence that SPA yields MLR models with better prediction performance than a genetic algorithm.

SPA works on the basis of a calibration (cal) and a validation (val) sets, consisting of instrumental response data ($\mathbf{X}$) and parameter values measured by a reference method ($\mathbf{y}$). The main operations in SPA consist of algebraic manipulations carried out on matrix $\mathbf{X}_{\text{cal}}$ (Kc × J), whose rows and columns correspond to Kc calibration samples and J spectral variables, respectively. Starting from a column $\mathbf{x}_0$ (which is associated to the initial variable of the selection), SPA determines which of the remaining columns has the largest projection on the subspace S_0 orthogonal to $\mathbf{x}_0$. This column, denoted by $\mathbf{x}_1$, can be regarded as the one that contains the largest amount of information not included in $\mathbf{x}_0$. At the next iteration, SPA restricts the analysis to subspace S_0, taking $\mathbf{x}_1$ as the new reference column, and proceeds with the steps described above. Thus, the selection criterion in SPA favours the minimization of collinearity between the variables. Moreover, no more than Kc variables can be selected in this manner. In fact, after each projection operation, the dimension of the column space of $\mathbf{X}_{\text{cal}}$ is reduced by one (that is, one degree of freedom is removed). Thus, after Kc projection operations all the column vectors of $\mathbf{X}_{\text{cal}}$ will have been projected onto the origin of the space, that is, $\mathbf{X}_{\text{cal}}$ will have become a null matrix.

The determination of the best initial variable (column of $\mathbf{X}_{\text{cal}}$) and the optimum number N of variables is carried out as follows. If N is fixed, J subsets of N variables can be selected, using each of the J available variables as a starting point for SPA. For each of those variable subsets, an MLR model is calibrated and the root-mean-square error of prediction in the validation set (RMSEV) is calculated as

$$\text{RMSEV} = \sqrt{\frac{1}{\text{Kv}}\sum_{k=1}^{\text{Kv}}(y_{\text{v}}^k - \hat{y}_{\text{v}}^k)^2} \tag{3}$$

where y_{v}^k and $\hat{y}_{\text{v}}^k$ are the reference and predicted values of the parameter of interest in the kth validation sample and Kv is the number of validation samples. The smallest RMSEV thus obtained is denoted by RMSEV$^*(N)$, where the star is used to indicate the best result for subsets of N variables. By repeating this procedure for $N = 1, 2, \ldots,$ Kc (note that N cannot be larger than Kc, as explained above) the optimum N can be obtained from the minimum of the RMSEV$^*(N)$ curve. To

Table 1
Partitioning of the samples in training and test sets

Set	Class			Total
	1	2	3	
Training	20	39	26	85
Test	9	10	10	29

save computational time, the analyst may interrupt the procedure before N reaches Kc if the reduction in RMSEV$^*(N)$ after a corner point is minor or if the curve starts to increase after a local minimum point.

3. Experimental

A set of 114 samples of lubricating oil (TURBO 15W40, Petrobras) for diesel engines in different stages of use was employed in this work. The samples were collected from an urban transportation company that operates in the city of Recife, Brazil.

Used lubricating oils for diesel engines display a very dark colour and a substantial amount of particulated matter, which prevents direct determinations in the NIR range. Attempts at minimizing this problem by means of centrifugation and filtration were unsuccessful. Attempts at reducing the optical path length were also unsuccessful. The samples were then diluted with toluene at the proportion of 1:5 (v/v). In order to inspect the spectra with minimum solvent influence, representative samples were also diluted in carbon tetrachloride. However, such an option would not be practical for routine use, because of its toxicity.

The NIR spectra were acquired in the 3996–14,000 cm^{-1} range (714–2500 nm) with an ABB Bomem MB 160D spectrophotometer fitted with a Hellma transflectance probe. A spectral resolution of 8 cm^{-1} and an optical path length of 2 mm were employed. The reference spectra were obtained with toluene or tetrachloride, according to the solvent used for dilution of the sample.

In the middle infrared, the spectra were acquired in the 650–4000 cm^{-1} range (2500–14,000 nm) with an FT-IR Perkin Elmer Spectrum GX spectrophotometer fitted with an ATR probe. A spectral resolution of 8 cm^{-1} was employed and air was used as reference.

All acquisitions, both in the NIR and MIR range, were carried out at room temperature (25 ± 1 °C).

3.1. Qualitative analysis

For classification purposes, the oil samples were grouped in three classes according to their stage of use: class 1 (short-term use—less than 5000 km), class 2 (medium-term use—from 5000 to 20,000 km) and class 3 (long-term use—more than 20,000 km). The samples were divided in training and test sets as shown in Table 1.

Classification was performed both with original and derivative spectra. The derivative spectra were obtained after smoothing by a Savitzky–Golay filter with a second-order polynomial and a 5-point window. Moreover, a preliminary elimination of variables with low signal-to-noise ratio was carried out by discarding the variables for which the maximum signal intensity over all derivative spectra did not exceed 10% of the maximum signal intensity in the entire data set. Furthermore, in the NIR derivative spectra, the spectral range closer to visible (10,130–14,000 cm^{-1}) was discarded because of the high level of noise caused by scattering.

3.2. Quantitative analysis

Determinations of kinematic viscosity at 40 °C were carried out according to the ASTM D445 method [2]. Two out of the 114 oil samples were deemed outliers because of abnormal viscosity values, which were ascribed to errors in the viscosity determination procedures.

The remaining 112 samples were divided into calibration, validation, and prediction sets with 64, 25, and 23 samples, respectively. The validation set was employed for the selection of PLS/PCR factors by external validation, and for the selection of wavelengths in SPA and GA. The prediction set was used for the final assessment and comparison of the models. The adopted figure of merit was the root-mean-square error in the prediction set (RMSEP).

The GA employed standard binary chromosomes with length equal to the number of wavelengths in the spectrum (a "1" gene indicates a selected wavelength) [22]. The fitness of each individual was taken as the inverse of the RMSEV (Eq. (3)) calculated by using the wavelengths coded in the chromosome. The probability of a given individual being selected for the mating pool was proportional to its fitness (roulette method). One-point crossover and mutation operators were employed with probabilities of 60 and 10%, respectively. Population size was kept constant, each generation being completely replaced by its descendants. The GA was carried out for 150 generations with 80 chromosomes each. Moreover, the algorithm was repeated 20 times, starting from different random initial populations. The best solution resulting from the 20 realizations of the GA was adopted.

A 2^3 factorial design was employed to assess the influence of pre-processing and variable selection procedures in the predictive ability of the resulting model. The factors under consideration were spectrum differentiation, smoothing (5-point Savitsky–Golay with second-order polynomial) and variable selection. For PLS and PCR, the low and high design levels for variable selection were no selection at all (i.e., use of full spectrum) and GA selection, respectively. For MLR, the low and high levels were SPA and GA selections, respectively.

4. Results and discussion

Fig. 1a presents spectra of toluene-diluted lubricating oils in three different stages of use. It is worth noting that the absorption of toluene, used as reference, is stronger than that of the oil, and therefore negative peaks are observed in the spectra. For comparison, Fig. 1b depicts the spectra of the same samples

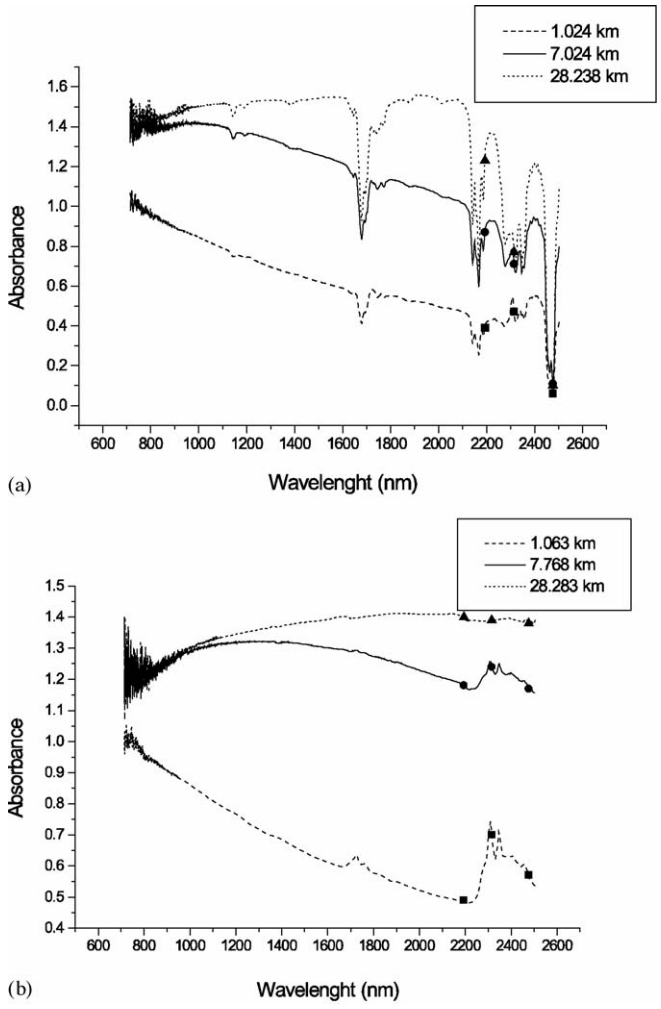

Fig. 1. Typical NIR spectra of (a) toluene-diluted and (b) carbon tetrachloride-diluted lubricating oils in different stages of use. The markers indicate the three wavelengths selected for qualitative analysis by QDA after pre-processing.

diluted with carbon tetrachloride, in which positive absorption bands appear, since carbon tetrachloride does not absorb in this region. As can be seen in both Fig. 1a and b, a positive baseline shift is associated with an increasing wear of the lubricant. Such a finding may be ascribed to the panchromatic absorption of particulate matter [32]. A related effect, also described in Ref. [32], consists of a decrease in the size of the absorption bands in Fig. 1b.

The spectra of the same lubricating oils in the MIR range are displayed in Fig. 2. By comparing Figs. 1 and 2, it can be seen that in the MIR range the peaks are narrower and more intense and that the baseline shift caused by particulate matter is less noticeable than in the NIR spectra. The region between 3000 and 4000 nm comprises low-intensity bands associated to the ring deformation of C–H in the aromatic ring superimposed to the high-intensity bands of ring deformations of CH_3-, CH_2- groups. The bands close to 6500 nm are distinctive of aromatic groups present in the samples. Bands of symmetric angular deformation of CH_2- groups, including CH_2–S bonds, are found in the region near 7500 nm. The bands ascribed to ring vibration of C–C bonds are weak and appear in the

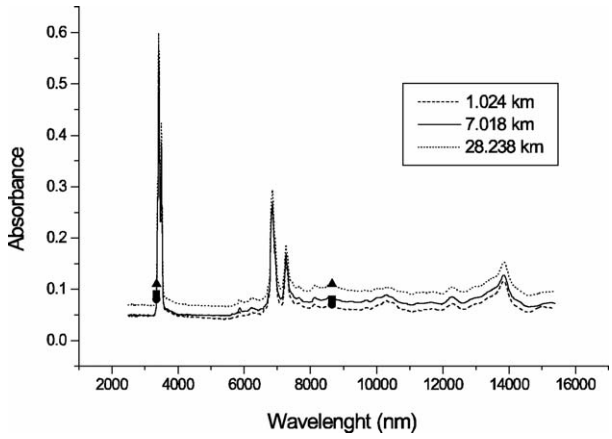

Fig. 2. Typical MIR spectra of lubricating oils in different stages of use. The markers indicate the two wavelengths selected for qualitative analysis by QDA.

Table 2
Number of classification errors in the MIR data set

	Original	Pre-processed
DA	2 (QDA, 2 wavelengths)	12 (LDA, 4 wavelengths)
KNN	6 ($k=28$)	14 ($k=1$)

For DA, the discriminant type (QDA or LDA) and the number of wavelengths are indicated, whereas for KNN, the number k of nearest neighbours is given.

region between 8300 and 12,500 nm. Finally, the region between 12,500 and 15,000 nm encompasses the absorption of several functional groups, including polynuclear aromatics, other aromatic groups and alkenes.

4.1. Qualitative analysis

Table 2 presents the classification results for DA and KNN in the MIR range. As can be seen, the best result was obtained with QDA by employing two wavelengths without pre-processing. In this case, only 2 out of 29 test objects were incorrectly classified, leading to a classification accuracy of 93%. The errors consisted of a class 2 and a class 3 objects included in classes 1 and 2, respectively. It is worth noting that, if the pre-processing is carried out, the number of errors increases both for DA and KNN. It could be argued that, in the MIR range, baseline information, which is removed by the derivative procedure, is important to discriminate the classes.

Table 3 presents the classification results in the NIR range. In this case, the best results for DA and KNN were obtained after the pre-processing procedures, unlike in the MIR range. It could be argued that baseline fluctuations in the NIR spectra cause a large within-class variability compared to the between-class

Table 3
Classification results for the NIR data set

	Original	Pre-processed
DA	8 (LDA, 1 wavelength)	2 (QDA, 3 wavelengths)
KNN	7 ($k=13$)	5 ($k=9$)

For DA, the discriminant type (quadratic or linear) and the number of wavelengths are indicated, whereas for KNN, the number k of nearest neighbours is given.

variability, which should be removed to improve the separation between the classes. The best result was obtained with QDA, as in the MIR data set, by employing three wavelengths. Again, only 2 out of 29 test objects were incorrectly classified (two class 3 objects included in class 2).

4.2. Quantitative analysis

The prediction results for kinematic viscosity at 40 °C employing NIR spectra and PLS, PCR, or MLR models were not satisfactory. Nonlinear calibration attempts using neural networks [33–35] were also unsuccessful. It could be argued that the radiation scattering and absorption by particulate matter, or possibly the sample dilution in toluene, may have masked the spectral features related to viscosity.

The prediction results obtained with MIR spectra and PCR/PLS models are shown in Table 4. On the overall, the PLS model predictions were more accurate when compared to PCR. Therefore, the discussion will be henceforth restricted to the PLS results.

A Pareto diagram for the effects calculated from Table 4 (PLS calibration) is presented in Fig. 3a. It is worth noting that the effects of interaction between factors are considerable. In order to obtain a better interpretation of the effects, a cube representation for the factorial design is presented in Fig. 3b.

An inspection of Fig. 3b reveals that a change from the low to the high level of the factors leads to an RMSEP increase in most cases. An exception that should be pointed out is the use of derivative and variable selection, in which case an RMSEP reduction of 4.4 cSt is observed when smoothing is not performed. The best result (smallest RMSEP) is obtained by using low levels for the three factors (4.2 cSt). Such a finding is in line with the conclusions of the classification study, in which the best results for the MIR data were also obtained without pre-processing.

Table 4
Factorial design matrix and PLS/PCR results for the MIR prediction of 40 °C kinematic viscosity

Factors				Levels	
				−	+
Derivative				No	Yes
Smoothing				No	Yes
Variable selection by GA				No	Yes
Trial	Factors			RMSEP (cSt)	
	1	2	3	PLS	PCR
1	−	−	−	4.2 (5)	4.7 (6)
2	+	−	−	5.6 (5)	6.7 (8)
3	−	+	−	4.3 (5)	4.8 (6)
4	+	+	−	4.8 (6)	6.4 (9)
5	−	−	+	4.9 (7)	4.4 (8)
6	+	−	+	8.9 (4)	10.3 (5)
7	−	+	+	5.6 (7)	5.7 (10)
8	+	+	+	4.5 (6)	4.6 (9)

The number of latent variables employed in each model is shown in parenthesis.

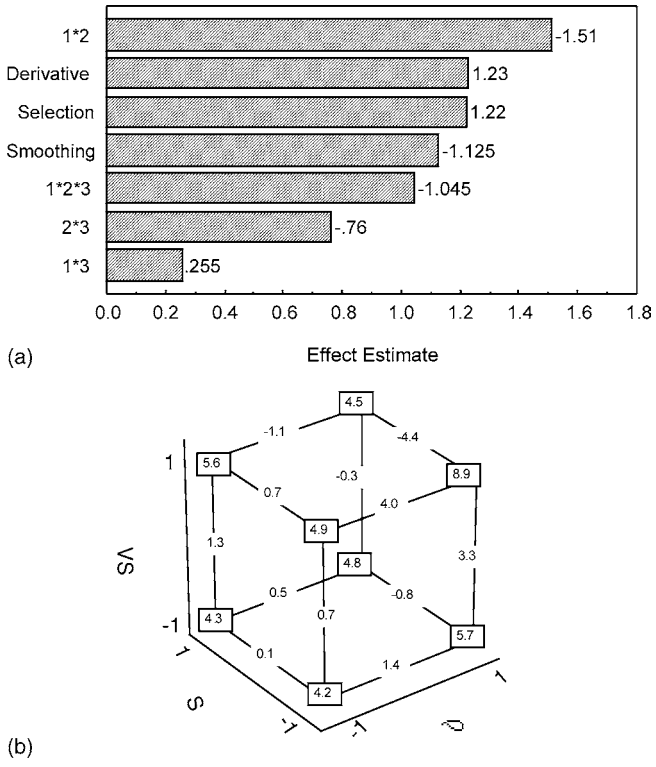

Fig. 3. (a) Pareto effect diagram for PLS results in the 2^3 factorial design: RMSEP values for the MIR prediction of 40 °C kinematic viscosity. (b) Cube representation for the 2^3 factorial design involving derivative (D), smoothing (S), and variable selection (VS) on the PLS results. The effects are expressed in terms of RMSEP values for the MIR prediction of 40 °C kinematic viscosity.

For the best settings of the PLS calibration, the graph of predicted versus observed values for the prediction samples is presented in Fig. 4.

Table 5 presents the factorial design performed for MLR calibration. The only difference from the design in Table 4 consists of the levels for the third factor. In this case, the selection of variables was carried out either by SPA (low level) or by GA (high level). It is worth noting that MLR cannot be directly applied to the full spectrum without variable selection because of ill-conditioning problems.

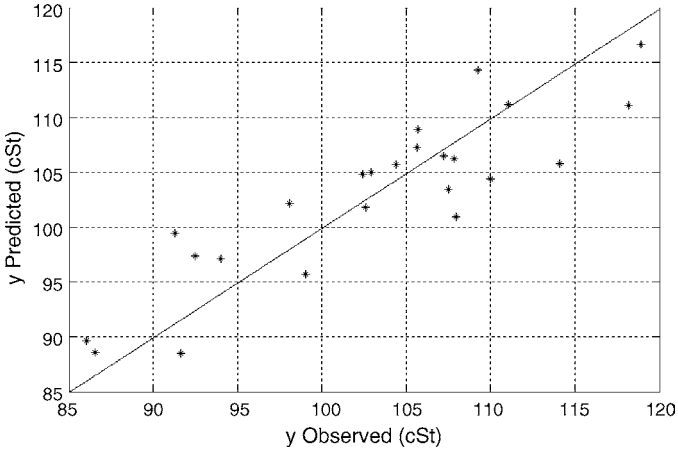

Fig. 4. PLS-MIR (without pre-processing) predictions of 40 °C kinematic viscosity versus reference values. A straight line was drawn to indicate the bisectrice of the quadrant.

Table 5
Factorial design matrix and MLR results for the MIR prediction of 40 °C kinematic viscosity

Factors	Levels	
	–	+
Derivative	No	Yes
Smoothing	No	Yes
Variable selection	SPA	GA

Trial	Factors			RMSEP (cSt)
	1	2	3	
1	–	–	–	5.1 (24)
2	+	–	–	7.6 (7)
3	–	+	–	3.8 (28)
4	+	+	–	5.9 (18)
5	–	–	+	4.9 (25)
6	+	–	+	5.4 (25)
7	–	+	+	5.0 (25)
8	+	+	+	6.1 (24)

The number of wavelengths employed in each model is shown in parenthesis.

A Pareto diagram and a cube representation for the effects calculated from Table 5 (MLR calibration) are presented in Fig. 5a and b, respectively. As in the PLS case, the effects of interaction between factors are substantial.

On average, the use of derivative increases the RMSEP by 1.6 cSt. Such an effect is more prominent when variable selection is performed by SPA (2.3 cSt average increase in RMSEP). It might be argued that the SPA result is more compromised by the use of derivative than the GA result because the SPA policy of selecting variables which are weakly correlated may favour the selection of noisy variables, a problem that is aggravated by the derivative calculation. In fact, the effect of changing the variable selection algorithm from SPA to GA decreases the RMSEP by 2.2 cSt, when the derivative is used without smoothing, which is the situation in which noise is maximally amplified by the pre-processing procedures. In the opposite situation (smoothing employed without the derivative), in which noise is maximally attenuated, the variable selection effect is also the opposite, that is, a 1.1 cSt increase in the RMSEP is observed when SPA is replaced with GA.

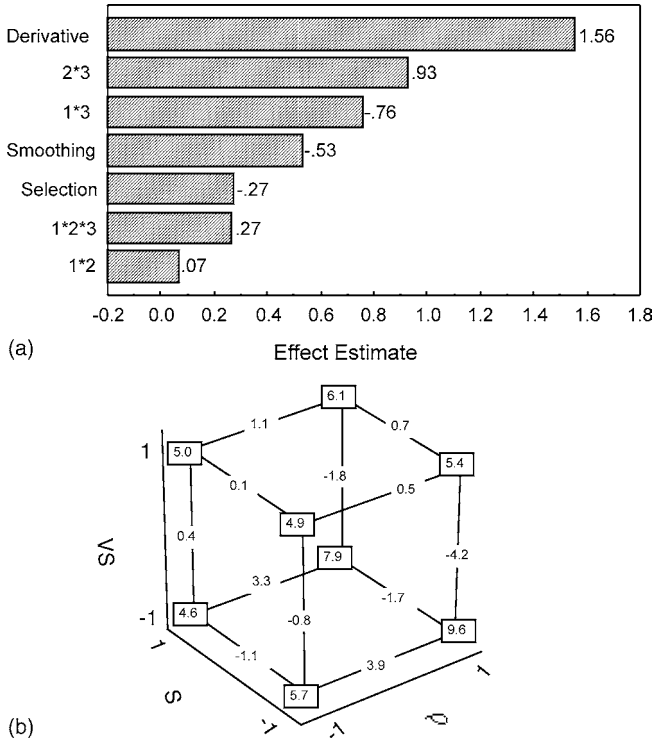

Fig. 5. (a) Pareto effect diagram for MLR results in the 2^3 factorial design: RMSEP values for the MIR prediction of 40 °C kinematic viscosity. (b) Cube representation for the 2^3 factorial design involving derivative (D), smoothing (S), and variable selection (VS) on the MLR results. The effects are expressed in terms of RMSEP values for the MIR prediction of 40 °C kinematic viscosity.

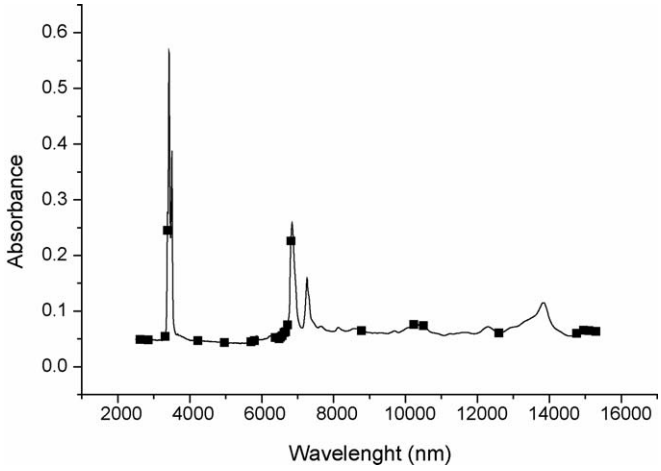

Fig. 6. Wavelengths selected by SPA for the MIR prediction of 40 °C kinematic viscosity.

Fig. 6 indicates the wavelengths that led to the best MLR result (RMSEP of 3.8 cSt), which was obtained without derivative, with smoothing, and with SPA variable selection. Such an outcome is slightly better than the best PLS result (RMSEP of 4.2 cSt), but the difference is not significant according to an *F*-test at 95% confidence level. Neural network models were also employed in an attempt to achieve better predictions. However,

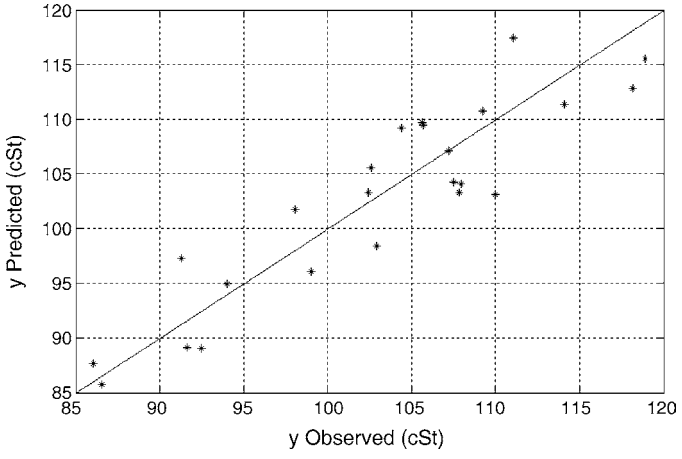

Fig. 7. APS-MLR (with smoothing) predictions of 40 °C kinematic viscosity vs. reference values. A straight line was drawn to indicate the bisectrice of the quadrant.

the results were similar to those yielded by the linear methods under study. For the best settings of the MLR calibration, the graph of predicted versus observed values for the prediction samples is presented in Fig. 7.

As the ASTM D445 norm does not present the reprodutibility for the determination of 40 °C kinematic viscosity for oils in service, the reference method repeatability was estimated in our laboratory. A relative standard deviation of 3.3% was obtained, which is comparable to the relative average errors obtained with the best PLS (3.5%) and MLR (3.2%) models.

5. Conclusions

This work presented two proposals for monitoring the service condition of diesel-engine lubricating oils by using infrared spectroscopy. In the first approach, the oil spectra were classified into three groups according to the stage of use. For this purpose, a variable selection algorithm was proposed to allow the use of simple discriminant analysis models. In this case, a classification accuracy of 93% was obtained both in the MIR and NIR ranges.

The second approach employed multivariate calibration methods to predict viscosity, which is the main control parameter for lubricants in service. In this case, the use of the NIR range was not successful regardless of the modelling method. Such a problem may be ascribed to the experimental methodology employed for spectra acquisition, which required the dilution of the samples because of the presence of particulated matter. This difficulty was circumvented by use of attenuated total reflectance (ATR) measurements in the MIR spectral range, in which an RMSEP of 3.8 cSt and a relative average error of 3.2% were attained. Those values can be considered satisfactory for monitoring the condition of lubricants in service.

The proposed methodologies may lead to substantial gains for companies that operate a large number of diesel engines, by allowing a more efficient condition-based replacement of the lubricating oil.

Acknowledgments

This work was supported by CAPES/PROCAD, FINEP/CTPETRO and CNPq (PRONEX grant and research fellowships). The authors also acknowledge the collaboration of Borborema Imperial Transportes Ltda, which provided the lubricant samples for this study.

Appendix A. Discriminability

In classification problems, the variables can be ranked on the basis of their ability to discriminate the classes under consideration. According to Duda et al. [14], the discriminability D_i of variable x_i can be quantified as:

$$D_i = \frac{S_{Bi}}{S_{Wi}} \tag{A.1}$$

where S_{Wi} and S_{Bi} are measures of the within-class and between-class dispersions for variable x_i, respectively. The within-class dispersion S_{Wi} is defined as

$$S_{Wi} = \sum_{j=1}^{C} s_{ij} \tag{A.2}$$

where s_{ij} is the dispersion of x_i in class j, calculated as

$$s_{ij} = \sum_{k \in I_j} [x_i^k - m_{ij}]^2 \tag{A.3}$$

where x_i^k denotes the value of x_i in the kth object and m_{ij} is the mean value of x_i in class j, that is:

$$m_{ij} = \frac{1}{n_j} \sum_{k \in I_j} x_i^k \tag{A.4}$$

The between-class dispersion S_{Bi} is defined as

$$S_{Bi} = \sum_{j=1}^{C} n_j [m_{ij} - m_i]^2 \tag{A.5}$$

where m_i is the average of x_i over all training objects.

References

[1] Standard Test Method for Flash and Fire Points by Cleveland Open Cup, D 92, ASTM (American Society of Testing Materials), 2001.
[2] Standard Test Method for Kinematic Viscosity of Transparent and Opaque Liquids (the Calculation of Dynamic Viscosity), D 445, ASTM (American Society of Testing Materials), 1994.
[3] C. Pasquini, J. Brazil. Chem. Soc. 14 (2003) 198.
[4] S. Macho, M.S. Larrechi, Trends Anal. Chem. 21 (2002) 799.
[5] M. Blanco, J. Pagès, Anal. Chim. Acta 463 (2002) 295.
[6] F.S.G. Lima, M.A.S. Araújo, L.E.P. Borges, Tribol. Int. 36 (2003) 691.
[7] M.I.S. Sastry, A. Chopra, A.S. Sarpal, S.K. Jain, S.P. Srivastava, A.K. Bhatnagar, Energy Fuels 12 (1998) 304.
[8] F.R. Van De Voort, J. Sedman, V. Yaylayan, Appl. Spectrosc. 58 (2003) 193.
[9] J. Dong, F.R. Van De Voort, V. Yaylayan, A.A. Ismail, D. Pinchuk, A. Brazeau, Lubr. Eng. 45 (2000) 30.
[10] A.D. Stuart, S.M. Trotman, K.J. Doolan, P.M. Fredericks, Appl. Spectrosc. 43 (1989) 55.
[11] A. Borin, R.J. Poppi, Vibr. Spectrosc. 37 (2005) 27.
[12] J. Paschoal, F.D. Barboza, R.J. Poppi, J. Near Infrared Spectrosc. 11 (2003) 211.
[13] A. Borin, Aplicação de quimiometria e espectroscopia no infravermelho no controle de qualidade de lubrificantes, Universidade Estadual de Campinas, Campinas, SP, 2003.
[14] R.O. Duda, P.E. Hart, D.G. Stork, Pattern Classification, 2nd ed., John Wiley, New York, 2001.
[15] W. Wu, Y. Mallet, B. Walczak, W. Penninckx, D.L. Massart, S. Heuerding, F. Erni, Chem. Intell. Lab. Syst. 329 (1996) 257.
[16] M. Kudo, J. Sklansky, Pattern Recogn. 33 (2000) 25.
[17] T. Naes, B.H. Mevik, J. Chem. 15 (2001) 413.
[18] N. Benoudjit, D. François, M. Meurens, M. Verleysen, Chem. Intell. Lab. Syst. 74 (2004) 243.
[19] U. Horchner, J.H. Kalivas, Anal. Chim. Acta 311 (1995) 1.
[20] J.H. Kalivas, N. Roberts, J.M. Sutter, Anal. Chem. 61 (1989) 2024.
[21] C.B. Lucasius, M.L.M. Beckers, G. Kateman, Anal. Chim. Acta 286 (1994) 135.
[22] R. Leardi, J. Chem. 15 (2000) 559.
[23] D.L. Massart, D. Jouan-Rimbaud, R. Leardi, O.E. De Noord, Anal. Chem. 67 (1995) 4295.
[24] V. Centner, D.L. Massart, O.E. deNoord, S. Jong, B.M. Vandeginste, C. Sterna, Anal. Chem. 68 (1996) 3851.

[25] H.C. Goicoechea, A.C. Olivieri, Analyst 124 (1989) 725.
[26] G.A. Bakken, T.P. Houghton, J.H. Kalivas, Chem. Intell. Lab. Syst. 45 (1999) 225.
[27] M. Forina, C. Casolino, C.P. Millan, J. Chem. 13 (1999) 165.
[28] B.K. Alsberg, D.B. Kell, R. Goodacre, Anal. Chem. 70 (1998) 4126.
[29] M.C.U. Araujo, T.C.B. Saldanha, R.K.H. Galvão, T. Yoneyama, H.C. Chame, V. Visani, Chem. Intell. Lab. Syst. 57 (2001) 65.
[30] R.K.H. Galvão, M.F. Pimentel, M.C. Araújo, U. Yoneyama, T.V. Visani, Anal. Chim. Acta 443 (2001) 107.
[31] M.C. Breitkreitz, I.M. Raimundo Jr., J.J.R. Rohwedder, C. Pasquini, H.A. Dantas Filho, G.E. José, M.C.U. Araújo, Analyst 128 (2003) 1204.
[32] J. McClelland, R.W. Jones, Lubr. Eng. 57 (2001) 17.
[33] Z. Ramadan, P.K. Hopke, M.J. Johnson, K.M. Scow, Chem. Intell. Lab. Syst. 75 (2005) 23.
[34] F. Estienne, F. Despagne, B. Walczak, O.E. de Noord, D.L. Massart, Chem. Intell. Lab. Syst. 73 (2004) 207.
[35] C. Ruckebusch, L. Duponchel, J.P. Huvenne, Chem. Intell. Lab. Syst. 62 (2002) 189–198.

Available online at www.sciencedirect.com
ScienceDirect
Talanta 70 (2006) 353–357
Talanta
www.elsevier.com/locate/talanta

Determination of clenbuterol by capillary electrophoresis immunoassay with chemiluminescence detection

Xinghu Ji [a], Zhike He [a,*], Xinping Ai [a], Hanxi Yang [a], Chuanlai Xu [b]

[a] *College of Chemistry and Molecular Sciences, Wuhan University, Wuhan 430072, PR China*
[b] *School of Food Science and Technology, Southern Yangtze University, Wuxi 214036, PR China*

Received 17 November 2005; received in revised form 16 February 2006; accepted 18 February 2006
Available online 11 April 2006

Abstract

A competitive immunoassay for clenbuterol (CLB) based on capillary electrophoresis with chemiluminescence (CL) detection was established. The method was based on the competitive reaction of horseradish peroxidase (HRP)-labeled CLB (CLB-HRP) and free CLB with anti-CLB antiserum. The factors affecting the electrophoresis and CL detection were systematically investigated with HRP as a model sample. Under the optimal conditions, the tracer CLB-HRP and the immunoassay complex were separated, and the linear range and the detection limit ($S/N = 3$) for CLB were 5.0–40 nmol l^{-1} and 1.2 nmol l^{-1}, respectively. The proposed method has been applied satisfactorily in the analysis of urine sample.

Keywords: Capillary electrophoresis; Chemiluminescence; Immunoassay; Clenbuterol

1. Introduction

Clenbuterol (4-amino-α-[(*tert*-butylamino)methyl]-3,5-dichlorobenzyl alcohol hydrochloride, CLB), a sympathomimetic drug with potent β-adrenoceptor stimulating properties, can effectively prevent and reverse bronchoconstriction and has been used for the treatment of the pulmonary diseases in veterinary and clinic medicine [1,2]. In recent years, it has been established that a number of β-agonists, including clenbuterol, may have repartitioning effects in meat-producing animals [3]. The flow of nutrients is apparently shifted from adipose tissue towards muscle tissue. The result is an improved lean meat deposition and higher production efficiency. However, the produced meat might contain residues of agonists, which is a real public health problem, and various intoxications have been described as being due to the consumption of meat products containing clenbuterol residue [4]. For reasons of public health and safety, CLB has been prohibited from being used in cattle feed in many countries [5]. Besides, clenbuterol is also abused as a doping agent in human athletes to improve their performance, as a result, it has been one of the prohibited substances by the International Olympic Committees [6,7]. It is implied that development of highly specific, reliable and reduced-cost methodologies for rapid determination of clenbuterol in diverse matrices is urgently needed. Various analytical methods have been reported to detect clenbuterol in animal tissues or urine [5,8]. The method currently used by most laboratories is gas chromatography–mass spectrometry (GC–MS). However, the derivatization step before injection is complicated and time-consuming [9]. High performance liquid chromatography (HPLC) offers advantages over GC to detect β-agonists. Ultraviolet (UV) detection is the most popular detection method applied in HPLC, but it is limited for the low sensitivity [10]. HPLC-MS is a powerful analytical method for the detection of clenbuterol, however, the complicated and expensive instrument does not belong to the facilities of average investigator [11]. Although enzymelinked immunosorbent assay (ELISA) technique is highly selective and sensitive, a primary drawback is the time-consuming and laborious incubation, washing and rinsing procedures [12]. As a result, these methods were limited to a certain extent in practice.

Capillary electrophoresis immunoassay (CEIA) combining the effective separation power of CE and the ligand specificity of IA has been proved to be a powerful technique for the separation and analysis of biological compounds [13]. Compared to conventional IA, CEIA is characterized by high efficiency, less samples, short analysis time, and easy automation. It has been successfully applied to determine certain tumor markers,

* Corresponding author. Tel.: +86 27 87162672; fax: +86 27 68754067.
E-mail address: zhkhe@whu.edu.cn (Z. He).

0039-9140/$ – see front matter © 2006 Elsevier B.V. All rights reserved.
doi:10.1016/j.talanta.2006.02.053

hormones and abuse drugs including human growth hormone (hGH), insulin, morphine, cortisol, digoxine and so on [14–16]. Chemiluminescence (CL) is being focused on its high sensitivity, easy operation, and inexpensive apparatus and reagents [17]. It has been widely applied in flow injection, LC, IA, and CE [18–22]. Especially, over the past decade, research in combining CE with CL detection has increased significantly [23,24]. Although CL detection method is very promising in CE–CL, little attention has been paid to its application in CEIA. Tsukagoshi et al. [25] demonstrated a CEIA experiment using mouse IgG and horseradish peroxidase (HRP)-labeled anti-mouse IgG antibody in a newly designed batch-type CL detection cell for CE. Wang et al. [26] successfully detected bone morphogenic protein-2 (BMP-2) in rat vascular smooth muscle (VSM) cells with noncompetitive format by CEIA based on enhanced CL detection. HRP-Ab_2-mAb-BMP-2 complex and free HRP were baseline separated and detected with the detection limits of 4.4×10^{-12} mol l^{-1} (53 zmol) for HRP and 6.2×10^{-12} mol l^{-1} (75 zmol) for BMP-2. CEIA based on CL was also successfully applied for the determination of the tumor Ag CA125 in human sera from health controls and patients associated with ovarian cancer [27]. All of these previous works reveal that the CEIA-CL method is a potential and promising analytical tool in biomedical analysis and clinical diagnosis.

In this research, a method for the determination of CLB was developed by CEIA with CL detection based on the competitive reaction between HRP labeled CLB and free CLB with a limited amount of anti-CLB antiserum. The results indicated that this method could be applied to the determination of free CLB in urine samples.

2. Experimental

2.1. Reagents

Luminol was obtained from the Chemistry Department of Shaanxi Normal University (Shaanxi, China), HRP and 30% hydrogen peroxide were purchased from Shanghai Chemicals (Shanghai, China), 4-iodophenol (PIP) was from ACROS Organics (New Jersey, USA), and clenbuterol hydrochloride (CLB) was from Sigma (St. Louis, MO, USA). Anti-CLB antiserum was provided by School of Food Science and Technology of Southern Yangtze University (Wuxi, China). All chemicals were of analytical grade or better, and ultrapure water (18.2 MΩ), purified on Water PRO PS system (Labconco, Kansas City, MO, USA), was used for the preparation of all the aqueous solutions. The electrophoresis buffer was 10 mmol l^{-1} NaH_2PO_4–Na_2HPO_4 buffer (pH 6.5), and the CL reaction buffer was 10 mmol l^{-1} NaH_2PO_4–Na_2HPO_4 buffer (pH 8.5) containing 0.5 mmol l^{-1} luminol, 40 mmol l^{-1} H_2O_2 and 1.2 mmol l^{-1} PIP. All solutions were filtered through 0.22 μm membrane filters before use.

2.2. Apparatus

The CE–CL apparatus was self-assembled in the laboratory and held in a light-tight box. A 50 cm capillary (Yongnian Reafine Chromatography Ltd., Hebei, China) with 50 μm i.d. and 375 μm o.d. used as the separation capillary was inserted into a 10 cm capillary with 530 μm i.d. and 690 μm o.d. used as the reaction capillary, on which a 1 cm detection window was made by burning off the coating. Both of the capillaries were installed in a tee, and the outlet of separation capillary was just positioned at the detection window, in front of which a photomultiplier tube (PMT) (R212, Hamamatsu) was situated. The CL reaction solution was also delivered into the tee by gravity with a PTFE tube (0.8 mm i.d.) and flowed in a sheath profile around the electrophoresis capillary, then reacted with analytes out from electrophoresis capillary at the detection window. The output from PMT was amplified and collected with N3000 chromatograph data system (Zhejiang University Star Information Technology Ltd, Zhejiang, China).

2.3. CE procedure

New separation capillary was treated successively with 1.0 mol l^{-1} NaOH, water, 1.0 mol l^{-1} HCl and water, and finally balanced with electrophoresis buffer overnight. Between runs, the capillary was flushed with electrophoresis buffer for 5 min. The sample was introduced by electrokinetic injection with 20 kV for 8 s, and electrophoresis separation was performed at 20 kV.

2.4. Preparation of HRP-labeled CLB

CLB was labeled with HRP following the procedure described by Degand et al. [28] with some modifications. Briefly, the CLB solution adjusted to pH 1.5 with 1.0 mol l^{-1} HCl reacted with $NaNO_2$ at 4 °C in the dark to form the diazo derivative of CLB. Then the whole solution was added dropwise to a limited HRP solution in 10 mmol l^{-1} phosphate buffer (pH 7.5) at 4 °C, and the pH of the mixture was continuously adjusted to 7.5 with 0.1 mol l^{-1} NaOH. After standing for 2 h at 4 °C, the mixture was adequately dialyzed against 0.01 mol l^{-1} phosphate buffer until the absorbance of CLB in the dialyzing phosphate buffer disappeared under the monitoring of a TU-1900 spectrophotometer (Purkinje General Instrument, Beijing, China). The conjugate was protected from light and stored at 4 °C until use.

2.5. IA protocol

The IA protocol was a competitive format. 20 μl of 1.0×10^{-7} mol l^{-1} CLB-HRP and 20 μl of 4.0 to 50 nmol l^{-1} CLB or urine samples were mixed with 10 μl anti-CLB antiserum in 200 μl small vials and then diluted with water (18.2 MΩ) to 100 μl. After incubating at 37 °C for 45 min, the mixture was analyzed by CE as described above.

3. Results and discussion

3.1. Effect of the pH and concentration of the running buffer

The pH of the running buffer affects the efficiency and the reproducibility of the capillary electrophoresis separation of

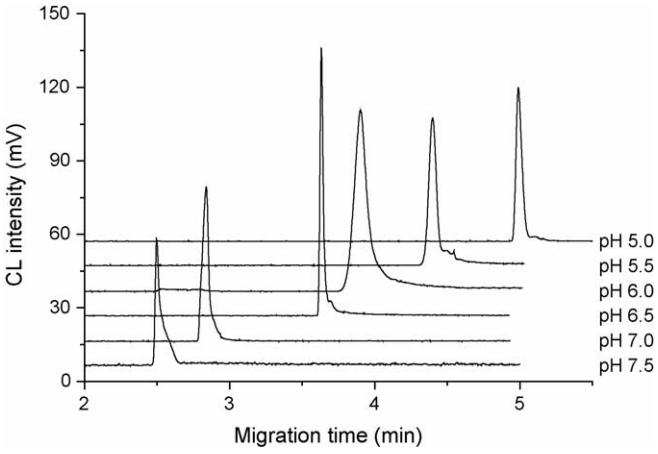

Fig. 1. pH effect of the running buffer on electrophoresis separation. A fused silica capillary (50 cm length, 50 μm i.d.) was used for CEIA. A 1.0×10^{-8} mol l^{-1} HRP used as model sample was electrokinetically injected with 20 kV voltage for 8 s, and the separation voltage was 20 kV. All curves were plotted with the same CL intensity scale, with a horizontal offset of the baseline for clarity.

proteins. Results from Fig. 1 showed that the increase in pH shortened the migration time of HRP because of the increase in the electroosmotic flow. At pH 6.5, the electropherogram peak of HRP is sharp and symmetrical, and the relative CL intensity calculated by peak height is the highest. The results may be related to that the isoelectric point of HRP is 6.5 [26]. In addition, the pH of the running buffer also affects the conformation of antigen and antibody. Therefore, the pH of the running buffer in the subsequent experiments was chosen to 6.5.

The effect of the running buffer with different ionic strengths ranging from 5.0 to 50 mmol l^{-1} was studied. It was found that increasing the ionic strengths of the buffer increased the migration time and the electrophoresis current. The best separation results were achieved in 10 mmol l^{-1} phosphate buffer.

3.2. Optimization of CL detection

The pH of the CL reaction buffer has an important effect on the CL intensity as shown in Fig. 2A. It was found that the CL intensity increased firstly and then decreased with the pH increasing. The maximal intensity presented at pH 8.5, which was similar to the situation in the conventional IA with CL detection [29]. So the following CL detections were at pH 8.5.

The influence of luminol concentration on the CL intensity was investigated. The results demonstrated that the CL intensity increased with increasing luminol concentration from 0.1 to 1.2 mmol l^{-1} (Fig. 2B). However, the background level increased and the signal-to-noise ratio reduced at higher concentration of luminol, and the concentration giving the best sensitivity was found to be 0.5 mmol l^{-1}.

The optimization of H_2O_2 concentration was given in Fig. 2C. The CL intensity rapidly increased in the range of 10–40 mmol l^{-1} and only slight changes in CL intensity were observed when the concentration of H_2O_2 was higher than 40 mmol l^{-1}. The optimal concentration of H_2O_2 was 40 mmol l^{-1}.

The enhancement degree of phenol derivatives as enhancers of the chemiluminescent reaction HRP-luminol-H_2O_2 is

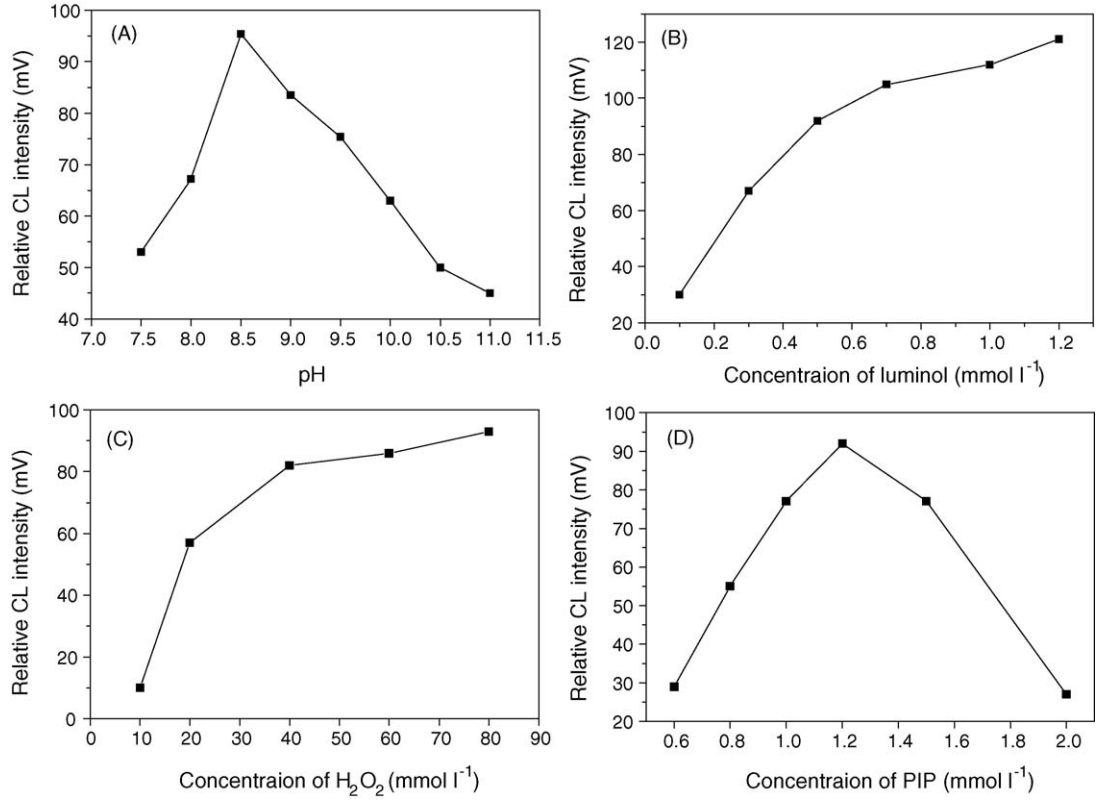

Fig. 2. Effects of pH (A), concentration of luminol (B), H_2O_2 (C), and PIP (D) on the CL detection. Other conditions as in Fig. 1.

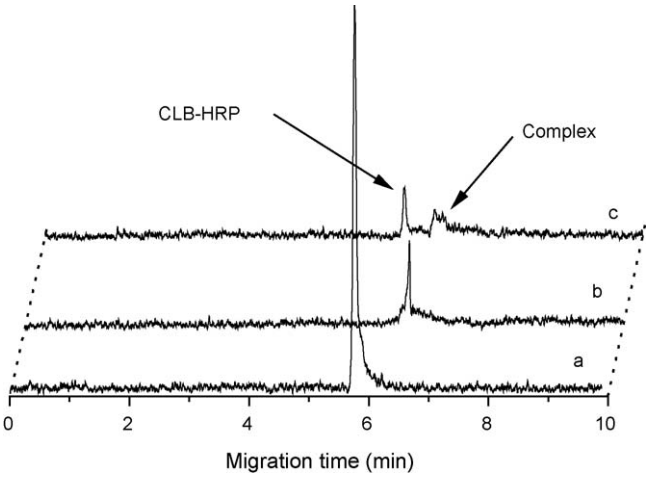

Fig. 3. Electropherograms of the competitive immunoassay for CLB: (a) 1.0×10^{-7} mol l^{-1} CLB-HRP without antiserum, (b) mixture of 1.0×10^{-7} mol l^{-1} CLB-HRP with antiserum, (c) 5.0×10^{-9} mol l^{-1} CLB competes with 1.0×10^{-7} mol l^{-1} CLB-HRP for antiserum. Running buffer, phosphate buffer (10 mmol l^{-1}, pH 6.5); CL solution, 0.5 mmol l^{-1} luminol, 40 mmol l^{-1} H_2O_2, and 1.2 mmol l^{-1} PIP in phosphate buffer (pH 8.5). Other conditions as in Fig. 1.

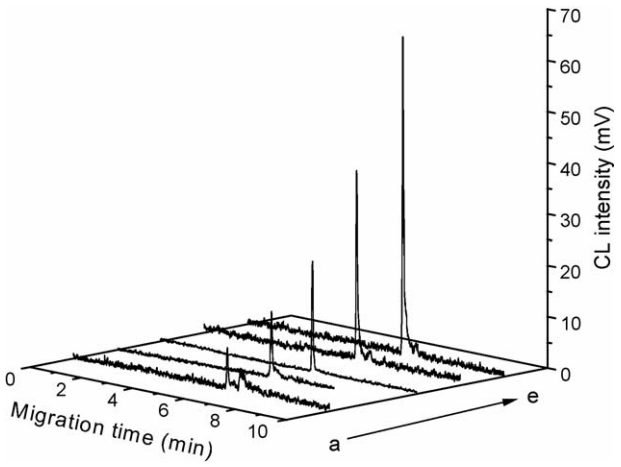

Fig. 4. Comparison of electropherograms of competitive CEIA from different concentrations of CLB. The concentrations from a to e were 5.0, 8.0, 15, 25, and 40 nmol l^{-1}, respectively. Conditions as in Fig. 3.

dependent on the enhancer concentration. PIP as presented enhancer, its influence on the CL intensity was investigated from 0.6 to 2.0 mmol l^{-1} (Fig. 2D). The result was that the CL intensity increased until the optimal concentration 1.2 mmol l^{-1} was reached, and decreased above this concentration.

3.3. Competitive CEIA for CLB

According to the IA procedure mentioned above, the competitive CEIA for CLB was performed under the optimal separation and CL detection conditions. Fig. 3 shows the typical electropherograms of the competitive immunoassays for CLB. The bottom electropherogram (Fig. 3a) was obtained by injection of tracer CLB-HRP. The central electropherogram (Fig. 3b) was obtained from mixing of a blank CLB sample (0 mol l^{-1}) and tracer CLB-HRP with CLB antiserum. The tracer was completely bound to antiserum to form complex, which was detected as a new peak later to that of tracer. When replacing the blank sample with diluted CLB solution, CLB in the sample competes with tracer CLB-HRP for a limited amount of antiserum, which leads to an increase in signal for free tracer and a decrease in the complex, as shown in the top electropherogram (Fig. 3c). The bound complex was resolved from the free tracer, which made the presented CEIA protocol into practice. Due to the difficulty in detecting the slight complex peaks in higher concentration CLB samples, the signals of the free CLB-HRP tracer were quantified (see below).

3.4. Calibration curve and detection limit

Fig. 4 is the CEIA electropherograms with different concentrations of CLB in the samples. As the concentration of CLB increased, the peak height of the immunocomplex in the electropherogram decreased and disappeared in higher concentration CLB sample while that of the tracer CLB-HRP increased proportionally. The linear calibration curve was obtained by plotting the peak height of tracer CLB-HRP against the concentration of CLB in the range of 5.0–40 nmol l^{-1} with a correlation coefficient of 0.9987 and the limit of detection was 1.2 nmol l^{-1} ($S/N = 3$).

3.5. Analysis of samples

The present method was applied in experiments of simulated samples with doping CLB in urine from healthy volunteer (Fig. 5). The bottom electropherogram was obtained from a blank urine sample, and the top one was from a urine sample doping 20 nmol l^{-1} CLB. The recoveries of the method were from 90 to 108%, and the RSD was less than 8% ($n = 5$).

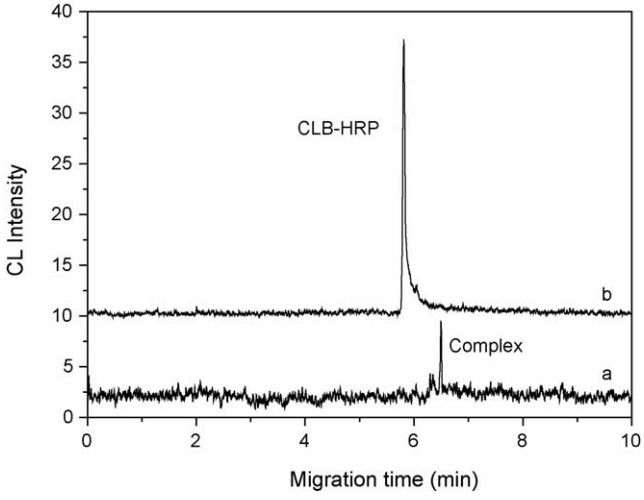

Fig. 5. Electropherograms of urine samples: (a) blank urine sample, (b) urine sample doping 20 nmol l^{-1} CLB. Conditions as in Fig. 3.

4. Conclusion

CEIA with CL detection based on a competitive format was performed, which was successfully used for the determination of β-agonist clenbuterol. Under the optimal conditions, the linear range and the detection limit ($S/N = 3$) for CLB were 5.0–40 and 1.2 nmol l^{-1}, respectively. The presented protocol paves another way for the pharmacokinetics, the analysis of drug residues and the monitor of prohibited substances.

Acknowledgements

The authors acknowledge the supports from National Natural Science Foundation of China (20299030-4, 20275028, 20575046), the National Key Basic Research and Development Program (973 Program 2002CB211800), Hi-tech Research and Development Program of China (863 Program 2002AA2Z2004) and Specilized Research Fund for the Doctoral Program of Higher Education (20050486026).

References

[1] K. Torneke, Vet. Res. Commun. 23 (1999) 41.
[2] I. Ziment, Chest 107 (1995) 198.
[3] D.J. Smith, J. Anim. Sci. 76 (1998) 173.
[4] A. Prezelj, A. Obreza, S. Pecar, Curr. Med. Chem. 10 (2003) 281.
[5] G.A. Mitchell, G. Dunnavan, J. Anim. Sci. 76 (1998) 208.
[6] P.N.R. Dekhuijzen, H.A. Machiels, L.M.A. Heunks, H.F.M. van der Heijden, R.H.H. van Balkom, Thorax 54 (1999) 1041.
[7] The World Anti-Doping Code, the 2005 prohibited list international standard, World Anti-Doping Agency, 2004. 9.
[8] A. Polettini, J. Chromatogr. B 687 (1996) 27.
[9] F. Ramos, A. Cristino, P. Carrola, T. Eloy, J.M. Silva, M.C. Castilho, M.I.N. da Silveira, Anal. Chim. Acta 483 (2003) 207.
[10] Y.R. Song, D.F. Wang, Y.P. Hu, X.X. Chen, Y.G. Jiao, D.Y. Hou, J. Pharm. Biomed. 31 (2003) 311.
[11] N. Van Hoof, D. Courtheyn, J.P. Antignac, M. Van de Wiele, S. Poelmans, H. Noppe, H. De Brabander, Rapid Commun. Mass Spectrom. 19 (2005) 2801.
[12] A. Roda, A.C. Manetta, F. Piazza, P. Simoni, R. Lelli, Talanta 52 (2000) 311.
[13] N.M. Schultz, R.T. Kennedy, Anal. Chem. 65 (1993) 3161.
[14] D. Schmalzing, S. Buonocore, C. Piggee, Electrophoresis 21 (2000) 3919.
[15] W.S.B. Yeung, G.A. Luo, Q.G. Wang, J.P. Ou, J. Chromatogr. B 797 (2003) 217.
[16] S.M. Lin, S.M. Hsu, Anal. Biochem. 341 (2005) 1.
[17] A. Roda, M. Guardigli, E. Michelini, M. Mirasoli, P. Pasini, Anal. Chem. 75 (2003) 463A.
[18] W.R.G. Baeyens, S.G. Schulman, A.C. Calokerinos, Y. Zhao, A.M.G. Campana, K. Nakashima, D. De Keukeleire, J. Pharma. Biomed. 17 (1998) 941.
[19] I.P.A. Morais, I.V. Toth, A.O.S.S. Rangel, Talanta 66 (2005) 341.
[20] C. Dodeigne, L. Thunus, R. Lejeune, Talanta 51 (2000) 415.
[21] M. Yamaguchi, H. Yoshida, H. Nohta, J. Chromatogr. A 950 (2002) 1.
[22] X.J. Huang, Z.L. Fang, Anal. Chim. Acta 414 (2000) 1.
[23] C. Kuyper, R. Milofsky, Trends Anal. Chem. 20 (2001) 232.
[24] R.G. Su, J.M. Lin, K. Uchiyama, M. Yamada, Talanta 64 (2004) 1024.
[25] K. Tsukagoshi, T. Nakamura, R. Nakajima, Anal. Chem. 74 (2002) 4109.
[26] J.H. Wang, W.H. Huang, Y.M. Liu, J.K. Cheng, J. Yang, Anal. Chem. 76 (2004) 5393.
[27] J.N. Wang, J.C. Ren, Electrophoresis 26 (2005) 2402.
[28] G. Degand, A. Bernes-Duyckaerts, G. Maghuin-Rogister, J. Agric. Food Chem. 40 (1992) 70.
[29] G.H.G. Thorpe, L.J. Kricka, S.B. Moseley, T.P. Whltehead, Clin. Chem. 31 (1985) 1335.

Available online at www.sciencedirect.com
ScienceDirect
Talanta 70 (2006) 358–363
Talanta
www.elsevier.com/locate/talanta

Study on pressurizing electroosmosis pump for chromatographic separation

Lei Wang, You-Zhao He *, Guo-Ni Fu, Yan-Yun Hu, Xiao-Kui Wang

Department of Chemistry, University of Science and Technology of China, Hefei, Anhui 230026, PR China

Received 25 November 2005; received in revised form 17 February 2006; accepted 18 February 2006
Available online 29 March 2006

Abstract

A porous core electroosmosis pump was studied and improved in accordance with the electroosmosis theory. Hexamethylene tetraamine (HMTA) was used as the additive of pump carrier solution to improve the flow rate stability and delivery efficiency. The influences of the electric field strength, porous core dimension and acetonitrile concentration of carrier solution on the pump flow rate and output pressure were investigated in detail. The improved electroosmosis pump can provide not only steady flow rate and large flow range, but also moderate output pressure. With the pump carrier solution of 0.5 mmol/L HMTA and the working voltage of 4950 V, the pump output pressure, flow rate and delivery efficiency achieved 1.1 MPa, 1.3 mL/min and 3.2 mL/(min mA), respectively. The pump can be employed for mobile phase delivery in the reversed-phase chromatographic separation of monolithic silica columns.

Keywords: Electroosmosis pump; Pressurization; Hexamethylene tetraamine; Reversed-phase liquid chromatography

1. Introduction

Electroosmosis is the liquid flow, in contact with a solid surface, under the influence of an applied electric field [1]. In the past decades, different electroosmosis pumps (EOPs) have been proposed, which can be classified as capillary EOP [2,3], packed capillary EOP [4–7] and porous core EOP [8–16].

The capillary EOP was developed by Dasgupta and Liu [2], and applied to a microanalysis system of flow injection analysis (FIA) and on-line electrostacking preconcentration as used in capillary electrophoresis. The capillary EOP was also employed in a sequential injection analysis (SIA) system that exhibited satisfied reproducibility for chemical reactions [3]. Since the electroosmotic flow (EOF) was generated in a capillary with the inner diameter of tens of micrometer, the flow rate and output pressure of the capillary EOP looked low, while its working voltage was rather high.

Guan and co-workers fabricated a capillary EOP with three fused-silica capillaries arranged in parallel and packed with silica particles. The packed capillary EOP could provide the flow rate from nL/min to μL/min and the output pressure of 45 MPa [4–7]. So the EOP possessed high output pressure, but restricted flow rate.

Based on the electroosmotic theory and experiments, He et al. fabricated a porous core EOP. The EOP can provide steady flow rate and large flow range, but low output pressure [8,9]. With the working voltage of 500 V, the flow rate and output pressure of the pump achieved 3.0 mL/min and 0.15 MPa, respectively. The EOP was employed in FIA, SIA and multicommutation analysis system for the separation, preconcentration and determination of inorganic ions [10–14], phenols [15] and trace anion surfactants [16] in water samples.

In this paper, an improved porous core EOP with 9.0 mm diameter and 6.0 cm length was constructed [17]. Hexamethylene tetraamine (HMTA) was evaluated as the additive of pump carrier solution to obtain stable flow rate and high delivery efficiency. The influences of electric field strength, porous core dimension and acetonitrile concentration of carrier solution on the pump flow rate and output pressure were investigated in detail. The proposed EOP has been employed for mobile phase delivery in the reversed-phase chromatographic separation of monolithic silica columns.

2. Experimental

2.1. Chemicals and solutions

All the reagents were of analytical grade. HMTA, anhydrous sodium carbonate (Na_2CO_3), hydrochloric acid (HCl), sodium

* Corresponding author. Tel.: +86 551 3607072; fax: +86 551 3603388.
E-mail address: yzhe@ustc.edu.cn (Y.-Z. He).

0039-9140/$ – see front matter © 2006 Elsevier B.V. All rights reserved.
doi:10.1016/j.talanta.2006.02.058

hydroxide (NaOH), polyethylene glycol (PEG, MW 10,000), urea, acetic acid glacial (HAc), acetonitrile, methanol, ethanol, phenol, benzene and toluene were purchased from Chemical Reagent Co. (Shanghai, China). Tetramethyl orthosilicate (TMOS) was obtained from Guibao Chemical Ltd. (Hangzhou, China). Chlorodimethyloctylsilane was purchased from Alfa Aesa (USA). Tri-distilled water was prepared by a SZ-3 distilled water system (Huxi Anal. Instr. Factory, Shanghai, China).

The porous core regeneration solutions included 0.1 mol/L Na_2CO_3, 1.0 mol/L HCl and 0.1 mol/L NaOH. The 0.5 mmol/L HMTA carrier solution (pH 9.5) was obtained by diluting 0.1 mol/L HMTA solution with tri-distilled water. These experimental solutions were filtered with 0.22 μm PTFE membrane before use. The 0.01 mol/L phenol and 0.01 mol/L benzene stock solutions were prepared by dissolving phenol and benzene in acetonitrile. The mixed analyte solution for chromatographic separation was prepared by diluting the stock solutions with acetonitrile further.

2.2. Instruments

DYY-12C electrophoretic power supply (Liuyi Instr. Factory, Beijing, China) provided the pump voltage from 20 to 5000 V dc. SX2-2.5-10 electric resistance furnace (Experiment Electr. Furnace Factory, Shanghai, China) was employed to prepare the porous core of the pump. SHZ (III) water-jet aspirator pump (Yingyu Yuhua Instr. Factory, Henan, China) was used to wash and regenerate the porous core. The micrographs of the porous core were measured by JSM-6700F field emission scanning electron microscope (JEOL, Japan). UV9100 spectrophotometer (Rayleigh Anal. Instr. Corp., Beijing, China) was employed as an UV detector measuring at 254 nm. A three-way solenoid valve (HP161T301, NResearch Inc., USA) introduced the analyte solution into the separation system. The output pressure of the pump was measured by a homemade pressure meter.

2.3. Fabricating and washing porous glass core

A 6.0 cm length and 9.0 mm diameter porous core of the EOP was prepared by sintering boric glass powder under high temperature. The scanning electron microscope (SEM) image of the porous core showed that the macropore diameters were in the range of 1.0–4.0 μm. The porous core was installed in a 9.1 mm i.d. boron glass tube and fixed by epoxy glue. The core column was washed or regenerated with 0.1 mol/L $NaHCO_3$, water, 1.0 mol/L HCl, water and 0.1 mol/L NaOH in turn by the water-jet aspirator pump, and then equilibrated by the carrier solution for 24 h.

2.4. EOP testing system

An EOP testing system, as shown in Fig. 1(a), consisted of one DYY-12C electrophoresis power supply, one homemade selection valve, one liquid pressure meter and the tested porous core EOP. The EOP included two pump chambers, two electrode cavities with platinum electrodes and one porous core column. Two tubular PTFE membranes (0.22 μm) were placed into the hollow electrode cavities to isolate bubbles produced in water electrolysis and conduct electric current. The maximal output pressure of the EOP was measured by turning off the output flow.

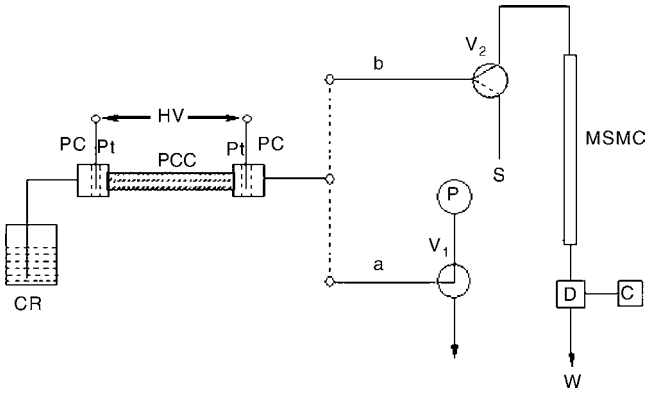

Fig. 1. Schematic diagram of EOP testing system (a) and chromatographic separation system (b). CR: carrier reservoir; PC: pump chamber; PCC: porous core column; HV: high-voltage power supply; Pt: platinum electrode; P: liquid pressure meter; V_1: selection valve; V_2: three-way solenoid valve; S: sample solution; MSMC: modified silica monolithic column; D: spectrophotometer; W: waste; C: computer.

2.5. Chromatographic separation performed by EOP

The chromatographic separation was performed by the EOP, as shown in Fig. 1(b). The separation system consisted of one electroosmosis pump, one solenoid valve, one silica monolithic column bonded with octylsilane, one spectrophotometer and a personal computer.

In the separation system, the porous core EOP was employed for mobile phase delivery. Its flow rate and flow direction could be controlled by the pump voltage and potential polarity, respectively. The injection volume of sample solution was regulated by the aspirating flow rate of the pump and the switch time of the valve. The silica monolithic column was prepared by sol–gel condensation with TMOS–HAc–PEG–urea in a 10 cm × 3 mm i.d. fused-silica tube, and chlorodimethyloctylsilane toluene solution was adopted to prepare C_8 stationary phase. The porosity and surface area of the silica monolithic column before modified with chlorodimethyloctylsilane were 60% and 540 m^2/g, respectively. The spectrophotometer was employed as an UV detector measuring at 254 nm and the absorbance data were transmitted to the computer.

3. Results and discussion

3.1. Influence factors for flow rate and output pressure of porous core EOP

The surface of the porous core is negatively charged because of the ionization of surface silanols. As a result, the solvated cations are accumulated in the diffusion layer of electric double

layer. When an external voltage is supplied, the cations, viz., counter ions, will migrate under both the actions of electric field and viscous friction, and drag the carrier solution through the porous core. Consequently, EOF can be generated in the micro-channels of the porous core, which can be treated as large numbers of tortuous micro-channels.

For each micro-channel of the porous core, the average EOF rate can be written as

$$q = \frac{\varepsilon\zeta E\pi a^2}{\eta} \tag{1}$$

where q is the average EOF rate in one micro-channel, ζ zeta potential, E the electric field strength, a the average radius of micro-channels and ε and η are the dielectric constant and viscosity coefficient of carrier solution, respectively.

The flow rate of the porous core EOP can be expressed as

$$Q = v_{\mathrm{eo}} \times A = \frac{\varepsilon\zeta EA}{\eta} = \frac{\varepsilon\zeta VA}{\eta L} \tag{2}$$

where Q is the flow rate of the EOP, A the effective cross-section area of porous core, V the working voltage and L is the physical length of porous core.

The equation indicates that the flow rate of EOP is related to the working voltage, zeta potential, the effective cross-section area and physical length of the porous core, the dielectric constant and viscosity coefficient of the carrier solution. For the same core material and carrier solution, large effective cross-section area and high electric field strength will enhance the pump flow rate.

Combining Eq. (1) with Poiseuille equation, the pressure difference between two ends of the porous core can be derived as

$$P_1 - P_2 = \frac{8\varepsilon\zeta El}{a^2} \tag{3}$$

where l is the characteristic length of the traveling flow in the micro-channel and P_1 and P_2 are the fore and back pressure of the porous core, respectively.

When the pump input is open and P_1 can be supposed to be zero, the maximal output pressure of the EOP can be expressed as

$$P_{\max} = \frac{8\varepsilon\zeta El}{a^2} \tag{4}$$

It implies that the maximal output pressure of the EOP depends on the electric field strength, the characteristic length of the porous core, zeta potential, the average radius of micro-channels and the dielectric constant of the carrier solution. So high output pressure of the EOP can be obtained by using high electric field, long porous core and small pore radius.

3.2. Effect of HMTA concentration on flow rate and delivery efficiency

In water carrier solution, the surface of the porous core is negatively charged as a result of partial silanol ionization. When a working voltage is applied to the EOP by the electrodes, hydrogen and hydroxyl ions will be generated in the anode and cathode area due to water electrolysis. Since the mobility of hydrogen ion is much faster than that of hydroxyl one, the pH value of the pump carrier solution and the surface charge density of the porous core will be reduced gradually, and make the pump flow rate decrease. To obtain a steady flow rate and high delivery efficiency, an appropriate additive should be introduced into the pump carrier to neutralize the hydrogen ions generated in water electrolysis.

In this paper, HMTA was selected as the additive of the pump carrier solution. For the organic alkali containing four amido-cyanogens, it can effectively neutralize the hydrogen ions and enhance the concentration of the protonized HMTA ions.

The delivery efficiency (R) of the EOP can be defined as the ratio of pump flow rate to working current

$$R = \frac{Q}{I} \tag{6}$$

where Q is the flow rate and I is the working current of the EOP. The influence of HMTA concentration on the pump flow rate and delivery efficiency was examined from 0.2 to 0.8 mmol/L with a fixed pump voltage of 880 V, as shown in Fig. 2.

Since HMTA is an organic alkali and can neutralize hydrogen ions, the carrier additive can effectively eliminate the influence of hydrogen ions on the surface charge density of the porous core during the pump operation. At the same time, the combination of HMTA and hydrogen ion can form the counter ion accumulated in the diffusion layer for EOF generation. In Fig. 2, the flow rate of the EOP increases with the HMTA concentration up to 0.5 mmol/L. When the concentration is higher than 0.5 mmol/L, the influence of the ion strength on the thickness of the diffusion layer becomes significant. For zeta potential is related to the thickness of electrical double layer, the further increase of HMTA concentration will reduce the thickness of electrical double layer, i.e. the zeta potential of the surface, and thus result in the decrease of the pump flow rate. In Fig. 2, both the pump flow rate and delivery efficiency can achieve the maximal values with 0.5 mmol/L HMTA. The relative standard deviation (R.S.D.) of

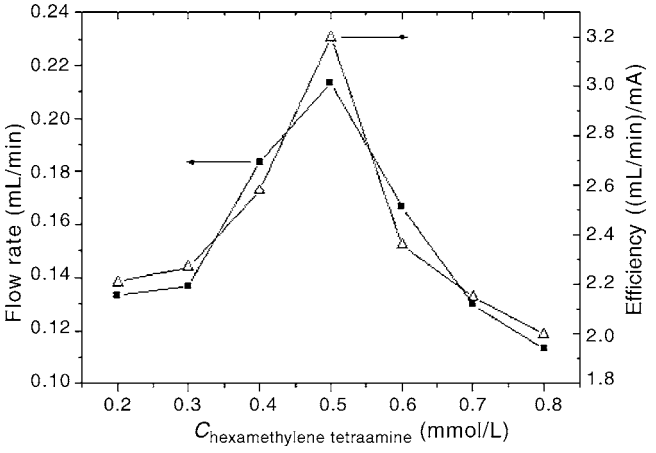

Fig. 2. Effect of HMTA concentration on pump flow rate and delivery efficiency. The diameter and length of the porous core are 9.0 mm and 6.2 cm, respectively. The working voltage of the electroosmosis pump is 880 V.

the pump flow rate is 4.3% in 4 h. So 0.5 mmol/L HMTA was selected as the pump carrier solution in this work.

3.3. Effect of electric field strength on flow rate and output pressure of EOP

The effect of electric field strength on the flow rate and output pressure of the EOP was examined. The experimental results showed that the flow rate of the pump was proportional to the electric field strength lower than 825 V/cm using a 6 cm porous core, which was consistent with Eq. (2). It manifests that the thermal effect of the EOP can be low enough with the electric field strength. Although the diameter of the porous core column in this work was smaller than those of our previous work [9] and in Zeng's paper [18], the flow rate per unit of electric field strength and cross-section area was higher and achieved 2.0×10^{-3} (mL/min)/[(V/cm) cm^2]. So the flow rate of the EOP can be adjusted by the electric field strength efficiently.

The maximal output pressure of the EOP can be measured by a liquid pressure meter after switching off the output flow. The experimental data indicated that a linear relation between the maximal output pressure and the electric field strength was obtained in the range from 100 to 825 V/cm, which was consistent with Eq. (4). The maximal output pressure of the EOP can be enhanced by increasing the applied electric field strength, but restricted by the maximum output voltage of the electrophortic power supply.

3.4. Effect of porous core dimensions on flow rate and output pressure of EOP

In the experiment of the porous core length, 9.0 mm diameter porous cores with different lengths were prepared to construct the EOPs. The influence of core length on the flow rate and maximal output pressure of the EOP were investigated, as shown in Fig. 3.

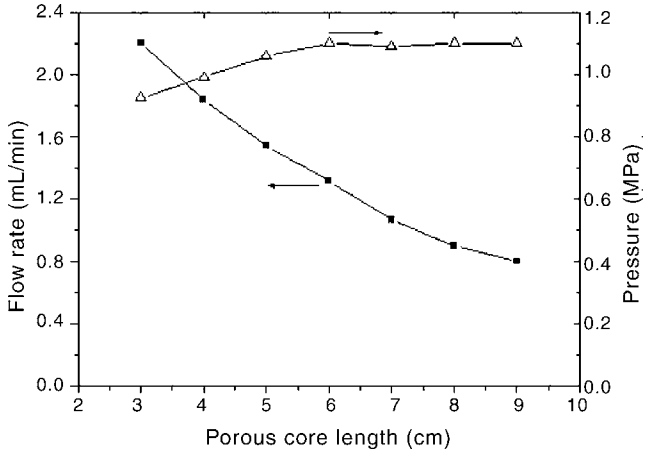

Fig. 3. Effect of porous core length on flow rate and maximal output pressure of EOP. The diameter of the porous core is 9.0 mm, the HMTA concentration is 0.5 mmol/L and the working voltage is 4950 V.

In Fig. 3, it showed that the flow rate of the EOP decreased with increasing the porous core length by using the pump voltage of 4950 V, which was limited by the maximum output voltage of the electrophoretic power supply. Since the electric field strength is the pump voltage divided by the porous core length, the increase of the porous core length will lead to the decrease of the electric field strength and the pump flow rate.

It also displayed that the pump output pressure increased with the porous core length in the range less than 6.0 cm. Among seven porous core lengths, 3.0 cm porous core gave the lowest output pressure of 0.93 MPa, whereas 6.0 cm porous core provided the highest pump pressure of 1.1 MPa. For the accumulative effect of the electroosmotic action and the reduction of the electric field strength, the maximal output pressure was enhanced with the porous core length from 3.0 to 6.0 cm. The results were consistent with those reported in refs. [7,8]. However, the maximal output pressure kept almost 1.1 MPa with the porous core length longer than 6.0 cm, because of the limited maximum voltage of the power supply and reduced electric field strength. So the porous core length was selected to be 6.0 cm in this work.

Three porous core columns with the diameters of 7.0, 8.0 and 9.0 mm were prepared to construct the EOPs in the core diameter investigation. The experimental results showed that the pump flow rate was dependent on the porous core diameter and consistent with Eq. (2). So 9.0 mm diameter core was used in the EOP construction.

The experimental results also displayed that the maximal output pressures with different core diameters were approximately the same under the fixed electric field strength. With the applied voltage of 5000 V, the porous core length of 6.0 cm and diameter of 9.0 mm, the maximal flow rate and output pressure of the porous core EOP could achieve 1.3 mL/min and 1.1 MPa, respectively. The working current and power was lower than 0.8 mA and 4 W, so the EOP could be operated continuously.

3.5. Effect of acetonitrile concentration on flow rate and output pressure of EOP

It is important that the EOP can be employed to drive the mobile phases of organic solvent and water mixture in liquid chromatography. Acetonitrile is the organic solvent used frequently in reversed-phase liquid chromatography. Meanwhile, acetonitrile is an effective solvent to generate electroosmotic flow in EOP system. Other organic solvents, such as methanol, tetrahydrofuran, acetone, were examined on their EOF rates. It could be found that the EOF rate generated with acetonitrile was the highest. Based on the reasons mentioned above, acetonitrile was adopted as the organic solvent of the mobile phase. In this paper, the effect of acetonitrile concentration in the mobile phase on the flow rate and the maximal output pressure was also investigated, as shown in Fig. 4.

The electroosmotic flow rate and maximal output pressure of the EOP are influenced by zeta potential, the dielectric constant and viscosity coefficient of the carrier solution, which can be changed by increasing the acetonitrile concentration in the

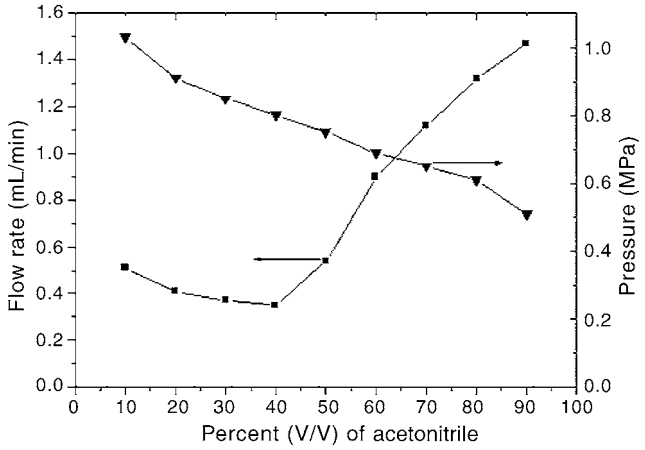

Fig. 4. Effect of acetonitrile concentration on flow rate and maximal output pressure. The diameter and length of the porous glass core are 9.0 mm and 6.0 cm, respectively. The HMTA concentration is 0.5 mmol/L and the working voltage is 4950 V.

carrier solution. In Fig. 4, the pump output pressure decreased with increasing the acetonitrile concentration, but the pump flow rate decreased firstly and then increased with the acetonitrile concentration.

3.6. Application of porous core EOP in chromatographic separation

To evaluate the practical application of the EOP, the porous core EOP was employed for the mobile phase delivery in chromatographic separation. The analytes of phenol and benzene were separated by a silica monolithic column bonded with C_8. The chromatogram driven by the porous core EOP is shown in Fig. 5.

Fig. 5 showed that phenol and benzene could be separated by the separation system with 35% (v/v) acetonitrile solution containing 0.5 mmol/L HMTA as the mobile phase. The separation efficiency was about 6000 plates/m for phenol. The peaks of phenol and benzene were relatively broad because of the low flow rate of the mobile phase supplied by the EOP. It may be that the porous core possesses relatively large radius of the microchannels resulting from the sintering temperature. So the output pressure of EOP and flow rate of the mobile phase could be lowered.

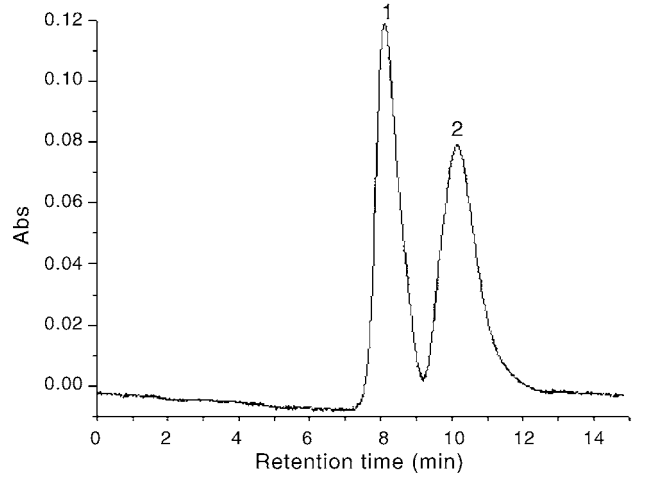

Fig. 5. Chromatogram of analyte separation by using porous core EOP. Separation conditions: Silica monolithic column polymerized in 10 cm × 3.0 mm i.d. fused-silica tube and modified with C_8; mobile phase, 35% (v/v) acetonitrile–water solution containing 0.5 mmol/L HMTA; injection voltage and time, 200 V and 2 s; detection wavelength, 254 nm; flow rate, 0.2 mL/min. Standard analytes: (1) 0.5 mmol/L phenol and (2) 1.0 mmol/L benzene.

The retention time of the analyte peaks in the chromatogram could display the flow rate stability of the EOP. The R.S.D. of retention time for phenol was 3.9% ($n = 4$). It implies the feasibility of the EOP application in the reversed-phase chromatography with silica monolithic columns.

4. Conclusion

In this paper, a porous core EOP was studied and improved to provide both sufficient flow rate and output pressure for the chromatographic separation. The effects of HMTA concentration on the flow rate and delivery efficiency of the EOP were examined and both the optimal values can be achieved with 0.5 mmol/L HMTA. After the investigation of the influences of the electric field strength, porous core dimension and acetonitrile concentration on the pump flow rate and maximal output pressure, an improved EOP was proposed and constructed. This pump can be used as mobile phase delivery in reversed-phase chromatography with silica monolithic columns.

However, the gases generated in water electrolysis may be accumulated in the hollow electrode cavities of the EOP, and thus influence the flow rate after 4 h. The improvement on convenient releasers and gas elimination is our due course. In addition, the modification method of the stationary phases should be improved to obtain high separation efficiency.

Acknowledgement

The authors thank the National Science Foundation of China (No. 20275035 and 29975026) for the financial supports to carry out this work.

References

[1] V. Pretorius, B.J. Hopkin, J.D. Schieke, J. Chromatogr. 99 (1974) 23.
[2] P.K. Dasgupta, S.R. Liu, Anal. Chem. 66 (1994) 1792.
[3] S. Liu, P.K. Dasgupta, Talanta 41 (1994) 1903.
[4] L.X. Chen, J.P. Ma, F. Tan, Y.F. Guan, Sens. Actuators B 88 (2003) 260–265.
[5] L.X. Chen, J.P. Ma, Y.F. Guan, Microchem. J. 75 (2003) 15.
[6] L.X. Chen, J.P. Ma, Y.F. Guan, J. Chromatogr. A 1028 (2004) 219.
[7] L.X. Chen, H.L. Wang, J.P. Ma, C.X. Wang, Y.F. Guan, Sens. Actuators B 104 (2005) 117.
[8] Y.Z. He, W.E. Gan, M. Zhang, M.Z. Zheng, R.H. Zeng, G. Jin, Chin. J. Anal. Chem. 26 (1998) 125.
[9] W.E. Gan, L. Yang, Y.Z. He, R.H. Zeng, M.L. Cervera, M. de la Guardia, Talanta 51 (2000) 667.
[10] L. Yang, Y.Z. He, W.E. Gan, X.Q. Lin, H.C. Zhang, Chin. J. Anal. Chem. 28 (2000) 248.
[11] L. Yang, Y.Z. He, W.E. Gan, M. Li, Q.S. Qu, X.Q. Lin, Talanta 55 (2001) 271.

[12] L. Yang, Y.Z. He, W.E. Gan, N. Deng, M. Li, X.Q. Lin, Chin. J. Anal. Chem. 29 (2001) 555.
[13] Y.Q. Zhao, Y.Z. He, W.E. Gan, L. Yang, Chin. J. Anal. Chem. 30 (2002) 440.
[14] Y.Q. Zhao, Y.Z. He, W.E. Gan, L. Yang, Talanta 56 (2002) 619.
[15] Y.H. Zhang, Y.Z. He, L.Q. Li, W.E. Gan, Chin. J. Anal. Chem. 30 (2002) 984.
[16] Y.Y. Hu, Y.Z. He, L.L. Qian, L. Wang, Anal. Chim. Acta 536 (2005) 251.
[17] Y.Z. He, X.K. Wang, N. Deng, L. Wang, F. Han, Electrokinetic-flow total analysis system, Chinese Patent, Application No. 200510038677.5 (2005).
[18] S.L. Zeng, C.H. Chen, J.G. Sntiago, J.R. Chen, R.N. Chen, R.N. Zare, J.A. Tripp, F. Svec, J.M.J. Fréchet, Sens. Actuators B 82 (2002) 209.

Available online at www.sciencedirect.com
ScienceDirect
Talanta 70 (2006) 364–369
Talanta
www.elsevier.com/locate/talanta

A fluorescent chemical sensor for Hg(II) based on a corrole derivative in a PVC matrix

Chun-Lian He [a,c], Feng-Lian Ren [a], Xiao-Bing Zhang [b,*], Zhi-Xiang Han [b]

[a] College of Chemistry and Chemical Engineering, Central South University, Changsha 410083, PR China
[b] State Key Laboratory of Chemo/Biosensing and Chemometrics, College of Chemistry & Chemical Engineering, Department of Chemistry, Hunan University, Changsha, Hunan 410082, PR China
[c] Medical College, Hunan Normal University, Changsha 410006, PR China

Received 27 December 2005; received in revised form 15 February 2006; accepted 18 February 2006
Available online 24 March 2006

Abstract

A fluorescent chemical sensor for Hg(II) using 5,10,15-tris(pentafluorophenyl)corrole (H_3(tpfc)) as fluorophore is described in this paper. The response of the sensor is based on the fluorescence quenching of H_3(tpfc) by coordination with Hg(II). H_3(tpfc) based sensor shows a linear response towards Hg(II) in the concentration range from 1.2×10^{-7} to 1.0×10^{-4} M, with a working pH range from 5.0 to 8.0. The response time for Hg(II) concentration $\leq 1.0 \times 10^{-5}$ M is less than 5 min. The sensor shows good selectivity for Hg(II) over alkali, and alkaline earth, and most of transition metal cations. The effect of the composition of the sensor membrane has been studied and the experimental conditions optimized. The corrole based sensor membrane can be easily regenerated just by washing with blank buffer solution after each measurement. The sensor has been used for determination of Hg(II) in water samples with satisfactory results.

Keywords: Corrole; Fluorescent sensor; Mercury(II) ion; Response characteristics

1. Introduction

Mercury, one of the most toxic elements in the world, represents a major toxicity to microorganisms and environment even in low concentrations. Inorganic mercury has been reported to produce harmful effects at 5 μg/l in a culture medium [1]. Once introduced into the marine environment, microorganisms convert it into methylmercury, a form of mercury being even more toxic to aquatic organisms and birds than the inorganic mercury, which eventually reaches the top of the food chain and accumulates in higher organisms, especially in large edible fish [2]. When consumed by humans, methylmercury triggers several serious disorders including sensory, motor and neurological damage [3]. For example, when ingested by a pregnant woman, methylmercury readily crosses the placenta and targets the developing fetal brain and central nervous system, which can cause developmental delays in children [4].

The development of methods for the determination mercury is, therefore, of significant importance for environment and human health. Several techniques for the determination of mercury ions in various samples have been reported over the past few years. They include spectrophotometry [5], atomic absorption spectrometry [6,7], inductively coupled plasma-mass spectroscopy (ICP-MS) [8], inductively coupled plasma-atomic emission spectrometry (ICP-AES) [9] and voltammetry [10,11]. These methods offer good limits of detection and wide linear ranges. However, most of these techniques necessitate the use of sophisticated and high cost apparatus and require complicated operation. They are not suitable for on-line or field monitoring. The past decades have seen increasing interest in development of optical chemical sensors for Hg^{2+} with different chemical transducers [12–18], as such sensors can offer advantages in terms of size, electrical safety, costs, no needing for a reference element and the fact that it is easy to carry out long distance transmission with the application of fiber optics. However, this type of sensors for mercury reported so far generally exhibits long response time, narrow working concentration range or moderate selectivity. New reports on fluorescence Hg^{2+} sensors based on different fluorophores are continually being published. It seems, however,

* Corresponding author.
E-mail address: xiaobingzhang89@hotmail.com (X.-B. Zhang).

0039-9140/$ – see front matter © 2006 Elsevier B.V. All rights reserved.
doi:10.1016/j.talanta.2006.02.051

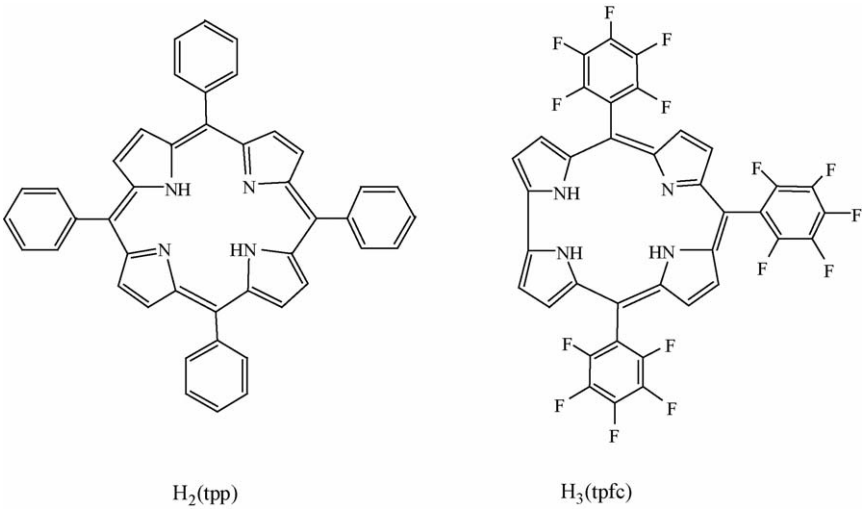

Fig. 1. Structure of H_2(tpp) and H_3(tpfc).

the scope of useful fluorophores for Hg^{2+} remains rather limited. Searching for new fluorophores with high selectivity towards Hg^{2+} as well as good photochemical property including excellent photostability, large Stokes shifts and high quantum yield is still a challenge for the analytical chemistry research efforts. Examples of recent advances along this line have been the synthesis of some new fluorophores which respond to Hg(II) with high selectivity [19–24]. Plaschke et al. [12], Zhang et al. [25] and Chan et al. [26] have reported fluorescence Hg^{2+} sensors based on porphyrin derivatives. This kind of fluorophores shows large Stokes shifts, and exhibits highly selective, sensitive and reversible fluorescence response towards Hg^{2+} over other metal ions. However, the regeneration for these porphyrins based sensors is rather complex, which needs washing first with acidic solution and then with blank buffer solution. Moreover, the fluorescence quantum yield of porphyrin is not high enough.

Corrole, a classical member of the porphyrinoid family, attracted very few research interests for decades until the first corrole synthesis started with commercially available reactants (pyrrole and aldehyde) was reported by two independent groups [27,28]. The stabilization of high oxidation states in transition metals is one of the most interesting features of corroles [29]. Another feature which has previously attracted limited attention is that some of them show good photophysical properties with strong fluorescence, large Stokes shifts and relatively long excitation (>400 nm) and emission (>600 nm) wavelengths that minimize the effects of the background fluorescence [30,31]. All these features make the corroles potential carriers for preparation of new optical chemical sensors. Thus, we tried to use 5,10,15-tris(pentafluorophenyl)corrole (H_3(tpfc); Fig. 1) as fluorophore to see whether the response characteristics of the fluorescent sensor towards Hg^{2+} could further be improved. H_3(tpfc) shows a higher fluorescence quantum yield ($\phi_f = 0.2$) than that of tetraphenylporphine (H_2(tpp)) ($\phi_f = 0.13$) [31]. Moreover, there is one more hydrogen atom bonded with the nitrogen of the tetrapyrrolic nucleus in H_3(tpfc) comparing to H_2(tpp) (Fig. 1). This might cause the distortion of the corrole macrocycle to result in increasing exposure of the pyrrole nitrogen lone pairs to solvent and be favorable for metal ion complexation, and therefore, decrease the response time of fluorophore towards Hg^{2+} [32]. Our experimental results show that the optode based on H_3(tpfc) shows fluorescence response towards Hg^{2+} with slightly wider linear concentration range and obviously shorter response time than that of porphyrin counterparts and comparable selectivity over other metal ions. Different from porphyrin based fluorescent chemical sensors which need washing first with acidic solution and then with blank buffer solution [25,26], corrole based sensor membrane can be easily regenerated just by washing with blank buffer solution after each measurement. The proposed sensor is preliminarily applied to the determination of Hg(II) in water samples with satisfactory results.

2. Experimental

2.1. Reagents

High molecular weight poly(vinyl chloride) (PVC), di-*iso*-octyl phthalate (DIOP), dibutyl-*o*-phthalate (DBP), dioctyl sebacate (DOS), trifluoroacetic acid (TFA), 2,3-dichloro-5,6-dicyano-l,4-benzoquinone (DDQ) and sodium tetraphenylboron (NaTPB) were obtained from Shanghai Chemicals (Shanghai, China) and used as received. H_2(tpp) was synthesized by Adler's method [33], [tetraphenylporphinato]zinc (Zn(tpp)) was prepared according to documented procedures [34] and both were identified by ^{1}H NMR, mass spectroscopy and UV–vis spectroscopy. Before being used, dichloromethane and benzaldehyde were subjected to simple distillation from K_2CO_3. Pyrrole was distilled at atmospheric pressure from CaH_2. Tetrahydrofuran (THF) was freshly distilled from sodium chips under argon with benzophenone/ketyl as indicator. Except when specified, other chemicals were of analytical reagent grade and used without further purification. Twice distilled water was used throughout all experiments.

2.2. Synthesis of H_3(tpfc)

H_3(tpfc) was synthesized by a modified procedure of literature [35]. In a 50 ml flask, pentafluorobenzaldehyde (196 mg, 1.0 mmol) was dissolved in 10 μl (12 μmol) of pre-prepared solution of TFA in CH_2Cl_2 (1:10, v/v) and stirred at room temperature for 5 min. Then fresh distilled pyrrole (105 μl, 1.5 mmol) was quickly added while stirring. After stirring for another 10 min at room temperature, the reaction mixture was dissolved in CH_2Cl_2 (10 ml) and a solution of DDQ (273 mg, 1.2 mmol) in toluene–THF (2 ml) was added, and stirred at room temperature for a further 5 min, then 2 g of silica was added and the solvent evaporated. The residue retained on silica was passed over short chromatographic column (silica, CH_2Cl_2:hexane, 1:2) to give crude product. Further purification by column chromatography (silica, hexane, then CH_2Cl_2:hexane, 1:5) and recrystallization from hexane afforded pure H_3(tpfc) (50 mg, 18.4%) as dark crystals. Spectroscopic and physical properties were in agreement with those reported in the literature [27].

2.3. Apparatus

All fluorescence measurements were carried out on a Perkin-Elmer LS55 luminescence spectrometer with excitation slit set at 5 nm and emission slit at 7.5 nm. A home-made poly(tetrafluoroethylene) flow-cell described elsewhere [25] and a bifurcated optical fiber (30 + 30 quartz fibers, diameter 6 mm and length 1 m) were used for the Hg(II) measurements. The excitation light was carried to the cell through one arm of the bifurcated optical fiber and the emission light collected through the other. A glass plate (diameter 10 mm) covered with sensing membrane was fixed on the top of the flow chamber by the mounting screw nut with the membrane contacted with the sample solution.

The standard solution of Hg(II) was obtained by serial dilution of 1.02×10^{-2} M $Hg(NO_3)_2$ solution and buffered with NaOAc–HOAc (pH 6.00). The pH measurements were carried out on a Mettler-Toledo Delta 320 pH meter.

2.4. Preparation of optode membrane

The optode membrane cocktail was prepared by dissolving a mixture of 1.5 mg of H_3(tpfc), 1.5 mg of NaTPB, 16 mg of PVC and 31 mg of DOS in 0.5 ml of freshly distilled THF. To improve the adhesion of the film, the glass plates (diameter 10 mm) were first activated by treatment with concentrated HNO_3 for 12 h, followed by 3% HF, and 10% H_2O_2 each for 30 min, and washed with distilled water and then with ethanol. A glass plate was then mounted on a spinning device and then rotated at a frequency of 600 rpm. Using a syringe, 0.1 ml of the membrane cocktail was sprayed to the center of the plate. A membrane of about 4 μm thickness was then coated on the glass slides and dried in ambient air at room temperature for 24 h before used.

2.5. Measurement procedure

Two arms of the bifurcated optical fiber were fixed in the detecting chamber of the spectrofluorometer to carry the excitation and emission light. The fluorescence intensity was measured with the maximal excitation wavelength of 420.0 nm and at the maximal emission wavelength of 643.0 nm. The sample solution was driven through the flow-cell by a peristaltic pump (Guokang Instruments, Zhejiang, China) at a flow rate of 1.4 ml min^{-1}. After each measurement, the flow-cell was washed with a NaOAc–HOAc buffer solution (pH 6.00) until the fluorescence intensity of the optode reached the original blank value.

3. Results and discussion

3.1. Fluorescence quenching of optode by Hg(II)

Fig. 2 shows the fluorescence spectra of H_3(tpfc) based optode membrane exposed to solutions containing different concentrations of Hg(II), which are recorded at λ_{ex} = 420.0 nm and λ_{em} = 550–750 nm. Owing to the conjugated double bond system and the high mobility of its π-electrons, H_3(tpfc) exhibits fluorescence emission at 615.0 and 643.0 nm when excited by the radiation of 420.0 nm. From Fig. 2 one can see that the fluorescence intensities of the optode membrane decrease with the increase of the concentration of Hg(II), which constitutes the basis for the determination of Hg(II) with the optical fiber sensor proposed in this paper.

3.2. Optimization of membrane compositions

Several optode membranes were prepared using different sensitive materials including H_3(tpfc), H_2(tpp) and Zn(tpp) with DOS as plasticizer to study the effect of sensing materials. The results are shown in Table 1.

From Table 1 one can see that the optode of H_3(tpfc) shows obviously better response characteristics towards Hg(II) than that of H_2(tpp) in terms of working concentration range and response time, while the optode based on Zn(tpp) shows no responses towards Hg(II). The effect of the structure of the

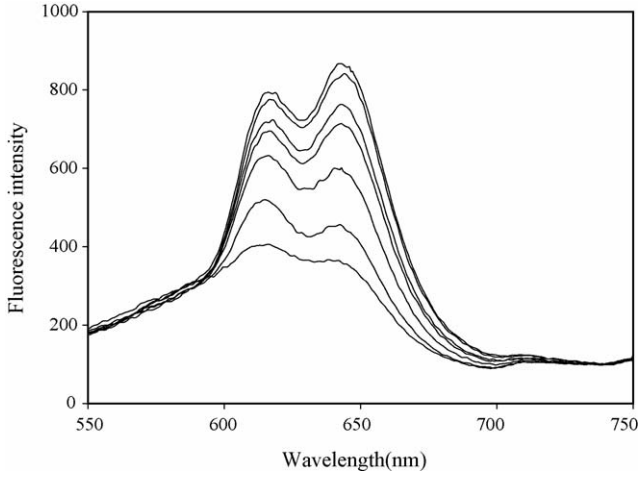

Fig. 2. Fluorescence emission spectra of the H_3(tpfc) sensing membrane in the presence of different concentrations of Hg(II): (1) 0 M; (2) 1.2×10^{-7} M; (3) 2.1×10^{-6} M; (4) 5.3×10^{-6} M; (5) 1.0×10^{-5} M; (6) 5.2×10^{-4} M; (7) 1.0×10^{-4} M.

Table 1
The effect of sensing materials on the response behavior of optodes

Optode	Sensing material	Working concentration range (M)	Response time (min)
1	H_3(tpfc)	1.2×10^{-7} to 1.0×10^{-4}	5
2	H_2(tpp)	5.6×10^{-6} to 2.5×10^{-4}	9
3	Zn(tpp)	No response	–

Membrane composition for each optode was: 3% sensing material, 3% NaTPB, 62% DOS and 32% PVC (w/w).

Table 2
The effect of plasticizers on the response behavior of optodes

Optode	Plasticizer	Working concentration range (M)
1	DOS	1.2×10^{-7} to 1.0×10^{-4}
4	DBP	2.0×10^{-6} to 1.5×10^{-4}
5	DIOP	4.2×10^{-6} to 1.0×10^{-4}

Membrane composition for each optode was: 3% H_3(tpfc), 3% NaTPB, 62% plasticizer and 32% PVC (w/w).

sensing materials to the optode response is obvious. From Fig. 1 one can see that there is one more hydrogen atom bonded with the nitrogen of the tetrapyrrolic nucleus in H_3(tpfc) comparing to H_2(tpp). On one hand, this kind of structure might cause the distortion of the corrole macrocycle, which is thought to result in increasing exposure of the pyrrole nitrogen lone pairs to solvent and be favorable for metal ion complexation and therefore, decrease the response time of fluorophore towards Hg^{2+} [32]; on the other hand, among the three hydrogen atoms, there is one which is easier to be deprotonated than other two hydrogen atoms on H_3(tpfc), leading to negatively charged form $[H_2(tpfc)]^-$, and facilitating the coordination with positively charged metal ions compared to H_2(tpp). Zn(tpp) has a central coordinating metal Zn that hinders the coordination of the Hg(II), which results in its inert response towards Hg(II).

Optodes with different plasticizers, DIOP, DBP and DOS were also prepared using H_3(tpfc) as the sensing membrane component. The results are shown in Table 2. Similar to the porphyrin based optode [25], the H_3(tpfc) based optode with DOS as the plasticizer gave the best response for Hg(II).

In the experiment, we also find that, with the addition of moderate amount of lipophilic ion, sodium tetraphenylborate, the response characteristics of the optode membrane are improved. The results are shown in Table 3.

From Table 3 one can see that the response concentration range of the optode membrane becomes wider and response time shorter as the amount of NaTPB in the optode membrane increases, which might be caused by the increasing hydrophilicity owing to the addition of NaTPB. This seems favorable for the Hg(II) approaching the solution/membrane interface and undergoing the reversible coordination/dissociation processes. However, the response concentration range of the optode membrane becomes narrower when the content of NaTPB is larger than 3%, which results in decreasing basic fluorescence intensity of the optode membrane. The experimental results show that the optode membrane composition consisting of 3% H_3(tpfc), 3% NaTPB, 62% DOS and 32% PVC (w/w) could provide the best response for Hg(II), which is chosen for further experiments.

Table 3
The effect of NaTPB on the response behavior of optodes

Optode	Content of NaTPB (%)	Working concentration range (M)	Response time (min)
6	0	5.1×10^{-6} to 2.2×10^{-4}	12
7	2	1.0×10^{-6} to 1.2×10^{-4}	6
1	3	1.2×10^{-7} to 1.0×10^{-4}	5
8	4	1.6×10^{-6} to 1.5×10^{-4}	5

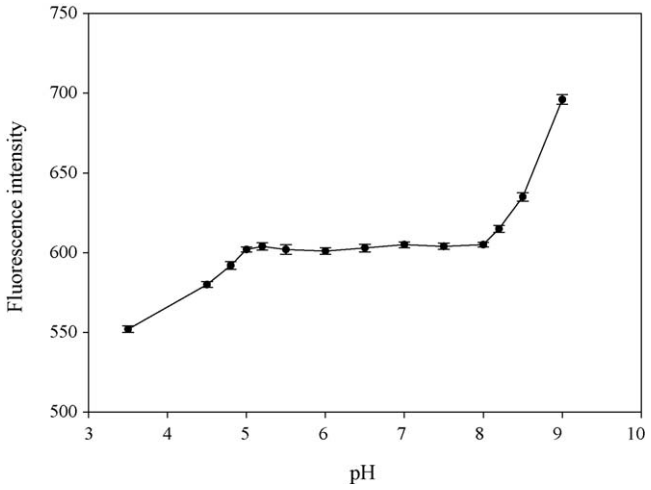

Fig. 3. Effect of pH on the determination of Hg^{2+} with proposed optode (the concentration of Hg^{2+} was fixed at 1.0×10^{-5} M; error bars were calculated with $n = 5$).

3.3. Effect of pH

The fluorescence intensity versus pH plot for the H_3(tpfc) optode shown in Fig. 3 was obtained by adjusting the solution pH with hydrochloric acid and sodium hydroxide and fixing the Hg(II) concentration at 1.0×10^{-5} M. In the alkaline condition, the high concentration of Hg(II) might cause precipitation of HgO. The experiment of the effect of pH on the response of the optode was carried out at a pH range from 3.0 to 9.0. It can be seen that, in the section of lower pH value, the fluorescence intensity of the optode decreased with decreasing pH value. This phenomenon might be caused by extraction of H^+ from aqueous solution into the optode membrane at high acidity, which caused the protonation of the nitrogen atom on H_3(tpfc) and decreased the mobility of its π-electrons. In the section of higher pH value, the increase of fluorescence intensity of the optode seems to be caused by the deprotonation of the nitrogen atom of tetrapyrrolic nucleus and formation of negatively charged $[H_2(tpfc)]^-$ [30]. Moreover, the partial precipitation of Hg(II) to HgO under strong basic condition might decrease the actual concentration of Hg(II) in the sample solution, which might also cause the increase of fluorescence intensity of the optode under basic condition. From Fig. 3 one can see that in a range of pH from 5.0 to 8.0, acidity does not affect the determination of Hg(II) with the proposed optode. In subsequent experiments, a pH 6.00 NaOAc–HOAc buffer solution was used.

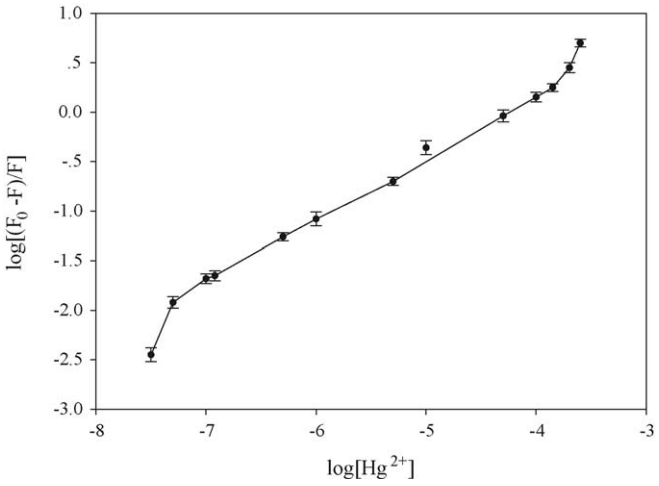

Fig. 4. Plot of $\log(\Delta F/F)$ as a function of the $\log[Hg^{2+}]$ (F_0 and F denote the fluorescence intensities of the optode membrane in the absence and presence of Hg(II), respectively; error bars were calculated with $n = 5$).

3.4. Response characteristics of the optode

The response curve of H_3(tpfc) based optode is shown in Fig. 4. In the Hg(II) concentration range of 1.2×10^{-7} to 1.0×10^{-4} M, the response of the sensor coincides with modified Stern–Volmer equation [25,36] with $\log(\Delta F/F)$ showing linear relationship with $\log[Hg^{2+}]$. With the Hg(II) concentration lower than 1.2×10^{-7} M, the response of the sensor follows the standard Stern–Volmer equation with $\Delta F/F$ showing linear relationship with $[Hg^{2+}]$. With the Hg(II) concentration larger than 1.0×10^{-4} M, there are no linear response characteristics observed, a stable complex between corrole and Hg(II) is expected to be formed. The regeneration of the optode became difficult when the Hg(II) concentration is larger than 1.0×10^{-4} M. The response time for Hg(II) concentration $\leq 1.0 \times 10^{-5}$ M is less than 5 min. The short-time stability of the optode was tested by recording the fluorescence intensity of 1.0×10^{-5} M Hg(II) over a period of 12 h for 20 measurements. A relative standard deviation of fluorescence reading of 1.6% was recorded. The proposed optode can be easily regenerated just by washing with blank buffer solution (NaOAc–HOAc, pH 6.00) after each measurement. All the regeneration process could be finished in 2 min, which indicated that the response of membrane to Hg(II) is reversible. The fluorescence intensity of the optode decreased 4% from the initial value after 100 measurement cycles (sensing of 1.0×10^{-5} M Hg(II) and regeneration with blank buffer solution). The optode could be stored in wet conditions without obvious change of the fluorescence intensity for at least one month, which implies that H_3(tpfc) is stable in a membrane contacting with water.

3.5. Selectivity

The interference of a number of common species for the fluorescence determination of Hg(II) was investigated. The experiments were carried out by fixing the concentration of Hg(II) at 1.0×10^{-5} M and then recording the change of the fluorescence intensity before and after adding the interferent into the Hg(II) solution buffered with a NaOAc–HOAc solution (pH 6.00). Experimental results show that most alkali and alkaline earth metal cations, and some transition metal cations such as Mn(II), Cd(II), Zn(II) and Al(III) exiting in concentration less than 1.0×10^{-2} M, do not show obvious interfering effect on the Hg(II) assay. Some other transition metal cations such as Fe(II), Fe(III), Ni(II), Cu(II) and Co(II) present in concentration less than 1.0×10^{-3} M do not show obvious interfering effect on the Hg(II) assay. However, Ag(I) exiting in the same concentration shows slight interfering effect on the Hg(II) assay. Further research shows that Ag(I) present in concentration less than 5.0×10^{-4} M can be tolerated. It causes slight interference when its concentration is above 5.0×10^{-4} M.

Table 4
Determination of Hg(II) in tap and river water samples with H_3(tpfc) based optode

Sample	Hg^{2+} spiked (M)	Hg^{2+} recovered (M)[a]	Recovery (%)
River water			
1	0	Not detected	–
2	5.0×10^{-7}	$(5.10 \pm 0.09) \times 10^{-7}$	102.0
3	2.5×10^{-6}	$(2.61 \pm 0.10) \times 10^{-6}$	104.4
4	1.0×10^{-5}	$(1.03 \pm 0.09) \times 10^{-5}$	103.0
Tap water			
1	0	Not detected	–
2	3.0×10^{-6}	$(2.98 \pm 0.08) \times 10^{-6}$	99.3
3	6.0×10^{-6}	$(6.05 \pm 0.06) \times 10^{-6}$	100.8

[a] Relative standard deviations were calculated with $n = 5$.

3.6. Preliminary analytical application

The application of the proposed method was evaluated for determination of Hg(II) in both tap and river water samples. The river water samples obtained from Xiang River were simply filtrated and showed that no Hg(II) was present in them. All the water samples were spiked with standard Hg(II) solutions at different concentration levels and then analyzed with proposed sensor. Results are shown in Table 4. One can see that recovery study of spiked Hg^{2+} determined by the H_3(tpfc) based optical fiber sensor shows satisfactory results. The present sensor seems useful for the determination of Hg(II) in real samples.

Acknowledgements

Financial support from the National Natural Science Foundation of China (Grants 20435003 and 20505008) is gratefully acknowledged.

References

[1] D.W. Boening, Chemosphere 40 (2000) 1335.
[2] M.V.B. Krishna, M. Ranjit, D. Karunasagar, J. Arunachalam, Talanta 67 (2005) 70.
[3] T.W. Clarkson, L. Magos, G.J. Myers, N. Engl. J. Med. 349 (2003) 1731.
[4] P. Grandjean, P. Weihe, R.F. White, F. Debes, Environ. Res. 77 (1998) 165.

[5] M.S. Hosseini, H. Hashemi-Moghaddam, Talanta 67 (2005) 555.
[6] J.V. Cizdziel, S. Gerstenberger, Talanta 64 (2004) 918.
[7] R.J. Huang, Z.X. Zhuang, Y. Tai, R.F. Huang, X.R. Wang, F.S.C. Lee, Talanta 68 (2006) 728.
[8] E. Curdova, L. Vavruskova, M. Suchanek, P. Baldrian, J. Gabriel, Talanta 62 (2004) 483.
[9] A.N. Anthemidis, G.A. Zachariadis, C.E. Michos, J.A. Stratis, Anal. Bioanal. Chem. 379 (2004) 764.
[10] H. Zejli, P. Sharrock, J.L.H.H. de Cisneros, I. Naranjo-Rodriguez, K.R. Temsamani, Talanta 68 (2005) 79.
[11] N.L. Dias, do Carmo F D.R., Talanta 68 (2006) 919.
[12] M. Plaschke, R. Czolk, H.J. Ache, Anal. Chim. Acta 304 (1995) 107.
[13] M. Ahmad, H. Hamzah, E.S. Marsom, Talanta 47 (1998) 275.
[14] A. Segura-Carretero, J.M. Costa-Fernandez, R. Pereiro, A. Sanz-Medel, Talanta 49 (1999) 907.
[15] C. Sanchez-Pedreno, J.A. Ortuno, M.I. Albero, M.S. Garcia, M.V. Valero, Anal. Chim. Acta 414 (2000) 195.
[16] B. Kuswandi, R. Narayanaswamy, Sens. Actuators B 74 (2001) 131.
[17] A. Safavi, M. Bagheri, Sens. Actuators B 99 (2004) 608.
[18] M. Shamsipur, M. Hosseini, K. Alizadeh, N. Alizadeh, A. Yari, C. Caltagirone, V. Lippolis, Anal. Chim. Acta 533 (2005) 17.
[19] A.B. Descalzo, R. Martinez-Manez, R. Radeglia, K. Rurack, J. Soto, J. Am. Chem. Soc. 125 (2003) 3418.
[20] E.M. Nolan, S.J. Lippard, J. Am. Chem. Soc. 125 (2003) 14270.
[21] X. Guo, X. Qian, L. Jia, J. Am. Chem. Soc. 126 (2004) 2272.
[22] A. Ono, H. Togashi, Angew. Chem. Int. Ed. 43 (2004) 4300.
[23] J.V. Ros-Lis, M.D. Marcos, R. Martinez-Manez, K. Rurack, J. Soto, Angew. Chem. Int. Ed. 44 (2005) 4405.
[24] S. Yoon, A.E. Albers, A.P. Wong, C.J. Chang, J. Am. Chem. Soc. 127 (2005) 16030.
[25] X.B. Zhang, C.C. Guo, Z.Z. Li, G.L. Shen, R.Q. Yu, Anal. Chem. 74 (2002) 821.
[26] W.H. Chan, R.H. Yang, K.M. Wang, Anal. Chim. Acta 444 (2001) 261.
[27] Z. Gross, N. Galili, I. Saltsman, Angew. Chem. Int. Ed. 38 (1999) 1427.
[28] R. Paolesse, L. Jaquinod, D.J. Nurco, S. Mini, F. Sagone, T. Boschi, K.M. Smith, Chem. Commun. (1999) 1307.
[29] Z. Gross, J. Biol. Inorg. Chem. 6 (2001) 733.
[30] J. Bendix, I.J. Dmochowski, H.B. Gray, A. Mahammed, L. Simkhovich, Z. Gross, Angew. Chem. Int. Ed. Eng. 39 (2000) 4048.
[31] A. Mahammed, Z. Gross, J. Inorg. Biochem. 88 (2002) 305.
[32] A.G. Cochran, P.G. Schultz, Science 249 (1990) 781.
[33] A.D. Adler, F.R. Longo, J.D. Finarelli, J. Org. Chem. 32 (1967) 476.
[34] G.D. Dorough, J.R. Miller, F.M. Huennekens, J. Am. Chem. Soc. 73 (1951) 4315.
[35] D.T. Gryko, B. Koszarna, Org. Biomol. Chem. 1 (2003) 350.
[36] W.H. Liu, Y. Wang, J.H. Tang, G.L. Shen, Q.R. Yu, Talanta 46 (1998) 679.

Available online at www.sciencedirect.com
ScienceDirect
Talanta 70 (2006) 370–376
Talanta
www.elsevier.com/locate/talanta

Applied analysis of lacquer films based on pyrolysis-gas chromatography/mass spectrometry

Rong Lu *, Yukio Kamiya, Tetsuo Miyakoshi **

Department of Industrial Chemistry, School of Science and Technology, Meiji University, 1-1-1 Higashi-Mita, Tama-ku, Kawasaki-shi 214-8571, Japan

Received 6 January 2006; received in revised form 18 February 2006; accepted 18 February 2006
Available online 29 March 2006

Abstract

Ancient lacquer film, a *Nanban* lacquer film, an old lacquer-ware object imported from an Asian country, and the Baroque and Rococo lacquer films were analyzed by pyrolysis-gas chromatography/mass spectrometry. Compared with the results of the natural lacquer film, it was revealed that the ancient lacquer film and *Nanban* lacquer film were made from *Rhus vernicifera*, and the old lacquer-ware imported from an Asian country was made from *Melanorrhoea usitata*. However, the Baroque and Rococo lacquer films obtained from the Doerner Institute in Munich, Germany were made from natural resins. 3-Pentadecylcatechol (MW = 320) (urushiol), 3-heptadecylcatechol (MW = 348) (laccol), and 4-heptadecylcatechol (MW = 348) (thitsiol) were the main products of the pyrolysis of *R. vernicifera*, *Rhus succedanea*, and *M. usitata*.

Keywords: Lacquer; Pyrolysis; Resin; Urishiol; Laccol; Thitsiol

1. Introduction

Lacquer is the only naturally occurring substance that is polymerized by an enzyme. It has been used in Asian countries for thousands of years as a durable and beautiful coating material [1,2]. Cultural treasures coated with lacquer have maintained their beautiful surfaces without loss of their original beauty for more than two thousand years [3,4]. However, it is well known that lacquer-ware is susceptible to ultraviolet irradiation [5–7]. Exposure to ultraviolet rays will cause the lacquer coating film to deteriorate, e.g., the film will flake off, lose its gloss, and crack [8,9]. Due to these characteristics, protection and restoration of lacquer-coated cultural treasures has become an important problem, and identification of the lacquer types in ancient coatings has also become very important for conservation and restoration studies. Therefore, an analytical method to determine the type of lacquer film is required.

There are three kinds of lacquer trees present in the Orient: *Rhus vernicifera* in China, Japan, and Korea, *Rhus succedanea* in Vietnam and Taiwan, and *Melanorrhoea usitata* in Thailand and Myanmar [10]. The saps of lacquer trees are composed of phenol derivatives, water, plant gum, glycoproteins, and the laccase enzyme. The phenol derivative of *R. vernicifera* lacquer is urushiol, of *Rhus succedanea* lacquer is laccol, and of *M. usitata* lacquer is thitsiol. The structures of urushiol, laccol, and thitsiol are shown in Scheme 1 [11,12].

Lacquer film is a cross-linked polymer that has been polymerized by laccase. Because lacquer films are insoluble in most solvents, only a few analytical techniques, such as solid NMR, FT-IR, and XPS, are available. However, most of these conventional techniques are time-consuming, demand large amounts of sample and frequently require several pre-treatments (such as solid NMR) [13]; further, they cannot obtain clear results (such as FT-IR) [14]. The pyrolysis-gas chromatography/mass spectrometry method is effective for analyzing lacquer film because this method can discriminate between the pyrolysis product of a lacquer sample and that of other natural resins [15–18].

Previously, we synthesized urushiol, laccol, and thitsiol analogues and successfully analyzed their films by pyrolysis-gas chromatography/mass spectrometry [19,20]. In this study,

* Corresponding author. Tel.: +81 44 934 7203; fax: +81 44 934 7203.
** Corresponding author.
E-mail addresses: lurong@isc.meiji.ac.jp (R. Lu), miya@isc.meiji.ac.jp (T. Miyakoshi).

0039-9140/$ – see front matter © 2006 Elsevier B.V. All rights reserved.
doi:10.1016/j.talanta.2006.02.050

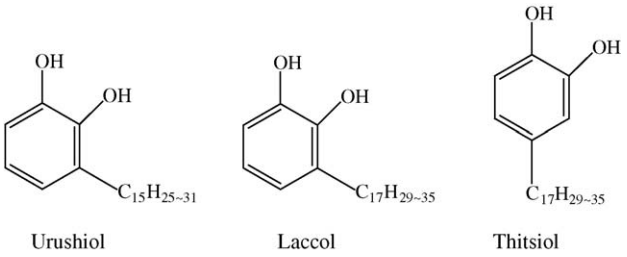

Scheme 1. Typical structures of urushiol, laccol, and thitsiol.

various ancient lacquer-wares were analyzed using pyrolysis-GC/MS, and the results were compared with the characteristics of the natural lacquer films to determine the kind of lacquer.

2. Experimental

2.1. General

The pyrolysis-gas chromatography/mass spectrometry measurements were carried out using a vertical micro-furnace-type pyrolyzer PY-2010D (Frontier Lab, Japan), an HP 6890 (Hewlett-Packard, Ltd.) gas chromatograph, and a HPG 5972A (Hewlett-Packard, Ltd) mass spectrometer. A stainless steel capillary column (0.25 mm i.d. × 30 m) coated with 0.25 mm of Ultra Alloy PY-1 (100% methylsilicone) was used for the separation. The sample (1.0 mg) was placed in a platinum sample cup. The cup was placed on top of the pyrolyzer at near ambient temperature. The sample cup was introduced into the furnace at 500 °C, then the temperature program of the gas chromatograph oven was started. The gas chromatograph oven was programmed to provide a constant temperature increase of 20 °C per min from 40 to 280 °C, then held for 10 min at 280 °C. The flow rate of the Helium gas was 18 ml/min. All the pyrolysis products were identified by mass spectrometry. The mass spectrometry ionization energy was 70 eV (EI-mode).

2.2. Materials

The three kinds of lacquer saps, *R. vernicifera*, *Rhus succedanea,* and *M. usitata,* were treated using the traditional *Nayashi* and *Kurome* methods as we previously reported [21] and coated on glass plates. They were allowed to polymerize in a humidity-controlled chamber at a relative humidity of 70–90% at 20 °C for 12 h, and then removed from the chamber and stored in the open air for 3 years.

The ancient lacquer film was obtained from the surface of a wooden dish extracted from an excavation site that dates back to the 17–18th century AD at *Kinenkanmae Iseki* on the Meiji University campus in Tokyo, Japan. A *Nanban* lacquer film from the 17th century AD and an old lacquer film imported from an Asian country during the 17–18th century AD were obtained from the surface of wooden crafts.

The *Baroque* and *Rococo* lacquer films were obtained from the wood surfaces of the Rococo church St. Alto in Altomunster, Munich, Germany.

3. Results and discussion

3.1. Py-GC/MS of R. vernicifera and Rhus succedanea lacquer films

The *R. vernicifera* and *Rhus succedanea* lacquer films were pyrolyzed at 500 °C. The total ion chromatogram (TIC) and mass chromatogram ($m/z = 320$) of the *R. vernicifera* lacquer film are shown in Fig. 1. Peak U-1 was identified as urushiol (MW = 320) based on the mass spectrum. The urushiol monomer was found in the pyrolysis product.

The TIC and mass chromatogram of $m/z = 320$ and $m/z = 348$ from the *Rhus succedanea* lacquer film are shown in Fig. 2. Peak L-1 was identified as laccol (MW = 348) by the mass spectrum. Laccol is the typical main component in *Rhus succedanea* lacquer sap.

Urushiol (MW = 320) was detected in both the *R. vernicifera* and *Rhus succedanea* lacquer films. The pyrolysis products clearly show a good correlation with the constituents of the respective lacquer saps. Mainly alkylcatechols and alkylphenols were observed as the thermally decomposed components of the terminal alkylcatechol-side chains of the lacquer films.

Based on the results obtained from these two specimens, it was possible to differentiate between the species. The alkylcatechols were detected in the mass chromatogram ($m/z = 123$) of the *R. vernicifera* and *Rhus succedanea* lacquer films as shown in Fig. 3. The alkylcatechols that have the longest side chains in *R. vernicifera* were pentadecylcatechols; however, those in the *Rhus succedanea* lacquer film were hepatadecylcatechols. In addition, the relative intensity of 3-heptylcatechol (C7) was the highest in the *R. vernicifera* lacquer film, whereas in the *Rhus succedanea* lacquer film, the 3-nonylcatechol (C9) had the highest intensity.

It has been reported that at the α- and β- positions, the double bonds of the olefines are most susceptible to thermal cleavage

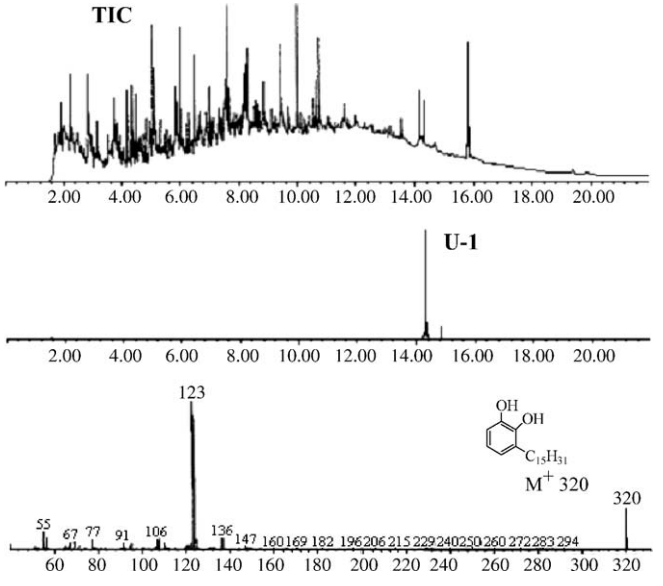

Fig. 1. Total ion chromatogram (TIC), mass chromatogram ($m/z = 320$) and mass spectrum (urushiol) of *Rhus vernicifera* lacquer film.

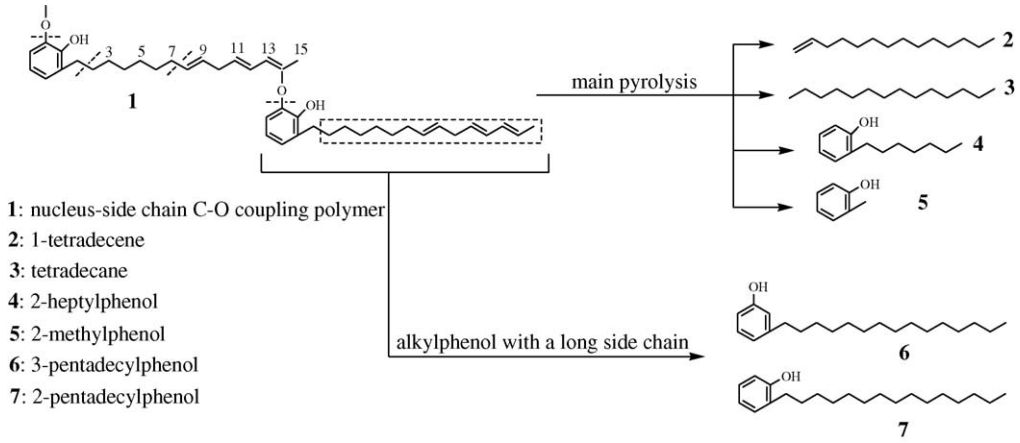

Scheme 2. Pyrolysis mechanism of urushiol polymer.

[22,23]. Therefore, as shown in Scheme 2, the highest yield of 3-heptylcatechol (C7) and 3-nonylcatechol (C9) can be attributed to the preferential cleavage at the α-position of the double bonds of the nucleus-14th and 16th chain C–O couplings of the urushiol and laccol polymers, respectively.

Alkyl phenols were detected in the mass chromatograms ($m/z = 108$) of the *R. vernicifera* and *Rhus succedanea* lacquer films, as shown in Fig. 4. The alkylphenols that have the longest side chains were the pentadecylphenols in the *R. vernicifera* lacquer film and the heptadecylphenols in the *Rhus succedanea* lacquer film. These are believed to be the products of pyrolysis of the nucleus-side chain C–O coupling for the urushiol and laccol polymers, respectively, because it has been inferred that dimerization of urushiol proceeds through laccase-catalyzed nucleus-side chain C–O coupling, as well as C–C coupling. Furthermore, because the C–O coupling polymers terminate mainly with alkyl- and monoalkenylcatechols, the pentadecylphenols and heptadecylphenols might be formed from such terminal groups, as shown in Fig. 4. Additionally, the relative intensity of 3-heptylphenol (C7) was the highest in the *R. vernicifera* lacquer film, whereas in the *Rhus succedanea* lacquer film, the 3-nonylphenol (C9) had the highest intensity. As shown in Fig. 5, the highest yield of heptylphenol (C7) and 3-nonylphenol (C9) can be attributed to the preferential cleavage at the α-position of the double bounds of the nucleus-14th and 16th chain C–O coupling for the urushiol and laccol polymers, respectively.

Fragments, such as the shorter side chains of the alkylcatechols and alkylphenols, were produced by thermal cleavage of the polymer at high temperatures. The relative intensity of 3-heptylphenol (C7) was highest in the *R. vernicifera* lacquer film, whereas in the *Rhus succedanea* lacquer film, the 3-nonylphenol was the highest.

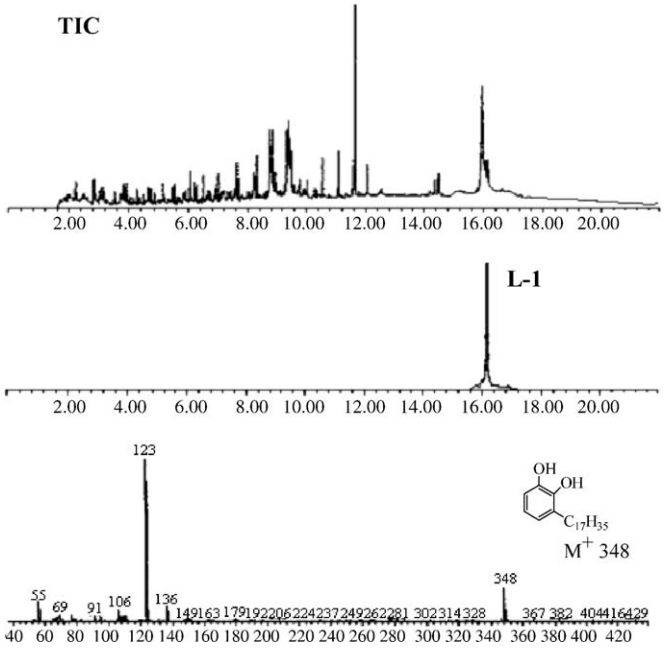

Fig. 2. Total ion chromatogram (TIC), mass chromatogram ($m/z = 348$), and mass spectrum (laccol) of *Rhus succedanea* lacquer film.

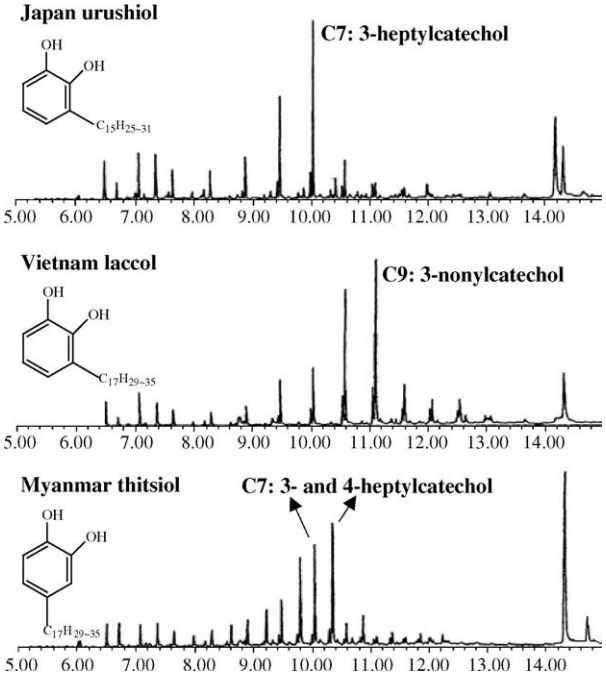

Fig. 3. Mass chromatograms ($m/z = 123$) of lacquer films from Japan, Vietnam, and Myanmar.

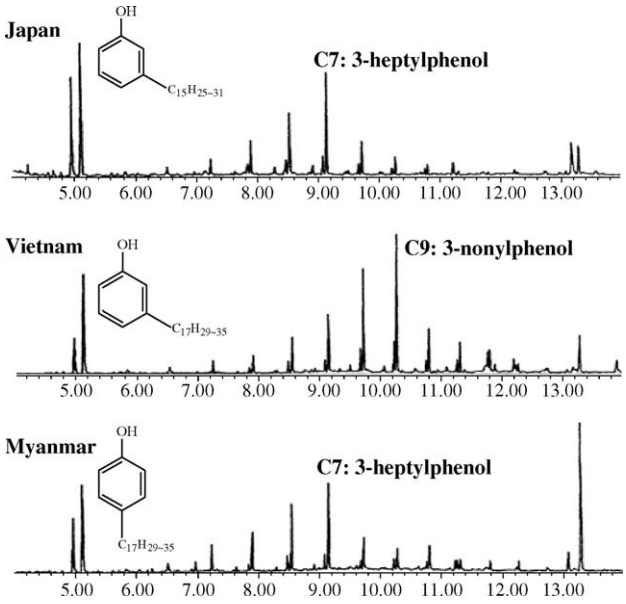

Fig. 4. Mass chromatograms ($m/z = 108$) of lacquer films.

3.2. Py-GC/MS analysis of M. usitata lacquer film

M. usitata is a lacquer tree that grows in Thailand and Myanmar. The main component of *M. usitata* is thitsiol, which contains 3- and 4-heptadecadienylcatechols, as well as a series of α- and β-positions.

The *M. usitata* lacquer film was pyrolyzed at 500 °C. Fig. 5 shows the TIC and the individual mass chromatograms at $m/z = 346$, 348, 310, 326, 338, and 354. Peaks 1, 2, 3, 4, 5, and 6 of the mass chromatograms were identified as 4-hepatadecenylcatechol (MW = 346), 4-hepatadecenylcatechol (MW = 348), 3-(10-phenyldecyl)phenol (MW = 310), 3-(10-phenyldecyl)catechol (MW = 326), 4-(10-phenyldodecyl)phenol (MW = 338) and 4-(12-phenyldodecyl)catechol (MW = 354), respectively. Because the C–O coupling polymers are terminated with 4-hepatadecenylcatechol, these compounds can be formed from such terminal groups.

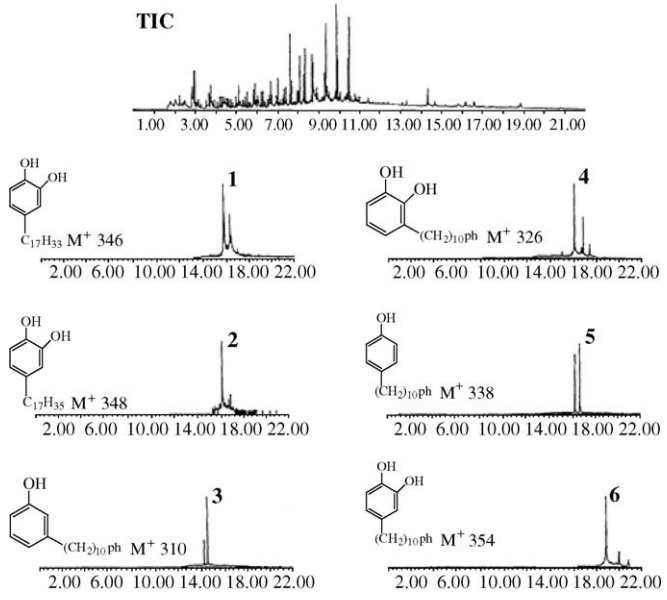

Fig. 5. TIC and mass chromatograms ($m/z = 346$, 348, 310, 326, 338, 354) of *Melanorrhoea usitata* lacquer film.

As shown in Fig. 3, a pair of peaks of the 3- and 4-alkylcatechols was detected in the mass chromatograms ($m/z = 123$) of the *M. usitata* lacquer films. The relative intensity of the 3- and 4-heptylcatechols (C7) was the highest in the pyrolysis products of the Myanmar lacquer. The highest yields of the 3- and 4-heptylcatechols were considered to be mainly due to cleavage at the α-position of the double bonds of the nucleus-8th and 12th chain C=O couplings for the thitsiol polymers. The alkylphenols detected are likely to be the pyrolysis products of the nucleus-side chain C–O coupling of the thitsiol polymers. The dimerization of the lacquer monomers is considered to proceed through the laccase-catalyzed nucleus-side chain C–O coupling as well as the C–C coupling. The yields of 3-heptylphenol (C7) were highest, as shown in Fig. 5. The α- and β-positions of the double bonds of the olefin are susceptible to thermal cleavage so that these highest yields are thought to be produced primarily by cleavage at the α-position of the double bonds of thitsiol, such as the 3- and 4-(8,11-heptadecadienyl)catechols. The existence of 3-pentadecylcatechol (MW = 320) (urushiol), 3-heptadecyl-catechol (MW = 348) (laccol), and 4-heptadecylcatechol (MW = 348) (thitsiol) in the pyrolysis products agrees with the characteristic components of the three kinds of lacquer saps, as shown in Table 1. Furthermore, the data acquired for the alkylcatechols and alkylphenols in the pyrolysis products allow the determination of whether the lacquer ware is actually produced from lacquer or some other resins.

3.3. Py-GC/MS analysis of ancient lacquer

It is sometimes extremely important to determine whether objects that are claimed to be lacquer-ware are actually created from lacquer sap or some other resins. Lacquer-ware can be precisely determined by the presence of urushiol or laccol with alkylcatechols and alkylphenols using pyrolysis-gas chromatography/mass spectrometry.

An ancient lacquer object obtained from an archeological site was identified using this method by comparison with

Table 1
Pyrolysis products of lacquer films

Species of lacquer film	Pyrolysis products		
	Monomer	Alkylcatechol	Alkylphenol
Rhus veinicifera	Urushiol	3-Heptylcatechol	3-Heptylphenol
Rhus succedanea	Laccol	3-Nonylcatechol	3-Nonylphenol
Melanorrhoea usitata	Thitsiol	3-Heptylcatechol, 4-heptylcatechol	3-Heptylphenol

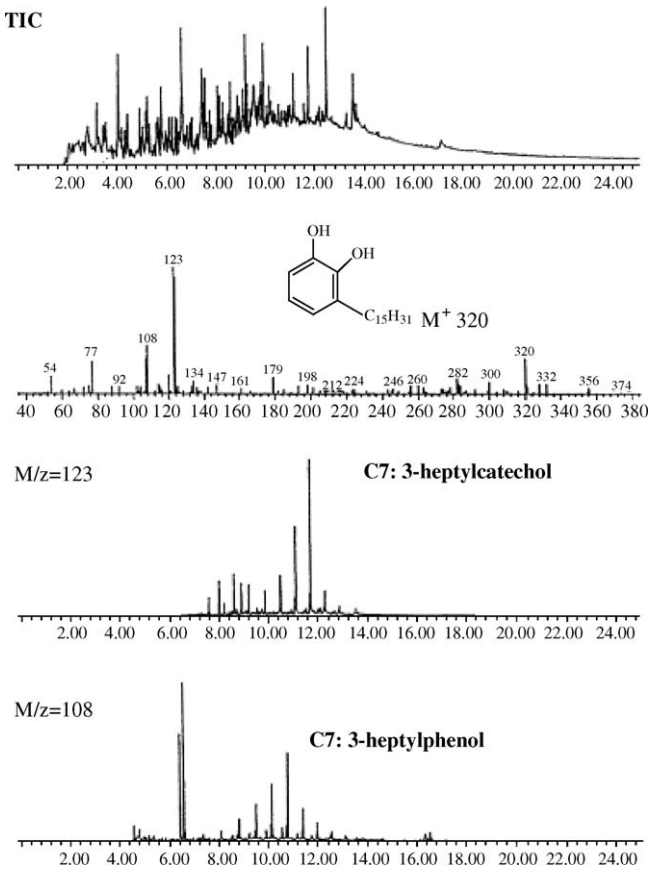

Fig. 6. Pyrolysis data of an ancient lacquer film excavated on the Meiji University campus in Tokyo, Japan.

natural lacquer films. This is a rapid technique that does not require large amounts of sample or sample preparation. The lacquer films were pyrolyzed at 500 °C. The TIC and mass chromatograms of $m/z = 320$ of the lacquer are shown in Fig. 6. Urushiol, 3-pentadecylcatechol (MW = 320), was identified as the monomer of the lacquer film based on the mass spectrum and retention time. This result was compared to those of the three types of oriental lacquers. 3-Pentadecylcatechol of MW = 320 is the saturated urushiol component, which is the monomer of the *R. vernicifera* lacquer. The monomers of the *Rhus succedanea* lacquer are laccol components such as 3-pentadecylcatechol of MW = 348. This was not detected in the ancient lacquer film except for the 3-pentadecylcatechol of MW = 320. The monomer of *M. usitata* lacquer is thitsiol, which has saturated and monoenyl side chains, such as 4-hepatadecylcatechol (MW = 348) and 3- and 4-(ω-phenylalkyl) phenols and catechols, and these components, except for the 3-pentadecylcatechol of MW = 320, were not detected in the ancient lacquer film.

In the TIC and mass chromatograms ($m/z = 108$) of the *Rhus succedanea* lacquer film, alkylphenols were also detected in the old lacquer film. However, two differences were found. The longest side chain of the alkylphenols was C17, and the relative peak intensity of the 3-nonylphenol (C9) was the highest in this film. The TIC and mass chromatograms ($m/z = 108$) of *M. usitata* were different from those of the old lacquer film. It was concluded that the lacquer film obtained from the archeological site is *R. vernicifera* lacquer.

3.4. Py-GC/MS analysis of Nanban lacquer-ware

The *Nanban* lacquer ware was identified using the Py-GC/MS method by comparison with the natural lacquer films. The TIC and the mass chromatograms of $m/z = 60$, $m/z = 123$, and $m/z = 108$ from the pyrolysis products of the sample are shown in Fig. 7.

The mass chromatograms of $m/z = 60$ indicated that the *Nanban* lacquer-ware included a drying oil [24], which was added to retard the rate of hardening and affected the physical properties of the film. The mass chromatograms of $m/z = 108$ and $m/z = 123$ of the pyrolysis products of the lacquer-ware are also shown in Fig. 7. The greatest abundance of peaks was from 3-heptylphenol (C7) and 3-heptylcatechol (C7), as revealed by the mass spectra. It was concluded that the *Nanban* lacquer was made from *R. vernicifera* lacquer sap. Urushiol was not detected because the surface of the *Nanban* lacquer-ware was oxidized by oxygen and light [25]. A type of wax was detected in the mass spectrum of the TIC from the pyrolysis products. It is considered that the wax was used to polish the surface of the lacquer-ware.

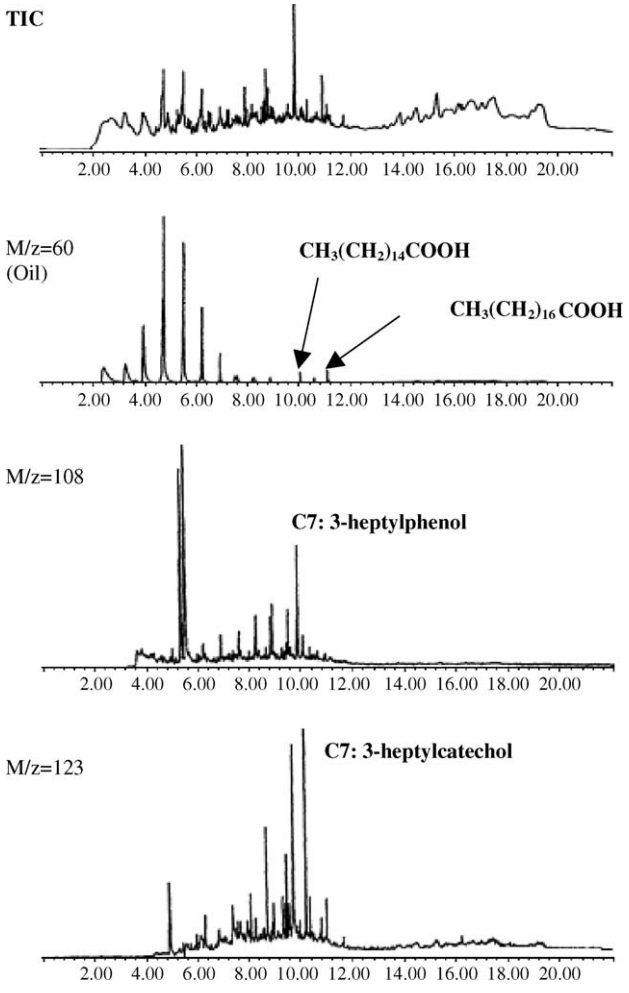

Fig. 7. Pyrolysis data of the *Nanban* lacquer film.

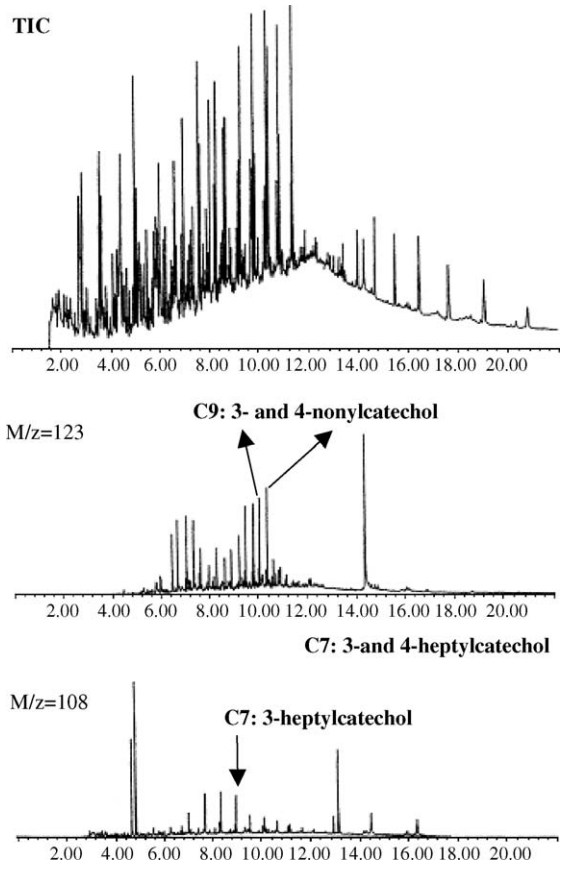

Fig. 8. Pyrolysis data of old lacquer-ware imported from Asia.

3.5. Py-GC/MS analysis of an old lacquer-ware imported from an Asian country

The lacquer-ware object imported from an Asian country was analyzed using the Py-GC/MS method and identified by comparison with the natural lacquer films. The TIC and mass chromatograms of $m/z = 123$ and $m/z = 108$ for the pyrolysis products of the sample are shown in Fig. 8. Alkylcatechols and alkylphenols were detected in the mass chromatograms. The greatest abundance of peaks was due to the 3- and 4-nonylcatechols (C9) and 3-heptylphenol (C7), as determined from the mass spectra. It is concluded that the lacquer-ware was produced using *M. usitata* lacquer sap. Thitsiol was not detected in the pyrolysis data because the surface of the lacquer-ware was oxidized by oxygen and the effect of light [17]. From the TIC and mass spectra of the pyrolysis products, a type of wax was detected. The wax was determined to be a type of bees-wax, as revealed by the mass spectra. The bees-wax was used to protect and polish the surface of the lacquer-ware.

3.6. Py-GC/MS analysis of baroque and rococo lacquer films

The Baroque and Rococo lacquer films were analyzed using the Py-GC/MS method and identified by comparison with the natural lacquer films. The lacquer components were not detected from the TIC on the mass chromatograms of the alkylcatechols

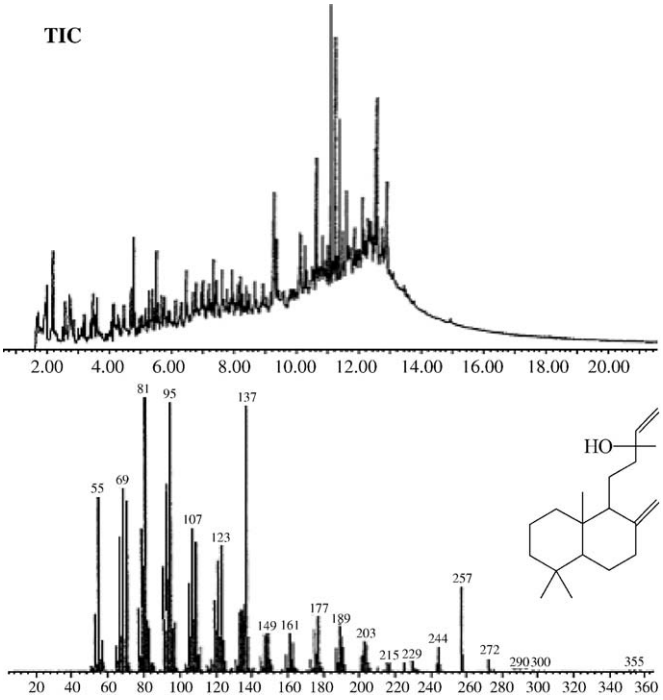

Fig. 9. Pyrolysis data of the Baroque and Rococo lacquer films.

of $m/z = 123$ and alkylphenols of $m/z = 108$ of the pyrolysis products. Monoterpene components and sesqueterpene components were detected [26] in the pyrolysis products of the lacquer ware as shown in Fig. 9. It is concluded that the lacquer ware was made from natural resins. The pyrolysis products of the Baroque and Rococo lacquer and natural resins using this method are under further investigation.

4. Conclusion

It was concluded that 3-pentadecylcatechol (MW = 320) (urushiol), 3-heptadecylcatechol (MW = 348) (laccol), and 4-heptadecylcatechol (MW = 348) (thitsiol) are the main products of the pyrolysis of *R. vernicifera*, *Rhus succedanea*, and *M. usitata*, respectively. Compared with the results of the natural lacquer film, the ancient lacquer film and *Nanban* lacquer film were assigned to *R. vernicifera*, the old lacquer-ware imported from an Asian country that was assigned to *M. usitata*. However, although they were also called "lacquer," the Baroque and Rococo lacquer films were identified as being made from a natural resin. The pyrolysis products clearly showed a good correspondence to the components of the lacquer sap. It was also revealed that the advanced pyrolysis-gas chromatography/mass spectrometry analytical method is useful for identifying and estimating the lacquer components and the original lacquer species. Py-GC/MS is a well-known method applied in various areas. Due to its ease of control, speed of analysis, and good reappearance, the Py-GC/MS method not only can be applied to lacquer films, organic coatings, and other materials that cannot be dissolved in solvents, but also to discriminate between lacquer and other resins for the conservation or restoration of lacquer-ware.

Acknowledgements

The authors are deeply grateful to Dr. M. Kuhlenthal of the Bavarian State Conservation Office in Munich, Germany, and Prof. S. Miura of the Tokyo National Research Institute of Japan, for their invaluable suggestions and discussions. Thanks to Dr. J. Kollor of the Doerner Institute in Munich, Germany, for the gift of the Baroque and Rococo lacquer films and Mr. K. Murose of the Mejiro Lacquer Institute of Research & Restoration in Tokyo, Japan, for donating of the ancient lacquer films. This work was partly supported by Research Project Grant A by the Institute of Science & Technology, Meiji University.

References

[1] E.J. Kidder, Ancient Peoples and Places, Thames and Hudson, Japan, 1959.
[2] Y. Kuraku, in: N.S. Brommelle, P. Smith (Eds.), Lacquer, Getty Conservation Institute, California, USA, 1988, p. 45.
[3] Y.M. Du, in: N.S. Brommelle, P. Smith (Eds.), Lacquer, Getty Conservation Institute, California, USA, 1988, p. 194.
[4] J. Hu, Conservation and Restoration of Cultural Property: Conservation of Far Eastern Objects, Tokyo National Research Institute of Cultural Property, Tokyo, Japan, 1980, p. 89.
[5] K. Toishi, T. Kenjou, Sikizai 40 (1967) 92.
[6] T. Ogawa, T. Yabu, M. Sakamoto, Kobunkazai no kagaku 38 (1993) 37.
[7] T. Egasira, T. Ichikawa, M. Sakamoto, T. Ogawa, Mater. Life 7 (1995) 78.
[8] M. Sasamori, T. Egashira, K. Kuwada, Ishikawaken kogyoushikenjyou kenkyuhoukoku 38 (1990) 38.
[9] J. Kumanotani, Sikizai 70 (1997) 813.
[10] J. Kumanotani, Prog. Org. Coat. 26 (1999) 163.
[11] T. Terada, K. Oda, H. Oyabu, T. Asami, Lacquer—the Science and Practice, Rikou Publisher, Tokyo, Japan, 1999, pp. 25–26.
[12] T. Miyakoshi, K. Nagase, T. Yoshida, Progress of Lacquer Chemistry, IPC Publisher, Tokyo, Japan, 2000, p. 53.
[13] J. Lambert, J. Frye, G. Carriveau, Archaeometry 33 (1991) 87.
[14] J. Kumanotani, Polym. Mater. 59 (1988) 278.
[15] N. Niimura, T. Miyakoshi, J. Onodera, T. Higuchi, Nippon Kagaku-Kaishi (1995) 724.
[16] N. Niimura, T. Miyakoshi, J. Onodera, T. Higuchi, J. Anal. Appl. Pyrolysis 37 (1996) 199.
[17] N. Niimura, T. Miyakoshi, J. Onodera, T. Higuchi, Rapid Comm. Mass Spectro. 10 (1996) 1719.
[18] Y. Kamiya, Y. Niimura, T. Miyakoshi, Bull. Chem. Soc. Jpn. 73 (2000) 2621.
[19] Y. Kamiya, T. Miyakoshi, J. Oleo Sci. 50 (2001) 865.
[20] Y. Kamiya, W. Sato, T. Miyakoshi, J. Oleo Sci. 51 (2002) 473.
[21] R. Lu, S. Harigaya, T. Ishimura, K. Nagase, T. Miyakoshi, Prog. Org. Coat. 51 (2004) 238.
[22] N. Niimura, T. Miyakoshi, J. Onodera, T. Higuchi, Int. J. Poly. Anal. Charact. 4 (1998) 309.
[23] N. Niimura, T. Miyakoshi, J. Onodera, T. Higuchi, Archaeometry 41 (1999) 137.
[24] N. Niimura, N. Kishi, T. Miyakoshi, J. Mass Spectrom. Soc. Jpn. 51 (2003) 229.
[25] Y. Kamiya, R. Lu, T. Kumamoto, T. Honda, T. Miyakoshi, Sur. Interf. Anal., in press.
[26] J. Kollor, B. Baumer, U. Baumer, Sonderheft Metalla, Deutsches Bergbau-Museum Bochum, Buchum, 1997, p. 85.

Available online at www.sciencedirect.com
ScienceDirect
Talanta 70 (2006) 377–382
Talanta
www.elsevier.com/locate/talanta

Investigation of the association behaviors between biliverdin and bovine serum albumin by fluorescence spectroscopy

Yan-li Wei [a], Jian-qing Li [a], Chuan Dong [a,*], Shao-min Shuang [a], Dian-sheng Liu [a,*], Carmen W. Huie [b]

[a] *School of Chemistry and Chemical Engineering, Key Laboratory of Chemical Biology and Molecular Engineering of Ministry of Education, Shanxi University, Taiyuan 030006, PR China*
[b] *Department of Chemistry and The Central Laboratory of the Institute of Molecular Technology for Drug Discovery and Synthesis, Hong Kong Baptist University, Kowloon Tong, Hong Kong, China*

Received 8 November 2005; received in revised form 15 February 2006; accepted 19 February 2006
Available online 31 March 2006

Abstract

The interaction between biliverdin and bovine serum albumin (BSA) has been studied by steady fluorescence spectroscopy, synchronous fluorescence and resonance light scanning spectra. The binding of biliverdin to BSA quenches the tryptophan residue fluorescence and the results show that both static and dynamic quenching occur together with complex formation. The binding constant and binding sites of biliverdin to BSA at pH 7.1 are calculated to be 3.33×10^8 L/mol and 1.54, respectively, according to the double logarithm regression curve. In addition, the distance between the biliverdin and BSA is estimated to be 1.25 nm using Föster's equation on the basis of the fluorescence energy transfer. Furthermore the synchronous fluorescence spectra show that the microenvironment of the tryptophan residues has not obvious changes, which obeys the phase distribution model. Finally, the thermodynamic data show that biliverdin molecules enter the hydrophobic cavity of BSA via hydrophobic interaction.

Keywords: Biliverdin; Bovine serum albumin; Tryptophan fluorescence quenching spectroscopy

1. Introduction

Protein plays an important role in life processes and investigation of the interaction between small molecules and protein has been the focus of extensive research in recent years. The binding between probes and proteins is of ever increasing importance in the pharmaceutical industry, sensor and scientific communities. Albumins, the most abundant protein in the plasma, are characterised by a low content of tryptophan and methionine, a high content of cysteine and preponderance of charged acidic and basic amino acids [1–3]. Serum albumins are the major soluble protein constituents of the circulatory system and have many physiological functions [4]. The most important property of this group of proteins is that they serve as a depot protein and as a transport protein for a variety of compounds. Bovine serum albumin (BSA) has been one of the most extensively studied of this group of proteins, especially of its structural homology with human serum albumin (HSA). BSA is made up of 637 amino acid residues, two of which are tryptophans located at positions 134 and 212 [5]. The structure of albumin at physiological pH is predominantly α-helical (67%) with the remaining polypeptide occurring in turns and extended or flexible regions between subdomains with no β-sheets [6]. The BSA molecule is made up of three homologous domains (I, II and III) which are divided into nine loops (L1–L9) by 17 disulfide bonds. Each of the domains can be divided into 10 helical segments, 1–6 for subdomain A and 7–10 for subdomain B. Domains I and II and domains II and III are connected through helical extensions of 10(I)–1(II) and 10(II)–1(III) creating the two longest helices in albumin. Trp-134 and Trp-212 are in the first and in the second domains, respectively.

From a biopharmaceutical point of view, one of the most important biological functions of albumins is their ability to carry drugs as well as endogenous and exogenous substances,

* Corresponding authors. Tel.: +86 351 7011322; fax: +86 351 7011322.
E-mail address: dc@sxu.edu.cn (C. Dong).

0039-9140/$ – see front matter © 2006 Elsevier B.V. All rights reserved.
doi:10.1016/j.talanta.2006.02.052

and numerous experiments with the aim of characterizing the binding capacity and sites of albumins have been carried out [7,8]. Albumin has a high affinity for fatty acids, amino acids, metals, drugs and pharmaceuticals. Albumin is also the key carrier or reservoir of nitric oxide, which has been implicated in a number of important physiological processes, including neurotransmission [9]. Understanding the full implications of the human genome project and the emerging field of proteomics has introduced new needs to further probe millions of protein interactions. Analysis is based on monitoring the change of a physicochemical property of the protein–probe system upon binding either directly (direct technique) or after separation of the bound and free probe (indirect technique). Among the direct techniques, fluorescence analysis is extensively used and considered to be superior to the indirect techniques (equilibrium and dynamic dialysis, ultrafiltration and gel filtration) because, for example, it does not disturb the binding equilibrium upon separation [10]. The spectral changes observed on the binding of fluorophores with proteins are an important tool for the investigations of the topology of binding sites, conformational changes and characterization of substrate to ligand binding [9]. Besides, determination of protein quantity in biological liquids is of great importance in biology and medicine [2] and fluorescent probes are successfully applied for this approach including Nano-Orange [10] and Ponceau 4R [11]. In addition, the resonance scattering technique has been widely used in the quantitative analysis of protein [12,13].

Biliverdin is reduced to bilirubin by biliverdin reductase. Bilirubin is a bile pigment that may have an important role as an antioxidant. Its antioxidant potential is attributed mainly to the scavenging of peroxyl radicals, and the major oxidation product of bilirubin in plasma is biliverdin. A circular dichroic electrochemical has been employed to study the interaction between bilirubin and bovine serum albumin [14]. Bilirubin has been used as an anti-precipitant against copper to investigate the copper–bilirubin complex [15]. However, few studies have dealt with the interaction between biliverdin and bovine serum albumin, especially by fluorescence spectroscopy. Biliverdin displays fluorescence emission with a maximum absorbance at 457 nm on excitation at 392 nm, which enhanced with the increasing bovine serum albumin. Critical literature survey reveals that attempts have not been made so far to investigate the mechanism of interaction of biliverdin with BSA and this is the first attempt made to probe the mode of association between biliverdin and BSA.

In this paper, the quenching of the intrinsic tryptophan fluorescence of BSA has been used as a tool to study the interaction of biliverdin with this transport protein in an attempt to characterize the chemical associations taking place. Meanwhile, several measurements including fluorescence quenching, absorption spectroscopy, resonance light scattering and synchronous fluorescence spectra serve as aids for better understanding the binding mechanism including hydrophobic interaction and aggregation at the surface of BSA. In addition, the conformational change of BSA is discussed on the basis of synchronous fluorescence spectra.

2. Experimental

2.1. Reagents

Albumin bovine fraction V (+99%, Acros Chemical Corporation) was purchased and used as received. The stock solution of 1×10^{-4} mol/L was prepared by dissolving the solid BSA in double distilled deionized water and stored at 0–4 °C, and diluted to 2×10^{-6} mol/L using Tris–HCl buffer (pH 7.1) when used. The stocking solution of 1×10^{-4} mol/L biliverdin (Frontier Scientific Inc. Chemical Corporation) was prepared by directly dissolving its crystal into 0.05 mol/L sodium hydroxide and stored at 0–4 °C. All other reagents were of analytical purity without further purification and prepared with doubly distilled deionized water.

2.2. Apparatus

The absorption measurement was performed with a UV-265 double-beam spectrophotometer (Shimadzu). The fluorescence and resonance light scattering spectra were carried out on a LS-50B spectrofluorometer (Perkin-Elmer) equipped with a 150 W Xenon lamp source and 1.0 cm quartz cell. The pH meter (pH-S 2 mode) used was made in the 2nd Instrument Factory of Shanghai, China. All experiments were carried out at 20 ± 1 °C.

2.3. Procedure

2.3.1. Fluorescence quenching measurements

The fluorescence intensities were recorded with a Perkin-Elmer LS-50B Luminescence Spectrophotometer using 2.5 nm excitation and 5 nm emission slit widths. To determine the linear concentration range for protein fluorescence, a series of BSA solutions with increasing concentrations (0–5 μM) were prepared in Tris–HCl buffer (pH 7.1). The maximum excitation wavelength (λ_{ex}) and maximum emission wavelength (λ_{max}) for BSA were 282 nm and 345 nm, respectively. The linear range of BSA fluorescence was between 0 μM and 4.4 μM. Therefore, 2 μM BSA was chosen as the concentration for fluorescence quenching experiments.

A dilution series of biliverdin (0.01–0.1 mM) were prepared in a 0.05 mol/L sodium hydroxide solution. For each data point, 0.25 mL of the biliverdin solution was added into 3 mL BSA solution, to give a final biliverdin concentration in the range 0.001–0.015 mM. The reaction time has been investigated and the results showed that 1 min was enough for the stabilization. So the change in fluorescence emission intensity was measured within 1 min of adding biliverdin to the BSA and the concentration of oxygen at the experimental conditions is maintained a constant. The addition of a constant volume of quencher to the protein solution avoided complications due to dilution effects within titration type experiments. Each measurement was repeated in triplicate and the mean and standard deviation were calculated. The fluorescence quenching data were plotted as relative fluorescence intensity against biliverdin concentration. For the calculation of quenching constants, the data were plotted as a Stern–Volmer plot of F_0/F against $[Q]$ and the quenching con-

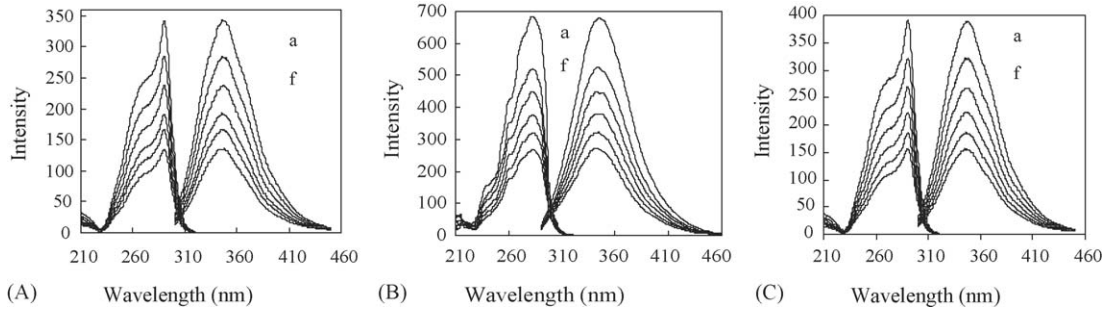

Fig. 1. The fluorescence spectra of BSA (2×10^{-6} mol/L) with the addition of biliverdin at different pH ((A) pH 4.0, (B) pH 7.1, (C) pH 10.0). The concentration of biliverdin (a → f): 0 μM, 1.25 μM, 1.875 μM, 2.5 μM, 3.125 μM and 3.8 μM.

stant was calculated by linear regression. The emission spectra of BSA were also recorded, to allow observation of any changes in the BSA spectra because of the addition of biliverdin at the same concentrations.

2.3.2. Resonance light scattering (RLS) and synchronous fluorescence spectra spectra measurements

By scanning both the excitation and emission monochromator of a common spectrofluorometer with $\Delta\lambda = 0$ nm, a resonance light scanning spectrum can be developed [16], which has been proved to be able to investigate the aggregation of small molecules and the long-range assembly of organic dyes on biological templates [16,17]. All RLS spectra were obtained by scanning simultaneously the excitation and emission monochromator (namely $\Delta\lambda = 0$ nm) from 250 nm to 700 nm with slit widths at 5 nm for the excitation and the emission.

The synchronous fluorescence spectra were obtained by scanning simultaneously the excitation and emission monochromator. The synchronous fluorescence spectra only show the tyrosine residues and the tryptophan residue of BSA when the wavelength interval ($\Delta\lambda$) is 15 nm and 60 nm, respectively [18].

3. Results and discussion

3.1. Fluorescence quenching

The fluorescence of BSA at different pH values with the addition of biliverdin as quencher was obtained (shown in Fig. 1) and the results showed that a gradual decrease in the fluorescence intensity of BSA was caused by quenching but there was no significant emission wavelength shift with the addition of biliverdin, which indicated that the microenvironment around tryptophan in BSA had not changed after interacting with biliverdin.

To interpret the data from fluorescence quenching studies, it is important to understand what kind of interaction takes place between the fluorophore (BSA) and the quencher (biliverdin). If it is assumed that the fluorescence quenching of BSA induced by biliverdin are dynamic quenching process, fluorescence quenching is described by the Stern–Volmer equation

$$\frac{F_0}{F} = 1 + k_q\tau_0[Q] = 1 + K_{SV}[Q] \quad (1)$$

where F_0 and F are the fluorescence intensities of BSA before and after the addition of the biliverdin, respectively, k_q the bimolecular quenching constant, τ_0 the lifetime of the fluorophore in the absence of quencher (for BSA, the lifetime of the fluorophore is approximately 5 ns [19]), $[Q]$ the concentration of biliverdin and K_{SV} is the Stern–Volmer quenching constant. Hence, Eq. (1) was applied to determine K_{SV} by linear regression of a plot of F_0/F against $[Q]$.

A linear Stern–Volmer plot is generally indicative of a single class of fluorophores, all equally accessible to the quencher. In many cases, the fluorophore can be quenched both by collision and by complex formation with the same quencher. When this is the case, the Stern–Volmer plot exhibits an upward curvature, concave toward the y-axis at high $[Q]$ [19], and F_0/F is related to $[Q]$ by the following modified form of the Stern–Volmer equation:

$$\frac{F_0}{F} = (1 + K_D[Q])(1 + K_{SV}[Q]) \quad (2)$$

where K_D and K_{SV} are the dynamic and static quenching constants, respectively. This modified form of the Stern–Volmer equation is second order with respect to $[Q]$, which accounts for the upward curvature observed at high $[Q]$ when both static and dynamic quenching occur.

In our research, both dynamic and static quenching were involved, which was demonstrated by the fact that the Stern–Volmer plot slightly deviated from linearity toward the y-axis at high biliverdin concentrations (Fig. 2). Quenching can also be caused by the formation of a complex between the two compounds after returning from the excited state and that is due to a specific interaction [20]. In the linear range of Stern–Volmer regression curve (see Fig. 2) the average quenching constants for biliverdin (having the lowest quenching effect) at pH 4.0, 7.1 and 10.0 are calculated to be $4.50 \times 10^6\ M^{-1}$, $2.23 \times 10^7\ M^{-1}$ and $4.58 \times 10^6\ M^{-1}$, respectively; thus k_q is $9.00 \times 10^{14}\ M^{-1}\ s^{-1}$, $4.46 \times 10^{15}\ M^{-1}\ s^{-1}$ and $9.16 \times 10^{14}\ M^{-1}\ s^{-1}$, respectively. These values are 10^4–10^5-fold higher than the maximum value possible for diffusion-limited quenching in water ($\sim 10^{10}\ M^{-1}\ s^{-1}$), which suggests that the quenching is not initiated by dynamic collision and that there is a specific interaction occurring between BSA and biliverdin.

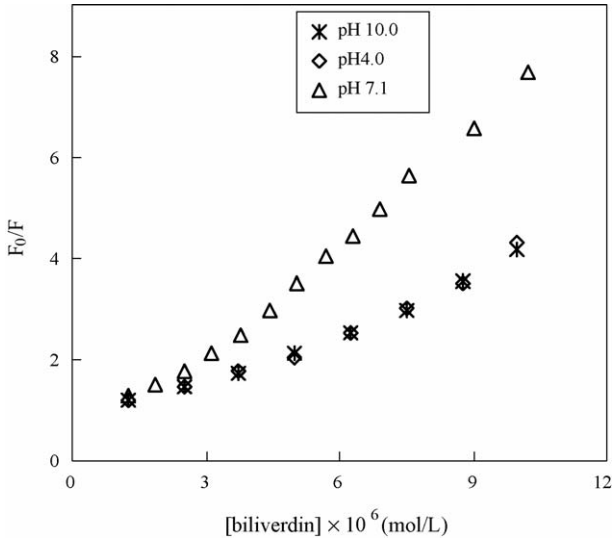

Fig. 2. Stern–Volmer plots describing BSA tryptophan quenching caused by biliverdin at different pH.

3.2. Binding constants of BSA with biliverdin

For the static quenching interaction, if it is assumed that there are similar and independent binding sites in the biomolecule, the binding constant (K_a) and the number sites (n) can be got from the double logarithm regression curve of $\log(F_0–F)/F$ versus $\log[Q]$ based on the following equation, which was deduced in previous report [21]:

$$\log \frac{F_0 - F}{F} = \log K_a + n \log[Q] \quad (3)$$

where K_a is the binding constant of biliverdin with BSA, which can be determined by the slope of double logarithm regression curve of $\log(F_0–F)/F$ versus $\log[Q]$ based on the Eq. (3). The double logarithm regression curve of BSA–biliverdin was linear in the whole small molecule concentration range measured and the binding constant K_a and binding sites n of biliverdin to BSA at pH 4.0, 7.1 and 10.0 were 7.38×10^7 L/mol and 1.46, 3.33×10^8 L/mol and 1.54, 8.79×10^7 L/mol and 1.48, respectively. It is obvious that the binding constant in neutral medium is larger than that in acidic and alkaline medium, while the binding sites are similar at different pH. It can be deduced that biliverdin is suitable for binding to BSA molecule in the neutral medium.

Pyrene is an extremely sensitive fluorescence probe for the micropolarity of organized media: the ratio of the first to the third fluorescence vibronic band (I/III) of pyrene is commonly used to probe the micropolarity of the organized media. As a kind of protein, BSA is present in form of a monomer, dimer and higher oligomers [22]. The values of I/III of pyrene were determined with the increasing of BSA and the results showed it decreased with the BSA concentration and finally approached a minimum value (not shown here). In addition, the monomer fluorescence (350–450 nm) and dimer fluorescence (450 nm) of pyrene existed simultaneously, and it can be deduced that BSA from Acros is a mixture of monomers and dimers. From the calculated binding sites of biliverdin to BSA, it can be deduced that in the BSA dimer there may be three binding sites for biliverdin.

3.3. The binding interaction force between BSA and biliverdin

The structure of a protein is usually determined by several binding interactions, including hydrophobic and electrostatic interactions, van der Waals forces, hydrogen bonds and covalent bonds between cysteines. BSA contains two tryptophan residues with intrinsic fluorescence; Trp-212 is located within a hydrophobic pocket of the protein and Trp-134 is located on the surface of the molecule. Furthermore, these residues are located in separate domains within the BSA molecule. This is significant because the quenching of tryptophan fluorescence does not show a preferential site of interaction, that is, the Stern–Volmer plot does not show deviation from linearity toward the x-axis at high biliverdin [19]. On the contrary, after the linear part, the Stern–Volmer plots show deviation toward the y-axis at high biliverdin concentrations, which is an indication that both static and dynamic quenching occur together with complex formation as discussed earlier [19]. The observation that there was interaction occurring between BSA and biliverdin and that both tryptophan residues were quenched with similar affinities suggests two simultaneous modes of interaction: (i) biliverdin molecules bind within the hydrophobic pockets of BSA and (ii) they surround the protein molecule.

The enthalpy is often taken to be a constant when the temperature of system is changed a little. The fluorescence quenching experiments of BSA by biliverdin were carried out at 293 K, 300 K and 308 K, respectively. The enthalpy and entropy were calculated to be 37.84 J/mol and 10.42 J/mol/K based on the Eqs. (4) and (5). Obviously, both the entropy and the enthalpy were larger than zero. So it can be concluded that the combination between BSA and biliverdin is mainly via the hydrophobic interaction [23].

$$\ln \frac{K_2}{K_1} = \frac{\Delta H}{R}\left(\frac{1}{T_1} - \frac{1}{T_2}\right) \quad (4)$$

$$\Delta G = \Delta H - T\Delta S = -RT \ln K \quad (5)$$

Since the enhancement of RLS is always associated with the aggregation and depends sensitively on the electronic properties of the individual chromophores, biliverdin has three weak RLS peaks at 313 nm, 351 nm and 459 nm. We have proved that BSA has very weak RLS signals in this medium even if its concentration reaches 1×10^{-3} mol/L. In contrast, a strong broad RLS band in this range can be observed for the mixture of biliverdin and BSA, indicating that the interaction between biliverdin and BSA has occurred. Since the enhancement of RLS is always associated with the aggregation and depends sensitively on the electronic properties of the individual chromophores, so it is reasonable to establish the aggregation mechanism of the biliverdin at the surface of BSA. Patra et al. [24] investigated the aggregation of bilirubin in the presence of BSA and definitely showed that the pigment in aqueous solution remained as a mixture of tetramer and monomer in equilibrium. The

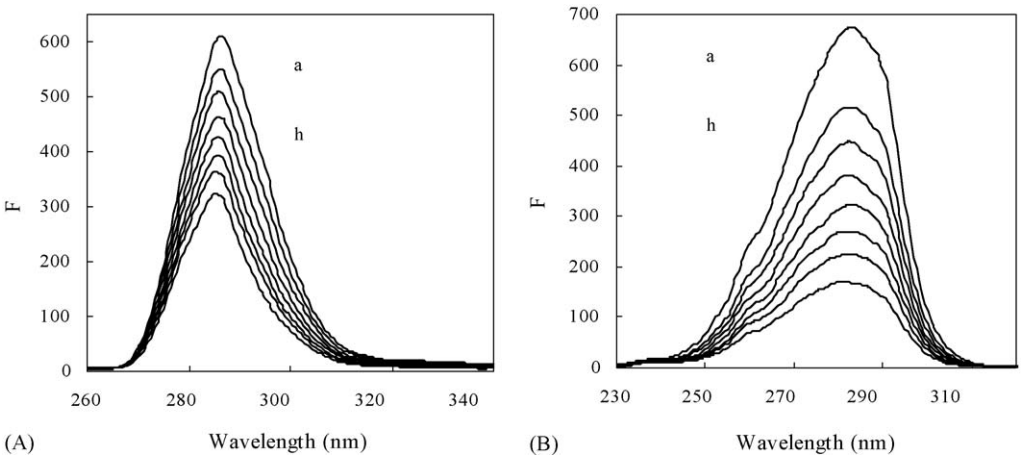

Fig. 3. The synchronous fluorescence spectra of BSA varying the concentration of biliverdin ((A) $\Delta\lambda = 15$ nm and (B) $\Delta\lambda = 60$ nm). The concentration of biliverdin (a → h): 0 μM, 1.25 μM, 1.875 μM, 2.5 μM, 3.125 μM, 3.8 μM, 4.425 μM and 5.05 μM.

aggregation mechanism of biliverdin in BSA system should be explored further. Based on these experimental results, a conclusion can be drawn that the tryptophan residue quenching by biliverdin has two simultaneous modes of interaction including the biliverdin molecules via the hydrophobic interaction entering the hydrophobic cavity of BSA and aggregating at its surface.

3.4. Calculating of binding location between biliverdin and BSA

The distance between biliverdin and tryptophan residue in protein was calculated according to Föster's non-radiative energy transfer theory [25]. Given the fluorescence quantum yield of tryptophan Φ is 0.118, the refractive index N of the medium is the average value of water (equal to1.333) and K^2 is 2/3 for a random orientation, by measuring and calculating the overlapping area between fluorescence emission spectra of BSA and UV absorbance of biliverdin. We can get the critical distance $R_0 = 1.01$ nm when energy transfer efficiency $E = 50\%$, and the actual distance r between them is 1.25 nm. The binding distance (r) is below 7 nm, which accord with the conditions of Föster's non-radiative energy transfer theory. These results indicate again the static quenching interaction between biliverdin and BSA and furthermore suggest that the binding reaction of biliverdin to BSA is through energy transfer which will quench the fluorescence of the protein. From $r = 1.25$ nm, it can be deduced the combination position may be located in a columnar hydrophobic cavity formed by the IV and dimensional structure of BSA [26]. While r is bigger than R_0, the static quenching happened much more possibly than non-radioactive energy transfer. So the static quenching mechanism caused by combining of drugs and protein is responsible mainly for the protein fluorescence quenching process.

3.5. The binding mode between BSA and biliverdin

The interactions of small molecules such as dyes and metal complexes with proteins are an area of considerable interest and activity. When a small molecule binds to protein, there could be a series of binding models: (a) Scatchard model [27], (b) phase distribution model [28] and (c) specific binding and non-specific binding [29].

The absorption of biliverdin at 373 nm was measured increasing the BSA and the value of the absorptive coefficient difference between free and combination ligand ($\Delta\varepsilon$) was calculated to be 5020 L/(mol cm). The absorption value at 373 nm was recorded fixing the concentration of BSA and varying the biliverdin, and the data was dealt with according to ref. [27]. The free concentration of biliverdin (C_F) was calculated on the basis of Eqs. (6) and (7).

$$C_B = \frac{\varepsilon_B C_T - A}{\Delta\varepsilon} \quad (6)$$

$$C_T = C_B + C_F \quad (7)$$

The value of n versus n/C_F is performed and a linear paralleled x-axis was obtained, which accords with the phase distribution model.

3.6. Effect of biliverdin on the protein conformation

Brustein et al. [18] considered that maximum emission wavelength (λ_{max}) of the tryptophan residues is relative to the polarity of microenvironment and the values of λ_{max} are 331 nm, 334 nm and 341 nm when the tryptophan residues located in hydrophobic medium, exposure in water partly and completely. The changes of maximum emission wavelength of the tryptophan residues will reflect the conformation changes of BSA. From Fig. 1, it can be seen that the emission of BSA does not shift with the increasing biliverdin. When considering the effect of biliverdin on the fluorescence spectra of BSA, the maximal emission wavelength of BSA does not apparently shift. This suggests no other change in the immediate environment of the tryptophan residues except the fact that the biliverdin are situated at close proximity to the tryptophan residue for the quenching effect to occur.

The observation that the protein conformation was not affected obviously with the addition of biliverdin was also demonstrated by synchronous fluorescence spectra. The syn-

chronous fluorescence spectra only show the tyrosine residues and the tryptophan residues of BSA when the wavelength interval ($\Delta\lambda$) is 15 nm and 60 nm, respectively. The tyrosine residues and the tryptophan residues of the fluorescence spectra of BSA at various concentrations of biliverdin are shown in Fig. 3(A and B), respectively. It can be seen that no significant shift change on the wavelength was observed, which indicated that the interaction of biliverdin with BSA does not affect the conformation of tryptophan and tyrosine micro-region.

4. Conclusions

Fluorescence method is an important tool for the investigation of the interaction between small probe molecule and protein. The fluorescence of BSA is mainly originated from the tryptophan residues, which can be quenched by biliverdin, and the results showed that both static and dynamic quenching occur together with complex formation. BSA is present in form of a monomer, dimer and higher oligomer. From the calculated binding sites between BSA and biliverdin, it can be deduced that in the BSA dimer there may be three binding sites for biliverdin. Biliverdin can enter the hydrophobic cavity of BSA via hydrophobic interaction and it also aggregates on the surface of BSA, but the microenvironment around the tryptophan residues has not obvious changes during the binding process. The binding mode of biliverdin to BSA is according to phase distribution model. The mechanism of the interaction between biliverdin and BSA is regarded as essential for using as a probe of the biomolecule, and the aggregation mechanism of biliverdin in BSA system should be explored in the future studies. Also, the possibility of BSA quantitative analysis using the RLS enhancement should be pursued based on more comprehensive and in-depth investigation of the basic mechanisms, on which a biosensing method for the determination of BSA can be further studied.

Acknowledgement

Financial support from the National Natural Science Foundation of China (NNSFC: 20575037) is gratefully acknowledged.

References

[1] R.T.A. McGillivray, D.W. Chung, E.W. Davie, Eur. J. Biochem. 98 (1979) 477.
[2] R.G. Reed, F.W. Putnam, T.J. Peter, Biochem. J. 191 (1980) 867.
[3] K. Hirayama, S. Akashi, M. Furuya, K.I. Fukuhara, Biochem. Biophys. Res. Commun. 173 (1990) 639.
[4] X.M. He, D.C. Carter, Nature 358 (1992) 209.
[5] T. Peter, Adv. Protein Chem. 37 (1985) 161.
[6] D.C. Carter, J.X. Ho, Adv. Protein Chem. 45 (1994) 153.
[7] M.A. Kessler, O.S. Wolfbeis, Anal. Biochem. 200 (1992) 254.
[8] J.S. Stamler, D.L. Singel, J. Loscalzo, Science 258 (1992) 1898.
[9] F. Moreno, M. Cortijo, G.J. Jiménez, Photochem. Photobiol. 70 (1999) 695.
[10] M.E. Georgiou, C.A. Georgiou, M.A. Kouppairs, Anal. Chem. 71 (1999) 2541.
[11] H. Zhong, J.J. Xu, H.Y. Chen, Talanta 67 (2005) 749.
[12] R.P. Jia, H.L. Zhai, Y. Shen, X.G. Chen, Z.D. Hu, Talanta 64 (2005) 355.
[13] X.F. Long, S.P. Liu, L. Kong, Z.F. Liu, S.P. Bi, Talanta 63 (2004) 279.
[14] H.Y. Bai, X.Q. Liu, Z.L. Zhang, S.J. Dong, Spectrochim. Acta A: Mol. Biomol. Spectrosc. 60 (2004) 155.
[15] S. Adhikari, R. Joshi, C. Gopinathan, Biochim. Biophys. Acta: Gen. Subjects 1380 (1998) 109.
[16] P.E. Pasternack, C. Bustamante, P.J. Colings, J. Am. Chem. Soc. 115 (1993) 5393.
[17] C.Z. Huang, Y.F. Li, X.D. Liu, Anal. Chim. Acta 375 (1998) 89.
[18] E.A. Brustein, N.S. Vedenkina, M.N. Irkova, Photochem. Photobiol. 18 (1973) 263.
[19] J.R. Lakowicz, Principles of Fluorescence Spectroscopy, second ed., Kluwer Academic/Plenum Publishers, New York, 1999, pp. 60, 121, 698.
[20] J.S. Johansson, R.G. Eckenhoff, L. Dutton, Anesthesiology 83 (1995) 316.
[21] M. Alain, B. Michel, D. Michel, J. Chem. Educ. 63 (1986) 365.
[22] J. Wen, T. Arakawa, J.S. Philo, Anal. Biochem. 240 (1996) 155.
[23] I.M. Klotz, J.M. Urquhart, J. Am. Chem. Soc. 71 (1949) 847.
[24] S.K. Patra, A.K. Mandal, M.K. Pal, J. Photochem. Photobiol. A: Chem. 122 (1999) 23.
[25] L.A. Sklar, B.S. Hudson, R.D. Simoni, Biochemistry 16 (1977) 5100.
[26] S. Dongchul, Y.K. Young, B.C. Jonathan, Process Biochem. 37 (2001) 521.
[27] G. Scatchard, I.H. Scheiberg, S.H. Armstrong, J. Am. Chem. Soc. 72 (1950) 535.
[28] P. Maria, P. Antonella, Talanta 38 (1991) 1099.
[29] T. Zenei, T. Hiroshi, Biochem. Pharmacol. 34 (1985) 1999.

Available online at www.sciencedirect.com
ScienceDirect
Talanta 70 (2006) 383–386
Talanta
www.elsevier.com/locate/talanta

Determination of antihelminthic drug pyrantel pamoate in bulk and pharmaceutical formulations using electro-analytical methods

Rajeev Jain *, Nimisha Jadon, Keisham Radhapyari

School of Studies in Chemistry, Jiwaji University, Gwalior 474011, India

Received 3 December 2005; received in revised form 20 February 2006; accepted 20 February 2006
Available online 5 June 2006

Abstract

Electrochemical behaviour of pyrantel pamoate has been studied by using different voltammetric and polarographic techniques in Britton Robinson buffer system. Differential pulse polarographic and cyclic voltammetric methods have been developed for the determination of drug in pharmaceutical formulation. A well-defined cathodic wave and one anodic peak were observed for the pyrantel pamoate in the entire pH range. Number of electrons transferred in the reduction process was calculated and the reduction mechanism postulated. The results indicate that the electrode process is reversible and diffusion controlled. The proposed method has been validated. The peak current is found to be linear over the concentration range 4×10^{-4} to 2×10^{-2} mol L^{-1}. The lower detection limit (LOD) and lower limit of quantitation (LOQ) is found to be 2.45×10^{-5} and 8×10^{-5} mol L^{-1}.

Keywords: Pyrantel pamoate; Electrochemical studies; Pharmaceutical formulation; Antihelminthic drug; DPP

1. Introduction

Multiple helminthic infections are frequently encountered in general population and especially in the Korean populations [1]. Rim et al. [2,3] and other workers have shown that pyrantel pamoate [A] is very effective against *A. lumbricoides*, hookworms, *T. orientalis* and *E. vermicularis*.

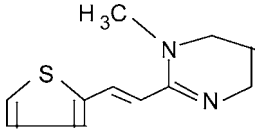

[A]

Pyrantel pamoate [1,4,5,6-tetrahydro-1-methyl-2-[2-(2-thienyl) ethenyl] pyrimi-dine] [A] could be effectively used to control serum mineral levels in children with intestinal parasitic infection [4]. Pyrantel pamoate shows maximum activity towards pigs as compared with its citrate form, i.e. pyrantel citrate [5]. Another interesting aspect of pyrantel pamoate is the improvement in appetite and growth in helminth-infected schoolboys 3 and 7 weeks after a single dose of pyrantel pamoate [6].

The anthelmic action of pyrantel pamoate is due to the inhibitions of neuromuscular transmissions, which paralyzes the helminth and force it to be expelled through the feces. Also it inhibits cholinesterases and it is poorly absorbed from gastrointestinal (GI) track. Side effects of pyrantel pamoate include skin rashes, abdominal cramps, diarrhea, nausea or vomiting, headache, dizziness, drowsiness and insomnia [7].

Pyrantel pamoate is the subject of a monograph in the US Pharmacopoeia USP [8]. The USP [8] on the other hand described chromatographic methods for both the drug and its formulations. Survey of literature reveals that pyrantel pamoate has been analyzed in bulk samples and pharmaceutical formulations by spectrophotometry [9] and in dog plasma by high performance liquid chromatography (HPLC) with a detection limit of 15–25 ng mL^{-1} [10]. HPLC was applied to the analysis of pyrantel pamoate in human plasma [11] using UV detector. Chromatographic methods developed for pyrantel pamoate [9,10] demand expensive equipment and could not be available in many laboratories.

Electrochemical methods [12,13], such as differential pulse polarography (DPP) [14,15], anodic stripping voltammetry

* Corresponding author. Tel.: +91 751 2346209; fax: +91 751 2346209.
E-mail address: rajeevjain54@yahoo.co.in (R. Jain).

0039-9140/$ – see front matter © 2006 Elsevier B.V. All rights reserved.
doi:10.1016/j.talanta.2006.02.061

(ASV) [16,17] and differential pulse voltammetry (DPV) [18,19] have been widely applied for the determination of pharmaceuticals. In general these methods offer high sensitivity, low limit of detection, easy operation and sometimes the use of simple instrumentation. The voltammetric behaviour of fenbendazole a benzimidazole-carbamate compound used for combating a broad spectrum of helmintic species in human and veterinary [20] at glassy carbon electrode [21] has been reported to exhibit a well-defined irreversible oxidation peak at 1.15 V versus SCE. Potentiometric determination of pyrantel pamoate has also been reported [22] using ion selective electrodes and detection limit of 1–2 $\mu g\,mL^{-1}$ of the drug has been claimed.

A perusal of literature reveals that so far no systematic and comprehensive electrochemical study of pyrantel pamoate has been undertaken. In the present study, the electrochemical behaviour of pyrantel pamoate has been studied using various electro-analytical techniques. Voltammetric methods have been developed for the determination of pyrantel pamoate in bulk samples. The results obtained are promising and demonstrate the utility of the developed method in determining the content of active substances in pharmaceutical preparations.

2. Experimental

2.1. Reagents and materials

Pyrantel pamoate (99% purity) was obtained from IPCA, pharmaceutical company, Ratlam, India and was used as-received. Tablets containing pyrantel pamoate (Nemocid) labeled 250 mg pyrantel pamoate were obtained from commercial sources. KCl (1 mol L^{-1}) solution was prepared in distilled water and used as supporting electrolyte. A stock solution of pyrantel pamoate (2×10^{-2} mol L^{-1}) was prepared in dimethyl formamide (DMF). The solutions for recording voltammograms were prepared by mixing appropriate volume of stock solution and buffer of varying pH. Britton Robinson buffers in the pH range 2.5–12.0 were prepared in distilled water by adding suitable amounts of 0.4 M NaOH solution (basic solution) to a stock solution composed of a mixture of 2.14 mL phosphoric acid, 2.472 g boric acid and 2.3 mL of glacial acetic acid (acidic solution). Solution was stirred after mixing and left overnight to attain equilibrium. All reagents used were Anal R grade.

2.2. Apparatus

The polarographic and differential pulse polarographic (DPP) measurements were carried out using the ELICO CL362 Polarograhic Analyser (India). The drop time of 1 s was electronically controlled using a 663 VA Stand from the company. The polarograms were recorded using a potential scan rate of 50 mV s^{-1}. A three-electrode system composed of a dropping mercury electrode (DME), saturated calomel electrode (SCE) as reference electrode and platinum as the auxiliary electrode was used. The solutions were purged with pure nitrogen gas for 10 min and then polarographed at ambient temperature.

The voltammetry experiments were performed using an EG&G Princeton Applied Research Model 273A potentiostat controlled by the model 270/250 Research Electrochemistry Software 4.30. A three-electrode system was composed of a glassy carbon-working electrode ($\phi = 2$ mm EG&G/PAR), Ag/AgCl reference electrode and a platinum auxiliary electrode.

To provide a reproducible active surface and improve the sensitivity and resolution of the voltammetric peaks the working electrode was polished with 0.5 μm alumina powder on a polishing cloth prior to each electrochemical measurement. Then it was thoroughly rinsed with methanol and double distilled water and gently dried with a tissue paper. The electrode cleaning procedures required only 2 min. All the solutions examined by electrochemical technique were purged for 10 min with purified nitrogen gas after which a continuous stream of nitrogen was passed over the solutions during the measurements. All measurements were carried out at room temperature. The pH metric measurements were made on Decible, Db-1011 digital pH meter fitted with a glass electrode and saturated calomel electrode as reference, which was previously standardized with buffers of known pH in acidic and alkaline medium. Ready made precoated TLC alumina plates from E Merck, Germany were used for TLC separation and IR spectra were recorded at Shimadzu Prestige IR 20.

2.3. Procedure

The amount of pyrantel pamoate present in each tablet was 250 mg. Excipients such as microcrystalline cellulose, hydroxypropyl methylcellulose, lactose and titanium dioxide are added to dosage forms. Ten tablets were weighted accurately and crushed to a fine powder. The accurately weighted quantities of these powders equivalent to 2.5 g of pyrantel pamoate were transferred to 50 mL volumetric flask. Dimethylformamide (99.5%) 40 mL was added to dissolve the active material. After sonicating and shaking the mixture for 30 min, it was completed to volume with the same solvent, mixed and centrifuged. An aliquot of the supernatant liquid was then transferred into a calibrated flask and a series of dilutions were prepared with BR buffers at pH 2–12 and mixed 1 mL KCl as supporting electrolyte having 50% DMF. The content of the drug in pharmaceutical preparations was determined using calibration graph.

3. Results and discussion

The voltammetric behaviour of pyrantel pamoate has been examined in the pH range 2.0–12.0 employing DC, DPV and CV techniques. A typical differential pulse polarogram has been depicted in Fig. 1. Pyrantel pamoate gave one well defined cathodic peak and one anodic peak at far off positive potential in the entire buffer range studied. The influence of several electrolytes (Phosphate & Britton–Robinson) on the analytical signal was also studied. With the rise in pH peak potential shifted towards more negative values indicating the participation of proton in the electrode process.

On the basis of the electrochemical reduction of pyrantel pamoate at DME, analytical method was developed involving DPP and DC for the determination of the drug. A linear relation between peak current and pyrantel pamoate conc. was found in

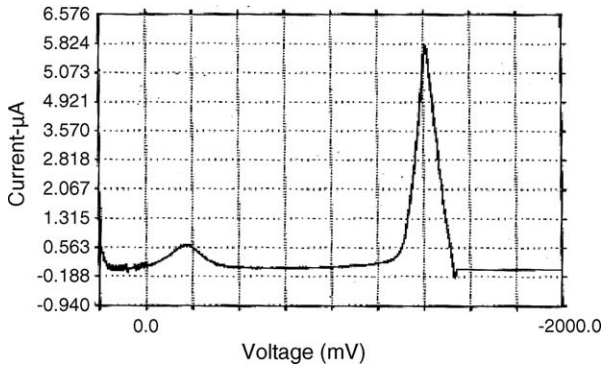

Fig. 1. Differential pulse polarogram for 4.00×10^{-4} mol L^{-1} pyrantel pamoate in Britton–Robinson buffer 4.6, pulse amplitude 50 mV s^{-1}.

the range 4×10^{-4} to 2×10^{-2} mol L^{-1}. The linear regression equation is expressed as $[i_p\ (\mu A) = (5.01 \times 10^3 \pm 2.0 \times 10^{-2})\ C(\text{mol L}^{-1}) - 15.47 \pm 1.5 \times 10^{-4}\ A]$, where i_p is peak current in µA and C is the concentration in mol L^{-1} with good correlation ($r^2 = 0.9931$).

The peak height increased linearly of both bulk and pharmaceutical formulation in pulse amplitude from 5 to 100 mV and the peak potential shifted towards positive potential.

The reversibility of the reduction process was studied at CV, where an anodic peak was obtained at far off positive potential in the entire pH range studied. Cyclic voltammograms at different concentrations of pyrantel pamoate at scan rate 50 mV s^{-1} at pH 7.9 are given in Fig. 2. As the peak current ratio ($i_p{}^{ox}/i_p{}^{red}$) is unity and independent of υ, it indicates reversible nature of the electrode process [23].

The study of the influence of scan rate shows that the peak current changes linearly with scan rate. The reduction peak is shifted to more negative potential and oxidation peak towards positive potential with increase in scan rate. From the plot of i_p versus $\nu^{1/2}$ (where i_p is the peak current and $\nu^{1/2}$ is scan rate) for oxidation linear regression equation is expressed as $[i_{pa}\ (\mu A) = (10.94 \pm 25\ \mu V)\ \nu^{1/2}(\text{mVs}^{-1}) + (4.2125 \pm 3 \times 10^{-4}\ A)\ i_{pa}]$ with good regression ($r^2 = 0.9915$) and reduction $[i_{pc}(\mu A) = -(11.195 \pm 25\ \mu V)\ \nu^{1/2}(\text{mVs}^{-1}) - (0.3481 \pm 3 \times 10^{-4}\ A) i_{pc}]$ wave between 50 and 500 mV s^{-1} with good correlation ($r^2 = 0.9915$), confirming the diffusion controlled nature of the electrode process.

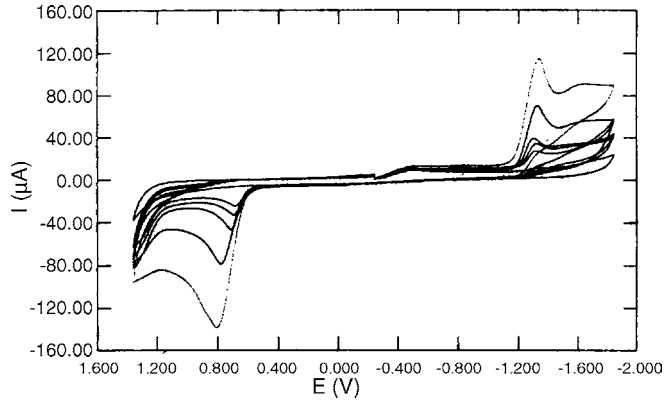

Fig. 2. Cyclic voltammograms at different concentrations (1×10^{-5} to 5×10^{-3} mol L^{-1}) of pyrantel pamoate at scan rate 50 mV s^{-1}, pH 7.9.

Further, diffusion-controlled and adsorption free nature of the electrode process in the buffer systems studied, is evidenced from the linear plot of i_m versus $t^{2/3}$ (where i_m is the maximum current in DPV, t is the drop time). According to the equation $i_p = 4\upsilon^x$, the x values 1 and 0.5 are expected for adsorption control and diffusion control reaction. The regression of i_p versus log $\upsilon^{1/2}$ gave a slope value of 0.99 indicating that the reduction current is diffusional in nature.

A comparison of limiting current at various pH indicates that the compound is reduced in pH range 2.5–12 by consuming identical number of electrons. The shift in E_p towards more negative potential with pH up to 8.0 was observed and after that there is almost consistency in peak potential. In the basic buffers of pH > 7.9, the curves are drawn out which may be due to the non-availability of protons and are not of any use for analytical purposes. This pH dependence of E_p till pH 8.0 suggests the participation of proton in rate determining step.

Controlled potential coulometry was carried out for the identification of reduction products. 2.0 mL of 1×10^{-2} mol L^{-1} solution of the electro-active species was placed in the cell and the electrolysis were carried out at a potential −1.4 V (versus Ag/$AgCl^-$) for respective compound at pH 7.0. During the electrolysis, solution were continuously stirred and purged with nitrogen. Cathodic peak has been attributed to the reduction of exo-cyclic unsaturated –C=C– bond in two electron process. Millicoulometry was employed to find out the number of electrons involved in the electrode process using the method of De Varies and Kroon [24] and was found to be two in the entire pH range studied. Pulse polarography and CV studies in conjunction with coulometric studies and TLC results confirm the formation of only one product. Before and after the electrolysis the products were analyzed by IR studies. The results indicate that the product is a saturated product of C=C bond.

4. Reaction mechanism

On the basis of DCP, DPP, CV, Cpc, coulometry, chromatographic and spectral studies following ECE type mechanism may be postulated for the reduction of pyrantel pamoate.

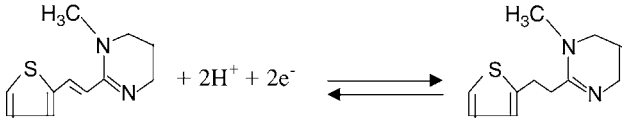

5. Analysis of pharmaceutical formulations

The applicability of the proposed voltammetric method for the sample dosage form was examined by analyzing Nemocid tablet (250 mg). The amount of the compound in the tablets was calculated by standard addition method. The accuracy and precise results obtained for the formulation pyrantel pamoate was found to be in good agreement with that of the declared values of drug taken from formulations. The effect of excipients on the voltammetric response of pyrantel pamoate was studied using

Table 1
Statistics and performance characteristics of the analytical method from the calibration data set

Standard				Tablet			
I (μA)	$(x-\bar{x})^2$	E (V)	$(x-\bar{x})^2$	I (μA)	$(x-\bar{x})^2$	E (V)	$(x-\bar{x})^2$
6.2785	0.00038	−1366	5.76	6.320	0.0003	−1371	0.16
6.2685	0.00009	−1366	5.76	6.3224	0.00007	−1372	0.36
6.2835	0.00006	−1366	5.76	6.300	0.00019	−1370	1.96
6.1637	0.009	−1372	12.96	6.2956	0.00033	−1372	0.36
6.3005	0.0017	−1372	12.96	6.332	0.00032	−1372	0.36
$\sum x$	$\sum (x-\bar{x})^2$	$\sum x$	$\sum (x-\bar{x})^2$	$\sum x$	$\sum (x-\bar{x})^2$	$\sum x$	$\sum (x-\bar{x})^2$
6.2589	0.0117	−1368.4	43.2	6.314	0.0094	−1371.4	3.2
R.S.D. = 0.0086		R.S.D. = 0.024		R.S.D. = 0.0024		R.S.D. = 0.0065	
CV = 0.86		CV = 0.24		CV = 0.24		CV = 0.065	

the above process. It was found that microcrystalline cellulose: hydroxypropyl, methylcellulose, lactose and titanium dioxide did not interfere with assay. Therefore, the proposed method can be used as a selective method.

6. Calibration graph and detection limit

A linear relationship was found over the concentration range 4×10^{-4} to 2×10^{-2} mol L^{-1}. The limit of detection is given by the expression LOD = 3 S.D./m [25], where S.D. is the standard deviation of replicate determination values and 'm' is the slope of the calibration curve. Now S.D. = 0.0086 and $m = 1.762 \times 10^{-1}$, hence LOD = 2.45×10^{-5} mol L^{-1}. The LOQ is defined as 10 S.D./m [25], and was found to be 8.17×10^{-5} mol L^{-1}. In order to validate and to obtain the precision and accuracy of the developed method, recovery studies have been carried out at different concentration levels. The amount of pyrantel pamoate present in corresponding solution was calculated from the calibration equation. The analysis of pyrantel pamoate in its pharmaceutical formulation exhibited the mean recovery of 100.4% and the relative standard deviation of 0.86% indicating adequate precision and accuracy of the proposed method. The performance data of the proposed method have been tabulated in Table 1. Furthermore, in an earlier spectrophotometric determination pyrantel pamoate [26] could be determined in the range 2.5–25 μg mL^{-1} but in the present developed electrochemical method it could be estimated to a level of 1.4 μg mL^{-1} without any prior extraction process which is the essential part of determination with other instrumental methods.

7. Conclusion

The proposed methodology provides a very sensitive and selective method of pyrantel pamoate analysis that was developed in this work allows quantitative determination of the compound in pharmaceutical dosage forms. The analytical results obtained by DPP and CV are adequately accurate and precise and are in good agreement with those obtained by other techniques. As low as 8×10^{-5} mol L^{-1} of pyrantel pamoate was accurately measured by the proposed methods. The main advantage of new method is its higher sensitivity and because of the possibility of higher sample dilution, less influence of matrix effects. Consequently, the proposed method has a potential of a good analytical alternative for determining pyrantel pamoate in pharmaceutical formulations.

References

[1] H.J. Rim, S.H. Lee, S.I. Lee, D.S. Chang, Korean J. Parasitol. 16 (1978) 14.
[2] H.J. Rim, J.K. Lim, Trans. Roy. Soc. Trop. Med. Hyg. 66 (1972) 170.
[3] H.J. Rim, J.K. Lim, Asian J. Med. 9 (1973) 393.
[4] J.L. Olivares, R. Fernandez, J. Heta, G. Rodrignez, A. Clavel, Dig. Dis. 21 (2003) 258.
[5] H. Bjorn, D.R. Hennessy, C. Fris, Int. J. Parasitol. 26 (1996) 1375.
[6] V. Hadju, L.S. Stephenson, K. Abadi, H.O. Mohammed, D.D. Bowman, R.S. Parker, Parasitology 113 (1996) 497.
[7] F.S.K. Barar, Essentials of Pharmacotherapeutics, S. Chand & Company Ltd., New Delhi, India, 2003, p. 459.
[8] The US Pharmacopocia, The National Formularly, USP 24. NF 19, USP Convention Inc. 12601, Twinbrook Parkway, Rockville, MD, 2005, p. 1678.
[9] G.A. Forcier, R.F. Mushinsky, R.L. Wagner Jr., J. Pharm. Sci. 60 (1971) 111.
[10] G. Morovjan, P. Csokan, L. Makromszki, E.A. Abdellah Nagy, K. Toth, J. Chromatorg. A 27 (797) (1998) 237.
[11] A.A. Fasanmade, A.O. Akamni, A.A. Olaniyi, A.A. Fasanmade, F. Jayo, Biopharm. Drug Dispos. 15 (1994) 527.
[12] A.J. Bard, H. Lund, Encyclopedia of Electrochemistry of the Elements, vol. XII, Marcel Decker, Inc., New York, 1978, p. 453.
[13] A.J. Bard, L.R. Faulker, Electrochemical Methods: fundamentals and applications, John Wiley & Sons Inc., New York, 2002, p. 213.
[14] F. Ibrahim, N. El-Enany, J. Pharm. Biomed. Anal. 32 (2003) 353.
[15] H. Abdine, F. Belal, Talanta 56 (2002) 97.
[16] A.M. Beltagi, J. Pharm. Biomed. Anal. 31 (2003) 1079.
[17] U. Tamer, N.P. Ozcicek, O. Atay, A. Yildiz, J. Pharm. Biomed. Anal. 29 (2002) 43.
[18] O.A. Razak, J. Pharm. Biomed. Anal. 34 (2004) 433.
[19] R.F. Torres, M.C. Mochon, J.C. Jimenez Sanchez, M.A. Bello Lopez, A.G. Perez, Talanta 53 (2001) 1179.
[20] D.S. Nakos, N.A. Botroglou, I.E. Psomas, J. Liq. Chromatogr. 19 (1994) 4145.
[21] M.F.D. Oliveria, N.R. Stradiotto, J. Pharm. Biomed. Anal. 30 (2002) 279.
[22] R. Aubeck, N. Hampp, Anal. Chim. Acta 256 (1992) 257.
[23] H. Lund, M.M. Baizer, Organic Electrochemistry, third ed., Marcel Dekker, NY, 1990, p. 131.
[24] T. De Varies, J.L. Kroon, J. Am. Chem. Soc. 75 (1953) 2484.
[25] B. Uslu, S.A. Ozkan, Anal. Chim. Acta 462 (2002) 49.
[26] K. Basavaiah, H.C. Prameela, Chem. Anal. 48 (2003) 327.

Available online at www.sciencedirect.com
ScienceDirect
Talanta 70 (2006) 387–391
Talanta
www.elsevier.com/locate/talanta

Simultaneous analysis of ellagic acid and coenzyme Q_{10} by derivative spectroscopy and HPLC

D. Venkat Ratnam, V. Bhardwaj, M.N.V. Ravi Kumar *

Department of Pharmaceutics, National Institute of Pharmaceutical Education and Research (NIPER), Phase-X, S.A.S. Nagar, Mohali 160062, Punjab, India

Received 1 February 2006; received in revised form 20 February 2006; accepted 20 February 2006
Available online 31 March 2006

Abstract

Antioxidants are gaining tremendous interest as chemopreventive as well as chemotherapeutic agents. Ellagic acid (EA) is a plant derived compound with very poor solubility in water and very low octanol/water partition coefficient and coenzyme Q_{10} (CoQ_{10}) is a highly lipophilic compound, which is synthesized in the body and can be derived from food supplements as well. The new insights in the combination therapy are promising a better future in many challenging diseases. Synergism is among the key advantages of combination therapy apart from decreased intensity of unwanted effects of a compound, increased patient compliance and reduction in cost of therapy. EA and CoQ_{10} supplementation in combination will be beneficial in strengthening the weakened antioxidant defense system in many diseases related to oxidative stress. Here we report first derivative UV spectroscopic and HPLC methods for the simultaneous analysis of these two agents in pharmaceutical preparations. Results obtained indicate that the derivative spectroscopy is as efficient as HPLC method in quantitative analysis. Retention of ellagic acid can be increased using PEG bonded column which is poorly retained on C_{18} column. PEG column can be used for rapid simultaneous analysis of EA and CoQ_{10}, which are having diverse physicochemical properties.

Keywords: Ellagic acid; Coenzyme Q_{10}; Derivative spectroscopy; HPLC; PEG bonded column

1. Introduction

Antioxidants are the substances which counter act free radicals and prevent the damage due to oxidants by crumbling them before they react with biological targets, preventing chain reactions or preventing the activation of oxygen to highly reactive products [1]. A hypothesis states that various common diseases of modern civilization are rooted in a chronic divergence between our ancient nutritional programming and our contemporary dietary input. A key disparity between dietary supply and physiological need may be in antioxidant nutrients [2]. Adding to this, in modern day environment people are exposed to a variety of toxins, which can be potent oxidants. If one combines the increasing environmental pressure of oxidants with unbalanced contemporary food supply, the value of antioxidant supplementation becomes apparent.

Ellagic acid (EA) and coenzyme Q_{10} (CoQ_{10}) are among the potential antioxidants, which can be formulated. These agents have been proved to have potential preventive and therapeutic effects in many diseases, where the oxidative stress has been implicated, like cancer, cardiovascular diseases, neurodegenerative disorders and in aging. EA is a naturally occurring polyphenolic constituent found in different fruits and nuts, like pomegranate, red raspberry, strawberry, blueberry and walnuts. It is the most explored phenolic acid compound, which is known to possess a variety of pharmacological and biological activities such as antioxidant, antimutagenic, antitumor, antihyperglyceamic and antiinfective effects. Several mechanisms are responsible for the above-mentioned effects, like increased detoxification of pre-carcinogens and/or active metabolism by inhibition of cytochrome P450 enzymes, stimulation of glutathione-S-transferase, ability to scavenge reactive metabolites of carcinogens. Preventing the destruction of the p53 gene by cancer cells thus inhibiting the mutagenesis and

* Corresponding author. Tel.: +91 172 2214683–89x2055; fax: +91 172 2214692.
E-mail addresses: mnvrkumar@niper.ac.in, mnvrkumar@yahoo.com (M.N.V.R. Kumar).

0039-9140/$ – see front matter © 2006 Elsevier B.V. All rights reserved.
doi:10.1016/j.talanta.2006.02.057

ability to mask the binding sites to be occupied by the mutagen or carcinogen by formation of adducts with DNA are among the other mechanisms [3–5].

On the other hand CoQ_{10} is an endogenous compound found in every cell. It is found in relatively higher concentrations in cells with high-energy requirements such as heart, liver, muscles and pancreas. It acts as a potent antioxidant by neutralizing the cell-damaging free radicals and it helps convert food into energy. Several studies have revealed the potentials of this compound in prophylaxis and therapy of various disorders related to oxidative stress. CoQ_{10} deficiency has been confirmed in patients with cardiovascular disorders and cancers. Animal studies have demonstrated that administration of CoQ_{10} reduces tumor size and increased survival in mice exposed to chemical carcinogens. In humans, high dose of CoQ_{10} (i.e. 390 mg per day) resulted in complete remission of metastatic breast cancer [6,7]. Circulating concentrations of this coenzyme decrease with age [8]. All these reports illustrate the advantages of CoQ_{10} supplementation.

EA and CoQ_{10} individually are reported to be good for cardiovascular complications and our interest is in identifying the synergism of this combination, keeping in mind the high cost of CoQ_{10}. The aim of the present study was to simultaneously analyze EA and CoQ_{10} using ultraviolet (UV) spectroscopy and high performance liquid chromatography (HPLC). The absorption of UV radiation by CoQ_{10} was very low when compared with that of ellagic acid at similar concentrations, which made it difficult for the analysis of these compounds simultaneously by zero order UV spectroscopy, where the absorbance values were utilized without derivatization. Derivative spectroscopy which is popularly used for the simultaneous analysis of pharmaceutical agents [9,10] was investigated for the analysis of these two agents. HPLC method was also developed for the simultaneous analysis of these agents using poly(ethylene glycol) (PEG) bonded stationary phase column. The derivative spectroscopic method was compared for the linearity, accuracy and precision with the HPLC method.

2. Experimental

2.1. Chemicals

Ellagic acid (assay 95%) was purchased from Sigma, US. Coenzyme Q_{10} is a gift sample from Tishcon Corporation (Westbury, NY). The solvents used for the first derivative UV method were of analytical grade and mobile phases used for HPLC method development were of HPLC grade. Wherever required water obtained from the reverse osmosis was utilized. Molecular weight of EA (320.20) is low when compared with that of CoQ_{10} (863). Partition coefficient of ellagic acid in octanol/pH 7 phosphate buffer is very low (0.27 ± 0.01) [3].

2.2. First derivative UV method

Standard stock solution of 50 μg/ml was prepared by dissolving accurately weighed amounts of EA and CoQ_{10} in required volume of methanol first and then the volume is made up with water such that the final solutions are of 40% methanol. Working standards were prepared using 40% methanol. UV scans were taken using a quartz cuvette with 1 cm path length. The solutions were scanned using double beam UV–vis spectrophotometer (Specord 200) from 190 to 500 nm at a speed of 50 nm/s. Then these were subjected to derivatization using WinAspect software to generate first derivative spectra with simultaneous smoothing of the scans at 25 base points. The wavelengths identified and implied for the development of this method were ^{1}D223 and ^{1}D383 nm for CoQ_{10} and EA, respectively (Fig. 1).

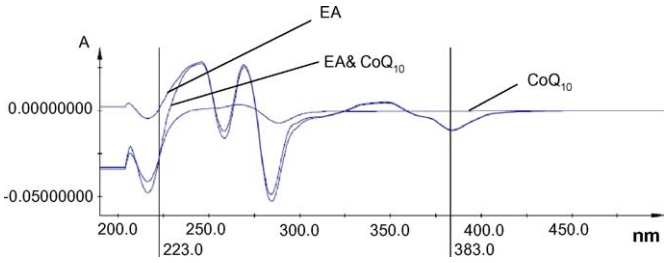

Fig. 1. First derivative spectra of ellagic acid, coenzyme Q_{10} and the mixture containing these two drugs. Zero crossing points can be seen as 223 nm for EA and 383 nm for CoQ_{10}. At these points mixture has the same value of interested compound for the analysis indicating least interference of the other compound.

2.3. HPLC method

A new HPLC method was developed for the simultaneous analysis of EA and CoQ_{10} using Supelco Discovery® HS PEG column, 25 cm × 4.6 mm, 5 μm (Supelco, Bellefonte, PA, USA) maintained at 40 °C. Elution of both the compounds is achieved using gradient mobile phase (Table 1). The mobile phase was acetonitrile–ethanol–5 mM potassium dihydrogen orthophosphate buffer (pH 2.5) (70:15:15, v/v/v) for 15 min except for 2.5–7 min where acetonitrile–ethanol (30:70, v/v) was used instead. Standard solutions and working standards were prepared in methanol. Analysis was performed using Waters HPLC system (717plus auto sampler and 600 controller) with Millenium software[32], coupled to photo diode array detector (996). Wavelengths 254 and 275 nm were selected, respectively, for EA and CoQ_{10} where they showed maximum absorbance. Mobile phases were filtered through 0.45 μm nylon filter and degassed using ultrasonic bath sonicator for 30 min before the experiment.

Table 1
Mobile phase gradient for HPLC method

Time (min)	Acetonitrile	Buffer[a]	Ethanol	Curve type[b]
0	70	15	15	1
2.5	70	15	15	1
7	30	0	70	1
15	70	15	15	1

[a] 5 mM potassium dihydrogen phosphate buffer (pH 2.5).
[b] As specified in Millenium software[32].

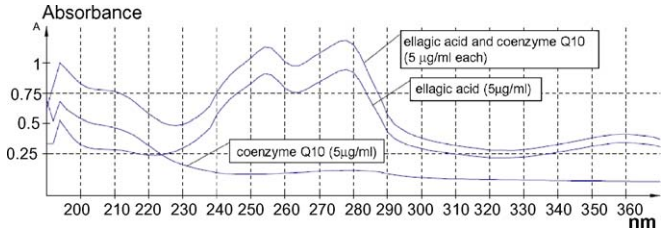

Fig. 2. Zero order UV scans of ellagic acid, coenzyme Q10 and the mixture containing these two drugs.

Table 2
UV method for the simultaneous analysis of EA and CoQ_{10}

Parameters	Values	
	Ellagic acid	Coenzyme Q_{10}
Linearity range (µg/ml)	0.5–14	0.5–20
Linearity (r^2)	0.9995	0.9993
Slope	0.0014	0.0027
Intercept	0.000205	0.000236

3. Results and discussion

3.1. First derivative UV method

The solubility of EA was found very low in water and buffer [11]. Hence, 40% methanol in water was used for preparing standard solution containing mixture of EA and CoQ_{10} 50 µg/ml each. Working standards of the mixture were prepared using 40% methanol. The zero order scan of mixture resembles the UV–vis scan of EA because CoQ_{10} absorption is poor when compared with the EA absorption from 220 to 500 nm, however, the mixture gives higher absorbance than EA alone. The absorption maxima (λ_{max}) of CoQ_{10} is 275 nm and EA was found to have multiple λ_{max} values at 254, 275 and 356 nm in 40% aqueous solution of methanol (Fig. 2). We found no specific peaks of these compounds in zero order UV spectrum, which forced us to deny zero order UV spectroscopy for the simultaneous analysis of EA and CoQ_{10}. Derivative spectroscopy, which is widely used to analyze the multi component systems was an option for the simultaneous detection of these two agents [9,10]. Other reason for our inclination towards derivative spectroscopy is the poor UV absorbing character of CoQ_{10} [12].

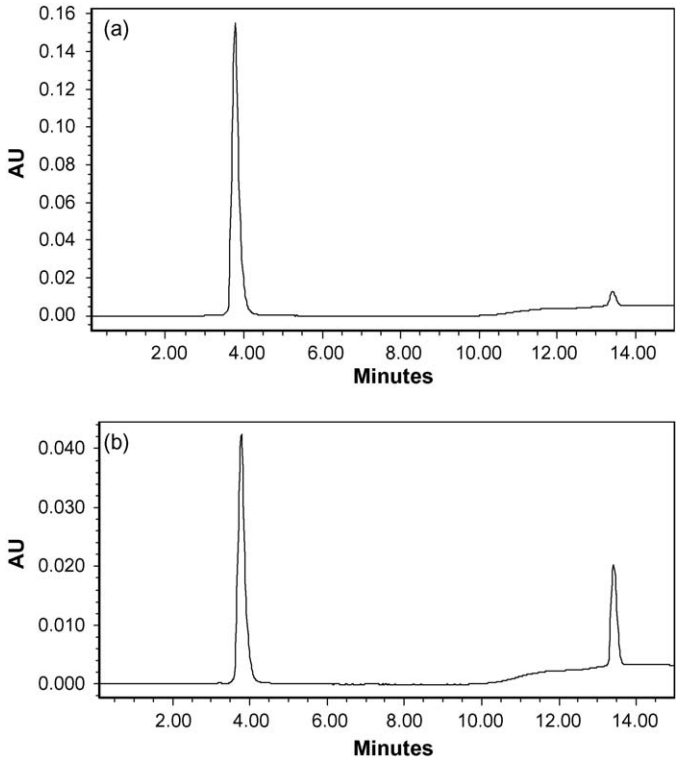

Fig. 3. Simultaneous analysis of EA and CoQ_{10} using HPLC method. Chromatograms extracted at (a) 254 nm and (b) 275 nm from PDA detector showing elution of EA and CoQ_{10} at 3.8 and 13.4 min after 10 µL injection of mixture containing EA and CoQ_{10} each 10 µg/ml.

Table 4
Analytical parameters of HPLC method for the simultaneous analysis of EA and CoQ_{10}

Parameters	Values	
	Ellagic acid	Coenzyme Q_{10}
Linearity range (µg/ml)	0.5–10	0.5–10
Linearity	0.9998	0.9997
Slope	148254	10985
Intercept	−2502	832

At the zero crossing point the compound will have zero value or negligible value throughout all the concentrations of the same and the zero crossing points for EA and CoQ_{10} were found to be 223 and 383 nm, respectively. Consequently, the wavelengths

Table 3
Intraday and interday variability of the simultaneous UV analytical method

Concentration (µg/ml)	Intraday[a]				Interday[b]			
	Ellagic acid		Coenzyme Q_{10}		Ellagic acid		Coenzyme Q_{10}	
	Accuracy	Precision	Accuracy	Precision	Accuracy	Precision	Accuracy	Precision
2	97.58	1.87	97.43	1.35	101.85	5.95	97.04	4.06
8	101.60	0.39	100.98	1.34	97.94	1.25	101.85	1.76
12	102.05	1.55	99.92	1.86	99.31	2.65	100.18	1.41

[a] For intraday variability triplicates were analyzed three times on a single day.
[b] For interday variability triplicates of the concentrations specified were analyzed on three consecutive days.

^{1}D223 and ^{1}D383 nm were selected for the estimation of CoQ_{10} and EA, respectively. The calibration curves were generated and validated for intra and interday variability.

EA showed good linearity (correlation coefficient r^2) of 0.9995 over a range of 0.5–14 μg/ml (1.56–43.72 μM), after 14 μg/ml (43.72 μM) the values deviated from the trend. CoQ_{10} showed linearity of 0.9993 over the range of 0.5–20 μg/ml (0.57–23.17 μM) (Table 2). The accuracy of the method was determined as the percentage recovery from the known concentration of sample and the precision is calculated as the percentage relative standard deviation of the samples analyzed at each concentration. These two parameters were evaluated for the intra as well as interday variability (Table 3). Good accuracy and precision were established with both the compounds.

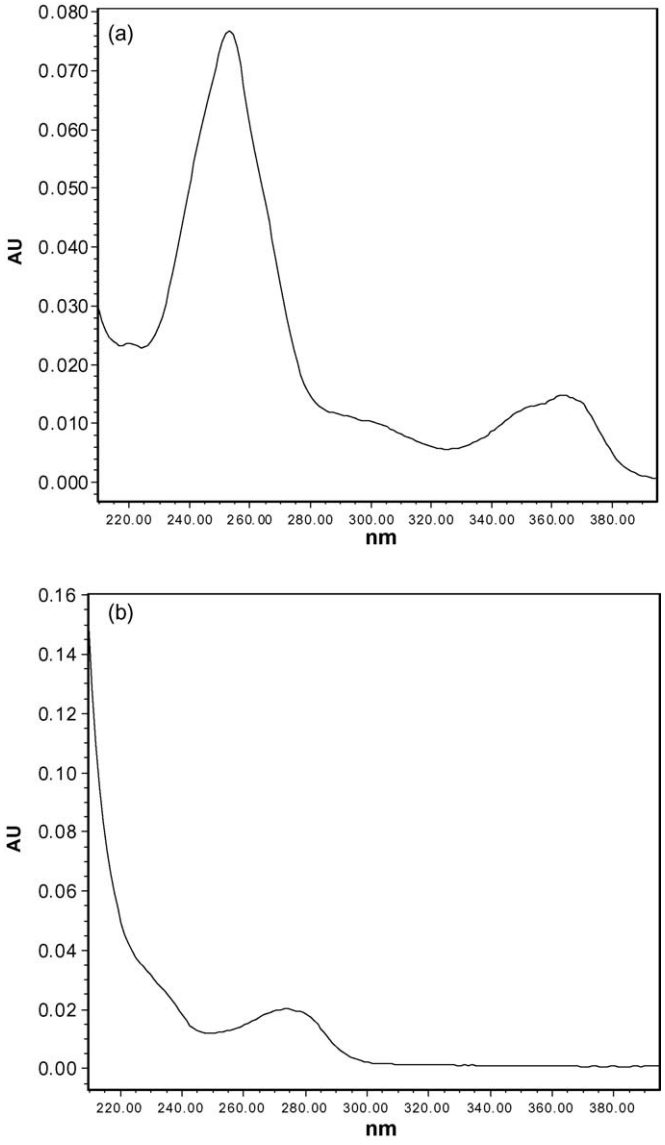

Fig. 4. UV spectra extracted at (a) 3.8 min and (b) 13.4 min from the PDA detector indicate the specificity of the respective peaks and confirm the elution of EA and CoQ_{10}, respectively.

Table 5
Validation parameters for the simultaneous analysis using HPLC

Concentration (μg/ml)	Accuracy (as %recovered)		Precision (as %R.S.D.)	
	Ellagic acid	Coenzyme Q_{10}	Ellagic acid	Coenzyme Q_{10}
6	100.03	105.09	1.75	2.83
4	100.16	102.38	1.28	2.09
1	99.78	98.01	3.34	5.16

3.2. HPLC method

A new HPLC method to simultaneously analyze ellagic acid and coenzyme Q_{10} has been developed and validated for selectivity, linearity, accuracy and precision. Ellagic acid retention on reverse phase C_{18} column is very poor and PEG bonded column was used for the analysis of ellagic acid previously [11]. CoQ_{10} is a lipophilic molecule and the retention of this molecule was found to be high and resulted in peak broadening on C_{18} column when the mobile phases used were polar in nature (data not shown). Usage of PEG bonded column facilitates the elution of CoQ_{10} relatively faster than the C_{18} column. Initially various combinations of isocratic mobile phases were tried out for the simultaneous analysis which demanded longer durations for the analysis. Gradient system with the composition specified in Table 1 resulted in successful elution of both compounds simultaneously with relative rapidity. The elution times for EA and CoQ_{10} were found to be 3.8 and 13.4 min, respectively (Fig. 3(a) and (b)). The specificity of the compounds was confirmed by observing the UV spectra of the compounds from start of the chromatogram peak till the complete elution (Fig. 4(a) and (b)). The linearity was good for both the compounds with r^2 values of 0.9998 and 0.9997 for EA and CoQ_{10} over a range of 0.5–10 μg/ml (Table 4). The method was validated for accuracy and precision as well (Table 5).

4. Conclusion

The developed first derivative UV and HPLC methods were accurate and precise for the quantitative estimation of the EA and CoQ_{10} simultaneously. Developed derivative spectroscopic method provides rapid simultaneous analysis of EA and CoQ_{10} and is as good as HPLC method. From the results it is evident that the PEG bonded column will be beneficial in increasing the retention of the poorly retained compound which supports our previous report [11]. PEG bonded phase provides hydrophilicity to the reverse phase C_{18} column and thus resulted in relative rapid elution of CoQ_{10} which is a lipophilic compound. Thus PEG column is a better option for the rapid simultaneous analysis of EA having poor retention and CoQ_{10} having high retention times.

Acknowledgements

Authors are thankful to Tishcon Corporation for the gift sample of CoQ_{10}. DVR acknowledges MS fellowship from NIPER. VB is grateful to NIPER for providing PhD fellowship. Startup

fund from NIPER to M.N.V. Ravi Kumar is gratefully acknowledged.

References

[1] A. Azzi, K.J.A. Davies, F. Kelly, FEBS Lett. 558 (2004) 3.
[2] I.F.F. Benzie, Comp. Biochem. Physiol. A: Mol. Integr. Physiol. 136 (2003) 113.
[3] A.C. Whitley, G.D. Stoner, M.V. Darby, T. Walle, Biochem. Pharmacol. 66 (2003) 907.
[4] R.W. Teel, G.D. Stoner, M.S. Babcock, R. Dixit, K. Kim, Cancer Detect. Prev. 9 (1986) 59.
[5] R.W. Teel, R.M. Martin, R. Allahyari, Cancer Lett. 36 (1987) 203.
[6] K. Lockwood, S. Moesgard, T. Yamamoto, K. Folkers, Mol. Aspects Med. 15 (1994) S231.
[7] K. Lockwood, S. Moesgard, T. Yamamoto, K. Folkers, Biochem. Biophys. Res. Commun. 212 (1995) 172.
[8] M. Turunen, J. Olsson, G. Dallner, Biochim. Biophys. Acta 1660 (2004) 171.
[9] A. Gursoy, E. Kut, S. Ozkirimli, Int. J. Pharm. 271 (2004) 115.
[10] J. Karpinska, Anal. Sci. 17 (2001) 249.
[11] I. Bala, V. Bhardwaj, S. Hariharan, M.N.V.R. Kumar, J. Pharm. Biomed. Anal. 40 (2006) 206.
[12] J. Karpinska, B. Mikoluc, J. Piotrowska-Jastrzebska, J. Pharm. Biomed. Anal. 17 (1998) 1345.

Available online at www.sciencedirect.com
ScienceDirect
Talanta 70 (2006) 392–396
Talanta
www.elsevier.com/locate/talanta

Microfluidic liquid–liquid extraction system based on stopped-flow technique and liquid core waveguide capillary

Meng Sun, Wen-Bin Du, Qun Fang *

Institute of Microanalytical Systems, Zhejiang University, Hangzhou 310028, China

Received 8 February 2006; received in revised form 22 February 2006; accepted 22 February 2006
Available online 18 April 2006

Abstract

In this work, a miniaturized liquid–liquid extraction system under stopped-flow manipulation mode with spectrometric detection was developed. A Teflon AF liquid-core waveguide (LCW) capillary was used to serve as both extraction channel for organic solvent flow and adsorption detection flow cell. Gravity induced hydrostatic pressure was used to drive the organic and aqueous phases through the extraction channels. During extraction process, a stable organic and aqueous phase interface was formed at the outlet of the capillary, through which the analyte in the flowing aqueous stream was extracted into the stationary organic solvent in capillary. The absorbance of the analyte extracted into the organic solvent was measured in situ by a spectrometric detection system with light emitting diode (LED) as light source and photodiode as absorbance detector. The performance of the system was demonstrated in the determination of sodium dodecyl sulfate (SDS) extracted as an ion pair with methylene blue into chloroform. The precision of the measured absorbance for a 5 mg L^{-1} SDS standard was 6.1% R.S.D. ($n = 5$). A linear response range of 1–10 mg L^{-1} SDS was obtained with 5 min extraction period. The limit of detection (LOD) for SDS based on three times standard deviation of the blank response was 0.25 mg L^{-1}.

Keywords: Microfluidic system; Liquid–liquid extraction; Stopped-flow technique; Liquid-core waveguide capillary

1. Introduction

Liquid–liquid (L–L) extraction is one of the most widely used tools for matrix isolation and analyte enrichment in analytical chemistry. However, the conventional L–L extraction procedure is time-consuming, labor-intensive, requires large amounts of toxic organic solvent, and often leads to emulsion formation and analyte loss. In recent years, various automated and miniaturized L–L extraction techniques, such as liquid-phase microextraction [1–16] and microfluidic chip based microextraction [17–25], have been developed to overcome these drawbacks. In 1996, Liu and Dasgupta [1] reported a L–L extraction system based on a 1.3 μL single droplet of organic solvent with an in situ spectrometric detector. Almost at the same time, Jeannot and Cantwell [2] reported a similar microextraction system with a microdrop (8 μL) of organic solvent suspended at the end of a Teflon rod immersed in a stirred aqueous sample solution. Thereafter, various L–L extraction systems based on single droplet of organic solvent were developed to perform sample pretreatment [3–8]. In most of these systems, L–L extraction under stopped flow manipulation mode was performed by forming a stationary organic solvent droplet immersed in a larger aqueous sample solution. Droplet volumes of the organic solvents were typically in the microlitres range and sample volumes consumed were in the millilitres range. However, the limitation of these systems is that the microdrops suspended on the needle or other holding devices are sometimes dislodged by the flowing aqueous sample during extraction process [9,15].

From 2000, Kitamori's group has reported a series of microfluidic chip systems performing L–L extraction based on formation of multiple phase laminar flows in microchannels [17–22]. More recently we reported a series of L–L extraction chip systems based on stopped flow and trapped droplet techniques [23–25]. The advantages of chip based solvent extraction systems are low consumption of sample and extractant in nL–μLs ranges and high extraction efficiency due to the microscale effect in microchannels. However, usually expensive equipment and complicated operation were required in the

* Corresponding author. Tel.: +86 571 88273496; fax: +86 571 88273496.
E-mail address: fangqun@zju.edu.cn (Q. Fang).

0039-9140/$ – see front matter © 2006 Elsevier B.V. All rights reserved.
doi:10.1016/j.talanta.2006.02.069

fabrication of L–L extraction chips, which may limit their further application in routine analysis.

In this work, a simple and robust microfluidic L–L extraction system under a stopped-flow manipulation mode was developed based on a Teflon AF LCW capillary without requirement for special microfabrication techniques. A stable L–L interface between the stationary organic solvent in the capillary and flowing aqueous sample was formed at the outlet of the capillary by adjusting the liquid level in reservoirs in the system. A miniaturized in situ spectrometric detector to monitor the absorbance of analyte extracted into the organic solvent was built also based on this capillary to achieve sensitivity comparable to other microextraction system [1] and conventional systems [26]. Aqueous solutions of SDS and chloroform were used, respectively, as samples and extractant to demonstrate the performance of the system.

2. Experimental

2.1. Chemicals

All chemicals were of analytical-reagent grade and deionized water was used throughout. The 100 mg L^{-1} methylene blue (MB) solution was prepared by dissolving 10 mg of MB and 2.83 g of $NaH_2PO_4{\cdot}2H_2O$ in 700 μL cons. H_2SO_4 and 25 mL methanol, and made up to 100 mL with water. The stock solution of sodium dodecyl sulfate (SDS, 100 mg L^{-1}) was prepared by dissolving 10 mg of SDS (Sigma–Aldrich) in 100 mL of water. The series of SDS standard solutions were prepared by sequentially diluting the stock solution with water. The working solution was prepared by mixing one portion of MB solution with three portions of SDS standard solution. All the solutions were prepared at least 24 h prior to use. Chloroform (Zhejiang Deyer Pharmaceutical Co., Hangzhou, China) was used as the extractant without further purification.

2.2. Apparatus

The microfluidic L–L extraction system is shown diagrammatically in Fig. 1. A 10 mm long glass tube (0.8 mm i.d., 1.2 mm o.d.) was used to supply the flowing channel for aqueous sample solution. A 6 mm long fused silica capillary (100 μm i.d., 375 μm o.d.) serving as sampling probe was connected to the inlet of the glass tube via a section of Tygon tubing (380 μm i.d., 900 μm o.d.). The outlet the glass tube was connected with a 70 mm long horizontal plastic tube (4.7 mm i.d., cut from a commercial 1 mL disposable syringe) used as waste reservoir via a 10 cm long Tygon tubing (1 mm i.d., 3 mm o.d.). A 0.4 mm-diameter hole was drilled on the sidewall of the glass tube using a 400 μm-diameter flat-tipped emery drill. A 15 mm long Teflon AF 2400 capillary (250 μm i.d., 500 μm o.d., Random Technologies, San Francisco, USA) was inserted through the hole 200 μm deep into the glass tube channel. The capillary served both as a LCW absorption detection flow-cell as well as an extraction channel for the organic solvent. The other end of the capillary was inserted into a perpendicular plastic tube (15 mm i.d., cut from a commercial 10 mL disposable syringe) that served as a reservoir for the organic solvent, positioned 500 μm from a 1 mm-diameter optical fiber inserted into the reservoir. All connections in the conduit system were sealed with epoxy. The sample vials were produced from the 0.2 mL Microtubes (Porex, Petaluma, USA) with 1.5 mm wide, 2 mm deep slot fabricated on the conical bottom of each tube for pass-through of the sampling probe.

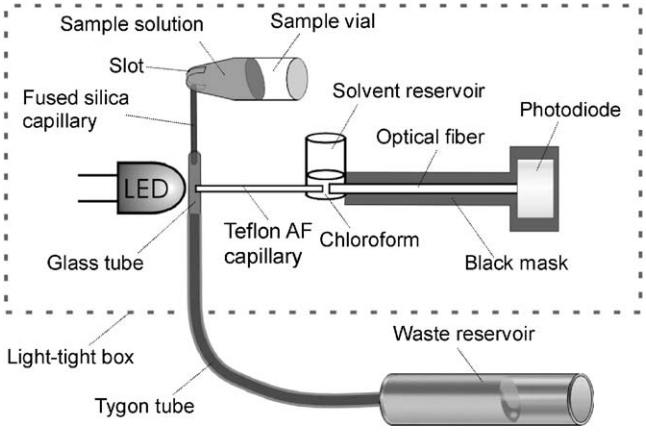

Fig. 1. Schematic diagram of the microfluidic L–L extraction system employing Teflon AF capillary liquid-core waveguide (not to scale).

A red LED (630 nm, Hangke Electronics Co., Hangzhou, China) was used as light source, positioned 2 mm from the Teflon AF capillary outlet to directly illuminate the capillary outlet through the sidewall of glass tube without further focusing. The light transmitted out from the capillary inlet was conducted by the optical fiber to a photodiode detector (Model OPT-301, with integrated amplifier, Texas Instruments, Tucson, USA). The Teflon AF capillary was masked from ambient light with black plastic tubing. The sections of conduit in the detection system were masked from ambient light using a light-tight box painted black inside. LabVIEW software (National Instruments, Austin, USA) was used to process the detection signals.

The L–L extraction system and detection system were fixed onto a platform, keeping the glass tube in upright position and the Teflon AF capillary in horizontal position, whereas the horizontally positioned waste reservoir was fixed onto another platform which could be perpendicularly moved to vary the position of the waste reservoir in relation to that of L–L interface at the outlet of the capillary.

For direct observing the stability of the L–L interface at the outlet of Teflon AF capillary, a stereo microscope (SZ-45B3, Sunny Instruments Co., NingBo) equipped with a CCD camera (YH-9628, Yonghui Technology Development Co., Shenzhen) was used.

2.3. Procedures

Before use, the conduits in the L–L extraction system were emptied. 100 μL blank solution and aqueous working solutions containing the ion-pair product were pipetted into separate horizontal sample vials. The L–L extraction was performed first by inserting the sampling probe through the slot of the blank solution vial. The aqueous solution driven by gravity flowed through

the glass tube, while the aqueous flow into the Teflon AF capillary was obstructed owing to surface tension effect produced by the hydrophobic properties of Teflon AF. Then the organic solvent reservoir was filled with 500 μL chloroform, which produced a liquid level of 3 mm relative to that of the capillary outlet. A stable aqueous/organic phase interface was formed at the outlet of the capillary based on surface tension by positioning the waste reservoir 4 mm below the capillary outlet. The L–L extraction and analysis for sample solution was performed by inserting the sampling probe into a sample vial instead of the blank vial. The ion-pair product extracted into the organic phase was in situ detected in this LCW capillary flow-cell. After one analytical cycle, the position of the waste reservoir was lowered to 30 mm below the capillary outlet for 5 s to wash out the organic solvent in the capillary, and then the waste reservoir was restored to its original position to obtain a fresh phase interface for the next analytical cycle.

3. Results and discussion

3.1. Design of the microfluidic L–L extraction system

In our previously reported miniaturized L–L extraction system [23–25], a stopped-flow manipulation mode was adopted to perform extraction in microfluidic chip with a "Y" shaped channel, which had the advantages of high enrichment factor and simple operation without requirement for organic/aqueous phase separation. In this work, the L–L extraction system was simplified by using a Teflon AF LCW capillary as a conduit to supply the organic solvent instead of using a chip with microfabricated channels, allowing the system to be built in routine laboratories without requirement for complicated microfabrication devices and operations. Owing to the hydrophobic property of Teflon AF, a stationary phase interface was easily formed at the capillary channel outlet by adjusting the liquid level in the reservoirs (See Section 3.2). In addition to serving as a conduit for organic solvent delivery, the Teflon AF capillary was also used as a flow-cell for the absorption detection making use of its waveguide properties when filled with aqueous solution. Such detection systems had been applied in long-path-length absorption spectrometry for microfluidic chips to improve sensitivity [27,28]. In the present system, for convenience, a 1.5 cm long Teflon AF capillary was used as a detection flow cell.

In the present L–L extraction system, hydrostatic pressure produced from difference in liquid levels between the sample/chloroform containers and the waste reservoir was employed to provide driving force for sample introduction and transfer as well as washout of chloroform from the capillary. Horizontal tubular sample vials and waste reservoirs were used to maintain stable hydrostatic pressure in the extraction channels during prolonged working periods. A slot was fabricated at the bottom of each sample vial to facilitate sample change. Owing to the low consumption of organic solvent (within several hundred nanoliters, see Section 3.3) during extraction process under the stopped-flow extraction mode, an upright reservoir was employed for organic solvent, in which the liquid level showed no observable changes during 3 h extraction periods.

3.2. Formation of stable L–L interface

In the present microfluidic L–L extraction system, there are four forces exerted on the L–L interface at the outlet of the capillary (as shown in Fig. 2), including the hydrostatic pressure f_o and f_a with different directions produced by the organic solvent reservoir and sample vial, and negative pressure f_w produced from the waste reservoir, as well as the surface tension f_s of the organic solvent at the capillary outlet. The combination of these forces f_c in the horizontal direction could be expressed as

$$f_c = f_o + f_w + f_a + f_{sp} \quad (1)$$

where f_{sp} is the vector force of surface tension f_s in the horizontal direction. When f_c is equal to zero, a stable stationary phase interface can be produced at the outlet of the capillary (as shown in Fig. 3b). If $f_c > 0$, the aqueous solution flows into the capillary to push the organic solvent back (as shown in Fig. 3a). If $f_c < 0$, the organic solvent overflows from the capillary outlet (as shown in Fig. 3c). Therefore, in the present system, the stability of the L–L interface is mainly governed by the liquid levels in the sample vial, waste and solvent reservoir. The former two liquid levels were decided by the vertical positions of the sample vial and waste reservoir, respectively, while the liquid level in the organic solvent reservoir was decided by the volume of organic solvent filled in the reservoir. The effects of the positions of the sample vial and waste reservoir on the stability of L–L interface were studied with the liquid level of solvent reservoir fixed at 3 mm above the L–L interface. The results (Fig. 4) show that corresponding to a defined sample vial position, a position range of approximately 4 mm of the waste reservoir usually existed (the shadowed section shown in Fig. 4), within which a stable phase interface could be obtained (i.e. $f_c = 0$). This is the result of self-adjustment of the organic solvent surface tension at the interface by changing its shape to counteract the position variation of waste reservoir within this range. With the raising of the sample vial position (i.e. to increase f_a), the position region of

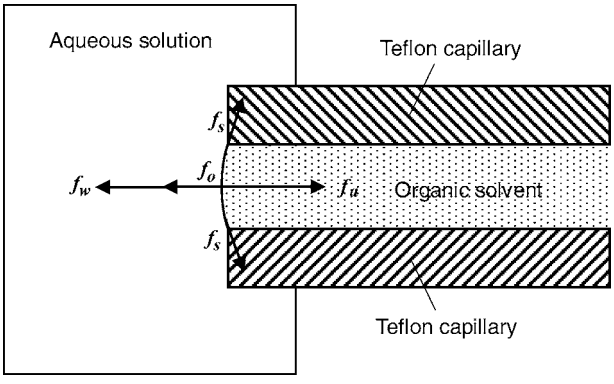

Fig. 2. Schematic diagram of different forces exerted on the liquid–liquid interface at the outlet of the capillary.

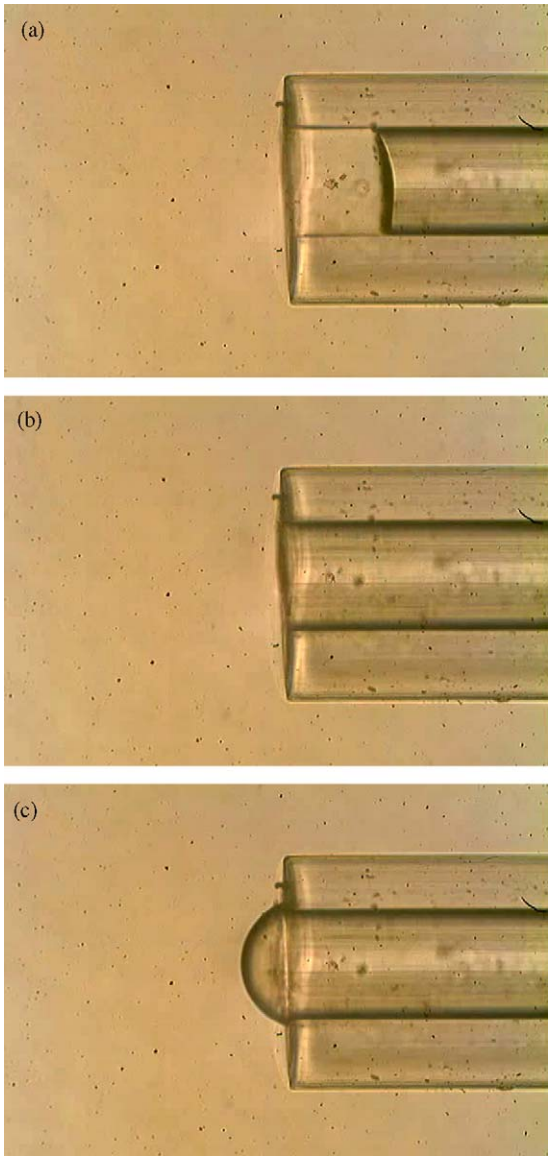

Fig. 3. CCD images of three typical states of the L–L interface at the outlet of capillary under different hydrostatic pressures.

waste reservoir required for stable interface shifted down (i.e. to increase f_w) to maintain the force equilibrium at the L–L interface.

In addition to the above experiments, the effects of the liquid level in the solvent reservoir and the position of the waste reservoir on the stability of L–L interface were studied. The results are shown in Fig. 5. Stable L–L interfaces were obtained within a position range of ca. 6 mm (the shadowed section shown in Fig. 5) of the waste reservoir, corresponding to a fixed liquid level in the chloroform reservoir. With the raising of liquid level in the chloroform reservoir (i.e. to increase f_o), the waste reservoir position required for stable interface shifted up (i.e. to decrease f_w) to maintain the force equilibrium at the phase interface.

Considering the consumption of sample and chloroform, a relatively low position for the sample vial and the liquid level of chloroform at 10 and 3 mm above the phase interface was

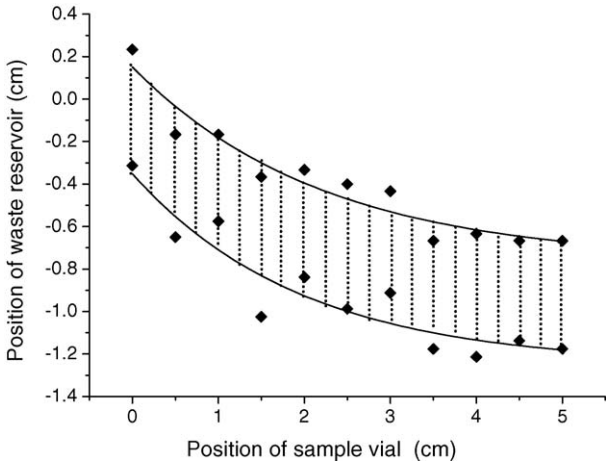

Fig. 4. Effects of positions of aqueous sample vial and waste reservoir on the stability of L–L interface. The liquid level in the chloroform reservoir was fixed at 3 mm above the interface. The positions of the sample vial and waste reservoir were evaluated in relation to that of L–L interface at the capillary outlet.

chosen in the present L–L extraction system, respectively, corresponding to a sample flow rate of 2.0 μL min^{-1} (70 μm s^{-1}). Under these conditions, an optimized position of 4 mm below the phase interface (expressed as −4 mm in Figs. 4 and 5) for the waste reservoir was chosen during the extraction process. This position is at the center of the region of waste reservoir positions that produced stable L–L interfaces.

3.3. Analytical performance

The analytical performance of the present microfluidic L–L extraction system was demonstrated in the determination of SDS with MB as reagent. Fig. 6 shows typical recordings of absorbance of 5 mg L^{-1} SDS during five repetitive extraction cycles. The absorbance response increased almost linearly with extraction time in the range of 0–5 min, beyond that the increase of response gradually levelled off, which implies that the L–L

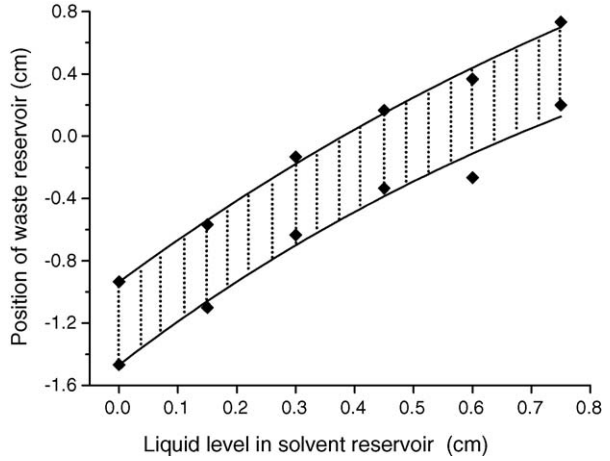

Fig. 5. Effects of liquid level of chloroform and position of waste reservoir on the stability of L–L interface. The position of the sample vial was fixed at 10 mm above the interface. The liquid level of chloroform and position of waste reservoir were evaluated in relation to that of L–L interface at the capillary outlet.

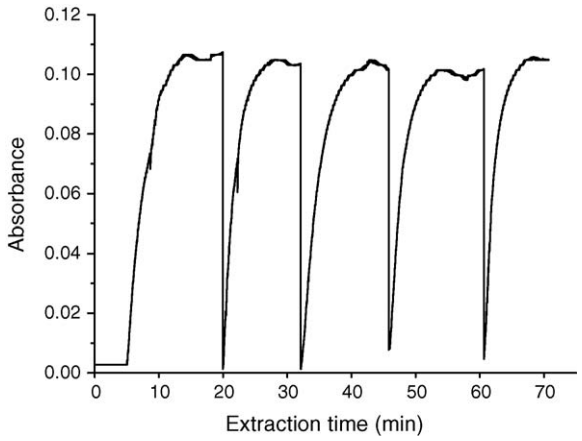

Fig. 6. Typical recordings of absorbance of 5 mg L^{-1} SDS during five repetitive extraction cycles to show the repeatability of the system.

extraction nearly reached equilibrium state. An extraction time of 5 min seemed to be a good compromise between detection sensitivity and analytical throughput. The precisions of a 5 mg L^{-1} SDS standard with extraction times of 5, 10 and 15 min were 6.1%, 3.9% and 3.8% R.S.D. ($n = 5$), respectively (Fig. 6). The analytical signal was found to be linearly related to the SDS concentration in the range of 0–10 mg L^{-1} within a 5 min extraction period: $A = 0.01936C - 0.00456$ ($r^2 = 0.9946$), where A is the absorbance response and C is the concentration of SDS solution in mg L^{-1}. The limit of detection (LOD) for SDS based on three times the standard deviation of the blank values was 0.25 mg L^{-1}. The shortest total analysis time for one cycle was 5.5 min, including 5 min extraction time and 0.5 min conduit washing and sample changing time. The consumptions of sample and organic solvent in one analytical cycle were 10 μL and 740 nL, respectively.

4. Conclusions

The present system proved to be an efficient, robust and organic solvent-economic means for achieving L–L extraction under stopped flow mode. The use of Teflon AF LCW capillary significantly facilitated the construction of the L–L extraction system and spectrometric detector in routine chemical laboratories. Such systems should be widely applicable for various analytical purposes involving L–L extraction with spectrometric detection. Although not pursued further in this work, the sample consumption of the system could be further reduced by decreasing the inner diameter of the aqueous phase channel, and sample consumption less than 1 μL is foreseeable.

Acknowledgement

This work was supported by Natural Science Foundation of China (20299030 and 20575059) and Research Foundation from Ministry of Science and Technology of China (2002AA2Z2042).

References

[1] H. Liu, P.K. Dasgupta, Anal. Chem. 68 (1996) 1817.
[2] M.A. Jeannot, F.F. Cantwell, Anal. Chem. 68 (1996) 2236.
[3] M.A. Jeannot, F.F. Cantwell, Anal. Chem. 69 (1997) 235.
[4] Y. He, H.K. Lee, Anal. Chem. 69 (1997) 4634.
[5] M. Ma, F.F. Cantwell, Anal. Chem. 71 (1999) 388.
[6] W.P. Liu, H.K. Lee, Anal. Chem. 72 (2000) 4462.
[7] B.O. Keller, L. Li, Anal. Chem. 73 (2001) 2929.
[8] V. Colombini, C. Bancon-Montigny, L. Yang, P. Maxwell, R.E. Sturgeon, Z. Mester, Talanta 63 (2004) 555.
[9] E. Psillakis, N. Kalogerakis, Trends Anal. Chem. 23 (2004) 1.
[10] J.F. Liu, J.B. Chao, G.B. Jiang, Anal. Chim. Acta 455 (2002) 93.
[11] S. Pedersen-Bjergaard, K.E. Rasmussen, Anal. Chem. 71 (1999) 2650.
[12] J.X. Wang, D.Q. Jiang, X.P. Yan, Talanta 68 (2006) 945.
[13] L. de Jager, A.R.J. Andrews, Anal. Chim. Acta 458 (2002) 311.
[14] X.M. Jiang, H.K. Lee, Anal. Chem. 76 (2004) 5591.
[15] L. Zhao, H.K. Lee, Anal. Chem. 74 (2002) 2486.
[16] P. Rodríguez-Sanmartín, A. Moreda-Piñeiro, A. Bermejo-Barrera, P. Bermejo-Barrera, Talanta 66 (2005) 683.
[17] M. Tokeshi, T. Minagawa, T. Kitamori, Anal. Chem. 72 (2000) 1711.
[18] T. Minagawa, M. Tokeshi, T. Kitamori, Lab Chip. 1 (2001) 72.
[19] A. Hibara, M. Tokeshi, K. Uchiyama, H. Hisamoto, T. Kitamori, Anal. Sci. 17 (2001) 89.
[20] M. Tokeshi, T. Minagawa, K. Uchiyama, A. Hibara, K. Sato, H. Hisamoto, T. Kitamori, Anal. Chem. 74 (2002) 1565.
[21] A. Hibara, M. Nonaka, H. Hisamoto, K. Uchiyama, Y. Kikutani, M. Tokeshi, T. Kitamori, Anal. Chem. 74 (2002) 1724.
[22] Y. Kikutani, H. Hisamoto, M. Tokeshi, T. Kitamori, Lab Chip. 4 (2004) 328.
[23] Q. Fang, H. Chen, Z.X. Cai, Chem. J. Chin. Univ. 25 (2004) 261.
[24] Q. Fang, H. Chen, Z.L. Fang, Ninth International Conference on Miniaturized Systems for Chemistry and Life Sciences, Boston, USA, 2005, p. 128.
[25] H. Chen, Q. Fang, X.F. Yin, Z.L. Fang, Lab Chip. 5 (2005) 719.
[26] R.D. Swisher, M.E. Bose, Standard Methods for the Examination of Water and Wastewater, American Public Health Association, Washington, DC, 1989, pp. 5–59.
[27] W.B. Du, Q. Fang, Z.L. Fang, Chem. J. Chin. Univ. 25 (2004) 610.
[28] W.B. Du, Q. Fang, Q.H. He, Z.L. Fang, Anal. Chem. 77 (2005) 1330.

Available online at www.sciencedirect.com
ScienceDirect
Talanta 70 (2006) 397–402
Talanta
www.elsevier.com/locate/talanta

Highly luminescent CdTe quantum dots prepared in aqueous phase as an alternative fluorescent probe for cell imaging

Jifang Weng [a,b], Xingtao Song [a], Liang Li [a], Huifeng Qian [a], Keying Chen [b], Xuemin Xu [b], Chengxi Cao [b], Jicun Ren [a,*]

[a] *College of Chemistry & Chemical Engineering, Shanghai Jiaotong University, 800 Dongchuan Road, Shanghai 200240, PR China*
[b] *College of Life Science & Biotechnology, Shanghai Jiaotong University, 800 Dongchuan Road, Shanghai 200240, PR China*

Received 1 December 2005; received in revised form 21 February 2006; accepted 23 February 2006
Available online 17 April 2006

Abstract

In this paper, our main aim is to explore the feasibility for application of luminescent CdTe quantum dots prepared in aqueous phase to live and fixed cell imaging. The highly luminescent CdTe quantum dots (QDs) were first prepared in aqueous phase using 3-mercaptopropionic acid (MPA) as a ligand, and then were covalently coupled to a plant lectin (UEA-1) and antibody anti-von Willebrand factors (anti-vWF) as fluorescent probes. Two probes QD-UEA-1 and QD-anti-vWF) were able to specifically bind the corresponding cell membrane receptor and cytoplasm immunogen, respectively. The good cell images were obtained in live cells and fixed cells using laser confocal scanning microscopy. Our preliminary results illustrated that CdTe QDs prepared in water phase were highly luminescent, water-soluble, stable, and easily conjugated with biomolecules since their surface were coated with MPA containing free carboxyl group. We predict that QDs prepared in water phase will probably become an attractive alternative probe in cellular imaging and bio-labeling.

Keywords: Aqueous phase; CdTe quantum dots; Cell imaging; HUVEC

1. Introduction

Semiconductor quantum dots (QDs) are nano-scale inorganic crystals in size range of 1–10 nm. Due to their quantum confinement of charge carriers in tiny spaces, QDs show some unique and fascinating optical properties, such as, sharp and symmetrical emission spectra, high quantum yield (QY), good chemical and photo-stability and size dependent emission wavelength turnability. When QDs are linked with bio-recognition molecules such as proteins [1–3], peptides [4–7] and nucleic acids [8–10], they will become promising attractive fluorescent probes in biological and medical fields such as bioassay, cell imaging and clinic diagnosis [9,11–17]. In 1998, two groups first reported that QDs could be used for imaging of cells as fluorescent probes [18,19]. Their pioneer work showed that QDs were brighter and more stable than rhodamin 6G. These excellent optical properties of QDs have received great interest in biological applications. Recently, QDs have been used as immuno-histochemical labels in fixed cell imaging, which mainly included the labeling of the breast cancer marker Her2 on the cell surface, staining of actin and microtubule fibers in the cytoplasm, and detection of nuclear antigens inside the nucleus [13]. In live cell imaging, Nie's group first illustrated that QDs labeled with transferrin could enter the cultured HeLa cells by endocytosis and recognized specific antibodies or antigens. Subsequently, some groups demonstrated that QDs were successfully used for targeting or tracking some membrane or transmembrane proteins, such as human and *Drosophila* serotonin transporters expressed in HeLa and HEK-293 cells [20], Glycine receptors in neurons [21], erbB/HER receptor in Chinese hamster ovary cells [22].

However, the QDs widely used in the bio-labeling, such as CdSe, CdTe nanocrystals and their core/shell alloys, are mostly synthesized in organic phase using high boiling point solvents such as trioctylphosphine (TOP) or trioctylphosphine oxide (TOPO) or a mixture of TOP and TOPO [23–27]. The

* Corresponding author. Tel.: +86 21 54746001; fax: +86 21 54741297.
E-mail address: jicunren@sjtu.edu.cn (J. Ren).

0039-9140/$ – see front matter © 2006 Elsevier B.V. All rights reserved.
doi:10.1016/j.talanta.2006.02.064

surfaces on the QDs prepared in organic phase were coated with TOP or TOPO, which forms a hydrophobic layer. Therefore, these QDs cannot be directly applied in bio-systems due to their hydrophobic surfaces. Usually, they need to replace the surface-capping molecules on nanoparticles using ligand exchange method. The exchange process was time-consuming and laborious, and frequently resulted in a significant decrease in quantum yield of QDs [19,28]. Additionally, it has been found that these hydrophilic QDs were not stable enough in aqueous solution after ligand exchange. Some surface modification techniques have been used to improve hydrophilicity and stability of QDs in aqueous solution. The modification often led to significantly increasing the diameter of QDs up to about 20–30 nm [29]. In contrast to organic synthesis, aqueous synthesis exhibits good reproducibility, low toxicity, inexpensive, and especially, the products prepared in water phase have excellent water-solubility, stability and biological compatibility [30]. However, QDs prepared in water phase usually possess low QY (3–10%) and wider the full width at half maximum (FWHM). In comparison with organic synthesis, no great attentions have been paid to aqueous synthesis for long time, and few applications were found so far. In recent years methods of preparing luminescent QDs in aqueous phase have significantly been improved by Weller and coworkers [30], Zhang et al. [31] and our group [32,33]. Using an autoclave with higher reaction temperature (180 °C) [31], micro-wave reactor with temperature controllable system [32], and optimization of aqueous synthesis conditions, [33] QY of QDs were dramatically enhanced up to 40–67%. These results demonstrated that aqueous synthesis method may become an attractive alternative to current syntheses of QDs in organic phase. To the best of our knowledge, it is not clear whether the QDs prepared in aqueous phase are able to be applied for live cell imaging as fluorescent probes. In this work, firstly, we want to prepare highly luminescent CdTe QDs in aqueous phase, and then evaluate that the feasibility of application of CdTe QDs conjugated with *Ulex europaeus* 1 (UEA-1) and anti-von Willebrand factor (anti-vWF) for imaging of human umbilical vein endothelial cells (HUVECs) using laser confocal scanning microscopy.

2. Materials and methods

2.1. Materials

3-Mercaptopropionic acid (MPA, >99%) was product of Fluka. $NaBH_4$ (96%), tellurium powder (99.999%, about 200 mesh) was obtained from Shanghai Reagent Company. *Ulex europaeus* 1 (UEA-1, gorse), anti-vWF and 1-ethyl-3-(3-dimethylaminopropyl) carbodiimide hydrochloride (EDC) were purchased from Sigma–Aldrich. The human umbilical vein endothelial cells (HUVECs) and cell media were from Cascade Biologics (Portland, USA). Other chemicals are of analytical grade (Sinopharm Chemical Reagent Co., Ltd., Shanghai, China; Shanghai Lingfeng Chemical Reagent Co., Ltd., Shanghai, China; Shanghai Chemical Reagent Co., Ltd., Shanghai, China). The ultrapure water with 18.2 MΩ/cm (Millipore Simplicity, USA) was used in all experiments.

2.2. Syntheses of CdTe QDs

Aqueous colloidal CdTe QDs solution was prepared using the reaction between Cd^{2+} and NaHTe solution in the presence of MPA as a stabilizer [32]. The synthesis reaction was expressed as following equation:

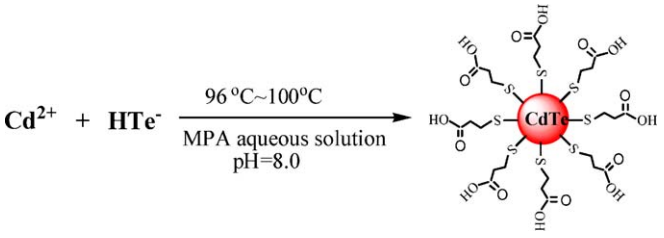

For preparation of Cd precursor solutions, a solution of $CdCl_2$ and MPA were mixed, and adjusted to pH 8 with 1 M NaOH. The typical molar ratio of Cd:Te:MPA was 2:1:4.8 in our experiments. This solution was placed in a three-necked flask and was deacerated with N_2 bubbling for 30 min. Under vigorous stirring, the prepared oxygen free NaHTe solution was injected. The resulting mixture solution was heated to 99–100 °C and refluxed to different time for controlling the size of CdTe QDs. In order to remove the excess MPA and cadmium ions, the CdTe QDs were precipitated using the same procedure described in the reference [34]. The CdTe QDs precipitates were rinsed with ethanol and dried by vacuum oven.

2.3. Spectral characterization of CdTe QDs

Emission spectra were collected using a Varian Cary spectrometer. Absorption spectra were collected using a Lambda 20 UV–visible spectrophotometer (Perkin-Elmer).

The QY of CdTe QDs was measured according to the method described in the references [35]. Briefly, Rhodamine 6G was served as a reference standard (QY = 95%), the absorbance for the standard and the CdTe colloid samples at the excitation wavelengths and the fluorescence spectra of the same solutions were measured, respectively. The integrated fluorescence intensity (that is, the area of the fluorescence spectrum) from the fully corrected fluorescence spectrum was calculated.

The areas of integrated fluorescence intensity versus absorbance were plotted. The plot obtained should be a straight line with a gradient M, which was used to calculate the quantum yield according to the following equation:

$$\phi_x = \phi_s \frac{M_x}{M_s} \left(\frac{\eta_x}{\eta_s} \right)^2 \quad (1)$$

where the subscripts ‘s’ and ‘x’ denote standard (such as rhodamine 6G) and test samples, respectively, ϕ is the QY, and η is the refractive index of the solvent. It should be noted that the excitation wavelength for measurements of QY was set at the excitonic absorption peak of the CdTe nanocrystal samples in our experiments.

2.4. Bioconjugation of CdTe QDs

MPA-coated CdTe QDs prepared in aqueous phase were conjugated to UEA-1 and anti-vWF using EDC as a coupling reagent. Firstly, 0.25 mg/ml CdTe QDs and 2 mg/ml EDC were reacted together for 5 min at room temperature, and then UEA-1 (or anti-vWF) was added into the reaction solution, further incubated for 2–4 h. Finally, the reaction was blocked by placing the mixtures in refrigerator at 4 °C. The mixtures were purified using ultra-filtration membrane (NMWL 50,000, Millipore, USA) according to the instruction of the manufacture.

Capillary electrophoresis with laser-induced fluorescence detector (CE-LIF) was used to confirm whether QDs were effectively conjugated with proteins. In the experiments, P/ACE-MDQ (Beckman Coulter Inc., Fullerton, CA, USA) instrument was used in normal polarity separation mode (anode at the injection side). The temperature of the separation capillary column was thermostated at 25 °C, and a 30 cm effective separation length capillary (40 cm total) with an i.d. of 75 μm was used for separation.

2.5. Cell culture

HUVECs were cultivated (37 °C, 5% CO_2) on coverslips in HEPES media containing 2% (v/v) fetal bovine serum, 1 μg/ml hydrocortisone, 10 ng/ml human epidermal growth factor, 3 ng/ml basic fibroblast growth factor, and 10 μg/ml heparin overnight.

2.6. Live cells treatments

When the cultured cells reached about 70% confluence, they were gently washed twice with PBS (pH 7.4), and blocked with 1% BSA for 20–30 min. After washing with PBS, cells were incubated with PBS containing 25 μg/ml of the conjugation complex (QD-UEA-1) or free QD in the incubator for 2–3 h. Finally, cells were washed three times with PBS containing 0.2% Tween-20 for 5 min each.

2.7. Fixed cells treatments

Cells were firstly fixed with 3.7% formaldehyde for 10 min, and then they were blocked with 1% BSA in PBS for 20–30 min. Consequently, fixed cells were incubated with PBS containing 12.5 μg/ml of the conjugation complex (QD-anti-vWF) at room temperature for 1–2 h. Finally, cells were washed three times with PBS containing 0.2% Tween-20 for 5 min each. Water-immersion objective was also used to take photos of cells in order to keep the shape integrity of cells.

2.8. Fluorescence microscopy

Images were collected with a Zeiss LSM 510 META laser confocal scanning microscopy with Achroplan 63X/0.95 water-immersion objective. Cells were imaged using 543 nm He-Ne laser excitation and a 560–615 nm BP emission filter. We observed the distribution of QD conjugates in the cells or on the cells surface using general scanning mode.

3. Results and discussion

3.1. Preparation of water-soluble CdTe QDs

The QDs used in bio-labeling should have high QY, good water-solubility and photo-stability. CdTe QDs were prepared in aqueous phase using the reaction between Cd^{2+} and NaHTe solution in the presence of MPA as a stabilizer. We systematically optimized the aqueous phase synthesis conditions, and significantly enhanced QY of CdTe QDs. A series of CdTe QDs with different emission wavelength (490–600 nm) were synthesized by controlling the reaction conditions. Fig. 1 shows the absorption and photoluminescence spectra of a typical CdTe QDs used in cell imaging in this study. The curve (A) presents the absorption spectrum and the curve (F) expresses the emission spectrum of QDs. The absorption spectrum indicates that CdTe QDs has a wider range of absorption, and the excitonic absorption peak is at 530 nm. The emission spectrum displays that the emission peak is at 560 nm, and this spectrum is characterized by good symmetry and relatively narrow spectral width. The QY of CdTe QDs was up to 50%. Furthermore, we observed that water-soluble CdTe QDs solutions were stable for at least 3 months at room temperature (about 20 °C) in the presence of MPA, which was similar to the reports in the references [36]. These data illustrated that CdTe QDs prepared in aqueous phase are high QY, water-soluble and stable, and probably are candidate fluorescent probes in bio-labeling.

3.2. Conjugation of CdTe QDs to UEA-1

Since CdTe QDs were prepared in aqueous phase using MPA as a stabilizer, their surface was coated with certain MPA. The thiol group of MPA is linked to the surface of CdTe QDs by thiol group-Cd coordination, and the functional carboxylic group is free, which can be easily coupled to biomolecules with amine groups, such as proteins, peptides and amino acids. EDC is a

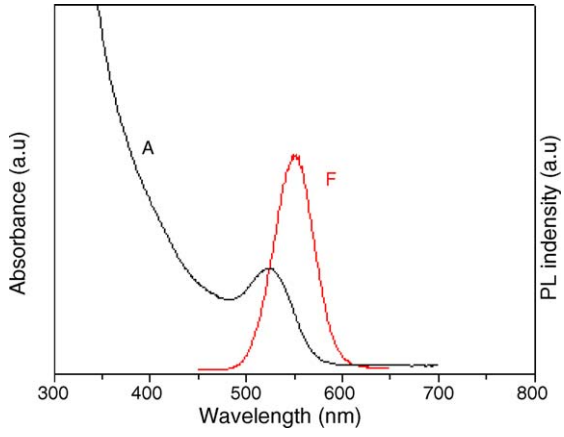

Fig. 1. Absorption (A) and emission spectra (F) of CdTe QDs used in the labeling experiments.

commonly used coupling agent that can link between amine groups of proteins and carboxylic group of some compounds [37,38]. In this work, EDC is chosen to conjugate proteins with CdTe QDs.

The coupling process is expressed as the following equation:

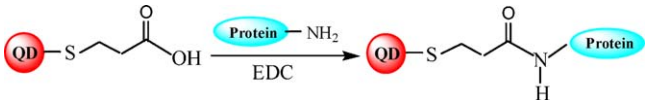

Capillary electrophoresis with LIF detector was used to confirm whether CdTe QDs were effectively conjugated with UEA-1 and anti-vWF.

Fig. 2 displays the electropherograms of the bare CdTe QDs and their conjugates. In the electropherograms 2A, the bare CdTe QDs displays sharp peak, and UEA-1 labeled with CdTe QDs shows a wide peak. Furthermore, the composition of QD-UEA-1 is markedly increased from 69 to 83% after purification using ultra-filtration membrane according to the peak area ratio. From Fig. 2B we can see that a majority of QDs are linked to the antibody anti-vWF, and the percentage of QD-anti-vWF is about 96% according to its peak area. This result shows that it is unnecessary to do the purification. These data demonstrated that both

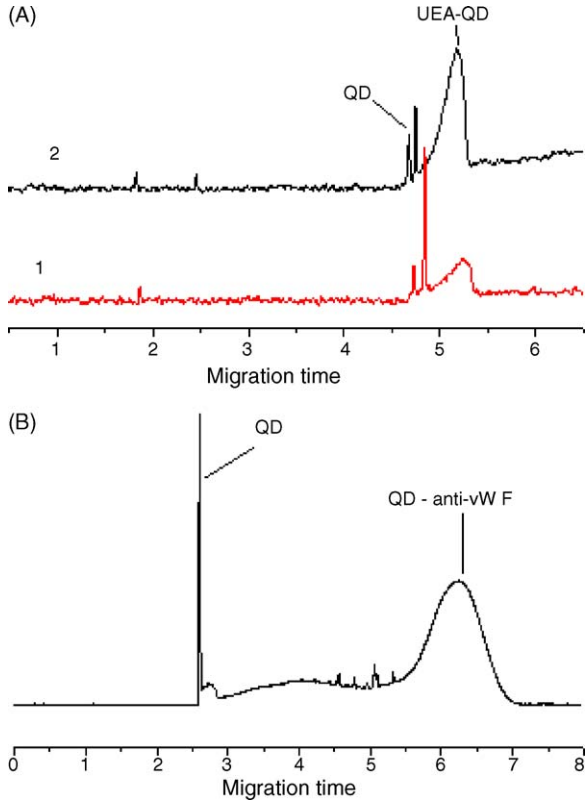

Fig. 2. Analysis of conjugates with QDs by capillary electrophoresis with LIF detector. In the electropherograms (A), the bare CdTe QDs displays sharp peak, and UEA-1 labeled with CdTe QDs shows a wide peak. Sample 1 was the original conjugates of QDs with UEA-1, and sample 2 was from purification of sample 1. The separation buffer was 3.13 mM $Na_2B_4O_7$ solution (pH 10.2). In the electropherograms (B), most of QDs were linked to the antibody anti-vWF. The separation buffer was 6.25 mM $Na_2B_4O_7$ solution (pH 10.1). Two samples were both injected into the capillary using pressure at 1 psi for 5 s.

UEA-1 and anti-vWF were successfully linked to CdTe QDs by reaction of the carboxylic groups on their surface with the amine groups of the protein.

3.3. Live cell imaging

Lectins are nonimmunoglobulin glycoproteins that can recognize and bind to specific sugar moieties on the cell membrane. They are involved in a variety of biological process, such as cell–cell and host–pathogen interactions and innate immune responses [39]. Lectins are usually derived from plants, animals, bacteria, or viruses, with plant lectins accounting for the majority of all lectins. *Ulex europaeus* 1, UEA-1, is one kind of lectins, whose carbohydrate specificity is α-L-fucose [40], and it has a high affinity for human vascular endothelial cells (HUVECs) surface glycoconjugates [41]. In this work, the water-soluble CdTe QDs conjugated-UEA-1 was visualized by confocal microscopy to be localized to the cell membrane.

We used confocal laser scanning fluorescent microscopy to confirm the binding of UEA-1 in HUVECs. Fig. 3A clearly shows the distribution and staining of QD-UEA-1 on the cell membrane. To confirm QD-UEA-1 specifically bound on the cell membrane, the contrast experiment was conducted using bare CdTe QDs at the same conditions, as shown in Fig. 3B. From Fig. 3B we observed nearly no bare QDs on the cell membrane, but only a few QDs dispersed in the cytoplasm, mostly in perinuclear region of the cells. This is because bare CdTe QDs prepared in aqueous phase possess smaller size, and easily dispersed in the cytoplasm after they entered the cell by endocytosis. Our results demonstrated that the QD conjugates could be used for imaging of live cells as fluorescence probes.

3.4. Fixed cell imaging

In this work, we want to apply QD-anti-vWF for the imaging of the fixed cells. The endothelial marker von Willebrand factor (vWF) is a plasma multimeric glycoprotein, and is synthesized exclusively in endothelial cells and stored in Weibel–Palade bodies. The vWF performs important functions in platelet adhesion, thrombosis and atherogenesis. Deficiency or dysfunction of vWF and maldistribution of the predominating multimeric forms of the protein characterizes several subtypes of the common hereditary bleeding disorder, von Willebrand Disease (vWD) [42]. The monoclonal anti-vWF specifically reacts with the cytoplasm of human endothelial cells from normal blood.

Fig. 4 showed images of HUVECs using QD-anti-vWF as a probe. We observed that QD-anti-vWF was distributed in the cytoplasm surrounding the nuclei, and targeted in the different parts of fixed cells. QD-anti-vWF could penetrate across the cell membrane and disperse in cytoplasm, due to that fixed cell membranes were demolished by formaldehyde. From Fig. 4, it is very clear that the QD-anti-vWF conjugates mostly distributed around the nuclei, which was similar with the reference [42] using FITC-anti-vWF. These data also demonstrated that CdTe

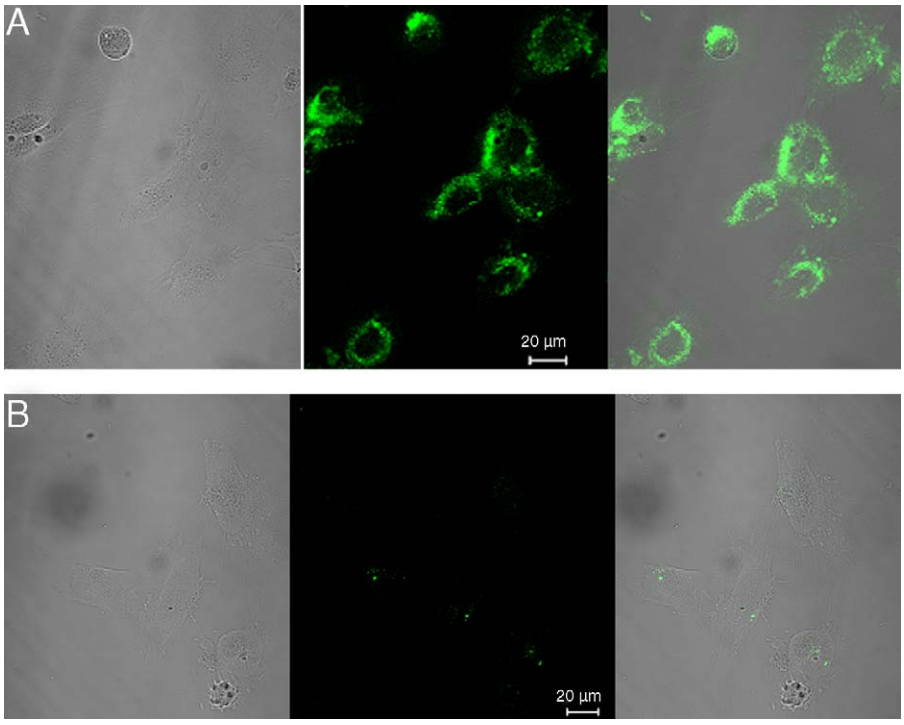

Fig. 3. Images of live cells membrane using QD bioconjugates. Confocal images of HUVECs stained with QD-UEA-1 (A), Confocal images of cells stained with QDs (B) (with same concentration and incubation time). In both panels, the left row represents the phase contrast image, the central row represents the fluorescence image, and the right row is an overlay of the left and central rows. Cells were incubated with all probes for 2–3 h. QD labeled UEA-1 were clearly visualized on the cell surface, while few free QDs were dispersed in the cytoplasm disorderly. The scale bars are 20 μm.

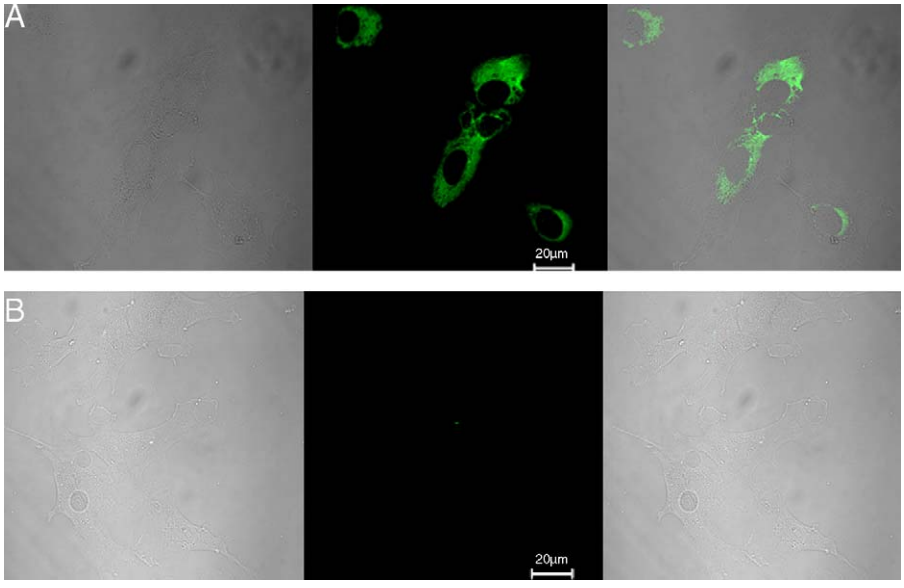

Fig. 4. Confocal images of fixed HUVEC cells incubated with anti-vWF conjugated QD (A) and bare QDs which the concentration was same with QDs in conjugates (B) as negative control. QD-anti-vWF was distributed in the cytoplasm, surrounding the nuclei. The scale bars are 20 μm.

QDs prepared in aqueous phase had the same imaging impact with common organic dyes (FITC) in fixed cells.

4. Conclusions

In this work, we demonstrated that highly luminescent CdTe QDs prepared in aqueous phase could be conveniently conjugated with glycoprotein and antibody, and the QDs linked with UEA-1 or anti-vWF was successfully used for the imaging of the live cells and fixed cells. Our results also showed that the QD probes were able to specifically bind the corresponding cellular membrane receptor in live cells, and dispersed in cytoplasm in fixed cells.

Compared to the currently used QDs prepared in organic phase, QDs prepared in water phase were low cost and water-soluble, and easily linked with biomolecules (such as proteins

and peptides). Our preliminary results illustrate that CdTe QDs prepared in water phase probably will become an attractive alternative probes in cellular imaging and bio-labeling.

Acknowledgements

This work was financially supported by the National Natural Science Foundation of China (No. 20271033, 90408014), the key project of National Natural Science Foundation of China (No. 20335020) and the Nano-Science Foundation of Shanghai (0452NM052, 05NM05002).

References

[1] F. Tokumasu, J. Dvorak, J. Microsc. 211 (2003) 256.
[2] M. Shingyoji, D. Gerion, D. Pinkel, J.W. Gray, F. Chen, Talanta 67 (2005) 472.
[3] X. Gao, Y. Cui, R.M. Levenson, L.W. Chung, S. Nie, Nat. Biotechnol. 22 (2004) 969.
[4] A.M. Derfus, W.C.W. Chan, S.N. Bhatia, Adv. Mater. 16 (2004) 961.
[5] M.E. Akerman, W.C. Chan, P. Laakkonen, S.N. Bhatia, E. Ruoslahti, Proc. Natl. Acad. Sci. 99 (2002) 12617.
[6] N. Gomez, J.O. Winter, F. Shieh, A.E. Saunders, B.A. Korgel, C.E. Schmidt, Talanta 67 (2005) 462.
[7] F. Chen, D. Gerion, Nano Lett. 4 (2004) 1827.
[8] M. Han, X. Gao, J.Z. Su, S. Nie, Nat. Biotechnol. 19 (2001) 631.
[9] D. Gerion, W.J. Parak, S.C. Williams, D. Zanchet, C.M. Micheel, A.P. Alivisatos, J. Am. Chem. Soc. 124 (2002) 7070.
[10] J.R. Taylor, M.M. Fang, S. Nie, Anal. Chem. 72 (2000) 1979.
[11] E.R. Goldman, A.R. Clapp, G.P. Anderson, H.T. Uyeda, J.M. Mauro, I.L. Medintz, H. Mattoussi, Anal. Chem. 76 (2004) 684.
[12] J.K. Jaiswal, H. Mattoussi, J.M. Mauro, S.M. Simon, Nat. Biotechnol. 21 (2003) 47.
[13] X. Wu, H. Liu, J. Liu, K.N. Haley, J.A. Treadway, J.P. Larson, N. Ge, F. Peale, M.P. Bruchez, Nat. Biotechnol. 21 (2003) 41.
[14] E.R. Goldman, G.P. Anderson, P.T. Tran, H. Mattoussi, P.T. Charles, J.M. Mauro, Anal. Chem. 74 (2002) 841.
[15] Q. Ma, X.G. Su, X.Y. Wang, Y. Wan, C.L. Wang, B. Yang, Q.H. Jin, Talanta 67 (2005) 1029.
[16] F. Zhang, C. Li, X. Li, X. Wang, Q. Wan, Y. Xian, L. Jin, K. Yamamoto, Talanta 68 (2006) 1353.
[17] J. Liang, S. Huang, D. Zeng, Z. He, X. Ji, X. Ai, H. Yang, Talanta 69 (2006) 126.
[18] W.C.W. Chan, S. Nie, Science 281 (1998) 2016.
[19] M. Bruchez Jr., M. Moronne, P. Gin, S. Weiss, A.P. Alivisatos, Science 25 (1998) 2013.
[20] S.J. Rosenthal, I. Tomlinson, E.M. Adkins, S. Schroeter, S. Adams, L. Swafford, J. McBride, Y. Wang, L.J. DeFelice, R.D. Blakely, J. Am. Chem. Soc. 124 (2002) 4586.
[21] M. Dahan, S. Levi, C. Luccardini, P. Rostaing, B. Riveau, A. Triller, Science 302 (2003) 442.
[22] D.S. Lidke, P. Nagy, R. Heintzmann, D.J. Arndt-Jovin, J.N. Post, H.E. Grecco, E.A. Jares-Erijman, T.M. Jovin, Nat. Biotechnol. 22 (2004) 198.
[23] Z.A. Peng, X. Peng, J. Am. Chem. Soc. 123 (2001) 183.
[24] R.E. Bailey, S.M. Nie, J. Am. Chem. Soc. 125 (2003) 7100.
[25] D.V. Talapin, S. Haubold, A.L. Rogach, A. Kornowski, M. Haase, H. Weller, J. Phys. Chem. B 105 (2001) 2260.
[26] L. Qu, Z.A. Peng, X. Peng, Nano Lett. 1 (2001) 333.
[27] L. Qu, X. Peng, J. Am. Chem. Soc. 124 (2002) 2049.
[28] H. Mattoussi, J.M. Mauro, E.R. Goldman, G.P. Anderson, V.C. Sundar, F.V. Mikulec, M.G. Bawendi, J. Am. Chem. Soc. 122 (2000) 12142.
[29] H.T. Uyeda, I.L. Medintz, J.K. Jaiswal, S.M. Simon, H. Mattoussi, J. Am. Chem. Soc. 127 (2005) 3870.
[30] N. Gaponik, D.V. Talapin, A.L. Rogach, K. Hoppe, E.V. Shevchenko, A. Kornowski, A. Eychmüller, H. Weller, J. Phys. Chem. B. 106 (2002) 7177.
[31] H. Zhang, Z. Cui, Y. Wang, K. Zhang, X. Ji, C. Lü, B. Yang, M.Y. Gao, Adv. Mater. 15 (2003) 777.
[32] L. Li, H.F. Qian, J. Ren, Chem. Commun. (2005) 528.
[33] L. Li, H.F. Qian, N.H. Fang, J. Ren, J. Luminesc. 116 (2006) 59.
[34] Z.Y. Tang, N.A. Kotov, M. Giersig, Science 297 (2002) 237.
[35] G.A. Crosby, J.N. Demas, J. Phys. Chem. 75 (1971) 991.
[36] J. Lovric, H.S. Bazzi, Y. Cuie, G.R. Fortin, F.M. Winnik, D. Maysinger, J. Mol. Med. 83 (2005) 377.
[37] S.P. Wang, N. Mamedova, N.A. Kotov, W. Chen, J. Studer, Nano Lett. 2 (2002) 817.
[38] A. Schroedter, H. Weller, Nano Lett. 2 (2002) 1363.
[39] M. Qaddoumi, V.H. Lee, Pharm. Res. 21 (2004) 1160.
[40] M. Tsokos, Leg. Med. 5 (2003) 73.
[41] C.K. Ozaki, M.D. Phaneuf, S.L. Hong, W.C. Quist, F.W. LoGerfo, J. Vasc. Surg. 18 (1993) 486.
[42] T. Royo, J. Martinez-Gonzalez, G. Vilahur, L. Badimon, Atherosclerosis 167 (2003) 55.

Available online at www.sciencedirect.com
ScienceDirect
Talanta 70 (2006) 403–407
Talanta
www.elsevier.com/locate/talanta

Microchip capillary electrophoresis coupled with an end-column electrochemiluminescence detection

Shou-Nian Ding, Jing-Juan Xu, Hong-Yuan Chen *

The Key Lab of Analytical Chemistry for Life Science, Department of Chemistry, Nanjing University, Nanjing 210093, China

Received 19 January 2006; received in revised form 22 February 2006; accepted 23 February 2006
Available online 31 March 2006

Abstract

An easy and universal wall-jet configuration for microchip CE-ECL detection system was constructed and investigated in this work. Two detection modes of pre-column and post-column were applied to the above system. TPA, tramadol and lidocaine were chosen as model analytes to estimate the system in both modes. The important operational parameters such as the concentration of luminescent reagent and the distance between the separation outlet and the working electrode were optimally obtained and compared for the first time.

Keywords: Microchip electrophoresis; Electrochemiluminescence; Tris(2,2′-bipyridyl)ruthenium(II)

1. Introduction

Many compounds such as oxalate, amino acids, amines, pharmaceuticals or protein can be sensitively detected via electrochemiluminescence (ECL) based on tris(2,2′-bipyridyl)ruthenium(II) ($Ru(bpy)_3^{2+}$) [1–5], thus meaning that this detection strategy may have widespread application in a variety of important areas[6–13].

Recently, some efforts have been reported to integrate capillary electrophoresis (CE) with the ECL detection [14–24]. Aqueous ECL of $Ru(bpy)_3^{2+}$ was often used to combine with CE to detect analytes due to its convenience. The appropriate mixing of $Ru(bpy)_3^{2+}$ and the separation buffer is critical in order to achieve good separation efficiency at maintaining high sensitivity all the while. Forbes et al. reported on-line electrogenerated $Ru(bpy)_3^{3+}$ chemiluminescent detection of β-blockers separated with CE [14]. Bobbit et al. reported in situ cell electrogenerated $Ru(bpy)_3^{3+}$-based chemiluminescence detection in CE [15,18]. Wang and co-workers reported a new technique for CE directly coupled with end-column electrochemiluminescence detection [19,20]. For these studies, two detection modes, pre-column mode and post-column mode, were applied for CE-ECL. For the pre-column mode, $Ru(bpy)_3^{2+}$ is added to the running buffer. For the post-column mode, $Ru(bpy)_3^{2+}$ is directly added to the cathodic cell. For common CE, the major shortcoming of the above modes is the excessive consumption of expensive $Ru(bpy)_3^{2+}$ reagent. To develop a solid-state ECL sensor in which $Ru(bpy)_3^{2+}$ is immobilized may offer an effective approach to resolve the above problem [25,26], however, its stability is a severe challenge. Meanwhile, the process of fabricating ECL sensors is tedious.

Microchip CE may offer another possibility to resolve such a problem. For microchip CE-ECL detection system, the separation time is much shorter than that for conventional CE-ECL, based on this fact, a series of the influences resulted from the variation of the experimental conditions such as the change of EOF in pre-column mode, a dilution of $Ru(bpy)_3^{2+}$ in post-column mode as well as excessive consumption of $Ru(bpy)_3^{2+}$, etc. should be minimized.

Up to now, reports on the microchip CE with ECL detection are very limited [25–31]. Manz and his co-workers reported a microfluidic system with indirect $Ru(bpy)_3^{2+}$ ECL detection of amino acids, based on a "U"-shape floating platinum electrode placed across the separation channel [29]. Wang and co-workers reported an ECL detector with microchip CE, which consisted of a poly(dimethylsiloxane) (PDMS) layer containing separation and injection channels and an electrode plate with an ITO electrode fabricated by a photolithographic method

* Corresponding author. Tel.: +86 25 83594862; fax: +86 25 83594862.
E-mail address: hychen@nju.edu.cn (H.-Y. Chen).

0039-9140/$ – see front matter © 2006 Elsevier B.V. All rights reserved.
doi:10.1016/j.talanta.2006.02.063

[25,30,31]. However, these microchip CE-ECL detection systems were complicated and to construct these detection systems was not only time-consuming and tedious but also need expensive special instruments. It is surprising that there are few reports on a simple, low-cost, end-column, wall-jet detector, which is widely used in electrochemically amperometric detection, for microchip CE-ECL.

In this work, a simple and universal wall-jet configuration for the microchip CE combined with an end-column ECL detection system was constructed and both detection modes, i.e. pre-column mode and post-column mode were applied to the microchip CE-ECL system. A 400 μm diameter glassy carbon disc electrode used as a working electrode and aligned with the outlet of separation channel electrochemically oxidizes the $Ru(bpy)_3^{2+}$ to the active $Ru(bpy)_3^{3+}$ form, which then reacts with analytes at the cathodic cell and produces light.

Since tramadol and lidocaine are often used for analgetic and local anesthetic, respectively, and with tertiary amine structures for $Ru(bpy)_3^{2+}$ ECL reaction, fast analysis of tramadol and lidocaine is of clinic importance for understanding the patient's medical process. Meanwhile, the $Ru(bpy)_3^{2+}$–TPA system has been well studied and shown to give rise to high ECL intensity. Therefore, TPA, tramadol and lidocaine were chosen as model compounds to characterize this microchip CE-ECL detection system in both modes.

2. Materials and methods

2.1. Chemicals and apparatus

All reagents used were commercially available and of analytical grade. Tripropylamine (TPA) and tris(2,2′-bipyridyl)ruthenium(II) chloride were purchased from Sigma–Aldrich (St. Louis, MO, USA) and used as received. Tramadol and lidocaine were obtained from Nanjing Pharmaceutical Institute (Nanjing, China). All solutions were prepared with twice-distilled water. The stock solutions were stored in the refrigerator (at 4 °C). All standard solutions and phosphate buffers (PBS) were prepared and filtered through a 0.22 μm membrane (Jasco, Dailian, China) before use.

Electrochemical measurements were performed with a three-electrode system comprising a platinum wire as auxiliary electrode, an Ag/AgCl (sat. KCl) electrode as reference electrode, and the glassy carbon disk electrode with a diameter of 0.4 mm as working electrode. The electrodes were connected to a CHI630A electrochemical workstation (Shanghai Chenhua Apparatus Corporation, China). All microchip CE-ECL emission detections were obtained by a Model MPI-A CE-ECL Analyzer Systems (Xi'an Remax Electronic High-Tech Ltd., Xi'an, China). The photomultiplier tube (PMT) was biased at 1000 V.

2.2. Applications of the microchip CE-ECL detection

Fig. 1 is the schematic diagram of the experimental setup and the detector was of the wall-jet configuration. The construction of the microchip CE-ECL platform is shown in Fig. 2. The platform body was made of polymethyl methacrylate material. The working electrode was aligned at the exit of the electrophoretic separation channel. No decoupler was employed for isolating the high separation electric field in this system. The glass chip shown in Fig. 2 consisted of a glass plate, with a 50 mm long separation channel and a 10 mm long injection channel (between the sample reservoir and the sample waste reservoir). The two channels crossed each other halfway between the sample and the sample waste reservoir and 45 mm from the outlet to yield a separation channel with an effective length of 45 mm. The channels were 60 μm width and 20 μm depth.

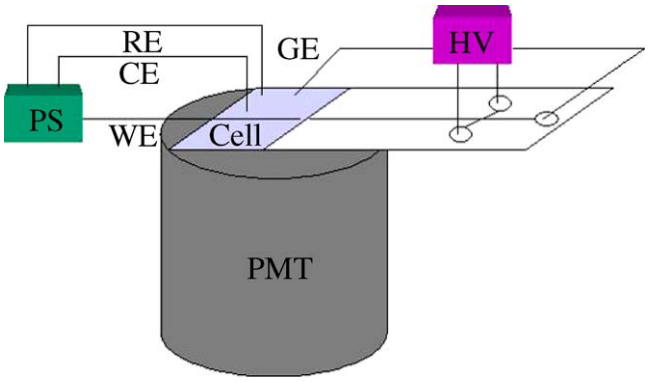

Fig. 1. Schematic diagram of the experimental setup: (WE) working electrode, (CE) counter electrode, (RE) reference electrode, (GE) ground electrode, (PS) potentiostat, (HV) high voltage, (PMT) photomultiplier tube. WE was a glassy carbon disk electrode with diameter of 0.4 mm; CE, GE were platinum wires; RE was Ag/AgCl (sat. KCl) electrode.

Alignment of the working electrode with the outlet of separation channel was quite important in the experiment. To accomplish alignment, the working electrode was aligned with the outlet of separation channel and fixed by a precisely three-dimensional adjustor (Shanghai Lian Yi Instrument Factory of Optical Fiber and Laser, Shanghai, China) with the precision of ±1 μm in each direction under the microscope with ruler. Meanwhile, the end of separation channel outlet of the glass microchip was rubbed away to a wedge shape with the thick-

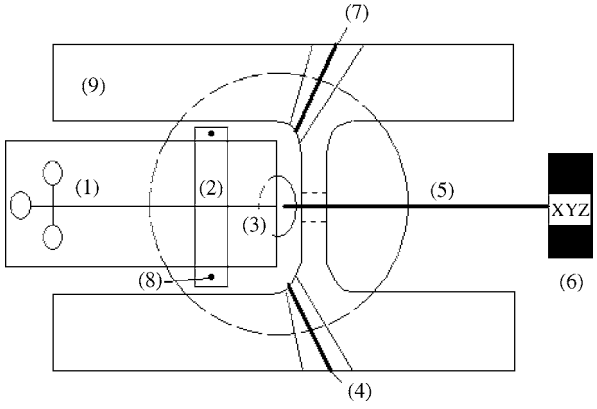

Fig. 2. The schematic diagram of the microchip CE-ECL platform by end-column mode. (1) glass microchip; (2) a piece of polymethyl methacrylate; (3) UV transparent optic glass; (4) counter electrode; (5) working electrode; (6) three-dimensional adjustor; (7) reference electrode; (8) screws; (9) polymethyl methacrylate body.

ness of 500 μm. The lower layer of the cell was made of a piece of UV transparent optic glass through which the photons were captured by the PMT. About 300 μL cathodic cell was obtained by the aid of Teflon thin films.

2.3. Electrophoresis procedure

A four-channel programmable high-voltage power supply (0–2000 V, Remax Electronic Co. Ltd., Xi'an, China) was applied to perform the electrokinetic sample injection and electrophoretic separation. The separation channel was treated before use by rinsing with 0.1 mol L^{-1} NaOH, twice distilled water, and 10 mmol L^{-1} PBS each for 5 min, then 10 mmol L^{-1} PBS (pH 9.0) with $Ru(bpy)_3^{2+}$ was used as running buffer. All these were carried out with the aid of a vacuum pump. In the experiments, external platinum wires were used to provide electrical circuit from the high voltage to the solutions in the reservoirs. Sample plugs were injected into the separation channel by applying a voltage of 200 V between the sample and sample waste reservoirs for 30 s with the buffer reservoir and the detection reservoir floating. Once the injection was completed, the high voltages of 1500, 800, 800 and 0 V were applied to the buffer reservoir, the sample reservoir, the sample waste reservoir and the detection reservoir for the sample separation.

3. Results and discussion

3.1. Detection potential for both modes

The detection and separation conditions can be optimized independently. In the format of microchip CE, electrochemical detection was easily affected by the high separation voltage. In this case, end-column detection modes were popular to minimize the influence of separation voltage, and the working electrode is positioned tens of micrometers from the exit of the separation channel. This distance allows sufficient decoupling of the working electrode and detector from the separation voltage. However, since the separation voltage is grounded within the detection reservoir, the remaining separation field causes potential shifts at the working electrode. Therefore, it is necessary to perform a cyclic voltammogram for a given analyte, under the exact separation conditions that will be employed, to determine the appropriate detection potential. Cyclic voltammogram of $Ru(bpy)_3^{2+}$ with separation voltage in pre-column mode was shown in Fig. 3. And it is similar to the cyclic voltammogram in post-column mode (not shown). The proper potential was chosen to bias at 1.2 V (versus Ag/AgCl), near the oxidation potential of $Ru(bpy)_3^{2+}$, in both pre-column mode and post-column mode.

3.2. Concentration of $Ru(bpy)_3^{2+}$ for both modes

However, the presence of $Ru(bpy)_3^{2+}$ in the CE electrolyte affects the separation and various buffer components (notably OH^-) affect the CL reactions. One of the most important detection parameters is the optimum concentration of $Ru(bpy)_3^{2+}$ added to the CE electrolyte. The concentration of $Ru(bpy)_3^{2+}$ in the electrolyte has a large impact on background CL signal and dynamic range; a lower concentration of $Ru(bpy)_3^{2+}$ leads to a lower background, while a high concentration of analyte may deplete the available $Ru(bpy)_3^{2+}$ at the outlet end of the separation channel leading to a non-linear working curve. Fig. 4 shows the S/N at each $Ru(bpy)_3^{2+}$ concentration for 1.0×10^{-4} mol L^{-1} TPA in pre-column mode (curve a). 1.5 mmol L^{-1} $Ru(bpy)_3^{2+}$ gives the best S/N, and has been used for all experiments in pre-column mode. However, in post-column mode, $Ru(bpy)_3^{2+}$ was directly added in the cathodic cell, which resulted in a dilution of $Ru(bpy)_3^{2+}$ near the surface of the working electrode by the running buffer flowed from the microchip, higher concentration of $Ru(bpy)_3^{2+}$ should be used. Fig. 4 (curve b) shows 5.0 mmol L^{-1} $Ru(bpy)_3^{2+}$ gives the best S/N in the post-column mode. Therefore 5.0 mmol L^{-1} $Ru(bpy)_3^{2+}$ has been chosen for all experiments in post-column mode.

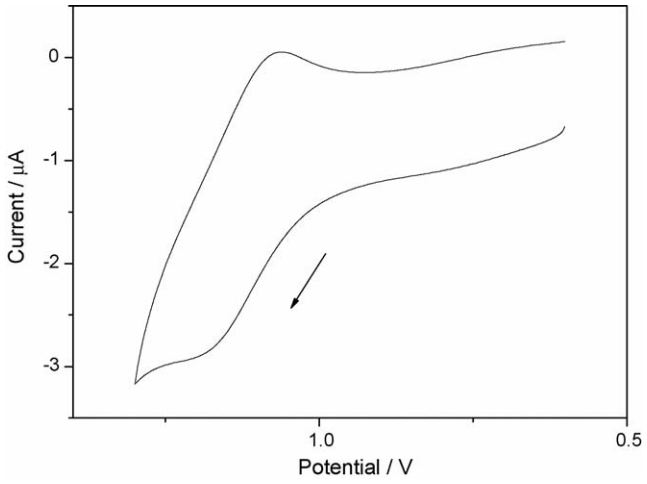

Fig. 3. Hydrodynamic cyclic voltammogram of 1.5 mmol L^{-1} $Ru(bpy)_3^{2+}$ in 10 mmol L^{-1} PBS running buffer with separation voltage. Scan rate, 100 mV/s. The distance between the separation channel outlet and the electrode was 30 μm.

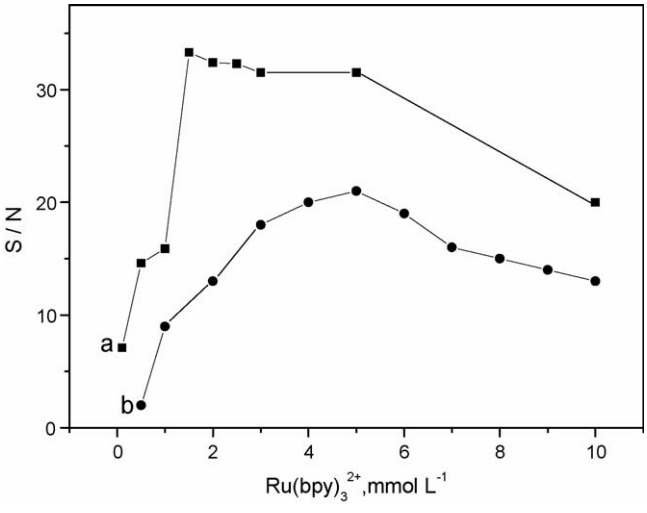

Fig. 4. Effects of concentrations of $Ru(bpy)_3^{2+}$ in the running buffer (a) and in the cathodic cell (b) on the signal-to-noise ratio for 1.0×10^{-4} mol L^{-1} TPA. The distances between the separation channel outlet and the electrode were 30 and 120 μm in the pre-column and post-column modes, respectively.

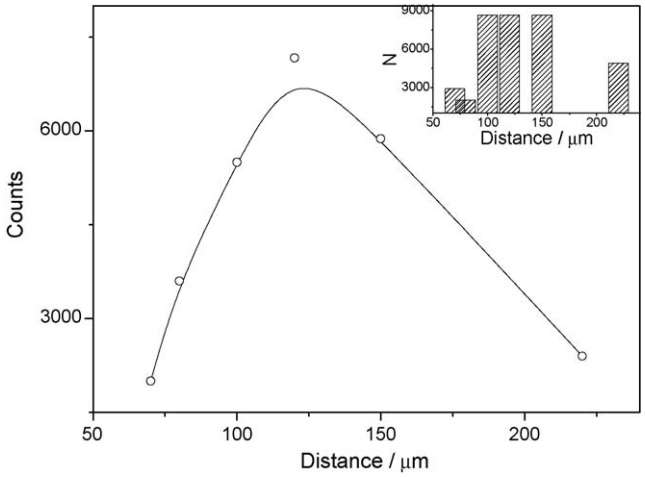

Fig. 5. 1.0×10^{-4} mol L^{-1} TPA ECL intensity and corresponding theory plates number (inset) in 5 mmol L^{-1} $Ru(bpy)_3^{2+}$ solution with the post-column mode.

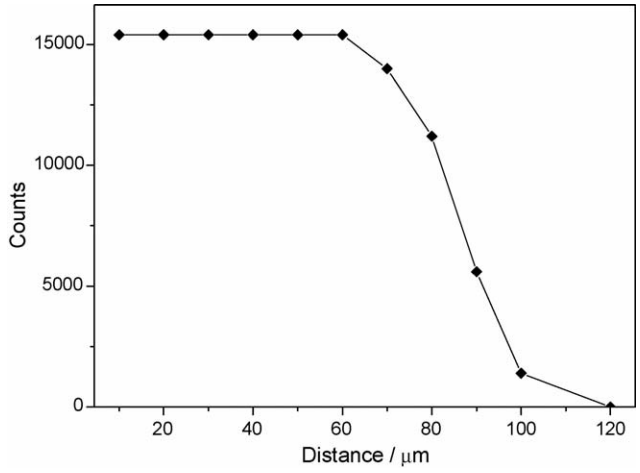

Fig. 6. Effects of the distance of separation channel outlet to electrode on peak height for 1.0×10^{-4} mol L^{-1} TPA in 10 mmol L^{-1} PBS. Separation voltage, 300 V/cm. Other conditions were the same as those in Fig. 3.

3.3. Effect of the distance between the outlet and the working electrode for both modes

For microchip CE-ECL detection system, the distance between the electrode and the capillary outlet is an important factor that influences the separation efficiency and detection sensitivity. Generally, large distance results in analyte band dispersion and loss of efficiency. Fig. 5 shows the effect of the outlet to electrode distance on the peak height and the theoretical plate numbers for TPA in post-column mode. For the distance smaller than 120 μm, the dispersion of CE buffer diluted the concentration of $Ru(bpy)_3^{2+}$ in the region of detection. For distance larger than 150 μm, a decrease of peak height of ECL was observed. The maximum ECL intensity was obtained at a distance of 120 μm. As a measure of separation efficiency, the theoretical plate numbers (*N*) were calculated on the basis of TPA signals for different outlet to electrode distances (the inset). The maximum *N* was only 9000 obtained for the distance from 100 to 150 μm. It can be explained that too large a distance results in a decrease of mass transport of analyte into the detection region.

For the pre-column mode, the optimum distance was greatly different. Fig. 6 shows the effect of the distance between the electrode and the separation channel outlet on peak height for TPA. It can be seen that the ECL intensities were found to be approximately independent of the positioning at the detector-to-outlet distances between 0 and 60 μm. For distances larger than 60 μm, the ECL intensities declined rapidly with increasing distance from the outlet of separation channel. The result indicated that the separation efficiency could be remained when the distance was less than the diameter of separation channel, which is consistent with the results obtained with amperometric detection [32–35]. This result can offer us a convenience in adjusting the distance between the detector and the outlet of separation channel and decrease the errors between two operations.

3.4. Electropherograms of both modes

Fig. 7 is the electropherograms of 1.0×10^{-4} mol L^{-1} TPA, 1.0×10^{-4} mol L^{-1} tramadol and 4.0×10^{-5} mol L^{-1} lidocaine in pre-column mode and in post-column mode. In post-column mode (a), only one peak can be obtained. TPA, tramadol and lidocaine cannot be separated and the theoretical plate numbers was only 9000. However, in pre-column mode, it can be seen that TPA, tramadol and lidocaine can be separated completely (b). And the theoretical plate numbers (*N*) were 91,000, 73,000 and 59,000 for TPA, tramadol and lidocaine, respectively. The poorer separation efficiency for the post-column mode was due to that $Ru(bpy)_3^{2+}$ was directly added in the cathodic cell, which resulted in a dilution of $Ru(bpy)_3^{2+}$ near the surface of the work-

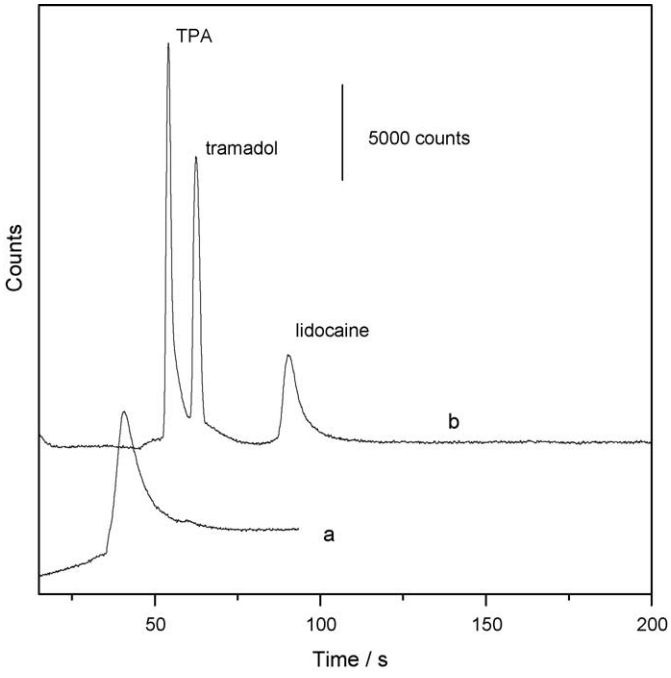

Fig. 7. Electropherograms of 1.0×10^{-4} mol L^{-1} TPA, 1.0×10^{-4} mol L^{-1} tramadol and 4.0×10^{-5} mol L^{-1} lidocaine in post-column (a) and pre-column (b) mode. Conditions: (a) 5.0 mmol L^{-1} $Ru(bpy)_3^{2+}$ in cathodic cell, 120 μm distance between the separation channel outlet and the electrode; (b) 1.5 mmol L^{-1} $Ru(bpy)_3^{2+}$ in running buffer, 30 μm distance between the separation channel outlet and the electrode.

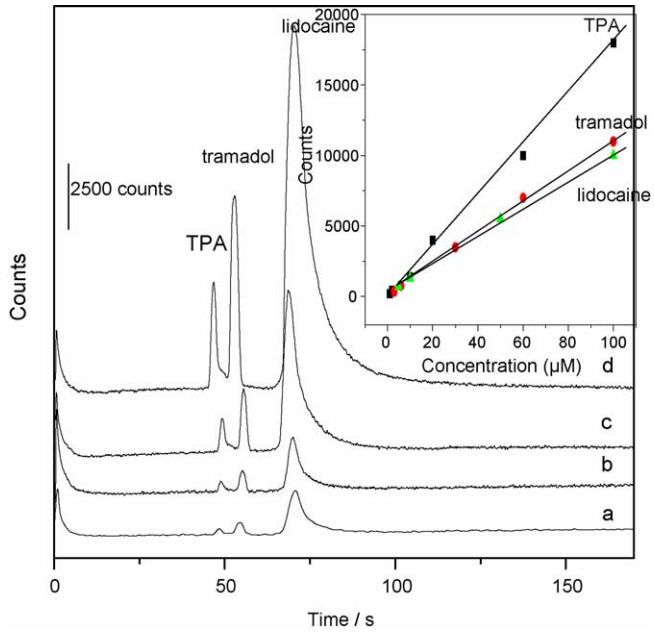

Fig. 8. Electropherograms of a mixture containing (a) 1.0×10^{-6} mol L^{-1} TPA, 3.0×10^{-6} mol L^{-1} tramadol and 5×10^{-6} mol L^{-1} lidocaine; (b) 2 times of (a); (c) 10 times of (a); (d) 20 times of (a). Other conditions were the same as those in Fig. 3.

ing electrode by the running buffer flowed from the microchip, and in order to maintain high concentration of $Ru(bpy)_3^{2+}$ near the working electrode, the distance from the outlet to the working electrode should be very large, while the large distance leads to the low separation efficiency and low theoretical plate numbers for the analytes diffusion.

3.5. Analytic performance in pre-column mode

Electropherograms of the mixtures of TPA, tramadol and lidocaine with different concentrations were shown in Fig. 8. The ECL intensities for detection of TPA, tramadol and lidocaine as a function of concentrations were found to be linear from 1.0×10^{-6} to 1.0×10^{-4} mol L^{-1} for TPA, 2.0×10^{-6} to 1.0×10^{-4} mol L^{-1} for tramadol, and 5.0×10^{-6} to 1.0×10^{-4} mol L^{-1} for lidocaine with the detection limits (S/N = 3) of 5.0×10^{-7} mol L^{-1} for TPA, 1.0×10^{-6} mol L^{-1} for tramadol, 3.0×10^{-6} mol L^{-1} for lidocaine, respectively.

4. Conclusion

$Ru(bpy)_3^{3+}$-based electrochemiluminescence detection coupling with microchip CE in a end-column configuration was investigated systematically. The optimal operational parameters for two detection modes, pre-column mode and post-column mode, for the microchip CE-ECL system were obtained and compared. And in pre-column mode, TPA, tramadol and lidocaine can be completely separated with high separation efficiency. Pharmaceuticals such as tramadol and lidocaine can be successfully detected by this detection system. The results in this work are instructive to facilitate ECL detection for application to micro total analytical system and show a good prospect for the determination of medicines in clinical analysis.

Acknowledgements

The support of this research by the National Natural Science Foundation of China (20475025, 90206037, 20575029) and the Natural Science Foundation of Jiangsu (BK 2004210) is gratefully acknowledged.

References

[1] I. Rubinstein, A.J. Bard, Anal. Chem. 55 (1983) 1580–1582.
[2] J.B. Noffsinger, N.D. Danielson, Anal. Chem. 59 (1987) 865–868.
[3] S.N. Brune, D.R. Bobbitt, Anal. Chem. 64 (1992) 166–170.
[4] T.M. Downey, T.A. Nieman, Anal. Chem. 64 (1992) 261–268.
[5] M. Zorzi, P. Pastore, F. Magno, Anal. Chem. 72 (2000) 4934–4939.
[6] K.A. Fahnrich, M. Pravda, G.C. Guilbault, Talanta 54 (2001) 531–559.
[7] R.D. Gerardi, N.W. Barnett, S.W. Lewis, Anal. Chim. Acta 378 (1999) 1–41.
[8] A.W. Knight, Trends Anal. Chem. 18 (1999) 47–62.
[9] W.Y. Lee, Mikrochim. Acta 127 (1997) 19–39.
[10] A.W. Knight, G.M. Greenway, Analyst 119 (1994) 879–890.
[11] J.G. Velasco, Bull. Electrochim. 10 (1994) 29–38.
[12] N.N. Rozhitskii, J. Anal. Chem. 47 (1992) 1288–1301.
[13] J.G. Velasco, Electroanalysis 3 (1991) 261–271.
[14] G.A. Forbes, T.A. Nieman, J.V. Sweedler, Anal. Chim. Acta 347 (1997) 289–293.
[15] X. Wang, D.R. Bobbit, Anal. Chim. Acta 383 (1999) 213–219.
[16] X. Wang, D.R. Bobbit, Talanta 53 (2000) 337–345.
[17] H.P. Hendrickson, P. Anderson, X. Wang, Z. Pittman, D.R. Bobbitt, Microchem. J. 65 (2000) 189–195.
[18] D.R. Bobbit, W.A. Jackson, H.P. Hendrickson, Talanta 46 (1998) 565–572.
[19] W. Cao, J. Liu, X. Yang, E. Wang, Electrophoresis 23 (2002) 3683–3691.
[20] W. Cao, J. Liu, H. Qiu, X. Yang, E. Wang, Electroanalysis 14 (2002) 1571–1576.
[21] M.-T. Chiang, M.-C. Lu, C.-W. Whang, Electrophoresis 24 (2003) 3033–3039.
[22] M.-T. Chiang, C.-W. Whang, J. Chromatogr. A 934 (2001) 59–66.
[23] X. Huang, R.N. Zare, S. Sloss, A.G. Ewing, Anal. Chem. 63 (1991) 189–192.
[24] S.-N. Ding, J.-J. Xu, H.-Y. Chen, Electrophoresis 26 (2005) 1737–1744.
[25] Y. Du, H. Wei, J. Kang, J. Yan, X.-b. Yin, X. Yang, E. Wang, Anal. Chem. 77 (2005) 7993–7997.
[26] S.-N. Ding, J.-J. Xu, W.-J. Zhang, H.-Y. Chen, Talanta, doi:10.1016/j.talanta.2006.01.017.
[27] W. Zhan, J. Alvarez, R.M. Crooks, J. Am. Chem. Soc. 124 (2002) 13265–13270.
[28] W. Zhan, J. Alvarez, R.M. Crooks, Anal. Chem. 75 (2003) 313–318.
[29] A. Arora, J.C.T. Eijkel, W.E. Morf, A. Manz, Anal. Chem. 73 (2001) 3282–3288.
[30] H. Qiu, J. Yan, X. Sun, J. Liu, W. Cao, X. Yang, E. Wang, Anal. Chem. 75 (2003) 5435–5440.
[31] X.-c. Zhao, T.-y. You, H.-b. Qiu, J. Yan, X. Yang, E. Wang, J. Chromatogr. B 810 (2004) 137–142.
[32] S.R. Wallenborg, K.E. Markides, L. Nyholm, Anal. Chim. Acta 344 (1997) 77–85.
[33] R.P. Baldwin, T.J. Roussel, M.M. Crain, V. Bathlagunda, D.J. Jackson, J. Cullapalli, J.A. Conklin, R. Pai, J.F. Naber, K.M. Walsh, R.S. Keynton, Anal. Chem. 74 (2002) 3690–3697.
[34] J. Wang, B. Tian, E. Sahlin, Anal. Chem. 71 (1999) 5436–5440.
[35] Y. Zeng, H. Chen, D.W. Pang, Z.L. Wang, J.K. Cheng, Anal. Chem. 74 (2002) 2441–2445.

Available online at www.sciencedirect.com
ScienceDirect
Talanta 70 (2006) 408–413
Talanta
www.elsevier.com/locate/talanta

Fast simultaneous spectrophotometric determination of naphazoline nitrate and methylparaben by sequential injection chromatography

Petr Chocholouš, Dalibor Šatínský, Petr Solich *

Department of Analytical Chemistry, Faculty of Pharmacy, Charles University, Heyrovského 1203, Hradec Králové 50005, Czech Republic

Received 20 January 2006; received in revised form 23 February 2006; accepted 23 February 2006
Available online 11 April 2006

Abstract

Fast simultaneous determination of naphazoline nitrate and methylparaben in pharmaceuticals using separation method based on a novel reversed-phase sequential injection chromatography (SIC) is described in this contribution as an alternative to classical HPLC. A Chromolith™ Flash RP-18e (25 mm × 4.6 mm) column (Merck®, Germany) and a FIAlab® 3000 system (USA) with a six-port selection valve and 5.0 ml syringe pump were used for sequential injection chromatographic separations in our study. The mobile phase used was methanol/water (40:65, v/v), pH 5.2 adjusted with triethylamine 0.8 μl ml^{-1} and acetic acid, at flow rate 0.9 ml min^{-1}. UV detection provided by DAD detector and two wavelengths were simultaneously monitored for increasing sensitivity of determination. Detector was set up at 220 nm for naphazoline nitrate and 256 nm for methylparaben and ethylparaben (IS). There is no necessity to use pre-adjustment of sample of nasal drops (only dilution with mobile phase) so the time of the whole analysis is very short. The validation parameters have shown good results: linearity of determination for both components (naphazoline nitrate and methylparaben), correlation coefficient >0.999; repeatability of determination (R.S.D.) in the range 0.5–1.6% at three different concentration levels, detection limits 0.02 μg ml^{-1} (naphazoline nitrate) and 0.20 μg ml^{-1} (methylparaben and ethylparaben), and recovery from the pharmaceutical preparations in the range 100.06–102.55%. The chromatographic resolution between peaks of compounds was more than 4.0 and analysis time was less than 4 min under the optimal conditions. The advantages and drawbacks of SIC against classical HPLC are discussed showing that SIC can be an advantageous alternative in many cases.

Keywords: Sequential injection chromatography; Monolithic column; Naphazoline nitrate; Methylparaben; Spectrophotometric determination

1. Introduction

In the last few years, special attention was given to sequential injection analysis (SIA), high versatile technique based on a programmable flow as an economical and expeditious alternative for the automation of analytical procedures [1]. SIA has been proposed by Růžička and Marshall as an efficient tool for automated liquid handling, especially performing of derivatisation reactions [2]. The technique is based on forward and reverse movement of a piston of syringe pump, which together with a multi-position selection valve enables precise sampling of chemicals into the system and propelling of the sequenced zones to the reactors and detector [3]. Automation, speed of the analysis and low consumption of sample and reagents are the most important features that favour the SIA technique for application in many fields of analysis, primarily by more complicated operations such as sample pre-treatment or monitoring of long lasting processes [4–6]. On the other side, SIA technique itself has generally one important drawback—it cannot primarily provide the separation procedure and analysis of multi-component samples.

This weak point was solved by coupling of short monolithic column [7] with SIA manifold. The new method called sequential injection chromatography (SIC) was recently successfully applied in the analysis of relatively simple multi-component samples like pharmaceuticals [8–11].

The use of monolithic columns (formed from a single piece of porous silica gel) enabling operation at high flow rates with lower back-pressure [12]. This feature can be used for integrating these columns into a SIA manifold and for extending the possibilities of SIA technique (the back-pressure limit range of the syringe pump in SIA apparatus is about 2.5 MPa).

The problem of determination of one analyte in the presence of other compounds or complex matrix using SIA method could be solved by using selective detectors or different analytical

* Corresponding author. Fax: +420 495 518 718.
E-mail address: solich@faf.cuni.cz (P. Solich).

0039-9140/$ – see front matter © 2006 Elsevier B.V. All rights reserved.
doi:10.1016/j.talanta.2006.02.065

tools. There can be mentioned fluorescence for determination of complex formed between naproxen and β-cyclodextrin in sample without any previous separation, extraction or other sample preparation [13], chemiluminescence for monitoring of glucose and penicillin during cultivations using specific reactions [14], selective sensors – ion selective electrodes sensitive to penicillin-G antibiotics for pharmaceutical products analysis [15], selective extraction – anion exchange solid phase micro-column for simultaneous determination of benzophenone-4 and phenylbenzimidazole sulphonic acid in sunscreen sprays [16], determination of organic acids and sugars in soft drinks by Fourier transform infrared spectroscopy [17], solid phase C18 RAM for direct determination of furosemide in serum [18], liquid–liquid microextraction using lab-on-valve (LOV) and a separating chamber for determination of diphenhydramine hydrochloride in pharmaceutical preparations and anionic surfactant in water samples [19], reaction columns—reduction copperised cadmium column for the determination of nitrate and nitrite in water samples [20,21], gas-diffusion unit for determination of ammonium in environmental samples [22], dialysis through a cellulose membrane was used to enable sample dilution and matrix separation to quantify pH, chloride and nickel in electrolytic baths [23], LOV format for simultaneous spectrophotometric determination of copper and iron in wastewater [24], lab-on-valve system using chelating Sepharose beads as sorbent material for the determination of ultra-trace levels of Cd^{2+}, Pb^{2+} and Ni^{2+} by electrothermal atomic absorption spectrometry [25], selective reaction of sulphate with barium-dimethylsulphonazo(III) for sulphate determination in automotive fuel ethanol [26] or use of special mathematical models—multivariate curve resolution with alternating least squares for simultaneous determination of analytes in the presence of interferents without the need to pretreat the sample [27].

Naphazoline nitrate (NN: 2-(1-naphthylmethyl)-2-imidazoline nitrate) depicted in Fig. 1, is an imidazolic α-sympathomimetic drug used like relatively long-lasting action nasal decongestive substance to threat rhinitis. Methylparaben

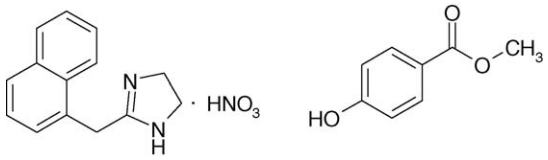

Fig. 1. Structure of naphazoline nitrate (A) and methylparaben (B).

(MP: methyl *p*-hydroxybenzoate) depicted in Fig. 1, is effective antibacterial and antifungal agent, which is commonly used as preservative in foods, beverages, cosmetics and pharmaceuticals.

Very recently, naphazoline salt was analysed by first-derivative UV spectrophotometry [28] and by chemometric assisted simultaneous spectrophotometric determination together with methyparaben, phenylephrine and diphenhydramine [29]. There has been no separation method found in the literature for simultaneous determination of NN and MP.

2. Experimental

2.1. Apparatus

2.1.1. Sequential injection system and monolithic column

A commercially available instrument FIAlab® 3000 system (FIAlab® Instruments Inc., Bellevue, USA) with a syringe pump (syringe reservoir 5.0 ml) and a 6-port selection Cheminert® valve (Valco Instrument Co., Houston, USA) was used. The manifold was equipped with fiber-optic UV–vis diode array detector USB 2000 (Ocean Optics Inc., Dunedin, USA), 10 mm Z-flow cell (Avantes, CO, USA) and UV light source D-1000-CE (Analytical Instrument Systems Inc., Flemington, USA). The whole SIC system was controlled by the program FIAlab® for Windows 5.0. Flow lines were made of 0.75 mm i.d. PTFE tubing. Mobile phases and samples were aspirated through the 6-port multi-position valve and then delivered to the monolithic column and to the detector. On-line sample separation was per-

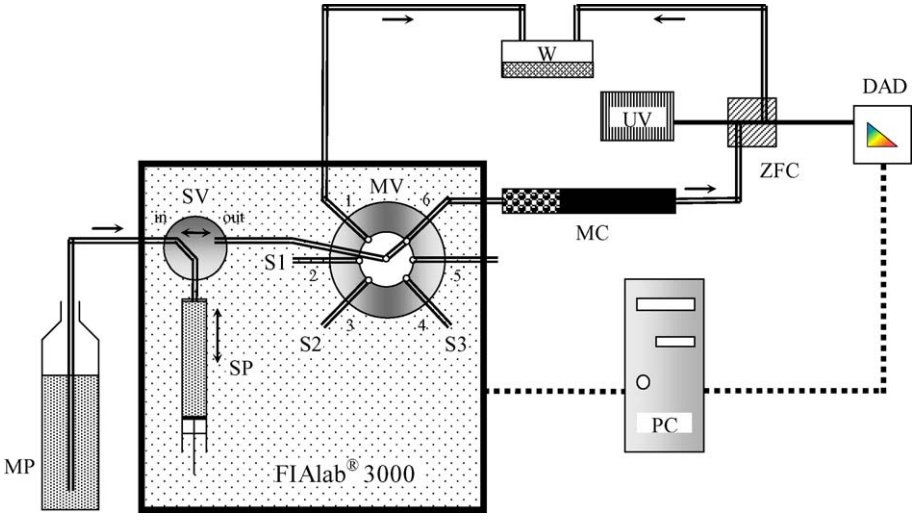

Fig. 2. Scheme of SIC set-up for determination of NN and MP. DAD, DAD detector; MC, monolithic column; MP, mobile phase; MV, 6-port multi-position valve; SP, syringe pump; SV, solenoid valve; S1–S3, Sample 1–3; PC, computer, UV, UV lamp, W, waste, ZFC, Z-flow cell.

formed on C-18 monolithic column Chromolith^{TM} Flash RP-18 (25 mm × 4.6 mm) (Merck, Darmstadt, Germany) coupled with monolithic precolumn (5 mm × 4.6 mm) (Merck). The Monolithic column with precolumn was placed between the multiposition valve and flow cell of the detector. A scheme of the sequential injection chromatography system with the monolithic column is depicted in Fig. 2.

2.1.2. HPLC apparatus

Preliminary experiments concerning the composition of mobile phase for precise separation were performed on HPLC system consisting of a pump (Ecom LCP 4100, Prague, Czech Republic), autosampler (Waters 717, Milford, USA), UV detector (Waters 486) and data processing software CSW v. 1.7 for Windows (Data Apex s.r.o., Prague, Czech Republic). Analyses were performed on the same above-mentioned column. Mobile phases of different composition were tested at flow rate 0.9 ml min^{-1} and the detector was set on 220 nm.

2.2. Reagents

Naphazoline nitrate was obtained from IVAX Pharmaceuticals s.r.o. (Czech Republic, PhEur3 grade quality), methylparaben was obtained from Zentiva, a.s. (Czech Republic, PhEur3 grade quality), ethylparaben was obtained from Sigma–Aldrich (Czech Republic, PhEur3 grade quality) and organic modifiers for mobile phase preparation were obtained from Sigma–Aldrich. Methanol (Chromasolv, for LC) was obtained from Sigma–Aldrich. All other used chemicals were of analytical grade quality. Millipore Milli-Q RG (Millipore s.r.o., Czech Republic) ultra pure water was used for preparing the solutions. Mobile phases were degassed by helium before use. Stock standard solutions were prepared in water with addition of methanol (5%) and were stored at 5 °C for 1 month. The final concentrations of the sample working standard solutions or reference standards for pharmaceutical preparations analysis were prepared by diluting the stock solution in the mobile phase.

2.3. Method and sample preparation

2.3.1. Mobile phase

The optimal mobile phase for separation of NN, MP and internal standard EP was methanol/water (40:65, v/v), pH 5.2 adjusted with triethylamine 0.8 μl ml^{-1} and acetic acid; flow rate 0.9 ml min^{-1} at ambient temperature. Volume of mobile phase used for one analysis was 3.5 ml. Mobile phase was degassed before application by means of helium.

2.3.2. Solutions and sample preparation

The tested pharmaceutical preparation was Sanorin® 0.5‰ (IVAX, Czech Republic) containing 500 μg of NN and 1000 μg of MP in 1.0 ml of nasal drops. Determination of the active substances in pharmaceutical was done by the following procedure: 1.00 ml of Sanorin® 0.5‰ solution was transferred to 50.00 ml calibrated flask; then 5.00 ml methanol and 1.00 ml of stock solution of internal standard ethylparaben was added. The sample was homogenized and dissolved by 5 min sonication; the time period 15 min was let for temperature stabilization, then the flask was filled to the mark with mobile phase and mixed. The comparative standard solution was the same for all the analysis and it was prepared diluting stock standard solution in 50.00 ml calibrated flask with 5.00 ml methanol and then the flask was filled to the mark with mobile phase and mixed. The final concentrations of the analytes in comparative standard solution were 10 μg ml^{-1} of NN, 20 μg ml^{-1} of MP and 20 μg ml^{-1} of EP. A volume of 10 μl of sample was analyzed by SIC system. Standards and samples were measured in triplicates and the mean peak height values were used for data acquisition.

3. Results and discussion

3.1. Method development and optimization

The incorporation of monolithic columns to SIA manifold has already been introduced in our previous works [7–11]. The main aim of the present study was to find optimal separation conditions of the sequential injection cycle for simple method of determination of NN and MP, and to explore practical suitability of this method for analysis in pharmaceutical solution. The optimization of mobile phase was started with Chromolith® Flash RP-18 column 25 mm × 4.6 mm and methanol/water (50:50, v/v) mobile phase. The mobile phases containing methanol as organic part have shown better separation of peaks and peak symmetry than acetonitrile containing mobile phases and the optimization was focused to make a proposal appropriate ratio of methanol/water mobile phase composition. In order to achieve a sufficient symmetry of the peaks together with a good separation of compounds and a short retention time, the optimal mobile phase for the separation of NN, MP was founded methanol/water (40:65, v/v), pH adjusted to 5.2 by means of triethylamine 0.8 μl ml^{-1} and acetic acid and flow rate of it 0.9 ml min^{-1}. Ethylparaben (EP) was chosen as a suitable internal standard. The sample injection volume was 10 μl. The proposed system enabled successful separation of target analytes in the time less than 4 min and total volume of mobile phase for one analysis was 3.5 ml. Standards and samples were measured in triplicates and the mean peak height values were used for data acquisition. The typical sequence of particular steps of the program is mentioned in Table 1 (action description of all parts of system). From the UV spectra of NN and MP in mobile phase, the optimal detection wavelength of 220 nm for NN and 256 nm for MP and internal standard EP was chosen. Peak height evaluation was performed using the FIAlab® software. Representative sequential injection chromatogram showing successful separation of active substances of Sanorin® 0.5‰ including internal standard is shown in Fig. 3.

3.2. Parameters of sequential injection chromatography process

The target compounds were successfully separated using the proposed procedure and basic chromatographic parameters were calculated from experimental data, such as retention times, peak

Table 1
The sequence of particular steps of the SIC control program for Sanorin® 0.5‰ determination (a single cycle)

Unit	Command	Parameter	Action
Solenoid valve	Valve in		Set valve position
Syringe pump	Set flow rate ($\mu l\,s^{-1}$)	100	
Syringe pump	Aspirate (μl)	3500	Mobile phase aspirated
Solenoid valve	Valve out		Set valve position
Multi-position valve	Valve port 2		
Syringe pump	Set flow rate ($\mu l\,s^{-1}$)	10	
Syringe pump	Aspirate (μl)	10	Sample aspirated
Multi-position valve	Valve port 6		
Syringe pump	Set flow rate ($\mu l\,s^{-1}$)	15	
Syringe pump	Dispense (μl)	1200	Elution of NN
Syringe pump	Set flow rate ($\mu l\,s^{-1}$)	15	
Syringe pump	Dispense (μl)	900	Elution of MP
Syringe pump	Set flow rate ($\mu l\,s^{-1}$)	15	
Syringe pump	Dispense (μl)	1400	Elution of EP

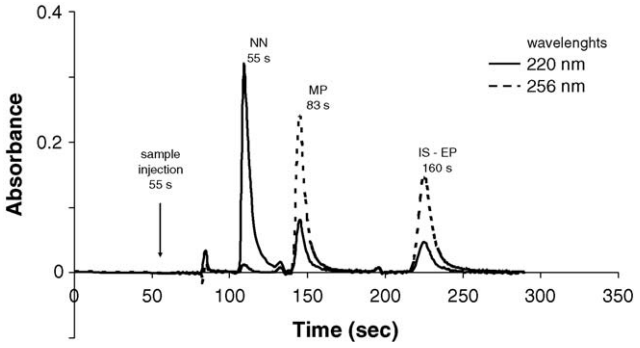

Fig. 3. SI chromatogram of the separation of active substances of Sanorin® 0.5‰ nasal drops. Mobile phase: methanol/water (40:65, v/v), pH 5.2 adjusted with triethylamine 0.8 $\mu l\,ml^{-1}$ and acetic acid, flow rate 0.9 $ml\,min^{-1}$ at ambient temperature, UV detection at 220 and 256 nm.

symmetry, number of theoretical plates and peak resolution; they are given in Table 2.

3.3. Validation and analytical parameters of the method

The developed method was validated in order to evaluate if adequate linearity, sensitivity, repeatability, recovery, selectivity, precision and accuracy had been achieved. Linearity was established with a series of working solutions prepared by diluting the stock solution with mobile phase to the final concentrations. Each concentration was injected in triplicate and the mean value of peak height was used for the calibration curve. The calibration graphs involved eight experimental points for NN (concentration range 0.065, 0.13, 0.26, 0.52, 1.04, 3.13, 6.25 and 12.50 $\mu g\,ml^{-1}$) and it is described by the following equation: $A = (0.0507 \pm 0.0004)c + (0.0019 \pm 0.0019)$ (where A is the absorbance and c the analyte concentration), the correlation coefficient was 0.9998; for MP and EP six experimental points (concentration range 1.30, 2.60, 5.20, 15.63, 31.25, 62.50 $\mu g\,ml^{-1}$) and they are described by following equations: MP $A = (0.0142 \pm 0.0002)c - (0.0179 \pm 0.0058)$, the correlation coefficient was 0.9996; and for internal standard EP: $A = (0.0088 \pm 0.0002)c - (0.0157 \pm 0.0047)$, the correlation coefficient was 0.9993. The limit of detection (LOD) was calculated by comparison of the three-fold variation of signal to noise ratio (3 S/N) obtained from analysis of the standards, and the limit of quantification (LOQ) was defined as the lowest measured quantity above which the analyte can be quantified at a given statistical level of (10 S/N). The system precision of the method was determined by preparing the standards of NN, MP and EP at three concentration levels (25, 50 and 250 times diluted drops) and peak heights for each compound were determined after processing each standard eight times. The method validation results obtained under the final conditions are shown in Table 3. The method was found to fulfill common requirements of accuracy, precision and linearity (calibration range with correlation coefficient >0.999, R.S.D. for repeated standard injections at three concentration levels ($n = 8$) less than 1.6%). To validate the precision of the method, a number of six different pharmaceutical sample solutions were used, which were prepared from the same batch and analyzed consecutively. This approach provides a means of covering the precision of the entire method, from sample preparation to data handling. The precision of the method calculated as R.S.D. of six sample determination, including sample preparation, was 1.45% for NN and 1.44% for MP. The mean values of found amount were average 99.41% of NN and 97.29% of MP. The accuracy of the method was carried out measuring of the pharmaceutical samples fortified with known quantity of the analytes (addition of 100% amount of the standards to pharmaceutical preparation). Spiked sample solutions and un-spiked sample solutions were compared for recovery evaluation. The method accuracy results—mean values of the

Table 2
Characterization of SIC process

	Nafazoline nitrate	Methylparaben	Ethylparaben
Retention time (s)	55	83	160
Peak symmetry	2.67	1.59	1.75
Number of theoretical plates	848.4	1418.3	2157.3
Peak resolution	$R_{NN/MP} = 4.0$	$R_{MP/EP} = 6.4$	

Table 3
Analytical parameters and method validation results

	Nafazoline nitrate	Methylparaben	Ethylparaben
Calibration range ($\mu g\,ml^{-1}$)	0.065–12.50	1.30–62.50	1.30–62.50
Correlation coefficient	0.9998	0.9996	0.9993
Limit of detection ($\mu g\,ml^{-1}$)	0.02	0.20	0.20
Limit of quantification ($\mu g\,ml^{-1}$)	0.06	0.60	0.60
System precision—drops diluted 25× (%)[a]	1.05	1.37	1.35
System precision—drops diluted 50× (%)[a]	1.36	0.87	0.52
System precision—drops diluted 250× (%)[a]	0.84	1.58	0.76
Repeatability of T_R (%)[a]	0.53	1.01	0.66
Method precision (%)[b]	1.45	1.44	
Accuracy—spike recovery (%)[c]	102.55	100.06	

[a] Relative standard deviation (R.S.D.) values were calculated for repeated standard injections ($n = 8$).
[b] R.S.D. for repeated injections of multiple sample preparations ($n = 6$).
[c] Spiked sample solutions.

Table 4
Comparison of HPLC and SIC

Characteristic	HPLC	SIC	Benefit SIC
Possibility of separation	Yes	Yes—simple mixtures[a]	No
Using of chromatographic columns	Yes	Only short monolithic[b]	No
Variability of detection	Yes	Yes	
Flow of mobile phase	Continual	Discontinual	Yes
Direction of flow of mobile phase	One way	Both ways + stop flow	Yes
Speed of mobile phase	Constant	Variable	
Consumption of mobile phase	High	Low (discontinual flow)[c]	Yes
Speed of the analysis	Average	Average	
Use of reagents (reactions)	Limited[d]	Yes	Yes
Pre-treatment of sample	Yes (restricted)	Yes	Yes
Automation of measurement	High	High	
Robustness of measurement	High	Average[e]	No
Data evaluation	Sophisticated	Simple	No
Reproducibility	High	High	
Cost of instrumentation	High	Low[f]	Yes
Portability of analyzer	No	Yes[g]	Yes

[a] From two to five substances.
[b] At present.
[c] Mobile phase is flowing during the separation only.
[d] Post-column derivatization.
[e] Sometimes problems with higher pressure in system, restriction in column lengths.
[f] Two to three times cheaper.
[g] Small-sized box.

recoveries were found as 102.55% for NN and 100.06% for MP. Assay values of recoveries show that the method allows direct determination of NN and MP in commercial dosage forms in the presence of other adjuvants.

3.4. Determination in pharmaceutical product

The method developed has been applied to the determination of NN and MP in nasal drops Sanorin® 0.5‰. The drops were commercially available on the Czech market. The interference effect of adjuvants (boric acid and ethylendiamine) was not observed. The samples were prepared by dilution 50 times with mobile phase containing IS. For analysis, a loop of three loads of comparative standard solution was programmed, three loads of first sample solution and three loads of second sample solution prepared from one pharmaceutical. The results of determination of samples (same batch) were in the range (96.78–101.59%) for NN and (95.37–99.26%) for MP of declared value. The procedure of sample preparation was simple, fast and achieving high precision and low sample and reagent consumption.

4. Conclusion

The proposed SIC system was proved to be a convenient and efficient tool for the separation and determination of naphazoline nitrate and methylparaben in pharmaceutical preparation (nasal drops). The simultaneous analysis of both compounds has never been described before. SIC technique shows several advantages as short time of analysis and possibility of on-line use of reagents in all steps of determination. The production of the waste and the consumption of solvents are lower than in HPLC methods (due to discontinual flow), this enable reduction of cost per analysis (at

least twice). Easy liquid manipulation not attainable by classical HPLC set up, dimensions of the SIC system and portability of analyzer provides the opportunity for analysis "on field".

On the other hand, SIC has several disadvantages like limited ability of separation due to short (only monolithic) column and limited amount of mobile phase available for one analysis due to the use of 5 ml syringe pump. Also robustness of SIC technique is not as high as in HPLC and data processing is rather elementary (only peak height at present). A comparison of different characteristics of HPLC and SIC together with their advantages/disadvantages is shown in Table 4.

The coupling of the commercial monolithic column with high separation performance at lower pressure to SIA manifold allows to carry out simple separations without an expensive instrumentation such as the HPLC. From this point of view, the low-pressure monolithic silica columns opened a new area offering separation analysis in highly flexible sequential injection systems. Moreover, the use of two wavelengths simultaneously in our method provides additional increasing of sensitivity of determination (measuring in wavelength of absorbance maximum of each compound). In summary, the SIC system can be an important tool for the rapid separation and quantification of several compounds in pharmaceutical analysis.

Acknowledgements

The authors gratefully acknowledge the financial support of the Czech Ministry of Education project no. MSM 0021620822 and project of the Grant Agency of Charles University, no. GA UK 315/2005/B-CH/FaF.

References

[1] C.E. Lenehan, N.W. Barnett, S.W. Lewis, Analyst 127 (2002) 997.
[2] J. Ruzicka, G. Marshall, Anal. Chim. Acta 237 (1990) 329.
[3] T. Gübeli, G.D. Christian, J. Ruzicka, Anal. Chem. 63 (1991) 2407.
[4] R.W. Min, J. Nielsen, J. Villadsen, Anal. Chim. Acta 312 (1995) 149.
[5] X.Z. Liu, S.S. Liu, J.F. Wu, Z.L. Fang, Anal. Chim. Acta 392 (1999) 273.
[6] P. Solich, H. Sklenářová, J. Huclová, D. Šatínský, U.F. Schaefer, Anal. Chim. Acta 499 (2003) 9.
[7] D. Šatínský, P. Solich, P. Chocholouš, R. Karlíček, Anal. Chim. Acta 499 (2003) 205.
[8] D. Šatínský, J. Huclová, P. Solich, R. Karlíček, J. Chromatogr. A 1015 (2003) 239.
[9] J. Huclová, D. Šatínský, R. Karlíček, Anal. Chim. Acta 494 (2003) 133.
[10] D. Šatínský, L. Santos, H. Sklenářová, P. Solich, M.C. Montenegro, A. Araújo, Talanta 68 (2005) 214.
[11] D. Šatínský, J. Huclová, R.L.C. Ferreira, M.C. Montenegro, P. Solich, J. Pharm. Biomed. Anal. 40 (2006) 293.
[12] H. Minakuchi, K. Nakanishi, N. Soga, N. Ishizuka, N. Tanaka, J. Chromatogr. A 762 (1997) 135.
[13] E.P. Zisiou, P.C.A.G. Pinto, M.L.M.F.S. Saraiva, C. Siquet, J.L.F.C. Lima, Talanta 68 (2005) 226.
[14] R.W. Min, J. Nielsen, J. Villadsen, Anal. Chim. Acta. 320 (1996) 199.
[15] E. Santos, A. Araújo, C. Couto, M.C. Montenegro, A. Kejzlarová, P. Solich, J. Pharm. Biomed. Anal. 36 (2004) 701.
[16] A. Chisvert, M.T. Vidal, A. Salvador, Anal. Chim. Acta 464 (2002) 295.
[17] H. LeThanh, B. Lendl, Anal. Chim. Acta 422 (2000) 63.
[18] J. Huclová, D. Šatínský, T. Maia, R. Karlíček, P. Solich, A. Araújo, J. Chromatogr. A 1087 (2005) 245.
[19] R. Burakham, S. Lapanantnoppakhun, J. Jakmunee, K. Grudpan, Talanta 68 (2005) 416.
[20] A. Cerdà, M.T. Oms, R. Forteza, V. Cerdà, Anal. Chim. Acta 371 (1998) 63.
[21] Z. Legnerová, P. Solich, H. Sklenářová, D. Šatínský, R. Karlíček, Water Res. 36 (2002) 2777.
[22] M.T. Oms, A. Cerdà, A. Cladera, V. Cerdà, R. Forteza, Anal. Chim. Acta 318 (1996) 251.
[23] J.E. da Silva, M.F. Pimentel, V.L. da Silva, M.C. Montenegro, A. Araujo, Anal. Chim. Acta 506 (2004) 197.
[24] S. Ohno, N. Teshima, T. Sakai, K. Grudpan, M. Polasek, Talanta 68 (2006) 527.
[25] X. Long, E.H. Hansen, M. Miró, Talanta 66 (2005) 1326.
[26] F.S. de Oliveira, M. Korn, Talanta 68 (2006) 992.
[27] A. Pasamontes, M.P. Callao, Trends Anal. Chem. 25 (2006) 77.
[28] J. Joseph-Charles, M. Bertucat, Anal. Lett. 32 (1999) 373.
[29] H.C. Goicoechea, A.C. Olivieri, Anal. Chim. Acta 453 (2002) 289.

Available online at www.sciencedirect.com
ScienceDirect
Talanta 70 (2006) 414–418
Talanta
www.elsevier.com/locate/talanta

Stripping of photoresist on silicon wafer by CO_2 supercritical fluid

Jian-Lian Chen [a,*], Yeoung-Sheng Wang [a], Hsin-I Kuo [a], Dun-Ying Shu [b]

[a] *Department of Occupational Safety and Health, Chung Shan Medical University, Taichung 40201, Taiwan*
[b] *Division of Nanoelectronic Device Technology, Electronics Research and Service Organization, Industrial Technology Research Institute, Hsinchu, Taiwan*

Received 5 January 2006; received in revised form 25 February 2006; accepted 25 February 2006
Available online 18 April 2006

Abstract

Supercritical CO_2-based fluid is not only being considered as environmentally benign medium for photoresist (PR) removal in electronic device manufacture, but also capable of challenging feature dimensions. Despite many attractive properties, clear supercritical CO_2 has little solvating power for PR. Here, two acetate modifiers were selective to add in the CO_2 and evaluated individual contribution to the overall stripping rate by factorial experiment design, which included four other factors with four level ranges for each one and concluded the best 90% extraction efficiency would be obtained under the optimized parameters: 2.5 min static time, 35 min dynamic time, 1.25 ml ethylacetate spiked, 125 °C oven temperature and 480 atm CO_2 pressure. As analyzing the variances of these contributors to this system, it disclosed that dynamics controlled the stripping mechanism before near 35 min purging but thermodynamics took over after then; and that increasing pressure was more competent for removing PR than increasing temperature. All supercritical extracts were from two commercial PR coated on two substrates and analyzed by UV absorption spectrometry. Removing PR coated on silicon oxide layer was easier than that on Al–Cu alloy one.

Keywords: Supercritical; Photoresist; Stripping; Factorial experiment design; Extraction; Alloy

1. Introduction

The microelectronics manufacture is the largest industry in the world and has continued to keep pace with Moore's law of exponential progress for decades [1,2]. Current practices use hazardous chemicals and enormous amounts of purified water during successive processing steps. It is estimated that a typical chip-fabrication plant where production of a 2 g microchip can consume 32 kg of water, 700 g of ultra-pure gases, 1.6 kg of fossil fuels, as well as 72 g of chemicals [3]. Besides the consideration of environmental safety and healthy impact, any alternative technologies are not just "greener" but provide valid technical advantage that meets innovative component design. Supercritical fluid (SF) technology is not surprisingly the prior candidate for the identification 2015 of the 2001 International Technology Roadmap for Semiconductors.

Increasing numbers of applications and successful commercial-scale processing involving SF with various cosolvents have been demonstrated in a variety of fields [4–8]. Achievable application of SF in integrated circuit manufacturing operations, including wafer cleaning, film deposition, photoresist (PR) developing, drying, and stripping, were reviewed [9–11]. Traditional PR wet-stripping techniques produce a large liquid waste stream than other steps in the IC process and will be likely the first SF application integrated into IC processing lines. SF remover of PR minimizes the use of hazardous solvents and eliminates rinsing and drying steps, thereby streamlining the manufacturing process and excluding the need for ultra-pure deionized water, thus reducing time, energy, and cost. Using this remover, moreover, presents the adaptation to the smallest features less than 100 nm because SF has zero surface tension and a gaslike viscosity. A group in Los Alamos National Laboratory developed a series of SF cleaning processes and carried out in collaboration with equipment makers to found a commercial device [12–16].

A favorable PR partition trend much more toward SF than the substrate surface indicates the high solubility of PR in SF medium and also a great success of quantitative extraction in a reasonable time and thereby a minimum SF consuming. The high compressibility of SF allows the solubility and diffusivity to

* Corresponding author. Tel.: +886 4 24730022; fax: +886 4 23248194.
E-mail address: cjl@csmu.edu.tw (J.-L. Chen).

0039-9140/$ – see front matter © 2006 Elsevier B.V. All rights reserved.
doi:10.1016/j.talanta.2006.02.066

be widely varied by simple pressure control of density. Temperature must simultaneously be optimized for solvating power since the detachment of adhesive PR solutes from matrices expands with increase temperature. The addition of suitable cosolvent into the SF usually lightly adjusts the polarity compatible to PR and remarkably facilitates PR removal from wafer. All SF parameters have to be coordinately optimized so that an extract of the desired composition could struggle kinetically against the binding matrices and inhabit a thermodynamically stable state in the modified SF. Since many variables have to be considered simultaneously in the SF PR stripping, factorial designs [17] and multilinear regression [18,19] both are formal optimization methods, excluding trial-and-error, namely univariate, procedure.

Here, we also present two factorial designs to optimize the stripping of two commercial PR on silicon oxide and metallized layers with two cosolvents added in SF-CO_2. Except the attempt to raise the extraction efficiency, an understanding of the fundamental mechanisms responsible for processing of PR stripping is desired.

2. Experimental

2.1. Reagents and chemicals

Dichloromethane (TCI, Tokyo, Japan), chloroform (TCI, Tokyo, Japan), methanol (TEDIA, HPLC/Spectro grade), ethanol (TEDIA, HPLC/Spectro grade), acetonitrile (Aldrich, Milwaukee, WI, USA), propylene glycol monomethyl ether acetate (PGMEA; Fluka, Switzerland), ethylacetate (EA; Merck, Darmstadt, Germany) and CO_2 supercritical fluid (Scott Speciality Gases, 99% purity) were solvents used.

2.2. Apparatus

The ISCO SFX 220 Extraction Systems consisted of an SFX 220 Extractor, a 260 D syringe pump, and an SFX 200 Controller, which controlled all pumping and extraction operations through six motor actuated valves. The operation limits for the system are 510 atm and 150 °C. Test tube clips were attached to the side of the extractor, allowing analytes to be conveniently collected in the tubes. To virtually eliminate sample plugging of the restrictor as it was routed from the analyte outlet to the collection vial, a restrictor temperature controller was set up for coaxially heated capillary with fixed flow rate, 1 ml min^{-1}. This controller heated the entire restrictor by passing an electric current through it for even heating. Jasco V530 spectrophotometer was for UV absorption measurement.

2.3. Wafer sample preparation

Two types of sample with different coating PR were prepared on the silicon wafer (200 mm diameter, 15–25 Ω cm, ⟨1 0 0⟩ face, Taisil Electronic Material Corp., Hsinchu, Taiwan). PR-A (ZEP 520, polyhydroxystyrene derivatives, Shin-Etsu Chemical Co. Ltd., Tokyo, Japan), 4000 A ± 5% thickness, was spin-coated on a silicon oxide layer, soft-baked at 90 °C for 30 s, and then hard-baked at 200 °C for 120 s. The oxide layer, 2000 A ± 4% thickness, was made by plasma enhanced chemical vapor deposition (PECVD). PR-B (YSB 663, polymethylstyrene derivatives, Nippon Zeon Co. Ltd., Tokyo, Japan), 6000 A ± 2.3% thickness, was spin-coated on an Al–Cu alloy layer (Al:Cu = 99.5:0.5), soft-baked at 90 °C for 30 s, and then hard-baked at 120 °C for 90 s. The alloy layer, 4000 A ± 5% thickness, was made by vacuum sputtering. These wafers coated with PR were cut into strips (4 cm × 1 cm) to be samples.

2.4. Solubility test

A strip PR-A sample were immersed in 20 ml solvent without stirring for 3 min. Seven solvents, including dichloromethane, chloroform, methanol, ethanol, acetonitrile, PGMEA, and EA, were tried. The suspended solutions were examined by spectrophotometer.

2.5. SF extraction (SFE)

Blank SFE test was preceded without sample inserted in extraction vessel and cosolvent added in, but with the collection solvent ready to mix the purging SF-CO_2. The collection solvent could be PGMEA or EA.

Two sets of four-level factorial design were employed to assess the significant five-factor (oven temperature, SF-CO_2 pressure, static extraction time, dynamic elution time, and the volume of organic modifier added directly to the solid samples) for optimizing SFE condition. One design was for PGMEA cosolvent added, the other for EA. The L16 orthogonal array tables, Tables 1 and 2 coordinately instructed the following 16 experiments for PGMEA cosolvent in their individual parameters, and Tables 1 and 3 for EA. For example, experiment no. 9 was assigned to the SFE parameters of 110 °C oven temperature,

Table 1
Design matrix for L16 (4^5) factorial experiments and results

Run	*A*	*B*	*C*	*D*	*E*	Absorbance[a]	Recovery (%)[b]
1	1	1	1	1	1	0.675	34.3
2	1	2	2	2	2	0.360	44.5
3	1	3	3	3	3	0.344	41.6
4	1	4	4	4	4	0.191	29.6
5	2	1	2	3	4	0.375	26.8
6	2	2	1	4	3	0.218	36.7
7	2	3	4	1	2	0.607	92.6
8	2	4	3	2	1	0.565	23.0
9	3	1	3	4	2	0.698	43.4
10	3	2	4	3	1	0.655	75.5
11	3	3	1	2	4	0.250	38.6
12	3	4	2	1	3	0.406	22.1
13	4	1	4	2	3	0.313	75.7
14	4	2	3	1	4	0.472	30.9
15	4	3	2	4	1	0.375	50.0
16	4	4	1	3	2	0.138	34.2

[a] The absorbance at 280 nm for the extract corresponding to the experimental conditions described in Table 2.

[b] The PR recovery corresponding to the experimental conditions described in Table 3.

Table 2
Factors on L16 factorial design with PGMEA spiked and their significant contribution

	A; oven temperature (°C)	*B*; CO_2 pressure (atm)	*C*; static time (min)	*D*; dynamic time (min)	*E*; spiked PGMEA (ml)
1	50 (0.392)[a]	500 (0.515)	15 (0.320)	25 (0.540)	0.75 (0.568)
2	80 (0.441)	400 (0.426)	10 (0.379)	20 (0.372)	0.50 (0.451)
3	110 (0.502)	300 (0.394)	5 (0.520)	15 (0.378)	0.25 (0.320)
4	140 (0.325)	200 (0.325)	0 (0.442)	10 (0.371)	0 (0.322)
SSF[b]	0.0675	0.0746	0.0883	0.0831	0.1695

[a] Datum in the parentheses presents the average response absorbance of individual factor.
[b] The sum of squares due to a factor.

Table 3
Factors on L16 factorial design with EA spiked and their significant contribution

	A; oven temperature (°C)	*B*; CO_2 pressure (atm)	*C*; static time (min)	*D*; dynamic time (min)	*E*; spiked EA (ml)
1	95 (37.5)[a]	500 (45.0)	7.5 (36.0)	40 (45.0)	1.50 (45.7)
2	105 (44.9)	490 (46.9)	5.5 (35.8)	35 (45.5)	1.25 (53.7)
3	115 (44.9)	480 (55.8)	4.0 (34.8)	30 (44.6)	1.00 (44.0)
4	125 (47.7)	470 (27.3)	2.5 (68.4)	25 (39.9)	0.75 (31.5)
SSF[b]	229.2	1709.2	3244.0	80.7	1011.7

[a] Datum in the parentheses presents the average response recovery of individual factor.
[b] The sum of squares due to a factor.

500 atm. CO_2, pressure, 5 min static time, 10 min dynamic time, and 0.50 ml PGMEA spiked.

In order to eliminate direct contact with sample and spread uniformly, cosolvent was spiked on the glass wool, which was inserted at the backside of strip sample, just before starting extraction. A collection vial containing 9 ml EA was ready for the extracted and eluted analytes to trap in. As violent venting began, the little loss due to the evaporation was made up to the 9 ml level, and then poured some mixtures into a UV cell for recovery evaluation. Recovery was the mole ratio of the SF extract in a collection vial with 9 ml EA to the room extract in a tube with 20 ml EA while the former strip sample was put in a extraction vessel and the later one in an open tube.

3. Results and discussion

3.1. PR solubility

In order to find a suitable solvent served as collectable medium positioned in the outlet and/or modifier added in the extraction vessel, several organic solvents were tested for their solubility of PR-A. Among the observations on them, dichloromethane and chloroform had very poor solubility; methanol, ethanol, and acetonitrile medium; PGMEA and EA well. The miscible solutions with soluble PR were examined by UV spectrophotometer, and showed spectrum in Fig. 1, which was free of solvent effect and indicated PGMEA was somewhat a better solvent than EA. The dissolved PR containing photoacid generators, which respond to trigger the solubility change of PR polymer in the exposed regions to make it substantially different from that in the unexposed regions, are sensitive to an appropriate range of wavelength; hence, the spectrometry is a direct and convenient way to quantify the extent of PR stripped by SF in the following sections. The 280 nm beam was chosen to be analyzed.

PGMEA and EA were candidates for the collection solvent. The concerned points would not only be the PR solubility, but also the reactivity with SF-CO_2, particularly its following influence on UV absorption measurement. PGMEA, which is originally used as a blending solvent for the PR-A manufacture, was simply assessed by blank SFE test. The curve for PGMEA in Fig. 2 shows a stable and slight increase in absorbance at 280 nm as increasing the purging time had really caused the difficulty in accurately determining the extraction efficiency. Despite the little adverse consequence, in fact, PGMEA, which was capable of the highest solubility among all verified solvents, was the most potential modifier to enhance the PR-A solubility upon SF-CO_2 flush. Especially, while a maximal efficiency of the PR

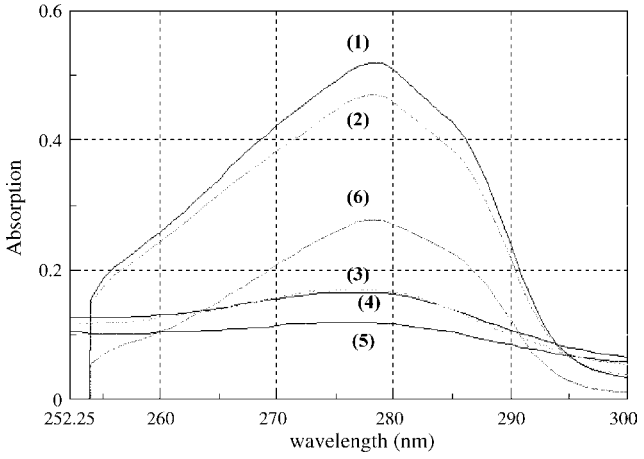

Fig. 1. UV absorption spectrum of hard-baked photoresist dissolving in organic solvent. (1) PR-A in PGMEA; (2) EA; (3) ethanol; (4) methanol; (5) acetonitrile; (6) PR-B, YSB 663 in ethylacetate.

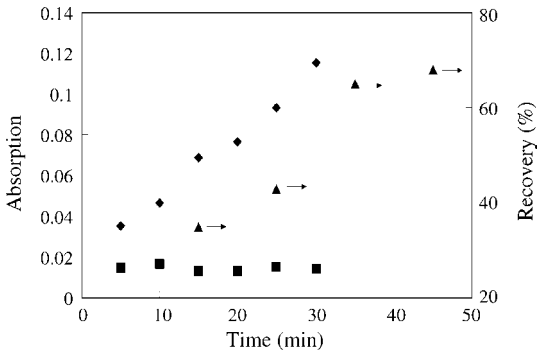

Fig. 2. Effects of the supercritical CO_2 purging time on the 280 nm absorption and the recovery of PR-B. (♦) Blank SFE test on the collection medium, PGMEA; (■) EA; (▲) the recovery under the condition, *A*4*B*3*C*4*D*2*E*3, defined in Table 3.

stripping is pursued by the IC fabrication, however PGMEA should be seriously considered. In Fig. 2 another absorption curve for EA exhibited the independence of purging time, so EA would be an adequate medium to collect PR-A and free of the spectrum interference from quantifying the PR stripping efficiency.

3.2. Factorial experiments

According to the judgment of above solubility examination, PGMEA and EA would be well prepared as modifiers in SF flush but properly scavenged only by EA. Through the experiments of factorial design, there shall be advised parameters of the optimized SF conditions for the efficient PR stripping and derivative studies of the effects of wafer matrix on the SF stripping process.

3.2.1. PGMEA modifier

On the basis of the methodical experimental plan in Table 1, 16 runs were conducted by the controllable factors defined in reasonable values in Table 2. Still within the safe limits of pressure and temperature set for the extraction vessel, the widely extended ranges, 200–500 atm and 50–140 °C, were favorable to obtain the adequately satisfactory SF density or dissolving power under overall consideration, without possibly exclusive trials. The arrangement of other parameters, such as modifier dose, static and dynamic span, was taking both the expense of fluids and spending time into account thus that should likewise be rational.

The measured 280 nm absorbance of 16 extracts, based on the L16 factorial design, was recorded in Table 1. Although the spectrometric results for each extract could not be correctly referred to the extraction efficiency as PGMEA would disturb the determination of PR-A in SF, it is believed that the trivial interference could be neglected because PGMEA was present only with little volume addition (0–0.75 ml), which is far less than the blank SFE test shown in Fig. 2, where PGMEA was used as collection medium (9 ml), and thus its adverse contribution to the absorbance in Table 1 would be minor. Therefore, instead of extraction efficiency, the absolute absorbance was assessed for the presentation of separate factors and their variances, and the assessment results were collective in Table 2. Here, the set of variables, *E*1*C*3*D*1*B*1*A*3, ranking in the order of obvious factors, was the best optimized conditions, upon which the ideal absorbance would be 0.985, or approximately 87% extraction efficiency. Through a proceeding examination, the success in the factorial design was confirmed as the five experimental recoveries, $85 \pm 5\%$, under the select condition were close to the estimated one. In comparison with the declaration issued by Los Alamos National Laboratory [16], where used the pre-mixed cosolvents, butylenes and propylene carbonates, and striping an obscure source of PR in a pulsed mode, a higher pressure (500 atm versus 200 atm) in our system was not only needed to maintain a certain SF density at higher temperature (110 °C versus 90 °C), but also might cause significant reductions in the glass transition temperature of PR polymer [20].

By overall checking the performance of each factor in Table 2, some clues to the stripping process could be disclosed. First of all, the effect of cosolvent addition was the most influential in determining the stripping efficiency because its sum of squares due to a factor (SSF) was the largest value. The significant contribution of four levels within the cosolvent factor showed $E1 > E2 > E3 \approx E4$; that is, the more volume the cosolvent was added, the more efficiently the PR-A was stripped. These meant that PGMEA, at least up to 0.75 ml spiked, was well miscible with SF-CO_2 and greatly facilitated PR-A removal from wafer matrix. According to the contribution ranking on the four levels, $C3 > C4 > C2 > C1$, it was found that the longer equilibrium time before purging, at least 10 min, could not enhance the stripping efficiency. Some unfavorable PR adsorption onto active surface, for examples of glass wool insert and extraction vessel wall, might happen if waiting time were too long. The suitable static time between 0 and 10 min was fully considered to dissolve the most amount of PR-A on wafer and deserve the less adsorption effect. As observing the curve of level contributions of the dynamic time factor, the purging time below 25 min seemed difficult to rid all matrices in the extraction vessel of PR-A while the waste flow rate was set at 1.0 ml min^{-1}. This is only 0.64 times the extraction vessel volume. With regard to the pressure and temperature variables, which coordinately determine the density as well as the polarity of SF-CO_2, the applied pressure was more crucial than the temperature within the level setting range in Table 2. This is also meant that the reductions in the glass transition temperature of PR-A polymer seemed more critical than the melt and flow of PR-A on wafer.

3.2.2. EA modifier

Although EA bore slightly poorer solubility of PR-A than PGMEA did in the room atmosphere, its actual function as cosolvent in SF was not definite. Taking advantage of the primary results from the factorial experiment design in Table 2, an improved design was submitted in Table 3. The level ranges for the factors of oven temperature, CO_2 pressure, and static time, were narrowed down to closely approach the ideal parameter, but those for dynamic time and spiked cosolvent volume were extended.

Without the misgiving of the disturbance to the absorption at 280 nm, the recovery through the SF-CO_2 flush could be simply calculated. The recoveries of 16 designed experiments guided

by Table 3 were compiled in Table 1, and their analysis on the significant contribution of each level as well as variances due to a factor was all incorporated in Table 3. By evaluating the rank in the SSF, the obvious factors were found in the order of *C*4*B*3*E*3*A*4*D*2, which was the superior stripping condition and the inferential prediction about the extraction efficiency would be 96%. Five repeat experiments under the select condition gave an average recovery of $90 \pm 3\%$ and approved of the success of the factorial experiment design. In contrast to the recovery as using PGMEA modifier, the moderate increase (90% versus 85%) was owing to the fine tuning in the factorial levels.

By checking the action of the four levels within the static time factor, which was the most obvious one, it was found that a preferable equilibrium time should be achieved before 2.5 min to lessen the PR-A adsorption. To realize the 100% stripping rate, a detailed reform system, including pipe and extraction vessel design, might be commended to absolutely resolve this issue. As for the consequence of SF properties to the stripping, the two factors, CO_2 pressure and oven temperature, became more decisive in this condition than that in Section 3.2.1, but pressure still had a lead over temperature. Here, the thermodynamic control prevailed over the dynamic one and thus the dynamic time was the least determinative factor, which contribution indeed reached nearly maximum just after through 30 min purging, namely near three times the extraction vessel volume. In respect of EA spiked volume, E2 presented the modified SF with the most suitable polarity to dissolve PR-A.

3.3. Stripping tests of PR-B on metallized wafers

With distinctive additive and surfactant, the PR-B material coating on Al–Cu alloy layer was lightly different from that on oxide layer. The concerned points included the adhesion energy, reflecting light intensification, resolution lines, etching requirement and so on. However, the main constituent polymer for both substrates could be the same and the stripping condition might also be. Utilizing the optimized parameters obtained from Section 3.2.2 study, the SF stripping for PR-B, which is also a polystyrene derivative like PR-A, on the Al layer was attempted to verify its potential applicability. The verification proceeded to the correlation between the extraction efficiency and purging time, and the relative curve was incorporated in Fig. 2. Unfortunately, only approximate 70% recovery was received even through 45 min collection. To acquire higher rate, a new factorial design would resolve the shortage, which apparently originated either from the polymer additives or adhesive layers. By the way, there was a saturate time close to 35 min, which imply the thermodynamic controlled these proceedings.

4. Conclusions

The potential for incorporation of stripping technology in microelectronics fabrication is high, and the presence of in-house SF-CO_2 systems may stimulate adoption of other application. Here we selected PGMEA and EA as cosolvent to enhance the SF solubility of PR. By factorial experiment design, the extraction efficiency best achieved 90% and revealed individual contribution of five controllable factors. With a strip sample in the confined extraction vessel, the equilibrium time was suggested not to exceed 2.5 min for more PR dissolving in the modified SF, which at most 1.25 ml cosolvent was suggested to add in. Dynamics controlled the stripping mechanism before near 35 min purging but thermodynamics took over after then. The reduction in glass transition temperature of PR polymer by raising SF-CO_2 pressure seemed more critical than the increase in oven temperature to melt the PR on wafer. The PR stripping strategic should consider substrates as a critical point. There is still a need of optimization and improvements in many ways, such as extraction vessel design, built-up materials, and flow path, to reduce the adverse effect of PR adsorption.

Acknowledgements

The authors thank the National Science Council of the Republic of China, Taiwan, for financial support.

References

[1] S. Luryi, J. Xu, A. Zaslavsky, IEEE (2002).
[2] G.E. Moore, Electronics 38 (1965) 114.
[3] E.D. Williams, R.U. Ayres, M. Heller, Environ. Sci. Technol. 36 (2002) 5504.
[4] M. Sihvonen, E. Jarvenpaa, V. Hietaniemi, R. Huopalahti, Trends Food Sci. Technol. 10 (1999) 217.
[5] K. Johns, G. Stead (Eds.), Supercritical Fluids for Coatings-from Analysis to Xenon. A Brief Overview, vol. 2, Kluwer Academic/Plenum Publishers, New York, NY, 1999.
[6] J. McHardy, S.P. Sawan, Supercritical Fluid Cleaning Fundamentals, Technology and Applications, Noyes, Westwood, NJ, 1998.
[7] A.I. Cooper, Adv. Mater. 13 (2001) 1111.
[8] J.L. Chen, C.Y. Liu, Anal. Chim. Acta 494 (2003) 125.
[9] J.W. King, L.L. Williams, Curr. Opin. Solid State Mater. Sci. 7 (2003) 413.
[10] G.L. Weibel, C.K. Ober, Microelectron. Eng. 65 (2003) 145.
[11] A. O'Neil, J.J. Watkins, Green Chem. 6 (2004) 363.
[12] J.B. Rubin, L.B. Davenhall, J. Barton, C.M.V. Taylor, K. Tiefert, IEEE/CMPT Int. Electro Manuf. Technol. Symp. 23rd, Institute of Electrical and Electronics Engineers, 1998, p. 308.
[13] J.B. Rubin, L.B. Davenhall, C.M.V. Taylor, L.D. Sivils, T. Pierce, IEEE International Symposium on Electronics and the Environment, Danver, MA, 1999, p. 13.
[14] L. Frazer, Environ. Health Perspect. 109 (2001) A383.
[15] L.B. Rothman, R.J. Robey, M.K. Ali, D.J. Mount, IEEE/SEMI Advanced Semiconductor Manufacturing Conference, 2002, p. 372.
[16] D.J. Mount, L.B. Rothman, R.J. Robey, M.K. Ali, Solid State Technol. 7 (2002) 103.
[17] F. Reche, M.C. Garrigos, A. Sanchez, A. Jimenez, J. Chromatogr. A 896 (2000) 51.
[18] M. Careri, L. Furlattini, A. Mangia, M. Musci, E. Anklam, A. Theobald, C. von Holst, J. Chromatogr. A 912 (2001) 61.
[19] J.L. Chen, C.Y. Liu, Anal. Chim. Acta 528 (2005) 83.
[20] S.P. Sawan, Y.T. Shieh, J.H. Su, G. Manivannan, W.D. Spall, Supercritical Fluid Cleaning: Fundamentals, Technology and Applications, Noyes Publications, Norwich, NY, United States, 1998.

Available online at www.sciencedirect.com
ScienceDirect
Talanta 70 (2006) 419–425
Talanta
www.elsevier.com/locate/talanta

A palm-sized surface plasmon resonance sensor with microchip flow cell

Hizuru Nakajima [a], Yuuki Harada [a], Yasukazu Asano [a], Tatsuro Nakagama [a], Katsumi Uchiyama [a,*], Toshihiko Imato [b], Nobuaki Soh [b], Akihide Hemmi [c]

[a] *Faculty of Urban Environmental Sciences, Tokyo Metropolitan University, 1-1 Minamiohsawa, Hachioji, Tokyo 192-0364, Japan*
[b] *Department of Applied Chemistry, Graduate School of Engineering, Kyushu University, 6-10-1 Hakozaki, Higashi-ku, Fukuoka 812-8581, Japan*
[c] *Mebius Advanced Technology, 3-31-6-105, Nishiogi-kita, Suginami-ku, Tokyo 167-0042, Japan*

Received 28 November 2005; received in revised form 26 February 2006; accepted 26 February 2006
Available online 3 July 2006

Abstract

A small-sized surface plasmon resonance (SPR) sensor with a microchip flow cell has been developed for the purpose of enhancing the sensitivity of the SPR detector for low molecular weight compounds. This portable differential SPR detector consisted of an LED, two cylindrical lenses, a round prism, a divided mirror, a CCD, electronics, and a polydimethylsiloxane/gold microchip with two flow paths (10 mm long, 1 mm wide, 20–100 μm deep). 3-Mercaptopropyltrimethoxysilane was used for sealing the microchip. The performance of the on-site orientated SPR detector was estimated using sucrose and IgA. A drastic change in the SPR intensity appeared. The depth of the flow cell was in inverse proportion to the SPR intensity. Compared to a conventional flow cell having the size of 10 mm (L) × 1 mm (W) × 1 mm (D), its sensitivity to 10% sucrose and 0.9 nM IgA increased about 11 and 39 times, respectively. This phenomenon seemed to be due to the increase in the substance on the SPR sensor based on its size effect. These results showed that the application of the microchip sensor for SPR measurement has the possibility for improvement of the SPR intensity for low molecular substances.

Keywords: Microchip; Surface plasmon resonance; Onsite analysis; Portable; Immune reaction; Immunoglobulin A

1. Introduction

Environmental pollution from toxic inorganic substances, such as mercury, cadmium, and sulfur dioxide, has almost vanished by the end of the 20th century in Japan. A possible solution of that from toxic organic substances, such as agricultural chemicals and environmental hormones, which can seriously affect the human body has been indicated by Carson and Colborn [1,2] for the left 21th century. Gathering information on biological pollution of the living body caused by toxic organic substances. In order to quickly solve the problems, an onsite detector for toxic low molecular organic compounds has been demanded for a long time.

Surface plasmon resonance methodology (SPR) is useful for protein interaction analysis because of its real time function and no-labeling detection for immune responses [3–7]. Therefore, it appears to be a strong candidate as an onsite instrument for low molecular organic substances. However, a weak point of the SPR methodology is the poor sensitivity to concentrations of low molecular substances because of its dielectric detection and it is a big instrument. Accordingly, the present SPR instruments were generally limited to use in a laboratory and for high polymer analysis. Up to now, SPR measurements of low molecular substances have been done using the competitive method [8]. As the competitive method involves the extra procedure of the addition of an antibody solution, the measurement systems become more complicated. Therefore, its extra procedure is unfavorable as an onsite analyzer. In our laboratory work, the direct sensitivity to low molecular substances, such as 2,4-dichlorophenol, was 0.1–1 mg/L at best. In order that the SPR methodology be put into practice in field analysis, downsizing of the instrument and improvement of the SPR sensitivity to low molecular substances are indispensable [21]. The downsizing of the SPR instruments was thought to be possible by introducing a divided mirror for constructing the differential style. Also,

* Corresponding author. Tel.: +81 426 77 2830; fax: +81 426 77 2821.
E-mail address: uchiyama-katsumi@c.metro-u.ac.jp (K. Uchiyama).

0039-9140/$ – see front matter © 2006 Elsevier B.V. All rights reserved.
doi:10.1016/j.talanta.2006.02.068

concerning the improvement of the detection limit, it was postulated that if a sample is fed to a sensing point at a faster flow rate, the SPR intensity would be increased over our former work [9]. Therefore, how fast the sample was supplied to the sensing point was thought to be an important factor for improvement of the SPR sensitivity. It is well-known that micro-fabrication of a flow cell helps improvement of the reaction efficiency [11–17] as the interaction between the solid-state sensing surface and the sample is intensified. Freundlich's equation of capillarity [20] suggests that as the pore size of the capillary decreases, the adsorption of a substance on the interior wall of the capillary increases thus the improvement of the sensitivity to the SPR signal by the SPR microchip sensor. Accordingly, if a portable SPR detector with a microchip sensor using a micro-fabrication technique was developed, the improvement of the SPR sensitivity to low molecular organic substances would be expected in the SPR measurement. Based on this background information, in this study, the downsizing of the SPR instrument and the improvement of the SPR sensitivity were mainly investigated and compared to our former data for developing the new optic system with the divided mirror and SPR microchip sensor for SPR onsite analysis.

2. Experimental

2.1. Materials

All reagents used in this study were of analytical reagent grade unless otherwise stated. Sucrose, sodium acetate, peptide synthesis grade *N*-hydroxysuccinimide (NHS), perchloric acid, and hydrofluoric acid were obtained from Wako Pure Chemical Industries (Osaka, Japan). Acetic acid, sodium dihydrogenphosphate, disodium hydrogenphosphate, ammonium fluoride, diammonium cerium(IV) nitrate, nitric acid, acetone, and ethanol were purchased from Kanto Chemicals (Tokyo, Japan). 3-Mercaptopropyltrimethoxysilane (MPTS) was obtained from GE Toshiba Silicones (TSL8380, Tokyo, Japan). 3-Mercaptopropionic acid was obtained from Tokyo Kasei Kogyo (Tokyo, Japan). 1-Ethyl-3-(3-dimethylaminopropyl)-carbodiimide hydrochloride (EDC) was purchased from DOJINDO (Kumamoto, Japan). The human IgA ELISA quantification kit was obtained from Bethyl Laboratories, Inc. (Montgomery, TX, USA). IgG was obtained from ICN Phrmaceuticals, Inc. (USA). For the microchip fabrication, a mask blank plate coated with a thin layer of 50 nm Cr/Cr_2O_3 (DUFR-2506 (p)-L) was obtained from ULVAC Equipment Sales, Inc. (Tokyo, Japan). The positive type photoresist (PMER P-RZ300), photoresist diluting solution (PMER P-R), and developer (PMER P-1S) were purchased from Tokyo Ohka Kogyo (Tokyo, Japan). The poly(dimethylsiloxane) (PDMS) prepolymer (Sylgard 184) and curing agent were received from Dow Corning (MI, USA). The cover glass (16 mm × 16 mm) with a thin gold layer (45 nm) was obtained from Eliotech (Tokyo, Japan). Water was purified using a Milli-Q system (Nihon Millipore, Tokyo, Japan). All buffers were filtered through a 0.45 μm membrane filter (JHWPO 4700, Nihon Millipore, Tokyo, Japan) and degassed with an aspirator before use.

2.2. Fabrication of master glass channel template

The preparation of the master glass template was performed using photolithography and a wet-chemical etching procedure followed by replication. Details of this procedure were described elsewhere [12]. Briefly, the mask blank plate (DUFR-2506 (p)-L) was coated with a thin layer of the positive type photoresist (40%, v/v PMER P-RZ300) using a spin coater (K-359 S-1, Kyowa Riken, Tokyo, Japan) at 600 rpm for 2 min and baked in an oven (ESPEC, Osaka, Japan) at 85 °C for another 15 min. A serpentine channel design (made by Illustrator 10 and printed out on a Kodak (Tokyo, Japan) Professional SUPRA III film) was transferred onto the mask plate by exposure to a long wavelength ultraviolet lamp (FLB-15, Toshiba, Japan) for about 2 min, followed by developing in a 20% (v/v) PMER P-1S solution for about 1 min. The template with the channel design was further baked at 85 °C for 15 min. The Cr/Cr_2O_3 layer was then removed with a mixture of 17% (w/v) diammonium cerium(IV) nitrate and 5% (v/v) perchloric acid solution to define the channel on the mask plate. After rinsing in 2 M HNO_3 for 5 min, a positive relief channel was obtained by etching the glass in 1 M NH_4F/1 M HF solution using an incubator (SN-M40S, NISSIN, Tokyo, Japan) at 25 °C for 22–110 min to produce a relief channel height of about 20–100 μm. After silanizing in 5% (v/v) trimethylchlorosilane/toluene for 24 h at room temperature, the master glass template was kept in a clean box before use.

2.3. Fabrication of PDMS/Au/glass microchip

First, an adhesive cellulose tape was fenced around the glass template and then four PEEK tubes (1/16 in. o.d., ca.10 mm long) were placed on a master glass template using water-soluble glue to define the reservoirs. A 10:1 weight mixture of the PDMS prepolymer and curing agent was thoroughly mixed. The mixture was degassed with a vacuum pump and then the mixture was poured onto the glass template with positive relief to form the channel. After curing at 60 °C for 60 min, the PDMS mold was peeled off from the master glass template and then exposed to plasma in a Sanyu Electron (Tokyo, Japan) Quick Coater SC-701 (etching mode, 3 mA for 30 s). The PDMS mold was immediately immersed in a 1% MPTS, 95% ethanol, and 20 mM acetate buffer (pH 4.5) mixture. After incubation for 60 min at room temperature, the PDMS mold was rinsed with a 95% ethanol/20 mM acetate buffer (pH 4.5) mixture and ethanol in this order. The PDMS mold was then attached to a cover glass with a thin gold layer and baked at 120 °C for 4 h. Finally, the four PEEK tubes were mounted in the device for sample installation and exhaust.

2.4. Differential optical system for onsite SPR measurement

Fig. 1 shows the main optical system for the present SPR detector. As shown in Fig. 1, the optical system used the Kretschmann configuration. The SPR detector consisted of a 770 nm light emitting diode (LED) (Hitachi, HE7601SG), two cylindrical lenses, a round prism (BK7), a divided mirror, a sensor, 2048 CMOS linear CCD (Sony, ILX551B), an electronic circuit, and a power source. The size and weight of the device

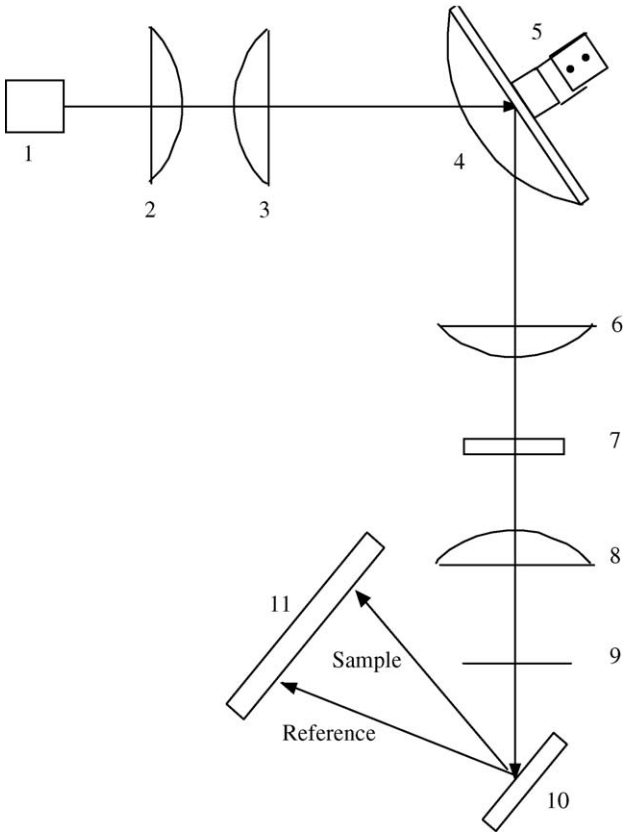

Fig. 1. Optical system for SPR microchip sensor: (1) LED light source; (2) plain convergingle ns; (3) cylindar lens; (4) prism; (5) SPR microchip sensor; (6) cylindar lens; (7) polarizer; (8) plain converging lens; (9) slit; (10) divided mirror; (11) linear CCD.

are 160 (W) × 100 (H) × 60 (D) mm and 770 g. Incident light at a 10° angle from the LED light source was converted into a linear wedge light by a cylindrical lens and was line-focused on the prism on which the sample and the reference sensor-cell were located at 0.5 mm intervals. The divided mirror is composed of two same-sized rectangular mirrors of 15 mm × 5 mm × 5 mm. The reflecting light of the sample and the reference from the prism were detected on the same number of CCD elements after adjusting the angle toward to the CCD element by the two controls of the divided mirror. The resonance angles based on the reflecting light from the sample and the reference were then determined and the remainder of the resonance angle of the reference and the sample to time (seconds) was monitored on the PC screen. As mentioned above, the greatest merit of the present optical system was the capability of the differential SPR on a single optical system by designing a divided mirror. The angular resolution of the present optic system was 0.0004°, which was obtained from an actual measurement using PBS as a blank [22].

2.5. SPR conditions

The conditions needed for a portable SPR detector are "simple, small, light, easy-handling, cheap, mobile, battery-driven, and so on. Fig. 2 shows the present SPR measurement system [18]. As shown Fig. 2, the system consists of a main body with an LED light source, an optical system, an electronic circuit, and a potential converter from 100 V/AC to 12 V/DC, a sensor guide, a double syringe pump (PHD2000, Harvard Apparatus, Holliston, MA, USA), an injector with a 300 μL loop (7725, Rheodyne, Cotati, CA, USA), a microchip sensor, and a Window's note type computer (Sony: PCG-9R6N) [18]. The contact between the sensor and the prism was done using matching oil (Type A: N_o = 1.5150, Cargille Laboratories, Inc., USA). Transmission of the data to the computer was done through an RS232C cable. When the measurement starts, the two SPRgrams, which display the relationship between the SPR intensities of the resonance angles of the sample and the reference, are continuously indicated on the PC monitor of the computer every 3 s for over 24 h. Also, all differential raw data are stored in a Microsoft Excel file. Other data processing functions such as the alarm, calibration function, and statistics quantity are under development. As mentioned above, the design of the divided mirror for the differential SPR measurement was available for downsizing of the detector and data processing without a time-lag. All experiments were done under the condition of 25 ± 1 °C, PBS running buffer, and flow rate of 20 μL/min.

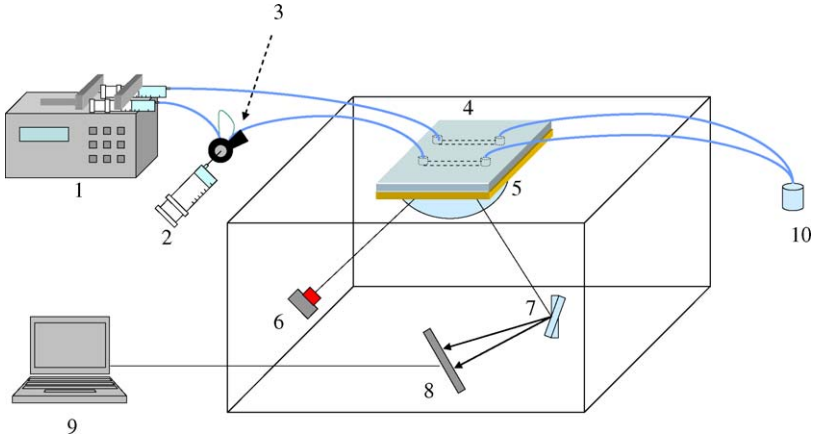

Fig. 2. Measurement system for microchip SPR sensor: (1) double syringe pump; (2) syringe; (3) sample injector; (4) microchip sensor; (5) prism 6: LED light source; (7) divided mirror; (8) linear CCD; (9) note type computer; (10) waste.

2.6. Immune detection

All reactions were performed using the flow system. First, a 5 mM 3-mercaptopropionic acid solution was pumped into the microchannel via an injection valve at the flow rate of 5 μL/min for 1 h and then a 400 mM EDC/100 mM NHS solution was introduced into the microchannel at the flow rate of 5 μL/min for 1 h. Next, the antibody (anti-IgA) solution was pumped into the microchannel at the flow rate of 5 μL/min for 1 h. Finally, the antigen (IgA) solution was introduced into the microchannel at the flow rate of 25 μL/min and the SPR response was monitored.

3. Results and discussion

3.1. SPRgrams

Fig. 3 shows the SPRgrams. A surface plasmon resonance was confirmed from the two SPRgrams. However, the SPR intensities of the two SPRgrams were slightly different. This is because the mechanical contact through the light interface (matching oil) between the sensor and the prism on the line focus was not even. The angle at the peak bottom gives the resonance angle. As soon as the sample is introduced to the sensor, its resonance angle immediately shifts to the higher side of the angle. The difference of both resonance angles corresponds to the concentration of organic substances.

3.2. Relationship between SPR intensity and sucrose concentration

Fig. 4 shows the relationship between the SPR intensity and 0–10% sucrose using the present SPR microchip sensor at the flow rate of 20 μL/min. A good linear calibration curve was obtained between the SPR intensity and sucrose concentration. The regression line was $y = 2.77\,e^{-1}x + 1.21\,e^{-2}$ for comparison with the regression line of $y = 2.59\,e^{-2}x - 1.47\,e^{-2}$ using the conventional flow cell the size of which was 10 mm × 1 mm × 1 mm ($L \times W \times D$), the slope of the present sensor became greater by ca. 11 times compared with the former data as shown Fig. 4. The correlation coefficient of the calibration curve was 0.986. For the SPR measurement, it has been defined that the amount of the substance adsorbed on the sensing area of 1 mm^2 is 1 ng for the angular change of 0.1° [19]. The detection limit of the SPR measurement depends on the angular resolution of the instrument. The developed detector has the angular resolution of 0.001° (angular resolution: 0.001°, S/N = 2). The sensing area of the microchip sensor was 0.1 mm^2 (chanel width: 1 mm, focus width: 0.1 mm). Accordingly, the detection limit for sucrose by the present SPR detector was thought to be ca. 30 ng if the margin should be regarded as 0.001 × 3. Based on these results, it was clarified that the integration of the microchip in the SPR measurement was useful for increasing the SPR intensity.

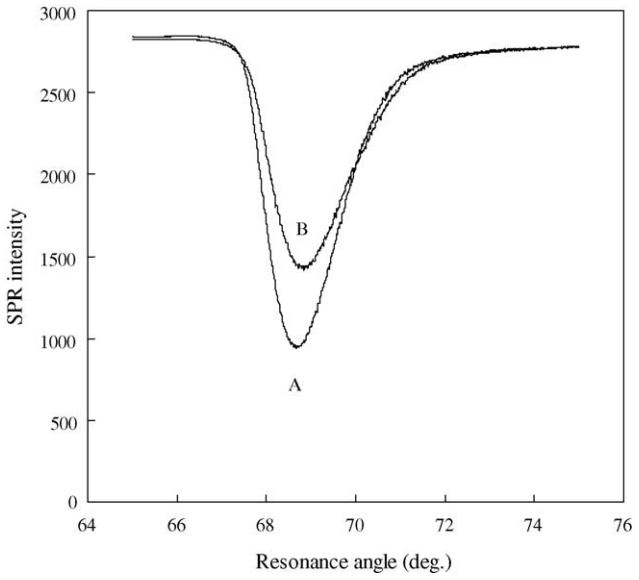

Fig. 3. SPRgrams: (A) sample channel and (B) reference channel. Both channels were filled with PBS (blank). Gold thickness: 45 nm; glass refraction index: 1.5150; wavelength: 770 nm; temperature: room temperature.

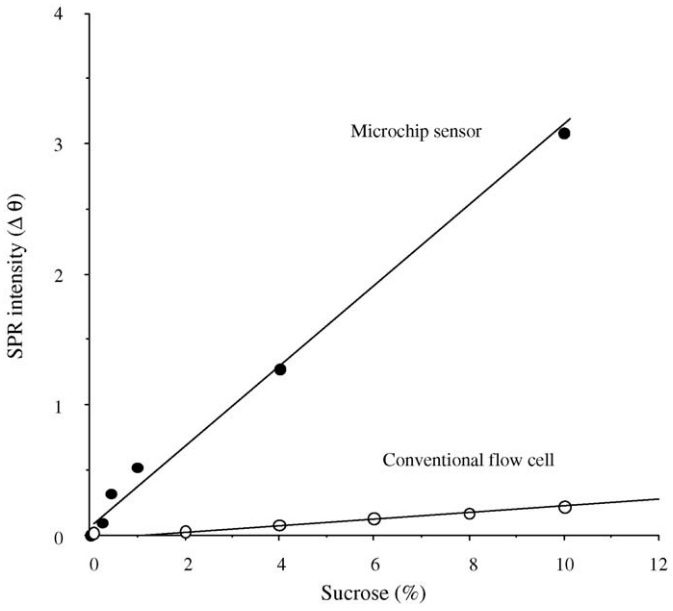

Fig. 4. Calibration curves for sucrose with SPR microchip sensor and conventional sensor: cell size, $L \times W \times D$ (mm); SPR microchip sensor (10 × 1 × 0.02), conventional flow cell (10 × 1 × 1); molecular weight of sucrose: 342

3.3. Effect of channel depth on SPR intensity

To prove the sensitivity improvement mentioned above, the effect of the chip depth on the SPR intensity was investigated after fabricating three sensors with different depths of 0.02, 0.04, and 0.1 mm. The evaluation was done by measuring the SPR intensity for 10% sucrose. Fig. 5 shows the effect of the channel depth on the SPR intensity. In there, a square is the reference data with the conventional flow cell having a depth of 1 mm. The SPR intensity was affected by the depth of the cell. As clarified in Fig. 5, the SPR intensity was in reverse exponential proportion to the channel depth and its regression line and coefficient factor were $y = 2.81 \times 10^{(-1.13x)}$ and $R^2 = 0.999$, respectively. It

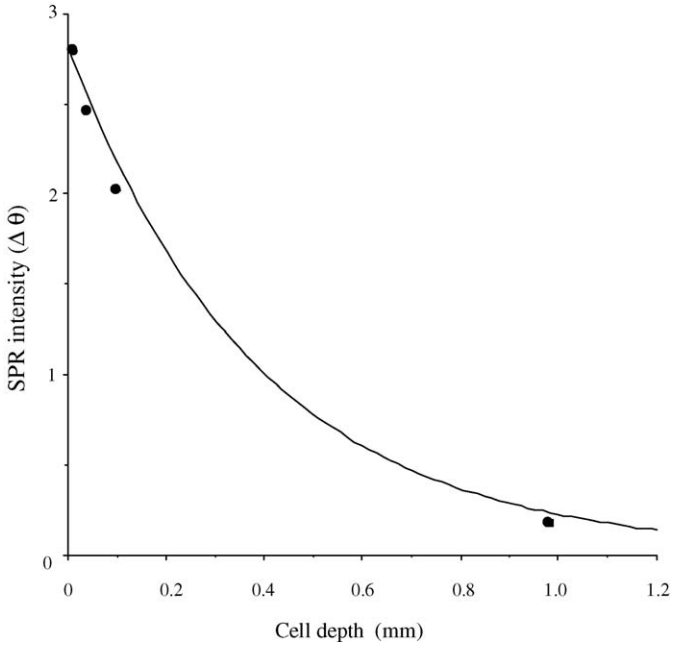

Fig. 5. Effect of cell depth on SPR intensity.

was clear that the deeper the channel depth, the smaller the SPR intensity. It was thought that the physical adsorption of sucrose on the sensor efficiently occurred as the liquid flow in a microcapillary became a laminar flow for the microchip to the turbulent flow of the conventional flow cell. As mentioned above, the size effect on the SPR intensity was clarified by this investigation.

3.4. Effect of flow rate on SPR intensity

The effect of the flow rate on the differential SPR signals was investigated for supplying the PBS buffer to the microchip sensor with the depth of 0.02 mm. The SPR intensity was affected by the flow rate. The value of the SPR intensity increased in proportion to the flow rate of the sample over 0–100 μL/min. As a result, the regression line was $y = 7.66\,e^{-4}x - 7.66$. The flow rate coefficient was $8\,e^{-4}$ °min/μL. This value was ca. 80 times greater compared with $1\,e^{-5}$ °min/μL for the convention flow cell. This result suggested that the sucrose was efficiently adsorbed on the sensing surface for the formation of a stable and slow flow by the microchip channel in proportion to the flow rate. Accordingly, the flow rate should be kept constant for the SPR measurement.

3.5. Reproducibility by SPR microchip sensor

To prove the repeatability of the SPR microchip sensor, the repeatability of the SPR microchip sensor was investigated by five random sample injections (6% sucrose) under the same conditions of Section 3.2. A coefficient of variation of 1.28% was obtained from the data shown in Table 1. The value was improved 5.5 times compared with that of the conventional flow cell. This improvement was thought to be because the SPR intensities of the sucrose by the chip effect increased.

Table 1
Reproducibility of SPR intensity obtained by 5 runs of 6% sucrose

Run no.	SPR intensity ($\Delta\theta$)
1	1.729
2	1.757
3	1.757
4	1.744
5	1.707

3.6. Application of SPR microchip sensor to immune detection

Immunoglobulin A (IgA) is a useful protein which prevents us from being affected by disease. Especially, it is well known as an indicator for a poor health condition and for some infectious diseases. Therefore, it is significant diagnostically to establish a simple onsite technology for measuring the IgA. To prove the possibility of the SPR microchip sensor for the immunoassay, the SPR microchip sensor was applied for the immunoassay of IgA. After immobilizing the anti-IgA antibody on a gold surface according to the already described procedure, the SPR measurement for IgA was done using the portable SPR detector developed for onsite SPR analysis. As shown in Fig. 6, a good linear calibration curve with the regression line, $y = 5.39\,e^{-1}x + 4.21\,e^{-2}$ was obtained between the SPR intensity and 0–0.9 nM IgA as shown Fig. 6. The slope of the calibration curve for IgA became ca. 39 times greater compared with $1.40\,e^{-2}$ for the IgG using the conventional flow cell. This shows the multiplier effect by the depth of the cell and the chemical binding force between IgA and the anti-IgA antibody on the solid sensor for SPR immunosensing. In our previous paper, the order of binding constant of bisphenol-A (MW: 225) was the same as that of IgG [10]. Molecular weight of IgG and IgA is

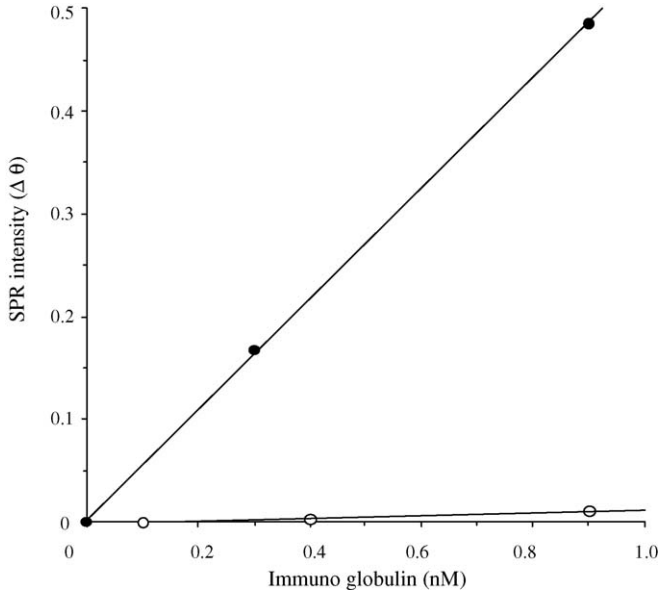

Fig. 6. Calibration curves for immunoglobulin A and G: (●) SPRmicrochip sensor (IgA, molecular weight: ca. 170,000); (○) conventional flow cell (IgG, molecular weight: ca. 150,000).

almost equal. Therefore, sensitivity for small molecular mass compound would be almost equal.

As mentioned above, the SPR microchip sensor and a portable SPR detector were developed and the basic properties were investigated and compared with those of the conventional flow cell. As a result, it was clarified that the SPR intensity was enhanced by introducing the microchip as a reaction field for the SPR detection from this investigation. It was thought that the microchip was useful as a means to increase the SPR intensity.

Why was the SPR intensity enhanced by the SPR microchip sensor? At present, we cannot give a definite answer to this question. However, we postulate the following five theories from our experimental results from the SPR microchip sensor.

(1) The flow in the microchip would become laminar.
(2) The flow coefficient increases.
(3) The flow rate became excessively fast (maybe, 17 mm/s as the calculated value at a 0.02 mm depth of the microchip) near the sensor surface.
(4) Mass transfer would be controlled by the chemical binding force (or the physical adsorption force) and the diffusion in the nanoarea on the sensor during the immuno reaction.
(5) The distribution of the substance might concentrate in the nano area on the SPR microchip sensor.

Freundlich's equation [20] of capillarity, which Freundlich developed from Thomson's formula from a gas to liquid, is well known for the solubility of a substance in a water droplet in the field of physical chemistry. We thought that the phenomenon from the SPR microchip sensor can be used with his equation. His equation is as follows:

$$\frac{RT}{M} \ln \frac{C_0}{C} = 2\frac{\gamma}{\rho r} \quad (1)$$

In the equation, R is the gas constant, T is the absolute temperature, M is the molecular weight, C_0/C is the relative solubility, γ is the surface tension, ρ is the density, and r is the radius of the droplet of water are given. Transforming Eq. (1), Eq. (2) is obtained:

$$\frac{C_0}{C} = e^{2\gamma M/\rho RT}\, e^{1/r} \quad (2)$$

where $e^{2\gamma M/\rho RT}$ is a constant. In Eq. (2), it is assumed that C/C_0 is the relative concentration change in the microchip sensor which has a depth of r. Fig. 7 shows a model of the SPR enhancement in the microchip channel if C and C_0 are the original concentration and the concentration in the nanoarea, respectively, near the sensing surface based on the data obtained by this investigation. As shown in Fig. 7, Eq. (2) might suggest that the lower the depth of the microchannel, the greater the relative concentration change in the microchannel. As a result, it was thought that the SPR intensity increased. Freundlich's equation of capillarity might provide creditability for our experimental results mentioned above.

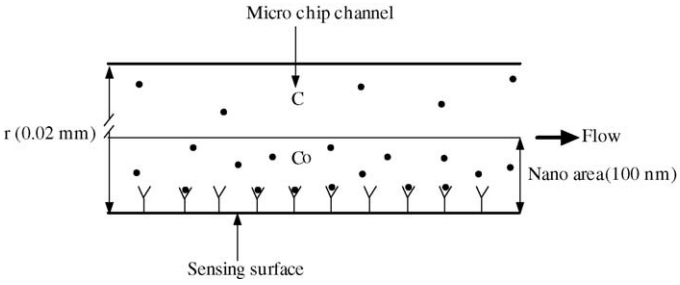

Fig. 7. A model of SPR enhancement on SPR micro chip sensor: (Y) antibody; (C) original concentration; (●) antigen; (C_0) concentration near sensing surface.

Table 2
Present performance obtained by portable SPR detector equipped with microchip sensor

Item	Conventional flow cell	Microchip
Repeatability for 6% sucrose (CV%, $n=5$)	6.4	1.3
Drift (°/1000 s)	0.0008	0.0006
Flow coefficient (°min/μL)	0.00001	0.0008
Regression line for sucrose	$y=2.59\,e^{-2}x - 1.47\,e^{-2}$	$y=2.77\,e^{-1}x + 1.21\,e^{-2}$
Correlation coefficient (R^2)	0.978	0.986
Regression line for immunoglobulin	$y=1.40\,e^{-2}x - 1.86\,e^{-3}$ (IgG)	$y=5.39\,e^{-1}x + 4.21\,e^{-2}$ (IgA)
Correlation coefficient (R^2)	0.987	1.000

4. Conclusions

Aiming at an SPR for on-site analysis, a portable SPR detector equipped with a microchip sensor has been developed. Its basic properties were investigated and related to the conventional data. As a result, the data shown in Table 2 were obtained by using a microchip sensor for the SPR measurement. As clarified in Table 2, the integration of the microchip sensor with the SPR measurement was useful for the improvement of the SPR detector's performance. The amplification effect of the SPR sensitivity would provide a high success rate for developing a highly sensitive SPR detector for low molecular substances for onsite use.

Acknowledgment

This research was partly supported by a Grant-in-Aid for Scientific Research (No. 16350047) from the Japan Society for the Promotion of Science (JSPS).

References

[1] R. Carson, Silent Spring, Mariner Books/Houghton Miffelin Company, USA, 1962, ISBN 0-618-24906-0.
[2] T. Colborn, D. Dumanoski, J.P. Myers, A Plume Book, Plume, USA, 1996, ISBN 0-452-27414-1.

[3] S. Lofas, M. Malmvist, I. Ronnberg, E. Stenberg, B. Liedberg, L. Ingermar, Sens. Actuators B 5 (1991) 79–84.
[4] E. Stenberg, B. Persson, H. Roos, C. Urbaniczky, J. Colloid Interface Sci. 143 (2) (1991) 513–526.
[5] U. Jonsson, M. Malmqvist, Adv. Biosens. 2 (1992) 291–336.
[6] C.S. Skjerpen, J. Weshe, S. Ossen, J. Biol. Chem. 277 (26) (2002) 23864–23871.
[7] U. Jonsson, M. Malmqvist, Adv. Biosens. 2 (1992) 291–336.
[8] D. Burakov, C.-W. Wong, C. Rachez, B.J. Cheskis, L.P. Freedman, J. Biol. Chem. 277 (26) (2002) 23864–23871.
[9] A. Hemmi, T. Imato, N. Soh, M. Sato, Y. Aoki, Y. Asano, C. Akasaka, S. Okutani, S. Ohkubo, N. Kaneki, K. Shimada, T. Eguchi, Development of Portable Differential SPR Detector Based on Single Optic System, Anal. Bioanal. Chem., submitted for publication.
[10] N. Soh, T. Watanabe, Y. Asano, T. Imato, Sens. Mater. 15 (8) (2003) 423–438.
[11] W. Xu, K. Uchiyama, T. Shimosaka, T. Hobo, Chem. Lett. (2000) 762–763.
[12] W. Xu, K. Uchiyama, T. Shimosaka, T. Hobo, J. Chromatogr. A 907 (2001) 279–289.
[13] K. Uchiyama, W. Xu, J. Qiu, T. Hobo, Fresenius J. Anal Chem. 371 (2001) 209–211.
[14] Y. Guo, K. Uchiyama, T. Nakagama, T. Shimosaka, T. Hobo, Electrophoresis 26 (2005) 1843–1848.
[15] K. Miyaki, Y. Guo, T. Shimosaka, T. Nakagama, H. Nakajima, K. Uchiyama, Anal. Bioanal. Chem. 382 (2005) 810–816.
[16] H. Nakajima, S. Ishino, H. Masuda, T. Shimosaka, T. Nakagama, T. Hobo, K. Uchiyama, Chem. Lett. 34 (2005) 358–359.
[17] H. Nakajima, H. Masuda, S. Ishino, T. Nakagama, T. Shimosaka, K. Arai, Y. Yoshimura, K. Uchiyama, Bunseki Kagaku 54 (2005) 817–823.
[18] PCT/JP2004/004428.
[19] E. Stenberg, B. Persson, H. Roos, C. Urbaniczky, J. Colloid. Interface Sci. 143 (1991) 513–526.
[20] F. Kitahara, Encyclopedia Chimica, vol. 408, no. 6, Kyoritsu Shuppan, Japan, 1961.
[21] Unpublished data.
[22] A. Hemmi, T. Imato, Y. Aoki, M. Sato, N. Soh, Y. Asano, C. Akasaka, S. Okutani, S. Ohkubo, N. Kaneki, K. Shimada, T. Eguchi, T. Oinuma, Sens. Acutuators B 108 (2005) 893–898.

Available online at www.sciencedirect.com
ScienceDirect
Talanta 70 (2006) 426–431
Talanta
www.elsevier.com/locate/talanta

Studies of the oxidation of palladium complexes by the advanced oxidation process
Pretreatment of model catalysts for precious metal analysis

D. Lynn Rodman, Nathan A. Carrington, Zi-Ling Xue *

Department of Chemistry, The University of Tennessee, Knoxville, Tennessee 37996-1600, USA

Received 7 February 2006; received in revised form 26 February 2006; accepted 26 February 2006
Available online 4 April 2006

Abstract

The advanced oxidation process (AOP) for the pretreatment of model palladium catalysts has been studied. Most standard metal analysis techniques are for metal ions free of organic ligands. Spent palladium catalysts contain organic ligands that need to be removed prior to analysis. AOP uses a combination of hydrogen peroxide and UV light to generate radicals that decompose such ligands, freeing up metals for further analysis. Palladium acetate $Pd(OAc)_2$, palladium acetylacetonate $Pd(acac)_2$, and tris(dibenzylideneacetone)dipalladium ($Pd_2(dba)_3$) were chosen as model precious metal catalysts for investigation. AOP was found to decompose ligands in $Pd(OAc)_2$, $Pd(acac)_2$ and give accurate Pd(II) quantification, while ligand decomposition and oxidation of Pd(0) to Pd(II) were demonstrated in treatments involving $Pd_2(dba)_3$. The effects of solubility of the palladium complexes, continuous addition of H_2O_2 during AOP treatments, sample pH, concentration of H_2O_2, and length of UV irradiation are reported.

Keywords: Palladium; Advanced oxidation process; Catalysts; Hydrogen peroxide

1. Introduction

Organometallic complexes have gained widespread use in catalysis over the past few decades. In particular, precious metal complexes have been used extensively as catalysts in many synthetic organic reactions [1–2] including industrial-scale reactions. As a result, spent precious metal catalysts are often contained in waste solutions from industrial-scale reactions. Before recycling the spent catalyst solutions to collect the spent precious metals, it is often necessary to determine the amount of precious metals in the solutions.

Metal catalysts often contain organic ligands, and standard analyses of metals by ion selective electrodes (ISEs) and other electrochemical techniques are, however, for metal ions free of organic ligands [3–6]. The organic ligands usually need to be decomposed or removed to free the metals prior to their qualitative and quantitative analysis. High-temperature processes such as graphite furnace atomic absorption spectroscopy or inductively coupled plasma atomic emission or mass spectrometry may be used to directly analyze metal complexes containing organic ligands [7–11]. These methods are usually costly and not suitable as a metal probe. In addition to organic ligands in precious metal catalysts, the presence of large amounts of organic species in spent catalyst solutions also makes quantitative analysis of precious metals a challenge.

Studies have been conducted to remove organic species in spent catalyst solutions. A method involving the use of supercritical water for oxidation of organic species was reported recently [12]. Other methods require the use of harsh acids to digest organic species [1d,13]. Although these methods have proven effective for the oxidation of metals as well as organic species, more environmentally benign and cost-effective methods are desirable.

The advanced oxidation process (AOP) has recently been investigated to convert organic compounds to CO_2 and H_2O. This process utilizes a combination of H_2O_2 and O_3 or UV radiation to generate highly potent hydroxyl radicals ($^{\bullet}OH$) [14] that oxidize even relatively stable substances [15]. AOP has thus been widely used in the decomposition of organic compounds and contaminants in drinking water and industrial wastewater

* Corresponding author.
E-mail address: xue@utk.edu (Z.-L. Xue).

0039-9140/$ – see front matter © 2006 Elsevier B.V. All rights reserved.
doi:10.1016/j.talanta.2006.02.067

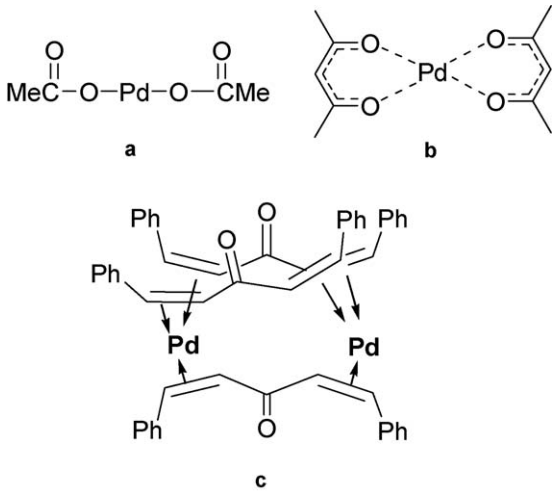

Scheme 1. Model Pd complexes studied in the current work: palladium(II) acetate (**a**); palladium(II) acetylacetonate (**b**); and tris(dibenzylideneacetone)-dipalladium(0) (**c**).

[14–17]. Many organic compounds have been oxidized and thus decomposed using AOP [16–19]. Although AOP has been used extensively for the oxidation of organic compounds, to our knowledge, it has been rarely used in the treatment of metal complexes.

When H_2O_2 is UV irradiated at wavelengths $\lambda < 300$ nm, homolytic splitting of the O–O bonds occurs, yielding $^{\bullet}$OH radicals (Eq. (1)) [15].

$$H_2O_2 \xrightarrow{h\nu} 2^{\bullet}OH \quad (1)$$

The radicals react with organic molecules to yield H_2O and CO_2 as main products. The UV radiation either decomposes or activates organic complexes as well, since most organic compounds absorb in the UV region, making the organic compounds more easily oxidized by $^{\bullet}$OH radicals. The reaction times of $^{\bullet}$OH radicals with organic compounds are short, usually less than a millisecond [15]. In addition to the formation of $^{\bullet}$OH from the UV irradiation of H_2O_2, these reactions yield several other reactive species such as hydroperoxyl or peroxyl radicals that also decompose organic compounds. In other words, the activation of H_2O_2 by UV irradiation or O_3 produces several radicals, all of which help decompose organic compounds.

We have investigated the conversion of palladium complexes to aqueous Pd(II) ions by the AOP reactions. The three complexes in Scheme 1 were chosen as models: $Pd(OAc)_2$ (**a**); $Pd(acac)_2$ (**b**); and $Pd_2(dba)_3$ (**c**). These three complexes are common catalysts in synthetic organic chemistry [1d–g]. $Pd_2(dba)_3$ (**c**) was chosen in part to test AOP as a means by which to oxidize Pd(0) in **c** to Pd(II). Our studies are reported here.

2. Experimental

2.1. Reagents

The chemicals used in the current studies, including H_2O_2 (Fisher, 30%; Kroger brand, 3%), *N*,*N*-dimethyl-4-nitrosoaniline (Acros, 99%), acetone (Fisher, certified ACS), glacial acetic acid (Mallinckrodt, analytical reagent), concentrated hydrochloric acid (Fisher, certified ACS), concentrated nitric acid (Fisher, certified ACS), sodium dodecyl sulfate (SDS, Fisher, certified ACS), Triton® X-100 (Acros) [20], $Pd(OAc)_2$ (**a**, Strem, 98+%), $Pd(acac)_2$ (**b**, Strem, 99%), and $Pd_2(dba)_3$ (**c**, Strem, 98%), and Pd atomic absorption standard solution (Acros, 1000.6 ppm Pd), were used as received. Deionized water (18 MΩ) was used in the preparation of all aqueous solutions and standards.

2.2. Analytical instrumentation

All UV–vis spectra were collected using a Hewlett-Packard 8452 photodiode array UV–vis spectrophotometer and a standard 1.0-cm quartz cuvette. Blank spectra of solutions containing all matrix components other than the analyte were recorded and subtracted from all subsequent spectra.

Atomic absorption (AA) analyses were performed using a Perkin-Elmer 5100 atomic absorption spectrophotometer using an air/acetylene flame under standard conditions [7–9] unless otherwise noted.

2.3. Photochemical reactor and UV lamp

The photoreactor (ca. 500 mL) used in the current studies consists of an outer vessel containing the sample, into which an Ace Glass quartz immersion well/water jacket housing the UV lamp is immersed. A port was incorporated to allow the use of a continuous addition funnel for H_2O_2 addition during UV irradiation. A second port allows air to enter the photoreactor. A UV source (450-W quartz medium-pressure mercury-vapor immersion lamp with a 5-in. arc length; Ace Glass 7825-34) was used.

2.4. Preparation and AOP treatment of samples

The three Pd complexes **a–c** were found insoluble in water. Studies were conducted to determine their solubilities in various organic solvents by the following process. Pd complex (20 mg) was weighed into each of several small glass vials. A minimal volume (<1 mL) of an organic solvent was added to each vial (one solvent per vial). The vials containing solvents with low solubilities of the Pd complex were discarded. The vials containing the solvent in which the Pd complex was soluble were kept for further investigation. The contents of these vials were then added to 100 mL of deionized water to determine if phase separation would occur. Suitable organic solvents were determined to be those in which the Pd catalyst would readily dissolve, and would exhibit no phase separation upon addition of water.

2.4.1. AOP treatment of palladium(II) acetate (*a*)

In the preparation of a typical sample of **a** for AOP treatment, $Pd(OAc)_2$ (**a**, 31.7 mg) was dissolved in acetone (700 μL). The solution was then added to water (200 mL) in the photochemical reactor. A 3:1 mixture of concentrated HCl and HNO_3 was then added to adjust pH to 0.75. H_2O_2 (30%, 5.0 mL) was

added to the reactor to bring the H_2O_2 concentration to 5.0 g/L. After shielding the photochemical reactor with aluminum foil, the sample was UV irradiated for 4.1 h. During the UV irradiation, H_2O_2 (5%, 100 mL) was added dropwise to replenish H_2O_2. After UV irradiation, the volume of the contents of the reactor was adjusted to 500 mL. Repeated $Pd(H_2O)_n^{2+}$ analyses by the *N*,*N*-dimethyl-4-nitrosoaniline method [21] showed that (98.5 ± 1.2)% of **a** had been converted to aqueous $Pd(H_2O)_n^{2+}$ ions. In a control sample of **a** that was not treated by AOP, only (79.1 ± 1.2)% of **a** existed as $Pd(H_2O)_n^{2+}$ ions. These results indicate that AOP treatment of the $Pd(OAc)_2$ is necessary for the accurate detection and quantification of Pd(II) in **a**.

Total Pd analysis for samples of **a** which were or were not treated by AOP were performed by AA. AA analyses of an AOP-treated sample and its control that was not treated by AOP detected (97 ± 3) and (99 ± 3)% of palladium, respectively, in the samples of **a**.

2.4.2. AOP treatment of palladium(II) acetylacetonate (*b*)

$Pd(acac)_2$ (**b**, 19.1 mg) was dissolved in glacial acetic acid (9.00 mL). The solution was added to deionized water (250 mL) in the photochemical reactor. A 3:1 mixture of concentrated HCl and HNO_3 was then added to adjust pH to 0.75. H_2O_2 (30%, 6.3 mL) was added to the reactor to make the H_2O_2 concentration 5.0 g/L. After shielding the photochemical reactor with aluminum foil, the solution was UV irradiated for 4.0 h. During the process, H_2O_2 (5%, 100 mL) was added dropwise to replenish H_2O_2. After UV irradiation, the volume of the contents of the reactor was adjusted to 500 mL. Repeated $Pd(H_2O)_n^{2+}$ analyses by the *N*,*N*-dimethyl-4-nitrosoaniline method showed that (98.2 ± 0.6)% of **b** had been converted to aqueous $Pd(H_2O)_n^{2+}$ ions. In a control sample of **b** that was not treated by AOP, only (89.5 ± 1.2)% of **b** existed as $Pd(H_2O)_n^{2+}$ ions. These results indicate that AOP treatment of the $Pd(OAc)_2$ sample gives more accurate detection and quantification of Pd in **b**.

AOP was also found necessary for the accurate quantification of Pd in **b** by atomic absorption (AA). AA analyses of an AOP-treated sample and its control that was not treated by AOP detected (99 ± 3) and (89 ± 3)% of palladium, respectively, in the samples of **b**.

2.4.3. AOP treatment of tris(dibenzylideneacetone)dipalladium(0) (*c*)

$Pd_2(dba)_3$ (**c**, 21.5 mg) was mixed with triton X-100 (0.150 mL) in a glass vial. This mixture was then added quantitatively to deionized water (300 mL) in the photochemical reactor. A 3:1 mixture of concentrated HCl and HNO_3 was then added to adjust pH to 0.13. H_2O_2 (30%, 5.0 mL) was added to the reactor to make the H_2O_2 concentration 5.0 g/L. After shielding the photochemical reactor with aluminum foil, the sample was UV irradiated for 5.8 h. During the process, H_2O_2 (4.7%, 125 mL) was added dropwise to replenish H_2O_2. After UV irradiation, the volume of the contents of the reactor was adjusted to 500 mL.

$Pd(H_2O)_n^{2+}$ analyses by the *N*,*N*-dimethyl-4-nitrosoaniline method showed that (90.0 ± 1.2)% of **c** had been converted to aqueous $Pd(H_2O)_n^{2+}$ ions. In a control sample of **c** that was not treated by AOP, no $Pd(H_2O)_n^{2+}$ ions were detected by the *N*,*N*-dimethyl-4-nitrosoaniline method. AOP treatments of $Pd_2(dba)_3$ (**c**) were repeated many times. However, quantitative oxidation of **c** was not reproducible. These results indicate that the oxidation of **c** and removal of its ligands is possible, but the process may not be complete.

AOP was also found necessary for the accurate quantification of Pd in **c** by atomic absorption (AA). AA analyses of an AOP-treated sample and its control that was not treated by AOP detected (99 ± 3)% and (16 ± 3)% of palladium, respectively, in the samples of **c**.

2.4.4. Continuous addition of H_2O_2 during UV irradiation

Continuous addition of H_2O_2 during UV irradiation was conducted by using an addition funnel that was offset from the photoreactor and shielded by aluminum foil. Such a design was made so that UV radiation from the photoreactor would not prematurely decompose H_2O_2 in the funnel. The flow rate was adjusted prior to the start of the UV irradiation.

2.4.5. Studies of the pH during AOP treatment of the Pd complexes

In order to determine the optimum pH and acid/acid combination for use during AOP, samples of $Pd(acac)_2$ (**b**) were investigated. $Pd(acac)_2$ (**b**, 19 mg) was dissolved in glacial acetic acid (9.00 mL). The solution was added to deionized water (250 mL) in the photochemical reactor. Sample pH was varied from 0 to 1 by addition of H_2SO_4, HCl, HNO_3, or aqua regia (a 3:1 mixture of HCl and HNO_3). H_2O_2 (30%, 6.3 mL) was added to each sample to make the H_2O_2 concentration 5.0 g/L. After shielding the photochemical reactor with aluminum foil, the solution was UV irradiated for 4.0 h. During the process, H_2O_2 (5%, 100 mL) was added dropwise to replenish H_2O_2. After UV irradiation, volume of the contents in the reactor was adjusted to 500 mL. Samples in which the pH was adjusted to 0.75 by aqua regia showed the lowest errors in both aqueous Pd(II) ((1.8 ± 0.6)%) and total Pd ((1 ± 3)%) analyses. Aqua regia was thus chosen for use in further experiments.

A control sample was prepared by adding $Pd(acac)_2$ (**b**, 19 mg) dissolved in glacial acetic acid (9.00 mL) to deionized water (250 mL) in a volumetric flask. Sample pH was adjusted to 0.75 by addition of aqua regia. There was no AOP treatment of this sample. Analyses of this control sample showed (10.5 ± 1.2) and (11 ± 3)% errors in aqueous Pd(II) and total Pd contents, respectively.

2.5. Analysis of total Pd and Pd(II)

All AOP samples and standards were prepared gravimetrically using standard analytical techniques. At the conclusion of the UV irradiation step, samples were quantitatively transferred and diluted in volumetric flasks. After dilution, samples were then analyzed for total palladium and aqueous Pd(II) content.

Total palladium in each sample was analyzed by AA spectroscopy using an air-acetylene flame. Standard solutions were prepared by serial dilution of a 1000.6 ppm Pd(II) AA standard solution and addition of necessary sample matrix components to each standard before diluting to the proper volume. The standard

curves were made by measuring the absorbance at 244.8 nm using a slit width of 0.20 nm with a lamp current of 15 mA during analysis of the standards and samples for total Pd [7–9].

Pd(II) in each sample was analyzed by UV–vis spectrometry using *N*,*N*-dimethyl-4-nitrosoaniline, a ligand selective for Pd(II) [21]. Upon addition of the ligand to a Pd(II) solution, a colored complex is formed. Pd(II) content in the standards and samples was determined by monitoring the absorbance at 496 nm in the UV–vis spectrum. Standards were prepared by serial dilution of a 1000.6 ppm Pd(II) AA standard solution and addition of the ligand and necessary sample matrix components to a volumetric flask.

3. Results and discussion

$Pd(acac)_2$ (**a**) and $Pd(acac)_2$ (**b**) are Pd(II) complexes. Our tests have shown that direct analysis of Pd before AOP treatment by the UV–vis and AA methods discussed earlier result in large errors, suggesting that the ligands in these complexes may interfere with detection of Pd(II). $Pd_2(dba)_3$ contains Pd(0) and thus requires both oxidation of Pd(0) to Pd(II) and the removal of the organic ligands before quantitative Pd analysis by established electrochemical or optical methods. AOP has thus been investigated to treat these Pd complexes.

Many AOP studies have been conducted using both O_3 and UV radiation to generate active $^{\bullet}OH$ radicals from H_2O_2. UV radiation was chosen as the method for activating H_2O_2 in the current studies. Advantages of using UV in our studies include the ease of generating UV radiation, low cost, and its potential for use in a portable sensor. Using ozone requires an ozone generator, and its use in a research laboratory may be associated with health risks, and lead to corrosion to laboratory equipment.

Our work reveals that, among the factors contributing to the efficiency of AOP, solubility of the complex in aqueous solution is the most important. Other factors include H_2O_2 concentration, length of UV irradiation, and sample pH.

3.1. Improving solubility of the Pd complexes in aqueous solution

AOP is an oxidation process conducted in aqueous solution using dilute H_2O_2 in water and UV radiation or O_3 as oxidants. Our studies have shown that, for the successful treatment by AOP, it is necessary that the compound be soluble or at least well dispersed in aqueous solution. For compounds that are water soluble, AOP may be readily applied. For compounds that are sparingly soluble in water, their AOP treatments may be challenging.

Most Pd complexes that are good catalysts are only soluble in organic solvents [1d]. All three Pd complexes (Scheme 1) investigated in the current studies, **a**–**c**, are insoluble in water [22–24]. Significant effort was made to develop methods to incorporate these complexes into aqueous solution.

Our initial studies to use surfactants to disperse $Pd(OAc)_2$ (**a**) show that a large amount of the surfactants needed to reach the critical micelle concentration to disperse the Pd complex likely exceeds the amount of organics that could be completely oxidized by AOP in our work, making subsequent accurate Pd analysis difficult [20].

We next investigated the approach using mixtures of an organic solvent and water to dissolve $Pd(OAc)_2$ (**a**). After investigating several solvents, acetone was found to work well in this approach. $Pd(OAc)_2$ in acetone and water was found to give a clear solution. In one solubility test, the sample was prepared by dissolving $Pd(OAc)_2$ (30 mg) in a small amount of acetone (700 μL). The solution was then added to 300 mL of water to give a homogeneous solution. Subsequent AOP treatment of this sample was successful, yielding values for total Pd and Pd(II) that were in a close agreement. The following may contribute to the success of this approach: (1) acetone molecules are much smaller than the bulky surfactant molecules; (2) acetone contains a carbonyl group that may have helped the oxidation of acetone in AOP; and (3) the total amount of organics (700 μL) is smaller than in samples containing the surfactants [20].

A similar method was used to dissolve $Pd(acac)_2$ (**b**) in mixed solvents. Several organic solvents were investigated, and $Pd(acac)_2$ was found to be soluble in glacial acetic acid. In one test, $Pd(acac)_2$ (**b**, 20 mg) was dissolved in glacial acetic acid (9 mL). This solution was then mixed with 300 mL of water to give a homogeneous solution. Subsequent AOP treatment of this sample was successful, yielding values for total Pd and Pd(II) that were in a close agreement. Acetic acid, as acetone, contains a carbonyl group, and is thus easier to oxidize than bulky surfactants. Even though a relatively large amount of glacial acetic acid was used here, it did not cause a problem for subsequent AOP treatment.

Tris(dibenzylideneacetone)dipalladium(0) [$Pd_2(dba)_3$, **c**] is soluble in few organic solvents [1d]. Of the solvents such as chloroform and toluene in which $Pd_2(dba)_3$ is soluble, none is miscible with water. The use of a surfactant was found to be the only method to disperse the complex in aqueous solution. Both sodium dodecyl sulfate (SDS) and triton X-100 [20] were investigated for dispersion of $Pd_2(dba)_3$ (**c**) in aqueous solution. Triton X-100 was found to work well for the dispersion of the complex. Subsequent AOP treatment of the $Pd_2(dba)_3$ (**c**)/triton X-100 samples show qualitatively that the ligand in **c** was removed from the metal, and Pd(0) in the complex was oxidized to Pd(II). However, the conversion during AOP was not complete, and unknown black solids were found in the AOP-treated mixture. The amount of surfactant (Triton X-100: 0.162 g) needed to reach the critical micelle concentration to disperse the Pd complex likely exceeds the amount of organics that could be oxidized by AOP. The use of surfactants thus made the complete oxidation of all organic species difficult.

3.2. Concentration of H_2O_2 during the AOP treatment

Earlier AOP studies showed that an H_2O_2 concentration of 5 g/L during the UV irradiation process was sufficient for the oxidation of several organic compounds [15]. The concentration of 5 g/L was also found to work well in the current studies. As is the case with other AOP systems, replenishing H_2O_2 during UV irradiation of the sample has been found to contribute to the overall efficiency of the process.

In many reported AOP studies, H_2O_2 is added at the beginning of the experiment before UV irradiation [15,16,25,26]. Our initial experiments were carried out similarly with an initial H_2O_2 concentration of 5 g/L. These experiments showed incomplete oxidation of the organic species and thus poor Pd(II) analysis. H_2O_2 may have been depleted during the reaction. We subsequently investigated continuous addition of H_2O_2 during the UV irradiation of $Pd(OAc)_2$ samples. H_2O_2 (30%, 5.0 mL) was added to samples i and ii (total volume: 300 mL) before UV irradiation to give an H_2O_2 concentration of 5 g/L. During the UV irradiation of samples i and ii, a 5% H_2O_2 solution (100 mL) was added dropwise to replenish H_2O_2. In control samples (iii and iv) without continuous H_2O_2 addition, H_2O_2 was only added prior to the UV irradiation so that the initial H_2O_2 concentration was 5 g/L. As shown in Fig. 1, the continuous addition of H_2O_2 was found to greatly increase the efficiency of the oxidation process and the removal of organic ligands. Nearly quantitative ($(99.0 \pm 0.5)\%$) conversion of the Pd complex in samples i and ii to aqueous Pd(II) was achieved. In comparison $(0.0 \pm 0.1)\%$ and $(17.8 \pm 0.1)\%$ of the Pd complex in samples iii and iv were converted to aqueous Pd(II).

3.3. Length of UV irradiation

Long UV irradiation is required to treat the water-insoluble palladium complexes, even when continuous addition of H_2O_2 is used during UV irradiation. **a** and **b** were investigated separately to determine the optimum UV irradiation length. Identical Pd samples of **a** or **b** were UV irradiated from 1 to 6 h. Samples treated for less than 4 h often did not yield quantitative analysis of aqueous Pd(II) by UV–vis spectroscopy using *N*,*N*-dimethyl-4-nitrosoaniline. UV irradiation of 4 h resulted in $(99.0 \pm 0.5)\%$ oxidation and removal of the ligands to give quantitative analysis of aqueous Pd(II) by UV–vis spectroscopy using *N*,*N*-dimethyl-4-nitrosoaniline. Longer UV irradiation was thus not investigated.

Several factors may contribute to the length UV irradiation time here: (1) there are organic solvents in **a** and **b**, and they need to be oxidized as well; (2) the Pd complexes **a** and **b** are insoluble in water, and, in mixed organic solvent/water, may have higher kinetic barriers for oxidation by water-based $^{\bullet}OH$ radicals; and (3) the volume of samples in the current work (~300–400 mL) is quite large, and the larger volume is expected to require longer AOP treatment.

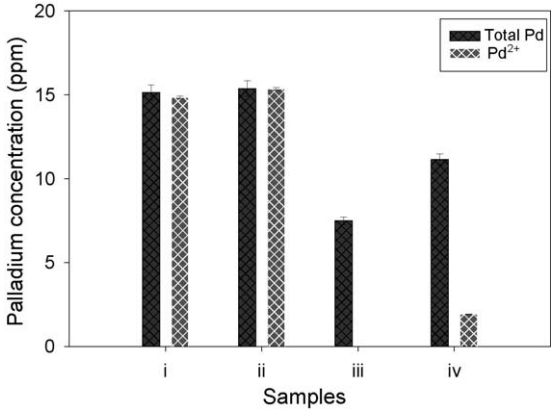

Fig. 1. Comparison of the total Pd and aqueous Pd(II) concentration after the AOP treatment of $Pd(OAc)_2$ samples i, ii, iii, and iv. H_2O_2 was continuously added during UV irradiation of samples i and ii. In control samples iii and iv, H_2O_2 was not continuously added during UV irradiation.

3.4. Effect of pH during AOP treatment

Initial AOP experiments involving the Pd complexes were conducted without adjustment of pH. Coatings and/or unknown black particles were often observed on the inside walls of the photoreactor. Analysis of the coatings/particles showed a significant amount of Pd content. Variation of solution pH during AOP treatment of $Pd(acac)_2$ (**b**) was subsequently investigated.

These studies show that lowering pH during the AOP treatment eliminates the formation of coatings and/or particles. Optimum results were obtained when sample pH was maintained in the range of 0.5–0.8. Several acids including HCl, HNO_3, and aqua regia (a 3:1 mixture of HCl and HNO_3) were used to lower pH. While neither HCl nor HNO_3 alone was found to greatly increase the amount of free Pd(II), the use of the combination of acids as aqua regia was found to give the best results ($(1.8 \pm 0.6)\%$ and $(1 \pm 3)\%$ errors in Pd(II) and total Pd analyses, respectively).

A control sample of **b** was prepared similarly, and its pH was adjusted to 0.75 by addition of aqua regia. There was no H_2O_2 addition or UV irradiation of this sample. The $(10.5 \pm 1.2)\%$ and $(11 \pm 3)\%$ errors in aqueous Pd(II) and total Pd analyses, respectively, in this control sample are larger than those in the sample of **b** that was treated by AOP. This finding indicates that the combination of low pH and AOP treatment are required for accurate Pd analysis. It should be noted that low pH ($pH < 2$) is often used in standard analytical procedures [27].

4. Concluding remarks

The AOP has proven to be a viable method to oxidize the ligands and organic species contained in model Pd catalyst complexes. The low solubility of these complexes in aqueous solution was a major challenge in the AOP treatment. The use of mixed organic solvent/water for $Pd(OAc)_2$ (**a**) and $Pd(acac)_2$ (**b**) is a good method to dissolve water-insoluble complexes for subsequent AOP treatment. Although treatment of Pd(0) complex **c** did not give good Pd analysis results, oxidation of **c** and removal of its ligands by AOP did occur. Its low solubility in many organic solvents makes it difficult to find mixed organic/water solvents for **c**.

Acknowledgments

The work was supported by the Measurement and Control Engineering Center (MCEC) at the University of Tennessee, a National Science Foundation Industry/University Cooperative Research Center (I/UCRC). The authors also thank Prof. X. Peter Zhang and Dr. Ying Chen for assistance with Pd samples, Profs. James Q. Chambers and Youngmi Lee for the use of UV–vis spectrophotometer.

Appendix A. Supplementary data

Supplementary data associated with this article can be found, in the online version, at doi:10.1016/j.talanta.2006.02.067.

References

[1] (a) For precious metal catalysts, see, e.g., (a) Vision 2020 Catalysis Report (www.ccrhq.org/vision/index/roadmaps/catrep.html);
(b) J. Halpern, Precious Met. 19 (1995) 411;
(c) S.S. Stahl, Science 309 (2005) 1824;
(d) R.F. Heck, Palladium Reagents in Organic Syntheses, Academic Press, New York, 1985;
(e) R. Singh, M.S. Viciu, N. Kramareva, O. Navarro, S.P. Nolan, Org. Lett. 7 (2005) 1829;
(f) J. Terao, A. Oda, N. Kambe, Org. Lett. 6 (2004) 3341;
(g) B.M. Trost, J. Xu, J. Am. Chem. Soc. 127 (2005) 17180.

[2] (a) R.T. Jacobsen, Chem. Eng. Prog. 101 (2005) 20;
(b) H. Meyer, M. Grehl, in: G.J. Antos, A.M. Aitani (Eds.), Catalytic Naphtha Reforming, second ed., Marcel Dekker, New York, 2004, pp. 459–475;
(c) P. Grumett, Platinum Met. Rev. 47 (2003) 163;
[d] X. Yang, T. Gegan, G. Hodge, G. Munzing, D. Pollick, 26 (2002) 84;
(e) C.G. Anderson, S.M. Nordwick, Precious Met. 19 (1995) 123.

[3] M. Aghamohammadi, N. Alizadeh, Anal. Chim. Acta 480 (2003) 299.

[4] J. Wang, K. Varughese, Anal. Chim. Acta 199 (1987) 185.

[5] J.B. Bharathibai, S.R. Rajagopalan, Analyst 117 (1992) 1623.

[6] G. Raber, K. Kalcher, C.G. Neuhold, C. Talaber, G. Kolbl, Electroanalysis 7 (1995) 138.

[7] B. Welz, M. Sperling, Atomic Absorption Spectrometry, third ed., Wiley, New York, 1999.

[8] Perkin Elmer Corporation, Anal. Methods Atomic Absorp. Spectr. (1996).

[9] D.A. Skoog, F.J. Holler, T.A. Nieman, Principles of Instrumental Analysis, fifth ed., Harcourt Brace, Philadelphia, 1998.

[10] H.E. Taylor, Inductively Coupled Plasma-Mass Spectrometry, Academic Press, New York, 2001.

[11] L. Qi, M.-F. Zhou, C.Y. Wang, J. Anal. Atom. Spectr. 19 (2004) 1335.

[12] (a) L. Ping, P.K. Dasgupta, Anal. Chem. 61 (1989) 1230;
(b) J.L. Capelo-Martínez, P. Ximénez-Embún, Y. Madrid, C. Cámara, Trends Anal. Chem. 23 (2004) 331;
(c) R. Ritsema, E. van Heerde, Fresenius J. Anal. Chem. 358 (1997) 838;
(d) R.H. Atallah, D.A. Kalman, Talanta 38 (1991) 167;
(e) P.G.C. Campbell, M. Bisson, R. Bougie, A. Tessier, J.P. Villeneuve, Anal. Chem. 55 (1983) 2246;
(f) C. Guéguen, C. Belin, B.A. Thomas, F. Monna, P.-Y. Favarger, J. Dominik, Anal. Chim. Acta 386 (1999) 155.

[13] R. Bock, A Handbook of Decomposition Methods in Analytical Chemistry, Wiley, New York, 1979.

[14] USEPA, Adv. Photochem. Oxid. Processes (1998).

[15] P. Schulte, A. Bayer, F. Kuhn, T. Luy, M. Volkmer, Ozone-Sci. Eng. 17 (1995) 119.

[16] M.E. Sigman, A.C. Buchanan III., S.M. Smith, J. Adv. Oxid. Technol. 2 (1997) 415.

[17] F.J. Castaldi, C.F. Richardson, B. Payne, in: Proceedings of the WEFTEC '96, vol. 3, 1996, p. 275.

[18] A. Safarzadeh-Amiri, Water Res. 35 (2001) 3706.

[19] F.J. Beltran, M. Gonzalez, J. Rivas, M. Marin, Ind. Eng. Chem. Res. 33 (1994) 125.

[20] See supplementary materials.

[21] P. Sarkar, P.K. Paria, S.K. Majumdar, J. Ind. Chem. Soc. 65 (1988) 117.

[22] Merck and Co., in: M.J. O'Neil, A. Smith, P.E. Heckelman (Eds.), The Merck Index, 13th ed., Whitehouse Station, New Jersey, 2001, p. 7056.

[23] Y. Takahashi, T. Ito, S. Sakai, Y. Ishii, Chem. Commun. 17 (1970) 1065.

[24] H. Kawazura, H. Tanaka, K.-I. Yamada, T. Takahashi, Y. Ishii, B. Chem. Soc. Jpn. 51 (1978) 3466.

[25] V. Kavitha, K. Palanivelu, Chemosphere 55 (2004) 1235.

[26] M.Y. Ghaly, G. Hartel, R. Mayer, R. Haseneder, Waste Manage. 21 (2001) 41.

[27] For example, in the ICP-AE or ICP-MS analysis of aqueous samples, the pH of the solutions is adjusted to <2 prior to analysis to minimize analyte precipitation. A.W. Varnes, in: Handbook of Instrumental Techniques for Analytical Chemistry, F.A. Settle (Ed.), Prentice Hall, Upper Saddle River, New Jersey, 1997, pp. 395–418.

Available online at www.sciencedirect.com
ScienceDirect
Talanta 70 (2006) 432–436
Talanta
www.elsevier.com/locate/talanta

Probing trace Pb^{2+} using electrodeposited *N*,*N*′-(*o*-phenylene)-bis-benzenesulfonamide polymer as a novel selective ion capturing film

Lei Zhang, Wei Li, Mianhong Shi, Jilie Kong *

Department of Chemistry, Fudan University Shanghai 200433, PR China

Received 30 December 2005; received in revised form 24 February 2006; accepted 27 February 2006
Available online 18 April 2006

Abstract

A novel film modified electrode for the determination of trace lead was developed in this work. The modified electrode was prepared by the electropolymerization of *N*,*N*′-(*o*-phenylene)-bis-benzenesulfonamide (PBSA) as the ion capturing reagent to create the functional film. The modified electrode shows a high selectivity towards Pb^{2+} over interfering cations, e.g. Cu^{2+}, Cd^{2+}, Co^{2+}, Ni^{2+}, Zn^{2+}, Cr^{2+}, and the calibration curve was linear in the concentration range of 2.0×10^{-9} to 1.0×10^{-7} M with correlation coefficient of 0.999. For 20 min accumulation, detection limit of 1.0×10^{-9} M was obtained at the signal to noise ratio of 3. Analytical availability of the modified electrode was demonstrated by the application for samples from pond water.

Keywords: *N*,*N*′-(*o*-phenylene)-bis-benzenesulfonamide (PBSA); Gold modified electrode; Stripping voltammetry; Selective Pb^{2+} detection

1. Introduction

Lead is one of the most abundant and certainly also one of the most toxic heavy metal ion causing environmental and health problems because of its stability in contaminated site and complexity of mechanism in biological toxicity, particularly dangerous for children leading to mental retardation when with abnormal concentration in bodily fluid. Thus, it is important to monitor the lead level in drinking water and in bodily fluids for the health of people. Compared the commonly used methods such as atomic adsorption spectrometry [1], atomic emission spectrometry [2–4], etc., stripping voltammetry, is one of the most favorable techniques for the determination of trace metal ions include lead ion because of its low cost and high sensitivity [5–8].

Electroanalytical approaches of film modified electrode towards the detection of trace mental ions have received considerable attention [9]. Wanekaya and Sadik used overoxidized polypyrrole film electrodes doped with 2(2-pyridylazo) chromotropic acid anion to determine lead [10]. Rahmam et al. reported the simultaneous determination of Hg^{2+}, Cu^{2+}, Pb^{2+} with an EDTA bonded conducting polymer modified electrode [11]. Because the selectivity of modified electrode for Pb^{2+} against other metal ions commonly presenting in biological systems, such as Cu^{2+} and Zn^{2+}, is very important, a new and simple approach of selective modified electrode became the pursuit of this work.

Kavallieratos et al. employed synthetic dansylamide, yielding from *o*-phenylenediammine and dansyl chloride, to extract trace Pb^{2+} from water and detected Pb^{2+} with fluorescence [12]. Meanwhile, high affinity of Pb^{2+} for *N*,*N*′-(o-phenylene)-bis-benzenesulfonamide (PBSA) (Scheme 1a), which is analogous to dansylamide, was confirmed by the same group [13]. Because of the fact that little attention was paid yet to employ any derivatives of *o*-phenylenediamine to probe Pb^{2+} electrochemically, a novel strategy to selectively sensing Pb^{2+} based on the electrodeposition of PBSA was presented in this work, triggered by the mentioned pioneer work.

The electrodeposited PBSA film, acting as the specific ion capturing matrix, was formed on Au electrode via scanning the potential between 0.0 and +1.0 V at 100 mV/s for several cycles. The formation of the electrodeposited film on Au was

* Corresponding author. Tel.: +86 21 65642138; fax: +86 21 65641740.
E-mail address: jlkong@fudan.edu.cn (J. Kong).

0039-9140/$ – see front matter © 2006 Elsevier B.V. All rights reserved.
doi:10.1016/j.talanta.2006.02.070

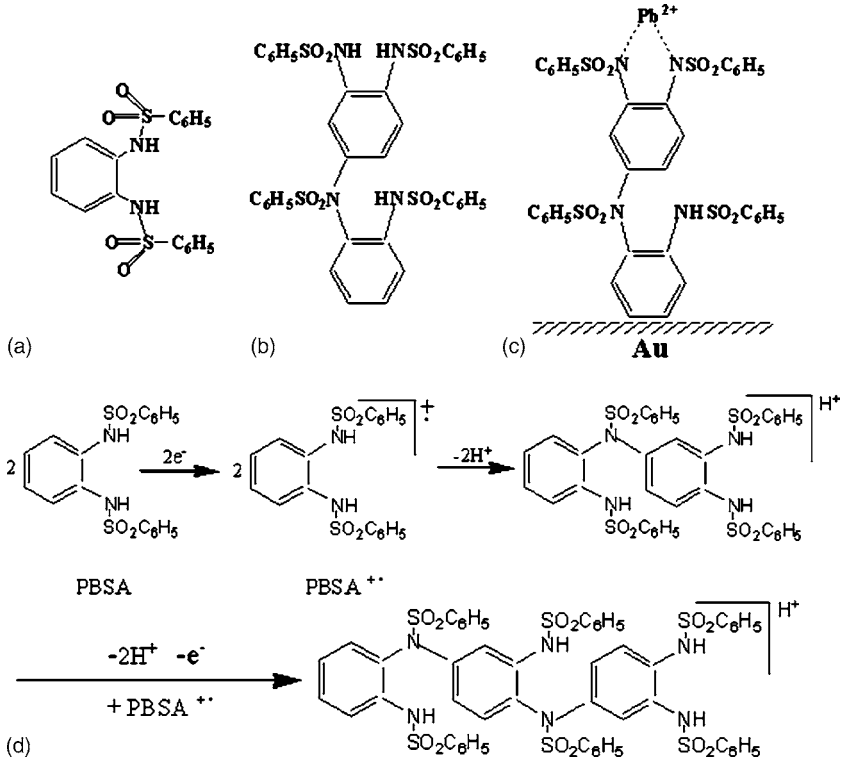

Scheme 1. (a) PBSA, (b) dimer of PBSA, (c) schematic electrodeposited film modified Au electrode with complexed Pb^{2+} and (d) schematic formation process of electrodeposited dimer or trimer of PBSA proposed from MALDI-TOF MS data [18].

confirmed by cyclic voltammetry (CV), electrochemical quartz crystal microbalance (EQCM) and MALDI-TOF MS. According to the result of MS, the main form of electrodeposited PBSA film was the dimer of PBSA (Scheme 1b). Thus, the modified electrode could be labeled as b-modified electrode (BME). The characteristic of BME was investigated for the chemical complexation/stripping of lead. Various experiment parameters that affected the sensitivity of BME, such as monomer amount, complex time and pH were optimized.

2. Experimental section

2.1. Reagents and apparatus

Standard metal ion (Cu^{2+}, Cd^{2+}, Co^{2+}, Ni^{2+}, Zn^{2+}, Cr^{2+} and Pb^{2+}) solutions of 100 mg/L (analytical grade) were purchased from Shanghai Chemical Co. Inc. and diluted step by step (1.0×10^{-4} to 1.0×10^{-9} M) to an adequate concentration immediately prior to use. Triethylamine (analytical grade) was redistilled before use. Other chemicals were of analytical grade and were used without further purification. Distilled water was obtained from Millipore Milli-Q water purification system.

Electrochemical measurements were performed on a CHI-1030 Electrochemical Workstation (Chenhua Co., Shanghai). A conventional three-electrode cell was applied, with saturated calomel electrode (SCE) as the reference electrode, a Pt wire electrode as the counter electrode and the electrodeposited film gold electrode as the working electrode.

EQCM measurements were carried out with QCM oscillators (gold disk area $A = 0.196\,cm^2$, CH Instrument) on a CHI-440 Electrochemical Crystal Microbalance (CH Instrument, Austin, TX, USA).

Mass spectra were recorded with AB 4700 Proteomics Analyzer (MALDI TOF/TOF MS) (reflect mode).

2.2. Synthesis and characterization of PBSA

PBSA was synthesized with good yields (65%) from o-phenylenediamine and benzene sulfochloride [14,15] and characterization with high-resolution ^1H NMR spectra (Bruker 500 MHz spectrometer, the sample was solved in dimethylsulfoxide) and Infrared spectra (Thermo-Nicolet Nexus 470). The data below confirmed the formation of PBSA.

^1H NMR (500 MHz, DMSO): δ 7.00 (4H, four protons of *o*-substituted aryl ring), 7.53–7.72 (10H, 5+5 protons of the two benzenesulphonyl groups), 9.36 (2H, 2 × NH–) [15]; IR (KBr) (cm^{-1}): 3276 (s), 3227 (s), 1598 (m), 1498 (s), 1410 (s), 1341 (s), 1285 (m), 1163 (s) etc. 3276 cm^{-1} (s) and 3227 cm^{-1} (s) belong to N–H; 1341 cm^{-1} (s) and 1163 cm^{-1} (s) belong to S=O [15].

2.3. Electrochemical polymerization

Prior to electropolymerization, a gold disk working electrode was polished on alumina powder (first with 1 μm, then with 0.3 μm, finally with 0.05 μm powder) aqueous suspension, followed by sonicating and rinsing with distilled water. 1 mM PBSA monomer solution was prepared in 0.2 M *p*-toluenesulfonate sodium solution which had 1 mM triethylamine to improve the water-solubility of monomer. The polymerization onto a gold electrode was carried out by cycling the potential

between 0.0 and +1.0 V, the scan rate was 100 mV/s, and the sweep segments was 40. After electropolymerization, the modified electrode was rinsed carefully with distilled water and dried with nitrogen.

2.4. Accumulation and voltammetric procedures

The modified electrode was immersed in 0.1 M ammonia buffer solution (pH 10.0) contained Pb^{2+} (10 mL) and the solution was stirred for 20 min without applying a reduction potential. The accumulation of the metal ions on the modified electrode was carried out chemically to avoid the affect of other interfering species reducible by applying the potential in the preconcentration solution. Although the accumulation time was a little long for electroanalysis, a good detection result could be obtained.

After accumulation of lead ion in the preconcentration solution, modified electrode was washed with 0.1 M ammonia buffer (pH 10.0) carefully to remove ions on modified electrode surface, then was transferred to a blank 10^{-4} M potassium hydroxide solution (pH 10.0) containing 10 mM potassium chloride. Before the stripping currents recorded, Pb (II) complexed on the modified electrode surface was reduced to Pb(0) at −1.2 V for 10 s in the blank solution without stir. Next, a differential pulse stripping voltammetry (DPSV) curve was recorded from −0.9 to 0.6 V in the blank solution with the potential scan rate 100 mV/s, pulse amplitude 50 mV and pulse duration 50 ms. DPSV exhibited the oxidation of Pb(0) to Pb(II) at about −0.31 V at modified electrode surface.

3. Results and discussion

3.1. Characterization of the electrodeposited film

Fig. 1a shows 20 cycles of cyclic voltammograms (CVs) recorded for the polymerization of a 1 mM monomer in a 0.2 M $CH_3C_6H_4SO_2ONa$ solution (polymerization parameters: cyclic scanning from 0.0 to 1.0 V, 100 mV/s). The CV exhibited one oxidation peak at +0.26 V during anodic scan, which is due to the oxidation of monomer to form the film on the electrode, confirmed by the result of EQCM. The current of this peak decreased gradually as the cycle numbers increased.

Fig. 1b shows the frequency and mass changes during electrodeposited process. The frequency decreased and the mass deposited on the electrode increased as time passed, which indicated the growth of the PBSA film on the electrode surface. After 2.4 s corresponding to 0.24 V of CV at the first segment, the mass increased dramatically, which indicated the electrodeposited film was formed on a large scale from about 0.24 V. In the next 19 cycles, the mass deposited on the electrode to every circle decreased gradually. After 20 cycles, the frequency change, Δf was found to be 665.8 Hz. Mass change, Δm, was calculated using the following equation [16]:

$$\Delta m = \Delta f \times 5.608\,(\mathrm{ng/cm^2})/\mathrm{Hz} \times 0.196\,\mathrm{cm^2}$$

where, Δf was the change in frequency, 5.608 (ng/cm^2)/Hz was the sensitivity factor calculated from the physical constant for quartz, and 0.196 cm^2 was the electrode area. The amount of the deposited film formed at the electrode surface after 20 cycles was calculated to be 0.732 μg.

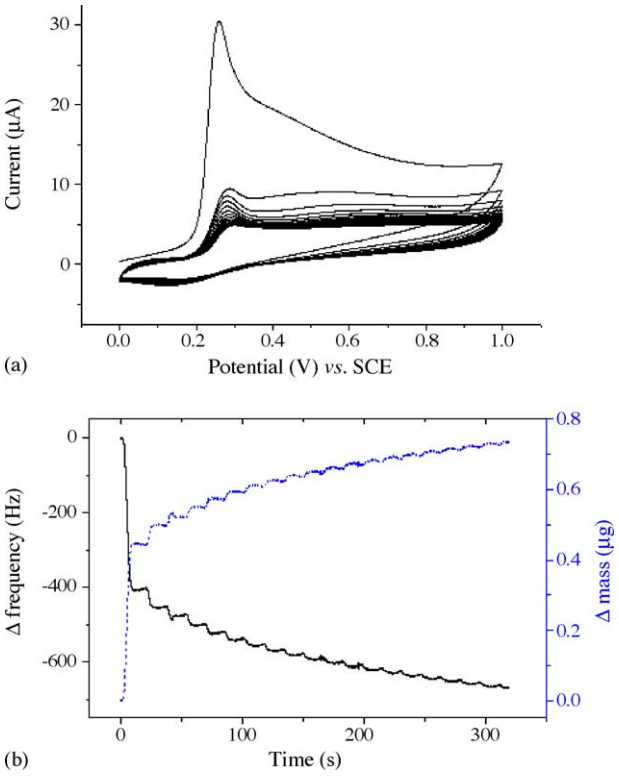

Fig. 1. (a) Consecutive CVs (20 cycles) recorded for the electrodeposited process of a 1 mM PBSA monomer in 1 mM $(C_2H_5)_3N$ and 0.2 M $CH_3C_6H_4SO_2ONa$ solution. (b) Frequency shift (solid line) and mass change (dash line) in electrodeposited process.

Thus, Fig. 1a and b demonstrated that PBSA film was fast formed after the oxidation of the monomer at 0.24 V. By mean of the result of EQCM, the thickness of the formed film was thus estimated as ca. 370 nm assuming that the density of the film was about 1.0 g cm^{-3} [17].

The formation of the electrodeposited film was also authenticated by mass spectrum (Fig. 2). The peak at *m/z* 797 with high

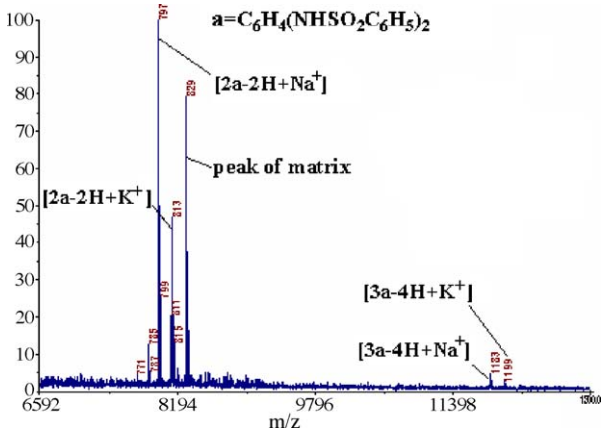

Fig. 2. MALDI-TOF mass spectra of BME in the presence of 8 mg/mL α-LHCA, 50% ACN, 0.1% TFA. *m/z* range 659–1300.

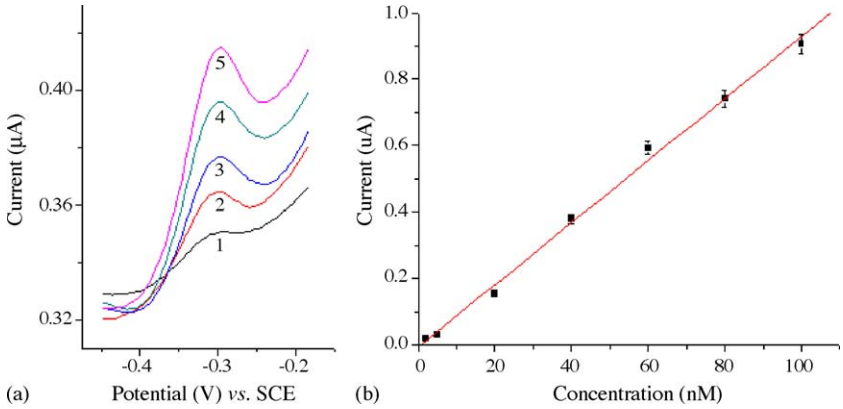

Fig. 3. (a) DPSV curves of BME recorded for (1) blank, (2) 2.0×10^{-9} M, (3) 3.0×10^{-9} M, (4) 4.0×10^{-9} M and (5) 5.0×10^{-9} M Pb^{2+} in KOH solution of pH 10.0 (accumulation 20 min in ammonia buffer of pH 10.0). (b) Calibration plot for Pb^{2+} from 2.0×10^{-9} to 1.0×10^{-7} M (each point stand for the average of three times of measurements).

intensity was assigned to the dimmer of **a**, i.e., **b** in Scheme 1. The peak at *m/z* 1183 with much less intensity was assigned to the trimer of **a**. The peak at *m/z* 829 was assigned to the peak of matrix cluster. The peaks at *m/z* 797 and 813 were assigned to peaks of [2**a**–2H + Na^+] and [2**a**–2H + K^+], respectively, while the peaks at *m/z* 1183 and 1199 were assigned to peaks of [3**a**–4H + Na^+] and [3**a**–4H + K^+] in turn. Above *m/z* 1200, no peaks were observed. It was reasonably concluded that the dominating component of the film was **b**, i.e., the dimer of **a**. The possible polymerization process was proposed in Scheme 1d according to the result of MS and the works of Losito et al. [18].

3.2. Optimization of polymerization and analytical conditions

The concentration of Pb^{2+} was fixed at 4.0×10^{-8} M in the further work to optimize the proposed system and operated as mentioned above. To investigate the influence of electropolymerization CV segments, four DPSV curves were recorded corresponding to 20, 40, 60, 80 segments, respectively. The anodic peak currents were found to be increased from 0.302 to 0.381 μA as the polymerized segments increased from 20 to 40. The further increase of segments above 40 did not give a noticeable rise in the peak currents for the oxidation of Pb^{2+}, which implying that the quantity of active ligand sites on the electrode did not go up greatly. There may be two reasons about it. First, the deposited amount of polymer to later every circle was less and less, which was confirmed by Fig. 1a; second, there was a steric hindrance of film coming from the former dimmer and trimer. Thus, the optimum number of electropolymerized segments for the analysis of lead was determined as 40.

The effect of accumulation time was studied in the range from 4 to 24 min under the previous condition. As the accumulation time increased from 4 to 20 min, the peak currents increased gradually from 0.06 to 0.382 μA, indicating an augment of lead ion combined on the BME. While, the anodic peak currents were found to be almost constant for longer time, suggesting that the active ligand sites were saturated by lead ion. Therefore, the optimum accumulation time for the BME was set at 20 min.

Considering that metal complexation reactions are pH dependent [19], so the effect of pH was also studied in this work. The DPSV anodic peak current gradually increased from 0.257 to 0.379 μA as pH increasing from 7.0 to 10.0, and reached the maximum at pH 10.0, then decreased beyond this value. So, the optimum pH of accumulation solution was fixed to 10.0.

3.3. Calibration plot and stability of the BME

The responses of the BME to series concentration standard solutions were investigated. And to avoid the memory effect of the BME, the electrode was spiked in 0.1 M HNO_3 for a few seconds after each measurement and then potential cycling in the blank solution until no peak was observed. Fig. 3a shows the voltammograms recorded for various concentration of Pb^{2+} ranging from 2.0×10^{-9} to 5.0×10^{-9} M and proves the excellent responses. And linear calibration plot was obtained in the concentration range from 2.0×10^{-9} to 1.0×10^{-7} M for Pb^{2+} and is shown in Fig. 3b. This linear dependence gave the regression equation of i_p (μA) = −0.006 + 0.009 [Pb^{2+}] with correlation coefficient of 0.999. The relative standard deviation at 4.0×10^{-8} M Pb^{2+} was found to be 5.9% ($n = 5$). The detection limit, estimated as three times the standard deviation of the background noise, was found to be 1.0×10^{-9} M.

The stability of the BME was also studied. In the first 20 days, the DPSV anodic peak current almost remained steady. And after 20 days, peak current gradually decreased, which was possibly due to the loss of film from the gold electrode on exposure to distilled water.

3.4. Selectivity of the BME and interference effects

The selectivity of the BME for the determination of lead ion was evaluated in this case. The BME was immersed in accumulation solution of pH 10.0 contained 4.0×10^{-8} M Pb(II), Cu(II), Cd(II), Co(II), Ni(II), Zn(II), Cr(II) for 20 min with stirring. After rinsed carefully, the BME was subjected to DPSV procedure in a blank solution. DPSV exhibited only two anodic peaks at about −0.31 and 0 V versus SCE, corresponding to the oxidation of Pb(0), Cu(0) to Pb(II), Cu(II), respectively.

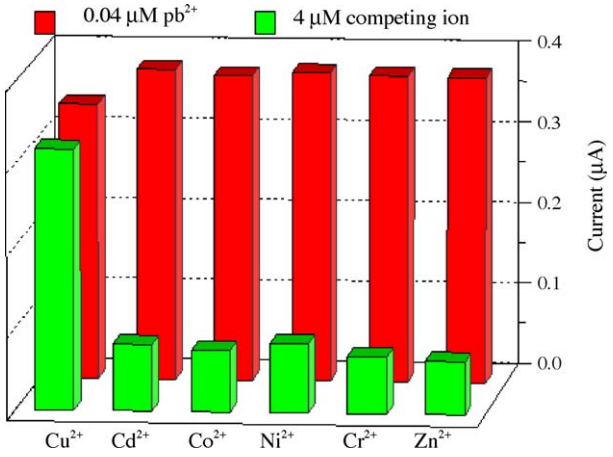

Fig. 4. DPSV peak currents of BME for 4.0×10^{-8} M Pb^{2+}, in the presence of selected metal ions 4.0×10^{-6} M, respectively, in 10^{-4} M KOH solution (pH 10.0).

Other metal ions did not show any response at this case. The DPSV peak current of Cu^{2+} is very small and about 1% of that of Pb^{2+}. To demonstrate precisely the selectivity of BME for Pb^{2+} over other metal ions, further experiment was done: six BMEs were immersed in six solutions of 4.0×10^{-8} M Pb^{2+} containing 4.0×10^{-6} M competing metal ion to accumulate Pb^{2+} and competing metal ion for 20 min, respectively. Fig. 4 shows that the DPSV peak current of Pb^{2+} is about 106% to that of 100-fold concentration Cu^{2+} and the proportions of the DPSV peak current of Pb^{2+} to that of 100-fold other competing metal ions respective were between 450% and 590%. Thus, the complex potential of BME with metal ions increases as follows: $Zn^{2+} < Cr^{2+} < Co^{2+} < Cd^{2+} < Ni^{2+} < Cu^{2+} \ll Pb^{2+}$.

The interference of other metal ions could also be concluded in this case, by comparing the two DPSV peak currents of Pb^{2+}: one obtained in the absence of competing metal ion, another obtained in the presence of that. With the presence of 4.0×10^{-6} M Cu, the recovery of 4.0×10^{-8} M Pb^{2+} was about 89%, indicating that 100-fold concentration Cu^{2+} could compete with Pb^{2+} for complexation with BME. However, with the presence of 100-fold concentration other metal ions respective, the recovery of Pb^{2+} ranged between 98% and 101%, implying 100-fold concentration other competing metal ions did not influence the accumulation of lead.

3.5. Standard reference material and real sample analysis

The availability of the BME was demonstrated by applying it to the determination of Pb^{2+} in standard reference material (GBWE 080398 water sample). The accumulation and stripping step were same as described above after the material was appropriately diluted. The result obtained by BME was 515 ppb Pb^{2+} (three samples, R.S.D. = 3.1%), while the certified value was 500 ± 20 ppb. BME was also applied successfully for the determination of lead ion in pond water, which collected in the campus of Fudan University. The samples were filtered and were adjusted to pH 10.0 with ammonia buffer. The result obtained by BME was 1.2 ppb Pb^{2+} (three samples, R.S.D. = 8.3%) in pond water. After added 12 ppb Pb^{2+} to sample, it was analyzed by BME and ICP-AES (IRIS Intrip, Thermo Elemental) in parallel. The result obtained by BME was 14.2 ppb Pb^{2+} (three samples, R.S.D. = 4.2%), while the result obtained by ICP-AES shows that 13.0 ppb Pb^{2+} (three samples, R.S.D. = 2.7%) was present in the pond water. The recovery of lead using BME was 108 ± 4% and the discrepancy between the two methods was 9.2%.

4. Conclusions

A high selective film for capturing Pb^{2+} was generated via electrochemical polymerization and further was developed to a modified electrode for trace Pb^{2+} probing. The linear range for the determination of lead using the BME was found as 2.0×10^{-9} to 1.0×10^{-7} M. The detection limit was estimated to be 1.0×10^{-9} M as three times the standard deviation of the background noise. The detection limit obtained here is very close to what obtained by the well-known Hg-based DPSV approach [20]. The BME was also applied to determine Pb^{2+} in practical samples and showed a good agreement with the result obtained with ICP-AES. So, a Hg-free method was supplied with compatible sensitivity but much higher selectivity, which holds the potential in quickly screening the Pb^{2+} pollution in environmental samples.

Acknowledgements

This work was supported by NSFC (20335040, 20475012, 20525519), 973 (2001CB510202) and TRAPOYT.

References

[1] I. Narin, M. Soylak, L. Elci, Talanta 52 (2000) 1041.
[2] Z. Horvath, A. Lasztity, I. Varga, Talanta 41 (1994) 1165.
[3] B. Marin, M. Valladon, M. Polve, A. Monaco, Anal. Chim. Acta 342 (1997) 91.
[4] R. MacIver, I. Leray, B. Valeur, Chem. Eur. J. 10 (2004) 4480.
[5] J. Wang, J.M. Lu, C. Yarnitzky, Anal. Chim. Acta 280 (1993) 61.
[6] A.M. Bond, R.W. Knight, O.G. Newman, Anal. Chem. 60 (1988) 2445.
[7] M.B. Gholivand, H.R. Nassab, H. Fazeli, Talanta 65 (2005) 62.
[8] S.M. Hassan, E.M. Elnemma, A.H.K. Mohamed, Talanta 66 (2005) 1034.
[9] J. Pei, M.T. Waeber, J. Buffle, Anal. Chem. 72 (2000) 161.
[10] A. Wanekaya, O.A. Sadik, J. Electroanal. Chem. 537 (2002) 135.
[11] M.A. Rahmam, Y. Shim, Anal. Chem. 75 (2003) 1123.
[12] K. Kavallieratos, J.M. Rosenberg, W.Z. Chen, J. Am. Chem. Soc. 127 (2005) 6514.
[13] K. Kavallieratos, J.M. Rosenberg, J.C. Bryan, Inorg. Chem. 44 (2005) 2573.
[14] L.H. Amundsen, J. Am. Chem. Soc. 59 (1937) 1466.
[15] P.K. Dubey, S.M. Kulkarni, R.V. Kumar, Indian J. Chem., Sec. B: Org. Chem. 41–46 (2002) 1305.
[16] T.Y. Lee, Y.B. Shim, Anal. Chem. 73 (2001) 5629.
[17] H.J. Choi, J.W. Kim, Polymer 40 (1999) 2163.
[18] I. Losito, F. Palmisano, P.G. Zambonin, Anal. Chem. 75 (2003) 4988.
[19] K. Kumar, K.V. Sukumaran, M.F. Tweedle, Anal. Chem. 66 (1994) 295.
[20] M.L. Tercier, N. Parthasarathy, J. Buffle, Electroanalysis 7 (1995) 55.

Available online at www.sciencedirect.com
ScienceDirect
Talanta 70 (2006) 437–443
Talanta
www.elsevier.com/locate/talanta

Flow injection on-line solid phase extractive preconcentration of palladium(II) in dust and rock samples using exfoliated graphite packed microcolumns and determination by flame atomic absorption spectrometry

R.S. Praveen [a], S. Daniel [a], T. Prasada Rao [a,*], S. Sampath [b], K. Sreenivasa Rao [c]

[a] *Trace Analysis Group, Regional Research Laboratory (CSIR), Trivandrum 695 019, India*
[b] *Inorganic and Physical Chemistry, Indian Institute of Science, Bangalore 560 012, India*
[c] *Institute of Scientific and Industrial Research (ISIR), Osaka University, 9-1 Mihogaoka, Ibaraki, Osaka 567-0047, Japan*

Received 18 January 2006; received in revised form 1 March 2006; accepted 1 March 2006
Available online 18 April 2006

Abstract

A sensitive and efficient flow injection preconcentration and matrix-separation technique using exfoliated graphite (EG) as column material was developed prior to flame atomic absorption spectrometry (FAAS) determination of palladium(II) in street/fan blade dust and rock samples. The method is based on the sorption of palladium(II)—diethylammonium dithiocarbamate chelate (which was found to be better among various thioligands) complex on to EG material and its subsequent elution with acidified methanol (0.01 M HCl in methanol). Using 8 ml of the sample, the detection limit achieved was 1.0 $\mu g\,l^{-1}$. The accuracy of the method developed was checked by analysing certified reference material SARM-7. The precision obtained for five successive determination of 100 $\mu g\,l^{-1}$ of palladium(II) was 2.4%. The performance of EG material was compared with allotropes of carbon in terms of pH, chelate concentration, weight of column material, sensitivity enhancement (w.r.t. conventional FAAS), detection limit, calibration range, selectivity and precision. Furthermore, performance of the EG material packed column was compared with commercially available C_{18} bonded silica gel/alumina columns for on-line FIA-FAAS determination of palladium(II).

Keywords: Palladium; Exfoliated graphite; Allotropes of carbon; Flow injection; FAAS; Street/fan blade dust; Rocks

1. Introduction

Noble metals especially, palladium is used as a precious metal in jewellery and as electrical contacts in telephone relays, printed circuits, as grids for electronic tubes and electrodes for high quality spark plugs and as catalyst in many industrial processes and automobiles [1]. However the emission of palladium into the environment is mainly associated with the production, operation and recycling of catalytic converters, production of jewellery and wastes of dental laboratories [2,3]. As the concentration levels of palladium in dust/rock samples lie in the range 0.1–0.5 $\mu g\,g^{-1}$ a preconcentration step is incorporated not only to enrich but also to separate the analyte from matrix [4]. Conventional off-line procedures for the preconcentration and separation, although effective, are usually time consuming and tedious, require large quantities of sample and reagents and are vulnerable to contamination and analyte losses [5]. The drive toward 'Green Chemistry' promotes techniques such as flow injection that are inherently low in reagent consumption, operate in a contaminated environment and produce minimal waste. An increase in awareness of the synergistic impact of chemicals on the environment and the environmental legislation provides an impetus for the increased use of flow injection (FI) based techniques in environmental analysis [5]. The salient features of various on-line FI preconcentration for palladium in conjunction with AAS since 2000 are summarized in Table 1 [6–12]. Lesniewska et al. [12] have preconcentrated palladium(II) from environmental samples by using ammonium pyrrolidine carbodithioate coated fullerene, C_{60} prior to determination by graphite furnace AAS. Barring the above reports

* Corresponding author.
E-mail address: tprasadarao@rediffmail.com (T.P. Rao).

0039-9140/$ – see front matter © 2006 Elsevier B.V. All rights reserved.
doi:10.1016/j.talanta.2006.03.001

Table 1
Summary of the essential features of FIA—flame atomic absorption spectrometric methods developed since 2000 for the determination of palladium(II)

Sl. No.	Chelating agent	Column material	Detection limit ($\mu g\,l^{-1}$)	Linear range ($\mu g\,ml^{-1}$)	Enrichment Factor	Application	Ref.
1.	Isodiphenyl thiourea (IDT)	IDT immobilized silica gel	4.7	0.20	–	Ni alloy, anode slime and $COCl_2$ solution	[6]
2.	2-Mercapto benzothiazole	Amidino thioureido silica gel	17	0.2–4.0	–	Secondary nickel alloy, anode slim, $COCl_2$ electrolytic solution	[7]
3.	Polyamine metal fix—chelamine resin	Polyamine metal fix-chelamine resin	9	–	20	Synthetic geological samples	[8]
4.	Polyamido-amine	Polyamidoamine immobilized silica gel	3.9	0.04–0.4	–	Metallurgical samples	[9]
5.	K^+ 18-Crown-6	–	16	–	29	Spiked blood & roadside dust samples	[10]
6.	Thiourea	Thiourea immobilized silica gel	21	Upto 3.0	15–20	Secondary nickel alloy, anode slime, $COCl_2$ electrolytic solution	[11]
7.	Ammonium pyrrolidine dithiocarbamate	Fullerene C_{60}	0.04	–	–	CRM, SARM-7	[12]
8.	Diethyl ammonium dithio carbamate	EG	1.0	Upto 0.2	80	Roadside dust & domestic fan blade & CRMs	[present method]

no other work has been done so far by using carbon or its allotropes (activated carbon (AC), fullerene, single walled carbon nanotubes (SWCNT) and multiwalled carbon nanotubes (MWCNT)) and exfloliated graphite (EG) as microcolumn packing materials in on-line FI preconcentration technique. Sampath et al. have prepared exfoliated graphite by chemical treatment followed by thermal shock as described in detail elsewhere [13–15]. However this material is employed for electrocatalytic and sensing application only. Now we propose the use of exfoliated graphite as a solid phase extractant material for the first time, by using it as a microcolumn packing material in on-line flow injection analysis, determination being done with FAAS.

2. Experimental

2.1. Reagents, standard solutions and samples

All reagents used were of analytical reagent grade. The thioligands investigated include thioglycollic acid (E-Merck, India), quinoline-8-thiol (Fluka, Germany), 2-thenoyltrifluoroacetone (Aldrich, USA), 1-(2-thiazolylazo)-2-naphthol (Aldrich, USA), 2-thiobarbituric acid (E-Merck, India), aminothiophenol (Fluka, Germany), toluene-3,4-dithiol (Aldrich, USA), 1-(2-thiazolylazo)-2-resorcinol (Aldrich, USA), sodium diethyl dithiocarbamate (E-Merck, Germany), ammonium pyrrolidine diethyldithiocarbamate (Fluka, Switzerland), diethylammonium dithiocarbamate (DDTC) (Aldrich, USA), thiosalicylic acid (E-Merck, Germany) and dithizone (Aldrich, USA). Activated carbon and fullerene were obtained from Aldrich, USA. SWCNT and MWCNT were obtained as a gift sample from Osaka University, Japan. The reagents were dissolved in 0.5 M of ammonia solution. Acidified methanol (pH ~2 with HCl) was used for elution of palladium–DDTC complex sorbed on various carbon sorbents. Prior to pH adjustment, 0.1 mol l^{-1} of ammonium acetate buffer was added.

2.2. Instrumentation

A Perkin-Elmer® Model AAnalyst™ 100 flame atomic absorption spectrometer (Perkin-Elmer Life and Analytical Sciences, Shelton, CT, USA) Deuterium background correction was used. Perkin-Elmer Lumina® palladium hollow cathode lamp was used. The above lamp was operated at 30 mA using 0.2 nm slit width. The wavelength used was 244.8 nm. A standard air-acetylene stainless steel burner and 10 cm path length system were operated at an air flow rate of 4.0 l min^{-1} and an acetylene flow rate of 1.0 l min^{-1}. The burner height was adjusted to about 30 mm from base for optimum sensitivity. The nebulizer uptake rate was adjusted to provide optimum response for conventional sample aspiration.

A Perkin-Elmer FIAS™—400 flow injection system connected to the spectrometer was used for on-line preconcentration of palladium (See Fig. 1 for schematic diagram). The automatic operation of the injection valve and two multichannel peristaltic pumps were programmed using the spectrometer software (Perkin-Elmer AA Winlab™ V 3.0). Tygon® peristaltic tubing was used to pump the sample and reagent solutions. A minimum length of PTFE tubing of 0.3 mm i.d. was used for all connections in order to minimize the dead volume. Home made conically shaped microcolumns were fabricated with internal diameter of 5 mm, capacity of 50 μl and sealed at both ends by Teflon septa having a hole in the middle. Commercailly available, conically shaped microcrocolumns of 50 μl capacity (Perkin-Elmer) C_{18} bonded silica gel and alumina columns were also used for comparison. Time resolved absorbance signals of palladium were displayed on the computer monitor and printed with peak height and integrated absorbance values.

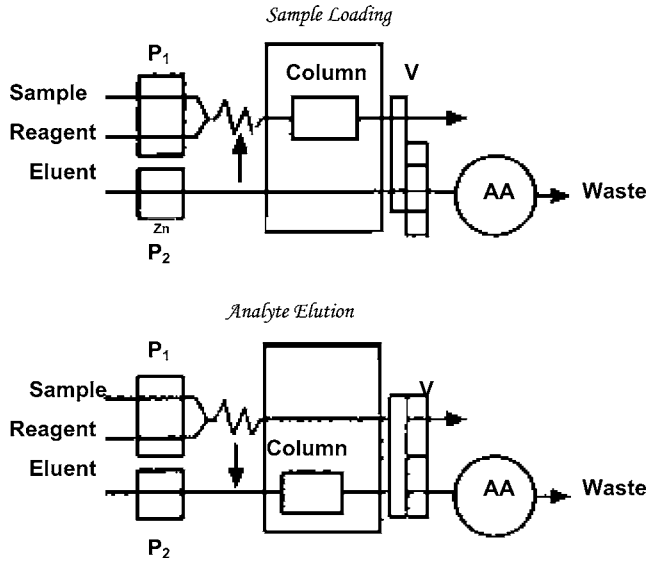

Fig. 1. Flow injection manifold for on-line preconcentration of palladium(II) V: injection valve; P_1 and P_2: peristaltic pumps with flow rates of 11.0 and 4.0 ml min^{-1}, respectively; AA: atomic absorption spectrometer.

2.3. Packing of microcolumns with carbon and its allotropes

EG and carbon and its allotrope materials were packed in between the septa of microcolumns. Acid resistant tubes (tygon) were used to pump the sample and chelating agents through a peristaltic pump (P_1), which get mixed before entering the microcolumn during loading mode (L). In eluent mode (E), acidified methanol was pumped using a peristaltic pump (P_2) through solvent resistant polyethylene tube and connected to the nebulizer of flame atomic absorption spectrometer (FAAS) through a short length tube to avoid dead volume (Fig. 1).

2.4. Analysis procedure

Sample and DDTC (0.001% in 0.5 M of ammonia) solutions (adjusted to pH 7.0 ± 0.2) were pumped at flow rates of 8 and 3 ml min^{-1}, respectively, through EG (1.4 mg) packed microcolumn via peristaltic pump, P_1 for one minute during load mode. The sorbed palladium(II)–DDTC complex was eluted with acidified methanol at a flow rate of 4 ml min^{-1} using peristaltic pump, P_2 and subjected to flame AAS determination. Calibration graphs were constructed by pumping sample solutions in the concentration range 0–200 μg l^{-1} of palladium(II). Unknown sample solutions were similarly subjected to flow-injection (FI) FAAS determination procedure described above and palladium(II) content was established using Perkin Elmer AA Winlab™ V 3.0 software by refering to calibration graph.

2.5. Analysis of certified reference material (SARM-7), street/fan blade dust samples and rock samples

The dust samples were collected from different road sides having dense traffic or from the fan blades fixed in houses located near busy traffic area in various cities of India by taking a representative sample using cone and quarter method. The samples were dried at 105 °C for 2 h, ground, sieved through a sieve of 200 mesh and then homogenized. A 0.1 g specimen of dust or SARM-7 or rock sample was weighed into a 100 ml beaker. In order to decompose it, the sample was heated at 100 °C with 2 × 10 ml of aqua regia and 1 ml of HF. After complete decomposition, the sample solution was cooled and diluted to ~20 ml. The pH of the solution was adjusted to ~3.0 by using NaOH/HCl and finally made up to 25 ml. These solutions were then subjected to FI preconcentrative separation and FAAS quantitation procedure by following the "Analysis procedure" described above. Furthermore, the samples were analysed by standard ICP-MS technique for verifying the results obtained by the FI-FAAS method developed in this paper.

3. Results and discussion

3.1. Optimization of experimental parameters for enrichment of palladium(II) from dilute aqueous solutions

3.1.1. Choice of chelating agent on palladium(II) sorption of EG

Palladium(II) was found to get enriched to an extent of ~7% in the absence of chelating agent using EG as column material, as 100 and 200 μg l^{-1} of palladium(II) gave absorption values of 0.011 and 0.022, respectively. On the other hand, the preconcentration of palladium(II) was systematically carried out by pumping metal ion and different chelating agents through microcolumn packed with EG material. The chelating agents investigated and the absorbance readings obtained for 0, 100 and 200 μg l^{-1} of palladium(II) are shown in Table 2. From the Table 2, it is clear that diethylammonium dithiocarbamate (DDTC) gave the highest absorbance

Table 2
FI-FAAS absorbance signals of 100 and 200 μg l^{-1} of palladium(II) obtained after on-line preconcentration and elution using EG packed microcolumns

Chelating agent	Absorbance		
	Blank	Palladium(II) concentration	
		100 μg l^{-1}	200 μg l^{-1}
None	0.000	0.011	0.020
Thiooxine	0.000	0.001	0.002
Toluene-3,4-dithiol	0.001	0.002	0.003
Thioglycollic acid	0.004	0.004	0.008
Thiobarbituric acid	0.003	0.006	0.008
1-(2-Thiazolylazo)-2-naphthol	0.001	0.006	0.013
Thenoyltrifluoroacetone	0.000	0.018	0.027
Thiosalicylic acid	0.000	0.011	0.017
1-(2-Thiazolylazo) resorcinol	0.001	0.021	0.041
Aminothiophenol	0.000	0.024	0.039
Ammonium pyrollidine dithiocarbamate	0.000	0.039	0.079
Dithizone	0.003	0.058	0.087
Sodium diethyl dithiocarbamate	0.001	0.066	0.145
Diethyl ammonium dithiocarbamate (DDTC)	0.000	0.160	0.320

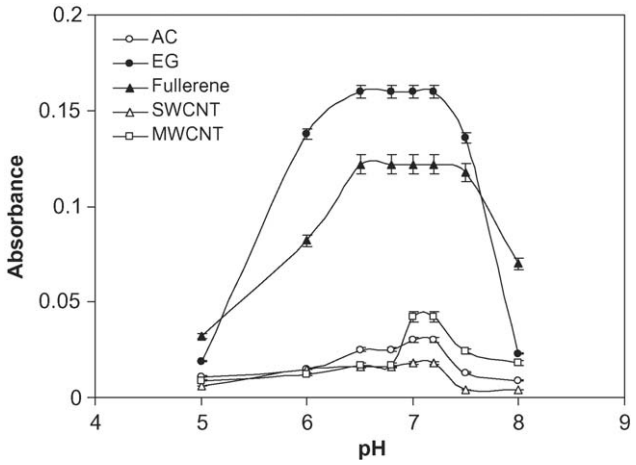

Fig. 2. Effect of pH on the analytical signal of 100 μg l^{-1} (a) and 200 μg l^{-1} (b) of palladium(II) (after subtracting the blank) eluted with acidified methanol after preconcentration on to carbon and its allotropes packed microcolumns in the presence of DDTC as chelating agent.

for palladium(II) compared to several other thioligands tested under identical conditions due to maximum recovery with DDTC.

3.1.2. Palladium(II) uptake with carbon and its allotropes as a function of pH

The pH of 0.002% diethylammonium dithiocarbamate (DDTC) solutions were adjusted in the range 5.0–8.0. Then, 0, 100 and 200 μg l^{-1} of palladium(II) and DDTC solutions were pumped through a microcolumn packed with carbon and its allotropes with a loading/preconcentration time of 1 min. Subsequently, the sorbed palladium(II)–DDTC complexes were eluted with acidified methanol and fed to the nebulizer of FAAS. The blank corrected absorbances obtained for 100 μg l^{-1} of palladium(II) as a function of pH is shown in Fig. 2. For all the materials, the optimum pH range is 6.8–7.2. The decrease in absorbance at pHs less than 6.8, may be due to the fact that DDTC is less stable under acidic conditions and at pHs greater than 7.2 there is competition between the formation of $Pd(OH)_2$ and palladium(II)–DDTC complex. Again, the preconcentration efficiency of palladium(II) in on-line mode with EG and carbon and its allotropes are in the order EG > Fullerene > MWCNT > SWCNT > activated carbon.

Table 3
Effect of DDTC concentration on FIA-FAAS absorbance signal of 100 μg l^{-1} of palladium(II) with carbon and its allotropes

DDTC concentration (%)	Absorbance				
	AC	EG	Fullerene	SWCNT	MWCNT
0.001	0.008	0.161	0.046	0.020	0.024
0.002	0.030	0.162	0.111	0.020	0.050
0.004	0.031	0.163	0.133	0.019	0.049
0.006	0.031	0.162	0.132	0.019	0.049

Therefore, the pH of the chelating agent solution was adjusted to 7.0 ± 0.2 in all subsequent studies.

3.1.3. Palladium(II) uptake with carbon and Its allotropes as a function of chelating agent concentration

The chelating agent (DDTC) concentration is varied from 0.0005% to 0.006% during on-line preconcentration of 0 and 100 μg l^{-1} of palladium(II) using carbon and its allotropes as sorbents with a loading/preconcentration time of 1 min. The blank corrected results obtained are shown in Table 3, from which it is clear that 0.002% DDTC gave higher absorbances for fullerene, MWCNT and SWCNT. On the other hand, 0.001% DDTC is enough for quantitative enrichment of palladium(II) using EG as column material. Again, the preconcentration efficiency of palladium(II) in on-line mode with EG and carbon and its allotropes are in the order EG > Fullerene > MWCNT > SWCNT > activated carbon as in the case of pH studies.

3.1.4. Effect of NH_3 concentration on dissolution of 0.001% DDTC

The ammonia concentration required for dissolving 0.001% DDTC was studied in the range 0.1–1.0 M. The studies indicate that concentration as low as 0.5 M of ammonia is enough for complete dissolution. Furthermore, the enrichment of palladium(II) with various column materials is independent of ammonia concentration in the range studied.

3.1.5. Influence of eluent and acidity of the eluent during elution of previously sorbed palladium(II)–DDTC complex on carbon and its allotropes

Of the various eluents acidified with 0.01 mol l^{-1} in HCl investigated viz. methanol, dimethyl formamide and dimethyl

Table 4
Comparison of FI-FAAS analytical data of microcolumns packed with carbon and its allotropes and C_{18} bonded silicagel/alumina microcolumns

Column material	Weight of column material (mg)	Sensitivity enhancement[a]	Detection limit (μg l^{-1})	R.S.D. at 100 μg l^{-1} (%)	Sample flow rate(ml)	Calibration range (μg l^{-1})
EG	1.4	80.0	1.0	2.4	8.0	0–200
Activated carbon	12.3	15	5.0	4.0	8.0	0–200
Fullerene	40	66.5	1.5	3.0	7.5	0–200
SWCNT	6.5	10	8.0	3.5	7.0	0–200
MWCNT	8	25	3.0	3.2	7.0	0–200
C_{18} bonded silica gel (commercial)	20	80.0	1.0	2.5	8.0	0–200
Alumina (commercial)	20	80.0	1.0	2.5	8.0	0–200

[a] Compared to FAAS signal.

sulphoxide, methanol gave highest FIA-AAS signal with carbon and its allotropes. Furthermore, with the acidity of the eluent (HCl) in the range 0.01–0.1 mol l^{-1}, it was possible to elute previously sorbed palladium(II) quantitatively. Hence, methanol acidified to 0.01 mol l^{-1} in HCl was chosen in subsequent studies.

3.2. Optimization of FI analysis flow conditions

High sample loading flow rates are important for efficient preconcentration and high sample throughput. In general, FI sample flow rates are limited by the back pressure produced by the column and/or sorption efficiency. The maximum sample flow rates without degradation in sorption efficiency are shown in Table 4. Higher flow rate through the peristaltic pump with the type of column used in this work will degrade the precision. The chelating agent flow rate (3 ml min^{-1}) should not be too low in order to ensure good mixing of chelating agent and sample solution. The sample flow rates shown in Table 4 were employed in subsequent studies as they are the maximum flow rates that can be employed without any back pressure.

An elution flow rate of 4.0 ml min^{-1} provided optimum sensitivity and elution peaks with minimum tailing. No provision was made to compensate for the lower flow rate delivered by the FI system; however, the transfer capillary to the nebulizer (PTFE, 0.3 mm i.d.) restricted the uptake rate to values close to flow rates provided by the FI system. Operating the nebulizer at this flow rate does not lower the sensitivity relative to a decrease in eluent flow rate due to the potential improvement in the nebulizer efficiency under starved conditions [16,17]. The lower eluent flow rate in the FI mode in comparison to the conventional free uptake rate of the nebulizer is also beneficial for droplet diameter distribution which results in smaller droplets and is therefore less prone to vaporization interferences [16].

3.2.1. Performance of the on-line preconcentration system

The characteristic data for the on-line preconcentration system with EG and carbon and its allotropes are shown in Table 4. The efficiency of SPE was investigated by analyzing for palladium(II) content of the column eluents. From the results obtained by repeated preconcentration, a retention efficiency of >99% was calculated for palladium(II) using EG. The SPE elution sequence is highly reproducible, giving an overall precision of 2.4% (R.S.D.), for five successive determinations of 100 μg l^{-1} palladium(II) (Table 4). With a loading time of 1 min, AC, EG, fullerene, MWCNT and SWCNT gave enrichment factors of 17-, 80-, 66.5-, 25- and 10-fold, respectively. A linear relationship up to 2 min was observed for all column materials (See Fig. 3). Linear calibration graphs were obtained for palladium(II) concentrations in the range 0–200 μg l^{-1} for all column materials. The detection limits corresponding to three times the standard deviation of the blank were found to be 5.0, 1.0, 1.5, 3.0 and 8.0 μg l^{-1} for palladium(II) with AC, EG, fullerene, MWCNT and SWCNT, respectively. The linear equations with regression

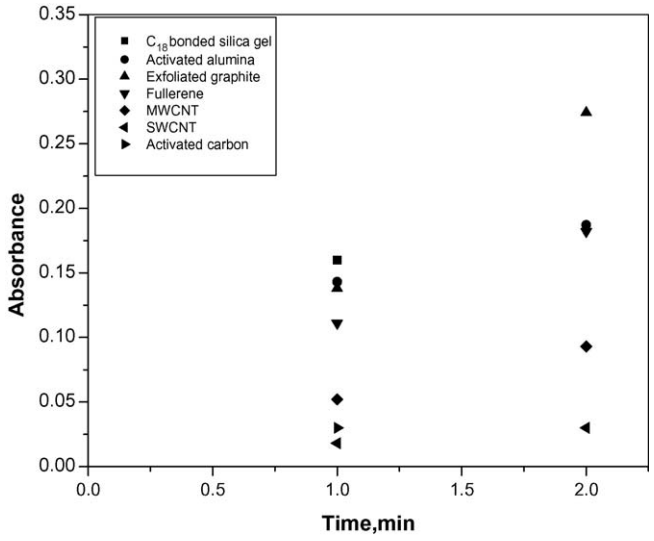

Fig. 3. Effect of loading time on analytical signal of 100 μg l^{-1} of palladium(II) (after subtracting the blank) eluted with acidified methanol after loading/preconcentration time of 1 and 2 min on to carbon and its allotropes packed columns in the presence of DDTC as chelating agent.

were as follows:

$$A_{AC} = 0.38C - 0.003, \qquad A_{EG} = 1.63C - 0.002,$$

$$A_{fullerene} = 1.32C + 0.003, \qquad A_{SWNT} = 0.19C - 0.003,$$

$$A_{MWNT} = 0.49C - 0.001$$

The correlation coefficients are 0.9918, 0.9999, 0.9993, 0.9877 and 0.9907, where A is the absorbance and C is the concentration of palladium(II) in mg l^{-1}. All statistical calculations were based on the average of triplicate readings for each standard solution in the given range. Furthermore, a 1 min loading/preconcentration time allows a sample frequency of 30 h^{-1}. Higher sensitivities can be obtained by modifying the method, i.e. using longer preconcentration period of 2 min at the expense of lower sample throughput.

Table 4 compares the various parameters related to sensitivity, precision and weight of column materials for EG, carbon and other allotropes of carbon, C_{18} bonded silica gel and alumina.

Table 5
Concentrations of catalytic converter constituents found both before and after passing through EG packed microcolumn ($n = 3$)

Ion	Concentrations in synthetic samples before passing through EG microcolumn (μg l^{-1})	Concentration found in eluate solution after on-line separation (μg l^{-1})
Fe(III)	85	0.30
Mg(II)	35	0.02
Ca(II)	35	0.07
Cu(II)	0.006	BDL[a]
Zn(II)	0.012	BDL[a]
Pb(II)	40	1.3
Ni(II)	0.07	BDL[a]

[a] BDL = below detection limit.

Table 6
Concentration of elements determined in street dust/domestic fan blade/rock samples by FAAS ($\mu g\,g^{-1}$)[a]

Ion	Street dust								Fan blade dust					
	Chennai		Tirupati		Delhi		Trivandrum		Chennai		Ernakulam		Rock	
	a	*b*	*a*	*b*	*a*	*b*	*a*	*b*	*a*	*b*	*a*	*b*	*a*	*b*
Fe(III)	5955 ± 120	150 + 30	9155 ± 180	33.3 ± 0.6	1956 ± 40	69.3 ± 1.4	2311 ± 45	25.3 ± 0.5	2222 ± 45	33.3 ± 0.6	4444 ± 90	86.7 ± 1.8	65.8 ± 1.3	100 ± 2.0
Zn(II)	2955 ± 60	10.6 ± 0.1	425 ± 8.5	6.8 ± 0.01	178.4 ± 3.5	7.3 ± 0.01	2730 ± 55	20.3 ± 0.4	2149 ± 42	21.7 ± 0.4	178.4 ± 3.6	10.7 ± 0.2	171.6 ± 3.4	7.0 ± 0.01
Ca(II)	6553 ± 125	0.5 ± 0.01	3906 ± 80	0.9 ± 0.01	4125 ± 85	0.9 ± 0.01	6563 ± 130	0.5 ± 0.01	7656 ± 150	0.9 ± 0.01	5313 ± 105	1.4 ± 0.02	187.5 ± 3.8	0.5 ± 0.01
Mg(II)	75.9 ± 1.5	0.1 ± 0.02	176.6 ± 3.5	1.1 ± 0.01	178.4 ± 3.6	1.1 ± 0.01	179.9 ± 3.6	1.8 ± 0.02	183.3 ± 3.6	1.6 ± 0.02	123.4 ± 2.4	0.2 ± 0.01	173.7 ± 3.4	1.8 ± 0.02
Cu(II)	27.9 ± 0.6	0.7 ± 0.04	172.1 ± 3.5	3.5 ± 0.01	55.8 ± 1.1	2.1 ± 0.01	158.1 ± 3.2	4.2 ± 0.06	232.6 ± 4.6	4.3 ± 0.08	51.2 ± 1.0	1.4 ± 0.02	27.9 ± 0.5	0.7 ± 0.01
Pb(II)	139.5 ± 2.6	14.0 ± 0.2	46.5 ± 0.9	20.9 ± 0.4	93.0 ± 1.8	20.9 ± 0.40	46.5 ± 0.9	14.0 ± 0.30	186.1 ± 3.8	14.0 ± 0.30	139.5 ± 2.8	13.9 ± 0.3	325.6 ± 6.5	20.9 ± 0.40

a: before passing through EG packed microcolumn; b: after passing through EG packed microlumn in presence of DDTC.
[a] Average of three determinations.

It is clearly seen from this Table that EG is a better choice as column material compared to other materials investigated during on-line FIA-FAAS determination of palladium(II).

3.3. Effect of neutral electrolytes and co-existing metal ions

The tolerance of maximum concentration of metal ions that can co-exist with palladium(II) and form complexes with DDTC on determination of 100 $\mu g\,l^{-1}$ palladium(II) were systematically studied with EG and carbon and its allotropes using FI-FAAS procedure described above. A deviation from the standard absorbance value greater than 3% was taken as interference. These studies indicate that 100-fold amounts of Cu(II), Zn(II), Mn(II), Cr(III), Fe(III) and Al(III) do not interfere with the determination of palladium(II) using EG, fullerene and SWCNT. Similar studies with other precious metals viz. Pt, Ru, Rh and Au present at 5-fold the concentration of palladium(II) do not have any deleterious effect on FIA-AAS signal of 100 $\mu g\,l^{-1}$ of palladium(II).These findings are quite comparable to commercially available C_{18} bonded silica gel and alumina microcolumns. On the other hand, in case of MWCNT, 10-fold amounts only can be tolerated. The constituents of the catalytic converter sample prepared synthetically was determined by AAS both before and after subjecting to online FIA-AAS separation/preconcentration procedure. The results obtained are shown in Table 5, from which it is clear that on-line FIA-AAS method developed in this work separates the catalytic converter matrix fairly well.

The concentrations of Fe(III), Zn(II), Ca(II), Mg(II), Cu(II) and Pb(II) present in four street dust samples, two fan blade dust samples and one rock sample solutions were determined before passing through EG packed microcolumn and in the eluent collected after on-line preconcentration/separation procedure and are compiled in Table 6. The results show that the concentration of matrix ions are very low in eluent owing to the lack of complexation and sorption on EG packed microcolumn during loading mode by DDTC, indicating that palladium(II) could be selectively preconcentrated prior to determination by FIA-FAAS.

3.4. Analysis of standard reference materials

The accuracy of the developed procedure was tested by analyzing standard reference material SARM-7 supplied by South African Bureau of Standards (SABS), South Africa. The sample was brought in to solution by following the procedure described in Section 2.5 and analysed by following the procedure described in Section 2.4.The results obtained were given in Table 7, from which it is clear that the amount of palladium present in reference material by the developed method is comparable to the value given by SABS, South Africa. Hence the developed method can be readily employed for routine monitoring of palladium(II) in real samples.

3.5. Analysis of street/fan blade dust and rock samples

Dust and rock samples collected from busy traffic areas of selected cities in India were mineralized and palladium(II)

Table 7
Analysis of SARM-7[a] certified reference material (supplied by SABS[b], South Africa)

Sample	Palladium found ($\mu g\,g^{-1}$), present method[a]		Certified value	Recovery (%), present method
	Added	Found		
SARM-7	0	1.59 ± 0.03	$1.53 + 0.032$	–
	0.8	2.39 ± 0.04		100
	1.61	3.20 ± 0.04		100.7

[a] SARM-7—South African Reference material.
[b] SABS—South African Bureau of Standards.

Table 8
Analysis of street/fan blade dust and rock samples

Sample	Palladium(II) found, $\mu g\,g^{-1}$		
	Present method[a]		ICPMS
	Found	95% Confidence interval	
Street dust			
Chennai	$0.48 + 0.05$	0.447–0.513	$0.50 + 0.01$
Tirupati	0.45 ± 0.04	0.424–0.476	0.44 ± 0.01
Delhi	0.25 ± 0.03	0.230–0.270	0.20 ± 0.01
Trivandrum	<0.3		<0.01
Fan blade dust			
Chennai	0.40 ± 0.04	0.374–0.426	0.42 ± 0.01
Ernakulam	0.21 ± 0.03	0.19–0.23	0.20 ± 0.01
Rock			
Trivandrum	0.11 ± 0.02	0.097–0.123	0.12 ± 0.01

[a] Average of three determinations.

content was determined using the General Procedure described above. The results obtained are shown in Table 8, which also shows the analytical values obtained by standard ICP-MS method. The satisfactory agreement of the results obtained by the developed FIA-FAAS method using EG column material with ICP-MS values indicate that FAAS in conjunction with on-line preconcentration method can be readily employed for routine monitoring of palladium(II) in dust and rock samples.

4. Conclusions

Comparison has been done between exfoliated graphite, activated carbon and different allotropes of carbon viz., activated carbon, fullerene, SWCNT and MWCNT as column materials during on-line flow injection preconcentrative separation prior to flame AAS determination. Among these, EG material is found to be better than AC and allotropes of carbon in terms of sensitivity enhancement, precision and detection limits. Furthermore, quite significantly 1.4 mg of EG material provides comparative tolerance limits for various metal ion species that usually co-exist in dust/rock samples compared to 10–40 mg of other materials. The sensitivity enhancement over conventional flame AAS for exfoliated graphite is comparable to commercially available C_{18} bonded silica gel or alumina columns which requires 20 mg of the respective materials to obtain analogous tolerance limits for palladium over other inorganic species. Of the various thioligands tested during the FI on–line preconcentration, diethyl ammonium dithiocarbamate was found to be best by offering a detection limit of $1.0\,\mu g\,l^{-1}$ in case of EG column material. The accuracy of the developed method was tested successfully by analyzing CRM of palladium viz. SARM-7 The palladium(II) content in street/fan blade dust and rock samples established by the developed method agree well with standard ICP–MS values. Studies are in progress to exfoliate MWCNT or SWCNT and in functionalize the allotropes of carbon and use them as column materials.

Acknowledgement

Authors, R.S. Praveen and Sobhi Daniel thank the Council of Scientific and Industrial Research (CSIR), New Delhi for awarding the Senior Research Fellowships.

References

[1] I.M. Kolthoff, P.J. Elwing, Treatise on Analytical Chemistry. Part II, 8, Interscience Publishers, New York, 1963, 384.
[2] K. Ravindra, L. Bencs, R. Van Grieken, Sci. Total Environ. 318 (2004) 1.
[3] M. Balcerzak, Noble metals, analytical chemistry, in: R.A. Meyers (Ed.), Encyclopedia of Analytical Chemistry, John-Wiley & Sons, Chichester, 2000, p. 8958.
[4] R.R. Barefoot, Trends Anal. Chem. 18 (1999) 702.
[5] P. Liu, Z. Su, X. Wu, Q. Pu, J. Anal. Atomic Spectrom. 17 (2002) 125.
[6] W. Xu, C. Richard, P.J. Sandford, A. Worsfold, G. Carlton, Hanrahan, Crit. Rev. Anal. Chem. 35 (2005) 237.
[7] P. Liu, Q. Pu, Z. Su, Analyst 125 (2000) 147.
[8] S. Zhang, Q. Pu, P. Liu, Q. Sun, Z. Su, Anal. Chim. Acta. 452 (2002) 223.
[9] M. Iglesias, E. Antico, V. Salvado, Talanta 59 (2003) 651.
[10] X. Wu, P. Liu, Q.S. Pu, Q. Sun, Z. Su, Talanta 62 (2004) 918.
[11] B. Dimitrova, K. Benkhedda, E. Ivanova, F. Adams, J. Anal. Atomic Spectrom. 19 (2004) 1394.
[12] B.A. Lesniewska, I. Godlewska, B.G. Zylkiewicz, Spectrochim. Acta, Part B 60 (2005) 377.
[13] P. Ramesh, S. Sampath, Anal. Chem. 72 (2000) 3369.
[14] P. Ramesh, S. Sampath, Chem. Commun. (1999) 2221.
[15] P. Ramesh, G.S. Suresh, S. Sampath, J. Electroanal. Chem. 561 (2004) 173.
[16] M. Sperling, S. Xu, B. Welz, Anal. Chem. 64 (1992) 3101.
[17] K.A. Tony, S. Karthikeyan, B. Vijayalekshmy, T. Prasada Rao, C.S.P. Iyer, Analyst 124 (1999) 191.

Available online at www.sciencedirect.com
ScienceDirect
Talanta 70 (2006) 444–448
Talanta
www.elsevier.com/locate/talanta

A simple and sensitive resonance scattering spectral method for determination of hydroxyl radical in Fenton system using rhodamine S and its application to screening the antioxidant

Ai-Hui Liang [a], Su-Mei Zhou [b], Zhi-Liang Jiang [a,b,*]

[a] *Department of Material and Chemical Engineering, Guilin University of Technology, Guilin 541004, China*
[b] *Department of Resource and Environmental Science, Guangxi Normal University, Guilin 541004, China*

Received 13 January 2006; received in revised form 5 March 2006; accepted 5 March 2006
Available online 18 April 2006

Abstract

Based on resonance scattering (RS) effect of rhodamine dye association particles, a new resonance scattering method for the determination of hydroxyl free radical from Fenton reaction was developed. In HCl–NaAc buffer solution, the $^{\bullet}OH$ of Fenton reaction oxidized the excess I^- to I_3^-. The I_3^- combined, respectively, with rhodamine B (RhB), butyl rhodamine B (b-RhB), rhodamine 6G (RhG) and rhodamine S (RhS) to form association particles that exhibit stronger resonance scattering effect at 420 nm and 610 nm. However, the RS peak at about 610 nm was interfered with its synchronous fluorescence peak at 580 nm for RhB, 580 nm for b-RhB, 560 nm for RhG and 560 nm for RhS, respectively. The concentration of H_2O_2 in the range of 0.648–21.6 μmol/L, 0.423–13.0 μmol/L, 0.216–13.0 μmol/L and 0.092–13.0 μmol/L was linear to its resonance scattering intensity at 420 nm. Its detection limit was 0.15 μmol/L, 0.10 μmol/L, 0.092 μmol/L and 0.044 μmol/L, H_2O_2, respectively. This RhS RS method was applied to selection of the antioxidant, with satisfactory results.

Keywords: Hydroxyl radicals; Rhodamine S; Association particles; Resonance scattering effect; Screening the antioxidant

1. Introduction

Free radical, such as hydroxyl radical $^{\bullet}OH$, super-oxide anion $^{\bullet}O_2^-$ and $RO^{\bullet}$, is one of important factor that cause the aging of human body and some diseases including cancer [1]. Among the free radicals, the hydroxyl radical has strong activity and is one of strong oxidant with good solubility in water. Fenton reaction between Fe^{2+} and H_2O_2 was considered to be one simple reaction to produce $^{\bullet}OH$, and it was also an important reaction system to treat waste water in environmental science. Recently, tea has been suggested to prevent some chronic diseases, such as cancer, and cardiovascular diseases, and its benefits are partly ascribed to its antioxidant components that scavenge hydroxyl radical, and the measurement of the scavenging percentage of the hydroxyl radical is helpful to identify tea quality. Therefore, it is important to develop a simple, rapid and sensitive method for the determination of hydroxyl radical in life science, environmental science and food science [2].

At present, several methods have been developed for the measurement of hydroxyl radical such as high-performance liquid chromatography (HPLC) [3–6], the electron spin resonance (ESR)-spin trapping method [7,8], chemiluminescence method [9–11], fluorescence method [12,13], spectrophotometer [14], capillary zone electrophoresis method [15] and so on. HPLC method can be determined hydroxyl radical indirectly, and has good selectivity, but its sensitivity was not very well. ESR was used to determine and investigate unpaired electron of free radicals and transition metal and its compound, but the cost of the method is too high. Chemiluminescence method, compared with ESR method and HPLC, was simple, fast and did not need expensive equipment. Lau et al. [16] measured indirectly hydroxyl radicals by the chemiluminescence method. This method employed the reaction between $^{\bullet}OH$ and methyl cyanide to product acheomycin(tetracycline). The fluorescence method has good sensitivity [12,13], it can be determined H_2O_2 in the range 0.10–2.0 μmol/L. However, the analytical reagent

* Corresponding author.
E-mail address: zljiang@mailbox.gxnu.edu.cn (Z.-L. Jiang).

0039-9140/$ – see front matter © 2006 Elsevier B.V. All rights reserved.
doi:10.1016/j.talanta.2006.03.002

was difficult to obtain. The spectrophotometric method for determination of •OH was also simple. However, the method has low sensitivity. For instant, Zhang et al. [17] described a spectrophotometric method for the determination of •OH by using methyl as a colored indicator of hydroxyl radical production. Quantitative determinations of its hydroxylated products can be performed using colorimetry.

Resonance scattering (RS) method has many advantages, including good selectivity, high sensitivity, simplicity and convenience, it has been used for determination of trace inorganic ions such as Ag, Cr, Se and some organic substances such as proteins and nucleic acid [18–24]. Recent studies indicated that not only some inorganic nanoparticles such as Au, Ag, Se and TiO_2 exhibit RS effect, but also some association complex particles also have RS effect and hypochromic effect, which have been applied to the determination of trace amount substances [24,25]. Rhodamine dyes (Rh), that is a type of stable and important analytical reagents, have been used in spectrophotometry, fluorescence, single sweep polarography and resonance scattering spectral analysis [25–28]. However, a RS method for the determination of hydroxyl radical does not seem to have been reported to date, according to the RS effect of rhodamine dye association particles. In this present work, we proposed a novel and sensitive and rapid RS method for determination of •OH using RhS. It was applied to investigate the tea and some antioxidants scavenging ability of hydroxyl radical, with satisfactory results.

2. Experimental

2.1. Apparatus and reagents

The Rayleigh scattering and synchronous fluorescence (SF) spectra were recorded with a model RF-540 spectrofluorophotometer (Shimadzu, Japan), using the synchronous scanning technique that the excited wavelength λ_{ex} was equal to the emission wavelength λ_{em} ($\lambda_{ex} = \lambda_{em}$). A model of TU-1901 dual beams spectrophotometer (Puxi Com., China) were used for recording the absorption spectra. A model NaNo-ZS90 nanosized and zeta potential analyzer (Malvem, GB) was used to record the diameter distribution of particles.

A 4.32×10^{-2} mol/L H_2O_2 standard solution was prepared by diluting 1.1 mL of 30.0% (v/v) H_2O_2 to 250 mL with double water, the concentration was standardized by $KMnO_4$ solution. A HCl–NaAc buffer solution and 0.020 mol/L KI were prepared. A 2.00×10^{-4} mol/L Fe^{2+} solution was prepared daily by diluting a 2.00×10^{-3} mol/L Fe^{2+} stocking solution that was prepared by $(NH_4)_2Fe(SO_4)_2{\cdot}6H_2O$. The rhodamine B (RhB), rhodamine S (RhS), rhodamine 6G (RhG) and butyl rhodamine B (b-RhB) concentrations were also prepared for 1.50×10^{-4} mol/L. A 2.50×10^{-5} mol/L sulfourea, 2.00×10^{-5} mol/L ascorbic acid, 40.0 μg/mL quercetin and 1.00×10^{-5} mol/L L-tryptophan were prepared.

Tea samples were prepared as follows, weighing 0.0603 g jasming tea, 0.120 g bitter tea, 0.0400 g firebrand tea of Yunnan and 0.150 g honeysuckle tea, respectively. And then place in boiling distilled water to boil for 30 min, then filtrated and placed to 100 mL solution, a 5.0 mL of the solution was taken out to dilute to 100 mL.

All of the reagents were of analytical grade and all of the water used throughout was double distilled.

2.2. Procedure

A certain volume of the HCl–NaAc buffer solution, 0.020 mol/L KI solution, certain volume of Fe(II) solution and certain volume of H_2O_2 standard solution were piped in a 10-mL graduated tube, then placed 1.50×10^{-4} mol/L RhB (or b-RhB, RhS, RhG) and mixed. The mixed solution was diluted to the mark of 5 mL with water and mixed thoroughly. The resonance scattering spectra can be obtained by using the synchronous scanning technique in a model RF-540 spectrofluorophotometer. The RS intensity (I) of each system was measured at 420 nm against a reagent blank (I_b), the value of ΔI ($=I - I_b$) was calculated. For the four systems, the resonance scattering intensities were all measured at 420 nm.

2.3. Measurement of the scavenging percentage of hydroxyl radical

In general, the antioxidant ability can be used the scavenging percentage (P) of hydroxyl radical to present it. Similar to the definition of the scavenging percentage of spectral method [11,29], this scavenging percentage (P) was defined as $P(\%) = [(I - I_s)/(I - I_b)] \times 100\%$, where I_s presents the RS intensity for the system containing H_2O_2 and scavenger, I the RS intensity for the system containing H_2O_2 and I_b represents the RS intensity in the absence of H_2O_2 and scavengers.

3. Results and discussion

3.1. Principle

There is very weak RS intensity at 420 nm for the Fe^{2+}–I^-–Rh, Fe^{3+}–I^-–Rh and I^-–Rh–H_2O_2 systems, owing to the three systems hardly producing hydroxyl radical to form association particles. Results showed that H_2O_2 did not oxidize rhodamine dyes and lead to fluorescence quenching. When H_2O_2 was added to the Fe^{2+}–I^-–Rh system, the system was produce hydroxyl radicals from Fenton reaction between H_2O_2 and Fe^{2+} [12], which reacted with excessive I^- and form I_3^-, the I_3^- reaction with Rh^+ to form the association particles $(Rh–I_3)_n$. Fig. 1 indicates the diameter distribution of $(RhS–I_3)_n$ particles. The means diameter is 650 nm. The $(Rh–I_3)_n$ particles exhibit RS effect at 420 nm. The RS intensity increased linearly with H_2O_2 concentration. According to reference [12] and our results, the main reactions is,

$$Fe^{2+} + H_2O_2 \rightarrow Fe^{3+} + {}^{\bullet}OH + OH^- \quad (1)$$

$${}^{\bullet}OH + I^- \rightarrow OH^- + I_2 \quad (2)$$

$$I_2 + I^- \rightarrow I_3^- \quad (3)$$

$$nRh^+ + nI_3^- \; (Rh–I_3)_n \quad (4)$$

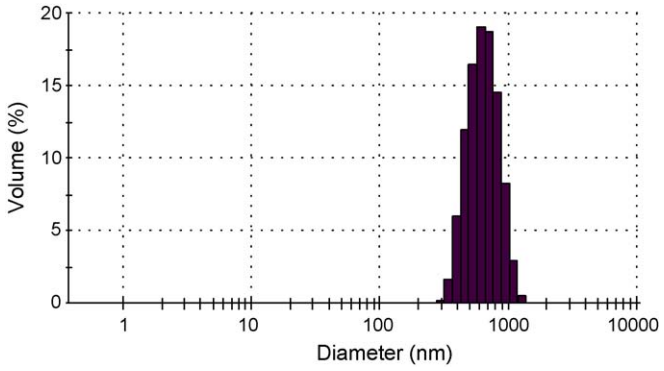

Fig. 1. The laser scattering graph of RhS particle system at pH 4.95, 3.00×10^{-3} mol/L KI, 4.00×10^{-5} mol/L Fe^{2+}, 3.00×10^{-5} mol/L RhS and 8.64 μmol/L H_2O_2.

Based on above reaction and RS effect of $(Rh–I_3)_n$, a new and sensitive resonance scattering method was proposed to measure hydroxyl radical.

3.2. Resonance scattering spectrum

The synchronous fluorescence spectrum indicated that RhB, RhS, RhG and b-RhB has a SF peak at 580 nm, 560 nm, 560 nm and 580 nm, respectively. The Rayleigh scattering of the RhS, and RhS–I^- and RhS–I^-–Fe^{2+} systems is very weak. After H_2O_2 is added into the RhS–I^-–Fe^{2+} system, the system (see Fig. 2c and d) exhibits three Rayleigh scattering peaks at 320 nm, 420 nm and 610 nm, respectively. Due to the influence of the scattering of the association particles, the SF peak at 560 nm becomes stronger. The RhG system is similar to the RhS system. However, the RhB and b-RhB system exhibits four Rayleigh scattering peaks at 320 nm, 420 nm, 530 nm and 610 nm, respectively. We have known that the strongest emission of the apparatus was at 470 nm [24], and the absorption of the free molecule in the particle system causes the scattering signal to decrease [25]. In Fig. 2c, the three SS peaks all became stronger, and the three peaks would be not appeared if the particles do not exist, which demonstrated that the three Rayleigh scattering peaks are RS peaks of $(RhS–I_3)_n$ association particles. Because there is strong RS effect at 420 nm, so, the Rayleigh scattering peak at 470 nm did not be observed in the systems [25]. The Rayleigh scattering signals at lower than 250 nm were very weak. It may be owing to the incidence light intensity of the light source being weak [25]. Although the RS peak at 610 nm was stronger, the synchronous fluorescence peak greatly affected it. Therefore, the RS intensity at 420 nm was measured for the four systems.

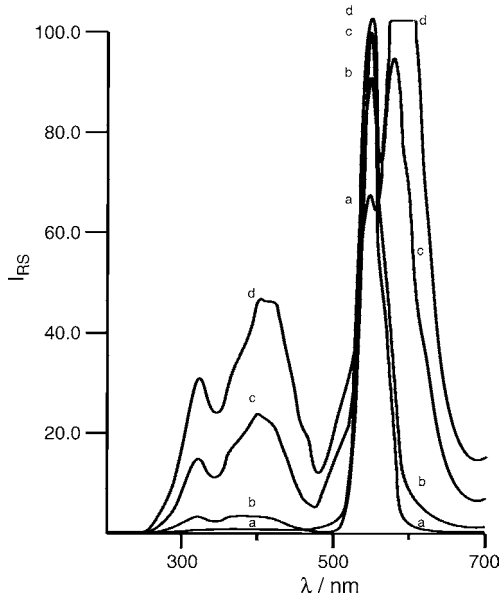

Fig. 2. RS spectra of RhS system at (a) pH 4.95, 3.00×10^{-3} mol/L KI, 4.00×10^{-5} mol/L Fe^{2+} and 3.00×10^{-5} mol/L RhS; (b) as in (a) with 1.08 μmol/L H_2O_2; (c) as in (a) with 4.32 μmol/L H_2O_2; (d) as in (a) with 10.8 μmol/L H_2O_2 (OR = 5, S = 2).

3.3. Effect of pH on the RS intensity

The effect of pH value on the ΔI was studied in the range of pH 0.65–5.20. Results showed that the RhB system was little affected by the pH. So a pH 4.19 was chosen for the RhB system. The other three systems reached their maximum ΔI value when the pH was in the range of 4.58–5.20. Therefore, a pH of 4.95 was all selected for the three systems. The influence of buffer solution volume on the ΔI was also tested, when the buffer volume was 0.80 mL for RhB and RhS, and 1.0 mL for RhG and b-RhB, the four systems all reached their maximum ΔI.

3.4. Effect of KI concentration

The effect of KI concentration on the ΔI showed that the ΔI increased with KI concentration from 0 mol/L to 2.00×10^{-3} mol/L. When concentration of KI reached 2.00×10^{-3} mol/L, the ΔI of the four systems increased slowly. Therefore, a 3.20×10^{-3} mol/L, 3.00×10^{-3} mol/L, 3.20×10^{-3} mol/L and 3.00×10^{-3} mol/L KI were chosen for the RhB, RhS, RhG and b-RhB systems, respectively.

3.5. Effect of Fe^{2+} concentration

Fe^{2+} is a good catalyst for the reaction. The ΔI was small in the absence of Fe^{2+}, and the ΔI increased with Fe^{2+} concentration in a range from 0 mol/L to 2.00×10^{-5} mol/L. When Fe^{2+} concentration was more than 2.00×10^{-5} mol/L, the ΔI values of the four Rh systems increased slowly. Hence, a 3.20×10^{-5} mol/L, 3.20×10^{-5} mol/L, 4.00×10^{-5} mol/L and 4.00×10^{-5} mol/L Fe^{2+} were selected for the RhB, RhG, RhS and b-RhB systems, respectively.

3.6. Effect of Rh concentration

The results of the Rh concentration on ΔI showed that when the Rh concentration was about 2.50×10^{-5} mol/L, the ΔI values of the four systems reached their maximum. Continue increasing Rh concentration, the ΔI values kept constant. However, when the concentrations of b-RhB and RhG were more than 3.00×10^{-5} mol/L, the ΔI values decreased

Table 1
Analytical feature of the Rh RS methods

System	Regress equation, C (μmol/L)	Linear range (μmol/L)	Correlation coefficient (r)	Detection limit (μmol/L)	R.S.D. (%)
RhB	$\Delta I = 2.52C_{H_2O_2} - 2.20$	0.648–21.6	0.9974	0.15	2.2
b-RhB	$\Delta I = 4.04C_{H_2O_2} - 0.32$	0.423–13.0	0.9984	0.10	2.0
RhG	$\Delta I = 4.35C_{H_2O_2} + 1.80$	0.216–13.0	0.9985	0.092	1.2
RhS	$\Delta I = 4.46C_{H_2O_2} - 1.40$	0.092–13.0	0.9990	0.044	2.4

Table 2
Effects of coexistence substances (CS)

Coexistent substance	Tolerance limit, $[m_{CS}]/[m_{H_2O_2}]$	Relative error (%)	Coexistent substance	Tolerance limit, $[m_S]/[m_{H_2O_2}]$	Relative error (%)
K^+	2290	+3.6	Pb^{2+}	35	+4.5
Ca^{2+}	1170	+4.8	F^-	90	+3.2
Mg^{2+}	100	−4.2	NO_3^-	30	+4.1
Zn^{2+}	80	+2.7	PO_4^{3-}	230	−4.6
Ni^{2+}	20	+4.4	ClO_3^-	900	−4.4
Co^{2+}	15	+4.6	Bitartrate	120	−4.6
Al^{3+}	50	+4.8	Br^-	160	+5.0
Mn^{2+}	110	+2.8	L-Arginine	20	+2.7
Ba^{2+}	1340	+4.1	$CO(NH_2)_2$	1700	+5.0
Hg^{2+}	3	+4.2	Cu^{2+}	6[a]	+5.0

[a] Containing 0.0010 mol/L EDTA.

weakly. Increasing the concentration of Rh further, in both systems precipitations appeared easily. Hence, a 3.00×10^{-5} mol/L RhB, 3.00×10^{-5} mol/L RhS, 2.80×10^{-5} mol/L RhG and 2.80×10^{-5} mol/L b-RhB were chosen for use.

3.7. Effect of reaction temperature and time

The effect of reaction temperature (20–40 °C) on the ΔI was considered. Results indicated that the ΔI changed weakly with the temperature. The operation was done at room temperature. The effect of time on ΔI for the four systems showed that the RhS system was more stable than others three systems and the reaction was fastest, almost the reaction finished within 5 min, meanwhile, kept almost constant 30 min. The ΔI of b-RhB and RhG systems kept constant within 20 min. The RhB system was also stable, but the system needed 15 min to reach the maximum ΔI. So, a reaction time of 15 min was chosen for use.

3.8. Relationship between hydroxyl radical concentration and ΔI

From the mechanism of reaction, the hydroxyl radical concentration was proportional to H_2O_2 concentration. So, we used H_2O_2 concentration to instead $^{\bullet}OH$ concentration to discuss. Results showed that the RS intensity increased with the H_2O_2 concentration. From Table 1, we known that the detection limit of RhS system was lower than the RhB, RhG and b-RhB systems, and the linear range was broader and the stability was good. Therefore, the RhS system was selected to determinate hydroxyl radical concentration. A 8.64 μmol/L H_2O_2 concentration was chosen to study the effect of scavenging, owing to it located in the middle of the linear range.

3.9. Effects of coexistence substances

In order to examine the effect of foreign ions on the determination of hydroxyl radical, the influence of a number of ions were investigated according to the procedure at a concentration of 0.294 μg/mL H_2O_2. The tolerance limit was defined as the content of substance that gives a relative error not more than ±5.0%. The results are summarized in Table 2. It can be seen that most of the ions normally present in water did not interfered with the determination of hydroxyl radical, which demonstrated the method has good selectivity.

3.10. Studying of the scavenging ability of some antioxidant on the hydroxyl radical

Sulfourea, ascorbic acid, L-tryptophan and quercetin are commonly used scavengers of hydroxyl radical. The four scavenging reagents were also used to detect the validity of this RS method. Fig. 3 indicated that the four scavenging reagents were good scavenging reagents and their scavenging activities of decreases in order, L-tryptophan > ascorbic acid > sulfourea > quercetin. Among of them, the scavenging percentage of the ascorbic acid and L-tryptophan were over 90%. These indicated that this RS method can be used to screen antioxidant.

3.11. Studying of the scavenging ability of some tea on the hydroxyl radical

According to the procedure, the scavenging percentage of some tea samples on the hydroxyl radical was investigated. Fig. 4 showed that the scavenging activity of jasming tea and honeysuckle was better, the two tea samples' scavenging percentage was over 90.0%.

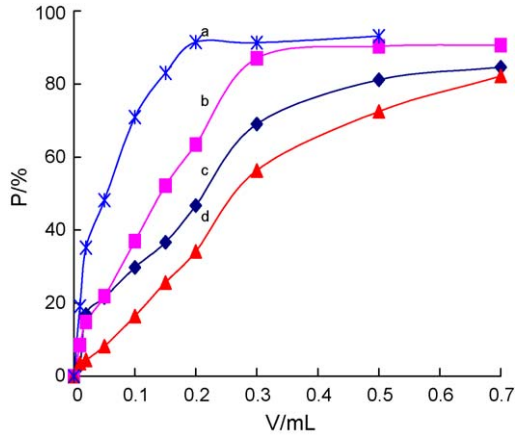

Fig. 3. Hydroxyl radical scavenged by L-tryptophan (a), ascorbic acid (b), sulfourea (c) and quercetin (d) at pH 4.95, 3.00×10^{-3} mol/L KI, 4.00×10^{-5} mol/L Fe^{2+}, 3.00×10^{-5} mol/L RhS and 6.48 μmol/L H_2O_2 (OR = 5, S = 2).

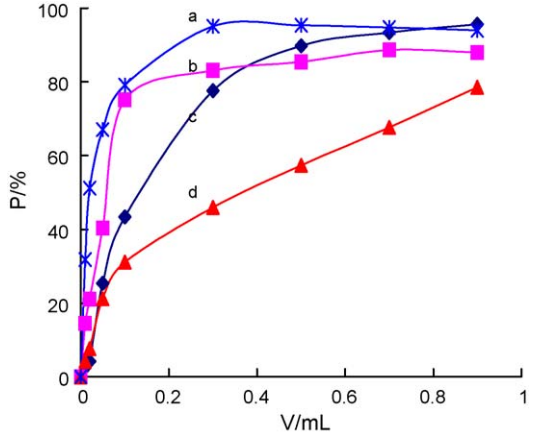

Fig. 4. Hydroxyl radical scavenged by honeysuckle (a), bitter (b), jasming (c) and firebrand teas (d) at pH 4.95, 3.00×10^{-3} mol/L KI, 4.00×10^{-5} mol/L Fe^{2+}, 3.00×10^{-5} mol/L RhS and 6.48 μmol/L H_2O_2 (OR = 5, S = 2).

4. Conclusions

A new and simple and sensitive resonance scattering spectral method for the determination of hydroxyl free radical was proposed, using Fenton reaction and KI–rhodamine S. The RS intensity at 420 nm was linear to H_2O_2 concentration in the range of 0.092–13.0 μmol/L. This RhS RS method was applied to screening the antioxidant of tea, with satisfactory results.

Acknowledgements

The investigation was supported by a grant from the Nature Science Foundation of Guangxi (No. 0575042) and Science Research Foundation of Guilin University of Technology is gratefully acknowledged.

References

[1] J.L. Mark, Science 235 (1987) 529.
[2] X. Yang, L.R. Kong, L.S. Wang, Environ. Chem. 22 (2003) 490.
[3] F.C. Cheng, J.F. Jen, T.H. Tsai, J. Chromatogr. B 781 (2002) 481.
[4] V.D.B. Viviane, V. Inge, D.B. René, F. Compernolle, C. Vinckier, J. Chromatogr. A 896 (2000) 135.
[5] B.B. Li, N.V. Blough, P.L. Gutierrez, Free Radic. Biol. Med. 29 (2000) 548.
[6] L. Diez, M.H.L.N. Livertoux, A.A. Stark, J. Chromatogr. B: Biomed. Sci. Appl. 763 (2001) 185.
[7] Z.R. Ma, B.L. Zhao, Z.B. Yuan, Anal. Chim. Acta 389 (1999) 213.
[8] K. Motohisa, K. Masahiko, I. Fukiko, Toxicol. Lett. 81 (1995) 73.
[9] S. Hanaoka, J.M. Lin, M. Yamada, Anal. Chim. Acta 426 (2001) 57.
[10] Y. Yoshiki, K. Okubo, M. Onuma, K. Igarashi, Phytochemistry 39 (1995) 225.
[11] Y.P. Zhao, W.L. Yu, D.P. Wang, X.F. Liang, T.N. Hu, Food Chem. 80 (2003) 115.
[12] X.F. Yang, X.Q. Guo, Anal. Chim. Acta 434 (2001) 169.
[13] B. Tang, L. Zhang, Y. Geng, Talanta 65 (2005) 769.
[14] K. Jana, S. Matija, P. Boris, Anal. Chim. Acta 431 (2001) 313.
[15] Q.J. Wang, D. Ding, N.N. Zhu, H. Li, P.G. He, Y.Z. Fang, J. Chromatogr. A 1016 (2003) 123.
[16] C. Lau, J.Z. Lu, M. Kai, Anal. Chim. Acta 503 (2004) 235.
[17] N.D. Zhang, W. Zheng, Y.Z. Peng, Chin. J. Anal. Chem. 31 (2003) 552.
[18] H. Zhong, J.J. Xu, H.Y. Chen, Talanta 67 (2005) 749.
[19] C.Z. Huang, Y.F. Li, Anal. Chim. Acta 500 (2003) 105.
[20] R.P. Jia, H.L. Zhai, Y. Shen, X.G. Chen, Z.D. Hu, Talanta 64 (2004) 355.
[21] L.Y. Wang, L. Wang, L. Dong, Y.L. Hu, T.T. Xia, H.Q. Chen, L. Li, C.Q. Zhu, Talanta 62 (2004) 237.
[22] X.F. Long, Q. Miao, S.P. Bi, D.S. Li, C.H. Zhang, H. Zhao, Talanta 64 (2004) 366.
[23] S.P. Liu, H.Q. Luo, Z.F. Liu, N.B. Li, Anal. Chem. 76 (2001) 3907.
[24] C.Y. Kang, D.L. Xi, S.M. Zhou, Z.L. Jiang, Talanta 68 (2006) 974.
[25] Z.L. Jiang, Nanoparticles and Resonance Scattering Spectroscopy, Guangxi Normal University Press, Guilin, 2003.
[26] A.H. Liang, Z.L. Jiang, B.M. Zhang, Q.Y. Liu, J. Lan, X. Lu, Anal. Chim. Acta 530 (2005) 131.
[27] Z.L. Jiang, F. Li, H. Liang, Acta Chim. Sin. 58 (2000) 1059.
[28] Z.L. Jiang, B.M. Zhang, A.H. Liang, Talanta 66 (2005) 783.
[29] L.M. Liu, G.W. Song, L.H. Liu, G.R. Fang, Chin. J. Anal. Chem. 31 (2003) 723.

Available online at www.sciencedirect.com
ScienceDirect
Talanta 70 (2006) 449–454
Talanta
www.elsevier.com/locate/talanta

Electro-oxidation of glucose at self-assembled monolayers incorporated by copper particles

Jia Zhao [a,b], Fang Wang [a], Jingjing Yu [a], Shengshui Hu [a,b,*]

[a] College of Chemistry and Molecular Sciences, Wuhan University, Wuhan 430072, China
[b] State Key Laboratory of Transducer Technology, Chinese Academy of Sciences, Beijing 100080, China

Received 13 January 2006; received in revised form 3 March 2006; accepted 5 March 2006
Available online 18 April 2006

Abstract

A novel copper incorporated self-assembled monolayers (SAMs) modified gold electrode (Cu/SAMs) for determination of glucose was developed by electrodepositing Cu particles on the SAMs of hexanethiol. The scanning electron microscopic (SEM) images showed that copper formed orbicular particles of nanosizes on the SAMs, which was much different from the fractal-like particles of copper formed at gold electrode. The Cu/SAMs film electrode exhibited high sensitivity to glucose oxidation and depressed responses towards some interferents of glucose in blood like uric acid and ascorbic acid. Under optimal working conditions, the oxidation current of glucose was proportional to the concentration of glucose in the range from 3.0 μM to 10 mM by amperometry with a low detection limit of 0.7 μM glucose (S/N = 3). This electrode was successfully applied to the determination of glucose in rat blood and the results were satisfactory.

Keywords: Self-assembled monolayers; Copper; Incorporate; Glucose

1. Introduction

In the past several decades, great attention has been paid to the electrochemical oxidation of glucose, in order to develop devices such as implantable bio-fuel cells for pacemakers or artificial hearts [1] and glucose sensors for an artificial pancreas [2]. In this field amperometric enzyme electrodes have been proved to be a powerful approach for the determination of glucose [3–6]. In place of dioxygen-coupled glucose assay methods—in which there are definitely some disadvantages suffered from both the variation in oxygen tension and the stoichiometric limitation of oxygen—there appears to the development of mediator-based 'second-generation' glucose biosensors. Recent interests have focused on the direct electrical communication between the GOD redox center and the electrode surface and fabricated so-called third generation glucose sensors. The other approach of using non-enzyme electrodes has received relatively less attention. There were reports of using metal [7–9], metal oxide [10], nanoparticles [11], ferricyanide [12] and polymer membrane [13,14] chemically modified electrodes (CME). Such electrodes are not as specific as glucose oxidase electrodes. However, their life times, temperature resistance, tolerance to oxygen disturbances are much better.

Recent research has demonstrated that coating electrode surfaces with organic films is an attractive approach for enhancing the power and scope of electroanalytical techniques. The studies of modified electrodes over the past two decades have resulted in a development, which might conceivably lead to the replacement of other electrode materials in practical electroanalysis [15–17]. Metal particles dispersed into an organic film have been recognized as effective electrocatalysts with good activity for various electrode reactions. There have been many studies on the incorporation of metal particles within organic films [18–20], such as polyaniline or polypyrrole. These studies showed that metal-organic electrodes are easy to prepare, stable for long time periods with good detection limits and wide linear range responses. Considerable efforts to date have focused on polymeric film encouraged us to find new organic materials.

Alkanethiols and dialkyl disulfides which can spontaneously form highly-ordered stable self-assembled monolayers (SAMs) on various metals have attracted substantial interest in analytical chemistry [21,22]. These SAM systems have been utilized

* Corresponding author. Tel.: +86 27 8721 8904; fax: +86 27 6786 4573.
E-mail address: sshu@whu.edu.cn (S. Hu).

0039-9140/$ – see front matter © 2006 Elsevier B.V. All rights reserved.
doi:10.1016/j.talanta.2006.03.004

for studying fundamental surface chemistry and interfacial processes. The existence of small electroactive pinholes in the otherwise blocking SAMs behave as an array of extremely small microelectrode, and it can be used to facilitate the determination of large heterogeneous electron-transfer rate constant [23–26]. However, there is no report about incorporation metallic particles within SAMs for electrochemical application. By controlling the electrodeposition time, copper microparticles are expected to develop predominately at the pinhole sites. As a result, mechanically stable self-assembled monolayers embedded by copper particles were fabricated. This electrode, designated as Cu/SAMs, exhibited catalysis toward the electro-oxidation of glucose in alkaline media and was successfully applied to the determination of glucose in rat blood.

2. Experimental

2.1. Chemicals

1-Hexanthiol (>98.0%) from Shanghai Reagent was dissolved in absolution ethanol to form a 1/1000 (v/v) solution for the self-assembly process. D-Glucose (purchased from Shanghai Reagent, China) was dissolved in water to prepare 0.5 M stock solution. All other chemicals were of analytical grade quality and used without further purification. 0.1 M NaOH electrolyte was prepared with doubly distilled water.

2.2. Apparatus and procedure

All voltammetric determinations were carried out with on a CHI 660A electrochemical analyzer (CH instrument company, Shanghai, China). All the experiments were carried out in a conventional electrochemical cell. The electrode system contained a copper deposition 1-hexanthiol SAM-modified polycrystalline gold disk working electrode (2 mm in diameter), a platinum wire counter electrode and a potassium chloride (KCl) saturated calomel reference electrode (SCE). Scanning electron microscopy (SEM) was done with a Hitachi X-650 microscope.

Electrochemical impedance spectroscopy (EIS) was carried out with the EG&G model 283 electrochemical workstation and an EG&G model 5210 lock-in amplifier (Princeton Applied Research) powered by Powersuit software. The equivalent circuit was deduced using ZsimpWin software produced by Echem Software. The impedance measurements were performed in the presence of 10 mM glucose as a redox probe. The supporting electrolyte was 0.1 M KCl. The EIS experiments were done at the formal potential (+0.70 V) at an amplitude of 10.0 mV (rms) with a wide frequency range of 100 kHz–0.1 Hz.

Infrared reflection–absorption spectra (IRRAS) of SAMs and Cu/SAMs immobilized on gold electrodes surfaces were obtained using a Magna-IR 550 spectrometer (Nicolet Instrument Corporation, USA). A spectrum of the bare gold surface was subtracted as background. Each spectrum resulted from the accumulation of 200 scans.

2.3. Preparation of the modified electrode

The gold electrode was firstly polished on a slush of 0.05 μm alumina (Al_2O_3). After sonicating in water for 5 min, the electrodes were treated with cyclic scanning in the potential range of −0.2 to 1.5 V at the scan rate of 100 mV s^{-1} in 1 M H_2SO_4 until stable signals were obtained. The area of the reduction peak at each bare gold electrode was compared to ensure that all the SAM-modified gold electrodes had the same effective area. Then the gold electrode was sonicated for 5 min in water and ethanol, respectively.

The monolayer films were typically formed by immediately immersing the pre-treated gold electrode into 1/1000 ethanol solution of 1-hexanthiol for 2 h, then rinsed with ethanol followed by distilled water to remove any excess amount of solvent. The copper–SAMs composites were prepared by depositing copper from 50 mM $CuSO_4$ with 0.1 M H_2SO_4 at an applied potential of −0.6 V for 20 s.

2.4. Preparation of plasma samples

The rat blood samples (obtained from College of Life Science, Wuhan University) were prepared according to the following procedure: 0.5 ml blood sample was diluted to 1 ml with doubly distilled water. Then 0.2 ml $CHCl_3$ was added and the mixture was sonicated for 5 min. After centrifuged at 4000 rpm for 10 min, the supernatant was collected and used within 2 h.

3. Results and discussion

3.1. Electrochemical characterization of the Cu/SAMs film electrode in alkaline solutions

Fig. 1 shows cyclic voltammograms of three different electrodes in 0.1 M NaOH over potential range between −1.0 and 0.8 V. Two pairs of redox peaks are observed at a bare gold electrode (Fig. 1c), the oxidation potentials are −0.1 and 0.4 V with the reduction potential at −0.2 and 0.1 V. Very similar

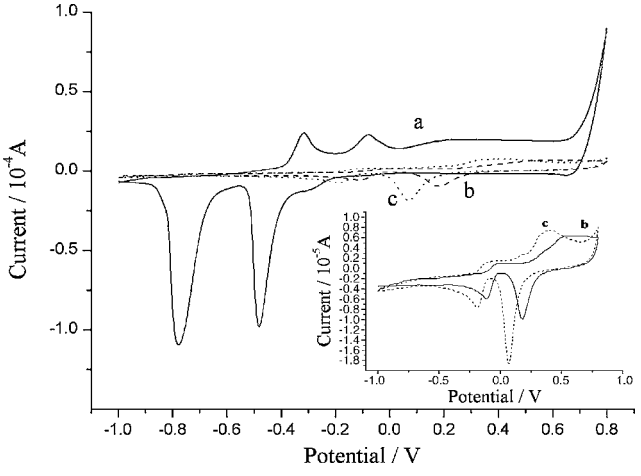

Fig. 1. Cyclic voltammograms of Cu/SAMs (a), SAMs modified electrode (b) and bare gold electrode (c) in 0.1 M NaOH. Scan rate: 50 mV s^{-1}.

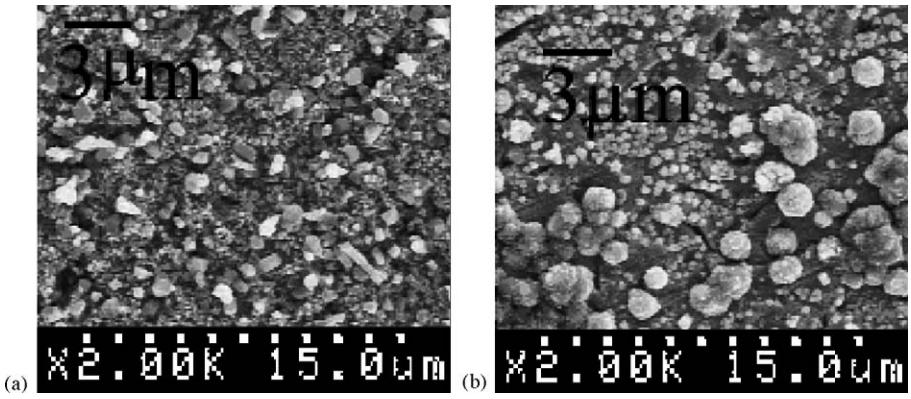

Fig. 2. SEM micrographs: Cu/Au film (a); Cu/SAMs film (b).

responses are observed at self-assembled monolayers modified gold electrode (Fig. 1b). But, the peak potentials observed at the SAMs are shifted positively, accompanied by the remarkable peak current decreased. Due to the block mass transfer by the hydrophobic layer of the SAM gold oxidation was inhibited. Even without suggestions concerning a detailed structure of the defects in the alkylthiol layer, the suppression of the peak current meant that the total area of uncovered gold is about 11% of the electrode area. After electrodeposition of copper at the SAMs, well-defined peaks are observed in the positive and negative scans (Fig. 1a). Anodic peaks at −0.35 and −0.1 V are attributed to the conversion of Cu to Cu(I), Cu(II), respectively. The large wave at about 0.2 V can be associated with the formation of soluble species (such as $HCuO_2^-$) during the oxidation of Cu. Interestingly, the Cu(II)/Cu(III) wave occurred at 0.50 V decreased rapidly on continued scanning due apparently to a very rapid film formation and passivation process, as described by Prabhu [27]. Examination of the reverse scan revealed, initially a small cathodic peak at 0.6 V, which has been attributed to the reduction of Cu(III) to Cu(II) [26]. The symmetric cathodic peaks at −0.46 and −0.78 V are ascribed to the transition of Cu(II) to Cu(I) and Cu(I) to Cu. The *I–E* characteristics of this voltammogram are in good agreement with those found in the literatures [13,27–31].

Infrared reflection–absorption spectrum (IRRAS) is a surface infrared technique for the study of configuration changes on surfaces. The bands in the IRRAS spectrum of the self-assembled monolayers incorporated by copper particles have shapes that are similar to those of the films of SAMs alone. These similarities suggested that Cu/SAMs retained near-native structure.

3.2. SEM images of Cu/SAMs and Cu/Au electrodes

Fig. 2 shows the SEM images of bare gold electrode modified with copper (Cu/Au) (a) and the Cu/SAMs (b), both achieved by reduction in 50 mM $CuSO_4$ for 20 s at −0.6 V. As can be seen, there are obvious morphological changes of copper sediment with and without self-assembled monolayers. Copper deposited in bulk area at bare gold substrate and corresponded to fractal-like structure. In contrast, near-perfect orbicular copper nanocrystals spread around the SAMs. In the Volmer-Weber growth process, the growth mechanism is instantaneous due to the large difference in the surface energies of the substrate and the deposited materials [32]. Copper–SAMs system in this work is supposed to bear an analogy with metal-polymer system which surface energy difference is much higher [33]. As Eliadis et al. [34] reported numerous monolayer defects provided the nucleation sites of deposited Cu. Following instantaneous growth mode the incoming copper atoms were expected to occupy all of the available nucleation sites on the substrate simultaneously at the very early instant of the start of the deposition process. Once all of the nucleation defects were occupied, further prolonging in the deposition time would only increase the size of the nanocrystals. Since the pinholes in the SAMs were surrounded by the hydrophobic tails of alkane, the growth of the deposited Cu should encompass the isolated Cu nucleation and form orbicular particles as showed in Fig. 2b.

3.3. Electro-oxidation of glucose at the Cu/SAMs film electrode

In the presence of 10 mM glucose, two anodic waves are observed at the SAMs electrode in cyclic potential scan between 0.0 and 0.8 V at a scan rate of 0.05 mV s^{-1} (Fig. 3c). By intercalation into the residual pinholes in the otherwise blocking

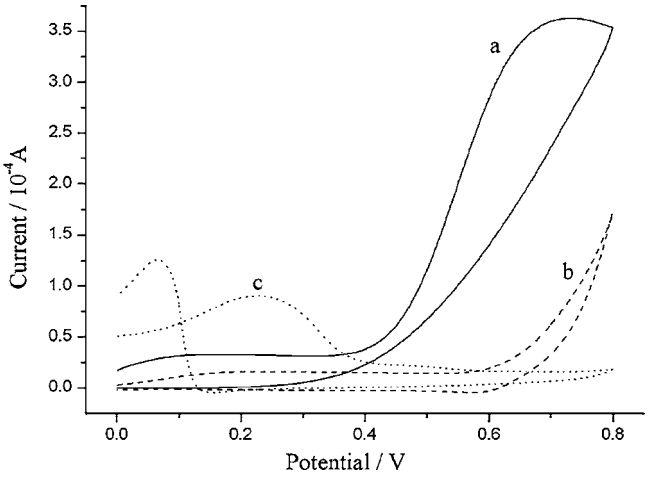

Fig. 3. Cyclic voltammograms of Cu/SAMs (a, b), SAMs modified electrode (c) in 0.1 M NaOH with (a, c) and without (b) 10 mM glucose.

monolayers, carbohydrate could undergo redox behavior with the gold substrate. Analogous redox waves were observed for other electroactive species at a SAM modified electrode with some defects [23,24]. When the copper–SAMs composite electrode is used, the electrocatalytical waves observed on SAMs electrode are disappeared, while a broad anodic peak centered at 0.65 V appears (Fig. 3a). No conspicuous peak can be seen at the corresponding potential when Cu/SAM is placed in blank solution (Fig. 3b). It is inferable that at a given applied potential copper loaded in the defect of the hydrophobic layers. Thus the glucose could not incorporate into the SAMs as without the Cu deposition and had no choice but turn to oxidize at the copper particles. Although the exact mechanism for the oxidation of carbohydrates at copper remain dispute, it is demonstrated herein that copper (II) and copper (III) surface species involved in the oxidation of glucose, as these species are present in this potential range [30].

EIS can give information on the impedance changes of the electrode surface during the modification process. A typical EIS plot contains a semicircle in the high-frequency region and a declining line with a slope of 1 in the low-frequency region. The semicircle in the EIS plot corresponds to a dynamic process, while the declining line stands for a diffusion process. From the composition of the EIS plot, useful information involved in the interface structure and important parameters about the dynamic process can be conveniently deduced. Fig. 4 shows the results of EIS for the bare gold electrode and two modified electrodes in the presence of 10 mM glucose. The Nyquist plots exhibit a semicircle in the whole frequency range and the Warburg impedance resulting from mass transfer disappeared. This suggested that the electrochemical reaction of glucose under this condition was mostly controlled by the dynamic processes. To obtain charge transfer (R_{ct}), the Randles circuit (inset of Fig. 4) was chosen to fit the obtained impedance data. Fig. 4a shows the impedance spectrum of the bare gold electrode and the R_{ct} for the glucose is 52.1 kΩ. The R_{ct} for the SAMs modified electrode shown in Fig. 4b is increased to 58 kΩ. When copper–SAMs composite is used to modify the electrode (Fig. 4c), R_{ct} sharply decreased to 3.24 kΩ. These results indicated that the deposition copper on the SAMs formed different kinetic barriers and could decrease the charge transfer resistance. As a result, the electrochemical response of glucose is greatly improved (consistent with the CV results in Fig. 3).

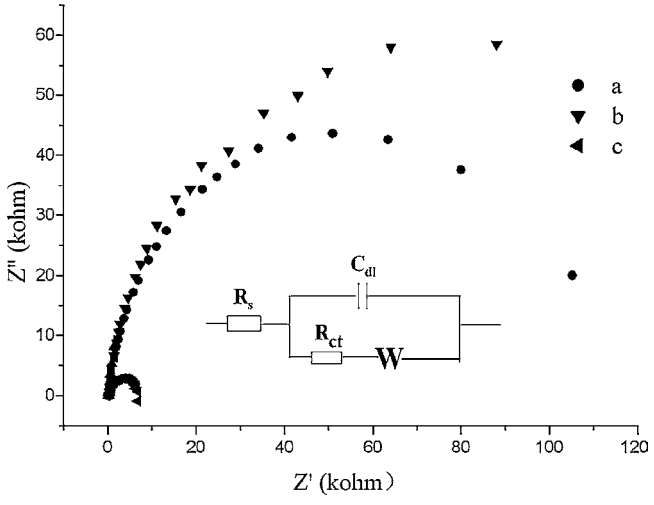

Fig. 4. Electrochemical impendence plots of: (a) bare gold electrode; (b) SAMs modified gold electrode; (c) Cu/SAMs modified electrode. Supporting electrolyte, 10 M glucose + 0.1 M NaOH. The electrode potential was 0.70 V vs. SCE; the frequency was from 100 kHz to 0.1 Hz and the amplitude was 10.0 mV (rms). Inset is the Randles circuit.

3.4. Effect of experimental conditions on voltammetric response

The effect of scan rate on the oxidation current of glucose at the Cu/SAMs composite-coated gold electrode in 0.1 M NaOH was tested by linear sweep voltammetry (LSV) (Fig. 5). In the range of 0.005–0.5 V s^{-1}, the anodic peak current (i_{pa}) varies linearly with the square root of the scan rate (ν) with a correlation coefficient of 0.9984. The linear regression equation is expressed as $i_P = 0.44 + 0.22\nu^{1/2}$ (i_P, μA; $\nu^{1/2}$, $(mV\,s^{-1})^{1/2}$). These results indicated that the electron transfer reaction was controlled by the diffusion of glucose. Meanwhile, the electrode reaction was totally irreversible, as confirmed from the lack of a reduction peak in the cyclic voltammograms and from the observation that the E_{pa} shift to more positive values with scan rate increasing in LSV.

It is well known that an alkaline medium is required for enhancing the electrocatalytic activity of several transition metals for the oxidation of carbohydrate [13,27,29,30]. This is in large part due to the fact that each of the oxidation processes results in the formation of passivating films or insoluble deposits of copper oxide or hydroxide species. Therefore, the effect of hydroxide concentration on the current signal was investigated by cyclic voltammetry (not shown here). There was a sharp decrease of a voltammetric response when the pH of the NaOH solution lowered than 13. Current signal of glucose was completely absent in a phosphate buffer solution at pH 8. During successive scans in high basic solution [35,36], the self-assembled

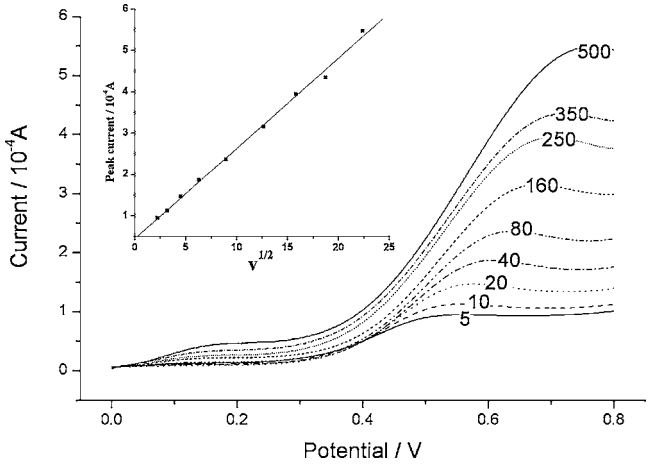

Fig. 5. Effect of scan rate on the oxidation of 10 mM glucose in 0.1 M NaOH at Cu/SAMs modified gold electrode. The numbers on the plots indicate the scan rate (mV s^{-1}). Inset is the plot of anodic peak current at about 0.7 V vs. square root of the scan rate. Other conditions are the same as Fig. 1.

monolayer would quantitatively desorption. Thus, a 0.1 M NaOH solution was selected for these experiments.

Experiment also showed that deposition time and deposition potential had apparent influences on the oxidation of glucose. When deposition potential shifted from 0 to −0.8 V, the formation of copper particles at the SAMs became easier. However, at too low potentials, the rate of the crystallization process was too fast and it was difficult to control both the size and the distribution of copper particles at the SAMs. Here, −0.6 V was selected as the deposition potential. The oxidation peak current increased with the gradual improving the deposition time in cupric salt solution. But the peak current increased at a much slower rate when the time exceeded 20 s. This might because that at the beginning of deposition copper preferentially decorated defects in the underlying SAMs. When the deposition time exceeds 20 s, further deposition only enlarges the size of Cu particles and copper gradually grows on the electron insulating organic film. Therefore an accumulation time of 20 s was suitable for this work.

Fig. 6 displays the amperometric response of the Cu/SAMs electrode to serial additions of glucose. This composite film electrode exhibits a rapid response to glucose additions, producing steady-state signals within 50 s. Glucose concentrations were varied from 3.0 μM to 10 mM and the oxidation peak current at about 0.6 V was recorded by employing linear sweep voltammetry (LSV). The current responses were plotted as a function of glucose concentration, a linear regression equation I_P (10^{-5} A) = 0.0423 + 1.116 × $c_{glucose}$ (10^{-4} M) was obtained with a correlation coefficient of r = 0.9975. The detection limit was 0.73 μM with a signal-to-noise of 3. The relative standard deviation (R.S.D.) of 6.5% for 10 mM glucose (n = 10) showed the good stability. The analytical performance of this electrode in electrochemical determination of glucose appears to be clearly superior in the sensitivity and linear range to that reported previously for other chemically modified electrodes [11,20].

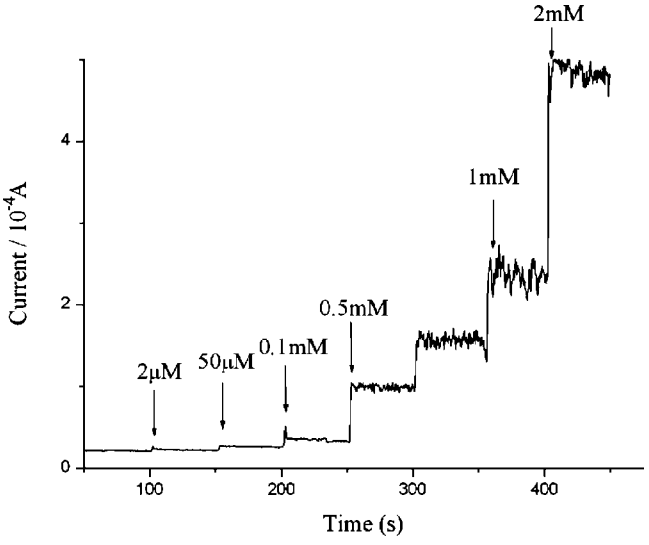

Fig. 6. Amperometric responses in 0.1 M NaOH at 0.7 V of sequential additions of glucose at Cu/SAMs modified Au electrode.

Table 1
Determination of glucose in blood samples

Sample no.	Spiked (mmol/l)	Found (mmol/l)	Recovery (%)	R.S.D. (%)
Real sample	–	4.27	–	–
1	0.238	0.251	105.3	5.62
2	0.476	0.471	98.95	2.14
3	0.714	0.683	95.66	3.54
4	0.933	0.902	96.68	6.54

R.S.D., relative standard deviation (three determinations).

3.5. Interferences

It is well known that surfactants can change the microenvironment of the electrode surfaces and improve electrode processes [21,22,37–41]. The effect of cationic surfactant, cetyltrimethylammonium bromide (CTAB), on glucose response was compared with both the SAMs/Cu and bare copper/Au electrodes. Upon addition of 0.5 mM CTAB to the solution, 1 mM glucose response of the Cu/Au electrode increased by 184.5%. In contrast, employing the Cu/SAMs electrode glucose response increased by 23.9% with the addition of the same concentration CTAB. Report indicated that glucose became anionic in 0.1 M NaOH [30]. When CTAB was present, such cationic surfactant adsorbed onto the substrate and electrostatic attracted negative charged glucose. With the increment of glucose molecule, current response was undoubtedly improved. Due to the hydrophobic interaction between SAMs and surfactant, Cu/SAMs film can elimination of such interference.

The oxidizable compounds such as ascorbic acid (AA) and uric acid (UA) are normally co-existed with glucose in real samples. In view of the physiological levels of glucose (3–8 mM) and the interfering agents (0.1 mM) [42], the amperometric response of the Cu/SAMs towards the addition of 3 mM glucose and 0.1 mM electroactive molecules was examined. Using the composite electrode the current signals for UA and AA were 1.1 and 2.2%, respectively, in comparison to that of glucose (480.5 μA).

3.6. Determination of glucose in mice blood

To illustrate the composite modified electrode application in practical analysis, it was used to detect glucose in rate blood samples. A rapid and stable amperometric response was obtained with the addition of 20 μl rate blood sample into 2 ml 0.1 M NaOH. Using standard additions method, the concentration of glucose in rat blood was calculated to approximately 4.27 ± 0.035 mmol (parallel measurements for three times), which was close to previous reports [43–45]. The recovered ratio on the basis of this method was investigated and the results were illustrated in Table 1. The good recoveries indicate that the determination of glucose using Cu/SAMs coated GCE is effective and sensitive.

4. Conclusion

A copper-dispersed self-assembled monolayers (SAMs) modified gold electrode was prepared. Infrared reflection–

absorption spectra (IRRAS) proved the SAMs, which was incorporated by Cu retained near-native structure. Cyclic voltammetry shows that this novel film electrode exhibits a sensing response towards glucose. In the range of 0.005–0.5 V s^{-1}, the anodic peak current varies linear with the square root of the scan rate. These results indicated that the electron transfer reaction was controlled by the diffusion of glucose. This Cu/SAMs film electrode showed good stability and responded linearly with glucose concentration from 3.0 μM to 10 mM, and a detection limit of 0.7 μm glucose (S/N = 3) was obtained.

Acknowledgement

This work was supported by the National Natural Science Foundation of China (nos. 60571042 and 30370397).

References

[1] L.A. Larew, D.C. Johnson, J. Electroanal. Chem. 262 (1989) 167.
[2] S.J. Updike, G. Hicks, Nature (London) 214 (1967) 986.
[3] D.R. Shankaran, N. Uehara, T. Kato, Biosens. Bioelectron. 18 (2003) 721.
[4] K. Krikstopaitis, J. Kulys, L. Tetianec, Electrochem. Commun. 6 (2004) 331.
[5] F. Hussain, D.J.S. Birch, J.C. Pickup, Anal. Biochem. 339 (2005) 137.
[6] M. Florescu, C.M.A. Brett, Talanta 65 (2005) 306.
[7] Y.B. Vassilyev, O.A. Khazova, N.N. Nikolaeva, J. Electroanal. Chem. 196 (1985) 127.
[8] A.E. Balzan, T. Iwasita, W. Vielstich, J. Electrochem. Soc. 134 (1987) 3052.
[9] K.B. Kokoh, J.M. Léger, B. Beden, et al., Electrochim. Acta 37 (1992) 1909.
[10] Y. Xie, C.O. Huber, Anal. Chem. 63 (1991) 1714.
[11] J.S. Ye, Y. Wen, W.D. Zhang, et al., Electrochem. Commun. 6 (2004) 66.
[12] N. Nath, M.P. Singh, Z. Phys. Chem. 224 (1963) 419.
[13] S.T. Farrell, C.B. Breslin, Electrochim. Acta 49 (2004) 4497.
[14] A. Zouanoui, O. Stéphan, M. Carrier, J.-C. Moutet, J. Electroanal. Chem. 474 (1999) 113.
[15] R.D. Rocklin, A.P. Clarke, M. Weizhandler, Anal. Chem. 70 (1998) 1496.
[16] L. Hua, L.S. Chia, N.K. Goh, S.N. Tan, Electroanalysis 12 (2000) 287.
[17] Y. Li, M.J. Yang, Y. She, Talanta 62 (2004) 707.
[18] D.E. Bartak, B. Kazee, K. Shimazu, T. Kuwana, Anal. Chem. 58 (1986) 2756.
[19] K.M. Kost, D.E. Bartak, B. Kazee, T. Kuwana, Anal. Chem. 60 (1988) 2379.
[20] F. D'Eramo, J.M. Marioli, A.H. Arévalo, Talanta 61 (2003) 341.
[21] C.G. Hu, S.S. Hu, J. Solid State Electrochem. 8 (2004) 947.
[22] B.Z. Zeng, F. Huang, Talanta 64 (2004) 380.
[23] N. Nakashima, T. Taguchi, Y. Takada, et al., J. Chem. Soc. Chem. Commun. 2 (1991) 232.
[24] D. Losic, J.G. Shapter, J.J. Gooding, Electrochem. Commun. 4 (2002) 953.
[25] E. Satatani, I. Rubinstein, J. Phys. Chem. 91 (1987) 6663.
[26] E. Sabatani, I. Rubinstein, J. Electroanal. Chem. 219 (1987) 365.
[27] S.V. Prabhu, R.P. Baldwin, Anal. Chem. 61 (1989) 852, and references therein.
[28] L.D. Burke, G.M. Bruton, J.A. Collins, Electrochim. Acta 44 (1998) 1467.
[29] M.Z. Luo, R.P. Baldwin, J. Electroanal. Chem. 387 (1995) 87.
[30] J.M. Marioli, T. Kuwana, Electrochim. Acta 37 (1992) 1187, and references therein.
[31] P. Luo, S.V. Prabhu, R.P. Baldwin, Anal. Chem. 62 (1990) 752.
[32] D.K. Sarkar, X.J. Zhou, A. Tannous, K.T. Leung, J. Phys. Chem. B 107 (2003) 2879.
[33] R. Krumm, B. Guel, C. Schmitz, G. Staikov, Electrochim. Acta 45 (2000) 3255.
[34] E.D. Eliadis, R.G. Nuzzo, A.A. Gewirth, R.C. Alkire, J. Electrochem. Soc. 144 (1997) 96.
[35] D.E. Weisshaar, B.D. Lamp, M.D. Porter, J. Am. Chem. Soc. 114 (1992) 5860.
[36] C.J. Zhong, M.D. Porter, J. Electroanal. Chem. 425 (1997) 147.
[37] J. Zhao, F.Q. Zhao, Z.Y. Chen, B.Z. Zeng, Electroanalysis 17 (2004) 1071.
[38] A. Navarro, F. Sanz, J. Colloid. Interf. Sci. 237 (2001) 1.
[39] B. Zeng, W.C. Purdy, Electroanalysis 11 (1999) 879.
[40] B. Ye, X. Zhou, Electroanalysis 8 (1996) 1165.
[41] O. Chailapakul, R.M. Crooks, Langmuir 11 (1995) 1329.
[42] B.H. Liu, R.Q. Hu, J.Q. Deng, Anal. Chem. 69 (1997) 2343.
[43] P.G. Salud, M.P. Rosa, P.G. Cuauhtémoc, et al., Pharmacol. Acta Helv. 72 (1997) 105.
[44] H. Nojiama, I. Kimura, F.J. Chen, et al., J. Nat. Prod. 61 (1998) 397.
[45] R.M. Perez, C. Perez, M.A. Zavala, et al., J. Ethnopharamacol. 71 (2000) 391.

Available online at www.sciencedirect.com
ScienceDirect
Talanta 70 (2006) 455–459
Talanta
www.elsevier.com/locate/talanta

Method optimization for quantitative analysis of octahydro-1,3,5,7-tetranitro-1,3,5,7-tetrazocine (HMX) by liquid chromatography-electrospray ionization mass spectrometry

Xiaoping Pan *, Kang Tian, Lindsey E. Jones, George P. Cobb

The Institute of Environmental and Human Health (TIEHH), Department of Environmental Toxicology, Texas Tech University, Lubbock, TX 79409-1163, USA

Received 2 February 2006; received in revised form 5 March 2006; accepted 5 March 2006
Available online 18 April 2006

Abstract

A simple, sensitive LC-ESI-MS method was optimized for quantitative analysis of octahydro-1,3,5,7-tetranitro-1,3,5,7-tetrazocine (HMX) in environmental samples. Under negative ionization mode, HMX can form adduct ions with various organic acids and salts, including acetic acid, formic acid, propionic acid, ammonium nitrate, ammonium chloride, sodium nitrite, and sodium nitrate. Acetic acid was chosen as additive and the ion, $[M + CH_3COO]^-$ with $m/z = 355$ was used for selective ion monitoring (SIM) in this study. Good sensitivity was achieved with low acetic acid concentration in the mobile phase and relatively low capillary temperature. The method detection limit was 0.78 pg for HMX in standard solution. Linearity ($R^2 > 0.9998$) was obtained at low concentrations (0.5–50 μg/L). This method has been used to determine HMX concentrations in water samples and lizard egg samples from an animal exposure study.

Keywords: Explosive; HMX; Liquid chromatography (LC); Electrospray ionization (ESI); Mass spectrometry (MS); Adduct ion; Water; Egg

1. Introduction

Octahydro-1,3,5,7-tetranitro-1,3,5,7-tetrazocine (HMX) (Fig. 1) is one of the most important explosives used in various military operations [1–4]. Limited animal studies indicate hepatic and central nervous system toxicities following HMX exposure [1]. However, HMX toxicity studies are limited compared to two other important explosives: RDX and TNT [5–7], especially in wildlife species such as reptiles. To aid in HMX toxicity studies, it is necessary to develop selective and sensitive analytical methods. In general, gas chromatography (GC) for nitramine explosive analysis, including HMX, is considered to be impractical due to their low vapor pressures and thermal liabilities [8]. Nevertheless, successful GC analysis of nitramine explosives using deactivated injection-port liners and short, wide-bore capillary columns has been reported [8]. Additionally, good GC separation of RDX and its derivatives from a DB-5 column was obtained using low injector temperature and fast carrier gas flow in our laboratory [9]. However, HMX failed to elute in the same system, probably due to its much lower vapor pressure than RDX (HMX: 10^{-14} Torr versus RDX: 10^{-9} Torr at 20 °C) [8]. As a good alternative, liquid chromatography coupled with different detectors has been widely employed for nitramine explosive analysis [10–13]. Compared with common analytical detection techniques, mass spectrometry detection is advantageous for its good sensitivity and selectivity. The formation of HMX adduct ions was commonly observed in many studies [14–17]. However, quantitative LC-ESI-MS analysis of HMX in real world samples is rare. The aim of this study was to optimize a LC-ESI-MS method for the trace quantification of HMX in environmental samples. Formation of HMX adduct ions with a variety of organic acids and salts were investigated, and critical LC-ESI-MS operation parameters such as additive concentration and heated capillary temperature were also optimized. This method has been applied to determine HMX concentrations in lizard egg extracts. Lizards

* Corresponding author. Tel.: +1 806 885 4567.
E-mail address: xiaoping.pan@tiehh.ttu.edu (X. Pan).

0039-9140/$ – see front matter © 2006 Elsevier B.V. All rights reserved.
doi:10.1016/j.talanta.2006.03.005

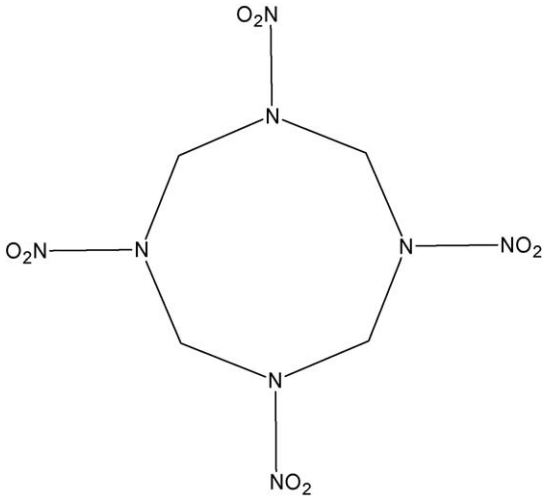

Fig. 1. Chemical structure of HMX (molecular weight = 296).

are among one of the most important bioindicator species for ecological risk assessment [18]. Eggs are generally deposited in their habitats, and developing embryos are susceptible to various environmental contaminants including HMX. Study of contaminant residue in egg is thus an important index for biomonitoring of potential adverse effects of contaminants on some wildlife populations [19].

2. Experimental

2.1. Chemicals and instruments

Standard HMX (CAS No. 2691-41-0; 99.0% pure) at a concentration of 1000 mg/L in acetonitrile was obtained from Supelco (Bellefonte, PA, USA). Methanol and glacial acetic acid (both HPLC grade), C18 cartridges (1 g), and PTFE syringe filter (0.2 μm) were from Fisher (Pittsburg, PA, USA). Ultra-pure water (>18 MΩ) obtained from a Barnstead NANOpure infinity system (Dubuque, IA, USA) was used for all aqueous solutions.

For instruments, the LC part was a Finnigan system including a vacuum membrane degasser, a gradient pump and an autosampler (San Jose, CA, USA). Chromatographic separation was achieved using a Supelco RP C18 column (4.6 mm × 250 mm, 5-μm packing) (Bellefonte, PA, USA). MS analyses were conducted using a Thermo-Finnigan LCQ advantage ion trap mass spectrometer. Helium was used as the damping gas for ion trap and nitrogen was the sheath and auxiliary gas for ion source. Some important LC-MS operation conditions are shown in Table 1.

2.2. LC-ESI-MS method optimization

To achieve better sensitivity, the LC-ESI-MS method was optimized. First, capacities of different organic acids and salts as additives in helping the formation of HMX adduct ion were investigated. Additives studies included acetic acid, formic acid, propionic acid, ammonium nitrate, ammonium chloride, sodium nitrite, and sodium nitrate. Additives were dissolved in the mobile phase and delivered at 0.5 mL/min, and HMX was injected continuously post-column at 5 μL/min using a syringe pump. These two streams mixed together at a "T" coupling unit and infused into the mass spectrometer interface.

Table 1
Some important optimized LC-ESI-MS operation parameters

LC conditions		MS conditions	
Mobile phase A	Methanol	Mode	Negative
Mobile phase B	0.5 mM aqueous acetic acid	Ion spray voltage (kV)	3.5
A:B	60:40 (v/v)	Sheath gas flow rate (L/h)	44.0
Flow rate	0.5 mL/min	Aux/sweep gas flow rate (L/h)	53.1
Injection	25 μL	Capillary voltage (V)	−6.3
		Capillary temperature (°C)	140.0
		Multipole 1 offset (V)	1.7
		Lens voltage (V)	25.6
		Multipole 2 offset (V)	7.0
		Multiple RF Amp (Vp-p, sp)	500.0

Based on HMX–acetate adduct ion, operation parameters such as ion spray voltage, sheath gas, and sweep gas were optimized using the "tune" function and was done by continuous after-column injection of HMX. Acetic acids at different concentrations in the mobile phase and heated capillary temperatures were optimized by changing the mobile phase manually and changing the heated capillary temperatures manually. For these two critical parameters, acetic acid concentration and heated capillary temperature, HMX was injected into LC column via autosampler and the signal responses as peak areas were recorded.

2.3. Method application

In order to further test the developed method, lizard eggs obtained from an ongoing HMX exposure study were analyzed. Lizards were dosed using HMX contaminated cricket daily, and eggs were collected during the experiment period. Eggs samples were extracted using a protocol reported previously with some modifications [20]. Briefly, egg samples (∼0.2 g each) were homogenized and dehydrated with 4–5 g of dried Na_2SO_4 using a small mortar and pestle. The soil sample–Na_2SO_4 mixture was then extracted using a Dionex Accelerated Solvent Extractor (Model 200, Salt Lake City, UT, USA) using 100% acetonitrile as extraction solvent. Extraction program is as follows: preheat 5 min, heat 5 min, and static extraction 5 min at constant temperature (100 °C) and pressure (1500 psi). Extracts (15–20 mL/sample) were then purged from cells into glass collection vials using nitrogen gas. The extract volume was reduced to ∼1 mL using a vortex evaporator for the following cleanup using a C18 cartridge. C18 cartridge was conditioned using 2× 3 mL acetonitrile, sample extract (∼1 mL) was then loaded

under gravity and eluates were collected. C18 cartridge was then rinse with 3× 1 mL acetonitrile and elutes were collected. The final extract volume was adjusted to 5 mL with acetonitrile. One milliliter from the 5 mL extracts was taken and diluted with water to 2 mL and then filtered through a 0.2 μm PTFE syringe filter into an autosampler vial for LC-MS analysis.

For LC-MS analysis, samples were injected into an LC column using an autosampler. The effluent from the LC column for the first 3 min was directed to waste via a six-port valve, and the fraction of the effluent between 3 and 9 min was directed to the electrospray interface of the mass spectrometer. LC effluent after 9 min was switched to waste.

3. Results and discussion

3.1. Choice of additives

ESI-MS detection requires the formation of charged species. HMX was difficult to ionize in the current ESI system due to a lack of acidic protons. In this case, additives are commonly employed to form adducts with the analyte [21]. Table 2 shows the relative ion abundance of HMX adduct ion when using different additives. Results indicate that acetate adduct ion is the most abundant ion at relatively low additive concentration (1 mM) in our system (Table 2). Given that salt should be avoided and the volatile additive concentration should be kept low in order to prevent ion source contamination, acetic acid was finally chosen to use in our system. However, the formation of a variety of HMX adduct ions provide more HMX identification possibilities. For example, in a severe formic acid contaminated system, ion $[M + HCOOH + CH_3COO]^-$ formed instead of $[M + CH_3COO]^-$, but this ion is relatively weak compared to use formic acid only as additive in such system (data not shown). In this case, formic acid is a convenient choice if sensitivity is not the primary concern.

Table 2
Relative HMX adduct ion abundances with different additives (1 mM in mobile phase B)

Candidate additives	Adduct ion	*m/z*	Ion relative abundance (%)
Formic acid	$[M + HCOO]^-$	341	30
Acetic acid	$[M + CH_3COO]^-$	355	100
Propionic acid	$[M + CH_3CH_2OO]^-$	369	45
Ammonium nitrate	$[M + NO_3]^-$	358	80
Ammonium chloride	$[M + Cl]^-$	331, 333	15
Sodium nitrite	$[M + NO_2]^-$	342	70
Sodium nitrate	$[M + NO_3]^-$	358	80

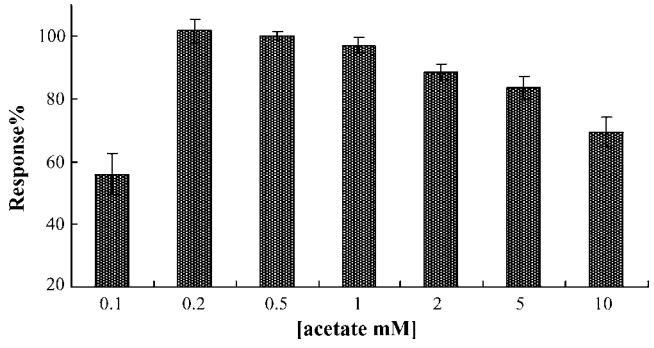

Fig. 2. Percent response vs. acetic acid concentration (mM) in mobile phase B. *Y* values were calculated as the ratio of signal values at certain acetate concentrations to the signal value obtained at 0.5 mM acetate in mobile phase B. Error bars indicate the standard deviation for triplicate injections. HMX injected: 50 μg/L.

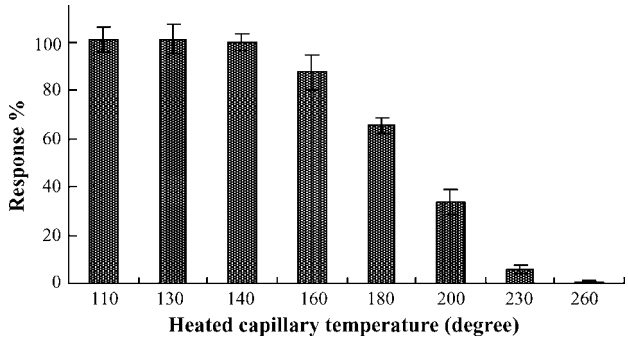

Fig. 3. Percent response vs. heated capillary temperature. *Y* values were calculated as the ratio of signal values at certain temperatures to the signal value obtained at 140 °C. Error bars indicate the standard deviation for triplicate injections. HMX injected: 2 μg/L.

3.2. Optimization of LC-ESI-MS operation conditions

Acetic acid concentration and the heated capillary temperature were found to be critical for other nitroamine detection,

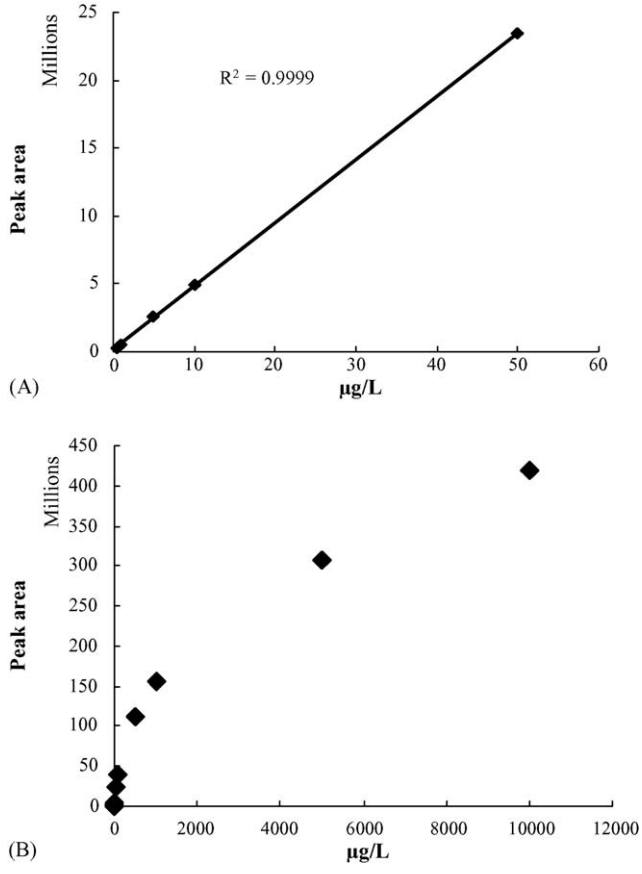

Fig. 4. Linearity of HMX calibration.

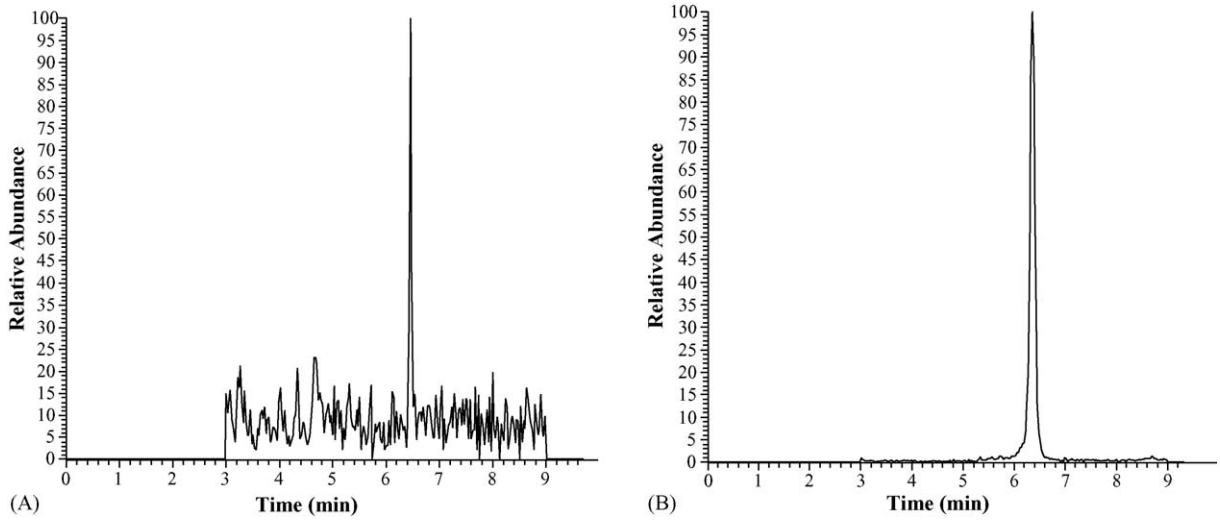

Fig. 5. LC-ESI-MS (SIM) chromatograms of (A) 0.1 μg/L HMX standard; (B) egg sample with 30.6 μg/L HMX incurred.

such as RDX [22], and thus were optimized manually. Fig. 2 shows that a relatively low concentration of acetic acid in mobile phase was optimum for adduct ion production, high concentration of acetic acid in mobile phase resulted in signal suppression. An acetic acid concentration of 0.5 mM was chosen as additive in the mobile phase (Table 1). Another important parameter is heated capillary temperature. Fig. 3 shows a relative low heated capillary temperature range was optimum for HMX analysis, so a heated capillary temperature of 140 °C was chosen for sample analysis (Table 1). HMX or the adduct ion may become unstable at a high capillary temperature. Similar patterns were also observed in RDX detection [22]. The "tune" function was used to optimize other essential parameters of the ESI-MS system. Important LC-MS operation conditions are summarized in Table 1.

3.3. Linearity and method detection limit (MDL)

Eleven concentrations of HMX, including 0.1, 0.5, 1, 5, 10, 50, 100, 500, 1000, 5000, and 10,000 μg/L, were prepared as standards in methanol/water solutions (v/v = 1:1). The standard samples were run using the optimized operation conditions. Good linearity was achieved at low concentrations and span 2 orders of magnitude (0.5–50 μg/L, $R^2 > 0.9998$) (Fig. 4A), using linear regression for seven runs on different days. The plot deviated from linearity at higher concentration (>100 μg/L) (Fig. 4B). Seven replicates of 0.10 μg/L HMX standards were prepared and analyzed to determine the MDL. The MDL, equal to the product of the standard deviation of seven replicates and the Student's value for a 99% confidence level ($t = 3.14$) [23], was 0.031 μg/L. With the injection volume of 25 μL, this equals an injected mass of 0.78 pg. Fig. 5A shows a representative chromatograph for 0.10 μg/L HMX.

3.4. Method application

This method was applied to analyze lizard egg extracts from an ongoing HMX exposure study. No significant matrix effect (ion suppression) was observed after cleanup and proper dilution. The detection limit of HMX in lizard egg samples was estimated as the follows: MDL × dilution factor (=50) and thus equal to 1.55 μg/kg. Fig. 5B shows an egg sample with 30.6 μg/L HMX incurred.

4. Conclusion

A sensitive and simple method for HMX quantification in environmental samples using LC-ESI-MS was reported. HMX can form different adduct ions with a variety of organic acids and salts in the ESI system. The same strategy may also apply to other nitramine explosives such as RDX. High sensitivity was achieved by adding a small amount of acetic acid to the mobile phase and operating at relatively low heated capillary temperature. This method has been applied to egg sample analysis. The detection limit of 0.78 pg for HMX is the lowest MDL achieved to date.

Acknowledgements

This work is funded by the Strategic Environmental Research & Development Program (SERDP), Project No. CU1235. Lizard eggs provided by Dr. Scott T. McMurry is highly appreciated. The authors also wish to thank Baohong Zhang, Haitao Luo, Qinsong Cai, Jia-Sheng Wang, Jun Liu, and Les McDaniel for assistant.

References

[1] ASTDR, Toxicological Profile for HMX, Agency for Toxic Substances and Disease Registry, US Department of Health and Human Services, Atlanta, GA, 1997.
[2] J.C. Pennington, J.M. Brannon, Thermochim. Acta 384 (2002) 163.
[3] D. Fournier, A. Halasz, S. Thiboutot, G. Ampleman, D. Manno, J. Hawari, Environ. Sci. Technol. 38 (2004) 4130.
[4] C.A. Groom, A. Halasz, L. Paquet, L. Olivier, C. Dubois, J. Hawari, Environ. Sci. Technol. 36 (2002) 112.
[5] M. Simini, R.T. Checkai, R.G. Kuperman, C.T. Phillips, J.E. Kolakowski, C.W. Kurnas, G.I. Sunahara, Pedobiologia 47 (2003) 657.

[6] G. Rosen, G.R. Lotufo, Environ. Toxicol. Chem. 24 (2005) 2887.
[7] S. Rocheleau, R.G. Kuperman, M. Martel, L. Paquet, G. Bardai, S. Wong, M. Sarrazin, S. Dodard, P. Gong, J. Hawari, R.T. Checkai, G.I. Sunahara, Chemosphere 62 (2006) 545.
[8] M.E. Walsh, T.A. Ranney, Determination of Nitroaromatic, Nitramine, and Nitrate Ester Explosives in Water Using SPE and GC-ECD, Comparison with HPLC, US Army Corps of Engineers, Cold Regions Research & Engineering Laboratory, 1998.
[9] X.P. Pan, B.H. Zhang, G.P. Gobb, Talanta 67 (2005) 816.
[10] K. Bratin, P.T. Kissinger, B.C. Briner, C.S. Bruntlett, Anal. Chim. Acta 130 (1981) 295.
[11] D.H. Fine, W.C. Yu, E.U. Goff, E.C. Bender, D.J. Reutter, J. Forensic Sci. 29 (1984) 732.
[12] T.F. Jenkins, P.H. Miyares, K.F. Myers, E.F. McCormick, A.B. Strong, Anal. Chim. Acta 189 (1994) 69.
[13] T.M. Chow, M.R. Wilcoxon, M.D. Piwoni, N.R. Adrian, J. Chromatogr. Sci. 42 (2004) 470.
[14] D.W. Berberich, R.A. Yost, D.D. Fetterolf, J. Forensic Sci. 33 (1988) 946.
[15] B. Casetta, F. Garofolo, Org. Mass Spectr. 29 (1994) 517.
[16] J. Yinon, J.E. McClellan, R.A. Yost, Rapid Commun. Mass Spectrom. 11 (1997) 1961.
[17] E. Holmgren, H. Carlsson, P. Goede, C. Crescenzi, J. Chromatogr. A 1099 (2005) 127.
[18] C.D. Klaassen, Toxicology: The Basic Science of Poisons, sixth ed., 2001, pp. 144–145.
[19] C.B. Pepper, T.R. Rainwater, S.G. Platt, J.A. Dever, T.A. Anderson, S.T. McMurry, J. Wildl. Dis. 40 (2004) 493.
[20] B.H. Zhang, X.P. Pan, G.P. Cobb, T.A. Anderson, J. Chromatogr. B 824 (2005) 277.
[21] X. Zhao, J. Yinon, J. Chromatogr. A 977 (2002) 59.
[22] X.P. Pan, B.H. Zhang, S.B. Cox, T.A. Anderson, G.P. Cobb, J. Chromatogr. A 1107 (2006) 2.
[23] SW846 Test Methods SW846, US EPA, Washington, DC, 2000.

Available online at www.sciencedirect.com
ScienceDirect
Talanta 70 (2006) 460–467
Talanta
www.elsevier.com/locate/talanta

A novel kinetic determination of dissolved chromium species in natural and industrial waste water

Ashraf A. Mohamed *, Ahmed T. Mubarak, Zakaria M.H. Marstani, Khaled F. Fawy

Department of Chemistry, Faculty of Science, King Khalid University, Abha 9033, Saudi Arabia

Received 21 February 2006; received in revised form 2 March 2006; accepted 5 March 2006
Available online 24 April 2006

Abstract

A highly sensitive, selective and simple kinetic method was developed for the determination of dissolved chromium species based on the catalytic effect of Cr(III) and/or Cr(VI) on the oxidation of 2-amino-5-methylphenol (AMP) with H_2O_2. The fixed time and initial rate variants were used for kinetic spectrophotometric measurements by tracing the oxidized product at 400 nm for 10 min after starting the reaction. Boric acid and Tween-40 exerted pronounced activating and micellar sensitizing effects on the studied redox reaction, respectively. The optimum reaction conditions were: 3.0 mmol l^{-1} AMP, 0.45 mol l^{-1} H_2O_2, 0.50 mol l^{-1} boric acid, 4 v/v% Tween-40, 10 mmol l^{-1} phosphate buffer and pH 6.45 ± 0.02 at 35 °C. Both Cr(III) and Cr(VI) ions exerted the same catalytic effect on the studied reaction. Linear calibration graphs were obtained for the determination of up to 6.0 ng ml^{-1} Cr with detection limits of 0.054 and 0.10 ng ml^{-1} Cr; following the fixed time and initial rate methods, respectively. The proposed method was successfully applied to the speciation and determination of trace levels of dissolved Cr(III) and Cr(VI) in natural and effluents of industrial waste water. The total dissolved Cr(III) and Cr(VI) species was determined first. In a second run, Cr(VI) was determined alone after precipitation of Cr(III) ions in presence of $Al(OH)_3$ collector, where Cr(III) is then determined by difference. Moreover, published catalytic–spectrophotometric methods for chromium determination were reviewed.

Keywords: Kinetic speciation of chromium; 2-Amino-5-methylphenol–hydrogen peroxide redox reaction; Micellar sensitization; Boric acid activator; Natural and industrial waste water

1. Introduction

Chromium speciation is receiving increased interests in environmental and biochemical studies. Chromium is known to exist in all oxidation states from 0 to VI, where Cr(III) and Cr(VI) are the most thermodynamically stable and commonly found forms. Chromium(III), at trace levels, is a micronutrient that plays an important role in the activation of insulin to maintain the correct levels of glucose in the blood; therefore, a 50–200 μg Cr(III) daily intake is recommended for adults [1]. However, Cr(VI) is of relatively high toxicity to humans, animals and aquatic life due to its carcinogenic and mutagenic properties [1–3]. Therefore, the US Environmental Protection Agency has regulated maximum levels (ML's) of 100 and 50 μg l^{-1} of total chromium and Cr(VI) in drinking and ground water, respectively. In Japan, the ML's of chromium in wastewater are 500 and 50 μg l^{-1} for total chromium and Cr(VI), respectively. Consequently, the development of low-cost, selective, sensitive and precise methods for the determination of ultra-trace levels of chromium species is important.

Sensitive techniques for the determination of chromium species include spectrophotometric [1–3], AAS [4–9], NAA [10], ICP-MS [11,12] and ICP-AES [13,14] analysis techniques that were frequently coupled with a prior preconcentration and/or separation steps. However, the high instrumental and operational costs and the high detection limits are common disadvantages of many of these methods. On the other hand, the well-known diphenylcarbazide (DPC) method is very

* Corresponding author: On leave from Department of Chemistry, Faculty of Science, Ain Shams University, Abbassia, Cairo 11566, Egypt.
Tel.: +966 507929119; fax: +966 7 2284783.
E-mail address: aamohamd@hotmail.com (A.A. Mohamed).

0039-9140/$ – see front matter © 2006 Elsevier B.V. All rights reserved.
doi:10.1016/j.talanta.2006.03.003

Table 1
General characteristics of catalytic–spectrophotometric methods for chromium determination

Reaction system	Dynamic range, ng ml^{-1} (detection limit)	Selectivity and remarks[a]	Reference
2-Amino-5-methylphenol–H_2O_2	0–6.0 (0.054), 0–6.0 (0.10)	FT_{10}, 10 mm cells IR	This work
2-Aminophenol–H_2O_2	0–7.0 (0.10)	FT_{10}, 50 mm cells	[17]
2-Aminophenol–H_2O_2	0.5–10	R_1, R_2, R_3, Act_1	[18]
Phenosafranin—H_2O_2	0–200 (29)	R_1, 100 °C, $FT_{10,5}$	[19]
Phenol red–H_2O_2	40–240 (40)	R_4, 100 °C, $FT_{20,5}$	[20]
PADMA [b] + DMA[b]–H_2O_2	0–120 (0.1)	na	[21]
Gallocyanine–H_2O_2	0–150	na	[22]
Indigo carmine–H_2O_2	(6)	R_1, Act_3	[23]
Methyl orange–H_2O_2	14–200 (14)	R_1, Act_4	[24]
Rhodamine B–H_2O_2	0–30 (7.2)	100 °C, $FT_{10,10}$	[25]
o-Toulidine–H_2O_2	(3.5)	R_1	[26]
1-Naphthylamine–H_2O_2	na	R_1, R_5, 80 °C, $FT_{30,1}$	[27]
Neutral red–H_2O_2	0–80	R_4, 100 °C, $FT_{15,5}$	[28]
Chrom blue black R–H_2O_2	0–750 (3.2)	R_1, 100 °C, $FT_{8,5}$	[29]
Catechol violet–H_2O_2	0–32 (1.28)	R_4, 70 °C, $FT_{6,3}$	[30]
Pyrogallol-5-sulphonate–H_2O_2	0.25–15.0 (0.024)	R_1	[31]
EHSMA [b] + MBTH[b]–H_2O_2	5–400 (2)	FIA	[32]
DMA[b] + MBTH[b]–H_2O_2	0.4–10	Act_2	[33]
o-Dianisidene–H_2O_2	0–40 (1.1)	R_1, R_5, R_6, 25 °C, FT_{30}	[34,35]
Fuchsin acid–H_2O_2	0–160 (5.7)	R_1, 85 °C, $FT_{13,5}$	[36]
I^-–H_2O_2	15–300	R_1, R_7	[37]
Alizarin green–Bromate	20–240 (3)	R_1, 70 °C, $FT_{8,5}$	[38]
Rhodamine B–Bromate	0–200 (1.24)	100 °C, $FT_{4,3}$	[39]
Ethylrhodamine B–Bromate	0–40 (1.66)	90 °C, $FT_{15,3}$	[40]
Amaranth–Chlorate	0–600 (23.6)	100 °C, $FT_{9,5}$	[41]
Carboxyazo I–IO_4^-	0–80 (0.82)	na	[42]
Ce^{IV}–As^{III}	10000–40000	R_1	[43]
Ce^{IV}–Te^{IV}	1–14	R_1, R_8, 70 °C, FT_{300}	[44]
Sb(III)–$[Fe(CN)_6]^{3-}$	5.2–1140	na	[45]

[a] IR, initial rate method. FT_x, a fixed time method where absorbance was measured after X min of mixing. $FT_{x,y}$, a fixed time method where the reacting mixture was kept at the specified temperature for X min. after which the reaction was quenched by cooling under running tap water for Y min. Act_x, in presence of an activator; X = 1, hexamine; 2, EDTA; 3, bipyridyl; 4, salicylic or citric acid. R_1, poor selectivity towards some ions, especially Ag^I, Co^{II}, Cu^{II}, Mn^{II}, Cr^{III}, Fe^{III}, Ru^{III}, V^V, Mo^{VI}, W^{VI}, Os^{VIII}, Br^- and/or I^- ions. R_2, initial rate method in presence of 1.0 mol l^{-1} NaCl as a salting out agent and a pH of 5.7. R_3, non-linear calibration graph. R_4, ion exchange was used to improve the selectivity. R_5, poor precision resulting from very high blank value. R_6, the reaction was carried out in an acetone-aqueous medium. R_7, a simultaneous determination of Cr^{VI} and W^{VI}. R_8, chromium was separated and pre-concentrated by extraction with 8-hydroxyquioline. FIA, flow injection analysis; na, data were not available.

[b] DMA = *N*,*N*-Dimethylaniline; MBTH = 3-methyl-2-benzothiazolinone hydrazone; PADMA = *p*-Amino-*N*,*N*-dimethylaniline; EHSMA = *N*-ethyl-*N*-(2-hydroxy-3-sulfopropyl)-3-methoxyaniline.

sensitive and was adopted as a standard for the determination of down to 10 μg l^{-1} Cr(VI) in natural and waste-waters [2,3]. Meanwhile, kinetic methods with spectrophotometric monitoring offer low cost and simple alternatives for the highly sensitive determination of traces of Cr(VI) and/or Cr(III) ions based on their effects on the oxidation of a substrate with a suitable oxidant such as H_2O_2 [15–37], bromate [38–40] chlorate [41], iodate [42], cerium(IV) [43,44], and ferricyanide ions [45], respectively. The general characteristics of these methods are shown in Table 1. However, the poor selectivity, poor precision and/or the high detection limits are common disadvantages.

The current paper describes an original method for the kinetic determination of ultra trace levels of Cr(III) and/or Cr(VI) based on their catalytic effect on the H_2O_2 oxidation of 2-amino-5-methylphenol. The nature of the products are inferred. The proposed method was successfully applied to the speciation and determination of trace levels of dissolved Cr(III) and Cr(VI) in natural and industrial waste water. Moreover, the published catalytic–spectrophotometric methods for chromium determination were reviewed.

2. Experimental

2.1. Apparatus and reagents

Absorbance measurements were performed on a Shimadzu UV-1601 PC spectrophotometer (Kyoto, Japan), equipped with a Shimadzu CPS 240A thermostated multi-cell positioner with a temperature stability of ±0.1 °C, using 10 mm matched cells. Eppendorf vary-pipettes (10–100, 100–1000 and 500–2500 μl) were used to deliver accurate volumes. pH measurements, with an accuracy of ±0.01, were made using a calibrated Hanna pH-mV meter model 211. A thermostated water bath, GFL 1003 type (Burgwedel, Germany), with an accuracy of ±0.1 °C, was also used. Ultrapure water was obtained from a Barnstead Nanopure diamond water purification system (Dubuque, IA, USA), and was used throughout.

All glassware and storage bottles were soaked in 10% HNO_3 overnight and thoroughly rinsed with water prior to use.

Unless otherwise stated, all chemicals were of ACS grade and were purchased from Aldrich (Milwaukee, WI) or Fluka (Buchs, Switzerland).

Stock standard solutions of 1000 μg ml^{-1} of Cr(III) and Cr(VI) were prepared from chromium(III) sulfate and potassium dichromate, respectively. Working standard chromium solutions were daily prepared from their respective stocks. A 30% hydrogen peroxide solution (Fluka) was used without dilution. A working solution of 10 mmol l^{-1} 2-amino-5-methylphenol (AMP) was daily prepared by dissolving 0.132 g $Na_2S_2O_5$ (Fluka) in about 80 ml water followed by the addition of 2.0 ml of 1.0 mg ml^{-1} EDTA, 5.0 ml of 1.0 mol l^{-1} H_2SO_4, 0.1228 g solid AMP (Aldrich) and stirring until complete dissolution. The resulting solution was diluted with water in a 100 ml volumetric flask, wrapped with an aluminum foil and stored at 4 °C, when not in use. A 200 ml composite buffer–activator–surfactant mixture, that is 20.0 mmol l^{-1} phosphate, 1.0 mol l^{-1} boric acid, 8.0 v/v% Tween-40 and 40 μg ml^{-1} EDTA, was prepared as follows: Dissolve 16.0 ml Tween-40 (Fluka) in about 150 ml water by vigorous stirring and gentle warming; add 0.40 g KH_2PO_4 (Aristar grade, BDH, Poole, UK), 0.151 g Na_2HPO_4 (Aristar), 12.37 g boric acid (Aristar) and 8.0 ml of 1.0 mg ml^{-1} EDTA and dissolve by stirring and gentle warming; after complete dissolution and cooling to room temperature, adjusted the pH to 6.45 ± 0.02 and dilute with water in a 200 ml volumetric flask. A 100 ml masking mixture (2% sulfamic acid and 2% citric acid) was also prepared and its pH was be adjusted to 6.45 ± 0.05. A collector solution for the co-precipitation of Cr(III) was prepared by dissolving 3.35 g of $AlCl_3 \cdot 6H_2O$ in 10 ml of 0.01 mol l^{-1} HCl and diluted to 100 ml in a volumetric flask.

2.2. Sample treatment for the determination of total dissolved chromium

Filter a 1.0 l of freshly collected water sample, using 0.45-μm membrane filter, acidify to pH 2.0 with HNO_3 and add 1.0 ml of the masking mixture. Acidified samples should be kept at 4 °C until the analysis step and analyzed with a maximum storage time of 24 h of collection [2,3]. However, just before the analysis step, re-adjust the sample pH to 6.4 ± 0.1.

2.3. Sample treatment for the determination of dissolved Cr(VI)

Filter a 1.0 l of freshly collected water sample, using 0.45-μm membrane filter, add 1 ml of the masking mixture, adjust the pH to 8.0 ± 0.1 using 1 M NaOH and keep at 4 °C until analyzed with a maximum storage time of 24 h of collection. Transfer a 75 ml aliquot of filtered sample to a 150 ml beaker and warm to 50–60 °C. Add 2.0 ml of the collector solution and adjust the pH to 8.0 ± 0.1 using 0.1 M NaOH solution, allow for coagulation, filter off and wash the precipitate with three 5 ml portions of water. Collect the filtrate and washings, adjust the pH to 6.4 ± 0.1, and dilute with water in a 100 ml volumetric flask.

2.4. Recommended procedure for the determination of dissolved Cr(III) and/or Cr(VI)

Use the treated samples for the determination of dissolved Cr(III) and/or Cr(VI). Transfer ≤460 μl of the sample solution to one of the thermostated spectrophotometric cells and dilute with water to 460 μl. Add 1500 μl of the composite buffer–activator–sensitizer mixture and 140 μl of the working H_2O_2 solution and shake well using a disposable Eppendorf tip. Leave the reacting mixture in the thermostated cell for 10 min then add 900 μl of the working AMP solution that's kept at 35 °C in the thermostated water bath and shake well. Record the absorbance–time graph at 400 nm, for 10 min against water as a reference. The value of A_{10} was used for fixed time calculations. The initial rate was calculated between 150 and 270 s of starting the reaction. The chromium concentration of the unknown sample is determined from a calibration graph, similarly prepared with the working standard Cr(VI) or Cr(III) solutions.

3. Results and discussion

The oxidation of 2-amino-5-methylphenol (AMP) with hydrogen peroxide was found to be a slow process that can be catalyzed by Cr(III) and/or Cr(VI) ions. The orange-yellow oxidized product exhibited a maximum absorbance at 400 nm against water as a reference (Fig. 1).

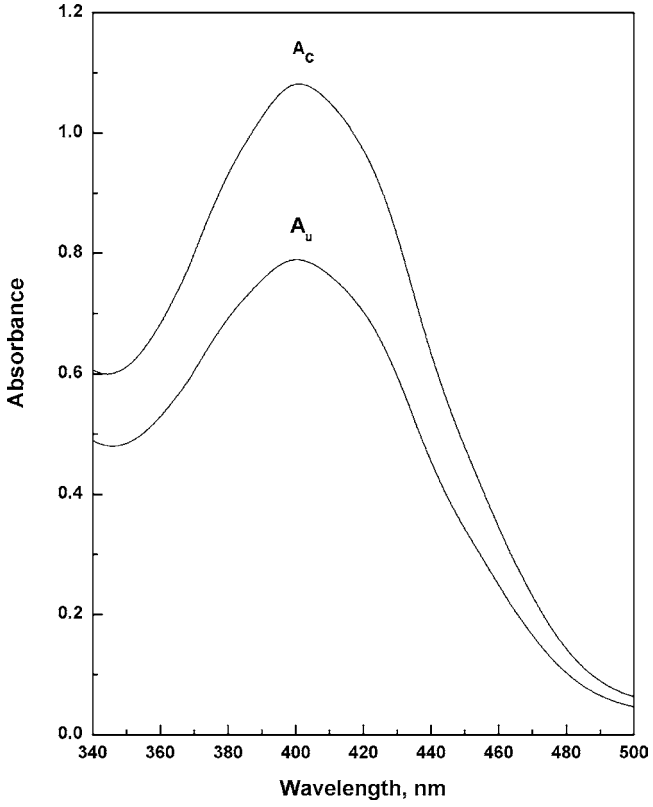

Fig. 1. Absorption spectra for the oxidation of 3 mmol l^{-1} 2-amino-5-methylphenol with 0.45 mol l^{-1} H_2O_2, following the recommended procedure, in the presence (A_c) or absence (A_u) of 3 ng ml^{-1} Cr(VI).

Chromium(VI) was used during preliminary optimization studies. The fixed time (after 10 min of mixing the reagents) and the initial rate kinetic methods were used to monitor the reaction. The absorbance–time graphs showed poor linearity up to 90 s thereafter good linearity was observed up to 480 s of starting the reaction; therefore, a lag time of 150 s was allowed for initial rate measurements that was made between 150 and 270 s.

Aqueous solutions of AMP, prepared by dissolving the reagent in dilute mineral acids were unstable and readily darkened after preparation because of their rapid auto-oxidation catalyzed by ultra-trace amounts of Co(II), Cu(II) and Fe(III) ions that may be found in the prepared solutions. Preliminary experiments showed that, sodium metabisulfite and EDTA acted as a stabilizer and a masking agent, respectively, and gave very stable AMP solutions. Namely, the sensitivity for chromium determination was not affected by metabisulfite and EDTA concentrations up to 500 and 50 $\mu g\,ml^{-1}$, respectively. Thus in order to overcome the instability of the AMP solution and confer enhanced selectivity for the proposed method, the working AMP solution was prepared as containing 1000 and 20 $\mu g\,ml^{-1}$ metabisulfite and EDTA, respectively.

3.1. Optimization of reaction conditions

The absorbances and initial rates of the catalyzed (A_c, k_c) and uncatalyzed (A_u, k_u) reactions gradually increased with AMP concentration resulting in maximum sensitivities, ($A_c - A_u$) and ($k_c - k_u$), at AMP concentrations $\geq$3.0 mmol l^{-1} (Fig. 2). Thus,

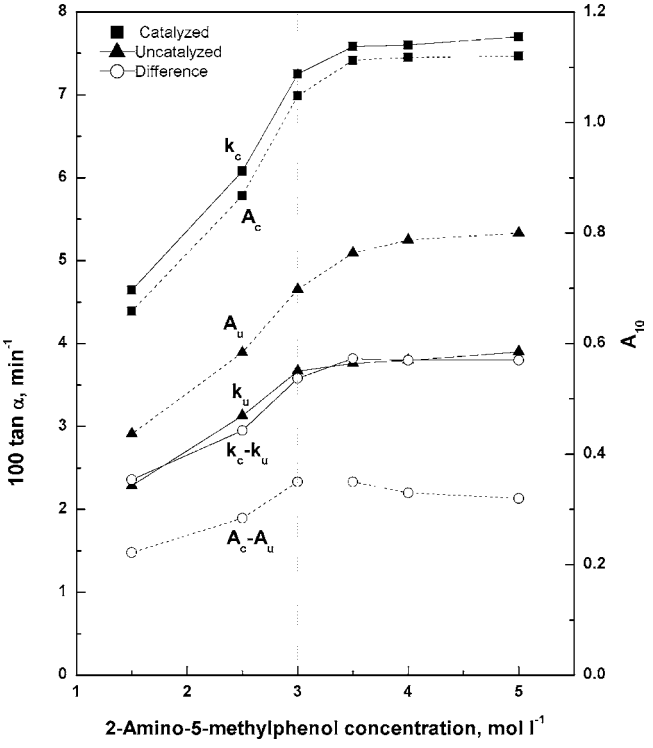

Fig. 2. Effect of 2-amino-5-methylphenol concentration. Except for the abscissa variable, conditions were those given in the recommended procedure. Absorbance values (- - -); rate values (—). Symbols were: k_c, A_c (■); k_u, A_u (▲); $k_c - k_u$, $A_c - A_u$ (◯).

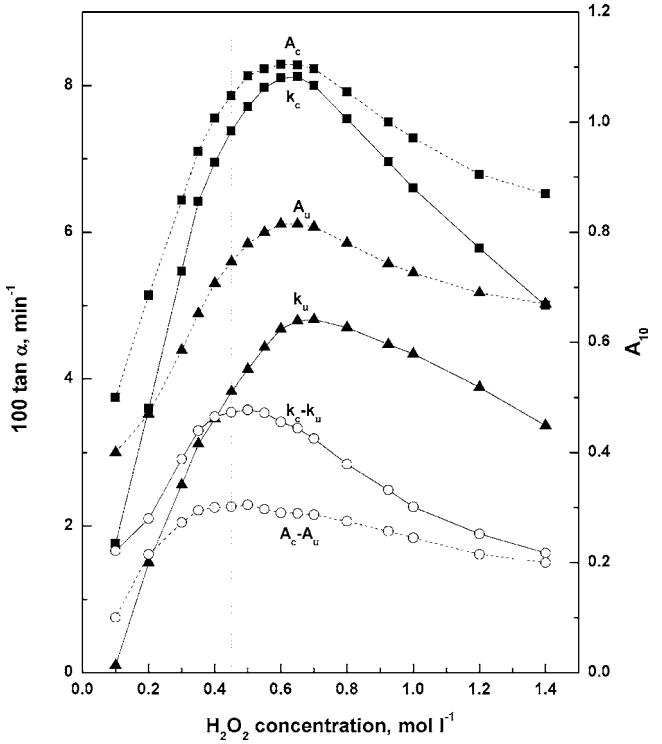

Fig. 3. Effect of hydrogen peroxide concentration. Except for the abscissa variable, conditions and symbols were those given in Fig. 2.

in order to have a high sensitivity and a low reagent blank, an AMP concentration of 3.0 mmol l^{-1} was adopted in the recommended procedure.

The absorbances and initial rates of the catalyzed (A_c, k_c) and uncatalyzed (A_u, k_u) reactions gradually increased with H_2O_2 concentration up to 0.6 mol l^{-1}; thereafter, it begin to decrease gradually. However, the sensitivities remained almost constant in the H_2O_2 concentration range of 0.40–0.50 mol l^{-1} (Fig. 3). Therefore, an H_2O_2 concentration of 0.45 mol l^{-1} was adopted in the recommended procedure.

Preliminary experiments showed that a working pH of about 6.5 gave high sensitivities. Therefore, phosphate buffer was adopted in the recommended procedure to enhance the selectivity of the proposed method. The absorbance and initial rate of the catalyzed reaction were maximum in the pH range 6.40–6.80 (Fig. 4). However, the sensitivities were maximum in the pH range 6.30–6.50; therefore, a pH of 6.45 ± 0.02 was adopted in the recommended procedure in order to provide a high sensitivity and a lower reagent blank.

The effect of varying (5.0–50.0 mmol l^{-1}) phosphate buffer concentrations was studied. It was found that the absorbances and initial rates of the catalyzed and uncatalyzed reactions and the sensitivities gradually decreased with increasing the buffer concentration. Therefore, a 10.0 mmol l^{-1} phosphate concentration was adopted in the recommended procedure in order to provide a high selectivity and a reasonable sensitivity. The gradual decrease of A_u, k_u, A_c and k_c may be attributed to an inhibitory effect of phosphate on the uncatalyzed and the Cr-catalyzed reactions. However, the gradual decrease in sensitivities ($A_c - A_u$ and $k_c - k_u$) revealed that high phosphate buffer concentrations

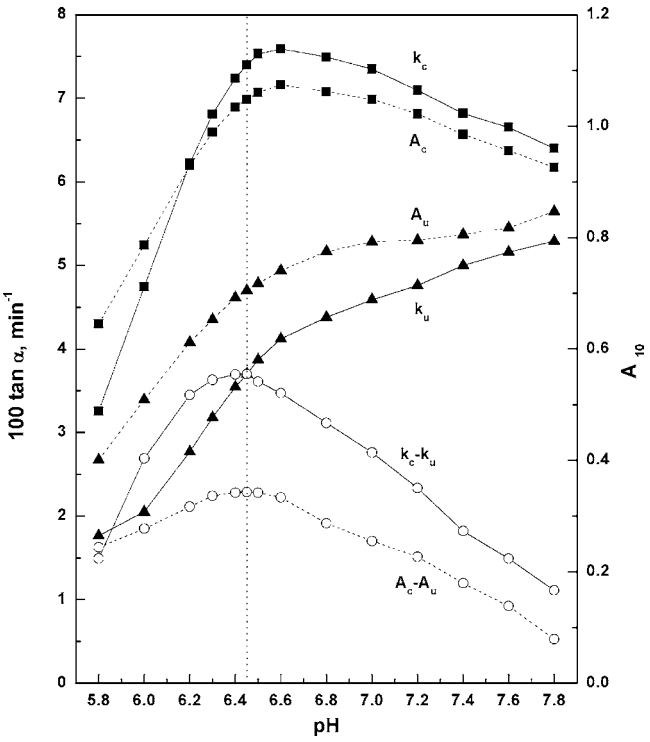

Fig. 4. Effect of pH. Except for the abscissa variable, conditions and symbols were those given in Fig. 2.

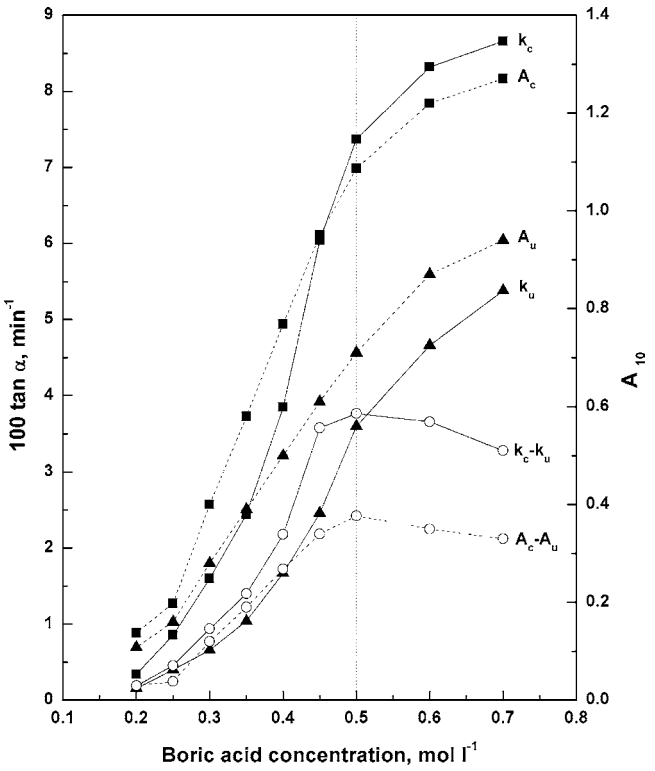

Fig. 5. Effect of boric acid concentration. Except for the abscissa variable, conditions and symbols were those given in Fig. 2.

exerted an inhibitory effect on the Cr-catalyzed reaction, probably by reducing the concentration of the catalytically active chromium species, via complexation.

The sensitivities ($A_c - A_u$ and $k_c - k_u$) could not be enhanced by the addition of variable concentrations of some activators, such as pyridine, 4-aminopyridine, 2,2′-bipyridyl, 1,10-phenanthroline, nitrilotriacetic acid, salicylic acid, citric acid, tartaric acid or 8-hydroxyquinoline. However, appreciable concentrations of Aristar grade boric acid greatly enhanced the absorbances and initial rates of the catalyzed and uncatalyzed reactions and also the sensitivities. Fig. 5, shows the effect of boric acid concentration at pH 6.45; where 0.50 mol l^{-1} concentration was adopted in the recommended procedure to give a high sensitivity and a moderate reagent blank. However, a 1500 μl volume of the buffer–activator–sensitizer composite solution was used because of the limited solubility of boric acid (solubility at 30 °C is 62.7 g $l^{-1} \cong 1.014$ mol l^{-1}). On the other hand, the increase of A_u and k_u with boric acid concentration may be attributed to a catalytic effect of boric acid on the oxidation of AMP to AMPZ and/or the hydrolysis of AMPZ to HMPZ (pp. 6,7). Meanwhile, the increase of A_c, k_c, $(A_c - A_u)$ and $(k_c - k_u)$ with boric acid concentration may be attributed partly to the above reasons and partly to its activating effect on the Cr-catalyzed reaction through weak complexation and formation of a more catalytically active chromium species. This is supported by the observation that appreciable concentrations of the strong complexing agent phosphate ion had decelerating effects on A_c, k_c, $(A_c - A_u)$ and $(k_c - k_u)$.

The effects of various surfactants of the cationic, anionic and nonionic types were investigated at concentration levels equal to or higher than their critical micellar concentrations. Thus, sodium dodecyl sulfate (SDS); cetylpyridinium chloride (CPC), benzyldimethylcetyl ammonium chloride (BDCAC), cetyltrimethylammonium hydrogensulfate (CTAHS), tetradecyltrimethylammonium hydrogensulfate (TTAHS), Triton X-100, and Tween-40 were tested. It was found that, SDS, CPC, BDCAC and Triton X-100 exerted slight decelerating effects; whereas, CTAHS and TTAHS had very slight accelerating effects. However, Tween-40 had pronounced accelerating effects that may be attributed to the proper organizing of reactants into and/or onto the highly organized assemblies of micelles. Therefore, the effect of Tween-40 concentration as a sensitizer was studied and resulted in a gradual increase in A_c, A_u and $(A_c - A_u)$. Namely, the presence of 0.25, 0.5, 1.0, 2.0, 4.0 and 5.0 v/v% of Tween-40 in the reaction cell gave sensitivity enhancements of 36, 68, 90, 123, 157 and 155%, respectively. Therefore, a 4 v/v% Tween-40 concentration was adopted in the recommended procedure.

Additions of up to 0.5 mol l^{-1} concentrations of Suprapur KCl or $NaNO_3$ had almost no effect on reaction sensitivities; however, A_c, k_c A_u, and k_u very slightly decreased with increasing the salt concentration.

The absorbances and initial rates of the catalyzed reaction (A_c, k_c) slightly depended on the order of addition; being slightly higher when AMP was added as the last reagent. Moreover, A_c and k_c values slightly increased with increasing the time of contact between Cr(VI) and H_2O_2, before the addition of AMP. For

example, in the determination of 3 ng ml^{-1} Cr(VI), the recoveries after 1, 3, 5 and 10 min of contact between Cr(VI) and H_2O_2, and before the addition of AMP, were 89, 93, 96 and 100%, respectively. This may be attributed to the formation of a more catalytically active species, probably oxodiperoxochromium(VI) [46,47]. Therefore, AMP was added as the last reagent, allowing a contact time of 10 min between Cr(VI) and H_2O_2, as adopted in the recommended procedure.

The absorbances and initial rates of the catalyzed and uncatalyzed reactions gradually increased with temperature. However, a working temperature of 35 °C was adopted in the recommended procedure because of its moderate sensitivity and reagent blank and its convenience for operation. The activation energies were calculated from linear regression analysis of Arrhenius plots. The activation energy for the uncatalyzed reaction was 11.13 kcal. mol^{-1}, whereas that for the reaction catalyzed by 3.0 ng ml^{-1} Cr(VI) was 8.29 kcal. mol^{-1}, showing efficient catalysis.

3.2. Study of interferences

The effects of potential interfering species, which generally accompany chromium in natural and waste water, were studied using 2 ng ml^{-1} Cr(VI). These species were tolerated to a great extent without any special precaution. All other species tested were tolerated at reasonably high concentrations; showing the high selectivity of the proposed method; especially when compared to the DPC standard spectrophotometric method [2,3]. The maximum tolerable concentrations of foreign species are shown in Table 2, where the tolerance level was defined as the concentration of foreign species that produced a change in the absorbance of the catalyzed reaction of less than 5%. The serious interference of nitrite ion was eliminated by the addition of sulfamic acid; that of Mo(VI) with citric acid and that of Hf(IV), Nb(V) and Ta(V) ions with EDTA, as described in the recommended procedure. Therefore, EDTA was included in the working solutions of AMP and the composite buffer–sensitizer–activator mixture. Moreover, a masking mixture of 2% of each of sulfamic and citric acids (at pH 6.45) was adopted in the recommended procedure.

3.3. Recovery of Cr(III), calibration graphs and detection limits

Both Cr(III) and Cr(VI) ions exerted the same catalytic effect on the studied reaction. Six replicate determinations of 0.1, 0.5, 1, 3 and 5 ng ml^{-1} Cr(III) or Cr(VI), following the recommended procedure, gave quantitative recoveries of ≥98.9% with relative standard deviations (R.S.D.%) ≤1.3% and Student's *t*-test values of ≥1.4, indicating that the proposed method may be equally applied to the determination of Cr(III) and Cr(VI) and that the *t*-test could not detect any systematic error revealing the high accuracy and precision of the proposed method (The tabulated *t*-value for the 95% confidence level and $n = 5$ is 2.78) [48].

Linear calibration graphs were obtained for the determination of up to 6.0 ng ml^{-1} of Cr(III) and/or Cr(VI); following both the fixed time and initial rate methods. The least square's equations for the calibration graphs were:

$$A_{10} = [0.700 \pm (2.04 \times 10^{-3})] + [0.1134 \pm (1.6 \times 10^{-4})][\mathrm{Cr}]$$

$$100 \tan \alpha = [3.70 \pm (3.95 \times 10^{-2})] + [1.234 \pm (1.4 \times 10^{-2})][\mathrm{Cr}]$$

where [Cr] is the Cr(III) or Cr(VI) concentration expressed in ng ml^{-1}. The correlation coefficients (*r*) were 0.9997 and 0.9995 and the detection limits, based on the $3S_b$-criterion [48], were 0.054 and 0.10 ng ml^{-1} Cr for the fixed time and initial rate methods, respectively.

3.4. Nature of the oxidation product

Oxidation of 2-aminophenols gave 2-aminophenoxazin-3-ones that under suitable conditions underwent hydrolysis to give 2-hydroxyphenoxazin-3-ones [49,50]. Thus, various 5-substituted-2-aminophenols reacted similarly, where the oxidative dimerization proceeded via elimination of a C_5-substituent from one phenol moiety to give the corresponding 2-amino-7-substituted-phenoxazin-3-ones that in most instances underwent hydrolysis to the corresponding 2-hydroxy-7-substituted-phenoxazin-3-ones [50]. Therefore, the intense orange-yellow colored product obtained in this work upon the H_2O_2 oxidation of AMP was attributed to the formation of 2-amino-7-methylphenoxazin-3-one (AMPZ) and/or 2-hydroxy-7-methylphenoxazin-3-one (HMPZ).

Table 2
Tolerance levels of foreign ions in the determination of 2 ng ml^{-1} Cr(VI)[a]

Tolerance level, μg ml^{-1}	Foreign species
>100	Acetate, citrate, oxalate, tartarate, sulfamic acid, catechol, glycerol, glucose, fructose, NO_3^-, F^-, Cl^-, Br^-, SO_4^{2-}, $S_2O_5^{2-}$, Na^+, K^+, NH_4^+, Ca(II), Mg(II), Al(III)
50	EDTA, CyDTA, Ba(II), Zn(II)[b], Fe(III)[b], As(III), As(V), Sn(IV)
20	SCN^-, SO_3^{2-}, Be(II), Sr(II), Zn(II)
10	NO_2^-[c], $S_2O_3^{2-}$, Ag^+, Hg^+, Ba(II), Cd(II), Cu(II), Hg(II), Ni(II), Pb(II), La(II), Zr(IV)
5	Co(II), Mn(II), Pd(II), Hf(IV), Nb(V), Ta(V), W(VI)
0.2	I^-, Ag^+, Fe(II), Fe(III), Ta(V), V(V), Mo(VI)[c]
0.02	NO_2^-, Sn(II), Mo(VI), Mn(VII)

[a] Reaction conditions are as given in the recommended procedure without co-precipitation in presence of $Al(OH)_3$ collector.
[b] After co-precipitation in presence of $Al(OH)_3$ collector.
[c] After addition of 30 μl of the masking mixture in the spectrophotometric cell.

The identity of the product was inferred from the following experiments: A 50 mmol AMP was treated with H_2O_2 at pH 6.45 in presence of phosphate and borate and the absence of Tween-40, which was omitted to avoid the formation of emulsion upon extraction with chloroform. The formed orange-yellow dye was extracted several times with chloroform until a colorless aqueous layer was left. The chloroform extract was concentrated by slow evaporation at 35 °C and the products were separated by column chromatography on a silica gel column with diethyl ether/petroleum ether 40–60 (1:4) as an eluent, dried under vacuum and characterized by ^{1}H NMR spectra. However, the aqueous layer was rendered alkaline by NaOH and distilled off. A portion of the distillate gave intense brown-orange ppt. with Nessler's reagent indicating the presence of ammonia. Another portion of the distillate was treated with alkaline $KMnO_4$, followed by acidification and dropwise addition of 2 ml of 5% Na_2SO_3 until complete decolorization adding few drops of Na_2SO_3 in excess. The resulting colorless solution gave intense pink color with Pararosaniline indicating the presence of methanol in the distillate. ^{1}H NMR spectra of the separated species revealed the presence of AMPZ [4.80 (NH_2, broad S), 2.35 (CH_3)] and HMPZ [10.69 (OH, broad S), 2.36 (CH_3)] in addition to the starting AMP. This may be attributed to the incomplete oxidation of AMP to AMPZ and the incomplete hydrolysis of AMPZ to HMPZ during the short reaction time of 10 min. Therefore, the overall reaction of AMP with H_2O_2 may be represented by the following equations:

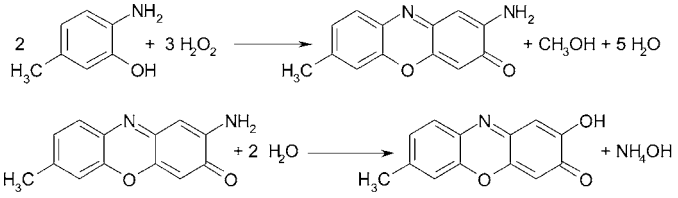

3.5. Speciation of chromium and application to natural and industrial waste water

The present method can equally determine Cr(III) and Cr(VI) ions in a given sample; therefore, speciation of chromium may be possible only after separation of Cr(III) and Cr(VI) that may be achieved by liquid chromatographic [4,5,11–14] or co-precipitation processes [6–9,17]. However, a prior co-precipitation step was adopted in the procedure as traces of Cr(III) may be co-precipitated quantitatively from slightly alkaline media, in presence of a collector such as the hydroxides of Ga(III) [6], Fe(III) [7], Hf(IV) [8], Zn(II) [9] or Al(III) [17]. Thus, $Al(OH)_3$ was the selected collector owing to its ability to give a quantitative and rapid co-precipitation of Cr(III) ions, while not creating interferences in the analytical determination due to its high tolerance level (see Table 2). The effects of the different precipitation variables on Cr(VI) recovery were thoroughly investigated. Quantitative co-precipitation of Cr(III) and recovery of Cr(VI) were obtained in the pH range 7.8–8.3 in presence of 30–200 μg ml^{-1} of Al(III) collector. Therefore, a pH of 7.90 ± 0.10, in the presence of 100 μg ml^{-1} Al(III) collector was adopted in the procedure in order to provide a reasonable amount of the collector. Such a co-precipitation step successfully enabled the quantitative separation of Cr(III) and Cr(VI) ions.

The implemented method was successfully applied to the determination of chromium species in effluents of plating and cement industries. The reliability of the proposed method to analyze such samples was checked by comparison with the reference air/acetylene FAAS method coupled with extraction of the ammonium pyrrolidinedithiocarbamate (APDC) complex into methyl isobutyl ketone [2]. The Cr(III) and Cr(VI) concentrations found by the proposed kinetic method were in good agreement with those obtained by the reference method as shown in Table 3 for samples No. 1 and 2. Moreover, the proposed method was applied to rain and polluted well-water samples from Abha

Table 3
Determination of chromium in natural and waste water samples

No.[a]	Cr(III)[b], ng ml^{-1}				Cr(VI)[b], ng ml^{-1}			
	Kinetic method			FAAS [2]	Kinetic method			FAAS [2]
	Added	Found ± S.D.	*R*%	Found ± S.D.	Added	Found ± S.D.	*R*%	Found ± S.D.
1	–	140.80 ± 2.70	–	145.5 ± 4.5	–	310.50 ± 4.80	–	318.5 ± 9.6
	200.0	335.60 ± 5.10	97.4	–	200.0	506.30 ± 6.90	97.9	–
2	–	30.72 ± 0.86	–	29.8 ± 1.6	–	17.80 ± 0.39	–	18.0 ± 1.1
	20.0	50.90 ± 1.24	100.9	–	20.0	37.76 ± 0.78	99.8	–
3	–	0.93 ± 0.04	–	–	–	0.82 ± 0.04	–	–
	1.0	1.89 ± 0.07	96.0	–	1.0	1.83 ± 0.06	101.0	–
4	–	11.52 ± 0.14	–	–	–	3.27 ± 0.09	–	–
	10.0	21.30 ± 0.19	97.8	–	10.0	13.40 ± 0.15	101.3	–
5	–	6.24 ± 0.12	–	–	–	4.58 ± 0.11	–	–
	10.0	16.42 ± 0.18	101.8	–	10.0	14.32 ± 0.18	97.4	–

[a] Samples no. 1 was waste effluent from plating industry; no. 2 was waste effluent from cement industry; no. 3, was rain water collected on the roof of King Khalid University building on 6 December 2005; no. 4 and 5 were well waters from Abha city. Sample pH's were: no. 1, 6.48; no. 2, 6.69; no. 3, 4.72; no. 4, 7.83; no. 5, 8.13.

[b] Concentration that is added to or found in 1 ml of original sample ($n = 5$).

city. Such samples could not be analyzed following the reference FAAS method as the chromium concentrations of these samples were below the determination limit of that method. Therefore, the reliability of the proposed method was checked by recovery experiments that gave quantitative recoveries (96.0–101.8%) with convenient reproducibility's (R.S.D. = 0.9–4.9%).

4. Conclusion

In comparison with the high cost techniques [10–14] for chromium speciation, the present work describes a very selective, simple, sensitive and low-cost method that can monitor concentrations of chromium species (III and/or VI) down to 0.054 ng ml^{-1} using a simple spectrophotometer. The advantageous sensitivity and selectivity make the proposed method a favorable competitive to the DPC standard spectrophotometric method [2,3] and the previously published catalytic–spectrophotometric methods (Table 1).

Acknowledgement

The financial support of King Abdulaziz City for Science and Technology (KACST) to project No. A.T. 22–80, from which this work is extracted, is gratefully acknowledged.

References

[1] ATSDR, Agency for Toxic Substances and Disease Registry, Toxicological Profile for Chromium, US Department of Health and Human Services, Atlanta, Georgia, 2000.
[2] E. Greenberg, L.S. Clesceri, A.D. Eaton (Eds.), Standard Methods for the Examination of Water and Waste-water, American Public Health Association, Washington, DC, 1995.
[3] American Society for Testing and Materials, Annual Book of ASTM Standards. Method No. D-1687, Vol. 11.01, ASTM, Philadelphia, 1995.
[4] A.S. Stasinakis, N.S. Thomaidis, T.D. Lekkas, Anal. Chim. Acta 478 (2003) 119.
[5] S. Yalcin, R. Apak, Anal. Chim. Acta 505 (2004) 25.
[6] S. Kagaya, J. Ueda, Bull. Chem. Soc. Jpn. 68 (1995) 2843.
[7] R.J. Keiber, J.D. Willey, S.D. Zvalaren, Environ. Sci. Technol. 36 (2002) 5321.
[8] J. Ueda, H. Satoh, S. Kagaya, Anal. Sci. 13 (1997) 613.
[9] A.C. Sahayam, J. Arunachalam, S. Gangadharan, Can. J. Anal. Sci. Spectrosc. 43 (1998) 4.
[10] W.Y. Feng, Q.F. Qian, W.J. Ding, Z.F. Chai, J. Radioanal. Nucl. Chem. 244 (2000) 321.
[11] F. Seby, S. Charles, M. Gagean, H. Garraud, O.F.X. Donard, J. Anal. Atom. Spectrom. 18 (2003) 1386.
[12] M.V. Balarama Krishna, K. Chandrasekaran, S.V. Rao, D. Karunasagar, J. Arunachalam, Talanta 65 (2005) 135.
[13] P. Liang, T.Q. Shi, H.B. Lu, Z.C. Jiang, B. Hu, Spectrochim. Acta B 58 (2003) 1709.
[14] T. Sumida, T. Ikenoue, K. Hamada, A. Sabarudin, M. Oshima, S. Motomizu, Talanta 68 (2005) 388.
[15] K.B. Yatsimirskii, Kinetic Methods of Analysis, Pergamon Press, London, 1966.
[16] D. Perez-Bendito, M. Silva, Kinetic Methods in Analytical Chemistry, Ellis Horwood, Chichester, 1988.
[17] A.A. Mohamed, S.A. Ahmed, M.F. El-Shahat, J. Trace & Microprob. Tech. 19 (2001) 297.
[18] S.U. Kreingol'd, A.N. Vasnev, J.V. Serebryakova, Zavod. Lab. 40 (1974) 6.
[19] Y. Cao, Fenxi-Shiyanshi 10 (1991) 22.
[20] Y.L. Cao, S.H. Chen, Lihua-Jianyan Huaxue-Fence 30 (1994) 177.
[21] H. Chen, X.Y. Huang, Fenxi-Huaxue 31 (2003) 87.
[22] R.H. He, J.H. Wang, Fenxi-Shiyanshi 19 (2000) 24.
[23] E.I. Jasinskiene, E.B. Bilidiene, Zh. Anal. Chem. 22 (1967) 741.
[24] E.I. Jasinskiene, E.B. Bilidiene, Zh. Anal. Chem. 23 (1968) 143.
[25] Y.Z. Cai, J. Huang, X.H. Yin, H.Y. Wu, Lihua-Jianyan Huaxue-Fence 38 (2002) 579.
[26] L.M. Kul'berg, Zavod. Lab. 7 (1938) 905.
[27] D. Li, Lihua-Jianyan Huaxue-Fence 25 (1989) 221.
[28] C.J. Liu, J.J. Jiang, Lihua-Jianyan Huaxue-Fence 29 (1993) 230.
[29] C.J. Liu, W. Zhang, Fenxi-Shiyanshi 13 (1994) 48.
[30] Z. Liu, X.Y. Wang, Fenxi Huaxue 24 (1996) 164.
[31] S.S. Mitic, G.Z. Miletic, A.N. Pavlovic, S.B. Tosic, Monatsh. Chem. 135 (2004) 927.
[32] M. Kaneko, M. Kurihara, S. Nakano, T. Kawashima, Anal. Chim. Acta 474 (2002) 167.
[33] S. Nakano, S. Hinokuma, T. Kawashima, Chem. Lett. (1983) 357.
[34] I.F. Dolmanova, G.A. Zolotova, T.N. Shekhovtsova, V.D. Bubelo, N.A. Kurdyukova, Zh. Anal. Khim. 33 (1978) 274.
[35] C. Reis, J. Carlos-de-Andrade, R.E. Bruns, R.C.C.P. Moran, Anal. Chim. Acta 369 (1998) 269.
[36] H.Z. Wu, Z.S. Zheng, G.B. Hu, F. Wang, Fenxi-Huaxue 20 (1992) 1445.
[37] Z.L. Zhu, C.Q. Han, Z.C. Gu, R.M. Chen, Analyst 119 (1994) 2251.
[38] H.Z. Wu, Z.S. Zheng, X.F. Guo, Y.H. Qiu, Fenxi-Huaxue 23 (1995) 821.
[39] J. Yan, Z.H. Xi, Z.J. Guo, Fenxi-Shiyanshi 19 (2000) 42.
[40] X. Zhao, Z.B. Li, Q.E. Cao, Lihua-Jianyan Huaxue-Fence 38 (2002) 285.
[41] Z.M. Zhang, Fenxi Huaxue 26 (1998) 325.
[42] J.H. Yu, Q.Y. Ou, C.Q. Shou, X.T. Zuo, Lihua-Jianyan Huaxue-Fence 40 (2004) 148.
[43] S.A. Chimatadar, G.S. Gokavi, S.T. Nandibewoor, J.R. Raju, Ind. J. Chem. A 27 (1988) 176.
[44] T. Fujinaga, T. Takamatsu, J. Chem. Soc. Jpn., Pure Chem. Sec. 91 (1970) 1165.
[45] S.T. Nandibewoor, V.A. Morb, J. Chem. Soc. Dalton Trans. (1995) 483.
[46] M.H. Dickman, M.T. Pope, Chem. Rev. 94 (1994) 569.
[47] P. Gili, A. Mederos, P.A. Lorenzo-Luis, E.M. de la Rosa, A. Munoz, Inorg. Chim. Acta 331 (2002) 16.
[48] J.C. Miller, J.N. Miller, Statistics for Analytical Chemistry, Ellis Horwood, Chichester, 1993.
[49] H.T. Nagasawa, H.R. Gutmann, M.A. Morgan, J. Biol. Chem. 234 (1959) 1600.
[50] N.H.P. Cnubben, B. Blaauboer, S. Juyn, J.J. Vervoort, I.M.C.M. Rietjens, Anal. Biochem. 220 (1994) 165.

Available online at www.sciencedirect.com
ScienceDirect
Talanta 70 (2006) 468–473
Talanta
www.elsevier.com/locate/talanta

Determination of trace Cd and Pb in environmental and biological samples by ETV-ICP-MS after single-drop microextraction

Li Li, Bin Hu *, Linbo Xia, Zucheng Jiang

Department of Chemistry, Wuhan University, Wuhan 430072, China

Received 13 January 2006; received in revised form 24 February 2006; accepted 3 March 2006
Available online 22 May 2006

Abstract

A method based on single-drop microextraction (SDME) combined with electrothermal vaporization (ETV)-ICP-MS was proposed for the determination of trace Cd and Pb. 8-Hydroxyquinoline (8-HQ) was employed as extractant dissolved in several microliters of chloroform and then an organic microdrop was formed at the tip of the microsyringe needle to extract the interest analytes. The vaporization behavior of the metal-8-HQ chelates in graphite furnace was investigated, and the ETV temperature program was optimized. The factors that influenced the extraction efficiency of target analytes (including pH value, flow rate of sample, extraction time and organic microdrop volume) were studied. Under the optimum conditions, the detection limits of the Cd and Pb were 4.6 and 2.9 pg mL^{-1} with the enrichment factor of 140-fold for Cd and 190-fold for Pb, respectively. The proposed method was applied successfully to the determination of trace Cd and Pb in environmental and biological samples. In order to validate the developed method, a certified reference material of GBW 08501 peach leaves was analyzed and the determined values obtained were in a good agreement with the certified values.

Keywords: Single-drop microextraction; Electrothermal vaporization; ICP-MS; Cadmium; Lead; 8-Hydroxyquinoline

1. Introduction

Cd and Pb have been well known as toxic elements for human and environment. By accumulation in bodies, Cd may induce dysfunction and reproductive deficiencies [1], and Pb may cause brain damage, kidney injury, seizures and anemia [2]. Therefore, there has been an increasing need for analytical chemists to evaluate the environmental and healthy quality based on accurate determination of Cd and Pb both in environmental samples and in biological samples.

In recent years, inductively coupled plasma-mass spectrometry (ICP-MS) has been used successfully for the rapid and simultaneous determination of trace metals in various samples due to its low detection limit, multi-element capability and wide linear range [3–5]. However, a certain preconcentration/separation process is usually imperative for the concentrations of target analytes in real samples are commonly too low or the sample matrix is too complicated to be determined directly by this instrumental technique.

Up to now, many articles have been published concerning the preconcentration/separation techniques for Cd and Pb in different samples, and solid-phase extraction [6,7], cloud point extraction [8,9] and HPLC [10] are among the most widespread used methods. Although relatively good analytical performance can be obtained with the above-mentioned pretreatment techniques, they have the disadvantages of complicated treatment procedure, large consumption of reagents and unsatisfactory enrichment factor.

Like the solid-phase extraction, liquid–liquid extraction (LLE) is another classic pretreatment technique that has been widely employed in analytical chemistry [11,12]. However, the conventional LLE uses large amounts of solvent and it is time-consuming to perform, which limits its further application. To overcome the disadvantages mentioned above, analytical researchers recently have been developing new "minimized" and "green" pretreatment methods. In 1996, Liu and Dasgupta [13] firstly used the term "solvent microextraction". They only used 1.3 μL chloroform as extraction reagent, thus decreased the environmental pollution greatly throughout the analytical pro-

* Corresponding author. Tel.: +86 27 87218764; fax: +86 27 68754067.
E-mail address: binhu@whu.edu.cn (B. Hu).

0039-9140/$ – see front matter © 2006 Elsevier B.V. All rights reserved.
doi:10.1016/j.talanta.2006.03.006

cedure. Meanwhile, Jeannot and Cantwell [14] introduced the single-drop microextraction (SDME) technique. In their another work [15], the authors investigated a convective–diffusive mass transfer model to interpret the kinetic procedure in this novel SDME technique. Bjergaard and Rasmussen [16] reported a microextraction method with a polypropylene hollow fiber as supporter and then the acceptor solutions inside the hollow fiber were analyzed by CE. The enrichment factor reached 75. Lee and co-workers combined the hollow fiber membrane-liquid-phase microextraction (HFM-LPME) with GC [17] or HPLC [18] to separate and determine aromatic compounds in various samples. Besides, headspace SDME [19] is another mode utilized extensively in analysis of compounds exhibiting high vapor pressure. Psillakis and Kalogerakis [20,21] have published two reviews that focus on basic extraction principles, technical set-up, recovery, enrichment, extraction speed, selectivity, applications and future trends in LPME. However, it should be noted that the overwhelming majority of research works on LPME are concentrated on the analysis of organic analytes but very few publications on the study of LPME for inorganic analytes were reported up to now. In our previous works, we developed a method that combined SDME with ETV-ICP-OES/MS for the determination of trace La [22], Be, Co, Pd and Cd [23], and speciation of Al [24]. It was shown that the microextraction techniques combined with microvolume sample introduction technique of ETV could be a very compatible coupling.

The aim of this work is to determinate trace toxic elements of Cd and Pb in environmental and biological samples by combining SDME with ETV-ICP-MS. The main parameters influencing the extraction efficiency and the analytical performance were systematically investigated and optimized. Finally, the proposed method will be validated by analyzing standard reference material and real samples.

2. Experimental

2.1. Reagents and standard solutions

According to standard methods [25], the standard stock solutions of Cd (1 mg mL^{-1}) and Pb (1 mg mL^{-1}) were prepared from analytical reagent grade (AR) $CdCl_2{\cdot}2.5H_2O$ and $Pb(NO_3)_2$, respectively. The standard working solutions of the metal ions were prepared by step dilution of standard stock solutions with high purity de-ionized water.

The buffer solution was a mixture of 0.01 mol L^{-1} potassium acid phthalate (AR, The Third Shanghai Reagent Factory, Shanghai, China) and potassium hydroxide (AR, The Third Tianjin Reagent Factory, Tianjin, China) and the pH value was adjusted approximately to 6.5.

The 0.1 mol L^{-1} solution of 8-hydroxyquinoline (8-HQ) was prepared by dissolved 0.3630 g 8-HQ (AR, Shanghai Chemistry Reagent Company, Shanghai, China) in 25 mL chloroform (AR, Shanghai Si Yi Chemicals Reagent Co. Ltd., Shanghai, China) and was stocked in fridge at 4 °C against light.

In order to eliminate the blank of trace analytes and other contaminants, all containers were dipped in 10% HNO_3 over 24 h and rinsed by high purity de-ionized water prior to use. And high purity de-ionized water obtained by a Labconco System (18.2 MΩ) was used throughout this work.

2.2. Apparatus

2.2.1. Microextraction system

SDME system has been described in our previous work [23]. A PFA tube (0.30 mm i.d.) was used to connect the extraction chamber (~0.2 mL volume) and an HL-2 pump (Shanghai Qingfu Huxi Instrument Factory, Shanghai, China), a 10-μL microsyringe (Gaoxin, Shanghai, China) was used as drop-holder and sample injection device.

2.2.2. ETV-ICP-MS apparatus

A modified commercially WF-4C graphite furnace (Beijing Second Optics, Beijing, China) was available as an electrothermal vaporizer and was connected to an Agilent 7500a ICP-MS (Agilent, Japan). Details on the modification of the graphite furnace and its connection with ICP-MS have been described previously [26].

The ICP-MS operating condition was optimized with conventional pneumatic nebulization method prior to connecting with ETV device. Pyrolytic graphite-coated graphite tubes were used throughout this work. The operating conditions for ETV-ICP-MS and the temperature program are summarized in Table 1.

2.3. Procedure

2.3.1. SDME procedure

After the extraction system has been filled with the sample solution, a 10-μL microsyringe was used to take 5 μL organic extraction solution (8-HQ-chloroform) without bubble. Then a 3–5 μL organic extraction solution was pushed out smoothly to form a drop right above the PFA tube outlet in the extraction chamber. As the sample solution flowed around the organic drop

Table 1
Operation condition of ICP-MS and temperature programs of graphite furnace for ETV–ICP–MS

Operation condition of ICP-MS	
RF power	1250 W
Outer gas flow rate	15 L min^{-1}
Intermediate gas flow rate	0.9 L min^{-1}
Nebulizer gas flow rate	0.7 L min^{-1}
Carrier gas flow rate	0.4 L min^{-1}
Sampling depth	7.0 mm
Sampler/skimmer diameter orifice	Nickel 1.0 mm/0.4 mm
Scanning mode	Peak-hopping
Dwell time	30 ms
Integration mode	Peak area
Sample introduction volume	3–5 μL
Temperature programs of graphite furnace for ETV–ICP–MS	
Drying step	100 °C, ramp 3 s, hold 3 s
Vaporization step	1800 °C, 4 s
Cooling step	50 °C, 5 s
Cleaning step	2300 °C, 3 s

continuously, the trace analytes were chelated with 8-HQ, and were extracted into the solvent drop from the sample solution simultaneously. After a period of extraction, the organic drop was withdrawn by the microsyringe and was then injected into the graphite furnace for further ETV-ICP-MS analysis.

2.3.2. ETV-ICP-MS analysis procedure

After the ETV unit was connected to the ICP-MS and the system was stabilized, the post-extraction drop in the microsyringe was directly introduced into the graphite furnace to analyze. The dosing pole was open to remove the water and organic solvent during the drying step of the temperature program, and it was sealed with a graphite probe 4 s prior to the vaporization step. At the same time, the data acquisition in ICP-MS was started to detect the analytical signal.

3. Results and discussion

3.1. Vaporization behavior of analytes and optimization of ETV temperature program

The vaporization behavior of 8-HQ chelates of Cd and Pb in graphite furnace was investigated. Fig. 1 is the signal profiles obtained by ETV-ICP-MS with (Fig. 1A and C) or without (Fig. 1B and D) 8-HQ as chemical modifier. As could be seen, a sharp and symmetrical peak could be detected at 1800 °C with 8-HQ as chemical modifier for Cd (Fig. 1A), and also a sharp vaporization signal occurred at 1800 °C without 8-HQ (Fig. 1B). But the signal intensity of Cd-8-HQ chelate (Fig. 1A) is much stronger than that without 8-HQ (Fig. 1B). Similarly, the signal intensity of Pb with 8-HQ (Fig. 1C) was much stronger than the signal intensity without 8-HQ (Fig. 1D). Although Cd and Pb are easily volatile elements, which make it unnecessary to decrease their vaporization temperature, the experimental results did demonstrate that the use of 8-HQ could surely improve the detection sensitivity of analytes.

Many factors may affect the signal intensity of analytes and therefore should be studied to get the highest sensitivity. Fig. 2 is the pyrolysis curves and vaporization curves of the analytes with 8-HQ as chemical modifier. As could be seen from the pyrolysis curves, the signal loss for both Cd and Pb occurred when the pyrolysis temperature was higher than 400 °C. Compared with the ashing temperature of 350 and 250 °C reported in literature [27], the pyrolysis temperature could be increased by 50 and 150 °C for Cd and Pb, respectively, in this work, which showed that 8-HQ could improve the thermal stabilization of Cd and

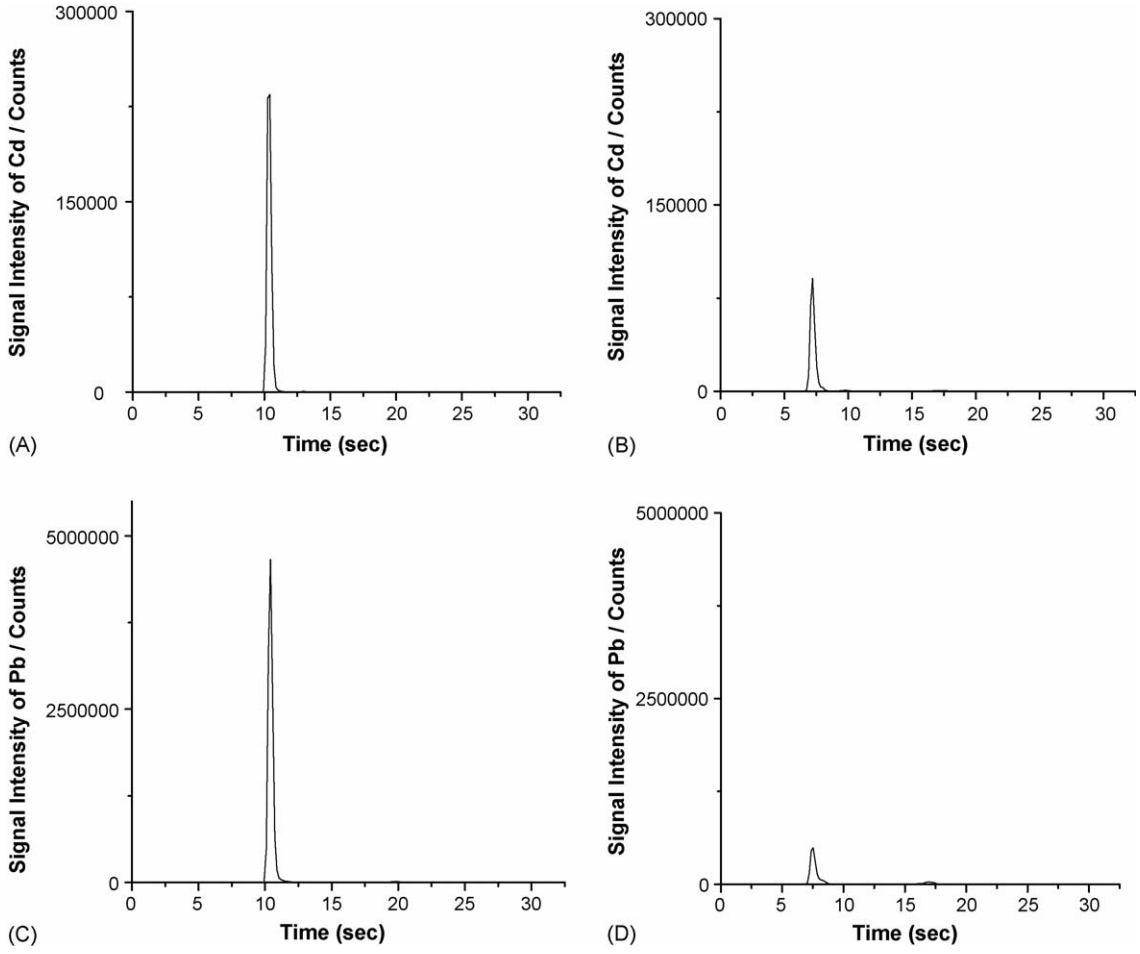

Fig. 1. Signal profiles of Cd and Pb: drying, 100 °C, ramp 3 s, hold 3 s; vaporization, 1800 °C, time 4 s. *Conditions*: (A) 25 pg Cd with 0.4 μmol 8-HQ as chemical modifier; (B) 25 pg Cd without 8-HQ; (C) 25 pg Pb with 0.4 μmol 8-HQ as chemical modifier; (D) 25 pg Pb without 8-HQ.

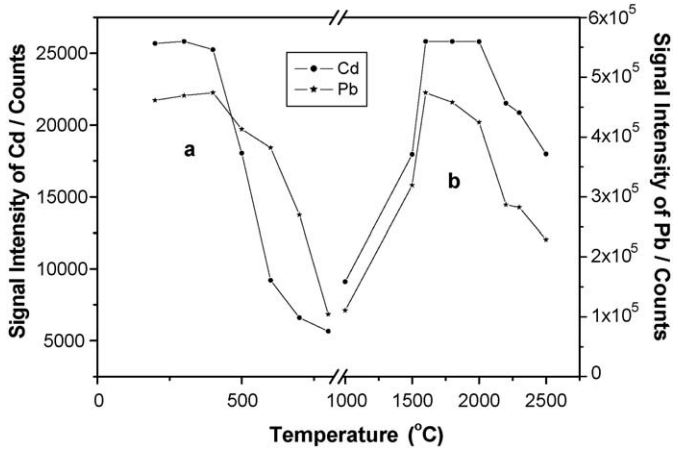

Fig. 2. Effect of pyrolysis and vaporization temperature on signal intensity. (a) Pyrolysis curve; (b) vaporization curve. *Conditions*: Cd and Pb 25 pg with 0.4 μmol of 8-HQ; drying, 100 °C, ramp 3 s, hold 3 s; vaporization time, 4 s.

Pb in ETV. The effect of pyrolysis time at ashing temperature of 200 °C was also studied, and no obvious signal loss was observed when the pyrolysis time was shorter than 15 s. It is found that the pyrolysis step is unnecessary for low temperature electrothermal vaporization; therefore, no pyrolysis process was employed in this work.

From the vaporization curves given in Fig. 2, it could be seen that the signal intensity of Cd and Pb increased noticeably with the increase of vaporization temperature from 1000 to 1600 °C. And the maximum signal intensity of Cd was obtained at 1600 °C and kept constant up to 2000 °C. With further increase of vaporization temperature above 2000 °C, the analytical signal intensity decreased rapidly, which was probably caused by the decomposition of metal chelates at high temperature. The strongest signal of Pb was obtained at approximately 1600 °C, and then the signal intensity began to drop gradually from 1600 to 1800 °C. After 1800 °C, a sharp decrease in signal intensity was found. For this reason, 1800 °C was selected as the vaporization temperature for simultaneous determination of Cd and Pb. The influence of the vaporization time on signal intensity was also studied. The results showed that the maximum signal intensity was achieved when the vaporization time was set to be greater than 3 s, which may indicate the complete vaporization of analytes in graphite furnace. So 4 s was selected as vaporization time in this work.

3.2. Optimization of extraction factors

Several factors that influence the extraction, such as sample pH value, sample flow rate, extraction time and organic drop volume, were investigated in details. For this purpose, 1.5 mL 0.01 mol L^{-1} buffer solution with 0.1 ng mL^{-1} Cd and Pb was employed as the test solution, and the μL level post-extraction drop was directly introduced in the graphite furnace for the determination.

3.2.1. Influence of sample pH

The influence of sample pH values on the extraction efficiency was investigated. It was found that Cd and Pb could be efficiently extracted into the organic solvent drop when the sample pH value was at the range of 6.0–7.0. The results were in accordance with the previous report in LLE [28]. The sample pH of 6.5 was selected in the further studies.

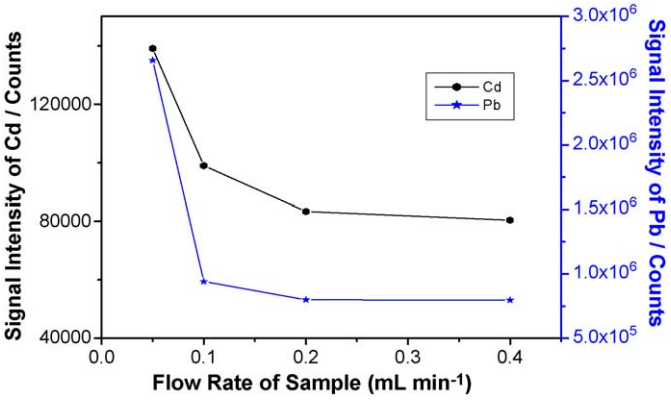

Fig. 3. Effect of sample flow rate on signal intensity. *Conditions*: Cd and Pb 0.1 ng mL^{-1}; aqueous volume, 1.5 mL; drop volume, 4 μL; extraction time, 15 min.

3.2.2. Influence of sample flow rate

The sample flow rate is a pretty crucial factor affecting the dynamic procedure of extraction according to the convective–diffusive mass transfer model [14]. As shown in Fig. 3, the analytical signal intensity decreased with the increase of sample flow rate, and the sample flow rate of 0.05 mL min^{-1} provided the highest extraction efficiency. The reason may be that the extraction dynamic rate is rather slow. On the other hand, 0.05 mL min^{-1} is preferable considering the stability of microdrop suspended at the tip of microsyringe needle. Therefore, a sample flow rate of 0.05 mL min^{-1} was selected in the work.

3.2.3. Influence of extraction time

With the sample flow rate of 0.05 mL min^{-1} and the organic microdrop volume of 4 μL, the effect of extraction time on the signal intensity was investigated and the experimental results are shown in Fig. 4. It could be seen that the signal intensity of analytes increased with the increase of extraction time within 20 min. When the extraction time was more than 20 min, remarkable dissolution of microdrop could be observed and thereby the analytical signal intensity decreased. Trading off the analytical speed and the extraction efficiency, an extraction time of 15 min was employed for the further study. It should be stressed that it did not reach extraction equilibrium with the extraction time of 15 min, so the calibration graph was also obtained by SDME.

3.2.4. Influence of drop volume

With the sample flow rate of 0.05 mL min^{-1} and the extraction time of 15 min, the influence of organic microdrop volume on the analytical signal intensity was studied. The results showed that no remarkable effect of organic microdrop volume on the analytical signal intensity was observed when it varied from 3 to 5 μL. Since the organic microdrop would easily fall off the

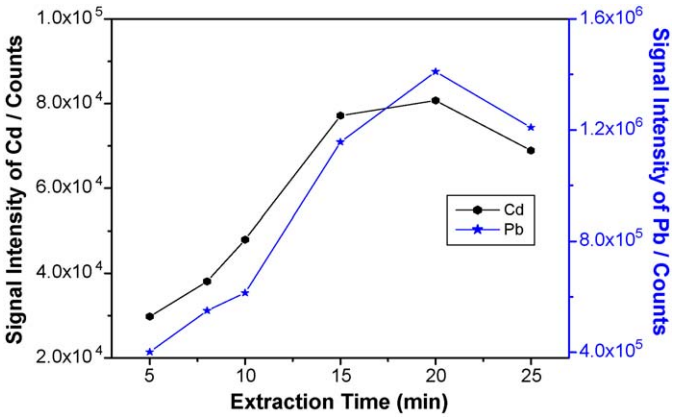

Fig. 4. Effect of extraction time on signal intensity. *Conditions*: Cd and Pb 0.1 ng mL^{-1}; sample flow rate, 0.05 mL min^{-1}; aqueous volume, 1.5 mL; drop volume, 4 μL.

needle with the volume of 5 μL, a droplet of 4 μL was selected in this work.

Based on the above results, the extraction conditions employed in this work are: pH value of 6.5, the sample flow rate of 0.05 mL min^{-1}, the extraction time of 15 min and the organic microdrop volume of 4 μL.

3.3. Interferences of coexisting ions

The coexisting ions commonly found in environmental and biological samples were added individually to the samples and the effects of coexisting ions on the analytical signal intensity were investigated. The results indicated that 2000 μg mL^{-1} Na^+, K^+, 1000 μg mL^{-1} Ca^{2+}, Mg^{2+}, 10 μg mL^{-1} Fe^{3+}, Zn^{2+} and 8 μg mL^{-1} Cu^{2+}, Al^{3+} had no obvious influence (error <15%) on the signal intensity of analytes.

3.4. Analytical performance

Under the optimized temperature program of ETV and the extraction conditions, the LODs of Cd and Pb with the enrichment factor of 140 and 190 are 4.6 and 2.9 pg mL^{-1}, respectively. Linearity was obtained between 0.01 and 50 ng mL^{-1} with $r^2 > 0.99$. Table 2 is the analytical performance data for the developed method.

Table 2
Analytical performance for SDME-ETV-ICP-MS determination of Pb and Cd

Element	LOD[a]		Actual enrichment factor[b] (fold)	R.S.D.[c] (%)
	Instrument (ng mL^{-1})	Method (pg mL^{-1})		
Cd	0.64	4.6	140	16
Pb	0.55	2.9	190	12

Sample volume is 1.5 mL and drop volume is 4 μL.
[a] Defined as three times the standard deviation of the blank signal ($n = 7$).
[b] Defined as the ratio of calibration slope after SDME and before SDME microextraction.
[c] Concentrations of Cd and Pb are both 0.1 ng mL^{-1} ($n = 7$).

3.5. Sample analysis

3.5.1. Environmental water and human serum samples analysis

Tap water (pH 7.4, Wuhan, China) and Lake water (pH 8.0, East Lake, Wuhan, China) were directly filtrated with a 0.45 μm membrane filter (Tianjin Jinteng Instrument Factory, Tianjin, China) and immediately adjusted to pH of 6.5. A 1.5-mL filtered aliquot of sample was used for further analysis.

One milliliter of healthy human serum (obtained from the Hospital of Wuhan University, Wuhan, China) was accurately measured into a clean and dry PTFE digest vessel, and then 2.5 mL ultrapure nitric acid and 0.5 mL 30% H_2O_2 were added into the vessel. The vessel was closed and positioned properly in an MDS-2003F microwave oven (Sineo Microwave Chemical Technology Co. Ltd., Shanghai, China). After digested according to a certain microwave digestion program, and cooled down to room temperature, the clear sample was heated to near dryness and diluted to 10 mL with buffer solution for determination.

Referring to the previous article [29], the microwave digestion program was performed in three steps: (1) 3 min at 200 W; (2) 5 min at 400 W; (3) 5 min at 600 W.

For sample analysis, the calibration was obtained using a standard solution subjected to the microextraction as well. Blank experiments were carried out using the same procedure without samples.

The environmental water and human serum samples analytical results along with the recovery for the spiked samples are listed in Table 3. As could be seen, the recoveries were within 96–119%. It should be pointed out that the Pb concentration in human serum is a little bit higher than that in healthy human

Table 3
Analytical results (mean ± S.D., $n = 3$) for Cd and Pb in environmental water and human serum samples

Sample	Added (ng mL^{-1})	Found (ng mL^{-1})	Recovery (%)
Tap water			
Cd	0	0.61 ± 0.06	
	0.5	1.20 ± 0.22	108
	2	2.55 ± 0.31	98
Pb	0	3.25 ± 0.47	
	0.5	3.78 ± 0.77	101
	2	5.19 ± 0.88	99
Lake water			
Cd	0	0.39 ± 0.08	
	0.5	1.06 ± 0.22	119
	2	2.70 ± 0.51	113
Pb	0	2.66 ± 0.32	
	0.5	3.22 ± 0.41	102
	2	4.87 ± 0.54	105
Human serum			
Cd	0	0.16 ± 0.02	
	0.5	0.67 ± 0.24	102
	2	2.07 ± 0.24	96
Pb	0	0.73 ± 0.13	
	0.5	1.28 ± 0.32	104
	2	2.71 ± 0.28	99

Table 4
Analytical results (mean ± S.D., $n = 3$) for Cd and Pb in peach leaves sample (GBW 08501)

Sample	Certified value ($\mu g\,g^{-1}$)		Analyzed value ($\mu g\,g^{-1}$)	
	Cd	Pb	Cd	Pb
GBW 08501 peach leaves	0.018 ± 0.008	0.99 ± 0.08	0.015 ± 0.006	1.03 ± 0.17

serum, the possible reason might be some contamination in the process of separating serum from whole blood in the hospital.

3.5.2. Validation of the method

In order to validate the developed method, a standard reference material of GBW 08501 peach leaves was employed. Proper amount of peach leaves (GBW 08501) was weighed and dried for 4 h at 90 °C. Then 50.0 mg dried sample was accurately weighed into a clean and dry PTFE digest vessel, adding 2.0 mL ultrapure nitric acid and 0.5 mL analytical grade hydrofluoric acid. The peach leaves were then digested by microwave irradiation with the same program as described above, and finally diluted to 5 mL with buffer solution for determination. Blank experiments were carried out using the same procedure without peach leaves.

Table 4 lists the determination values for Cd and Pb obtained by the developed method and the certified values; as could be seen, a good agreement between the determined values and the certified values was obtained.

4. Conclusions

A method combining SDME and ETV-ICP-MS to determine trace toxic elements of Cd and Pb is described and it has some outstanding advantages: (1) the operation of SDME is simple and less toxic to environment; (2) the combination of SDME and ETV possesses low absolute LOD, high enrichment factor and is especially suitable for the determination of trace/ultra trace elements in the samples with complicated matrix; (3) 8-HQ could be used both as extractant and as chemical modifier, and the analytical sensitivity could be improved greatly.

Acknowledgements

Financial supports from National Nature Science Foundation of China and NCET, MOE of China are gratefully acknowledged.

References

[1] H. Boiteau, A. Pineau, Cadium, in: H.A. Mc Kenzie, L.E. Smythe (Eds.), Quantitative Trace Analysis of Biological Materials, Elsevier Science Publishers B.V., 1988, p. 543.
[2] T.R. Daher, Anal. Chem. 67 (1995) 405R.
[3] K.W. Warnken, G.A. Gill, L.S. Wen, L.L. Griffin, P.H. Santschi, J. Anal. At. Spectrom. 14 (1999) 247.
[4] T. Tanaka, Y. Ando, T. Saitoh, M. Hiraide, J. Anal. At. Spectrom. 17 (2002) 1556.
[5] E. Vassileva, C.R. Quetel, Anal. Chim. Acta 519 (2004) 79.
[6] Z.H. Xie, F.Z. Xie, L.Q. Guo, X.C. Lin, G.N. Chen, Sep. Sci. 28 (2005) 462.
[7] M. Tuzen, K. Parlar, M. Soylak, J. Hazard. Mater. 121 (2005) 79.
[8] T.D. Maranhao, D.L.G. Borges, da Veiga MAMS, A.J. Curtius, Spectrochim. Acta 60B (2005) 667.
[9] J.R. Chen, S.M. Xiao, X.H. Wu, K.M. Fang, W.H. Liu, Talanta 67 (2005) 992.
[10] G. Yang, Z. Li, H. Shi, J. Wang, J. Anal. Chem. 60 (2005) 480.
[11] T. Hayashita, H. Sawano, T. Higuchi, M. Indo, K. Hiratani, Z.Y. Zhang, R.A. Bartsch, Anal. Chem. 71 (1999) 791.
[12] J. Yoshinaga, M. Morita, J.S. Edmonds, J. Anal. At. Spectrom. 14 (1999) 1589.
[13] H.G. Liu, P.K. Dasgupta, Anal. Chem. 68 (1996) 1817.
[14] M.A. Jeannot, F.F. Cantwell, Anal. Chem. 68 (1996) 2236.
[15] M.A. Jeannot, F.F. Cantwell, Anal. Chem. 69 (1997) 235.
[16] S.P. Bjergaard, K.E. Rasmussen, Anal. Chem. 71 (1999) 2650.
[17] Y. He, H.K. Lee, Anal. Chem. 69 (1997) 4634.
[18] L.M. Zhao, L.Y. Zhu, H.K. Lee, J. Chromatogr. A 963 (2002) 239.
[19] V. Colombini, C.B. Montigny, L. Yang, P. Maxwell, R.E. Sturgeon, Z. Mester, Talanta 63 (2004) 555.
[20] E. Psillakis, N. Kalogerakis, Trends Anal. Chem. 21 (2002) 53.
[21] E. Psillakis, N. Kalogerakis, Trends Anal. Chem. 22 (2003) 565.
[22] Y.L. Wu, Z.C. Jiang, B. Hu, Chem. J. Chin. Univ. 24 (2003) 1793.
[23] L.B. Xia, B. Hu, Z.C. Jiang, Y.L. Wu, Y. Liang, Anal. Chem. 76 (2004) 2910.
[24] L.B. Xia, B. Hu, Z.C. Jiang, Y.L. Wu, L. Li, R. Chen, J. Anal. At. Spectrom. 20 (2005) 441.
[25] G.Q. Guo, Handbook of Analytical Chemistry, vol. 1, second ed., Chemical Industry Press, Beijing, 1997, p. 309 (in Chinese).
[26] S.Z. Chen, T.Y. Peng, Z.C. Jiang, Z.H. Liao, B. Hu, J. Anal. At. Spectrom. 14 (1999) 1723.
[27] N.N. Meeravali, S.J. Kumar, J. Anal. At. Spectrom. 13 (1998) 647.
[28] J. Stary, Anal. Chim. Acta 28 (1963) 132.
[29] F. Cubadda, A. Raggi, Microchem. J. 79 (2005) 91.

Available online at www.sciencedirect.com
ScienceDirect
Talanta 70 (2006) 474–478
Talanta
www.elsevier.com/locate/talanta

Short communication

Pipette tip solid-phase extraction and gas chromatography–mass spectrometry for the determination of mequitazine in human plasma

Takeshi Kumazawa [a,*], Chika Hasegawa [a], Xiao-Pen Lee [a], Akemi Marumo [a], Natsuko Shimmen [a], Akira Ishii [b], Hiroshi Seno [c], Keizo Sato [a]

[a] *Department of Legal Medicine, Showa University School of Medicine, 1-5-8 Hatanodai, Shinagawa-ku, Tokyo 142-8555, Japan*
[b] *Department of Legal Medicine, Fujita Health University School of Medicine, Kutsukake-cho, Toyoake, Aichi 470-1192, Japan*
[c] *Department of Legal Medicine, Aichi Medical University School of Medicine, Nagakute-cho, Aichi 480-1195, Japan*

Received 27 December 2005; received in revised form 21 February 2006; accepted 21 February 2006
Available online 2 May 2006

Abstract

Mequitazine has been found to be extractable from human plasma samples using MonoTip C_{18} tips, inside which C_{18}-bonded monolithic silica gel was fixed. Human plasma (0.1 mL) containing mequitazine and cyproheptadine as an internal standard (IS) was mixed with 0.4 mL of distilled water and 25 μL of 1 M potassium phosphate buffer (pH 8.0). After centrifugation of the mixture, the supernatant fraction was extracted to the C_{18} phase of the tip by 25 repeated aspirating/dispensing cycles using a manual micropipettor. The analytes retained on the C_{18} phase were then eluted with methanol by five repeated aspirating/dispensing cycles. Without evaporation and reconstitution, the eluate was injected into a gas chromatograph injector and detected by a mass spectrometer with selected ion monitoring in the positive-ion electron impact mode. The separation of mequitazine and the IS from each other and from impurities was generally satisfactory using a DB-1MS capillary column (30 m × 0.32 mm i.d., film thickness 0.25 μm). The recoveries of mequitazine and the IS spiked into plasma were more than 90.0%. The regression equation for mequitazine showed excellent linearity in the range of 0.2–200 ng 0.1 mL^{-1}, and the detection limit was 0.05 ng 0.1 mL^{-1} of plasma. The intra-day and inter-day coefficients of variation for mequitazine in human plasma were not greater than 8.16 and 9.24%, respectively. Accuracy for the drug was in the range of 90.0–97.4%. The data obtained from determination of mequitazine in human plasma after oral administration of the drug are also presented.

Keywords: Mequitazine; Pipette tip solid-phase extraction; Gas chromatography; Mass spectrometry

1. Introduction

Mequiazine is a phenothiazine derivative, which has been described as a potent, non-sedative and long-acting histamine H_1 antagonist, and is widely used for the treatment of allergic reactions, such as hay fever, urticaria and allergic rhinitis [1,2].

Mequitazine has usually been extracted from human body fluids by liquid–liquid extraction (LLE) with organic solvents such as chloroform [3], diethyl ether [3,4], hexane [5] and dichloromethane–isopropanol–ethyl acetate (1:1:3) [6] before its analysis by gas chromatography (GC)–mass spectrometry (MS) [4–6] or high-performance liquid chromatography (HPLC) [3]. However, there are several disadvantages associated with conventional extraction procedures such as LLE [7–11]. These procedures are time-consuming and tedious. Moreover, the large amount of organic solvents used in the extraction procedure causes problems with regard to health and the environment.

Micropipette tip based micro-SPE is now an essential tool for purification, concentration and selective isolation (by affinity and metal chelate) of proteins and peptides in the study of genomics, proteomics and metabolomics [12–15]. To minimize the required volume of solvents as well as samples, SPE is available in a miniaturized format such as the SPE pipette tip. Several manufacturers have developed SPE pipette tips, such as the ZipTip and NuTip, that can be used for the purification of small amounts of proteins or peptides [16,17]. Recently, a new SPE pipette tip, the MonoTip C_{18} tip, was developed in Japan for the purification of proteins and peptides from aqueous samples [18]. In this device, monolithic silica (diameter 2.8 mm, thickness 1 mm), consisting of continuous mesoporous (pore-size, 20 nm) silica skeletons ∼10 μm in size and 10–20-μm through-pores, is fixed in the end of the 200-μL pipette tip; the monolithic silica

* Corresponding author. Tel.: +81 3 3784 8140; fax: +81 3 3787 6418.
E-mail address: kumazawa@med.showa-u.ac.jp (T. Kumazawa).

0039-9140/$ – see front matter © 2006 Elsevier B.V. All rights reserved.
doi:10.1016/j.talanta.2006.02.059

surface is modified chemically with the C_{18} phase. The sample solution is aspirated and dispensed through the MonoTip C_{18} tip for extraction of analytes using the micropipettor before HPLC or HPLC–MS analysis. An advantage of the MonoTip C_{18} tips for sample preparation is that extraction can be carried out more easily and rapidly than with the conventional SPE cartridges. The small bed volume and sorbent mass within the MonoTip C_{18} tip allow for the use of a reduced solvent volume, smaller elution volume, reduced time for the evaporation step and higher throughput.

A number of pipette tip SPE methods have been published for the extraction of peptides and proteins from biological samples [12–14,16–18]. Van Hout et al. [19] reported pipette tip SPE–GC for lidocaine and diazepam in phosphate buffer, but not in biological samples. In this paper, we report the establishment of recommendable pipette tip SPE procedure for determining mequitazine from human plasma samples using the MonoTip C_{18} tip and GC–MS analysis.

2. Experimental

2.1. Materials

The chemical structures of mequitazine and cyproheptadine as an internal standard (IS) examined in this study are shown in Fig. 1. Mequitazine was provided by Asahi Kasei Pharma Co. (Tokyo, Japan). Cyproheptadine hydrochloride was purchased from Sigma Chemicals (St. Louis, MO, USA). The MonoTip C_{18} tips (200 μL pipette-tip volume, C_{18}-bonded monolithic silica gel with a diameter of 2.8 mm and thickness of 1 mm) were purchased from GL Sciences Inc. (Tokyo). Other common chemicals used were of highest purity commercially available. Drug-free whole blood samples were obtained from healthy volunteers and were centrifuged at 1300 × *g* for 10 min at 4 °C in the presence of EDTA-2Na as an anticoagulant. Plasma was decanted, and stored at −80 °C until use. The drug-free plasma was used to prepare plasma samples containing mequitazine and the IS, and also used as blank samples.

2.2. Preparation of standard solutions

Stock standard solutions of mequitazine and the IS were prepared separately by dissolving an appropriate amount of each compound in methanol to achieve a concentration of 1 mg mL^{-1}.

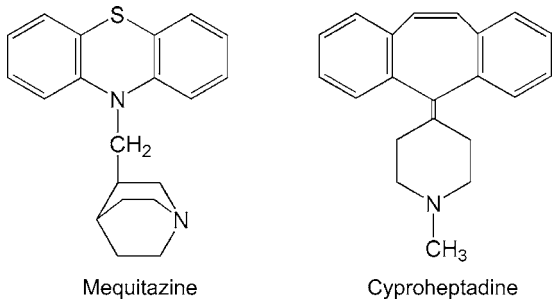

Fig. 1. Chemical structures of mequitazine and cyproheptazine (IS) used in this study.

Working standard solutions of the compounds were prepared by serial dilution of the stock standard solutions with methanol. These working standard solutions were then used for making spiked plasma samples.

2.3. GC–MS conditions

All analyses were performed using a Shimadzu GC-2010 gas chromatograph interfaced with a Shimadzu QP-2010 quadrupole mass spectrometer (Shimadzu Corp., Kyoto, Japan). The GC–MS was operated with the interface temperature at 250 °C and the ionization source temperature at 280 °C. The mass spectrometer was tuned on a daily basis using perfluorotributylamine. A solvent delay of 5 min was set to protect the filament from oxidation. Chromatographic separation was achieved using a DB-1MS fused silica capillary column (30 m × 0.32 mm i.d., film thickness 0.25 μm, J&W Scientific, Folsom, CA, USA). Helium was used as carrier gas at a flow rate of 2.0 mL min^{-1}. An AOC-20i autoinjector (Shimadzu Corp.) was used to inject 2 μL of standard solution or extract into the GC–MS. The gas chromatograph was equipped with a split/splitless injection port operated at 250 °C. The samples were injected in the splitless mode and the splitter was opened after 1 min. The gas chromatograph oven temperature was initially held at 120 °C for 1 min and then temperature-programmed at 20 °C min^{-1} to 300 °C. The mass spectrometer was operated in the positive-ion electron impact (EI) mode. EI mass spectra were obtained at an ionizing energy of 70 eV and emission current of 60 μA. In order to select the monitoring ion for mequitazine and the IS, mass spectra were obtained from injections of working solutions of the analyte standards into the GC–MS. For each compound the following ions were observed: *m/z* 124 and 322 for mequitazine; *m/z* 287, 96 and 215 for the IS. Base peak ions (underlined) were used for quantification of mequitazine and the IS by the selected ion monitoring (SIM) mode.

2.4. Sample preparation

Extraction of mequitazine and the IS from human plasma was achieved using a MonoTip C_{18} micropipette tip. After attaching the tip onto a Pipetman P200 microliter pipette (Gilson SAS, Villiers-le-Bel, France), preconditioning of the tip was done by aspirating and dispensing (to waste) 200 μL of methanol and then 200 μL of distilled water through the tip. For new tips, this procedure was repeated twice to reduce background noise. To 0.1 mL of a plasma sample containing mequitazine and the IS were added 0.4 mL of distilled water and 25 μL of 1 M potassium phosphate buffer (pH 8.0). After centrifugation of the mixture at 10,000 × *g* for 10 min, the supernatant fraction was decanted into a clean sample tube (1.5 mL). A 200-μL aliquot of the supernatant was aspirated into the conditioned MonoTip C_{18} tip and dispensed back into the same sample tube. These two steps together are referred to as one aspirating/dispensing cycle. In this work, the extraction of mequitazine and the IS onto the C_{18} phase of the tip was performed by 25 repeated aspirating/dispensing cycles. The tip was then washed by aspirating

200 μL of distilled water and dispensing the eluate to waste. After washing, the tip was placed on a vacuum manifold and dried under vacuum for 3 min to remove any traces of water. Finally, mequitazine and the IS were eluted from the tip into an autoinjector vial (200 μL) by five repeated aspirating/dispensing cycles of 100 μL of methanol. A 2-μL aliquot of the eluates was subjected to GC–MS analysis.

2.5. Evaluation for recovery, quantification and linearity

The recoveries were calculated by comparing the chromatographic peak areas obtained from the extracts of the spiked plasma samples with those obtained by direct GC injection of non-extracted authentic compound dissolved in methanol, and determined at two to three different concentrations of the compounds. Regression equation for mequitazine extracted from human plasma were obtained by fitting the ratio of the peak area of the analyte to that of the IS (10 ng) against concentrations of the analyte. Concentrations of the calibrators ranged from 0.2 to 200 ng 0.1 mL^{-1} for mequitazine (10 calibrators: 0.2, 0.5, 1, 2, 5, 10, 20, 50, 100 and 200 ng 0.1 mL^{-1}). Intra-day coefficient of variation (CV) and accuracy were determined by replicate analysis of six sets of plasma samples spiked with four different concentrations of mequitazine (0.5, 5, 50 and 200 ng 0.1 mL^{-1}). The same procedure was repeated on 5 different days to determine the inter-day CV and accuracy. The detection limit was determined in such a way that the analyte spiked in plasma yielded a response signal that was at least three times the backgrounds noises.

2.6. Administration of mequitazine to volunteers

A therapeutic oral dose of mequitazine (6 mg) was administered orally to two healthy volunteers, a 28-year-old female (40 kg body weight) and a 27-year-old male (60 kg body weight). Informed consent was obtained from the subjects after explanation of the nature and aims of this study. Whole blood samples were collected at pre-dose (0 h) and then 5 h after drug administration, and transferred to centrifuge tubes containing EDTA-2Na. Blood samples were centrifuged at 1300 × *g* for 10 min to obtain plasma. Plasma samples were stored at −80 °C until analysis.

3. Results and discussion

3.1. Optimization of extraction conditions for MonoTip C_{18} tips

The number of aspirating/dispensing cycles is the critical parameter for extraction recovery in the pipette tip SPE method using the MonoTip C_{18} tips. The extraction profiles of mequitazine and the IS were examined by plotting analyte recovery from the plasma samples versus the aspirating/dispensing cycles (Fig. 2). The extraction of the compounds reached equilibrium after 25 aspirating/dispensing cycles. We thus decided the number of aspirating/dispensing cycles of extraction at 25 cycles (roughly 1.5 min). In the elution process, mequitazine and

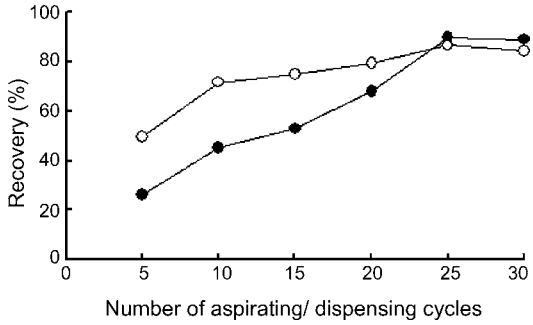

Fig. 2. Effect of number of aspirating/dispensing cycles on the extraction of mequitazine (●) and IS (◯) from human plasma by the MonoTip C_{18} tips. The amount of each compound spiked into 0.1 mL of plasma was 50 ng. Each point represents the mean of duplicate determinations.

the IS were eluted from the MonoTip C_{18} tip into an autoinjector vial (200 μL) by aspirating/dispensing of 100 μL of methanol through the tip several times. The results showed that the number of aspirating/dispensing cycles for desorption was not significant for the compounds tested (Fig. 3). However, to achieve sufficient recovery within a short period of time, five repeated aspirating/dispensing cycles (roughly 10 s) of 100 μL of methanol were used in the elution step.

In the present study, all extraction procedures including conditioning, sampling (extraction), washing, drying and elution by the MonoTip C_{18} tips required approximately 8 min. In addition, the eluate from the MonoTip C_{18} tips was directly injected into a GC injector without evaporation and reconstitution steps; this is particularly important in view of rapid and simple analysis. However, the time required to manually perform conventional cartridge SPE was reported to be >20 min [20–22]. Therefore, the use of the MonoTip C_{18} tips is recommended for rapid extraction of mequitazine from human samples.

3.2. Reliability of the method

We have demonstrated the quantitative analysis of mequitazine with cyptoheptadine as the IS. The best way to select an IS is to use a stable isotope-labeled analyte. Since such an IS for mequitazine is not commercially available, an alternative approach was taken. The chromatographic retention, extractability and ionization behavior of the IS should match

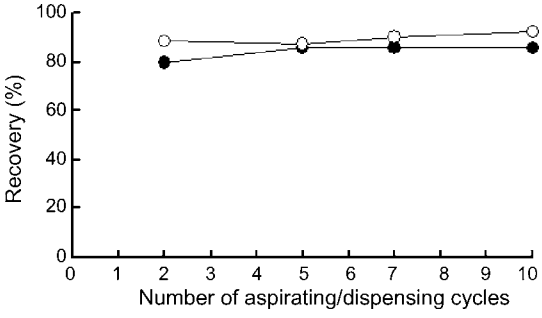

Fig. 3. Effect of number of aspirating/dispensing cycles on the elution of mequitazine (●) and IS (◯) extracted from human plasma by the MonoTip C_{18} tip. The amount of each compound spiked into 0.1 mL of plasma was 50 ng. Each point represents the mean of duplicate determinations.

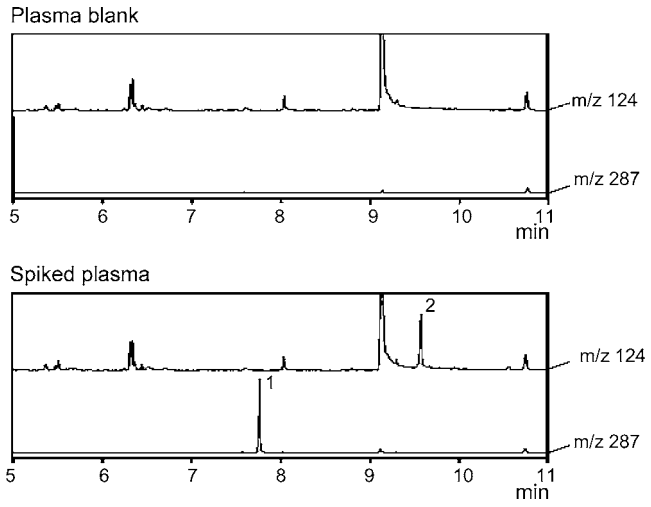

Fig. 4. SIM chromatograms for mequitazine and IS extracted from human plasma by the MonoTip C_{18} tips. The amounts of mequitazine and IS spiked into 0.1 mL of plasma were 5 and 10 ng, respectively. Peaks: (1) IS and (2) mequitazine.

those of mequitazine. In preliminary trials, other antihistamines were assessed for the selection of the IS, and cyproheptadine was found to fulfill these criteria sufficiently. Moreover, the co-existence of both mequitazine and cyproheptadine in a sample is rare clinically. Therefore, cyptoheptadine was chosen as the IS in the quantitative analysis of mequitazine from human plasma.

Fig. 4 shows SIM chromatograms obtained for extracts from 0.1 mL of human plasma in the presence (5 ng of mequitazine and 10 ng of the IS) or absence of the compounds. Distinct peaks appeared for two compounds, and the retention times for the IS and mequitazine were 7.92 and 9.58 min, respectively (Fig. 4, lower panel). While some impurity peaks were observed for the blank plasma, no interfering peaks were found around the peaks of the test compounds (Fig. 4, upper panel).

Recoveries of mequitazine and the IS from plasma samples using the present method are presented in Table 1. Recoveries of mequitazine and the IS were 90.0–91.3 and 93.5–94.7%, respectively. The calibration curve for mequitazine from plasma showed good linearity in the ranges of 0.2–200 ng 0.1 mL^{-1}. The equation and regression coefficients were: $y = 0.1874x + 0.0538$ and $r = 0.9999$. The detection limit of the drug was estimated to be 0.05 ng 0.1 mL^{-1} plasma. The intra-day and inter-day CVs are shown in Table 2. The intra-day and inter-day CVs at all concentrations examined were less than 8.16 and 9.24%, respectively. The accuracy values for intra-day and inter-day study were in the range of 90.0–97.4%.

3.3. Application of the method to dosed human samples

In addition to spiked human plasma, the present method was applied to human plasma samples collected from oral administration of mequitazine. Typical SIM chromatograms obtained for plasma samples from a female volunteer are shown in Fig. 5. The drug concentration in the plasma of the female volunteer was 0.97 ng 0.1 mL^{-1} at 5 h after administration, and that of the male volunteer was 0.82 ng 0.1 mL^{-1}. These concentrations in plasma were within therapeutic levels [4,5,23].

Table 1
Recovery data of mequitazine and cyproheptadine (IS) from human plasma

Compound	Amount added (ng 0.1 mL^{-1})	Amount extracted (ng 0.1 mL^{-1})[a]	Recovery (%)
Mequitazine	500	457 ± 27.5	91.3
	50	45.7 ± 3.66	91.4
	5	4.50 ± 0.29	90.0
Cyproheptadine	50	47.4 ± 1.12	94.7
	5	4.67 ± 0.16	93.5

[a] Values are mean ± S.D. of four to five experiments.

Table 2
Intra- and inter-day coefficients of variation (CV) and accuracy for mequitazine from human plasma

Amount added (ng 0.1 mL^{-1})	Amount detected (ng 0.1 mL^{-1})	Accuracy (%)	CV (%)
Intra-day[a]			
200	195 ± 8.21[c]	97.3	4.22
50	47.1 ± 3.18	94.2	6.75
5	4.50 ± 0.27	90.0	6.03
0.5	0.49 ± 0.04	97.4	8.16
Inter-day[b]			
200	183 ± 14.6[c]	91.7	7.97
50	45.0 ± 3.19	90.6	7.08
5	4.76 ± 0.44	95.2	9.24
0.5	0.46 ± 0.04	92.6	9.03

[a] Intra-day CV was calculated from measurements of six spiked samples on the same day.
[b] Spiked plasma were kept at 4 °C and analyzed on 5 separate days, with one sample each day.
[c] The values are mean ± S.D.

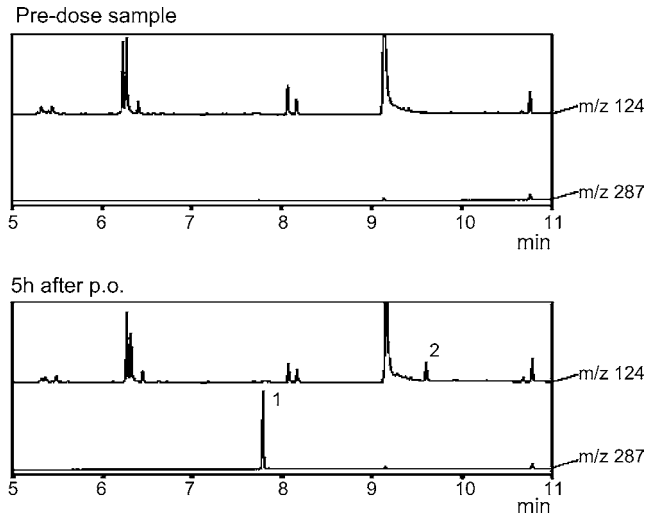

Fig. 5. SIM chromatograms obtained from extracts of plasma of a female volunteer at 5 h after oral administration of 6 mg of mequitazine. The amount of cyproheptadine used as IS was 10 ng for 0.1 mL of plasma. The key numbers are the same as specified in Fig. 4.

4. Conclusion

We were able to extract and detect mequitazine in human plasma samples by pipette tip SPE with the MonoTip C_{18} tips and GC–MS. Compared to LLE and conventional SPE, the present pipette tip SPE technique reduced sample extraction time and organic solvent consumption. Under optimized conditions, good recovery, linearity and reproducibility were obtained. The present results on the extraction of mequitazine by MonoTip C_{18} tips suggests its applicability to a number of other drugs in the fields of therapeutic drug monitoring, clinical toxicology and forensic toxicology.

Acknowledgement

This study was supported in part by a grant-in-aid from the Ministry of Education, Science, Sports and Culture of Japan.

References

[1] A. Uzan, G. Le Fur, C. Malgouris, J. Pharm. Pharmacol. 31 (1979) 701.
[2] A.N. Nicholson, Lancet ii (1983) 211.
[3] N.A. El-Ragehy, A.M. Badawey, S.Z. El Khateeb, J. Pharm. Biomed. Anal. 29 (2002) 121.
[4] J.-B. Fourtillan, J. Girault, S. Bouquet, M.-A. Lefèbvre, J. Chromatogr. 309 (1984) 391.
[5] O.-S. Kwon, H.-J. Kim, H. Pyo, S.-J. Chung, Y.B. Chung, Arch. Pharm. Res. 28 (2005) 1190.
[6] H. Maurer, K. Pfleger, Arch. Toxicol. 62 (1988) 185.
[7] D.L. Mayer, J.S. Fritz, J. Chromatogr. A 773 (1997) 189.
[8] T. Kumazawa, X.-P. Lee, K. Sato, O. Suzuki, Anal. Chim. Acta 492 (2003) 49.
[9] X.-P. Lee, T. Kumazawa, J. Sato, Y. Shoji, C. Hasegawa, C. Karibe, T. Arinobu, H. Seno, K. Sato, Anal. Chim. Acta 492 (2003) 223.
[10] M. Abdel-Rehim, J. Chromatogr. B 801 (2004) 317.
[11] C. Hasegawa, T. Kumazawa, M. Fujishiro, X.-P. Lee, A. Marumo, Y. Shoji, J. Sato, H. Seno, K. Sato, Anal. Lett. 38 (2005) 1379.
[12] M.G. Pluskal, A. Bogdanova, M. Lopez, S. Gutierrez, A.M. Pitt, Proteomics 2 (2002) 145.
[13] T. Keough, M.P. Lacey, R.S. Youngquist, Rapid Commun. Mass Spectrom. 16 (2002) 1003.
[14] N.S. Tannu, J. Wu, V.K. Rao, H.S. Gadgil, M.J. Pabst, I.C. Gerling, R. Raghow, Anal. Biochem. 327 (2004) 222.
[15] J. Šalplachta, P. Řehulka, J. Chmelík, J. Mass Spectrom. 39 (2004) 1395.
[16] Micropipette Tip-Based Sample Preparation for Bioanalysis, LCGC North America, 2005 (http://www.lcgcmag.com/lcgc/).
[17] M. Palmblad, J.S. Vogel, J. Chromatogr. B 814 (2005) 309.
[18] S. Miyazaki, K. Morisato, N. Ishizuka, H. Minakuchi, Y. Shintani, M. Furuno, K. Nakanishi, J. Chromatogr. A 1043 (2004) 19.
[19] M.W.J. van Hout, R.A. de Zeeuw, G.J. de Jong, J. Chromatogr. A 858 (1999) 117.
[20] O. Suzuki, T. Kumazawa, H. Seno, H. Hattori, Med. Sci. Law 29 (1989) 242.
[21] Z. Huang, S. Zhang, J. Chromatogr. B 792 (2003) 241.
[22] A. Marumo, T. Kumazawa, X.-P. Lee, K. Fujimaki, A. Kuriki, C. Hasegawa, K. Sato, H. Seno, O. Suzuki, J. AOAC Int. 88 (2005) 1655.
[23] P. Ylitalo, K. Nieminen, G. Wilén-Rosenqvist, J.-B. Fourtillan, J. Girault, L. Ylitalo, J.S. Pukander, P.H. Karma, Int. J. Clin. Pharm. Res. IX (1989) 305.

Available online at www.sciencedirect.com
ScienceDirect
Talanta 70 (2006) 479
Talanta
www.elsevier.com/locate/talanta

Erratum

Erratum to "DNA mutation analysis based on capillary electrochromatography using colloidal poly(*N*-isopropylacrylamide) particles as pseudostationary phase" [Talanta 68 (3) (2006) 940–944]

Joon Myong Song [a,*], Amit Asthana [b], Dong Pyo Kim [b,**]

[a] *College of Pharmacy, Seoul National University, Seoul 151-742, South Korea*
[b] *Department of Fine Chemical Engineering and Chemistry, Chungnam National University, Daejon 305-764, South Korea*

The publisher regrets that the project number in the acknowledgement was mistyped. The corrected Acknowledgment is reproduced below.

Acknowledgement

This work was supported by Korea Research Foundation Grant (KRF-2004-042-C00085).

DOI of original article:10.1016/j.talanta.2005.06.052.
* Corresponding author. Tel.: +82 2 880 7857; fax: +82 2 874 8928.
** Corresponding author. Fax: +82 42 821 6695.
E-mail addresses: jmsong@cnu.ac.kr (J.M. Song), dpkim@cnu.ac.kr (D.P. Kim).

doi:10.1016/j.talanta.2006.08.001

Available online at www.sciencedirect.com
ScienceDirect
Talanta 70 (2006) 480
Talanta
www.elsevier.com/locate/talanta

Corrigendum

Corrigendum to "Determination of gentamicin in pharmaceutical formulations using peroxyoxalate chemiluminescent detection in flow-injection analysis" [Talanta 69 (3) (2006) 763–768]

José M. Ramos-Fernández, Ana M. García-Campaña, Fermín Alés-Barrero, Juan M. Bosque-Sendra *

Department of Analytical Chemistry, Faculty of Sciences, University of Granada, E-18071 Granada, Spain

The author regrets that during the processing of the above paper an error occurred in one of the author's names. The author list is reproduced correctly above.

DOI of original article:10.1016/j.talanta.2005.11.008.
* Corresponding author. Tel.: +34 958 248435; fax: +34 958 243328.
E-mail address: jbosque@ugr.es (J.M. Bosque-Sendra).

doi:10.1016/j.talanta.2006.08.002

Talanta

The International Journal of Pure and Applied Analytical Chemistry

Publication information: *Talanta* (ISSN 0039-9140). For 2006, volumes 68–70 are scheduled for publication. Subscription prices are available upon request from the Publisher or from the Regional Sales Office nearest you or from this journal's website (http://www.elsevier.com/locate/talanta). Further information is available on this journal and other Elsevier products through Elsevier's website: (http://www.elsevier.com). Subscriptions are accepted on a prepaid basis only and are entered on a calendar year basis. Issues are sent by standard mail (surface within Europe, air delivery outside Europe). Priority rates are available upon request. Claims for missing issues should be made within six months of the date of dispatch.

Orders, claims, and journal enquiries: please contact the Customer Service Department at the Regional Sales Office nearest you:
Orlando: Elsevier, Customer Service Department, 6277 Sea Harbor Drive, Orlando, FL 32887-4800, USA; phone: (+1) (877) 8397126 [toll free number for US customers], or (+1) (407) 3454020 [customers outside US]; fax: (+1) (407) 3631354; e-mail: usjcs@elsevier.com
Amsterdam: Elsevier, Customer Service Department, PO Box 211, 1000 AE Amsterdam, The Netherlands; phone: (+31) (20) 4853757; fax: (+31) (20) 4853432; e-mail: nlinfo-f@elsevier.com
Tokyo: Elsevier, Customer Service Department, 4F Higashi-Azabu, 1-Chome Bldg, 1-9-15 Higashi-Azabu, Minato-ku, Tokyo 106-0044, Japan; phone: (+81) (3) 5561 5037; fax: (+81) (3) 5561 5047; e-mail: jp.info@elsevier.com
Singapore: Elsevier, Customer Service Department, 3 Killiney Road, #08-01 Winsland House I, Singapore 239519; phone: (+65) 63490222; fax: (+65) 67331510; e-mail: asiainfo@elsevier.com

USA mailing notice: *Talanta* (ISSN 0039-9140) is published monthly by Elsevier B.V. (P.O. Box 211, 1000 AE Amsterdam, The Netherlands). Annual subscription price in the USA US$ 3,628 (valid in North, Central and South America), including air speed delivery. Application to mail at periodical postage rate is pending at Jamaica, NY 11431.
USA POSTMASTER: Send address changes to *Talanta*, Publications Expediting Inc., 200 Meacham Avenue, Elmont, NY 11003.
AIRFREIGHT AND MAILING in the USA by Publications Expediting Inc., 200 Meacham Avenue, Elmont, NY 11003.